THE JOURNAL
OF
CHEMICAL PHYSICS

VOLUME 21, NUMBER 2 FEBRUARY, 1953

Low Temperature Spectroscopy in the Farther Ultraviolet Region*

W. J. POTTS, JR.†
Department of Chemistry, University of Chicago, Chicago, Illinois
(Received September 15, 1952)

Methods are presented which make possible quantitative spectroscopic measurements at liquid nitrogen temperatures from the visible region to as far as 1670A in the ultraviolet region.

THE importance of ultraviolet spectroscopic measurements at low temperature is well known. At the temperature of liquid nitrogen (77°K) absorption spectra often become much sharper.[1] Also, the use of rigid transparent media at low temperature allows the study of phosphorescence of many organic molecules, whose long-lived emission could not otherwise be observed, because of collision quenching.[2] A common technique for low temperature spectroscopy has been the use of a rigid glass. This consists of some mixture of solvents which is transparent over a reasonable portion of the ultraviolet spectrum and which forms a stable glass upon cooling with liquid nitrogen. A mixture of ether, isopentane, and alcohol, often referred to as EPA in the literature, has found the widest use as such a glass. Although the use of EPA has been very fruitful in obtaining spectra of molecules which absorb in the nearer ultraviolet region (above about 2200A), it is not applicable in shorter wavelength regions because ether and alcohol become opaque in path lengths of a centimeter or so. The purpose of this paper is to demonstrate that hydrocarbon glasses make investigation of the farther ultraviolet region possible at low temperatures.

HYDROCARBON GLASSES

To achieve a satisfactory glass which will show reasonable transmission into the Schuman region of the ultraviolet, use must be made of a mixture of carefully purified paraffin hydrocarbons. Mixtures of other compounds either do not have the desired transmission in the far ultraviolet, will not form glasses, or do not dissolve organic molecules. Of the numerous possible mixtures of paraffin hydrocarbons that form low temperature glasses,[3] three of use are 3-methylpentane (alone), a mixture of 3-methylpentane and isopentane, and a mixture of methylcyclohexane and isopentane.

A one centimeter path of 3-methylpentane alone has usable transmission to about 2000A at room temperature and to about 1900A at low temperature. The glass formed at 77°K is not too satisfactory, because of its high "hardening point"; that is, the glass "sets" at a temperature somewhat above 77°K, and with further cooling the contraction either causes the glass to crack if in a closed cell, or else forms a very deep "meniscus" if in an open tube.

More satisfactory glasses are formed by the mixtures of isopentane with methylcyclohexane or 3-methylpentane. Almost any proportion in either mixture forms a satisfactory glass. Thus it is advantageous to make the proportion of isopentane high, and thereby utilize the high transmission of isopentane.

A mixture of 6 parts isopentane and one part methylcyclohexane makes a very stable glass with good transmission properties. Even better in all respects is a mixture of 6 parts isopentane and one part 3-methylpentane. The latter "sets" at a temperature only a little above that of liquid nitrogen, and thus gives very little trouble in contraction after hardening. The over-all contraction (from the liquid at room temper-

* Presented before the Annual Symposium on Molecular Structure and Spectroscopy, Ohio State University, Columbus, Ohio, June 9–13, 1952.

† AEC Predoctoral Fellow, University of Chicago.

[1] Sinsheimer, Scott, and Loofbourow [J. Biol. Chem. 187, 299 (1950)] list the causes of spectral sharpness at low temperature. The authors review various techniques of low temperature spectroscopy, and give several references.

[2] Discussed at length by M. Kasha, Chem. Revs. 41, 401 (1947).

[3] Dr. M. Kasha, in an unpublished work, lists several.

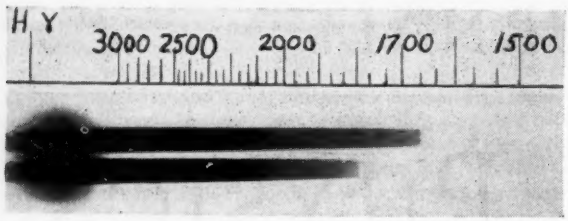

FIG. 1. Comparison of solvent transmission at room and low temperature. Bottom exposure is transmission of a 1.27-cm path of a mixture of one part 3-methylpentane and 6 parts isopentane. Top exposure is transmission of the same mixture at liquid nitrogen temperature. The scale is in angstrom units.

ature to the rigid glass at 77°K) is 22±2 percent for all these mixtures, including EPA.

Obtaining useful and reproducible transmission in low temperature glasses throughout the ultraviolet region is an experimental problem of no small magnitude. There are several seemingly trivial precautions, often neglected by most authors, which have little effect in the ultraviolet region above about 3000A, but which must be followed to obtain reproducible transmission below about 2800A, and to obtain *any* transmission in the region 2100 to 1700A.

The design of apparatus is important. Of course, a suitable spectrograph must be employed. Spectrographs with large quartz optics are usually too slow below 2200A to be suitable for low temperature work. Below 2000A a vacuum spectrograph should be employed.

The light path should pass through as few optical parts as possible, other than the hydrocarbon glass. Thick and numerous windows are to be avoided, and all optical surfaces should be flat, with the exception of lenses. The ultraviolet light should not pass through any distance of the liquid nitrogen refrigerant, for although centimeter paths of liquid nitrogen transmit light to 1750A, it is difficult to keep liquid nitrogen pure, and bubbles can become quite troublesome.

The hydrocarbons that make up the glass must be highly purified for use in the farther ultraviolet. Suitable methods for purification of the hydrocarbons mentioned in this paper have been discussed.[4]

By far the most important precaution to be followed to obtain useful transmission in low temperature glasses is to remove thoroughly all the dissolved air before freezing and to seal the hydrocarbon mixture from the air so that none redissolves during nor after freezing. If this is not done, the hydrocarbon mixture shows far worse transmission at low temperatures than at room temperature. But if the air is removed prior to freezing, a glass results having farther ultraviolet transmission than at room temperature, and having sufficient reproducibility to be employed for quantitative low temperature spectra.

Figure 1 is a reproduction of a plate used to determine the room temperature and low temperature transmission of the mixture of one part 3-methylpentane and 6 parts isopentane. The scale is in angstrom units. The bottom exposure of Fig. 1 shows transmission of the mixture at room temperature, using the apparatus described below. The top exposure is the same hydrocarbon mixture, but at liquid nitrogen temperature as an optimum rigid glass. The exposure times are equal. Note that the low temperature transmission limit extends about 100A farther into the ultraviolet: to 1670A. This limit is some 500A lower than any transmission limit for low temperature rigid glasses appearing in earlier literature. Because the 6 to 1 isopentane-3-methylpentane glass, hereafter referred to as 3PIP, is superior in all respects to other hydrocarbon glasses studied, it has been employed by the author for actual spectroscopic measurements.

A possible explanation for this increased transmission limit at low temperature is that the hydrocarbon molecules, during the cooling process (22 percent contraction), assume a more compact internal configuration.[5] It is entirely possible that there is no spectral transition of any strength in the region between 1700 and 1800A from this configuration.

That the increased transmission at low temperatures is due to the molecules all being in their lowest vibrational state is probably an erroneous explanation. A simple calculation shows that if this is the cause, the

TABLE I. Transmission properties of some spectroscopic solvents used in the farther ultraviolet.

Compound	Transmission limit at room temperature, 1-cm path	Transmission limit at room temperature, 0.14 mm path	Transmission limit of cm path of low temperature glass		Purification	Storage properties
C_2H_5OH	*ca* 2100A[a]	1890A[a]	2 C_2H_5OH + 5 iso-C_5H_{12}	*ca* 2200A	Dist fr CaO	poor
$(C_2H_5)_2O$	2130	1980[a]	5 $(C_2H_5)_2O$		Dist fr Na	poor
H_2O	1870[a]	1785[a]	...		Redist fr $KMnO_4$	good
n-C_7H_{16}	1950[b]	1720[b]	...		Tr w H_2SO_4	good
n-C_8F_{18}	*ca* 1800[c]	1580[c]	...		Fract dist	good(?)
3-Me-C_5H_{12}	1950[b]	1720[b]	1 3-Me-C_5H_{12}		Tr w H_2SO_4, SiO_2	good
iso-C_5H_{12}	1770[b]	1720[b]	6 iso-C_5H_{12}	1670	Tr w H_2SO_4, SiO_2	good
Me-Cyclo-C_6H_{12}	2100[b]	1780[b]	1 Me-Cyclo-C_6H_{12}	1700	Tr w H_2SO_4, SiO_2	good

[a] H. B. Klevens and J. R. Platt, J. Am. Chem. Soc. **69**, 3005 (1947).
[b] See reference 4.
[c] H. B. Klevens and J. R. Platt, J. Chem. Phys. **16**, 1168 (1948).

[4] W. Potts, J. Chem. Phys. **20**, 809 (1952).
[5] In the discussion following the papers of Disc. Faraday Soc. **10**, Part I, 125 ff. (1951), this possibility is pointed out.

molar extinction of the molecules in their first (or higher) excited vibrational states must be about 10^6, prohibitively high for such electronic systems. Furthermore, this would not explain why the transmission limit of a short path of hydrocarbon at room temperature is poorer than a path 100 times as long is at low temperature.

Table I gives a summary of ultraviolet transmission limits of some spectroscopic solvents under various conditions. Data are for purest solvents in all casses.

Hydrocarbon glasses, unfortunately, do not seem as satisfactory as EPA (ether, isopentane, alcohol mixture) for phosphorescence studies. Visual observation of benzene and naphthalene phosphorescence shows shorter phosphorescent lifetimes in hydrocarbon glasses than in EPA. This is probably caused by viscosity dependent quenching, the EPA presumably being more viscous at liquid nitrogen temperature than the hydrocarbon glasses studied. Varying the component porportions in hydrocarbon glasses will change their viscosities at low temperature, but the disturbing trend observed is that the better the ultraviolet transmission of the glass, the more undesirable its quenching action. This curious result deserves further investigation. Still lower temperatures (liquid hydrogen) may be helpful.

APPARATUS AND METHODS FOR THE FAR ULTRAVIOLET

The apparatus for low temperature absorption spectra in the farther ultraviolet is shown in Fig. 2. *A* is the actual absorption cell: a brass tube ½ in. long with very thin (0.2 mm) quartz windows (*C'*) cemented onto the ends. (The cement is Araldite, manufactured by Ciba Pharmaceutical Company. It was the only cement found by the author which is not attacked to more than negligible extent by organic solvents, and which does not crack at liquid nitrogen temperatures. Care must be exercised in the making of metal to glass type joints with this cement. If they are to withstand low temperatures, they must be made in such a way that the strain due to the different thermal expansions is taken up; this is accomplished here by the use of very thin pieces of quartz.) Sapphire windows, ⅛ in. thick *C* are cemented with Araldite onto the glass end of the hydrogen lamp *P* and onto a glass tube, which is in turn connected to the spectrograph with a Housekeeper seal *E*. *B* is an ordinary Pyrex beaker with round holes cut in opposite sides, the space around the holes being plugged with a mixture of vacuum putty and stopcock grease *D*. Sylphons *F* make connections to the entrance of the vacuum spectrograph *H*. The lower sylphon allows positioning of the entrance window under vacuum, and the upper one is for the shutter control *G*. The tube by which the cell is filled *J* is attached to a Kovar seal *K*, in turn attached to a male ground glass joint *L*. *M* is a stopcock in the upper vent tube; it is lubricated with silicone grease.

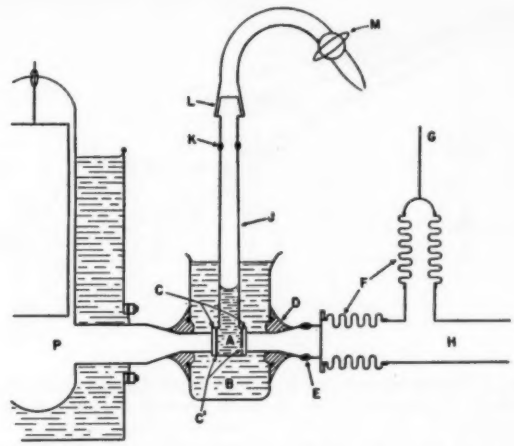

FIG. 2. Apparatus used to obtain far ultraviolet low temperature absorption spectra.

The spectrograph used is a Cario-Schmitt-Ott vacuum fluorite spectrograph, which has been described previously in the literature.[6] Ilford type Q1 plates, 4 in.×¾ in., are employed. Four exposures may be put on one plate. A liquid nitrogen trap must be put in the vacuum pump line of the spectrograph, so that vapors from the pump will not condense and accumulate on the inside of the sapphire entrance window.

The light source is a standard hydrogen capillary discharge tube, with power input of about 300 volt-amperes.

Spectra are made as follows: The beaker and cell are put in place, and then the loaded and evacuated spectrograph is pushed snugly against the cell, holding it against the window of the hydrogen lamp. The space between the beaker and the glass tubes is plugged up with putty. Silicone grease (less soluble in hydrocarbons than Lubriseal, for example) is lightly applied to the lower part of the male ground joint at the top of the cell. The hydrocarbons which will form the rigid glass are mixed, and the cell is filled to about half way up the tube *J* (to allow for contraction of the glass when cooled). Then the vent tube is fitted on the ground joint in such a way that the lower portion is lubricated. With the stopcock *M* open, the hydrocarbon mixture is now gently boiled by heating the cell with a small electric resistance wire heater encased in a glass tube. This removes the air dissolved in the hydrocarbons. If one limits study to molecules of essentially high boiling point compared to the hydrocarbon solvent (bp of isopentane=29°C), this boiling process introduces only a small error in the concentration of the solution whose spectrum is being taken. As is obvious from Fig. 2, the glass attachments on the top of the cell are so arranged that stopcock lubricant will not be washed into the cell by refluxing hydrocarbon. When the hydrocarbon mixture has been boiling so that vapor has been issuing from the tip of the vent tube for 1 or 2

[6] Platt, Ruşoff, and Klevens, J. Chem. Phys. 11, 535 (1943).

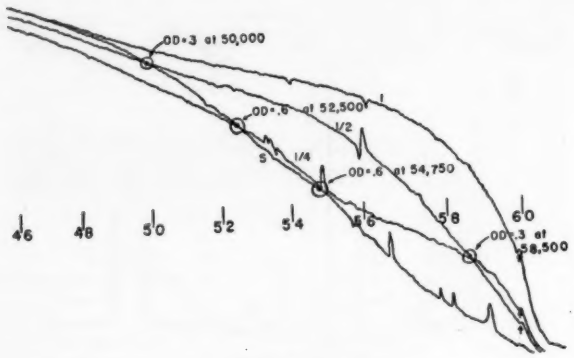

FIG. 3. Densitometer tracings of a typical plate from the far ultraviolet apparatus. Scale is in thousands of wave numbers. Curve marked *S* is that of the sample being studied. Curves marked 1, ½, ¼ are, respectively, those of the equal, ½-, and ¼-time blanks. Small peaks marked with arrows on the far right of the curves result from the 1672 emission line of molecular hydrogen. Other sharp peaks in the curves result from local flaws in the emulsion of the plate.

minutes, the stopcock *M* is closed, the heater removed, and the beaker filled with liquid nitrogen. Of course, in such a vessel liquid nitrogen boils out quite rapidly, but the heat leaks are not so large that a rigid glass cannot be formed, nor a spectrum taken. After allowing ample time for the sample to freeze (3 or 4 minutes is probably sufficient, but 10 are allowed), the exposure is immediately made.

A quantitative low temperature spectrum is made in the following manner. Solutions of known concentration of the compound to be studied are made up in 3-methylpentane. (These same solutions can be used for room temperature spectra, using conventional methods, or for the far ultraviolet, the methods of Jacobs and Platt.[7]) One volume of these solutions with six volumes of isopentane is make into 3PIP glass at 77°K, and its spectrum taken as described above. Then on the same plate three exposures, of equal, one-half, and one-fourth the time used for the above solution are made with a blank of 3PIP glass. The resulting plate is traced on a recording densitometer. Where the curve of the solution crosses the ½-time blank curve, the optical density of the solute is taken as equal to $0.3(-\log\frac{1}{2}=0.3)$; where the solution curve crosses the ¼-time blank curve, as equal to 0.6. Usually, no attempt is made to interpolate between curves, and reciprocity law failure is neglected, as the variance in optical density blanks gives a much larger error than reciprocity law failure. The maximum error of the blank at the far end of the ultraviolet region is about 0.1 optical density units, being somewhat less in the nearer ultraviolet. An estimate of the amount of this error is made by noting how well the curves of the solution exposure and of the equal time blank exposure coincide in a region where the solute is not absorbing. By an appropriate estimation, the error can be cut to about 0.05 optical density units. A sample set of densitometer curves from a typical plate are shown in Fig. 3.[8]

Wavelength calibrations have been made with Hg emission lines (below 1700A). From plates of these spectra a dispersion curve is determined with a precision comparator. From these data a plot of wavelength *vs* mm distance from the bright green line of atomic hydrogen (Hβ) is made. From this dispersion curve a plastic wavelength scale was made for visual examination of plates. The dispersion curve times the ratio of the paper speed and plate travel speed in the recording densitometer gives the wavelength calibration of the densitometer curves.

A MORE VERSATILE APPARATUS FOR THE NEARER ULTRAVIOLET REGION

While the method just described is quite satisfactory for the farther ultraviolet region, it is convenient to have some low temperature device in keeping with the above design principles but which is more versatile, such that it may be used in conjunction with ordinary quartz spectrographs or adapted to a spectrophotometer. Toward this end the apparatus in Fig. 4 was developed.

The device shown here is essentially a brass Dewar with cell built into it in such way that the light beam does not go thru the liquid nitrogen refrigerant. *A* is the absorption cell; the *B*'s are threaded holes to take the inner window assemblies. Each assembly is a threaded brass ring with a thin quartz window *P* cemented into it with Araldite cement. A slot is cut in the outer end of the ring to take an oversized screwdriver, so that the window may be screwed securely against a Teflon gasket resting on the shoulder at the

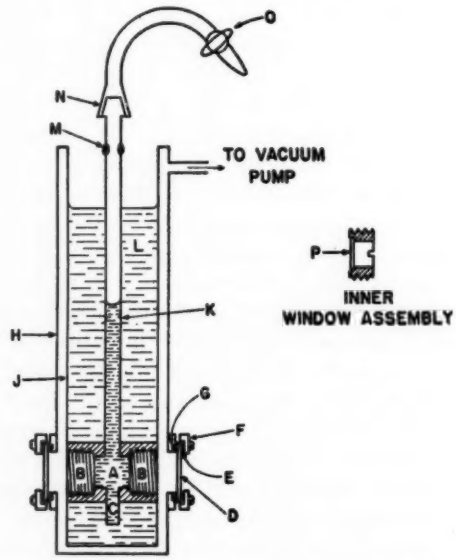

FIG. 4. Low temperature absorption apparatus for the nearer ultraviolet region.

[7] L. E. Jacobs and J. R. Platt, J. Chem. Phys. **16**, 1137 (1948).

[8] The molecule absorbing here is tetramethylethylene. Complete data on its spectrum will be discussed in a forthcoming paper.

junction of *A* and *B*. The space between the outer and inner walls of the vessel *H* and *J* is evacuated to form a Dewar. (A liquid nitrogen trap is placed in the pump line to keep pump vapors from entering the vacuum jacket, where they might condense on the inner windows.) The outer quartz windows *D* are placed between rubber O rings *G* and rubber gaskets *E*, and held in place by the brass ring *F*. It is seen that liquid nitrogen *L* completely surrounds the cell, but the light beam does not pass through any refrigerant.

The upper glass assembly and the method of filling the cell and preparing the rigid glass sample are the same as those employed in the far ultraviolet apparatus. First, a vacuum is applied to the Dewar, and then liquid hydrocarbon solution is added so that filling tube *K* is about half full. The upper glass assembly is put in place, a heater is inserted, and the solution gently boiled; stopcock *O* is closed and finally liquid nitrogen is added. During a longer run of any kind, liquid nitrogen must be replaced from time to time.

Not shown in the drawing are four circular copper fins which are soldered to the outer can between the top of the vessel and the outer windows. These fins allow heat to leak into the lower portion of the outer can, keeping the outer windows warm enough so that water from the atmosphere does not condense upon them. On very humid days it is necessary to blow warm air gently on the outer windows to prevent fogging.

The device described above has been used successfully in a Beckman model DU quartz spectrophotometer. Figure 5 shows the top view of the arrangement. *A* is the brass Dewar cell of Fig. 4, which sets on base *B*; *B* slides on rods *C*. Control *D* moves the cell in and out of the light beam (between *E*, the monochromator light exit, and *F*, the photocell housing entrance). The box *G* holding the assembly is made to fit the Beckman instrument in the same way as other standard cell housings. A cover, which fits around the brass Dewar cell, slides with the Dewar, making the assembly light tight. It is usually necessary to pass warm air through the housing to prevent fogging of the outer windows.

A spectrum is taken by filling the Dewar cell with a 3PIP glass blank at low temperature, and taking its optical density (relative to air) *vs* wavelength curve. The process is repeated with a glass containing a known concentration of the molecule to be studied, and subtracting the two optical density curves gives the optical density curve of the solute molecule.

The largest error in this set-up is the poor reproducibility of the blank optical density curve. Other errors are believed small compared to this. The variance between successive optical density blank curves is less than 0.02 OD units above 2700A (entirely satisfactory), about 0.02 units at 2600A, gradually increasing to about 0.08 OD units at 2100A (rather poor). The error throughout the curve is always in the same direction, however. That is, if the curve is about 0.02 OD units "high" at 2600A, it will be about 0.06 OD units "high" at 2300A, about 0.08 at 2100A. Thus, when subtracting a blank curve from a solution curve, one can compare the optical densities in some region where the solute molecule has negligible absorption, and "adjust" the blank curve so it coincides with the solution curve in this region. With this correction method the error is probably reduced to less than 0.04 OD units at 2100A, and correspondingly less at higher wavelengths.

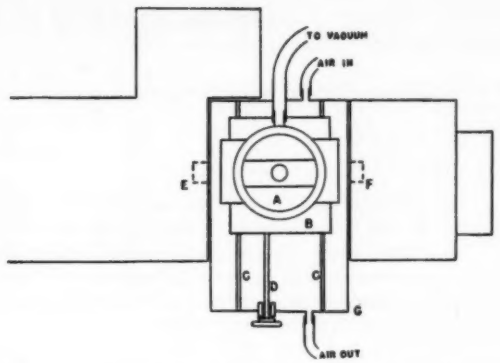

FIG. 5. Top view of housing which adapts the low temperature absorption cell to a Beckman spectrophotometer.

CONCLUSIONS

In comparing this method with the far ultraviolet method described above, it is the author's opinion that for low temperature absorption spectra above 2200A the Beckman method just described is most satisfactory, while below 2200A the fluorite vacuum spectrograph is indicated. With these two methods it is now possible to obtain reasonably quantitative absorption spectra at liquid nitrogen temperatures from the visible region throughout the ultraviolet region to 1670A.

ACKNOWLEDGMENT

The author wishes to thank Professor J. R. Platt for many helpful suggestions, and Mr. I. Kalberg, physics department machinist, whose cooperation was most helpful in design and construction of apparatus.

On the Stability of Metallo-Organic Compounds

H. H. JAFFÉ AND G. O. DOAK
Venereal Disease Experimental Laboratory, U. S. Public Health Service, School of Public Health, University of North Carolina, Chapel Hill, North Carolina

(Received August 20, 1952)

It is pointed out that serious difficulties are encountered in preparing organic compounds of the transition elements. The hypothesis is proposed that these difficulties are caused by insufficient stability of the carbon-metal bonds involved. Some rough calculations based on Mulliken's "magic formula" are used to test this hypothesis. The results obtained indicate that carbon-metal bonds formed by the transition elements are extremely weak. The calculations further suggest that carbon-metal bonds involving the alkali and alkaline earth metals are largely ionic.

ORGANIC chemists have long attempted the preparation of metallo-organic compounds[1] of the transition elements.

The formation of ethyl iron (II) iodide has been reported,[2] but the compound has not been isolated and the evidence for its existence is not convincing.* No other compound containing an alkyl group linked to a transition element has been described. Compounds of titanium[3] and chromium[4] linked to aromatic radicals have been isolated and analyzed. The preparation of aromatic compounds of iron[5] and manganese[6] has also been reported, but the evidence presented for their existence is not conclusive.

A possible reason for the difficulties encountered in preparing metallo-organic compounds of the transition elements may be that the covalent metal-carbon bond is not sufficiently stable, while the electronegativity difference between the metals and carbon is insufficient to lead to a stable ionic bond. This paper presents some calculations to show that this statement is a reasonable hypothesis. Mulliken's "magic formula"[7] will be used as a basis for the present considerations. Unfortunately, the evaluation of all the terms in this formula is difficult, even for some of the simplest metallo-organic compounds, and impractical if a series of third-row metals is involved. Furthermore, exact calculations by the "magic formula" would require choice of specific compounds, and thus greatly complicate a general discussion of the Me−C bond.

The most important term in the "magic formula" is $\sum X_{ij}$; this summation contains just one X_{ij} term for each bond. Since we are dealing with elements with relatively large electronegativity differences, the RE-term (i.e., in this case the ionic resonance energy) may also be of considerable importance. All other terms in the "magic formula" will be neglected. This neglect may be partially justified because the considerations in this paper concern energies of dissociation, not of atomization. In the case of aromatic compounds the RE-term should also include the resonance energy due to π-bonding. This resonance energy will be particularly important for compounds of the transition elements, since low energy d orbitals are available for π-bond formation.[8] No π-bonding energies will be considered in this paper, and hence the calculations will apply directly only to aliphatic compounds, and to the σ-bond in aromatic compounds.

The X_{ij}'s which make the major contribution to the bond energies, have the following form:[9]

$$X_{ij}=AS_{ij}\bar{I}_{ij}/(1+S_{ij}). \quad (1)$$

They depend, aside from a constant A, only on the overlap integrals S and the average ionization potential $\bar{I}$. Accordingly, an approximate picture of the variation of the Me−C bond energy can be obtained by studying the variation of S_{ij}, $\bar{I}_{ij}$ and *RE*. The variation of these quantities in going along the third (first long) row of the periodic table will be investigated. For comparison the corresponding values for the second (last short) row will also be calculated.

OVERLAP INTEGRALS

All overlap integrals (OI) used in this paper are based on Slater non-orthogonal atomic orbital wave functions (AO). Although such OI do not always give good agreement of calculated with experimental quantities,[10] we are interested mostly in trends and orders of magnitude, and we believe that these OI are adequate for this purpose.

[1] The term metallo-organic compounds will be used in this paper to refer only to compounds in which a metal atom is linked directly to a carbon atom in an alkyl or aryl group.

[2] A. Job and R. Reich, Compt. rend. **174**, 1358 (1922).

* *Note added in proof:*—While the work was in progress, a stable organic iron compound, *bis*cyclopentadienyl iron, has been described by T. J. Kealy and P. L. Paulson [Nature **168**, 1039 (1951)]. These authors give a detailed criticism of the earlier claims (references 2 and 5) to the preparation of organic compounds of iron. The conclusions reached in this paper are not contradicted by the stability of *bis*cyclopentadienyl iron, since this compound appears to involve a rather special type of binding [See H. H. Jaffé, J. Chem. Phys. **11**, 156 (1953) and references cited there].

[3] D. F. Herman and W. K. Nelson, J. Am. Chem. Soc. **74**, 2693 (1952).

[4] F. Hein, J. prakt. Chem. **153**, 160 (1939).

[5] G. Champetier, Bull. soc. chim. France **47**, 1131 (1930).

[6] H. Gilman and J. C. Bailie, J. Org. Chem. **2**, 84 (1937).

[7] R. S. Mulliken, J. Phys. Chem. **56**, 295 (1952).

[8] H. H. Jaffé, Abstracts 122nd Meeting, American Chemical Society, Atlantic City, New Jersey, September, 1952.

[9] See Eq. (22) of reference 7.

[10] See, e.g., R. S. Mulliken, J. Am. Chem. Soc. **72**, 4493 (1950); J. Chem. Phys. **19**, 900, 912 (1951).

The OI required for this study were the $S(2te, x)$, where $2te$ stands for the $2s2p^3$ hybrid AO of carbon, and x stands for $3s$, $3p\sigma$, $3d\sigma$, $4s$, and $4p\sigma$ AO of the metals, and for various hybrids of these AO. Some of these OI were calculated from published tables and formulas,[11] others were computed in this laboratory.[12] The parameters (ρ and τ)[13] needed for calculation of OI for the specific bonds were found in the usual manner.[11] Gordy's bond distances were used.[14] The hybrid AO OI were computed by known procedures.[11]

The method used does not permit straightforward computation of OI involving AO with $n=4$. Therefore, $n=4$ OI were obtained as averages of the corresponding OI for $n=3$ and $n=5$. This procedure appears justifiable since the OI being averaged usually do not differ materially.

Many recent authors believe that monovalent elements do not normally utilize pure s or p orbitals for σ-bond formation, but rather that some hybrids of s and p orbitals are involved.[15] Mulliken has shown that even a small amount of hybridization greatly affects the OI.[10] Accordingly, we have assumed sp bonding for sodium and copper and sp^3 bonding for the halogens. Values assuming pure s and p bonding, respectively, are given for comparison. The calculations for potassium are based on pure s bonding. The conclusions reached are not changed if either sp or sd bonding is assumed for this element.

IONIZATION POTENTIALS

The ionization potentials (IP) involved in the "magic formula" are averages of the mean IP of the atoms involved. These mean IP in turn are weighted means of the IP of the valence AO of the elements.[7] Unfortunately, such valence AO IP do not appear to be available for the elements of the first long period. Since the valence AO IP probably depend largely on the IP of the element in the ground state, it appears satisfactory to use ground state IP. This approximation is further justified by the wide variation of ground state IP encountered in going along a row of the periodic table. Furthermore, we are interested only in major trends, not in small differences. Accordingly, the IP used in this paper are the average of the ground state IP of the metal and the sp^3 AO IP of carbon.[7]

IONIC RESONANCE ENERGIES

According to Pauling,[16] the ionic resonance energy (IRE) can be calculated from electronegativity differences:

$$\text{IRE} = (x_A - x_B)^2. \qquad (2)$$

The electronegativities used were taken from Bellugue and Daudel,[17] since these authors report values for all the elements of interest in this paper.

TABLE I.

Element[a]	Assumed hybridization[b]	$S(2te, h)$[c]	IP[d,e]	X_{ij}/A[d,f]	IRE[d,e]
Na (IA)	sp	0.397	5.11	2.67	4.00
	(s)	(0.236)			
Mg (II)	sp	0.508	7.61	3.58	2.56
Al (IIIB)	sp^2	0.585	5.96	5.76	1.56
Si (IVB)	sp^3	0.615	8.10	4.14	0.72
P (VB)	sp^3	0.616	11.0	4.70	0.42
S (VIB)	sp^3	0.624	10.31	4.61	0.00
Cl (VIIB)	sp^3	0.586	12.96	4.85	0.36
	(p)	(0.443)			
K (IA)	s	0.145	4.32	1.14	4.41
Ca (IIA)	sd	0.244	6.09	1.94	3.42
Sc (IIIA)*	sd^2	0.377	6.7	2.80	1.32
Ti (IVA)*	sd^3	0.383	6.81	2.84	0.90
V (VA)*	sd^3	0.368	6.76	2.75	1.69
Cr (VIA)*	sd^3	0.340	6.74	2.60	1.82
Mn (VIIA)*	sd^3	0.337	7.40	2.56	1.56
Fe (VIII)*	sd	0.316	7.83	2.58	0.90
Co (VIII)*	sd	0.293	8.5	2.51	0.72
Ni (VIII)*	sd	0.291	7.61	2.40	0.72
Cu (IB)	sp	0.474	7.68	3.43	0.42
	(s)	(0.290)			
Zn (IIB)	sp	0.534	9.36	4.01	1.44
Ga (IIIB)	sp^2	0.583	5.97	3.62	1.10
Ge (IVB)	sp^3	0.592	8.09	4.05	1.21
As (VB)	sp^3	0.591	10.5	4.49	0.42
Se (VIB)	sp^3	0.566	9.70	4.23	0.01
Br (VIIB)	sp^3	0.596	11.5	4.51	0.12
	(p)	(0.420)			

[a] The figures in parenthesis following the elements refer to the column in which these elements occur in the periodic table. Elements marked * are transition elements.
[b] These states of hybridization are assumed as most probable. The results would not be changed appreciably by assuming different states of hybridization. Replacement of d orbitals by p orbitals, however, would usually materially increase S; this effect would be largely counter-balanced by the promotion energy required.
[c] h stands for the appropriate hybrid orbital.
[d] In electron volts.
[e] The notation is explained in the text.
[f] See Eq. (1).

DISCUSSION

Table I lists the overlap integrals and ionization potentials together with the X_{ij} calculated from Eq. (1). The X_{ij} for the Me−C bond for the transition elements are appreciably smaller than the corresponding values for the elements of groups IB to VIIB. At the same time no major differences of the ionic resonance energies of these two groups of elements are noted. These facts strongly suggest that the difficulties encountered in the preparation of metallo-organic compounds of the transition elements can be explained by thermodynamic instability of the Me−C bonds involved. This view is further supported by the properties of organic copper compounds. From the relative values of the X_{ij}, these compounds are expected to be more stable than organic compounds of the transition elements, but less stable

[11] Mulliken, Rieke, Orloff, and Orloff, J. Chem. Phys. **17**, 1248 (1949).
[12] The newly computed values are tabulated in the appendix, together with necessary formulas.
[13] The notation in this paper is that of reference 11, as modified by C. C. J. Roothaan and K. Rüdenberg, J. Chem. Phys. **19**, 1445, 1459 (1951).
[14] W. Gordy, Phys. Rev. **69**, 604 (1946).
[15] See, e.g., J. Duchesne, Trans. Faraday Soc. **46**, 187 (1950); J. Chem. Phys. **19**, 246 (1951); **20**, 540 (1952).
[16] L. Pauling, *The Nature of the Chemical Bond* (Cornell University Press, Ithaca, New York, 1944), second edition, Chapter II.
[17] J. Bellugue and R. Daudel, Rev. sci. **84**, 541 (1946).

than organic compounds of the elements of groups IIB to VIIB. This order of stability is in accord with experimental fact.

The stability of organic compounds of potassium, sodium, and calcium cannot be explained on the basis of the values of X_{ij}. However, for these metals the IRE are very much larger than for the remaining elements. Consequently, the bonds will be largely ionic in character, and the stability of organic compounds of these elements depends primarily on the ionic binding energy.

It may be profitable at this point to inquire into the reason for the relatively low values of X_{ij} obtained for the elements forming no stable metallo-organic compounds. Analysis of the calculations shows that no single factor is determining. The integrals $S(2te, 4s)$ are relatively small for these elements; the $S(2te, 3d\sigma)$ are small for some. Moreover, the former increase while the latter decrease in going from left to right across the periodic table, so that small values of one are associated with larger values of the other. All transition elements possess somewhat smaller IP than the elements forming stable metallo-organic compounds. The contribution to the bond strength from the IRE is of the same order of magnitude in both groups.

It should be pointed out here that the calculations presented in this paper are not intended to indicate small differences in bond energies. Too many approximations are made to permit more than qualitative conclusions. However, it is believed that a ready explanation is given for the difficulties long experienced by organic chemists

TABLE II. $S(2s, 5s)$.

ρ	$\tau=-0.75$	-0.5	-0.25	-0.125	0.0	0.125	0.25	0.5	0.75
0.0	0.284	0.802	0.973	0.891	0.732	0.540	0.350	0.089	0.006
0.5		0.797			0.730			0.091	
1.0	0.284	0.783	0.946	0.871	0.723	0.542	0.359	0.097	0.007
1.5		0.763			0.712			0.105	
2.0	0.284	0.732	0.872	0.814	0.695	0.542	0.378	0.116	0.010
2.5		0.699			0.671			0.129	
3.0	0.284	0.661	0.769	0.724	0.639	0.524	0.389	0.141	0.014
3.5		0.619			0.600			0.154	
4.0	0.280	0.575	0.635	0.608	0.555	0.480	0.382	0.164	0.020
4.5		0.528			0.504			0.175	
5.0	0.270	0.480	0.499	0.481	0.452	0.411	0.351	0.179	0.027
5.5		0.433			0.398			0.182	
6.0	0.255	0.386	0.371	0.361	0.344	0.327	0.300	0.183	0.034
6.5		0.342			0.294			0.181	
7.0	0.235	0.300	0.261	0.250	0.247	0.247	0.242	0.176	0.040
7.5		0.261			0.205			0.170	
8.0	0.212	0.225	0.176	0.166	0.167	0.176	0.185	0.162	0.046
9.0	0.189	0.165	0.114		0.108		0.134	0.142	0.050
10.0	0.166	0.118	0.071	0.064	0.067	0.077	0.094	0.121	0.053
12.0	0.124	0.058	0.025	0.022	0.023	0.029	0.042	0.080	0.055
14.0	0.089	0.027	0.005	0.006	0.007	0.010	0.015	0.048	0.053
16.0	0.063	0.012	0.003	0.002	0.002	0.003	0.006	0.027	0.049

TABLE III. $S(2s, 5p\sigma)$.

ρ	$\tau=-0.75$	-0.5	-0.25	-0.125	0.0	0.125	0.25	0.5	0.75
0.0	0.000	0.000	0.000	0.000	0.000	0.000	0.000	0.000	0.000
0.5		0.038			0.139			0.030	
1.0	−0.012	0.076	0.224	0.267	0.271	0.239	0.182	0.061	0.005
1.5		0.112			0.388			0.092	
2.0	−0.014	0.149	0.400	0.473	0.485	0.436	0.341	0.124	0.012
2.5		0.181			0.558			0.156	
3.0	−0.005	0.209	0.501	0.587	0.607	0.561	0.457	0.187	0.020
3.5		0.235			0.629			0.215	
4.0	+0.010	0.247	0.520	0.601	0.629	0.599	0.512	0.241	0.031
4.5		0.253			0.608			0.261	
5.0	0.026	0.253	0.473	0.540	0.571	0.563	0.507	0.277	0.043
5.5		0.247			0.522			0.287	
6.0	0.037	0.235	0.389	0.436	0.467	0.477	0.456	0.292	0.055
6.5		0.220			0.409			0.291	
7.0	0.045	0.202	0.294	0.324	0.351	0.373	0.379	0.287	0.067
7.5		0.183			0.296			0.278	
8.0	0.048	0.163	0.209	0.225	0.246	0.273	0.295	0.267	0.077
9.0	0.048	0.126	0.140		0.163		0.218	0.237	0.084
10.0	0.046	0.094	0.090	0.092	0.103	0.124	0.154	0.202	0.090
12.0	0.038	0.049	0.033	0.032	0.038	0.048	0.069	0.135	0.095
14.0	0.030	0.023	0.011	0.010	0.011	0.016	0.028	0.083	0.092
16.0	0.023	0.011	0.003	0.003	0.003	0.005	0.010	0.047	0.083

TABLE IV. $S(2p\sigma, 5s)$.

ρ	$\tau=-0.75$	-0.5	-0.25	-0.125	0.0	0.125	0.25	0.5	0.75
0.0	0.000	0.000	0.000	0.000	0.000	0.000	0.000	0.000	0.000
0.5		0.115			0.001			−0.013	
1.0	0.123	0.228	0.145	0.073	0.010	−0.029	−0.044	−0.024	−0.003
1.5		0.334			0.032			−0.034	
2.0	0.228	0.428	0.299	0.178	0.067	−0.013	−0.052	−0.040	−0.005
2.5		0.506			0.111			−0.043	
3.0	0.310	0.565	0.430	0.293	0.158	+0.050	−0.019	−0.043	−0.007
3.5		0.603			0.202			−0.039	
4.0	0.361	0.619	0.494	0.368	0.237	0.122	+0.034	−0.033	−0.009
4.5		0.617			0.261			−0.025	
5.0	0.384	0.598	0.481	0.379	0.272	0.170	0.081	−0.016	−0.009
5.5		0.567			0.271			−0.006	
6.0	0.383	0.528	0.413	0.337	0.259	0.183	0.108	+0.002	−0.009
6.5		0.483			0.241			0.010	
7.0	0.367	0.435	0.323	0.268	0.217	0.167	0.114	0.017	−0.008
7.5		0.388			0.191			0.023	
8.0	0.340	0.341	0.233	0.195	0.165	0.137	0.104	0.028	−0.007
9.0	0.307	0.245	0.159		0.116		0.086	0.031	−0.005
10.0	0.280	0.190	0.103	0.085	0.076	0.072	0.066	0.034	−0.003
12.0	0.207	0.094	0.039	0.031	0.029	0.030	0.033	0.029	+0.000
14.0	0.150	0.044	0.013	0.010	0.009	0.011	0.014	0.020	0.002
16.0	0.107	0.020	0.004	0.003	0.003	0.004	0.006	0.013	0.003

TABLE V. $S(2p\sigma, 5p\sigma)$.

ρ	$\tau=-0.75$	-0.5	-0.25	-0.125	0.0	0.125	0.25	0.5	0.75
0.0	−0.284	−0.802	−0.973	−0.891	−0.732	−0.540	−0.350	−0.089	−0.006
0.5		−0.778			−0.714			−0.091	
1.0	−0.266	−0.706	−0.849	−0.785	−0.658	−0.500	−0.337	−0.095	−0.007
1.5		−0.596			−0.568			−0.099	
2.0	−0.204	−0.461	−0.526	−0.501	−0.447	−0.372	−0.280	−0.102	−0.010
2.5		−0.315			−0.308			−0.101	
3.0	−0.132	−0.172	−0.140	−0.145	−0.163	−0.177	−0.166	−0.096	−0.013
3.5		−0.044			−0.026			−0.088	
4.0	−0.063	+0.064	+0.168	+0.149	+0.093	+0.021	−0.042	−0.073	−0.015
4.5		0.148			0.186			−0.058	
5.0	−0.009	0.208	0.335	0.316	0.252	0.162	+0.069	−0.040	−0.016
5.5		0.247			0.291			−0.023	
6.0	+0.030	0.267	0.375	0.359	0.307	0.229	0.138	−0.006	−0.016
6.5		0.272			0.304			+0.009	
7.0	0.054	0.267	0.336	0.323	0.288	0.234	0.164	0.022	−0.014
7.5		0.253			0.263			0.033	
8.0	0.067	0.235	0.281	0.253	0.233	0.203	0.164	0.042	−0.012
9.0	0.073	0.191	0.190		0.170		0.135	0.052	−0.009
10.0	0.072	0.147	0.128	0.120	0.115	0.113	0.106	0.055	−0.006
12.0	0.064	0.079	0.051	0.045	0.045	0.049	0.055	0.048	−0.003
14.0	0.051	0.039	0.018	0.015	0.015	0.018	0.024	0.034	+0.004
16.0	0.038	0.018	0.006	0.004	0.004	0.006	0.010	0.021	+0.007

in attempting to prepare organic compounds of transition elements.

APPENDIX

In the course of the present investigation the following Slater AO overlap integrals had to be derived: $S(2s, x)$ and $S(2p\sigma, x)$ with $x=5s$, $5p\sigma$ and $3d\sigma$. The OI for $x=5s$, $5p\sigma$ were computed from published formulas,[11] and are tabulated Tables II to V. The formulas for $x=nd\sigma$ were derived by standard methods,[11,18] and are given below:

$$S(n_a s, n_b d\sigma)=(1/4)(5)^{\frac{1}{2}}N_a N_b (R/2)^{m_a+m_b+1}\int_1^\infty\int_{-1}^1 [3(1-\xi\eta)^2-(\xi-\eta)^2] \times(\xi+\eta)^{m_a-1}(\xi-\eta)^{m_b-3}(\xi^2-\eta^2)e^{-\rho(\xi+\eta\tau)}d\eta d\xi, \quad (3)$$

$$S(n_a p\sigma, n_b d\sigma)=(1/4)(15)^{\frac{1}{2}}N_a N_b (R/2)^{m_a+m_b+1}\int_1^\infty\int_{-1}^1 (1+\xi\eta) \times[3(1-\xi\eta)^2-(\xi-\eta)^2](\xi+\eta)^{m_a-2}(\xi-\eta)^{m_b-3}(\xi^2-\eta^2)e^{-\rho(\xi+\eta\tau)}d\eta d\xi. \quad (4)$$

[18] H. H. Jaffé, J. Chem. Phys. 20, 258 (1952).

TABLE VI. $S(2s, 3d\sigma)$.

ρ	$\tau=-0.75$	-0.5	-0.25	-0.125	0.0	0.125	0.25	0.5	0.75
0.0	0.000	0.000	0.000	0.000	0.000	0.000	0.000	0.000	0.000
0.5		−0.003			0.014			0.012	
1.0	−0.006	−0.010	0.013	0.033	0.053	0.068	0.071	0.046	0.009
1.5		−0.015			0.114			0.096	
2.0	−0.013	−0.013	0.065	0.129	0.187	0.229	0.237	0.156	0.031
2.5		−0.006			0.258			0.218	
3.0	−0.014	+0.003	0.137	0.230	0.317	0.379	0.396	0.277	0.065
3.5		0.018			0.358			0.325	
4.0	−0.011	0.029	0.183	0.282	0.375	0.446	0.473	0.359	0.096
4.5		0.040			0.377			0.386	
5.0	−0.006	0.047	0.190	0.277	0.361	0.431	0.470	0.398	0.125
5.5		0.051			0.332			0.398	
6.0	0.000	0.053	0.165	0.231	0.296	0.358	0.406	0.385	0.146
6.5		0.053			0.257			0.374	
7.0	+0.001	0.050	0.129	0.172	0.218	0.268	0.317	0.352	0.160
7.5		0.047			0.181			0.327	
8.0	0.003	0.043	0.092	0.118	0.147	0.195	0.231	0.300	0.167
9.0	0.004	0.034	0.064		0.094		0.157	0.245	0.168
10.0	0.004	0.026	0.039	0.046	0.056	0.075	0.104	0.192	0.165
12.0	0.004	0.014	0.014	0.015	0.018	0.026	0.041	0.110	0.148
14.0	0.004	0.007	0.005	0.004	0.005	0.008	0.014	0.058	0.124
16.0	0.003	0.003	0.001	0.001	0.001	0.002	0.005	0.029	0.100

TABLE VII. $S(2p\sigma, 3d\sigma)$.

ρ	$\tau=-0.75$	-0.5	-0.25	-0.125	0.0	0.125	0.25	0.5	0.75
0.0	0.000	0.000	0.000	0.000	0.000	0.000	0.000	0.000	0.000
0.5		−0.082			−0.225			−0.084	
1.0	−0.022	−0.143	−0.308	−0.365	−0.387	−0.370	−0.316	−0.151	−0.024
1.5		−0.171			−0.456			−0.193	
2.0	−0.029	−0.169	−0.342	−0.404	−0.434	−0.428	−0.382	−0.208	−0.040
2.5		−0.143			−0.344			−0.198	
3.0	−0.025	−0.105	−0.173	−0.204	−0.218	−0.233	−0.234	−0.170	−0.044
3.5		−0.062			−0.087			−0.132	
4.0	−0.016	−0.022	+0.019	+0.034	+0.029	+0.005	−0.034	−0.089	−0.040
4.5		+0.012			0.121			−0.048	
5.0	−0.006	0.038	0.137	0.173	0.183	0.162	+0.113	−0.010	−0.033
5.5		0.057			0.217			+0.022	
6.0	+0.001	0.067	0.174	0.212	0.229	0.218	0.180	0.047	−0.023
6.5		0.073			0.223			0.066	
7.0	0.005	0.074	0.160	0.191	0.207	0.207	0.186	0.079	−0.013
7.5		0.072			0.184			0.087	
8.0	0.008	0.067	0.125	0.145	0.159	0.165	0.159	0.091	−0.005
9.0	0.009	0.055	0.089		0.109		0.122	0.088	+0.002
10.0	0.009	0.043	0.059	0.064	0.070	0.078	0.086	0.077	0.008
12.0	0.009	0.023	0.022	0.022	0.024	0.029	0.037	0.052	0.015
14.0	0.007	0.012	0.008	0.007	0.007	0.009	0.014	0.030	0.016
16.0	0.005	0.005	0.005	0.002	0.002	0.003	0.009	0.016	0.015

The OI for the orbital $d\sigma$ along the z axis can easily be shown to be identical to those for the four equivalent d orbitals if they are oriented so as to have correct symmetry for σ-bond formation.

Equations (3) and (4) can be evaluated in terms of A's and B's,[11] leading to the following expressions for the integrals of interest:[19]

$$S(2s, 3d\sigma)=(1/4)(5)^{\frac{1}{2}}\mathfrak{N}_{2,3}[-A_5(B_0-3B_2)-A_4(5B_1-3B_3)+A_3(3B_0-4B_2-3B_4)+A_2(3B_1+4B_3-3B_5)-A_1(3B_2-5B_4)-A_0(3B_3-B_5)], \quad (5)$$

$$S(2p\sigma, 3d\sigma)=(1/4)(15)^{\frac{1}{2}}\mathfrak{N}_{2,3}[-A_5(B_1-B_3)-A_4(B_0+B_2)-A_3(B_1+3B_5)+A_2(3B_0+B_4)+A_1(B_3+B_5)-A_0(3B_2-B_4)]; \quad (6)$$

and for $\rho=0$:

$$S(n_a s, n_b d\sigma)=S(n_a p\sigma, n_b d\sigma)=0. \quad (7)$$

The integrals were evaluated from Eqs. (5) to (7) for a number of values of the parameters ρ and τ, and are tabulated in Tables VI and VII.

[19] The $\mathfrak{N}_{n_a, n_b}$ are given in reference 18.

Electric Polarizability of Polar Ions*

KAROL J. MYSELS
Department of Chemistry, University of Southern California, Los Angeles 7, California
(Received July 28, 1952)

Polar ions are compared with well-known uncharged dipoles with respect to their polarizability and the contribution to the dielectric constant of their solutions. It is shown that (1) hydrodynamic forces exerted by the solvent on the solvated ion have to be taken into account in any kinetic discussion of dielectric behavior. (2) For ions having a symmetrical shape the polarizability is the same as that of an uncharged dipole obtained by adding, at the center of symmetry of the ion, a neutralizing charge. (3) The same effective dipole enters into the thermodynamic considerations of unsymmetrical ions. (4) The dipole analogy may be extended to the general case, leading to a rigorous but implicit expression. (5) As a first approximation, the polarizability of an ion is an indication of its dissymmetry.

THE relation between the electrical symmetry and the polarizability of a molecule has become a familiar part of our knowledge. This relation, as first formulated by Debye,[1] deals with molecules possessing an electrical dissymmetry, but only treats those with no net charge.[2]

The calculation of the polarizability of any molecule from the dielectric constant of a solution or of a liquid can be considered separately, and has been formulated a century ago for nonpolar liquids by Clausius and Mossotti.[3] More recently the problem for polar liquids such as water, has been successfully treated.[4–7]

The influence of ions upon the dielectric constant of solutions has been treated, for example, by Debye, Huckel, Onsager, and Falkenhagen,[8] but the work of these authors deals only with symmetrical ions.

In recent years the technique of dielectric constant measurements has been extended to quite conducting solutions[9–11] and made possible the study of uncharged dipoles in the presence of symmetrical ions. These systems are usually treated as simply mixtures of the two components.

The experimental study of solutions containing unsymmetrical or polar ions has also been made possible by this recent advance, and such measurements have been made on solutions of charged inorganic complexes[12] and of proteins.[13] It was found that these unsymmetrical ions have large effects upon the dielectric constant as would be expected intuitively when one realized that when an unsymmetrical ion is moved through a liquid by the action of an electrical field, it will be twisted[14] reversibly out of its equilibrium orientation and thus store electrical energy. It becomes thus polarized and contributes to the dielectric constant like a dipole. However, the classical theory of dipoles, which is based on the premise that the dipole possess no net charge,[2] cannot be applied to such an ion. The dielectric constant of the solution will, of course, be influenced by the polarization of unsymmetrical ions in the same way as by classical dipoles.

A thermodynamic treatment for special cases of such unsymmetrical ions from the point of view of the activity of the ion has been made by Kirkwood,[15] but he does not relate his treatment to a study of the polarizability of such an ion.

This led therefore to the necessity of analyzing quantitatively the relation between the structure of an unsymmetrical ion and its electrical polarizability. For the most important case of ions, such as spheres and ellipsoids, whose shape (but not the charge) has a center of symmetry, these considerations lead to the classical Debye formula provided that the dipole moment of the particle is calculated including a neutralizing charge located at the center of symmetry. For more complicated shapes, the result is an analogous expression which cannot be integrated explicitly and which involves the knowledge of the hydrodynamic properties of the particle. We shall treat the two cases separately.

* Based in part on the Ph.D. thesis of K. J. Mysels, Harvard University, 1941, and briefly mentioned in E. J. Cohn and J. T. Edsall, *Proteins, Amino Acids and Peptides* (Reinhold Publishing Company, New York, 1943), p. 552.

[1] P. Debye, *Polar Molecules* (Chemical Catalog Company, New York City, 1929).

[2] Reference 1, p. 23.

[3] O. F. Mossotti, Mem. Mathem. fisica Modena, **24**, II, 49 (1850); R. Clausius, *Die Mechanische Warmetheorie*, (Friedrich Vieweg and Sohn, Braunschweig, 1879), Vol. II, p. 62. See reference 1, p. 11.

[4] J. Wyman, Chem. Revs. **19**, 213 (1936).

[5] L. Onsager, J. Am. Chem. Soc. **58**, 1486 (1936).

[6] J. G. Kirkwood, Ann. N. Y. Acad. Sci. **40**, 315 (1940).

[7] J. N. Wilson, Chem. Revs. **25**, 377 (1939).

[8] H. Falkenhagen, *Electrolytes* (Oxford University Press, London, 1934).

[9] J. Wyman, Jr., Phys. Revs. **35**, 623 (1930).

[10] R. Furth, Z. Physik. **22**, 98 (1924); Handb. biol. Arbeitsmeth. **IIIB**, 835 (1929). See also W. J. Shutt, Trans. Faraday Soc. **34**, 467 (1938).

[11] J. L. Oncley, J. Am. Chem. Soc. **60**, 1115 (1938); Chem. Revs. **30**, 433 (1942); J. D. Ferry and J. L. Oncley, J. Am. Chem. Soc. **63**, 272 (1941).

[12] A. B. Lamb and K. J. Mysels, J. Am. Chem. Soc., **67**, 468 (1945).

[13] J. L. Oncley in E. J. Cohn and J. T. Edsall, *Proteins, Amino Acids and Peptides*, (Reinhold Publishing Co., New York, 1943), p. 552–3.

[14] Birefringence resulting from such twisting of ions has been observed by W. Kuhn and H. Kuhn, Helv. Chim. Acta **27**, 493 (1944).

[15] J. G. Kirkwood, J. Chem. Phys. **2**, 351 (1934); J. G. Kirkwood and F. H. Westheimer, J. Chem. Phys. **6**, 506, 513 (1938).

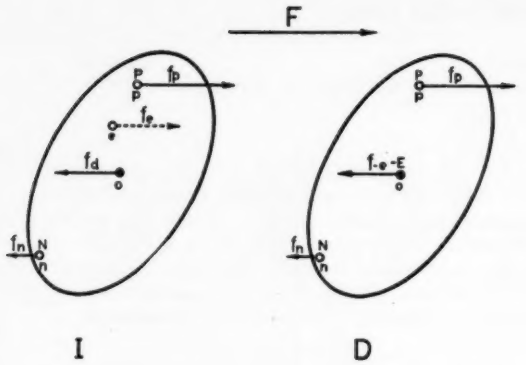

FIG. 1. I is an ion of symmetrical shape but unsymmetrical charge; D is a dipole which gives the same contribution to the dielectric constant.

I. ION WHOSE SHAPE HAS A CENTER OF SYMMETRY

Let us consider the two particles shown in Fig. 1. I is an ion having symmetrical shape with a center of symmetry at o and unsymmetrical positive and negative charges such that the resultant of all positive charges is a charge P located at p while N at n corresponds to the negative charges. Thus this ion has a net charge $E=P+N$. D is a classical uncharged dipole which differs from I only in having a neutralizing charge $-E$ located at point o. D therefore has no net charge but has a dipole moment which we may call $\mathfrak{y}$.

When these two particles are placed in a viscous, nonconducting liquid and an electric field $\mathbf{F}$ is applied, the dipole D will be subject to forces acting on the charges, namely, $\mathbf{f}_p=\mathbf{F}P$, $\mathbf{f}_n=\mathbf{F}N$, and $\mathbf{f}_e=-\mathbf{F}E=(\mathbf{f}_p+\mathbf{f}_n)$. The net resultant of these forces being zero, the dipole will not drift away from its original position but will only twist under the torque which is equal to $\mathfrak{y}\times\mathbf{F}$.

The ion I on the other hand will be subject to two unequal forces exerted by the field upon the positive and negative charges, namely, $\mathbf{f}_p=P\mathbf{F}$ and $\mathbf{f}_n=N\mathbf{F}$. The resultant of these two forces will be a force $\mathbf{f}_e=(\mathbf{f}_p+\mathbf{f}_n)$ which may be considered as applied at a point e the center of charge.

Under the influence of this force $\mathbf{f}_e$, the ion accelerates and in a viscous medium such as water soon reaches a constant velocity so that inertia effects can be neglected.

Once this constant velocity is reached, the viscous drag resulting from forces acting upon the whole surface of the ion, and which can be represented by a single force $\mathbf{f}_d$, must be equal in magnitude and opposite in direction to the net driving force $\mathbf{f}_e$. For reasons of symmetry, $\mathbf{f}_d$ may be considered as applied at point o. Thus the ion I, once it drifts with uniform velocity, is subject to no net force but only to the couple formed by $\mathbf{f}_p$, $\mathbf{f}_n$, and $\mathbf{f}_d$ which is exactly the same as the couple which causes the twisting of the dipole D and produces the same torque $\mathfrak{y}\times\mathbf{F}$.

The ion I and the dipole D are both subject to identical thermal agitation which tends to keep them oriented randomly and to identical torques which tend to align them with the field. Hence their orientation will not be completely random but will tend to be on the average somewhat oriented with the field according to a Boltzman distribution. Both are then polarized and store some electric energy which is released when the field is removed and they both return to a random orientation. Changes in orientation occur by rotation of both particles around their center of symmetry o and storage and release of electric energy is due, therefore, to the movement of charges around o. Therefore the neutralizing charge $-E$ located at point o, which differentiates D from I, makes no contribution to this energy since it does not move. Hence both particles store and release the same amount of energy and are polarized to the same extent.

Thus we have found the dipole D which has the same polarizability as the ion I of symmetrical shape and differs only by the presence of a neutralizing charge at the center of symmetry. The polarizability of this dipole, and hence of the ion, is given by Debye's theory as

$$\alpha=\mu^2/3kT. \tag{1}$$

II. THE GENERAL CASE

The above reasoning is somewhat loose in accepting without further proof that both the viscous drag is applied at, and rotation centered on, point o (the result, as will be shown later, is nevertheless correct). This reasoning is also clearly not applicable to ions of unsymmetrical shape. To bring out the complications involved, let us consider an aneroid-shaped ion shown in Fig. 2 which has a charge at its center o. When an electric field is applied and the ion drifts to the right, the viscous forces are applied unsymmetrically, and their resultant is not at o but at some point d the center of drag. As a result, the ion will rotate clockwise around o without producing any electric work. If we were to place a neutralizing charge at d, we would obtain the same rotation (for this position of the ion), but it would involve electrical energy.[16]

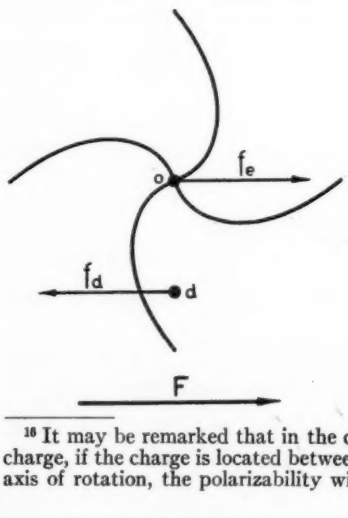

FIG. 2. An aneroid-shaped ion has a center of symmetry o, but the viscous drag is applied at point d.

[16] It may be remarked that in the case, for example, of a single charge, if the charge is located between the center of drag and the axis of rotation, the polarizability will be negative. That is, the

Thus it becomes apparent that if we wish to draw an analogy between an ion and a dipole, we will have to consider two dipoles—one subject to the same torque and another whose rotation produces the same electric effects.

Directional Distribution

To discuss the general case, let us consider an ion (Fig. 3) having no center of symmetry, a resultant of positive charges P at p, of negative charges N at n, and hence subject in a field $\mathbf{F}$ to forces $\mathbf{f}_p=\mathbf{F}P$ and $\mathbf{f}_n=\mathbf{F}N$ applied at these points. These forces cause the ion to drift and, together with the viscous drag,[17] $\mathbf{f}_d=(-\mathbf{f}_p-\mathbf{f}_n)$ to acquire a constant velocity.[18] The ion is then subject to a couple formed by the forces $\mathbf{f}_n$, $\mathbf{f}_p$, and $\mathbf{f}_d$ which exert a torque which we may call $\boldsymbol{\mu}_d\times\mathbf{F}$.

We may interpret $\boldsymbol{\mu}_d$ as the moment of a dipole which would differ from our ion by having a neutralizing charge $-E=(-P-N)$ at a "center of drag" d where the viscous resulting force $\mathbf{f}_d$ is applied. The value of $\boldsymbol{\mu}_d$ will depend on the position of d which will in general depend upon the orientation of the ion with respect to the field, i.e., upon the angle θ which a fixed direction in the ion makes with the field $\mathbf{F}$ and the angle ω which defines the rotation of the molecule around this fixed direction (Fig. 4).

The directional distribution of the ion will not be random but will follow the Boltzmann function $Ae^{U/kT}$. The rotational potential energy U of our ion is $-\boldsymbol{\mu}_d\cdot\mathbf{F}$. Thus the fraction of molecules oriented within small angles $d\omega$ with $d\Omega$ will be

$$\frac{1}{8\pi^2}[\exp\boldsymbol{\mu}_d\cdot\mathbf{F}/kT]d\omega d\Omega, \qquad (2)$$

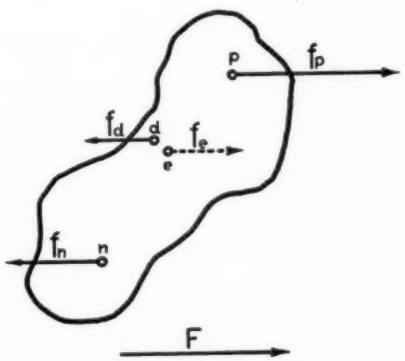

FIG. 3. An ion without center of symmetry.

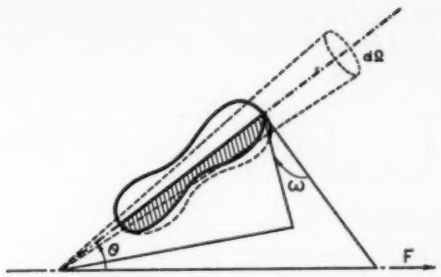

FIG. 4. The hydrodynamic properties of a completely unsymmetrical ion depend on both θ and ω

the factor $1/8\pi^2$ being introduced to make the total number of ions equal to unity.

Electric Moment

The translational drift of a polar ion is analogous to that of a simple ion and gives rise only to an irreversible degradation of electrical energy. It is only the rotational movement which leads to a reversible polarization in the bulk of the solution. This rotational movement is effected around some momentary axis of rotation **A**.

The electric energy dW produced by rotation around this axis **A** is the product of the field strength by the sum ($\boldsymbol{\mu}_a$) of the moments of all charges with respect to this axis:

$$dW=d\boldsymbol{\mu}_a\times\mathbf{F},$$

where $\boldsymbol{\mu}_a=P\mathbf{r}_{ap}+N\mathbf{r}_{an}$, and $\mathbf{r}_{ap}$ is the distance from p to the axis **A**.

We may again interpret $\boldsymbol{\mu}_a$ as the moment of a dipole which differs from our ion by having a neutralizing charge $-E$ on the axis A (but not necessarily at the center of drag). The value of $\boldsymbol{\mu}_a$ will (like that of $\boldsymbol{\mu}_d$) depend on the angles θ and ω defining the position of the ion in the field. Such a moment will have a contribution in the direction of the field equal to $\boldsymbol{\mu}_a\cdot\mathbf{F}/\mathbf{F}$.

Combining this expression for the effective moment with Eq. (2) for the rotational distribution and integrating, we obtain for the average effective moment of the ion

$$\bar{m}=\frac{1}{8\pi^2F}\int\int(\exp\boldsymbol{\mu}_d\cdot\mathbf{F}/kT)\boldsymbol{\mu}_a\cdot\mathbf{F}d\omega d\Omega.$$

Expansion in a power series in F yields

$$\bar{m}=\frac{1}{8\pi^2F}\int\int\boldsymbol{\mu}_a\cdot\mathbf{F}d\omega d\Omega$$

$$+\frac{1}{8\pi^2F}\int\int(\boldsymbol{\mu}_d\cdot\mathbf{F})(\boldsymbol{\mu}_a\cdot\mathbf{F})/kTd\omega d\Omega+\cdots.$$

The first term must be zero since it does not depend on $\mathbf{F}$ and since $\boldsymbol{\mu}_a$ is constant as θ changes. Terms higher than the second may be neglected for low values of $\mathbf{F}$ such as are used in dielectric constant measurements.

torque caused by the field will produce a current which will flow against the field. This, of course, could never occur with an ordinary dipole.

[17] This force $\mathbf{f}_d$ is the resultant of *all* the translational viscous forces; that is, those referred to as vertical lift forces, horizontal drag forces, and the viscous resistance force corresponding to the lift force.

[18] This motion is not necessarily parallel to the field although the electric forces and the opposing viscous forces, which we represent by $\mathbf{f}_d$, are parallel to the field. Only the component of motion parallel to the electric field can contribute to the electrical polarizability.

Hence the second term alone is significant. Noting that in a homogeneous field $d\Omega = 2\pi \sin\theta d\theta$, we have therefore

$$\bar{m} = \left(\frac{1}{4\pi kTF}\right) \int_0^{2\pi} \int_0^{\pi} (\mathfrak{y}_d \cdot \mathbf{F})(\mathfrak{y}_a \cdot \mathbf{F}) \sin\theta d\theta d\omega.$$

The polarizability is then $\alpha = \bar{m}/F$.

This is the simplest general expression for the average electric moment of the ion. It cannot be simplified further unless some information is available about the variation of $\mathfrak{y}_d$ and $\mathfrak{y}_a$ with the orientation of the ion. If sufficient information is available, $\bar{m}$ may be calculated explicitly. Thus in the case of an ion of zero net charge (a classical dipole) $\mathfrak{y}_d = \mathfrak{y}_a = \mathfrak{y}$ and $\bar{m} = \mu^2 F/3kT$ as calculated by Debye.

Case of Ions Having a Symmetrical Shape

We can now give a more rigorous proof of the formula (1) for the polarizability of an ion whose shape has a center of symmetry o.

Because of the symmetry of the shape, viscous forces resisting rotation may be considered as composed of a series of torques applied at diammetrically opposed points and symmetrical with respect to point o. Therefore all axes of rotation must pass through o, and we may write

$$\mathfrak{y}_a = P\mathbf{r}_{np} + E\mathbf{r}_{no} = \mathfrak{y}.$$

The center of drag may, however, be located away from the center of symmetry since translational forces need not be symmetrical. We can introduce an auxiliary moment $\mathfrak{d}$ such that

$$\mathfrak{y}_d = P\mathbf{r}_{np} + E\mathbf{r}_{no} - E\mathbf{r}_{od} = \mathfrak{y} + \mathfrak{d}.$$

The expression for the average electric moment thus becomes

$$\bar{m} = \frac{1}{4\pi kTF} \int_0^{2\pi} \int_0^{\pi} (\mathfrak{y} \cdot \mathbf{F})^2 \sin\theta d\theta d\omega + \frac{1}{4\pi kTF} \int_0^{2\pi} \int_0^{\pi} (\mathfrak{y} \cdot \mathbf{F})(\mathfrak{d} \cdot \mathbf{F}) \sin\theta d\theta d\omega.$$

Symmetry of the molecule and of the field requires, however, that

$$\mathfrak{d}(\omega, \theta) = \mathfrak{d}(\omega + \pi, \theta + \pi) = \mathfrak{d}(\omega, -\theta) = \mathfrak{d}(\omega + \pi, \pi - \theta),$$

which gives a series of equations such as

$$\int_0 \int_0^{\pi/2} (\mathfrak{y} \cdot \mathbf{F})(\mathfrak{d} \cdot \mathbf{F}) \sin\theta d\theta d\omega = -\int_{\pi}^{2\pi} \int_{\pi/2}^{\pi} (\mathfrak{y} \cdot \mathbf{F})(\mathfrak{d} \cdot \mathbf{F}) \sin\theta d\theta d\omega.$$

(This means for the aneroid of Fig. 2 that for every ion such as the one shown in the figure, there is another one obtained by a 180° rotation around a horizontal axis which will tend to rotate counterclockwise when moved to the right.)

The second integral is therefore zero so that

$$\bar{m} = \mu^2 F/3kT \quad \text{and} \quad \alpha = \mu^2/3kT,$$

as deduced previously.

III. RELATION TO KIRKWOOD'S STUDY

Kirkwood[15] considers a spherical ion having a complex charge distribution, and calculates the activity of such an unsymmetrical ion when surrounded by ordinary ions. He introduces Q_1, the square of the "dipole" moment,

$$Q_1 = \sum_{k=1}^{m} \sum_{i=1}^{m} e_k e_i \mathbf{r}_k \mathbf{r}_i \cos\theta_{ki},$$

e_i and $\mathbf{r}_i$ being, respectively, a point charge and its distance from the center of the sphere.

Substituting the vectors $\mathfrak{y}_k = e_k \mathbf{r}_k$ and $\mathfrak{y}_i = e_i \mathbf{r}_i$, this becomes in our notation

$$Q_1 = \sum_{k=1}^{m} \mathfrak{y}_k \cdot \sum_{i=1}^{m} \mathfrak{y}_i = \mathfrak{y}^2,$$

where $\mathfrak{y} = \sum \mathfrak{y}_k = \sum \mathfrak{y}_i = P\mathbf{r}_{po} + N\mathbf{r}_{no}$.

We have therefore arrived at the same result for the effective dipole moment of such a molecule from our kinetic approach that Kirkwood introduced into his thermodynamic treatment.[15] Although it would be very difficult to show this for a general case, it is reasonable to assume that the same dipole moment is always effective, except at very high frequencies where inertia effects become important.

IV. CONCLUSION

The importance of the shape factor and of hydrodynamic forces which we have considered will depend on the structure of the ion. If the positive and negative charges P and N of the ion are large compared with their differences, the net charge E of the ion, and are widely distant, the influence of our auxiliary charges will be small, and interpretation of the polarizability in terms of electrical structure alone will give a good approximation. If, on the contrary, E is of the same order of magnitude as P and N, and the ion shape is very unsymmetrical, the effect of the hydrodynamic forces and apparent dipole on the polarizability may be very noticeable. Thus, hydroxopentaminecobaltic ion, $Co(NH_3)_5OH^{++}$, may be a case where the dissymmetry of shape of the hydrated ion causes a high dielectric increment.[12] Thus a high electrical polarizability can always be attributed to a high dissymmetry which may be either of shape or of charge or of both.

The "dissymmetry" effect of ions need not be, of course, the only dielectric effect of the ion in solution. It may be accompanied by, and superimposed upon, other effects such as the Debye saturation effect and the Debye-Falkenhagen ionic cloud deformation effect. For very dissymmetrical ions, the dissymmetry effect should, however, overshadow the others.

ACKNOWLEDGMENT

Professor J. L. Oncley of Harvard Medical School has, over the years, spent a great deal of time in discussing this problem with the author who acknowledges gratefully that many of the ideas here presented were suggested by him and that many errors have been omitted upon his advice.

THE JOURNAL OF CHEMICAL PHYSICS VOLUME 21, NUMBER 2 FEBRUARY, 1953

The Effects of Interactions in Real Polymer Chains

F. BUECHE
Department of Physics, University of Wyoming, Laramie, Wyoming
(Received August 20, 1952)

The effect of interactions between the segments of a polymer chain on the size of the molecule has been calculated. Two approaches have been used. The first is a direct probability calculation using an exponential interaction energy between segments. The second follows the original approach of Flory but solves the problem to a different approximation. Both methods lead to essential agreement with Flory's result for small and moderate interactions. A probable reason for the spurious results found by others is proposed.

INTRODUCTION

A FEW years ago, P. J. Flory presented a theory of polymer chain configurations in dilute solutions.[1] In that paper he arrived at the conclusion that a coiling polymer molecule will be extended throughout a larger volume in good than in poor solvents. This general conclusion has been widely accepted since it is amply verified by experiment. However, some disagreement has existed about the details of Flory's result.

The chief point of disagreement is centered about the way in which the polymer expansion in good solvents should vary with the molecular weight. If we represent the polymer's mean square end to end distance calculated on the basis of no interaction by $\langle R_0^2\rangle$ and with interaction by $\langle R^2\rangle$, then in general $\langle R^2\rangle=\alpha^2\langle R_0^2\rangle$ where α is an expansion factor. (See Fig. 1.) Flory concluded that $\alpha^5-\alpha^3=CM^{\frac{1}{2}}$ where M is the molecular weight of the chain and C is a constant which characterizes the polymer-solvent interaction.

Other authors[2] have concluded from other types of calculations that α should be independent of M for M large. Whereas Flory used an approximate statistical thermodynamic approach, most of these other authors have used a straight statistical method. The available experimental data seem to favor Flory's result.[1] However, some authors are not in agreement with this.[2]

In this paper, we shall give two alternate calculations of this molecular expansion effect. The first, given in Sec. I, starts from simple basic assumptions and does not involve the use of thermodynamics. In Sec. II we give a somewhat modified treatment of Flory's original calculation.

[1] P. J. Flory, J. Chem. Phys. 17, 303 (1949). See also P. Flory and T. Fox, J. Am. Chem. Soc. 73, 1904 (1951); and Mandelkern, Krigbaum, Scheraga, and Flory, J. Chem. Phys. 20, 1392 (1952).

[2] Hermans, Klamkin, and Ullman, J. Chem. Phys. 20, 1360 (1952). This paper gives a rather complete summary of the work done on this problem. For that reason, we shall not give a complete list of references here.

SECTION I

For mathematical convenience, we postulate a chain composed of Z freely orienting segments. These segments will be assumed to have a length which is not fixed but which is exponential in nature. That is to say, if one end of a segment is at a point 0, 0, 0, the probability that the other end is in a volume element $d\xi$, $d\eta$, $d\nu$ is given by

$$C\exp\left[-\frac{3}{2a^2}(\xi_n^2+\eta_n^2+\nu_n^2)\right]d\xi_n d\eta_n d\nu_n.$$

It may be shown that such a chain behaves much like a chain of fixed bond length equal to a.

If we were to ignore interactions of these segments one with another, the probability of a given chain configuration would be

$$dP_0=C'\exp\left[-\frac{3}{2a^2}\sum_{n=1}^{z}(\xi_n^2+\eta_n^2+\nu_n^2)\right]d\tau.$$

The probability that the chain ends are separated by a distance x, y, z is obtained after multiplying by

$$\Delta=C''\int\int\int_{-\infty}^{\infty}\exp[-2\pi i\{t_x(\textstyle\sum\xi_n-x)+\cdots+\cdots\}]dt_x dt_y dt_z$$

and integrating over all ξ, η, and ν.

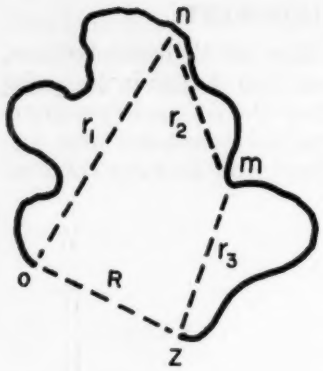

FIG. 1. Diagram illustrating the symbols used in the text.

This is true since this integral is a representation of a delta function which is unity for $\sum\xi_n=x$, $\sum\eta_n=y$, $\sum\nu_n=z$ and zero otherwise.[3]

But if interactions are present, there will be a potential energy between two approaching segments. The total potential of the whole chain will be assumed to have the form

$$V=\epsilon\sum_{2}^{N}\sum_{1}^{j-1}\exp[-\gamma^2 r_{ij}^2],$$

where $\gamma^2=3/2a^2$ and where r_{ij} is the distance between the i and j segments and ϵ is an interaction energy. Its value is a measure of the *difference* in interaction between two segments when far separated and when adjacent. The value of ϵ will depend upon molecular weight. This is due to the fact that there is a probability that the two segments under consideration will be near other polymer segments both when r is large and small. This effect should not be important for all except the lowest molecular weights. To preserve simplicity, it will be neglected for the present time.

With the above factor put in, one has for the probability of an end to end chain separation of x, y, z

$$P(x,y,z)=C\int_{\xi}\int_{\eta}\int_{\nu}\exp[-\gamma^2\sum_{1}^{Z}(\xi_n^2+\eta_n^2+\nu_n^2)]\cdot\Delta\left(1-\frac{\epsilon}{kT}\sum\sum\exp(-\gamma^2 r_{ij}^2)\right)d\tau.$$

To get this we have expanded the factor $\exp(-V/kT)$. Our answer will be restricted by this assumption to small interactions.

It might be well to point out here that, besides the mathematical formalism involved, the above expression differs in a major respect from most of the non-Flory derivations thus far proposed. These other theories have, put in a qualitative fashion, constructed the probability in such a way that the nth segment takes up a position in the potential field of the previous undisturbed $n-1$ segments. No provision is made for the fact that the nth segment influences the preceding $n-1$ segments or that the next $Z-n$ segments will influence the nth segment. By using the total energy of the chain, we have avoided this approximation.

To proceed, we need to evaluate the above integrals. This may be done and the result for Z not too small turns out to be, writing R for the end to end chain distance,

$$P(R)\cong C\left(\frac{(\pi)^{\frac{1}{2}}}{\gamma}\right)^{3Z-1}\left\{\frac{\exp(-\gamma^2R^2/Z)}{Z^{\frac{1}{2}}}-\frac{\epsilon}{kT}\sum\sum\frac{\exp[-\gamma^2R^2/(Z-j+i-1+\ln 2)]}{(j-i)^{\frac{1}{2}}(Z-j+i-1+\ln 2)^{\frac{1}{2}}}\right\}.$$

This expression is rather formidable because of the double sum. Actually, we are only interested in $\langle R^2\rangle$ and so we need only evaluate

$$\langle R^2\rangle=\frac{\int_0^\infty P(R)R^4dR}{\int_0^\infty P(R)R^2dR}.$$

This turns out to be

$$\langle R^2\rangle\cong R_0^2\left(1+\frac{\epsilon}{ZkT}\sum\sum(j-i)^{-\frac{1}{2}}\right),$$

where terms in higher powers of ϵ/kT have been dropped and $R_0^2\equiv 3Z/2\gamma^2$. From this,

$$\langle R^2\rangle\cong R_0^2\left(1+\frac{2\epsilon}{kT}Z^{\frac{1}{2}}\right).$$

This means that Flory's α would be given by

$$\alpha^2=\left(1+\frac{2\epsilon}{kT}Z^{\frac{1}{2}}\right).$$

Such a result is not far from agreement with Flory's relation that

$$\alpha^2=\left(1+\frac{c}{\alpha^3}Z^{\frac{1}{2}}\right).$$

In fact, for α-values near unity the two results are essentially the same. The discrepancy at large values of α may be due to the approximation made in expanding the energy factor. Or, since Flory's derivation makes a number of major approximations, the difference may be due to one of these. To investigate this latter possibility, we shall carry through Flory's derivation in a somewhat different fashion. This is done in the next section.

Before going on with that we should mention that the above result for α is in direct contradiction to a qualitative approach which has led many people to state that the interaction effect must decrease with increasing

[3] S. Chandresekhar, Revs. Modern Phys. **15**, 1 (1943).

molecular weight. The fallacy in that argument is pointed out in the appendix where we give an exceedingly simple but less rigorous derivation of the above relation.

SECTION II

Flory has given several alternative derivations of his relation and Simha has given another.[1,4] All of these lack preciseness due to the fact that each neglects to some extent the fact that the chain is a single entity. It has been this feature in the Flory derivation which has often met with criticism. We shall here carry out Flory's derivation without making such an assumption.

Consider a polymer chain having Z freely orienting segments. Call one end the zero segment. Counting from that end there will be a length of chain leading to the mth segment where $m \leqslant Z$. We shall also need to talk about an intermediate segment, the nth, for which $n<m$.

Flory, from quite general considerations, has shown that if Ω_0 is the total number of chain configurations possible when interaction is neglected and Ω is the number actually possible, then

$$\ln(\Omega/\Omega_0)=\sum_R N(R)\ln[Nf(R)W(R)/N(R)].$$

In this expression $W(R)$ is the chain end distribution function without interference, i.e.,

$$W(R)dR=\left(\frac{\beta^2}{\pi Z}\right)^{\frac{3}{2}}\exp[-\beta^2R^2/Z]4\pi R^2dR,$$

where β^2 is $3/2l^2$ where l is the bond length. $N(r)$ is the actual number of molecules having a chain end separation of R. This is taken to be $N(R)=NW(R/\alpha)$. The quantity $f(R)$ is defined as the ratio of number of configurations actually allowed to a chain of end to end separation R as compared to the number available without interaction.

It is the quantity $f(R)$ which we intend to calculate in a more rigorous fashion than has been done previously. To do this, we first calculate the probability that the nth segment occupies the same position as the mth segment for a fixed end to end distance of the chain. Call this P_n. Now if we think of the number of ways in which the mth segment may be placed in solution preserving the fixed end to end chain position, we see that this number is reduced by a factor $(1-\sum_{n<m} P_n)$ over the number without interference. The total reduction in configurations for a chain with fixed end separation will be

$$f(R)=\prod_{m=1}^{Z}(1-\sum_{1}^{m-1}P_n)\cong\exp[-\sum_{1}^{Z}\sum_{1}^{m-1}P_n].$$

This approximation invalidates the treatment at extremely large interactions. However, this approximation is much better than the one used in Sec. I. To calculate P_n, consider the molecule shown in the figure. The probability of the configuration shown is

$$C\exp\left\{-\frac{\beta^2r_1^2}{\alpha_1^2n}-\frac{\beta^2r_2^2}{\alpha_2^2(m-n)}-\frac{\beta^2r_3^2}{\alpha_3^2(Z-m)}\right\},$$

where C is a normalization constant adjusted so that the integral of the above over all values of r_1, r_2, and r_3 consistent with the end separation R is unity. Some ambiguity arises in connection with the factors α_1, α_2, and α_3 which are expansion factors for the three portions of the chain. Obviously, they cannot in general be equal to α and to each other.

We shall work out the problem for two approximations to these α values. First, consider the case of small interactions so that $f(R)$ may be computed on the basis of $\alpha_1=\alpha_2=\alpha_3=1$.

P_n is given by the integral of the above expression over all r_1 and r_3 consistent with the fact that R remains fixed and that segment n overlaps segment m. This means $r_2\cong 0$ and so the integral over r_2 results in a factor v, the excluded volume due to one segment. If the segments are considered to be spheres, v is 8 times the volume of one segment. Carrying out the other integrations leads to

$$P_n=v\left[\frac{Z\beta^2}{\pi(m-n)(Z-m+n)}\right]^{\frac{3}{2}}\exp\left\{-\frac{R^2\beta^2}{Z}\frac{(m-n)}{(Z-m+n)}\right\},$$

which gives $f(R)$ directly.

We actually want

$$\ln(\Omega/\Omega_0)=\sum_R N(R)\ln[NW(R)f(R)/N(R)].$$

This may be evaluated most simply by first carrying out the integration over R. After doing the R, n, and m integrations, one finds

$$\ln(\Omega/\Omega_0)=N\ln(\alpha^3/N)-\tfrac{3}{2}(\alpha^2-1)N+\frac{v\beta^3}{\pi^{\frac{3}{2}}}Z^{\frac{1}{2}}(4\alpha-2N^{\frac{1}{2}}).$$

Since we are really interested in the most probable value of α and since the above expression is merely proportional to the entropy of the system, we find α by differentiating $\ln(\Omega/\Omega_0)$ with respect to α and equating to zero. This leads to

$$\alpha^2=1+\frac{4}{3}\left(\frac{3}{2\pi}\right)^{\frac{3}{2}}\frac{v}{l^3}Z^{\frac{1}{2}}\alpha.$$

For α near unity, where the above approximations hold, this is essentially the same as Flory's previous result and the result of Sec. I.[5]

[4] Weissberg, Simha, and Rothman, J. Research Natl. Bur. Standards 47, 298 (1951).

[5] In the particular case where the segments are considered spherical, the quantity $vZ^{\frac{1}{2}}/l^3$ may be replaced by the alternate quantity $8V/qM(M/R_0^2)^{\frac{1}{2}}M^{\frac{1}{2}}$, where V is the volume occupied by the polymer molecule and q is the molecular weight of a freely orienting chain segment. If the segments are considered as cylinders, the above value should be multiplied by 0.5.

A better approximation applicable to a wider range of α may be obtained as follows: In the evaluation of P_n, the major portion of the integral is seen to occur for small values of $m-n$. To a good approximation, we can therefore take $\alpha_2=1$. However, α_1 and α_3 should be quite closely given by α since both n and $Z-m$ will in general be of the order of Z. To this approximation ($\alpha_1=\alpha_3=\alpha$, $\alpha_2=1$), one then finds in a manner similar to above that

$$\alpha^4-\alpha^2=\frac{48}{69}\left(\frac{3}{2\pi}\right)^{\frac{1}{2}}\frac{v}{l^3}Z^{\frac{1}{2}}\left(1+\frac{2}{3\alpha^2}+\frac{1}{4\alpha^4}\right).$$

This again for α near unity is the same as Flory's result. It does not quite agree at very large values of α due to the difference between $\alpha^5-\alpha^3$ and $\alpha^4-\alpha^2$. The correct value is still in doubt due to the fact that both results are not exact for large α. However, this is of minor importance until large extensions of the molecule owing to long range interactions are encountered. Also, in that case, the chain end to end distance can no longer be assumed to be Gaussian. The only known case at present where this is important is for highly charged polyelectrolytes. It is hoped to clarify this point further, but until that is done we suggest that Flory's value be used.

Unfortunately, the method used in this section, i.e., finding α from the entropy, is very sensitive to the choice of α_1, α_2, and α_3. A better approach may be to notice that the true probability for a chain end to end separation of R is given by $P(R)\sim W(R)f(R)$.

The value of $\langle R^2\rangle$ and therefore of α^2 is found by evaluating

$$\langle R^2\rangle=\frac{\int P(R)R^2dR}{\int P(R)dR}.$$

Until now, this has only been done for small interactions resulting from integration difficulties, but the same answer as above is found in the approximation of α near unity.

CONCLUSION

The above treatment of the excluded volume effect confirms in essentials the results previously found by Flory. Some uncertainty still exists as to the proper behavior at very large expansions of the molecule. For all practical cases except highly charged polyelectrolytes, Flory's result is satisfactory although his numerical constant may be slightly in error. This has been shown both by a completely different derivation and also by the fact that the removal of the most objectional points in this original derivation still leaves the answer essentially unchanged. It would appear that the disagreement with Flory's result which has been found by others is derived from the fact that a portion of the interaction effect has been neglected by them as was pointed out in Sec. I of this paper.

ACKNOWLEDGMENT

Most of this work was done while the author was employed as a Research Associate at Cornell University on a contract sponsored by the Office of Rubber Reserve, R.F.C.

I am indebted to Professor P. J. Flory and Professor P. Debye for discussions on various points connected with this work.

APPENDIX

The following reasoning is often used to show why Flory's relation must be wrong. Consider the molecule as an equivalent sphere of diameter R. This sphere contains Z segments. Since its volume is $(1/6)\pi R^3=(1/6)\pi Z^{\frac{1}{2}}l^3$, one finds that the density of segments in the sphere decreases as $Z^{-\frac{1}{2}}$. Because of this, the effect of interaction must also decrease (or at most remain constant) with increasing molecular weight. Therefore, α^2 cannot increase as a positive power of Z.

To show why this reasoning is false, consider the same spherical model of the molecule. Suppose two segments when in the same cell have a potential energy ϵ, zero energy otherwise. In the molecular sphere of diameter R there are $(1/6)\pi R^3/v_0$ cells of volume v_0. From straight probability theory, the average number of cells which contain two segments is Z^2 times $\frac{1}{2}$, divided by the total number of cells. Therefore, the total energy of the system will be

$$\frac{3}{\pi}\frac{v_0Z^2}{R^3}\epsilon.$$

This is the salient feature for if $R^2\sim Z$, we see that the interaction energy increases with increasing Z. To observe the consequences of this, we have that the probability of an end to end separation of R will be

$$P(R)=C\exp\left[-\frac{3R^2}{2l^2Z}-\frac{3\epsilon v_0}{\pi kT}\frac{Z^2}{R^3}\right]R^2.$$

Since we desire the most probable value of R, we differentiate $P(R)$ with respect to R and equate to zero. After making the substitution that $R^2=\alpha^2R_0^2=\alpha^2(2l^2Z/3)$, we have

$$\alpha^5-\alpha^3=\frac{9}{2\pi}\left(\frac{3}{2}\right)^{\frac{1}{2}}\left(\frac{v_0}{l^3}\right)\frac{Z^{\frac{1}{2}}}{kT}.$$

Again we see that for α approaching unity this is equivalent to the answer found in Sec. I. Since no expansion of the exponential has been made here, we would expect that perhaps the $\alpha^5-\alpha^3$ representation is the more accurate for large α-values.

Second-Order Transitions and Critical Phenomena

ROBERT L. SCOTT
Department of Chemistry, University of California, Los Angeles 24, California
(Received July 14, 1952)

Second-order transitions occur when a system which is completely ordered at low temperatures (degree of order $s=1$) changes gradually to a disordered state, ultimately reaching $s=0$ at the critical or Curie temperature T_c. Elementary theories always predict that $s^2 \propto (1-T/T_c)$ and predict limiting heat capacities at T_c which are finite and much smaller than those observed. Experimental data on liquid-liquid and liquid-vapor critical phenomena fit a relation in which the cube of s, not the square, is proportional to $1-T/T_c$. A crude argument, using this empirical equation, leads to the conclusion that the heat capacity rises sharply, probably reaching infinity at the Curie temperature. Experimental data on ammonium chloride and on quartz fit a relation in which the anomalous heat capacity is proportional to an inverse power of $(1-T/T_c)$.

THE resemblance between the critical phenomena associated with the equilibrium between liquid and vapor in a one-component system or between two liquid phases in a two-component system and second-order phase transitions such as those in β-brass, liquid helium, ammonium chloride, and iron has long been known. However, the fact that this correspondence is essentially complete has frequently been obscured, partly because of differing terminology, but mostly because different aspects are emphasized in different situations. Thus, in the case of liquid-vapor equilibria, we normally confine our attention to the separate thermodynamic properties of each of the two coexistent phases; in the case of order-disorder transitions, we measure thermodynamic properties (e.g., the heat capacity) of the entire system. Actually, as we shall see, information obtained from observing one class of these phenomena can prove useful in interpreting the behavior of other classes.

Common to all these phenomena is the existence of two segregated "phases" at a low temperature. This segregation may be between two macroscopically distinct regions of space (liquid-vapor or liquid-liquid equilibrium), between two interlaced superlattices (order-disorder phenomena), between two different regions of "momentum space" (liquid helium), etc. In all of these, as the temperature is raised, molecules are transferred from one "phase" to the other, and as a result the difference in character between the two "phases" becomes less and less marked until at the critical temperature or *lambda*-point, the two become identical in properties and we have a single phase.

In each of these cases, it is possible to define a degree of order s which measures the difference between the two conjugate "phases." For liquid-vapor equilibrium this may be defined as $(\rho_l-\rho_g)/2\rho_c$ [or better as $(\rho_l-\rho_g)/(\rho_l+\rho_g)$?], where ρ_l and ρ_g are the densities of liquid gas, respectively, and ρ_c is the critical density. In simple liquid-liquid systems, and in simple order-disorder phenomena, s is merely $|x'-x''|$ where x' and x'' are the mole fractions of a particular component in the two "phases." An analogous concept can doubtless be defined for other systems of interest.

Most of the theoretical studies of these phenomena have concentrated upon the symmetrical systems, those in which the two conjugate "phases" are more or less mirror images of each other, e.g., liquid-liquid phase separation and order-disorder effects in 1−1 binary alloys. The correspondence between the "regular solution" treatment of liquid-liquid miscibility[1] and the Bragg-Williams treatment[2] of order-disorder in β-brass is exact, and the quasi-chemical refinements[3] of these are essentially identical.

The "ordered" two-phase system has a lower energy than the "disordered" one-phase system, and, according to any of the simple theories, the amount of this energy difference per mole is, at least to a good first approximation, proportional to s^2:

$$E(s)-E(0)=-As^2. \tag{1}$$

The constant A is then the difference in energy per mole between the one-phase system and the completely ordered two-phase system. (For the liquid-liquid case, it is just the energy of formation of the one-phase mixture, from the two pure liquids.)

The disordered state ($s=0$) is clearly the one of higher entropy, so it must be the stable high temperature form just as the completely ordered state ($s=1$) must be the stable form at the low temperature limit.

We note from Eq. 1 that the energy necessary to increase the disorder by an amount Δs is directly proportional to s and consequently decreases with decreasing s. This means that the less order there is the easier it is to introduce more disorder. Because of these "cooperative" phenomena, an "acceleration" in the disordering process sets in (a kind of "autocatalysis" with increasing temperature) and we observe second-order transition phenomena, in particular the sharp rise in the heat capacity just below the critical temperature

[1] See for example, J. H. Hildebrand and R. L. Scott, *Solubility of Nonelectrolytes* (Reinhold Publishing Corporation, New York, 1950), third edition, especially pp. 41–45, 253–269.
[2] W. L. Bragg and E. J. Williams, Proc. Roy. Soc. (London) **A145**, 699 (1934); **A151**, 540 (1935).
[3] For a resumé of the quasi-chemical theories and extensive references, see R. H. Fowler and E. A. Guggenheim, *Statistical Thermodynamics* (Cambridge University Press, Cambridge, England, 1939), pp. 358–366, 576–581.

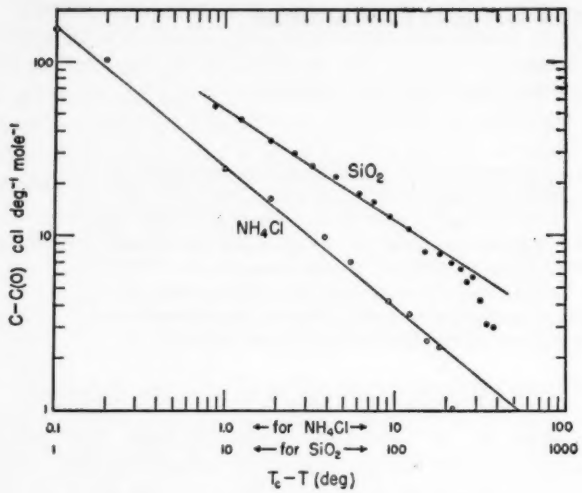

FIG. 1. Heat capacities near the critical temperature.

and its discontinuous drop to a low value at that temperature.

From Eq. 1, it follows that the anomalous heat capacity is given by

$$C(s)-C(0)=\frac{d[E(s)-E(0)]}{dT}=-A\frac{ds^2}{dT}=-B\frac{ds^2}{d\theta}, \quad (2)$$

where $\theta=T/T_c$ and $B=A/T_c$. The critical temperature T_c and the constant A are related, so B should be a more-or-less universal constant (in the Bragg-Williams or regular solution models, it is $R/2$ per mole).

All of the "classical" theories, crude or refined, derive s as a function of θ by use of the van der Waals principle of "continuity of states," or its equivalent. This invariably[4] leads to a relation

$$s^2=K_1(1-\theta)+K_2(1-\theta)^2+\cdots, \quad (3)$$

where K_1, K_2, etc., are constants. Substitution of Eq. 3 into Eq. 2 leads to a finite limiting value for $C(s)-C(0)$ as $T\rightarrow T_c$ ($3R/2$ in the simple Bragg-Williams theory, a somewhat larger value in more refined treatments) and a finite limiting slope on the low temperature side ($dC/d\theta=12R/5$ in the simple B-W theory, slightly steeper if refined). Actually the anomalous heat capacity is confined to a narrower range and reaches a higher peak than any of these theories predict. Further refinements account for only a small part of the discrepancy between the original B-W theory and experiment.

Recent studies on critical phenomena in liquid-liquid and liquid-vapor systems suggests a possible explanation for these difficulties. Guggenheim[5] has shown that the conjugate densities of A, Kr, Xe, N_2, O_2, CO, and CH_4 fit with surprising accuracy the simple formula

$$1-\theta=[ks]^3, \quad (4)$$

where $k=0.57$. Zimm found the same cubic relation for the coexistence curve in his careful study[6] of the carbon tetrachloride-perfluoromethylcyclohexane system fitting the data with $k=0.64$. More recently he has shown[7] that a similar curve with $k=0.6$ can account for the measurements on aniline-cyclohexane by Rowden and Rice.[8]

This apparently general cubic relation is at obvious variance with the parabolic relation (Eq. 3) deduced from "classical" models. The explanation for this is still unknown, but a possible approach towards a satisfactory theory of critical phenomena has recently been suggested.[9]

These results suggest that the use of Eq. 3 in the theory of second-order transitions is a basic error,[10] and that we might better use Eq. 4. If Eq. 4 is solved for s^2 and substituted into Eq. 2, we obtain

$$C(s)-C(0)=\tfrac{2}{3}Ak^{-2}(1-\theta)^{-\frac{1}{3}}. \quad (5)$$

It should be emphasized that we have not derived Eq. 5 in any rigorous way. It is unreasonable to expect that the as yet imperfectly understood factors which produce Eq. 4 will not require some modification in Eq. 2; this might produce a final result quite different from Eq. 5. Moreover, it is clear that the right-hand side of Eq. 3 (and consequently that of Eq. 5 as well) is only the leading term of a power series, so we cannot expect to apply it far from the critical point.

Equation 5 predicts that $C_v\rightarrow\infty$ as $\theta\rightarrow 1$, a conclusion not inconsistent with experimental results. Moreover, since the total energy associated with the disordering process is fixed [$E(0)-E(1)=A$], any model which predicts such a sharp peak in the anomalous heat capacity will also explain the comparative narrow range of temperatures to which the anomalous behavior is confined.

It is hard to compare experimental heat capacity measurements with Eq. 5 because of (a) the sensitivity of the heat capacity (near $\theta=1$) to the exact choice of T_c, (b) the uncertainty concerning the best choice of a function for $C(0)$, and (c) uncertainty concerning the range of θ over which Eq. 5 might be valid. Figure 1 shows data for ammonium chloride[11] from −51.7°C to the λ-point (taken as −30.3°C) and for crystalline quartz[12] from 202.8°C to its λ-point (taken as 580°C). The $C(0)$ function for the former was estimated by means of a linear relation which fits the experimental points at low temperatures and at temperatures well above the critical point: $C(0)=18.8-0.06(T_c-T)$ cal

[4] The proof of this statement will be found on pp. 316–318 of reference 3.

[5] E. A. Guggenheim, J. Chem. Phys. **13**, 253 (1945).

[6] B. H. Zimm, J. Phys. and Colloid Chem. **54**, 1306 (1950).

[7] B. H. Zimm, J. Chem. Phys. **20**, 539 (1952).

[8] R. W. Rowden and O. K. Rice, J. Chem. Phys. **19**, 1423 (1951).

[9] B. H. Zimm, J. Chem. Phys. **19**, 1019 (1951). See also J. E. Mayer, J. Chem. Phys. **19**, 1024 (1951).

[10] Equation 3 is still quoted as if it were an established fact. See, for example, P. J. Price, J. Chem. Phys. **19**, 1281 (1951), Eq. 7.

[11] Simon, von Simson, and Ruhemann, Z. physik. Chem. **129**, 339 (1927).

[12] H. Moser, Physik. Z. **37**, 737 (1936).

deg^{-1} mol^{-1}. Experimental data on quartz glass[12] were used to obtain $C(0)$ for the latter. The log-log plots are reasonably good straight lines, but the slope is not the -0.33 predicted by Eq. 5 (-0.8 for NH_4Cl, -0.65 for SiO_2).

Heat capacity data on other systems (e.g., β-brass, nickel, liquid helium) give results not inconsistent with these if due allowance is made for the uncertainties cited above. Information on the heat capacities of substances in the region of liquid-vapor critical phenomena is extremely meager, the few experiments[13,14] which have been performed being hard to interpret because of uncertainties about $C(0)$ and the probability of non-equilibrium effects.

More careful studies are clearly needed, especially on the heat capacities of two-phase liquid-liquid systems.

[13] D. B. Pall, J. W. Broughton, and O. Maass, Can. J. Research **B16**, 230 (1938), (ethylene).
[14] A. Michels and J. C. Strijland, Physica **16**, 813 (1950) (carbon dioxide).

THE JOURNAL OF CHEMICAL PHYSICS VOLUME 21, NUMBER 2 FEBRUARY, 1953

Entropy Changes in Free Radical Reactions

A. F. TROTMAN-DICKENSON
Chemistry Department, The University, Manchester, England
(Received August 28, 1952)

The entropies of alkyl and other simple free radicals may be estimated with sufficient accuracy to make informative calculations about the equilibria involved in the reactions of these radicals. Such calculations have been made for metathetical reactions, the decomposition of saturated molecules, and the decomposition of free radicals. The method provides a means of obtaining knowledge about reactions which are not readily susceptible to direct experimental investigation. The deviations of the frequency factors of some unimolecular decompositions from a value of $10^{13\pm1}$ are discussed.

ONE of the principal reasons for studying free radical reactions is that they are, because of their formal simplicity, very suitable for testing theories of chemical kinetics.

Free radical reactions may be divided into three classes represented by the equilibria (1), (2), and (3)

$$R'-+AR''\leftrightarrows R'A+R''-, \quad (1)$$

$$R'R''\rightleftarrows R'-+R''-, \quad (2)$$

$$R'-A-B-\leftrightarrows R'-+A=B. \quad (3)$$

Type (1) represents a metathetical reaction, type (2) represents the decomposition of a saturated molecule and the combination of two radicals, and type (3) represents the addition of a radical to a double bond and the decomposition of a radical into a smaller radical and an unsaturated molecule. At the present time examples of all these types of free radical reaction are known; in some cases it has been possible to measure their rate constants and even to obtain their frequency factors and activation energies, but in very few cases have the forward and reverse processes for the same reaction been quantitatively studied. This discussion will be confined to a consideration of the "temperature independent" factors of reactions of the types (1), (2), and (3).

It has been found that the Arrhenius equation

$$k=A\exp(-E/RT)$$

adequately describes the variation of the velocity constant of a gas reaction with temperature (the symbols have their usual meaning). Hence for the reaction

$$A+B\underset{k_b}{\overset{k_f}{\rightleftarrows}}C+D,$$

$$-RT\ln k_f/k_b=(E_f-E_b)-RT\ln A_f/A_b=\Delta H-T\Delta S$$

$$R\ln A_f/A_b=\Delta S.$$

This relation is strictly true if the activation energy is defined by

$$RT^2(d\ln k/dT)=E,$$

and the temperature independent factor is defined by

$$RT\ln A=\partial(RT^2\ln k)/\partial T.$$

These definitions relate to a particular temperature, whereas experimentally A and E are derived from the integrated form of the Arrhenius equation. However, it has been found that for gas phase reactions, these two derivations give the same values for A and E within the limits of experimental error. In addition the most popular theories indicate that for bimolecular and unimolecular reactions, the form of the temperature dependence of the A factors should be the same and hence the ratio A_f/A_b will be temperature independent. This type of treatment results from the work of Van t'Hoff and has been recently used by Dainton and Ivin[1] when discussing polymerization reactions, though they arrive at the same expression by consideration of

[1] F. S. Dainton and K. J. Ivin, Trans. Faraday Soc. **46**, 331 (1950).

the theory of absolute reaction rates, which is unnecessary.

Here we will calculate values of ΔS and hence of A_f/A_b for a number of reactions for which either A_f or A_b are known. The entropies of the radicals are often not known accurately, but because of the symmetry of many of the reactions, many of the errors which may occur resulting from arbitrary assumptions about the character of the radicals balance out and fairly definite conclusions may be drawn. Unless it is specifically stated to the contrary, the calculations have been carried out using entropies at 298°K; where it is convenient the calculations have been repeated for temperatures closer to those at which the reactions were studied experimentally. It can be seen that this does not alter the character of the results. The evaluation of entropy changes involves a knowledge of three species (a) of ordinary saturated molecules, (b) of atoms, and (c) of free radicals.

(a) The entropies of ordinary saturated molecules are taken from the tables published by the National Bureau of Standards.[2]

(b) The entropies of atoms may be calculated to the desired accuracy by the use of standard methods.

(c) The entropies of the large free radicals R, that is, other than ethyl and methyl, are taken as being the same as those of the compounds RH with an allowance made of the electron degeneracy of the radical owing to the presence of an unpaired electron. In most cases this is probably a very good approximation, for the translational entropy because of the very small differences in mass; for the rotational entropy because of the small change in the moments of inertia and because the symmetry number is unlikely to vary by more than a factor of two; and for the vibrational entropy because although an inversion vibration analogous to that in ammonia may make a considerable contribution to the vibrational entropy of an alkyl radical, this entropy is only a small fraction of the total. As an illustration of this point let us consider the entropy of a methyl radical (neglecting for the moment the contribution of the electron degeneracy). We have the following figures, at 298°K.

$$S^0(\text{methane}) = 44.5 \text{ eu}, \quad S^0(\text{ammonia}) = 45.9 \text{ eu},$$

for a planar methyl radical (symmetry number 6)

$$S^0_{\text{trans}}(\text{methyl}) = 34.1 \text{ eu}, \quad S^0_{\text{rot}}(\text{methyl}) = 9.9 \text{ eu},$$

for a methyl radical with a very high inversion frequency

$$S^0_{\text{trans}} + S^0_{\text{rot}} + S^0_{\text{vib}}(\text{methyl}) = 44.1 \text{ eu},$$

for a methyl radical with very low inversion frequency

$$S^0_{\text{trans}} + S^0_{\text{rot}} + S^0_{\text{vib}}(\text{methyl}) = 45.5 \text{ eu}.$$

From these figures it can be seen that the value of 45.5 eu which has been adopted here for the total entropy of the methyl radical, may be too low but can hardly be too high.

Similarly the value adopted for the ethyl radical of 56.3 eu may be seen to be about as small a value as could reasonably be selected when compared with $S^0_{C_2H_6} = 54.9$ eu, $S^0_{C_2H_4} = 52.5$ eu, and $S^0_{CH_3NH_2} = 57.7$ eu.

We can now use these values to derive the A factors of reactions which are not in general experimentally accessible. It will be seen that in some cases there is an experimental value which agrees satisfactorily with that calculated.

1. METATHETICAL REACTIONS

(a) The Reactions of Methyl Radicals with Alkanes

A large number of reactions of the type

$$CH_3 + RH \rightarrow CH_4 + R-$$

have been studied[3] and it has been found[4] that the A factors are of the order of 10^{11} (all velocity constants are given in g mole, cc and sec). Since the entropy change in these reactions is almost zero, reactions of the type

$$R + CH_4 \rightarrow CH_3 + RH$$

will also have A factors of the order of 10^{11}. Hence the A factor for the reaction

$$C_2H_5 + CH_4 \rightarrow C_2H_6 + CH_3$$

may be expected to be of the order of 10^{11}. It is therefore very surprising that Ivin and Steacie[5] find that $A = 10^{13.3}$ for the very similar reaction

$$C_2H_5 + C_2H_5 \rightarrow C_2H_4 + C_2H_6.$$

(b) The Reactions of Hydrogen Atoms with Alkanes

In these reactions the entropy change is not zero because of the large difference between the entropies of the hydrogen atom and the hydrogen molecule. Rather exact calculations may be made for the equilibrium

$$H + CH_4 \underset{k_b}{\overset{k_f}{\rightleftarrows}} H_2 + CH_3,$$

because of the simplicity of the species. We find that $A_f \geqslant 10A_b$ in good agreement with the latest experimental data which indicates that A_f is between 10 and 100 times as great as A_b.[6] It has often been assumed when the results of hydrogen atom reactions studied by the Wood-Bonhoeffer method are considered

[2] Natl. Bur. Standards (U. S.), Circ. C. 461, 1947, Washington D. C.

[3] A. F. Trotman-Dickenson and E. W. R. Steacie, J. Chem. Phys. **19**, 329 (1951).

[4] R. Gomer and G. B. Kistiakowsky, J. Chem. Phys. **19**, 85 (1951).

[5] K. J. Ivin and E. W. R. Steacie, Proc. Roy. Soc. (London) **A208**, 25 (1951).

[6] E. W. R. Steacie, *Atomic and Free Radical Reactions* (Reinhold Publishing Corporation, New York, 1947); T. G. Majury and E. W. R. Steacie, J. Chem. Phys. **20**, 197 (1952).

that reactions of the type

$$H+RH\rightarrow H_2R$$

have frequency factors of the order of 10^{13}. If that assumption is correct the frequency factors of the back reactions for alkyl radicals should be 10^{12}, since $A_b/A_f\approx 1/10$.

2. UNIMOLECULAR DECOMPOSITIONS

Szwarc and his collaborators have recently measured the rates of a large number of reactions of the type

$$R'R''\underset{k_b}{\overset{k_f}{\rightleftarrows}}R'+R'',$$

and in some cases have been able to measure the frequency factors of the reactions. When this has been impossible very fruitful interpretations of the data have been obtained by assuming that A_f is constant for a series of similar reactions in which R′ is unchanged. We will consider two series, the alkyl benzenes and the bromomethanes.

(a) The Alkyl Benzenes

In treating the alkyl benzenes it has been assumed that the entropy of the benzyl radical is the same as that of toluene, however, this doubtful assumption does not affect conclusions about variations among members of the series. The results are given in Table I. The variation of A_b(calc) in this table is not in agreement with the general belief that the association of more complex radicals will involve a lower A factor. To obtain a value of A_b of 10^9 would mean that A_f would be 3×10^{12}, this value of A_f combined with the experimental value for k_f leads to an activation energy consistent with an equality of strengths for the C_2H_5-H and $n-C_3H_7-H$ bonds, which is a more reasonable result than that of $D(C_3H_7-H)-D(C_2H_5-H)=4$ kcal given by Szwarc and Leigh (see Table I, references c and d).

(b) The Bromomethanes

Similar calculations for the decompositions of the series of bromomethanes[7] have been made on the assumption that $S_{RH}=S_R-$. A_f has been taken as 10^{13}, there being good experimental evidence that this value is correct for CH_3Br and CCl_3Br. The results in the table are probably reliable and form a series which conforms with the general idea that the association of more complex radicals involves lower A factors:

Reaction	A
CH_3+Br	4×10^{11}
CH_2Br+Br	1×10^{11}
$CHBr_2+Br$	3×10^{10}
CBr_3+Br	7×10^9.

[7] M. Szwarc and A. H. Sehon, Proc. Roy. Soc. (London) **A209**, 110 (1951).

TABLE I. A factors for the decomposition of alkyl benzenes.

Substance	A_f(expt)	A_f/A_b at 298°K	A_f/A_b at 1000°K	A_b(calc) 1000°K
Toluene	10^{13} [a]	40	240	4×10^{10}
Ethyl benzene	10^{13} [b]	1000	2900	3×10^9
n-Propyl benzene	3×10^{12} [c]	2500	2300	1×10^9
n-Butyl benzene	3×10^{14} [d]	3000	3000	1×10^{11}

[a] M. Szwarc, J. Chem. Phys. **16**, 128 (1948).
[b] M. Szwarc, J. Chem. Phys. **17**, 431 (1949).
[c] C. H. Leigh and M. Szwarc, J. Chem. Phys. **20**, 403 (1952).
[d] C. H. Leigh and M. Szwarc, J. Chem. Phys. **20**, 407 (1952).

(c) The Combination of Alkyl Radicals

Only two rate constants and A factors have been determined for the combination of radicals in the gas phase. They relate to the combination of methyl and the combination of ethyl radicals. From these results the *minimum* values of the A factors for the symmetrical decomposition of ethane and n-butane may be calculated with certainty and are given in the table.

	A	
	This work	Original authors
Decomposition of ethane	1×10^{17}	2×10^{15}
Decomposition of butane	1.5×10^{17}	6×10^{15}

The values given by the original authors are rather low because Ivin and Steacie[5] seem to have chosen an improbably low value for the entropy of the ethyl radical, and Gomer and Kistiakowsky[4] used the equilibrium constant calculated by Glasstone, Laidler, and Eyring,[8] who made no allowance for the electron degeneracy of the free radicals and so obtained an answer which is probably too small.

3. THE DECOMPOSITION OF FREE RADICALS

Bywater and Steacie[9] have studied the decomposition of the free radicals produced by the mercury photosensitization of ethane, propane, and 2-methyl propane and determined the activation energies of the decompositions on the assumption that the dimerization of the free radicals requires no activation energy. In each of these cases it is possible to estimate from the experimental data the number of alkyl radicals decomposing and the number dimerizing, the error being of the order of 20–30 percent. If these two quantities are known, then it is possible[10] to calculate the relative values of the rate constant k_{4f} and k_5 for the reactions (4) and (5) by using the

$$RA\underset{k_{4b}}{\overset{k_{4f}}{\rightleftarrows}}R+A \qquad (4)$$

$$2RA\xrightarrow{k_5}(RA)_2, \qquad (5)$$

[8] Glasstone, Laidler, and Eyring, *Theory of Rate Processes* (McGraw-Hill Book Company, Inc., New York, 1941), p. 263.
[9] S. Bywater and E. W. R. Steacie, J. Chem. Phys. **19**, 172, 319, 326 (1951).
[10] A. F. Trotman-Dickenson, J. Chem. Phys. **19**, 261 (1951).

formula $dR/dt/d(RA)_2/dt=k_{4f}/k_5^{\frac{1}{2}}$. Since the activation energy of reaction ($4f$) is known a maximum value of A_{4f} may be obtained by supposing reaction (5) to take place on every collision. The annexed table given the values found for A_{4f}.

Reaction	A_f	A_b	
$C_2H_5 \rightarrow C_2H_4+H$	2×10^{14}	2×10^{13}	(6)
$C_3H_7 \rightarrow C_2H_4+CH_3$	3×10^{9}	6×10^{6}	(7)
$C_4H_9 \rightarrow C_3H_6+CH_3$	1×10^{9}	1×10^{5}	(8)

By the methods outlined above the entropy changes in these reactions may be found, and hence A_{4b} calculated; the values found are given in the table. Full experimental data to check these calculations are not yet available, but two pieces of work provide some comparison.

Melville and Robb[11] have found that the collision yield for the reaction of hydrogen with ethylene at room temperature is 10^{-3}, this would agree with the above results if the activation energy for the reaction is 3 kcal. From Bywater and Steacie's activation energy for the decomposition, and Stevenson's[12] bond strengths the activation energy for the addition may be calculated as 2 kcals.

Trotman-Dickenson and Steacie[13] found that at 180°C the addition of a methyl radical to ethylene took place at the same speed to within a factor of two or three as the abstraction of a hydrogen atom. The rate constant for the abstraction reaction is 3×10^6 g mole^{-1} cc sec^{-1}. Our slight knowledge of bond strengths and activation energies for the decomposition of radicals indicates that reaction (7_b) will have very small or zero activation energy. If the reaction requires zero activation energy then $A_{7b}=3\times10^6$ in remarkable agreement with the value calculated above.

The frequency factors for the decomposition of the propyl and butyl radicals differ markedly from the value of 10^{13} which has been regarded as a norm. Two other cases of such low frequency factors in similar reactions are known, as has been pointed out by Trotman-Dickenson[10]; they are the decomposition of the radicals of dimethyl ether and of methyl alcohol,

$$CH_2OCH_3 \rightarrow CH_3CH_2O$$

$$CH_2OH \rightarrow CH_2O+H,$$

where the maximum possible values for the A factors were found to be 1.5×10^{10} and 1.7×10^{10}, respectively. In all of these cases the errors are probably quite large and amount to about one power of ten. Consequently although the fact that the frequencies factors are very low is well established, little reliance can be placed on the exact numerical values.

The decomposition of ethane and butane discussed above are examples of the opposite phenomenon for they have very high frequency factors. The experimental data seem very reliable and a minimum value for the frequency factor has been deliberately calculated. A further somewhat similar example of a high frequency factor has recently been confirmed by Carrington and Davidson,[14] who find that the reaction

$$N_2O_4 \rightarrow 2NO_2$$

has a frequency factor of about 10^{16} if the reverse reaction has no energy of activation.

These two classes of deviation of the A factor of a reaction from the accepted value of $10^{13\pm1}$ raise considerable problems. It may be that special explanations apply to these cases, for example, the decompositions of radicals in which one fragment has to rearrange to form an unsaturated compound are slightly reminiscent of the cases of *cis-trans* isomerism in which low frequency factors were found. Harman and Eyring[15] suggested that this effect might be the cause of the A factors which are found for the propagation reactions in polymerizations, those reactions are the reverse of the decompositions. However, Baxendale and Evans[16] have shown that in this case the low A factors are understandable in terms of the ordinary theory of absolute reaction rates. They show in the same manner that for reactions in solution the symmetrical decomposition of a polymer molecule should have an A factor of approximately 10^{13}, if the combination (or disproportionation) of two polymer radicals has an A factor of 10^{11}. This is in marked contrast to the behavior of ethane and butane discussed above. The reason for this is that the large polymer molecules and radicals cannot rotate freely but only librate or vibrate. Since these forms of motion are little affected by the size of the species there is no effect to correspond to the loss of rotational entropy in the case of the combination of two small radicals.

The author wishes to thank Professor M. G. Evans and Dr. M. Szwarc for numerous discussions.

[11] H. W. Melville and J. C. Robb, Proc. Roy. Soc. (London) **A202**, 181 (1950).
[12] D. P. Stevenson, Disc. Faraday Soc. **10**, 35 (1951).
[13] A. F. Trotman-Dickenson and E. W. R. Steacie, J. Chem. Phys. **19**, 169 (1951).
[14] T. Carrington and N. R. Davidson, J. Chem. Phys. **19**, 1313 (1951).
[15] R. A. Harman and H. Eyring, J. Chem. Phys. **10**, 557 (1942).
[16] J. H. Baxendale and M. G. Evans, Trans. Faraday Soc. **43**, 210 (1947).

The Configurations of Rotational Isomers and Their Normal Frequencies*

SAN-ICHIRO MIZUSHIMA, TAKEHIKO SHIMANOUCHI, ICHIRO NAKAGAWA, AND AKIHISA MIYAKE
Chemical Laboratory, Faculty of Science, Tokyo University, Hongo, Tokyo

(Received August 20, 1952)

Normal frequencies of molecular configurations of different azimuthal angles of internal rotation have been calculated for various molecules showing rotational isomerism. It has been shown that one can tell fairly accurately the value of azimuthal angle by comparing the observed frequencies (especially the skeletal deformation frequencies) with those calculated for different configurations. The sum rule for the rotational isomers similar to that for isotopic molecules has been derived and has been shown to be very useful in assigning the observed frequencies. The product rule for rotational isomers derived in our previous paper has also been applied to this problem and has been shown to be useful in determining the azimuthal angles of rotational isomers.

DURING the past years we have reported structural investigations of molecules with axes of internal rotation, e.g., 1,2-dihalogenoethanes. The results of our measurements of the Raman effect, infrared absorption, dipole moment, and electron diffraction has shown that such a kind of molecule exists in the *trans*- and the *gauche*-forms in the gaseous and the liquid states and of these only the *trans*-form persists in the solid state.[1] This is in good agreement with the experimental results obtained by other investigators, including Pitzer, Gwinn, Glockler, Bernstein, Sheppard, Rank, and Cleveland.

The determination of the *trans*-form or the more stable form of 1,2-dihalogenoethane was made as early as 1934, but it took several more years before we could determine the *gauche*-form or the less stable form.[2] The reason is that the determination of the *gauche*-form cannot be carried out so straightforwardly as in the case of the *trans*-form. So far, the *gauche*-form has been determined by observing the spectral change with change of state, electron diffraction patterns, dipole moment values, etc., but the use of the frequency values of the Raman lines or the infrared absorption peaks have not yet been made, although the existence of rotational isomers was first proved from the observation of vibrational spectra. In the present paper, we shall report how far we can discuss the problem of rotational isomerism by the use of vibrational frequencies of different configurations.

SECULAR EQUATION

The potential function of a molecule of the type

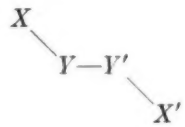

will be expressed in the following form, if we assume the Urey-Bradley field and neglect the interaction between X and X' atoms which are far apart from each other:

$$V=L_0R_0(\Delta R)+\tfrac{1}{2}K_0(\Delta R)^2+L_1r_0(\Delta r)+\tfrac{1}{2}K_1(\Delta r)^2 +L_1'r_0'(\Delta r')+\tfrac{1}{2}K_1'(\Delta r')^2+MR_0r_0(\Delta\alpha) +\tfrac{1}{2}HR_0r_0(\Delta\alpha)^2+M'R_0r_0'(\Delta\alpha')+\tfrac{1}{2}H'R_0r_0'(\Delta\alpha')^2 +Nq_0(\Delta q)+\tfrac{1}{2}F(\Delta q)^2+N'q_0'(\Delta q')+\tfrac{1}{2}F'(\Delta q')^2,$$

where R, r, r', q, and q' are the interatomic distances, YY', XY, $X'Y'$, $Y'X$ and YX'; α and α' are the bond angles $\angle XYY'$ and $\angle X'Y'Y$; and R_0, r_0, r_0', q_0, q_0', α_0, and α_0' are their equilibrium values. Further, K_0, K_1, K_1', H, H', F, F', L_0, L_1, L_1', M, M', N, and N' are force constants, and of these L_0, L_1, L_1', M, and M' can be expressed in terms of N and N'.

If we set up the secular equation

$$|\mathbf{GF}-\mathbf{E}\lambda|=0 \qquad (1)$$

according to Wilson's method,[3] the kinetic energy

TABLE I. Sums of squared frequencies of rotational isomers.

Molecule	$\Sigma\nu_i^2$(*trans*)	$\Sigma\nu_i^2$(*gauche*)	Difference (%)
ClH_2C-CH_2Cl[a]	4.964×10^7	4.955×10^7	0.2
BrH_2C-CH_2Br[b]	4.896×10^7	$\left\{\begin{matrix}4.851\times10^7\\ \sim4.892\times10^7\end{matrix}\right\}$	1.0~0.1
BrD_2C-CD_2Br[c]	2.807×10^7	2.810×10^7	0.1
$ClHC=CHCl$[d]	2.740×10^7	2.732×10^7(*cis*)	0.3
$ClDC=CDCl$[d]	1.710×10^7	1.706×10^7(*cis*)	0.2
ClH_2C-CH_2Cl(skeletal)[e]	2.32×10^6	2.19×10^6	5.6
BrH_2C-CH_2Br(skeletal)[f]	1.96×10^6	1.86×10^6	5.1
ClH_2C-CH_2Br(skeletal)[g]	2.14×10^6	2.02×10^6	5.6
ClH_2C-CH_2I(skeletal)[h]	2.01×10^6	2.11×10^6	5.0
$ClH_2C-COCl$(skeletal)[i]	4.74×10^6	4.71×10^6	0.6
$BrH_2C-COCl$(skeletal)[i]	4.53×10^6	4.48×10^6	1.1
$BrH_2C-COBr$(skeletal)[i]	4.39×10^6	4.40×10^6	0.2

[a] The frequencies (cm^{-1}) used in this calculation are as follows: *trans*-form: A_g(2956, 1442, 1302, 1054, 753, 301), A_u(3002, 1124, 766), B_g(3002, 1263, 991), B_u(2956, 1451, 1229, 708, 223); *gauche*-form: A (2956), 1428, 1309, 1032, 653, 264, 3002, 1143, 881, 125), B (3002, 1207, 943, 2956, 1428, 1280, 676, 411).

[b] *trans*-form: A_g(2972, 1438, 1255, 1053, 659, 190), A_u(3018, 1087, 753), B_g(3018, 1169, 732), B_u(2974, 1441, 1186, 589, 170); *gauche*-form: A (2953, 1419, 1276, 1019, 551, 231, 3005, 1104, 898), B (3005, 1104 or 1278, 836, 2953, 1419, 1243, 583, 355).

[c] *trans*-form: (2187, 1155, 992, 907, 607, 188, 2290, 779, 564, 2290, 919, 712, 2174, 1061, 900, 564, 170); *gauche*-form: (2174, 1141, 1014, 947, 518, 230, 2290, 791, 712, 2290, 791, 686, 2174, 1051, 975, 526, 318).

[d] Data of H. J. Bernstein and D. A. Ramsey, J. Chem. Phys. **17**, 556 (1949).

[e] *trans*: (1052, 754, 300, 709, 223); *gauche*: (1031, 654, 265, 677, 411).

[f] *trans*: (1053, 660, 190, 589, 170); *gauche*: (1019, 551, 231, 583, 355).

[g] *trans*: (1052, 726, 251, 630, 214); *gauche*: (1023, 665, 385, 568, 251).

[h] *trans*: (1046, 707, 232, 576, 186); *gauche*: (1107, 660, 368, 511, 232).

[i] Nakagawa, Ichishima, Kuratani, Miyazawa, Shimanouchi, and Mizushima, J. Chem. Phys. **20**, 1720 (1952).

* Presented at the Atlantic City Meeting of the American Chemical Society, September, 1952.

[1] As to the previous works see the references given in: Mizushima, Morino, and Shimanouchi, J. Phys. Chem. **56**, 324 (1952); and Mizushima, Morino, Watanabe, Shimanouchi, and Yamaguchi, J. Chem. Phys. **17**, 591 (1949).

[2] Mizushima, Morino, and Higashi, Sci. Papers Inst. Phys. Chem. Research Tokyo, **25**, 159; **26**, 1 (1934). See also reference 9.

[3] E. B. Wilson, J. Chem. Phys. **7**, 1047 (1939); **9**, 76 (1941).

matrix **G** and the potential energy matrix **F** for the normal vibrations of this molecule will be expressed as

$$\mathbf{G}=\begin{vmatrix} \mu_0+\mu_0' & & & & \\ \mu_0\cos\alpha_0 & \mu_0+\mu_1 & & & \\ \mu_0'\cos\alpha_0' & 0 & \mu_0'+\mu_1' & & \\ -\rho_0\mu_0\sin\alpha_0 & -\rho_1\mu_0\sin\alpha_0 & \rho_1\mu_0'\sin\alpha_0'\cos\theta & \rho_1^2\mu_0'+\rho_0^2\mu_1+\rho_{10}^2\mu_0 & \\ -\rho_0'\mu_0'\sin\alpha_0' & \rho_1'\mu_0\sin\alpha_0\cos\theta & -\rho_1'\mu_0'\sin\alpha_0' & -(\rho_s\mu_0+\rho_s'\mu_0')\cos\theta & \rho_1'^2\mu_0+\rho_0'^2\mu_1'+\rho_{10}'^2\mu_0' \end{vmatrix},$$

$$\mathbf{F}=\begin{vmatrix} K_0+a_0F+a_0'F' & & & & \\ cF & K_1+a_1F & & & \\ c'F' & 0 & K_1'+a_1'F' & & \\ \rho_1d_0F & \rho_0d_1F & 0 & H+bF & \\ \rho_1'd_0'F' & 0 & \rho_0'd_1'F' & 0 & H'+b'F' \end{vmatrix},$$

where μ_0, μ_0', μ_1, and μ_1' are the reciprocals of masses of the atoms, Y, Y', X, and X', respectively, and θ the azimuthal angle of internal rotation. Further,

$$\rho_0=(R_0/r_0)^{\frac{1}{2}} \qquad c=s_0s_1-t_0t_1(N/F)$$
$$\rho_0'=(R_0/r_0')^{\frac{1}{2}} \qquad c'=s_0's_1'-t_0t_1'(N'/F')$$
$$\rho_1=(r_0/R_0)^{\frac{1}{2}} \qquad d_0=t_1s_0+t_0s_1(N/F)$$
$$\rho_1'=(r_0'/R_0)^{\frac{1}{2}} \qquad d_0'=t_1's_0'+t_0's_1'(N'/F')$$
$$\rho_{10}^2=\rho_1^2+\rho_0^2-2\cos\alpha_0 \qquad d_1=t_0s_1+t_1s_0(N/F)$$
$$\rho_{10}'^2=\rho_1'^2+\rho_0'^2-2\cos\alpha_0' \qquad d_1'=t_0's_1'+t_1's_0'(N'/F')$$
$$\rho_s=\rho_1'(\rho_1-\rho_0\cos\alpha_0) \qquad s_0=(\rho_0-\rho_1\cos\alpha_0)/\rho_{10}$$
$$\rho_s'=\rho_1(\rho_1'-\rho_0'\cos\alpha_0') \qquad s_0'=(\rho_0'-\rho_1'\cos\alpha_0')/\rho_{10}'$$
$$a_0=s_0^2+t_0^2(N/F) \qquad s_1=(\rho_1-\rho_0\cos\alpha_0)/\rho_{10}$$
$$a_0'=s_0'^2+t_0'^2(N'/F') \qquad s_1'=(\rho_1'-\rho_0'\cos\alpha_0')/\rho_{10}'$$
$$a_1=s_1^2+t_1^2(N/F) \qquad t_0=\rho_1\sin\alpha_0/\rho_{10}$$
$$a_1'=s_1'^2+t_1'^2(N'/F') \qquad t_0'=\rho_1'\sin\alpha_0'/\rho_{10}'$$
$$b=t_0t_1-s_0s_1(N/F) \qquad t_1=\rho_0\sin\alpha_0/\rho_{10}$$
$$b'=t_0't_1'-s_0's_1'(N'/F') \qquad t_1'=\rho_0'\sin\alpha_0'/\rho_{10}'.$$

In the case of the symmetrical molecule

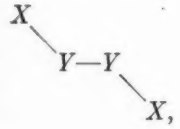

G and **F** can be factored into $\mathbf{G}_a$, $\mathbf{G}_b$, $\mathbf{F}_a$, and $\mathbf{F}_b$ as follows:

$$\mathbf{G}_a=\begin{vmatrix} 2\mu_0 & & \\ \sqrt{2}\mu_0\cos\alpha_0 & \mu_1+\mu_0 & \\ -\sqrt{2}\rho_0\mu_0\sin\alpha_0 & -\rho_1\mu_0\sin\alpha_0(1-\cos\theta) & \rho_0^2(\mu_1+\mu_0)+2\mu_0(\rho_1^2-\cos\alpha_0)(1-\cos\theta) \end{vmatrix},$$

$$\mathbf{F}_a=\begin{vmatrix} K_0+2a_0F & & \\ \sqrt{2}cF & K_1+a_1F & \\ \sqrt{2}\rho_1d_0F & \rho_0d_1F & H+bF \end{vmatrix},$$

$$\mathbf{G}_b=\begin{vmatrix} \mu_1+\mu_0 & \\ -\rho_1\mu_0\sin\alpha_0(1+\cos\theta) & \rho_0^2(\mu_1+\mu_0)+2\mu_0(\rho_1^2-\cos\alpha_0)(1+\cos\theta) \end{vmatrix},$$

$$\mathbf{F}_b=\begin{vmatrix} K_1+a_1F & \\ \rho_0d_1F & H+bF \end{vmatrix}.$$

TABLE II. Force constants (in 10^5 dynes/cm) and calculated and observed frequencies (in cm^{-1}).

K(CH₂−CH₃) =4.0	H(CH₃−CH₂−CH₃) =0.20	F(CH₃...CH₃) =0.33
K(CH₂−OH) =4.6	H(CH₃−CH₂−OH) =0.20	F(CH₂...OH) =0.65
K(CH₂−Cl) =2.9	H(CH₃−CH₂−Cl) =0.17	F(CH₃...Cl) =0.49
K(CH₂−Br) =2.4	H(CH₃−CH₂−Br) =0.15	F(CH₃...Br) =0.40
K(CH₂−CH₂) =3.7	H(Cl−CH₂−Cl) =0.13	F(Cl...Cl) =0.64
	H(Br−CH₂−Br) =0.10	F(Br...Br) =0.47

N/F = N'/F' = −0.1

	Obs	Calc		Obs	Calc
CH₃−CH₂−CH₃	1155}[a]	919	CH₃−CH₂−OH	434[b]	427
	867}			882}	{947
	372	380		1050}	{1070
	1053}	1044		1096}	
	923}				
Cl−CH₂−Cl	700[c]	661	CH₃−CH₂−Cl	1030}[d]	995
	283	289		968}	
	736	773		656	708
				335	342
Br−CH₂−Br	576[c]	541	CH₃−CH₂−Br	1027}[d]	991
	174	174		960}	
	637	658		560	595
				292	293
Cl−H₂C−CH₂−Cl (*trans*)	1052[e]	1008	Cl−H₂C−CH₂−Cl (*gauche*)	1031[e]	1006
	754	754		654	674
	300	287		265	252
	709	741		677	738
	223	226		411	421
Br−H₂C−CH₂−Br (*trans*)	1053[e]	994	Br−H₂C−CH₂−Br (*gauche*)	1019[e]	994
	660	662		551	564
	190	182		231	209
	589	620		583	634
	169	181		355	353
Cl−H₂C−CH₂−OH (*trans*)	1055[f]	1080	Cl−H₂C−CH₂−OH (*gauche*)	1035[f]	1069
	942	965		942	958
	751	755		662	711
	394	361		477	471
	259	265		294	279

[a] H. L. McMurry and V. Thornton, J. Chem. Phys. **18**, 1515 (1950).
[b] Mizushima, Morino, Kitasato, and Nakamura, Proc. Imp. Acad. Tokyo **16**, 549 (1940).
[c] G. Herzberg, *Infrared and Raman Spectra of Polyatomic Molecules* (D. Van Nostrand Company, Inc., New York, 1945).
[d] N. Sheppard, J. Chem. Phys. **17**, 79 (1949).
[e] Mizushima, Morino, and Shimanouchi, Sci. Paper Inst. Phys. Chem. Research Tokyo **40**, 87 (1942); see also J. Chem. Phys. **17**, 591 (1949).
[f] Mizushima, Shimanouchi, Miyazawa, Abe, and Yasumi, J. Chem. Phys. **19**, 1477 (1951).

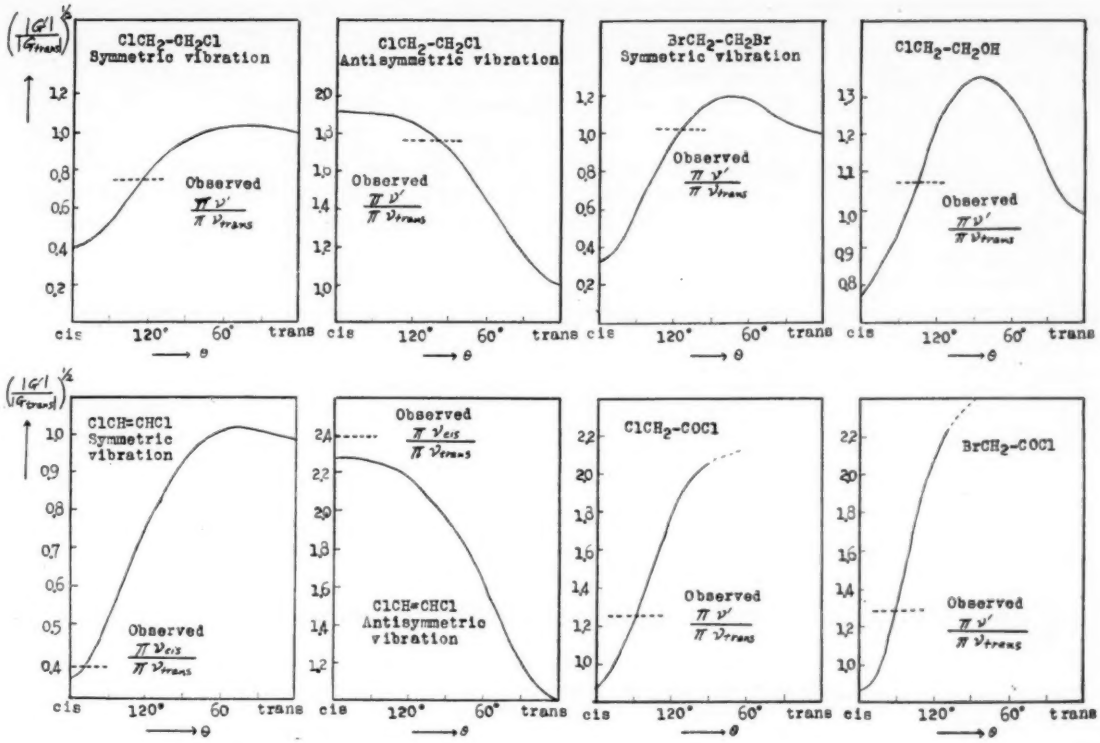

FIG. 1. The calculated values of $|\mathbf{G}'|/|\mathbf{G}(trans)|$ and the observed values of $\Pi\nu'/\Pi\nu_{trans}$.

SUM RULE

Let the solutions of the secular Eq. (1) be $\lambda_1, \lambda_2, \cdots, \lambda_n$. Then we have[3]

$$\sum_{i=1}^{n} \lambda_i = \sum_{k,l=1}^{n} G_{kl}F_{kl}. \tag{2}$$

If we neglect the interaction between the X and X' atoms in the potential energy expression, all the elements F_{kl} corresponding to G_{kl} containing the azimuthal angle θ, vanish and the right-hand side of Eq. (2) becomes independent of the azimuthal angle θ of internal rotation. We have, therefore,

$$\sum_{i=1}^{n} \lambda_i = \text{constant}.$$

Since $\lambda_i = 4\pi\nu_i^2$, this is rewritten as

$$\sum_{i=1}^{n} \nu_i^2 = \text{constant}. \tag{3}$$

This can be called as the sum rule for rotational isomers similarly as in the case of the sum rule for isotopic molecules.[4] In order to see if this relation actually holds, we have made numerical calculations for the rotational isomers of 1,2-dichloroethylene, 1,2-dihalogenoethanes, and monohalogenoacetylhalides. As shown in Table I, the sum of the squared frequencies remains the same for both kinds of the rotational isomers. It is worthy of note that we can apply the sum rule for such a molecule as 1,2-dichloroethylene in which the interaction between the two chlorine atoms may be considered to be much larger than that in 1,2-dichloroethane. For the latter substance this rule is applied quite satisfactorily as can be seen from Table I.

The difference in the sum of the squared skeletal frequencies between the *trans*- and the *gauche*-forms amounts to about 5 percent as shown in the latter half of the table. This difference is reduced to about 0.5 percent, if we take into account the hydrogen vibrations. Thus it is evident that this rule lays down a reliable criterion to test the correctness of the frequency assignment.

PRODUCT RULE

The product of normal frequencies of a molecular configuration can be expressed as[3]

$$2\pi \prod_{i=1}^{n} \nu_i = (|\mathbf{G}||\mathbf{F}|)^{\frac{1}{2}}. \tag{4}$$

If, therefore, we neglect the interaction between X and X' atoms in the potential energy expression, the F matrix becomes common to both of the rotational isomers, and we have for the frequencies ν_i and ν_i' of the two rotational isomers the following relation:

$$\prod_{i=1}^{n} \nu_i / \prod_{i=1}^{n} \nu_i' = (|\mathbf{G}|/|\mathbf{G}'|)^{\frac{1}{2}}. \tag{5}$$

[4] J. C. Decius and E. B. Wilson, J. Chem. Phys. **19**, 1409 (1951).

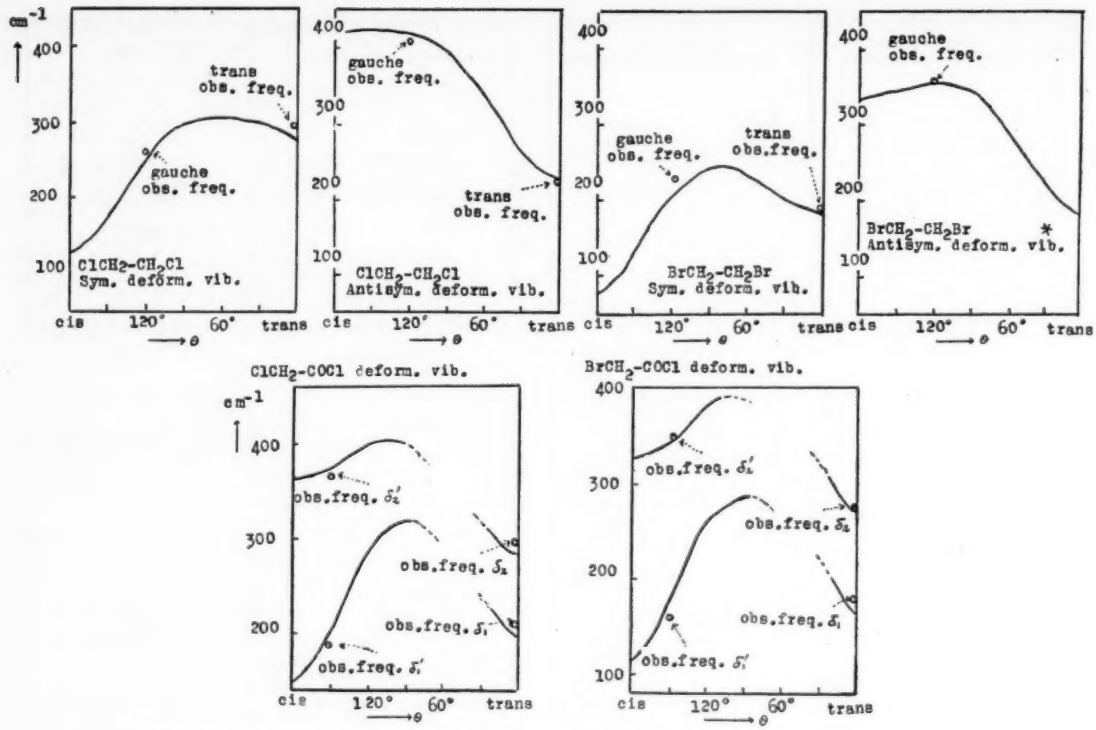

FIG. 2. Dependence of skeletal deformation frequencies of azimuthal angle θ. (The antisymmetric vibration of the *trans*-form of $BrCH_2-CH_2Br$ has not been observed.)

This product rule for rotational isomers was first derived by us[5] in 1942 and later on reported by Bernstein independently.[6] In Fig. 1 are shown the calculated values of the right-hand side of Eq. (5) or the square roots of ratios of G's of different azimuthal angles to that of the *trans* at which the origin of the azimuthal angle θ has been taken. As can be seen from the figure the ratios of the products of observed frequencies of 1,2-dichloroethane, 1,2-dibromoethane, 1,2-dichloroethylene, ethylene chlorhydrin, chloracetyl chloride, and bromacetyl chloride agree very well with the theoretical values at the azimuthal angles corresponding to the other stable molecular configurations so far determined by the various methods.[1]

CALCULATION OF SKELETAL FREQUENCIES

One of us calculated normal frequencies of many simple molecules by use of the Urey-Bradley field and found good agreement with the observed values.[7] For the more complex molecules, it is often impossible to take into account motions of all the atoms contained in the molecules, and we can only calculate the normal motions of skeletons, neglecting the individual motions of hydrogen atoms. Even in this case, the frequencies can be calculated quite satisfactorily if we introduce suitable corrections for the values of force constants. In Table II are shown the force constants corresponding to such skeletal vibrations, and the frequencies calculated therefrom are compared with those observed in the Raman effect and infrared absorption.

Of the normal frequencies of rotational isomers, skeletal deformation frequencies depend more conspicuously upon the azimuthal angle of internal rotation, and, therefore, these frequencies can be used for the determination of molecular configuration of rotation isomers more profitably. In Fig. 2 are shown the calculated frequencies for the skeletons of 1,2-dichloroethane, 1,2-dibromoethane, chloracetyl chloride, and bromacetyl chloride at various azimuthal angles. From the comparison of these theoretical values with those of the observed skeletal deformation frequencies, we can confirm our previous conclusion that the *gauche*-form is the second stable form for 1,2-dichloroethane and 1,2-dibromoethane. Further, we see that in the case of chloracetyl chloride and bromacetyl chloride the second stable configuration has an azimuthal angle larger than that of the *gauche*-form of 1,2-dihalogenoethane.

As described above, we can use frequency values for the determination of the configurations of rotational isomers, if we can assign the frequencies appropriately. For the assignment we can make use of the spectral changes on solidification, on vaporization, on solution, and with the change of temperature.[1] For example, the marked simplification of the spectrum on solidification which was first observed by us in 1936,[8] has often been

[5] Mizushima, Morino, and Shimanouchi, Sci. Papers Inst. Phys. Chem. Research Tokyo **40**, 87 (1942); T. Shimanouchi, Bull. Inst. Phys. Chem. Research Tokyo **23**, 371 (1944).

[6] H. J. Bernstein, J. Chem. Phys. **17**, 256 (1949).

[7] T. Shimanouchi, J. Chem. Phys. **17**, 245, 734, 848 (1949).

[8] Mizushima, Morino, and Noziri, Nature **137**, 945 (1936).

used for this purpose since then. The sum rule can be used for the confirmation of the correctness of the assignment, as stated above.

We have also seen that the product rule for rotational isomers can be used for the determination of the molecular configuration. The determination of the azimuthal angle becomes more accurate if we know the configuration of one of the rotational isomers exactly. For example, in 1,2-dihalogenoethanes we could determine the *trans*-configuration very accurately from the Raman measurement in the solid state,[9] and accordingly, the azimuthal angle of the *gauche*-configuration could be determined fairly accurately from the vibrational frequencies assigned to this configuration through the application of the product rule. Evidently, in order that the product rule may be applied to such molecules, the force constants corresponding to the interactions between the movable groups must be small as compared with K, H, F, etc., but the potential function need not be of the Urey-Bradley type.

The error due to neglect of the coupling between the torsional motion and the deformation frequencies or that between the skeletal frequencies is estimated to be less than 10 percent. The accuracy in the determination of the azimuthal angle would thus be estimated as about $\pm 10°$.

[9] S. Mizushima and Y. Morino, Proc. Indian Acad. Sci. **8**, 315 (1938) (The Raman Jubilee Volume).

THE JOURNAL OF CHEMICAL PHYSICS VOLUME 21, NUMBER 2 FEBRUARY, 1953

The Infrared Spectra of Oriented Rhombic Sulfur Crystals with Polarized Radiation

GORDON M. BARROW
Department of Chemistry, Northwestern University, Evanston, Illinois
(Received June 5, 1952)

The infrared spectra, in the rock salt region, of oriented sections of single rhombic sulfur crystal have been obtained. The spectra of sections perpendicular to the c axis of the crystal, the 001 type planes, have been compared, under ordinary radiation with those of sections parallel to the c axis, 110 type planes. Most bands in the region investigated, 700 to 1500 cm^{-1}, show differences in intensity in the two spectra. With a 110 section and radiation polarized at various angles, similar changes in intensity were observed. Both experiments lead to similar conclusions regarding the direction of the oscillating dipole in the vibrations giving rise to the observed bands. Assignments of the infrared active species (B_2 or E_1) in these bands are given but no attempt is made to explain them in terms of the fundamental vibrations.

THERE have been several investigations of the infrared[1,2] and Raman[3,4] spectra of the S_8 sulfur molecule. The assignment of the observed bands to fundamental vibrations and to overtones and combinations of these is still somewhat unsatisfactory.

Sulfur can readily be obtained in fairly large crystals which are not unduly difficult to handle. Furthermore, the crystal structure has been completely worked out.[5] It, therefore, seemed likely that a study of the variation of the band intensities of different crystal planes, with and without an infrared polarizer, would provide additional useful information. Barnes[1] has already pointed out in his investigation of the spectrum from 500 cm^{-1} to 80 cm^{-1} that the spectra of crystal sections of different but undetermined orientations showed small but real differences.

Since the previous investigations have shown that all the fundamental vibrations occur at frequencies below about 500 cm^{-1}, the present work with a rocksalt prism instrument is concerned only with measurements on combination and overtone bands.

In the rhombic crystal the crown-like sulfur molecules are arranged in layers, on edge, perpendicular to the c axis of the crystal. A view of the crystal along the c axis, therefore, shows only the edges of the crowns, while a view perpendicular to the c axis shows, effectively, some of the molecules in an edge view and some full faced. The changes in the intensities of the infrared bands in spectra taken along these directions, i.e., with radiation incident on the 001 and 110 type planes, are reported here.

EXPERIMENTAL

Crystals

The sulfur crystals were grown by the slow evaporation at room temperature of a carbon disulfide solution of sublimed sulfur. The crystals so obtained had the usual well developed 111 type faces and were up to several cubic centimeters in size. The orientations of the crystals were determined entirely from the angles of the developed faces. Sections were taken through clear, and presumed perfect, parts of the crystals parallel to the 001 and 110 planes. The 110 plane sections were also ob-

[1] R. B. Barnes, Phys. Rev. **39**, 562 (1932).
[2] H. J. Bernstein and J. Powling, J. Chem. Phys. **18**, 1018 (1950); and erratum **19**, 139 (1951).
[3] C. S. Venkateswaran, Proc. Indian Acad. Sci. **4A**, 345 (1936).
[4] H. Gerding and R. Westrick, Rec. trav. chim. **62**, 68 (1943).
[5] B. E. Warren and J. T. Burwell, J. Chem. Phys. **3**, 6 (1935).

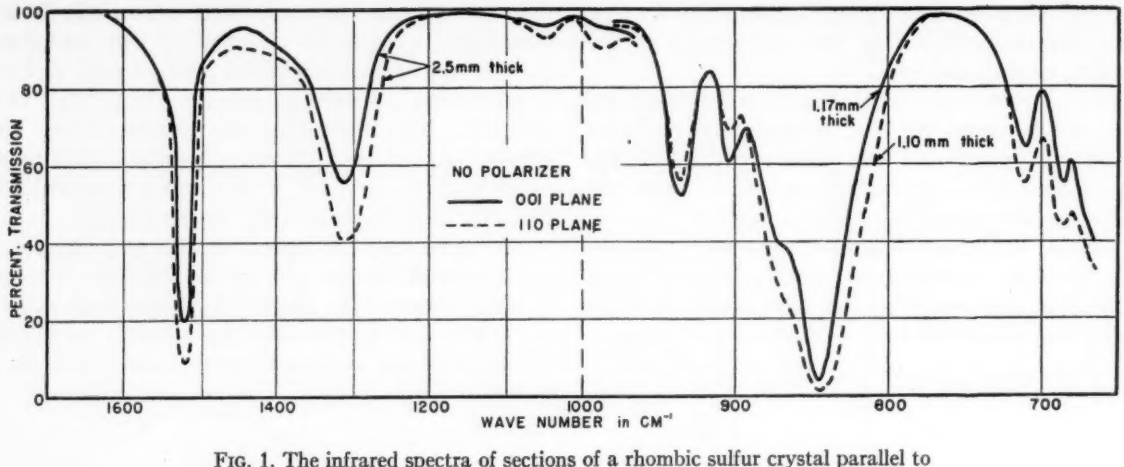

FIG. 1. The infrared spectra of sections of a rhombic sulfur crystal parallel to the 001 and 110 planes taken with ordinary radiation.

tained by polishing down, at an angle of 18°, sections cut parallel to the developed 111 faces. Sections taken from different crystals gave entirely consistent results.

The only satisfactory method found for cutting these rather brittle crystals was by means of a carborundum wheel glass saw. The cuts so obtained were rough but could be readily polished with rouge and water on a polishing cloth. The oriented sections so obtained were usually 1 to 2 cm by about 0.5 cm, with thicknesses from about 1 to 3 mm. In addition, a section parallel to the 111 face was obtained large enough so that it could be rotated in the light path. The changes in band intensities with orientation of this section, the polarizer remaining fixed, paralleled those obtained with fixed 110 type sections, with the polarizer rotated.

Spectra

The spectra were measured with a Beckman IR–2T instrument using a rocksalt monochromator. The crystals masked with a piece of aluminum foil were mounted immediately in front of the entrance slit in what is normally the gas cell compartment.

The polarizer consisted of eight sheets of 0.25-mm silver chloride inclined at an angle of 25° to the incident radiation. The sheets were slotted in a $4\frac{1}{4}$-in. Bakelite box (inside dimensions 1 in.×1 in.) which was centered in a 2 in. diameter brass cylinder. The unit was placed, on supports on which it could be rotated, in the gas cell compartment of the instrument.

The transmission varied considerably in regions free from absorption bands because of changes in the reflectivity of the sulfur crystal and losses in the instrument due to polarization and deviation of the light beam. In all cases, therefore, a smooth but somewhat arbitrary 100-percent transmission curve was drawn based on the regions of the spectra free from absorption bands.

Spectra of two types were obtained. First, spectra were taken of sections parallel to the 001 and 110 planes with ordinary (not polarized) radiation. Figure 1 gives two such spectra for sections of similar thickness. Second, spectra of the 110 type sections were obtained with the incident radiation polarized at various angles. Spectra with polarizer angles of 0° and 90° are shown in Fig. 2.

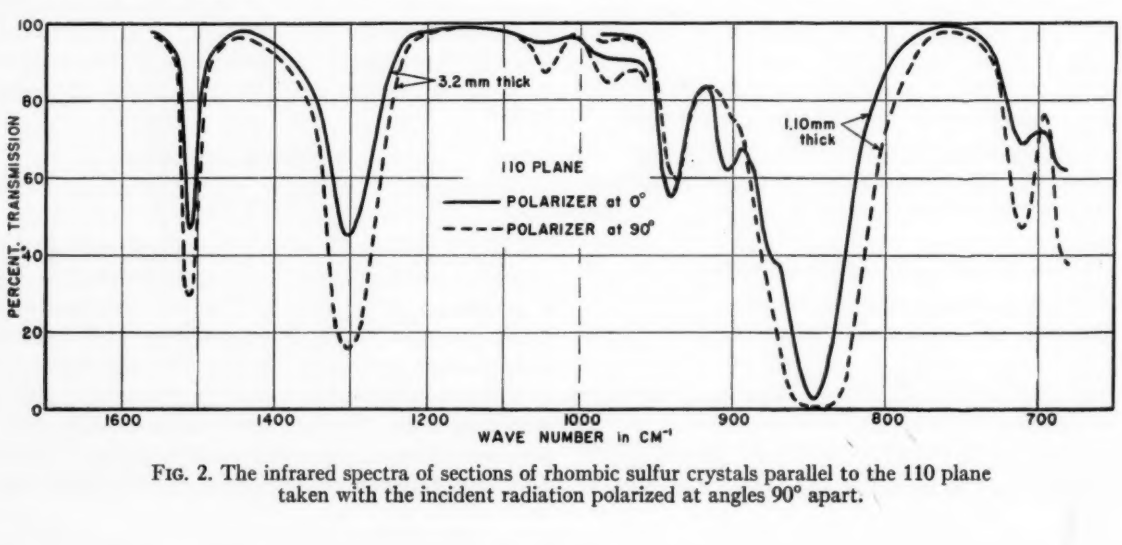

FIG. 2. The infrared spectra of sections of rhombic sulfur crystals parallel to the 110 plane taken with the incident radiation polarized at angles 90° apart.

DISCUSSION

The crown-like eight membered rings of the sulfur molecule have been shown[5] to be arranged on edge in layers perpendicular to the c axis of the crystal. The crowns of these layers are successively parallel and perpendicular to the 110 type planes. Figure 3 shows schematically the arrangement of the molecules viewed in the direction of the incident light in the sections studied. These sections were placed, as shown, before the vertical entrance slit of the instrument. The relative direction of the electric vector of the polarized incident radiation is also given in Fig. 3.

A vibration of the S_8 molecule[6] will be infrared active if its representation contains either the B_2 or E_1 irreducible representation.[7] The oscillating dipole moment for vibrations of these species are, respectively, parallel and perpendicular to the fourfold symmetry axis of the molecule. The representation of an overtone or a combination can also contain both the B_2 and E_1 representations with the result that the dipole moment change of the vibration will have components both parallel and perpendicular to the molecular axis.

The spectra of the 001 and 110 type sections, with the incident radiation not polarized, will be considered first. In the 001 section every molecule is oriented such that an oscillating dipole either parallel or perpendicular to the molecular axis can interact with the incident radiation. In the 110 section, however, half the molecules (those shown full face in Fig. 3) are so oriented that a component of the dipole change parallel to the symmetry axis of the molecule cannot interact with the incident radiation. The perpendicular component of the oscillating dipole of these molecules can, on the other hand, react with both components of the electric vector of the incident light. A vibration in which the dipole change is parallel to the molecular axis should then be about twice as intense in the spectra of the 001 plane as in that of the 110 plane. One which is active due to a perpendicular dipole change should be about three halves as intense in the 110 plane spectra as in those of the 001 plane.

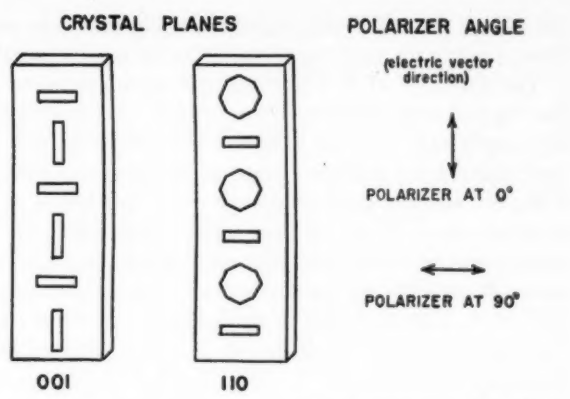

FIG. 3. Schematic representation of the arrangement of the S_8 molecules in the 001 and arrangement of the S_8 molecules in the 001 and 110 type sections investigated and the relative directions of the electric vector of the incident radiation for given polarizer angles.

The variation in intensity of the absorption bands of the 110 section with the angle of polarization of the radiation follow a similar pattern. With the polarizer at 0° (Fig. 3) the electric vector of the radiation can interact with only the perpendicular dipole component of the full faced layer of molecules and only the parallel component of the molecules seen edgewise. With the polarizer at 90° the incident radiation interacts again with the perpendicular component of the full faced molecules but now also with the perpendicular component of the molecules viewed edgewise. A vibration with a dipole component perpendicular to the molecular symmetry axis should, therefore, show an intensity varying from a given value at 0° to about twice that value at 90°.

The spectra of Figs. 1 and 2 show, indeed, that these correlations can be made. The results are collected in Table I. The conclusions concerning the direction of the oscillating dipole moment for a given band obtained from the variation in intensity of that band either with ordinary radiation incident on different crystal faces or with differently oriented polarized radiation on the 110 type section are in complete agreement. As is expected, the change in appearance of the spectra in going from

TABLE I. Symmetry of the infrared bands of S_8 above 680 cm^{-1}.

Frequency cm^{-1}	More intense band Plane	Polarizer angle	Observed infrared active species
680	110(?)	90°(?)	E_1(?)
711	110(?)	90°	E_1
846	110	90°	E_1
870	...	...	B_1(?)
903	001	0°	B_1
937	(001)	(0°)	B_1, E_1
986	110	90°	E_1
1047	110	90°	E_1
1305	110	90°	E_1
1512	110	90°	E_1

[6] The argument that follows is based on the treatment of the oriented molecules of the crystal without regard for any crystal effects. This view has been discussed for the case of naphthalene by G. C. Pimentel and A. L. McClellan, J. Chem. Phys. **20**, 270 (1952). The selection rules of the isolated S_8 molecule are assumed valid for the molecules in the crystal. The directional effects observed for the different planes investigated and for the different angles of polarization are interpreted in terms of the two types of orientation of the molecules in the crystal. This simple treatment is open to criticism on the basis that the effect of the unit cell and site symmetry on the spectrum of the free molecule, i.e., splittings of fundamental vibrations and possibly new selection rules, has been ignored. However, in view of the weak interactions to be expected between sulfur molecules and the essentially perpendicular arrangement of the differently oriented molecules, it is expected that the more detailed methods [see R. S. Halford, J. Chem. Phys. **14**, 8 (1946); D. F. Hornig, J. Chem. Phys. **16**, 1063 (1948); and H. Winston and R. S. Halford, J. Chem. Phys. **17**, 607 (1949)], which would in general be required, would not in this case show anything new. The validity of this procedure can be further discussed when a more complete spectrum is obtained.

[7] S. Bhagavantam and T. Venkatarayudu, Proc. Indian Acad. Sci. **8A**, 101, 115 (1938).

the 001 to the 110 type plane is not so great as in going from a polarizer angle of 0° to 90° with the 110 section.

The shoulder at 870 cm^{-1} on the strong band at 846 cm^{-1} is not sufficiently well resolved to be assigned with any certainty but the symmetrical shape of the 846 cm^{-1} band for a polarizer angle of 90° suggests that the 870 cm^{-1} band is then relatively weak and hence of the parallel type. There is also some uncertainty in the assignment of the band at 680 cm^{-1} since it appears as a shoulder on a strong band, of undetermined character at 659 cm^{-1}. The variation in the intensity of the band at 937 cm^{-1} has been carefully studied at polarizer angle intervals of 20° from 0° to 180°. For a 1.10-mm section, $\log I_0/I$ for the band maximum increased steadily from a value of 0.21 at 90° to 0.25 at 0° or 180°, while the position shifted slightly to higher frequencies. The small change in intensity of this band compared with all the other bands and with the change expected for a B_2 or E_1 type vibration indicates that the band contains both of these species.

The only other bands easily studied as detailed functions of polarizer angle are those at 1305 and 1512 cm^{-1}. From the arguments given above these bands are assigned a dipole change perpendicular to the molecular axis. It follows that the full faced molecules will contribute a constant absorption for changes in the polarizer angle. The contribution from molecules seen edgewise, however, should vary from an amount equal to the contribution of the full faced molecules for a polarizer angle of 90° to zero for an angle of 0°. The dotted curve of Fig. 4 shows the calculated variation in total intensity for a contribution of the full faced molecules of $\log I_0/I = 0.122$. The two full inner curves give the constant contribution and the variable contribution separately. The points along the outer curve are the experimental values of $\log I_0/I$ for peak intensity of the 1305-cm^{-1} band and a crystal thickness of 1.10 mm, while those on the inner curve were obtained by subtracting 0.122 from the experimental values. The results for the 1512 cm^{-1} band are similar but because of the sharpness of the band the scatter in peak intensities is rather greater. The results of Fig. 4 show that the 1305 cm^{-1} band intensity is caused almost entirely by a perpendicular type oscillating dipole. A comparison has also been made of the intensities of the 1305 cm^{-1} band in the spectra of the 1.10-mm section parallel to the 110 plane and the 1.17-mm section parallel to the 001 plane. After correction for the difference in thickness, a ratio of $\log I_0/I$ for the 110 plane to that for the 001 plane of 1.4 was obtained. This agrees well with the predicted ratio of 1.5.

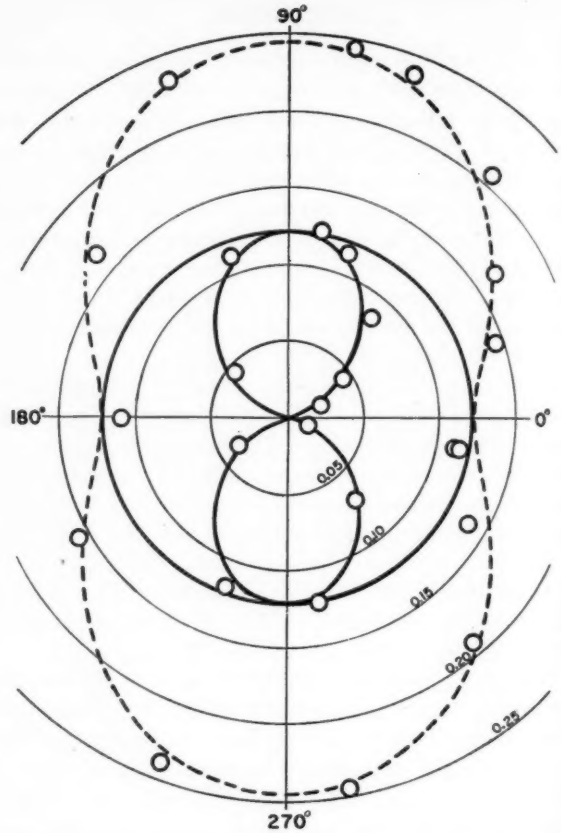

FIG. 4. $\text{Log} I_0/I$ for the 1305 cm^{-1} band of a 1.10-mm section parallel to the 110 plane. ------ calculated total $\log I_0/I$. ------ calculated variable and constant parts of $\log I_0/I$. ○ outer, observed $\log I_0/I$; inner, observed minus 0.122.

The symmetry species of the infrared active components of the bands studied are listed in Table I. The observed and previously assigned[2] symmetries of several of these bands are in disagreement. In the future we hope to be able to extend our measurements to much lower frequencies and to obtain direct information about the symmetry of some of the fundamental bands. No attempt, therefore, is now made to explain the origin in terms of fundamental vibrations of those bands for which the assigned and observed symmetry are different. Since it has been shown that information obtained with the infrared polarizer duplicates that obtained from ordinary spectra of the different crystal sections investigated here, it should be possible to obtain information on the nature of a vibrational band at lower frequencies than are transmitted by the silver chloride polarizer.

An Investigation of the Thermoluminescence of Fluorite Colored by X-Ray Irradiation

JOHN J. HILL AND JACK ARON
Lewis Laboratory, National Advisory Committee for Aeronautics, Cleveland, Ohio
(Received June 16, 1952)

The thermoluminescence resulting when calcium fluoride crystals colored by x-ray irradiation are heated, has been investigated in the region from 3200 to 6500A. First, the form of the emission spectrum was determined by the use of a spectrophotometer in conjunction with a photomultiplier tube as a detector, and fifteen emission bands were observed of which seven weak ones had not previously been reported. The peaks of these bands occurred at 3430, 3650, 3710, 3790, 3810, 4150, 4270, 4370, 4570, 4780, 4890, 5230, 5350, 5430, and 5740A. Second, continuous annealing curves or "glow curves" were obtained for the strongest emission bands by raising the temperature of the crystal at a constant rate and recording the intensity of the emitted light at the peak of each band. The maxima of the glow curves thus recorded fall into two groups. In group 1, three maxima located at approximately 197, 285, and 310°C were observed. In group 2, five intensity maxima could be distinguished, the lowest occurring at approximately 70°C and the highest at 245°C. The corresponding activation energies were calculated, and in two cases were checked by carrying out the annealing at fixed temperatures. These results are consistent with the assumption that two distinct types of imperfections are responsible for the thermoluminescence of calcium fluoride. The optical absorption appears to be the result of the imperfections associated with group 2.

INTRODUCTION

THE properties of a real crystal deviate quite notably from those of the (hypothetical) perfect crystal whose characteristics are fairly well known from a theoretical viewpoint. An understanding of the behavior of real crystals requires, therefore, a knowledge of the effects of lattice imperfections on such properties. In general, unfortunately, it is quite difficult to produce imperfections of a known type or to determine the nature of those already present in a given crystal. The situation with regard to ionic crystals is, however, rather favorable in this regard because, as is well known, upon irradiation of such crystals with x-rays, some of the imperfections present manifest themselves by a coloration of the crystal, that is, by a change in the optical absorption spectrum.[1] In addition, it has been recently found that new imperfections are formed as a consequence of the irradiation. This is substantiated by such investigations as those by Esterman, Leivo, and Stern,[2] and by Hacskaylo and Groetzinger[3] in which it was established than the density of ionic crystals decreases upon irradiation.

Irradiated crystals usually display several absorption bands, and it is generally accepted that at least some of these bands are due to electrons trapped in negative ion vacancies and to positive holes trapped in positive ion vacancies. These types of imperfections are referred to as color centers.

Recently, Barile,[4] in investigating the kinetics of the annealing of the imperfections responsible for four absorption bands in fluorite, found that they all decay in nearly the same fashion, apparently indicating that the imperfections responsible are interrelated. In order to obtain a deeper insight, it was decided to apply another approach to the study of these color centers, namely, to investigate thoroughly the thermoluminescence and especially its kinetics.

There are two previous studies of the thermoluminescent spectrum of such crystals. Iwase,[5] using a photographic plate as a detector in his spectrometer, investigated the emission spectrum in the region from 3500A to 6000A and found that it was composed of six bands (see Table I). He observed only the brightest bands and did not attempt to study the annealing of the thermoluminescence. He found that pairs of bands showed an approximately constant energy difference,

TABLE I. Wavelength of the peaks of thermoluminescent CaF_2 emission bands[a] in the region from 3200 to 6500A.

Band	Group	λ observed	λ(Iwase[b])	λ(Rwatschew[c])
A	1	3430A (v. weak)	···	2800A
B	1	3650 (v. weak)	···	3000A
C	1	3710 (v. weak)	···	···
D	–	3790 (v. weak)	···	···
E	1	3810	3800	···
F	1	4150	4200	···
G	–	4270 (weak)	···	···
H	1	4370	4360	···
I	–	4570 (weak)	···	···
J	2	4780	4800	4750
K	–	4890	···	···
L	1	5230	···	5100
M	2	5350	···	5350
N	1	5430	5420	5480
O	2	5740	5740	5780

[a] The system of designating the emission bands is arbitrary and of course bears no relation to the usual nomenclature for absorption bands of the color centers.
[b] See reference 5.
[c] See reference 6.

[1] See, for example, F. Seitz, Revs. Modern Phys. **18**, 384 (1946); P. W. Pohl, Physik. Z. **39**, 36 (1938); N. F. Mott and R. W. Guerney, *Electronic Processes in Ionic Crystals* (Oxford University Press, London, 1940).
[2] Esterman, Leivo, and Stern, Phys. Rev. **75**, 627 (1949).
[3] M. Hacskaylo, and G. Groetzinger, Phys. Rev. **87**, 789 (1952).
[4] S. Barile, J. Chem. Phys. **20**, 2 (1952).
[5] E. I. Iwase, Nature **131**, 909 (1933).

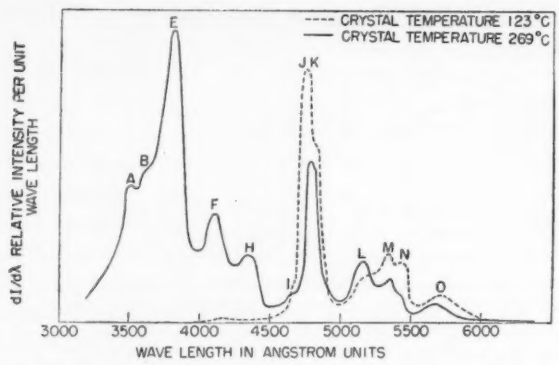

FIG. 1. The thermoluminescent spectrum of fluorite crystals colored by irradiation with x-rays, showing the values of the peak intensities which would be reached at approximately five minutes after heating to 123°C (dotted curve) and to 269°C (solid curve) as obtained by corrections based upon observed decay characteristics.

and proposed that the emission originated at two energy levels with a separation of 0.67 ev. Rwatschew[6] (see Table I) used as a detector a photographic plate in the region from 4500A to 6000A and a photosensitive Geiger Mueller counter in the region from 2000A to 3500A. He found two additional emission bands in the visible region as well as two in the ultraviolet. By using the counter without the monochromator, he obtained some integral decay curves for the luminescence in the ultraviolet region at 180°C and 20°C.

Recent advancements in the technique of using photomultiplier tubes in conjunction with devices for recording fast pulses afford means for recording very low light intensities. We decided, therefore, to make use of this system for detecting radiation in our study of the thermoluminescence.

In general, there are two techniques employed to study annealing. In the first method, the temperature is held constant and the process is investigated as a function of time. Such experiments performed at different temperatures allow the activation energy for the process to be determined without any further assumptions. The condition of constant temperature cannot in practice be fulfilled in the initial stage of the experiment. For this reason, it is preferable in many cases to use a second method, namely, that of continuous annealing (which has, however, a disadvantage to be discussed below). In this method, the temperature is increased at a constant rate and the measured quantity recorded as a function of temperature. In the case of the study of thermoluminescence, the method involves obtaining a so-called glow curve by heating the irradiated crystal at an approximately uniform rate and recording the intensity of the emitted light as a function of the temperature (or time). For a process involving only one activation energy, the decay rate of the centers and hence the intensity of emission increases with temperature while the total number of available emission centers decreases with temperature. Thus, at some specific temperature an intensity maximum or glow peak will occur. The temperature at which the maximum occurs is determined by the activation energy or trap depth of the emission center producing the luminescence. When several activation energies are involved, then several intensity maxima will occur. From the number and positions of these maxima, the number of emission levels and their activation energies or trap depths can be obtained. According to P. Schwed,[7] the method of continuous annealing has the disadvantage that the smallest difference between two activation energies which can be just distinguished is 50 percent larger than in the case of annealing at constant temperature. The interpretation of the glow curves is, in many cases, complicated by the fact that due to the width of the emission bands, the radiation measured at one peak may contain contributions from nearby emission bands.

APPARATUS

The apparatus for investigating the thermoluminescence consisted of a small furnace, a monochromator, and a photomultiplier, all enclosed in a light-tight box. As a monochromator, the optical system of a Beckman spectrophotometer was used. The light source of the spectrophotometer was replaced by a small electric furnace in which the crystals were heated and the phototube was replaced by a 5819 type photomultiplier tube.

The output pulses of the photomultiplier were fed into a linear amplifier and discriminator. The pulses passed by the discriminator were counted by a commerical counting rate meter, whose output was recorded on a strip recorder and also monitored with a scale of 4096 counter. The counting rates were always sufficiently high that statistical variations were negligible, but low enough that no saturation effects were encountered.

Because only a small amount of light was produced by the luminescent crystal of which only a small portion was passed by the monochromator, it was necessary to reduce the dark count as much as possible. For this reason, all cables and units were carefully shielded, line noise was reduced by the use of Sola transformers and filters, and the photomultiplier unit was packed in dry ice to reduce the thermal noise.* These precautions enabled us to use the amplifier with a 0.2-microsecond rise time at its full gain of approximately 3500. The discriminator was arbitrarily ad-

[6] W. P. Rwatschew, J. Phys. (U.S.S.R.) 6, 141 (1942).

[7] P. Schwed, NACA Report RM E51G24.

* The elimination of noise is more important here than in the case of the counting of scintillations due to nuclear particles. In the present case the individual pulses which were to be recorded, were due to single photons and therefore to single photoelectrons. These are much more difficult to distinguish from the random noise pulses than are the much higher pulses resulting from the simultaneous emission of a large number of photoelectrons generally encountered in scintillation counters.

justed to give a background count of about five per second.

To facilitate the rapid determination of the spectral distribution of the radiation emitted, the prism of the monochromator was equipped with an electric motor drive, the speed of which was such that the whole range was covered in about fifteen minutes. By means of a contact coupled to the shaft of the drive and a second pen on the recorder, calibration marks were made on the record at predetermined wavelengths during the operation of the scanner.

EXPERIMENTAL PROCEDURE

All the specimens studied were synthetic CaF_2 crystals† cut into pieces of approximately 4×4×8 mm and irradiated at room temperature for about an hour with a beryllium window x-ray tube operated at 45 kilovolts and 30 milliamperes. Samples used in the annealing studies were stored in dry ice immediately after irradiation until the beginning of the experiment.

To determine the general features of the emission spectrum, a sample was placed in the furnace which had been preheated to 123°C, and the spectrum recorded after the sample had reached a constant temperature. This was repeated at 269°C. Then, in order to determine its detailed structure, each emission band observed was scanned separately using a freshly irradiated crystal. The wavelength of the peak was determined by averaging the readings for both directions of scanning thus eliminating lag in the counter rate meter.

The glow curves of the individual emission bands were obtained by setting the monochromator at the wavelength corresponding to the peak of the band and raising the temperature of the furnace containing the crystal at a fairly uniform rate of about 0.2°C per second starting at room temperature. In order to reduce light loss, the crystal was covered by aluminum foil on five faces. While the glow curve was being recorded, the temperature of the crystal, determined by means of a small thermocouple mounted on its surface, was entered manually on the same chart at approximately 10°C intervals. Continuous annealing curves or glow curves for each of the more intense emission bands of the spectrum were obtained in this manner.

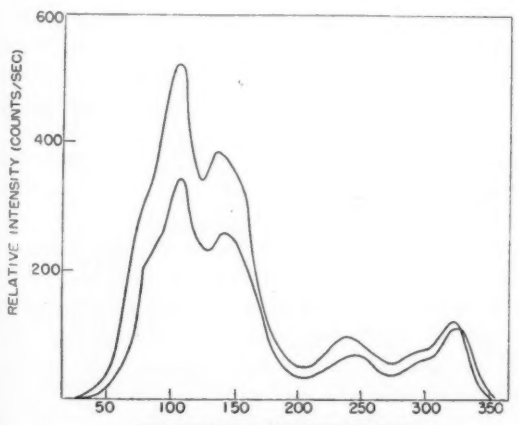

FIG. 2. Glow curves for the *M*-emission band of two thermoluminescent fluorite crystals which had decayed for several hours at room temperature prior to the annealing measurements.

† The crystals were obtained from the Harshaw Chemical Company of Cleveland, Ohio.

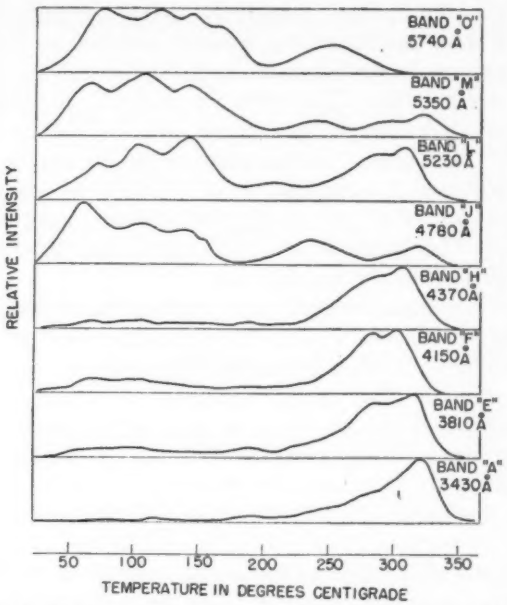

FIG. 3. Glow curves for the main emission bands of thermoluminescent fluorite colored by irradiation with x-rays at room temperature and preserved at dry ice temperature prior to the beginning of the continuous annealing.

RESULTS

Emission Spectrum

The intensity per unit wavelength $dI/d\lambda$, as a function of λ is shown (in arbitrary units) in Fig. 1. The intensity has been corrected approximately for the nonlinear dispersion of the monochromator, for the wavelength dependence of the photomultiplier sensitivity,[8] and for the decay of the luminescence during the run. The intensities shown are values attained at a time of about five minutes after the heating began, as calculated on the basis of the results of our study of the decay.

Table I lists the wavelengths of the peaks of the spectral emission bands, which were obtained by averaging the results of scanning the individual peaks separately. As explained above, these values are more exact than those which can be obtained from Fig. 1.‡ Table I also contains the results of Iwase[5] and Rwatschew.[6]

Annealing of Individual Bands

The results of our observations concerning the annealing of the individual emission bands are shown in

[8] RCA Data Handbook.

‡ The weaker peaks do not even appear in this figure.

Figs. 2 and 3. The annealing curves represented in Fig. 2 were taken for two different crystals at 5350A, the peak of the *M*-emission band. Each curve shows at least six maxima. (The term "maximum" is used exclusively in connection with glow curves while the term "peak" is reserved for a maximum in the spectrum.) The fact that the maxima occur at the same temperatures in both curves indicates the reproducibility of the results. The positions of the maxima are practically independent of the heating rate.

The annealing curves for the eight strongest emission bands are shown in Fig. 3, normalized so that the intensity of the highest maximum is unity.

It appears that every maximum occurring in the curves can be assigned to one of seven temperatures. These characteristic temperatures can be divided into two groups. Group 1 consists essentially of two temperatures, both above 250°C, associated with the prominent maxima seen in curves *A*, *E*, *F*, and *H*. Group 2 is made up of the five temperatures associated with the maxima shown in curve *O*. The temperatures of the maxima in each group are given in Table II. It might be reasonable to assume that the members of a given group can be associated with a given type of imperfection and always occur together. Thus the two groups have a different origin and cannot both be present in a single band. If one accepts this point of view, the fact that all seven maxima occur prominently in the three remaining curves (*M*, *L*, and *J*) of Fig. 2, can then be explained on the basis that each of them contains contributions from at least one spectral band belonging to a different group than that of the band at whose peak the monochromator is set. This overlapping results from the finite half-width of adjacent bands in the spectrum. For example, the form of curve *M* can be explained by assuming that bands *M* and *N* overlap, that the maxima of band *M* belong to group 2, and that those of band *N* belong to group 1. This assignment is consistent with the results shown in Fig. 1, since the relative prominence of band *M* is much greater in the low temperature curve of that figure as would be expected from the fact that the maxima of group 1 occur at higher temperatures than those of group 2. In a similar fashion, the other prominent bands have been assigned (Table I). The seven maxima discussed do not necessarily exhaust all those present. In particular, it appears that the group 1 contains one other maximum besides the two mentioned, namely, that associated with the very small hump occurring at 197°C in curves *A*,*E*, *F*, *H*, and *L* of Fig. 2.

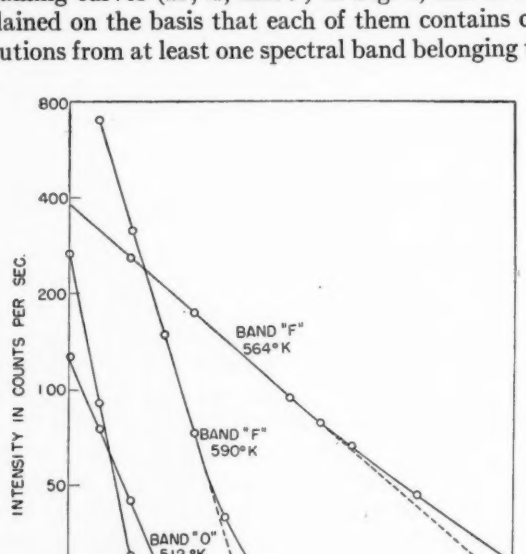

FIG. 4. Constant temperature annealing curves for the "*O*" and the "*F*" bands at temperatures of 512°K and 526°K and of 564°K and 590°K, respectively, after the removal of the lower energy luminescence.

In order to obtain the activation energy associated with a given maximum of the annealing curve, it is necessary to know the order of the annealing process in question. This was determined experimentally in two cases by measuring the rate of decay of the *O*-band at two temperatures near 246°C, and of the *F*-band at two temperatures near 310°C. The decay curves obtained should correspond to the 246°C and the 310°C maxima (which are, respectively, the highest in groups 2 and 1) since the annealing processes occurring at lower temperatures are completed while the crystal is being heated up to the temperature in question. The results of the measurements are given in Fig. 4 on a semilog plot. Each of the curves is essentially composed of two straight lines of slightly different slopes indicating the existence of two first order processes of slightly different activation energies. It should be noted that in each case the process with the higher activation energy makes only a small contribution to the total intensity. This and the small separation of the activation energies account for the fact that these two activation energies are not resolved by the method of continuous annealing.

For continuous annealing in the case of a single first-order process, the activation energy E (which for the following is assumed to be the only one present) may be obtained from the equation[7]

$$E = kT_{\max} \ln(12\nu/r), \tag{1}$$

where k is Boltzmann's constant, $T_{\max}$ is the temperature at which the intensity of the emitted radiation takes on its maximum value, r is the rate of heating in °K/sec, and ν is the jump frequency of the process in $\sec^{-1}$. The quantity ν in general is not known and in principle it is better to use instead the following equation,[9] which does not require a knowledge of ν:

$$E = kT_{\max}^2/\tau, \tag{2}$$

[9] F. Urbach, "Preparation and characteristics of solid luminescent materials," *Cornell Symposium* (John Wiley and Sons, Inc., New York; Chapman and Hall, Ltd., London, 1948).

TABLE II. Activation energies for the thermoluminescence displayed by CaF_2 colored by irradiation with x-rays.

Group	Continuous annealing T_{max} in °K	τ in °K	$E=kT_{max}^2/\tau$ in ev	$E=kT_{max}\log(70\nu)$ in ev[a]	Annealing at fixed temperatures T_a' and T_a'' T_a' in °K	$E=kT_a'\log(\nu/r)$ in ev[a]	T_a'' in °K	$E=kT_a''\log(\nu/r)$ in ev[a]
1	470			1.40				
	559			1.65				
					564	1.69	590	1.70
	583	15.5	1.87	1.72				
					564	1.70	590	1.74
2	342			0.98				
	380			1.09				
	415			1.20				
	433			1.27				
					512	1.49	526	1.50
	519	18.0	1.28	1.51				
					512	1.51	526	1.55

[a] Taking $\nu=10^{13}$/sec.

where τ is given by

$$\tau=(1/I_{max})\int_{T_{max}}^{\infty} I(T)dT. \quad (3)$$

$I(T)$ is the intensity of the light emitted at the temperature T, and

$$I_{max}=I(T_{max}). \quad (4)$$

Because of the overlapping of curves corresponding to different activation energies, the quantity τ could not be determined except in the case of the highest temperature maximum of each group. The values obtained for E in these two cases are given in Table II. This table contains, furthermore, the values of E for all the maxima computed on the basis of the usual assumption that $\nu=10^{13}$/sec and that the process involved is of the first order. As a further check, the decay curves of Fig. 4 were used to determine the values of E corresponding to the two decay processes associated with each curve. For this purpose use was made of the equation

$$E=kT_a\log(\nu/\rho),$$

where T_a is the constant temperature at which the annealing experiment was performed and

$$\rho=-(dI/dt)/I,$$

dI/dt being the time rate of change of I. In this case ν was again taken as being equal to 10^{13}/sec. The two values of E thus obtained for each of the two maxima in the glow curves are given in Table II.

It may be noted that the value of E found by the different methods enumerated are in fairly good agreement with one another, the largest discrepancy being associated with the values based on the actual measurement of τ. These last values are likely to be in error, however, because of the fact that the temperature measurements made in this experiment are accurate only to a few degrees, so that τ, and consequently E, could be in error by 20 or 30 percent from this cause (although an error of a few degrees in the temperature measurement causes no more than one percent error in T_{max}). However, the discrepancy might also partly arise from the fact that the actual value of ν may be quite different from 10^{13} sec^{-1}.

DISCUSSION

As remarked before, it seems reasonable to conclude that at least two different types of imperfections are present in irradiated fluorite which accounts for the existence of the two groups of activation energies. By comparing the thermoluminescence activation energies with those found for the optical absorption, it is possible to associate these latter with group 2. Thus Barile[4] distinguished four activation energies for the absorption, of which he was able to measure three with values of 1.19, 1.25, and 1.38 ev. We tentatively identify these with those of group 2 occurring at 1.20, 1.27, and 1.51 ev. This last, of course, is really composed of two different activation energies, that is, 1.50 and 1.52 ev, so that there are four activation energies involved just as in Barile's work. (It may be remarked that, at the temperatures Barile used, the defects with activation energies of 0.98 and 1.09 ev, would anneal very quickly and could not have been detected.) One further similarity between the thermoluminescence and the optical absorption may be mentioned. Just as we found that all the emission bands of group 1 follow essentially the same annealing curve, so Barile found that there were at least four absorption bands following the same annealing curves.

The fact that there is more than one activation energy in a group is not puzzling in the case of thermoluminescence because of the possibility that the activation energies in this case are those required to raise the electrons from one of the several different metastable states to a common emission level. In this picture, however, the absorption frequency is associated with the energy required to raise an electron from one of these metastable states to some excited level. Consequently, there should be associated with each activation energy an individual absorption band. In view of

the Franck-Condon principle the differences between the energies of these absorption bands may be much smaller than the differences in the corresponding activation energies so that it might, therefore, be very difficult to resolve the various bands.

In order to check this idea, S. Barile and the authors, undertook measurements of the absorption coefficient at the temperature of dry ice and were able to resolve the absorption band at 2280A into two bands. These two bands had also been found by S. Smakula.[10]

ACKNOWLEDGMENT

The authors are indebted to Dr. Gerhart Groetzinger and Dr. Philip Schwed for valuable discussions.

[10] S. Smakula (private communication).

THE JOURNAL OF CHEMICAL PHYSICS VOLUME 21, NUMBER 2 FEBRUARY, 1953

Neutron Diffraction and Atomic Distribution in Liquid Lead and Liquid Bismuth at Two Temperatures

PAUL C. SHARRAH*
Department of Physics, University of Arkansas, Fayetteville, Arkansas

AND

G. PEDRO SMITH
Metallurgy Division, Oak Ridge National Laboratory, Oak Ridge, Tennessee

(Received August 8, 1952)

Neutron diffraction patterns have been obtained on liquid lead and liquid bismuth at two temperatures. The patterns differ only slightly at the different temperatures, the main peak being slightly shorter and broader and shifted slightly to smaller angles at the higher temperatures. The diffraction patterns have been analyzed to obtain information on the atomic distribution. The first main peak in the distribution curve for liquid lead is at 3.40A and represents about 9.4 atoms. The first main peak in the curve for liquid bismuth is at 3.35A and represents about 7.7 atoms. The second most prominent concentration of atoms occurs at 6.6A for both lead and bismuth.

INTRODUCTION

THIS work was undertaken with the purpose of obtaining neutron diffraction patterns on liquid lead and liquid bismuth at two temperatures and of analyzing these patterns in order to obtain information on the atomic distribution in the liquid. These two elements have conveniently large neutron scattering cross sections. Bismuth and lead are the only liquid metals which have been studied by neutron diffraction[1] and, in the case of lead, the results differ somewhat from those obtained by x-ray diffraction methods.[2] The previous neutron diffraction work with these liquids made use of an instrument with a spread in angle and wavelength. While this arrangement did help to overcome the disadvantage of a low neutron beam intensity, it introduced complications in the interpretation of the data. It was hoped that the neutron spectrometer[3] available would be capable of giving good patterns because of its relatively intense well-defined monochromatic beam and the relative simplicity of obtaining experimental results.

EXPERIMENTAL

The equipment used consisted of a neutron spectrometer and recording system[3] and a special furnace to hold the metal in the liquid state at a controlled temperature.

The neutron diffraction spectrometer consisted of a monochromatizing crystal with collimating slits, a monitoring system for maintaining a neutron beam of nearly constant intensity, a BF_3 slow neutron proportional detector arranged to scan the diffracted beam out to about 110 degrees, and the associated electronic circuits and recording system. A copper crystal reflecting a relatively strong neutron beam of 1.16A from the (111) planes was employed to give the patterns used in the analysis. The wavelength spread was about 2 percent at the center of the beam, and the sensitive angle of the detector was about 2 degrees. The BF_3 neutron detector scanned through the diffraction angles at a rate of 8 degrees per hour for most of this work, and the pulses from it operated the rate meter and recording potentiometer. The data were obtained in the form of a chart showing counts per minute against scattering angle.

Two preliminary low temperature runs on liquid bismuth were made using a heating system which applied heat to one end of the sample. The remainder of the low and all the higher temperature runs were

* Research participant, Metallurgy Division, ORNL.
[1] O. Chamberlain, Phys. Rev. 77, 305 (1950).
[2] H. Hendus, Z. Naturforsch. 2A, 505 (1947).
[3] Made available by H. Levy and S. W. Peterson, similar to that described by E. O. Wollan and C. G. Shull, Phys. Rev. 73, 830 (1948).

made using a furnace constructed in the following manner. A copper bar mounted concentric to an aluminum vacuum chamber held the sample tubes in a one-half inch hole in its center. A milled slot through the copper bar permitted the incident and diffracted neutron beams to pass practically unobstructed. The thickness of the wall of the aluminum cylinder was about $\frac{1}{32}$ inch where the neutron beam passed through it. The heat was supplied by two heating coils, one at each end of the bar, supplying about 250 watts at the higher temperatures used. Four or five sheets of aluminum foil surrounded the furnace as a radiation shield. Chromel-Alumel thermocouples imbedded in the bar were used to measure and control the temperature. The actual temperature of the sample probably cannot be specified closer than 10°C. A mechanical pump was used to maintain a sufficiently low pressure within the aluminum container to reduce the heat loss. Water cooling was provided at each end of the aluminum cylinder. The samples were contained in aluminum or vitreous quartz tubes with an inside diameter of about one centimeter and a wall thickness of 0.3 mm for the aluminum tubes and about 0.5 mm for the quartz tubes. Any appreciable quantities of oxide in the lead (99.94 percent) and bismuth (99.999 percent) samples were removed by bubbling hydrogen through the molten material held at 500°C for about 12 hours. The samples were then sealed in the aluminum or quartz sample holders. The lead samples were sealed in the open air, and the bismuth samples were sealed in a dried helium atmosphere.

Five satisfactory diffraction patterns were obtained using liquid bismuth and three using liquid lead. Two of the bismuth samples were contained in 24S aluminum tube samples holders and three were in quartz tubes. A number of attempts using 2S aluminum to hold the bismuth failed. Quartz was the only type of sample holder used for the liquid lead.

Four of the runs on liquid bismuth were at 300°C and one was at 550°C. All of the patterns except one were made using a wavelength of 1.16A and extended to $\sin\theta/\lambda$ equal to 0.7. One pattern was made using a value of 0.71A which gave experimental intensity data to $\sin\theta/\lambda$ equal to 1.15, but the graph was essentially constant from $\sin\theta/\lambda$ equal to 0.7 to 1.15.

THEORY AND METHOD OF ANALYSIS

The atomic distributions in the liquid lead and bismuth were determined through an analysis similar to that used with x-rays,[4] based on the theory of Zernike and Prins[5] and Debye and Menke.[6] The atomic distribution equation may be written

$$4\pi R^2\rho(R)=4\pi R^2\rho_0+\frac{2R}{\pi}\int_0^{s_0} si(s)\sin Rs\,ds. \quad (1)$$

A similar equation with different notation has been used to analyze neutron diffraction patterns.[1] In the above equation the variable R is the distance measured from any given atom in the liquid, $\rho(R)$ is the atomic density function, and the constant ρ_0 is the average density of atoms in the liquid. The variables and the function $i(s)$ are defined by the following equations:

$$s=(4\pi\sin\theta)/\lambda, \quad i(s)=(I-K)/K,$$

where I is the experimentally determined diffraction curve, corrected for sample-holder scattering, background, and incoherent and diffuse scattering;[6] and K is the coherent intensity which would be expected if no interference effects were present. K is assumed to be a constant in accord with the essentially isotropic nature of slow neutron scattering.

The upper limit of integration s_0 in Eq. (1) is the value of s at the limit of the range of $\sin\theta/\lambda$ for which scattering data were obtained ($\sin\theta/\lambda=0.70$, or $s_0=8.79$). The upper limit of integration as used in the theory is infinity. However, the interference effects had essentially disappeared for s greater than 8.79 as shown by the run made with neutrons of wavelength 0.71A. Thus the $i(s)$ function is assigned the value zero beyond s equal to 8.79, and the integral beyond this value vanishes.

The form of the equation given in reference (1) can be used if the value of the bound cross section for scattering is known and if the differential scattering cross section is obtained from the diffraction curve by an absolute measurement. Equation (1) avoids the necessity for these absolute measurements and was used in the work reported here.

Values of K were obtained by two different methods. In the first method it was assumed that K is equal to the limiting value which the measured scattering approaches at large values of $\sin\theta/\lambda$. These limiting values are shown in Figs. 1(a) and 2(a) as those solid horizontal lines about which the intensity curves oscillate. The value of K is then read from the ordinate scale in the same units as that for the graph itself. A second method for evaluating K made use of the criterion that $\int_0^{s_0} s^2 i(s)ds$ should equal $-2\pi^2\rho_0$. This condition is obtained from Eq. (1) by making the assumption that $\rho(R)$ should approach zero as R approaches zero.

The analysis consisted finally in the evaluation of the integral in Eq. (1) for many values of R over the range of interest. This was carried out by numerical integration for values of R up to 9A.

RESULTS

Four of the diffraction patterns obtained are shown in Figs. 1(a) and 2(a). These patterns have been corrected for the scattering by the quartz sample holder and background, also shown in the figures. The sharp drop in the intensity curves near the origin

[4] N. S. Gingrich, Revs. Modern Phys. 15, 90 (1943).
[5] F. Zernike and J. Prins, Z. Physik 41, 184 (1927).
[6] P. Debye and H. Menke, Physik. Z. 31, 797 (1930).

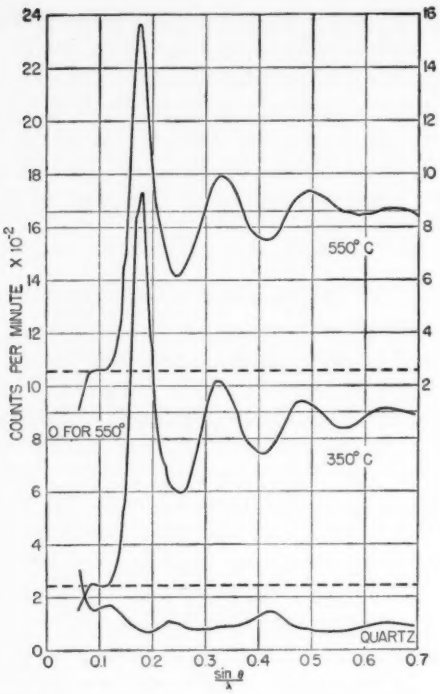

FIG. 1(a). The neutron diffraction patterns for liquid lead at 350°C and 550°C.

should have no significance since the accuracy of the patterns at such small angles is poor due to the proximity of the incident neutron beam. The sample holder correction did not take into account the absorption which would result when the quartz tube is filled with the molten metal and thus may be somewhat larger than it should be. A practically level step in the intensity patterns at the small values of the scattering angle was assumed to represent the incoherent scattering, and any diffuse background that might be present and a constant of this amount was subtracted from each of the curves. This amounted to moving the origin of the ordinate scale to the dotted lines shown on Figs. 1(a) and 2(a). No absorption correction was applied as it was calculated to be practically constant with angle. No account has been taken of any possible effects of multiple scattering, but this was not considered to be too serious with the sample sizes used.

Diffraction patterns obtained on the same material at the same temperature were practically identical.

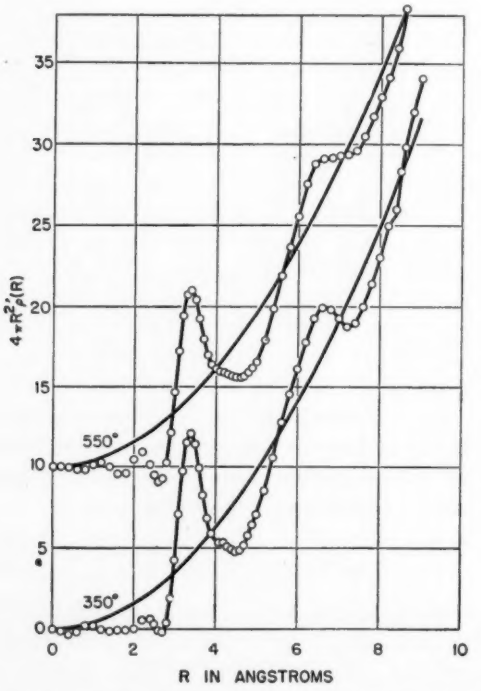

FIG. 1(b). The atomic distribution curves for liquid lead at 350°C and 550°C.

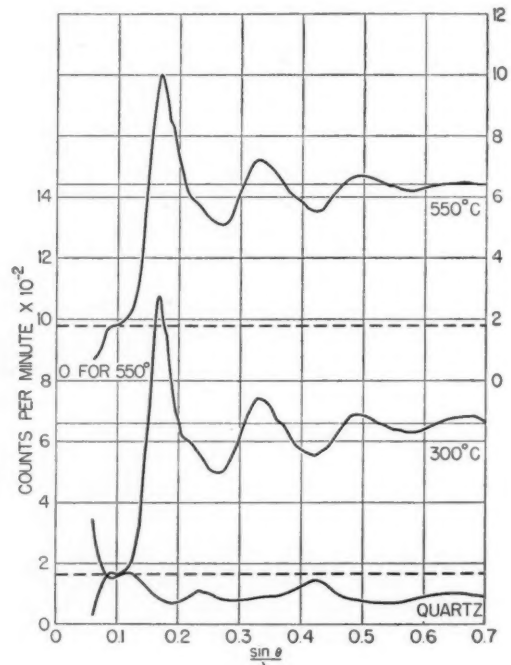

FIG. 2(a). The neutron diffraction patterns for liquid bismuth at 300°C and 550°C.

At each temperature the diffraction pattern consists of one prominent peak and several much smaller secondary peaks. The differences between the patterns at the two temperatures are small. The main peak shifts to slightly smaller values of $\sin\theta/\lambda$ and is shorter at the higher temperature. The secondary peaks are slightly less prominent at the higher temperature. The positions of the maxima and minima in the diffraction patterns are summarized in Table I.

The atomic radial distribution curves shown in Figs. 1(b) and 2(b) were calculated using values of K obtained by the first method mentioned above. The values of K obtained by the second method gave distribution patterns which were only slightly different from those shown with the exception of lead at 550°C for which the two values of K were identical.

The distribution patterns each show a pronounced peak with center between 3.0 and 3.5A. The height of this peak is slightly greater at the lower temperatures. The curves do not fall to zero after this first peak, a characteristic of the results found on all liquid metals and noble gases. A second prominent concentration of atoms occurs at 6.6A for both lead and bismuth. There is some indication of a very small peak at about 4.5A on the bismuth curves and at 4.3A on the lead curves, similar to that observed on many of the curves published.[1,2,4] Theory would predict the possibility of small subsidiary peaks located symmetrically about

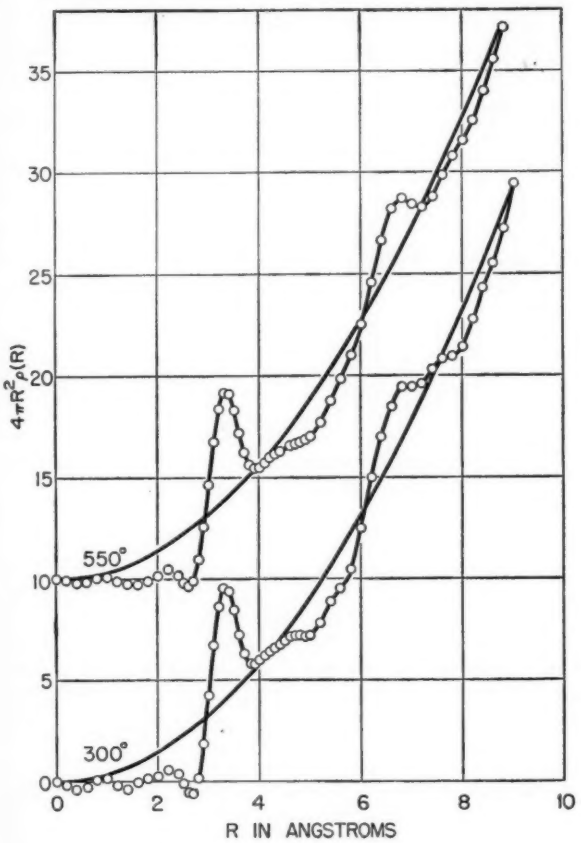

FIG. 2(b). The atomic distribution curves for liquid bismuth at 300°C and 550°C.

any strong peak on the distribution curve resulting from the fact that the experimental data extend over a finite range of the variable s.[7] These small peaks are located at a distance from the main peak which would indicate that they are probably caused by this effect. Table II summarizes the peak positions for the distribution curves. The positions of the concentrations in the distribution curves compare well in general with those reported by other workers using x-ray techniques.[2] The positions shown for the first concentration were obtained by locating the center of the peak, but the positions shown for other regions of excess on the curves can only be estimated approximately.

[7] C. Finbak, Acta Chem. Scand. 3, 1279 (1949); 3, 1293 (1949).

TABLE I. Values of $\sin\theta/\lambda$ at diffraction pattern maxima and minima.

Substance	Max	Min	Max	Min	Max	Min	Max
Lead 350°C	0.180	0.25_0	0.32_5	0.41_0	0.48_5	0.56	0.65
Lead 550°C	0.175	0.24_5	0.33_0	0.41_5	0.49_0	0.57	0.65
Bismuth 300°C	0.175	0.26_5	0.33_0	0.42_0	0.49_5	0.57	0.65
Bismuth 550°C	0.170	0.27_0	0.33_0	0.42_5	0.49_5	0.58	0.65

The area under the atomic distribution curve $4\pi R^2\rho(R)$ between any two values of R gives the number of atoms within that range. It is especially significant to assign the number of atoms represented by the first peak on the curve. This was done by projecting the right side of the peak down to the base line in such a manner that the resulting peak is approximately symmetrical and by then determining its area. Values

TABLE II. Atomic concentration positions in angstroms. (Values in ( ) from references)

Substance	First	Second
Lead 350°C	3.40	6.6
Lead 550°C	3.40	6.6
Bismuth 300°C	3.35	6.8
Bismuth 550°C	3.35	6.8
Lead 375°C[a]	(3.40)	...
Lead 390°C[b]	(3.4)	(6.4)
Bismuth 340°C[a]	(3.32)	...
Bismuth 310°C[b]	(3.2)	(6.7)

[a] See reference 2.
[b] See reference 1.

obtained for the area of this peak are influenced considerably by the manner in which the projection is done but seem to consistent among themselves. Table III shows the results obtained along with those given by others. Also listed is the number of atoms surrounding any given atom in the liquid out to the distances shown.

Some remarks about the effect of systematic errors on the features and accuracy of the distribution curves can be made. Small subsidiary peaks may be produced in the manner described above.[7] An error in the origin

TABLE III. Atoms in first peak and atoms to distances shown. (Values in ( ) from references)

Substance	Peak	3.5	4.0	4.5	5.0	5.5	6.0
Lead 350°C	9.4	5.3	9.3	11.9	14.5	19.1	26.1
Lead 550°C	9.5	5.1	9.0	11.8	14.6	18.6	25.1
Bismuth 300°C	7.7	4.6	7.8	11.0	14.5	18.4	23.3
Bismuth 550°C	7.5	4.6	7.7	10.6	13.9	17.8	23.1
Lead 375°C[a]	(8)	...	...	...	...	...	...
Lead 390°C[b]	(12±1)	...	...	...	...	...	...
Bismuth 340°C[a]	(7–8)	...	...	...	...	...	...
Bismuth 310°C[b]	...	...	(8.0)	...	...	...	...

[a] See reference 2.
[b] See reference 1.

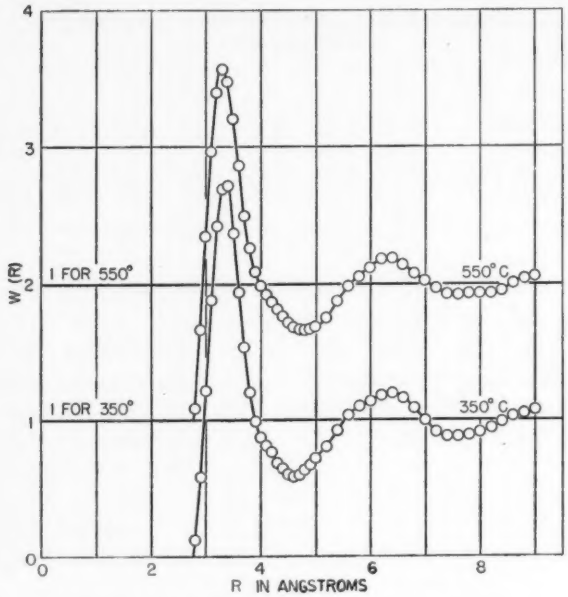

FIG. 3. The probability function $W(R)$ for liquid lead at 350°C and 550°C.

of the ordinate scale of the corrected intensity pattern caused by an over correction for sample holder, background, incoherent, or diffuse scattering will cause the values of the integral in Eq. (1) to be too large. A sample calculation indicates that this error in the value of the integral for our data will be of the order of 20 percent if the total correction applied was two times the proper value. On the other hand, an error in the value of K will produce an error in the value of the integral of equal percent; and, in addition, certain small oscillating terms which vary as $\sin Rs_0/R^2$ at small values of R and as $-\cos Rs_0/R$ at large values of R. No attempt is made here to analyze these and other possible errors completely. It should be pointed out that an error in the integral in Eq. (1) will cause the area of the first peak in the distribution curves to be changed but apparently by a smaller factor. A sample calculation indicates that an error of 20 percent for the values of the integral will cause the area of the first peak in our results shown in Figs. 1(b) and 2(b) to be in error by only about 5 percent, but the magnitude of this error is quite sensitive to the manner in which the right side of the peak is extended to the axis.[8]

Figures 3 and 4 are graphs of the Menke probability function $W(R)$. These were obtained by making use of the relation $W(R)$ equal $\rho(R)/\rho_0$ and give the relative probability of finding atoms at a given distance R from the origin atom.

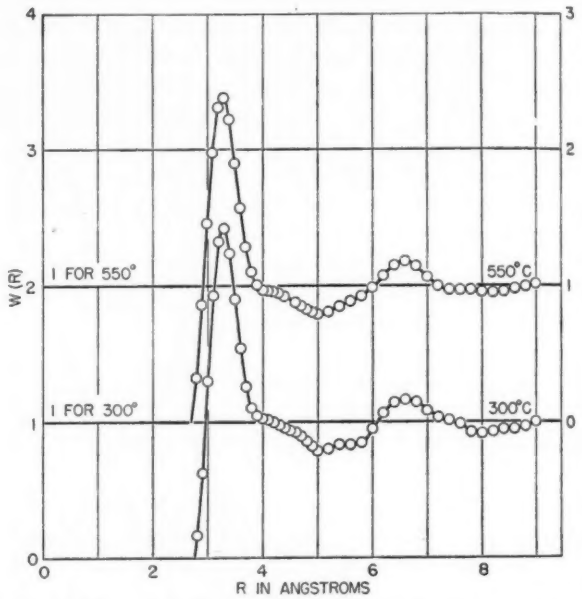

FIG. 4. The probability function $W(R)$ for liquid bismuth at 300°C and 550°C.

ACKNOWLEDGMENTS

The authors wish especially to thank Dr. J. V. Cathcart for assisting in preparing the metal samples, Dr. H. A. Levy and Dr. S. W. Peterson for making time available for the use of the neutron spectrometer and for their assistance in conducting the experimental work, and Dr. C. L. Perry for making arrangements for the evaluation of the integral in Eq. (1).

[8] The work of Danilova, Danilov, and Spektor, Doklady Akad. Nauk. S.S.S.R. 82, 561 (1952) has just come to our attention. Atomic distribution curves were obtained on liquid tin, bismuth, and lead using x-rays and the method of balanced filters. The number of atoms in the first peak is given as 11 for lead and 7–7.5 for bismuth. The small persistent secondary peaks between 4.0 and 5.0A are quite prominent.

The Effect of 1470A Irradiation of Nitrogen-Hydrogen Mixtures and of Ammonia*

M. H. J. WIJNEN AND H. AUSTIN TAYLOR
New York University, University Heights, New York, New York
(Received August 20, 1952)

The characteristics of a xenon resonance lamp were studied, using carbon dioxide as an actinometer, to determine the influence of the xenon pressure in the lamp on the intensity of the 1470A radiation. The xenon sensitized photosynthesis of ammonia was studied both in static and in flow systems. No ammonia could be detected. Some experiments on the photolysis of ammonia at 1470A are reported and discussed. The present work furnishes the first direct chemical evidence rejecting the value of 171.3 kcal per mole as the dissociation energy of nitrogen.

IN 1928 Lewis[1] demonstrated that ammonia was produced when active nitrogen, prepared by electrodeless discharge was mixed with hydrogen atoms, produced in a Wood's discharge tube. When either the nitrogen or the hydrogen in a mixture was activated alone no ammonia resulted. Lewis concluded that ammonia is produced only when both nitrogen atoms and hydrogen atoms are present.

The energy equivalent of the xenon resonance radiation at 1470A is 194.5 kcal per mole. The value of the dissociation energy of the nitrogen molecule is variously considered as: 171.3, 226.4, or 273.7 kcal.[2] If the smallest value is correct, nitrogen atoms should be produced by xenon photosensitization at 1470A. The presence or absence of ammonia in a xenon sensitized nitrogen-hydrogen mixture after exposure to 1470A radiation can thus be decisive concerning the lowest suggested value of the nitrogen dissociation energy.

EXPERIMENTAL

The apparatus used in this study, illustrated in Fig. 1, is built around a xenon resonance lamp described by Dacey and Hodgins[3] which employs a very thin quartz tube to contain the discharge and yet transmit the 1470A radiation. The method of filling the lamp and the reaction cell is apparent from the diagram. The lamp was operated on 60-cycle current from a 5000-v transformer whose primary windings were connected to a variac. An operating current of 100 ma was used throughout the experiments. The pressure of the gas mixture in the reaction cell was measured on a manometer. Small gas pressures in the lamp or cell could be measured accurately in a McLeod gauge down to a pressure of 0.5 micron. After illumination of the nitrogen-hydrogen mixture in the reaction cell the gas was pumped off through the gas burette, while cooling the trap with liquid nitrogen. Any reaction products formed such as ammonia or hydrazine would have been condensed in the trap and could be brought over to the gas burette by filling the small mantel around the burette with liquid nitrogen. It was thus possible to determine the amount of condensables formed during the reaction. A small removable trap permitted the collection of the gas after freezing, for identification, using Nessler's reagent for ammonia and gold chloride for hydrazine.

RESULTS AND DISCUSSION

A. Carbon Dioxide

The photolysis of carbon dioxide was studied to obtain information about the characteristics of the xenon resonance lamp. Groth[4] has suggested that at 1470A one molecule of carbon dioxide decomposes per light quantum absorbed. In the experiments performed, residual carbon dioxide was condensed in liquid nitrogen and the pressure of the noncondensable gases, carbon monoxide and oxygen, was measured. Knowing the volume of the reaction system, the number of molecules of carbon dioxide decomposed per second could be calculated. Accepting a quantum yield of unity this number of molecules of carbon dioxide decomposed per second is the number of quanta emitted per second by the lamp. Dacey and Hodgins[3] state that they used mixtures of xenon and neon in the lamp, neon serving to conduct heat away from the electrodes. Since no

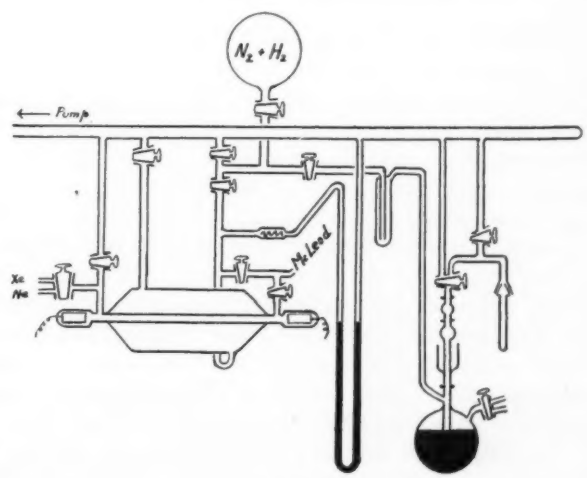

FIG. 1.

* This work has been made possible through the support and sponsorship of the Geophysics Research Division of the Air Force Cambridge Research Center under Contract No. AF 19(122)–426.
[1] B. Lewis, J. Am. Chem. Soc. **50**, 27 (1928).
[2] See Kistiakowsky, Knight and Malin, J. Am. Chem. Soc. 73, 2972 (1951) and G. Glockler, J. Chem. Phys. **19**, 124 (1951).
[3] J. R. Dacey and J. W. Hodgins, Can. J. Research **B28**, 90 (1950).
[4] W. Groth, Z. physik Chem. **B37**, 207 (1937).

TABLE I.

No.	Press of xenon in lamp in mm	Reaction vessel: Press of xenon in micron	Reaction vessel: Press of CO_2 in mm	Quanta/sec 10^{-14}
10	0.66	42	11.8	1.34
11	1.09	40	11.9	1.92
16	1.43	47	12.0	51.50
17	1.44	37	9.3	44.30
15	1.46	45	11.8	48.00
21	1.52	36	11.9	61.10
18	1.53	40	15.3	45.80
20	1.53	50	9.2	13.70
19	1.61	43	9.9	29.91
9	1.69	40	10.8	8.05
14	1.90	42	12.0	2.65
12	2.40	44	11.3	12.90
13	3.55	38	11.0	0.86

observable cooling occurred in the present lamp when neon was added and since the operation of the lamp was not impaired by its omission, neon was not used. The electrode chambers were covered with copper foil and cooled in a stream of compressed air. Table I lists the results of a series of experiments to determine the light intensity of the lamp using an approximately constant reaction mixture of 10 mm carbon dioxide and 40 microns xenon, the lamp operating on pure xenon at various pressures.

Examination of the data in Table I shows a pronounced peak in light intensity for xenon pressures of about 1.5 mm in the lamp. These pressures are the pressures of xenon in the lamp before operation. Once the lamp is burning it is quite impossible to follow the changes in pressure that occur. The lamp heats up and the pressure consequently increases. On the other hand, it is known that the xenon in the lamp, while operating, slowly disappears. This may be attributed to adsorption on or absorption in the electrodes and to "clean-up" as observed in electrodeless discharge of gases.

B. Nitrogen-Hydrogen Mixtures

A mixture of hydrogen and nitrogen in the ratio 3:1 was prepared and subjected to 1470A irradiation under the conditions specified in Table II. In none of these runs was any ammonia or hydrazine detectable after exposure, even when xenon, in amounts previously shown capable of absorbing all the xenon resonance light, was present as a sensitizer. In experiment 25, for example, the xenon thus added is less than 0.01 percent of the total mixture. Nevertheless, 92 percent of the xenon was recovered in the analysis after irradiation. Since ammonia is considerably less volatile than xenon under the analytical conditions it seems certain that ammonia, had it been formed in amounts greater than 0.001 percent of the total, would have been detected.

The absence of ammonia in the irradiation products might be the result of the instability of NH_2 or NH radicals. As a partial test of this a series of experiments was carried out to study the photolysis of ammonia under the influence of 1470A radiation. These experiments are described in the next section. It is important now to note that no hydrazine could be detected. This might suggest a great instability of the NH_2 radicals. F. O. Rice[5] recently presented evidence indicating that the NH radical is very unstable.

If nitrogen atoms are formed in the mixtures used, the production of ammonia will depend on the stationary concentrations of these intermediate radicals. If these are extremely small, ammonia might be detectable only by a rapid removal and collection over a period of time.

A circulating pump was therefore introduced into the system. During the irradiation the gas mixture was circulated through a liquid nitrogen trap to freeze out any ammonia and hydrazine if formed. Six experiments were carried out with irradiation times varying from 60 to 220 minutes and total nitrogen-hydrogen pressures between 20 to 70 mm Hg. All experiments were photosensitized by adding small amounts of xenon to the nitrogen-hydrogen mixture. No traces of ammonia or hydrazine were found. It has already been stated that it seemed certain that ammonia could be detected if it were formed in amounts greater than .001 percent of the total pressure. It is known[1] that ammonia is formed from nitrogen and hydrogen when both gases are activated by an electric discharge. To obtain a second test on the sensitivity of the analysis system therefore a nitrogen-hydrogen mixture was passed first, through the discharge lamp then through a liquid nitrogen trap. The ratio was $N_2/H_2=4$, as suggested by Storch and Olson.[6] The pressure of the gas mixture in the lamp was about 1 mm Hg and about 1 cc of gas passed per minute through the lamp. Ammonia was detected after 50 minutes.

C. Ammonia

As already indicated, some experiments were carried out to investigate the photolysis of ammonia at 1470A. The main aim was to see whether any hydrazine would be formed. The fact that no traces of hydrazine were detected agrees with investigations on the ammonia photolysis in the region 1900–2500A, where only after many precautions was the formation of hydrazine

TABLE II.

No.	Duration of irradiation in sec	$P_{\text{xenon in lamp}}$	$P_{\text{xenon in reaction cell}}$	$P_{N_2+H_2}$ in mm
23	2400	1.5 mm	None	36
24	3000	1.52 mm	12 microns	34
25	6000	1.5 mm	52 microns	87
26	8520	1.5 mm	108 microns	125

[5] F. O. Rice and M. Freamo, J. Am. Chem. Soc. **73**, 5529 (1951).
[6] H. H. Storch and A. R. Olson, J. Am. Chem. Soc. **45**, 1605 (1923).

shown.[7] Although of little importance to the present investigation it is interesting to study in detail the results given in Table III. Most authors agree that the over-all reaction for the photolysis of ammonia may be written

$$2NH_3+xE\rightarrow N_2+3H_2.$$

If we accept this equation, the number of molecules of ammonia decomposed per second was calculated using the same technique as in the case of carbon dioxide (section *A*). Experiments 33, 34, and 35 give the results of a straight photolysis; experiments 27 to 32 those of a photosensitized decomposition. The xenon pressure in the lamp was kept constant to obtain the same light intensity throughout all experiments. Tests with carbon dioxide as actinometer indicated that the intensity of the lamp was within experimental error the same before and after these experiments.

The results in Table III clearly indicate an increase in the number of molecules of ammonia decomposed with increasing ammonia pressure even in the xenon photosensitized decomposition.

Dacey and Hodgins[3] showed that xenon at pressures as low as 3 microns can absorb all the 1470A light. The increase in yield must be accounted for by an increase in quantum yield for ammonia decomposition with increasing pressure. This has been shown to be true in the photolysis of ammonia at wavelengths of about 2000A.[8]

Accepting a quantum yield of unity for the decomposition of carbon dioxide at 1470A quantum yields for the ammonia decomposition (φNH_3) are obtained varying from 2 to 11 depending on the pressure of ammonia in the reaction vessel. Two other values[4,9] for φNH_3 at low wavelengths are mentioned in the literature. These data are summarized in Table IV and show that the values for φNH_3 found in this work are considerably larger than those obtained by Groth and by Harteck and Oppenheimer. Several factors may have caused this difference.

In this work the discharge tube is surrounded by the reaction vessel. Since the discharge tube gets quite hot during operation a temperature gradient probably exists inside the reaction vessel with perhaps a maximum temperature of 200°C in the center and a temperature of about 50°C at the surface. The actual reaction temperature was therefore well above room temperature. This might lead to a quantum yield for ammonia several times larger than the one observed by Groth and by Harteck and Oppenheimer, who are presumed to have worked at room temperature. An increase in quantum yield in the photo decomposition of ammonia with temperature has been reported by several authors[8,10] at longer wavelengths.

TABLE III. Photolysis of ammonia at 1470A.

No.	Duration of irradiation in sec	P_{xenon} in lamp in mm	P_{xenon} in reaction vessel	P_{NH_3} in reaction vessel	Number of molec. decomposed per sec
30	600	1.52	42 microns	4.4 mm	$1.36\ 10^{16}$
32	900	1.51	42 microns	9 mm	$3.2\ 10^{16}$
27	1500	1.52	40 microns	11 mm	$2.24\ 10^{16}$
31	900	1.54	50 microns	14.5 mm	$0.94\ 10^{16}$
28	1500	1.54	48 microns	25 mm	$4.8\ 10^{16}$
29	660	1.54	40 microns	68.8 mm	$5.75\ 10^{16}$
33	1380	1.52	None	5.8 mm	$2.02\ 10^{16}$
34	900	1.54	None	16.3 mm	$2.64\ 10^{16}$
35	960	1.52	None	29.7 mm	$2.98\ 10^{16}$

TABLE IV.

Source	φNH_3	Wavelength	P_{NH_3}	Temp.	Intensity of lamp based on $\varphi CO=1$
Harteck and Oppenheimer	0.5	1470 and 1295A	1 atmos	room temp?	1.5×10^{17} quanta/sec
Groth	0.17	1470 and 1295A	1 atmos	room temp?	1.7×10^{16} quanta/sec
This work	2–11	1470A	4.4→68.8 mm Hg	about 150°C	5×10^{15} quanta/sec

The values of φNH_3 in Table IV are based on the assumption that in the photolysis of carbon dioxide the quantum yield of carbon monoxide production is unity at 1470 and at 1295A. In suggesting this Groth accepted that at these wavelengths φNH_3 would be equal to 0.17 as found by Wiig and Kistiakowsky[10] at about 2100A and that the quantum yield of ozone formation in oxygen would be equal to two as found by Noyes[11] in the region 1720–1900A. This suggestion, however, has lost much of its validity since Groth did not then accept a decomposition of the carbon monoxide molecule which he later[12] proves to take place at 1295A.

Experimental data,[13] furthermore, indicate an increase of φNH_3 with light of higher energy. This would suggest that there is no certainty about the actual value of φCO and that very probably in carbon dioxide photolysis φCO will not be the same for the two wavelengths 1470 and 1295A, since the monoxide decomposes at the shorter wavelength only.

There also exists the possibility that φCO might vary with carbon dioxide pressure, light intensity, and pressure. Summarizing the results on the photolysis of ammonia the quantum yields reported are of a relative nature. The change in quantum yield with pressure, however, is to be expected from data on the photolysis of ammonia at longer wavelengths.

The fact that no ammonia is produced by photosensitization, either in a static system or in a flow system where traces of ammonia could be frozen out to

[7] A. Koenig and Th. Brings, Z. physik Chem. Bodenstein Festband, 541 (1931).

[8] M. Vaupee, Bull. soc. chim. Belges **53**, 179 (1944).

[9] P. Harteck and F. Oppenheimer, Z. physik Chem. **B16**, 77 (1932).

[10] E. O. Wiig and G. B. Kistiakowsky, J. Am. Chem. Soc. **54**, 1806 (1932). W. Kuhn, J. Chem. Phys. **23**, 521 (1926); Compt. rend. **177**, 956 (1923). Ogg, Leighton, and Bergstrom, J. Am. Chem. Soc. **56**, 318 (1934).

[11] W. A. Noyes, Jr., J. Am. Chem. Soc. **52**, 559 (1930).

[12] Faltings, Groth, and Harteck, Z. physik Chem. **B41**, 15 (1938).

[13] L. S. Kassel and W. A. Noyes, Jr., J. Am. Chem. Soc. **49**, 2495 (1927).

prevent decomposition by photolysis, indicates that the energy available in the lamp was not sufficient to break the nitrogen bond. This is further confirmed by showing that ammonia was produced when nitrogen and hydrogen mixtures were lead through the lamp where both gases could be activated or split into atoms by the available high energies of the discharge.

The energy equivalent of the xenon resonance radiation is 194.5 kcal. Failure to produce ammonia indicates that the energy of the nitrogen bond is greater than 194.5 kcal and will be either 226.4 or 273.7 kcal per mole. The present work gives the first direct chemical evidence rejecting the value of 171.3 kcal for the dissociation energy of the nitrogen bond. Recent physical investigations[2] and theoretical considerations[2] lead to a similar conclusion and suggest either 226.4 or 273.7 kcal per mole as the dissociation energy for the nitrogen bond in N_2.

THE JOURNAL OF CHEMICAL PHYSICS VOLUME 21, NUMBER 2 FEBRUARY, 1953

The Representation of Gas Properties in Terms of Molecular Clusters*

HAROLD W. WOOLLEY
National Bureau of Standards, Washington, D. C.
(Received July 7, 1952)

The equation of state of a gas in virial form is derived from the equilibrium constants for the formation of molecular clusters. It is indicated that by choosing effective Lennard-Jones parameters independently for clusters of various numbers of molecules, the actual virial coefficients may be represented more satisfactorily. Results for the third virial coefficient are shown for A, N_2, CO, CO_2, CH_4, C_2H_4, CF_4, and Xe.

THE virial coefficients which occur in the equation

$$PV/RT=1+B/V+C/V^2+D/V^3+E/V^4+\cdots \quad (1)$$

are related to the equilibrium constants for the formation of clusters of molecules. In attempting to fit experimental virial coefficients to parameters representing intermolecular forces, it is necessary to recognize that the higher virials include contributions resulting from interactions among several different types of clusters. It would appear that the choice of force law parameters related to a given virial coefficient is most appropriately made in regard to the equilibrium constant for the formation of a cluster of the greatest number of molecules that is associated with the given virial coefficient, retaining such parameters for smaller clusters as were obtained from the data for the lower order virial coefficients.

The problem may be considered in the following manner. At low pressure for which the virial development applies strictly, the formation of clusters of n molecules of the gas X is in accord with the equation

$$nX \rightleftarrows X_n \quad (2)$$

for which the equilibrium constant K_n is given by

$$K_n=\frac{(PX_n)}{(PX)^n}, \quad (3)$$

where Px_n is the partial pressure due to the component made up only of clusters of n molecules.

Adding the partial pressures, the total pressure is obtained as

$$P=\sum_n(Px_n). \quad (4)$$

If V is molar volume for an ideal gas, then $1/V=P/RT$ is a representation of density in that it is proportional to the number of molecules per unit volume. The number of molecular clusters per unit volume for the general case under consideration is similarly proportional, for each size of cluster, to $(Px_n)/RT$. The contribution of each size cluster to the density is then proportional to $n(Px_n)/RT$. The total mass of gas in a given volume is the sum of the masses of its constituents, so the density is the sum of the densities of the various cluster components. Thus it is indicated that

$$\frac{1}{V}=\sum_{n=1} n(Px_n)/RT. \quad (5)$$

A question may possibly arise as to the use of the ideal gas law in regard to each component gas of clusters of a given size. The point to be made is that any non-ideality for such a component gas of clusters is due to the close approach between its individual clusters and either single molecules or other individual clusters, and during the time of close approach each combined cluster so formed is simply one of the larger clusters and is completely accounted for in that way. In the present attempt to represent how pressure depends on molecular aggregation, one notices that there is an ordinary effect of clustering occurring as an increase in concentration due to the presence of larger aggregates. A second effect is that in which the molecules exclude other molecules

* This work was supported in part by the National Advisory Committee for Aeronautics.

from given configurations of close approach. This second effect provides a contribution of reversed sign. The present treatment is closely related to a number of papers on the subject. A paper by Kahn and Uhlenbeck[1] presents a derivation of fundamental relations involved and includes a representation extending through the second and third virial coefficients equivalent to that to be obtained here.

From Eqs. (4) and (5), the compressibility factor is obtained directly as

$$\frac{PV}{RT}=\frac{\sum_n P_{X_n}}{\sum_n nP_{X_n}}. \tag{6}$$

Bringing in the definition of the equilibrium constants, this becomes

$$\frac{PV}{RT}=\frac{\sum_n K_n(P_X)^n}{\sum_n nK_n(P_X)^n}, \quad \text{with } K_1\equiv 1. \tag{7}$$

As the denominator is P_X times the derivative of the numerator with respect to P_X, and as the numerator is equal to the total pressure, P, Eq. (7) may be written as

$$\frac{PV}{RT}=\frac{P}{P_X(dP/dP_X)}=\frac{P}{P_X}\frac{dP_X}{dP}. \tag{8}$$

By inversion of the series $P=\sum K_n(P_X)^n$, a series for

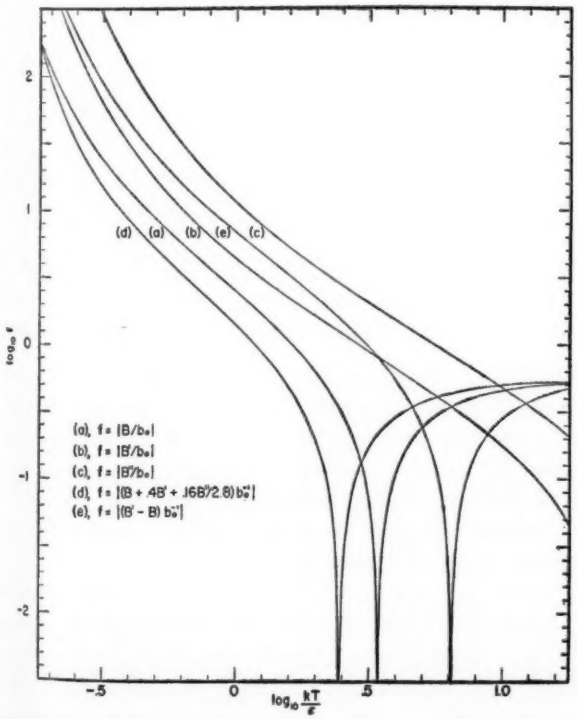

FIG. 1. Curves for the fitting of Lennard-Jones parameters for molecular pairs having 6–12 potentials.

[1] B. Kahn and G. E. Uhlenbeck, Physica 5, 399 (1938).

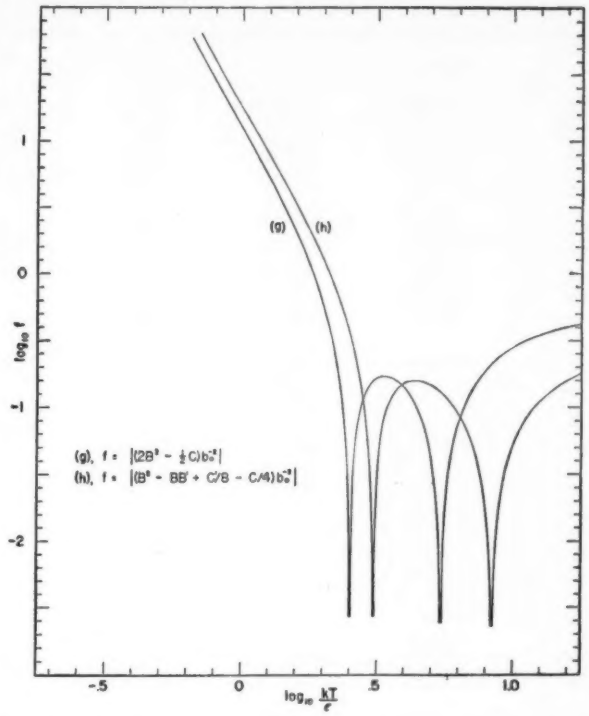

FIG. 2. Curves for the fitting of Lennard-Jones parameters for trimolecular clusters involving 6–12 pair potentials.

P_X is obtained:

$$\begin{aligned}P_X=P&-K_2P^2+(2K_2^2-K_3)P^3\\&+(-5K_2^3+5K_2K_3-K_4)P^4\\&+(14K_2^4-21K_2^2K_3+3K_3^2\\&\qquad+6K_2K_4-K_5)P^5+\cdots.\end{aligned} \tag{9}$$

Straightforward evaluation of Eq. (8) for PV/RT on the basis of this representation for P_X gives

$$\begin{aligned}PV/RT&\\=1&-K_2P+(3K_2^2-2K_3)P^2\\&+(-10K_2^3+12K_2K_3-3K_4)P^3\\&+(35K_2^4+10K_3^2-60K_3K_2^2+20K_2K_4-4K_5)P^4\\&+(-126K_2^5+280K_2^3K_3-105K_2K_3^2-105K_2^2K_4\\&\qquad+30K_3K_4+30K_2K_5-5K_6)P^5+\cdots.\end{aligned} \tag{10}$$

This can be compared with

$$\begin{aligned}PV/RT=1&+B(P/RT)+(C-B^2)(P/RT)^2\\&+(D-3BC+2B^3)(P/RT)^3\\&+(E-4BD-2C^2+10B^2C-5B^4)\\&\times(P/RT)^4+(F-5BE-5CD+15B^2D\\&\quad+15BC^2-35B^3C+14B^5)(P/RT)^5\cdots,\end{aligned} \tag{11}$$

giving

$$\begin{aligned}B&=-K_2RT\\C&=[4K_2^2-2K_3](RT)^2\\D&=[-20K_2^3+18K_2K_3-3K_4](RT)^3\\E&=[112K_2^4+18K_3^2-144K_3K_2^2\\&\qquad+32K_2K_4-4K_5](RT)^4\cdots.\end{aligned} \tag{12}$$

TABLE I. Calculated points for Figs. 1 and 2.

τ	$\log_{10}\tau$	(a)	(b)	(c)	(d)	(e)	(g)	(h)
0.2	−0.6989	2.0437	2.6677	3.4713	1.9713	2.7603		
0.25	−0.6021	1.6831	2.1997	2.9269	1.5203	2.3151		
0.3	−0.5229	1.4453	1.8843	2.5525	1.2463	2.0191		
0.4	−0.3979	1.1398	1.4810	2.0658	0.9212	1.6441		
0.5	−0.3010	0.9405	1.2285	1.7585	0.7183	1.4090		
0.6	−0.2218	0.7922	1.0511	1.5430	0.5675	1.2417		
0.7	−0.1549	0.6730	0.9168	1.3813	0.4444	1.1129	1.6633	1.8163
0.8	−0.0969	0.5722	0.8098	1.2539	0.3380	1.0081	1.4520	1.5989
0.9	−0.0458	0.4839	0.7214	1.1497	0.2425	0.9197	1.2679	1.4138
1.0	0	0.4045	0.6462	1.0622	0.1542	0.8430	1.1027	1.2512
1.1	0.0414	0.3317	0.5810	0.9871	0.0707	0.7750	0.9511	1.1052
1.2	0.0792	0.2639	0.5234	0.9215	−0.0097	0.7138	0.8092	0.9715
1.3	0.1139	0.1998	0.4719	0.8635	−0.0885	0.6578	0.6744	0.8472
1.4	0.1461	0.1386	0.4253	0.8114	−0.1669	0.6062	0.5443	0.7302
1.5	0.1761	0.0795	0.3828	0.7643	−0.2461	0.5581	0.4171	0.6188
1.6	0.2041	0.0220	0.3436	0.7214	−0.3276	0.5129	0.2909	0.5116
1.7	0.2304	−0.0345	0.3073	0.6819	−0.4127	0.4702	0.1641	0.4075
1.8	0.2553	−0.0904	0.2735	0.6454	−0.5035	0.4296	0.0344	0.3054
1.9	0.2788	−0.1462	0.2419	0.6115	−0.6028	0.3908	−0.1006	0.2043
2.0	0.3010	−0.2023	0.2122	0.5797	−0.7147	0.3536	−0.2447	0.1033
2.1	0.3222	−0.2591	0.1840	0.5500	−0.8466	0.3177	−0.4033	0.0014
2.2	0.3424	−0.3172	0.1573	0.5220	−1.0126	0.2829	−0.5865	−0.1028
2.3	0.3617	−0.3771	0.1320	0.4955	−1.2485	0.2492	−0.8160	−0.2106
2.4	0.3802	−0.4394	0.1076	0.4704	−1.7073	0.2163	−1.1570	−0.3241
2.5	0.3979	−0.5050	0.0848	0.4466	−1.8595	0.1842	−2.3089	−0.4460
2.6	0.4150	−0.5749	0.0626	0.4238	−1.3535	0.1527	−1.3445	−0.5807
2.7	0.4314	−0.6506	0.0415	0.4021	−1.1415	0.1218	−1.0773	−0.7355
2.8	0.4472	−0.7340	0.0210	0.3813	−1.0097	0.0913	−0.9478	−0.9255
2.9	0.4624	−0.8283	0.0013	0.3614	−0.9160	0.0613	−0.8720	−1.1882
3.0	0.4771	−0.9384	−0.0177	0.3423	−0.8444	0.0315	−0.8251	−1.6940

Parameters for the Lennard-Jones type forces between molecules may be obtained so as to give an approximate fit for a number of properties. Using formulas given by Lennard-Jones, various writers have tabulated values of the second virial coefficient for a pair energy of

$$V_2=4\epsilon[(r_0/r)^{12}-(r_0/r)^6].$$

Such a tabulation[2] including several derived quantities may be used in fitting the pressure dependence at low pressure for PV/RT, internal energy, specific heat, velocity of sound, and the value of the Joule-Thomson coefficient at low pressure. The method of selecting the parameter values is an extension of that used by Lennard-Jones, in which logarithms of the experimental and theoretical quantities are plotted against logarithms of the absolute temperature and of kT/ϵ, respectively. The experimental values on one sheet are compared with the theoretical values on another sheet by laying one sheet over the other and viewing them both at the same time, having a top sheet that is partly transparent. Using the abbreviations B' for TdB/dT and B'' for T^2d^2B/dT^2, the theoretical values to be plotted *vs* $\log_{10}kT/\epsilon$ are (a) for the compressibility, $\log_{10}|B/b_0|$; (b) for the internal energy, $\log_{10}|B'/b_0|$; (c) for the specific heat, $\log_{10}|B''/b_0|$; (d) for the sound velocity, $\log_{10}|b_0^{-1}[B+(\gamma^0-1)B'+B''(\gamma^0-1)^2/2\gamma^0]|$; and (e) for the Joule-Thomson coefficient; $\log_{10}|b_0^{-1}(B'-B)|$, b_0 being the usual value $2\pi Nr_0^3/3$. The quantity (d) is of use in such a plot if γ^0 is independent of temperature. The experimental data to be plotted *vs* $\log_{10}T$ are

$$\log_{10}|(1-PV/RT)RT/P|_{P=0},\quad \log_{10}|(E-E^0)/P|_{P=0},$$
$$\log_{10}|(C_p/R-C_p{}^0/R)RT/P|_{P=0},$$
$$\log_{10}|(a/a_0-1)RT/P|_{P=0},$$

and $\log_{10}\mu_0C_p{}^0$, respectively, where "a" is the velocity of sound. The super-position of the two graphs permits direct reading of $\log_{10}b_0$ and $\log_{10}\epsilon/k$ as the difference in numerical values for corresponding points on the graphs. This procedure also reveals directly the degree of theoretical consistency among a large body of experimental data of various kinds.

Values for the third virial coefficient for a 6-12 Lennard-Jones type gas have been given by Bird, Spotz, and Hirschfelder[3] together with first and second derivatives. Their values for the third virial coefficient when combined with values for the second virial coefficient, give equilibrium constants for the formation of a cluster

[2] H. W. Woolley and W. S. Benedict, forthcoming report, National Bureau of Standards.

[3] Bird, Spotz, Hirschfelder, J. Chem. Phys. 18, 1395 (1950).

TABLE I.—*Continued.*

τ	$\log_{10}\tau$	(a)	(b)	(c)	(d)	(e)	(g)	(h)
3.1	0.4914	−1.0736	−0.0361	0.3238	−0.7872	0.0020	−0.7960	−1.7786
3.2	0.5052	−1.2534	−0.0539	0.3061	−0.7402	−0.0273	−0.7793	−1.3271
3.3	0.5185	−1.5355	−0.0712	0.2889	−0.7006	−0.0565	−0.7716	−1.1418
3.4	0.5315	−2.3686 *	−0.0879	0.2724	−0.6667	−0.0857	−0.7710	−1.0332
3.5	0.5441	−1.7222	−0.1042	0.2564	−0.6373	−0.1148	−0.7761	−0.9614
3.6	0.5563	−1.3902	−0.1200	0.2408	−0.6115	−0.1440	−0.7859	−0.9112
3.7	0.5682	−1.2137	−0.1354	0.2258	−0.5886	−0.1733	−0.8000	−0.8750
3.8	0.5798	−1.0951	−0.1505	0.2111	−0.5682	−0.2028	−0.8179	−0.8488
3.9	0.5911	−1.0074	−0.1652	0.1969	−0.5500	−0.2326	−0.8392	−0.8300
4.0	0.6021	−0.9377	−0.1795	0.1831	−0.5333	−0.2628	−0.8643	−0.8166
4.2	0.6232	−0.8336	−0.2072	0.1565	−0.5045	−0.3243	−0.9251	−0.8025
4.4	0.6434	−0.7577	−0.2337	0.1313	−0.4803	−0.3881	−1.0020	−0.8005
4.6	0.6628	−0.6992	−0.2592	0.1072	−0.4597	−0.4552	−1.0995	−0.8072
4.8	0.6812	−0.6523	−0.2838	0.0842	−0.4420	−0.5264	−1.2271	−0.8204
5.0	0.6990	−0.6138	−0.3075	0.0621	−0.4266	−0.6033	−1.4077	−0.8390
5.2	0.7160	−0.5814	−0.3304	0.0409	−0.4131	−0.6881	−1.7153 *	−0.8622
5.4	0.7324	−0.5538	−0.3527	0.0205	−0.4012	−0.7836	−3.886	−0.8894
5.6	0.7482	−0.5300	−0.3743	0.0008	−0.3906	−0.8951	−1.7224	−0.9203
5.8	0.7634	−0.5092	−0.3953	−0.0181	−0.3812	−1.0320	−1.4299	−0.9550
6	0.7782	−0.4909	−0.4157	−0.0365	−0.3727	−1.2142 *	−1.2623	−0.9934
6.5	0.8129	−0.4535	−0.4647	−0.0800	−0.3549	−2.0477	−1.0201	−1.1086
7	0.8451	−0.4347	−0.5111	−0.1204	−0.3410	−1.1686	−0.8792	−1.2605
7.5	0.8751	−0.4020	−0.5553	−0.1582	−0.3298	−0.9285	−0.7833	−1.4799
8	0.9031	−0.3836	−0.5978	−0.1939	−0.3207	−0.7933	−0.7127	−1.8931 *
9	0.9542	−0.3560	−0.6784	−0.2598	−0.3071	−0.6366	−0.6149	−1.6325
10	1.0000	−0.3364	−0.7548	−0.3199	−0.2977	−0.5451	−0.5501	−1.2692
12	1.0792	−0.3114	−0.9003	−0.4272	−0.2864	−0.4408	−0.4707	−0.9953
14	1.1461	−0.2969	−1.0429	−0.5224	−0.2808	−0.3828	−0.4253	−0.8700
16	1.2041	−0.2881	−1.1902	−0.6094	−0.2783	−0.3462	−0.3973	−0.7972
18	1.2553	−0.2827	−1.3516	−0.6909	−0.2776	−0.3214	−0.3794	−0.7504
20	1.3010	−0.2795	−1.5427	−0.7685	−0.2781	−0.3039	−0.3677	−0.7183

*—— denotes discontinuity.

(a): $\log_{10}|B/b_0|$; (b): $\log_{10}|B'/b_0|$; (c): $\log_{10}|B''/b_0|$; (d): $\log_{10}\left|\left(B+0.4B'+\frac{0.16}{2.8}B''\right)\Big/ b_0\right|$; (e): $\log_{10}|(B-B')/b_0|$; (g): $\log_{10}|(2B^2-C/2)/b_0^2|$; (h): $\log_{10}|[B^2-BB'-C/4+C'/8]/b_0^2|$.

of three molecules in the following manner:

$$K_3=(b_0/RT)^2[2(B/b_0)^2-0.5C/b_0^2]. \quad (13)$$

The pressure dependence of the Joule-Thomson coefficient at low pressure furnishes data which can also be used similarly on the basis of the relations

$$\begin{aligned}-(RT)^2T dK_3/dT&=4B(B-B')-C+0.5C'\\&=0.5C_p^0RT(d\mu/dP)_0\\&\quad-(3B+0.5B''R/C_p^0)(B'-B) \quad (14)\end{aligned}$$

to determine the parameters for a cluster of three molecules. Thus if values of

$$\log_{10}|b_0^{-2}(2B^2-0.5C)|$$

and

$$\log_{10}|b_0^{-2}[B(B-B')-C/4+C'/8]|$$

(i.e., of $\log_{10}|(RT/b)^2K_3|$ and $\log_{10}|\frac{1}{4}(RT/b)^2TdK_3/dT|$) computed on the basis of the 6–12 Lennard-Jones potential are plotted against $\log_{10}kT/\epsilon$ and if on another sheet a plot against $\log_{10}T$ is made of

(g) $$\log_{10}|2B^2-C/2|$$

and of

(h) $$\log_{10}|C_p^0RT(d\mu/dP)_0/8-(3B/4+B''R/8C_p^0)(B'-B)|$$

or of the latter's equivalent

$$\log_{10}|(B'-B)[RT(d\mu/dP)_0/8\mu_0-3B/4-B''R/8C_p^0]|,$$

then the differences between abscissas and between ordinates of the theoretical and experimental curves when they are superposed gives $\log_{10}\epsilon/k$ and $2\log_{10}b_0$, from which ϵ/k and b_0 may be obtained directly for the cluster of three molecules and used for calculations of K_3 and its derivatives. In preparing these K_3 plots, it is appropriate to use the calculated values of B and its derivatives with experimental values of C, μ_0, and $(d\mu/dP)_0$.

It may be remarked that there is no basic theoretical reason why the parameters for the cluster of three should be identical with those for pairs. In fitting the best available experimental results for a number of molecules it has been found that by making quite small changes in the parameters for the cluster of three, the fit

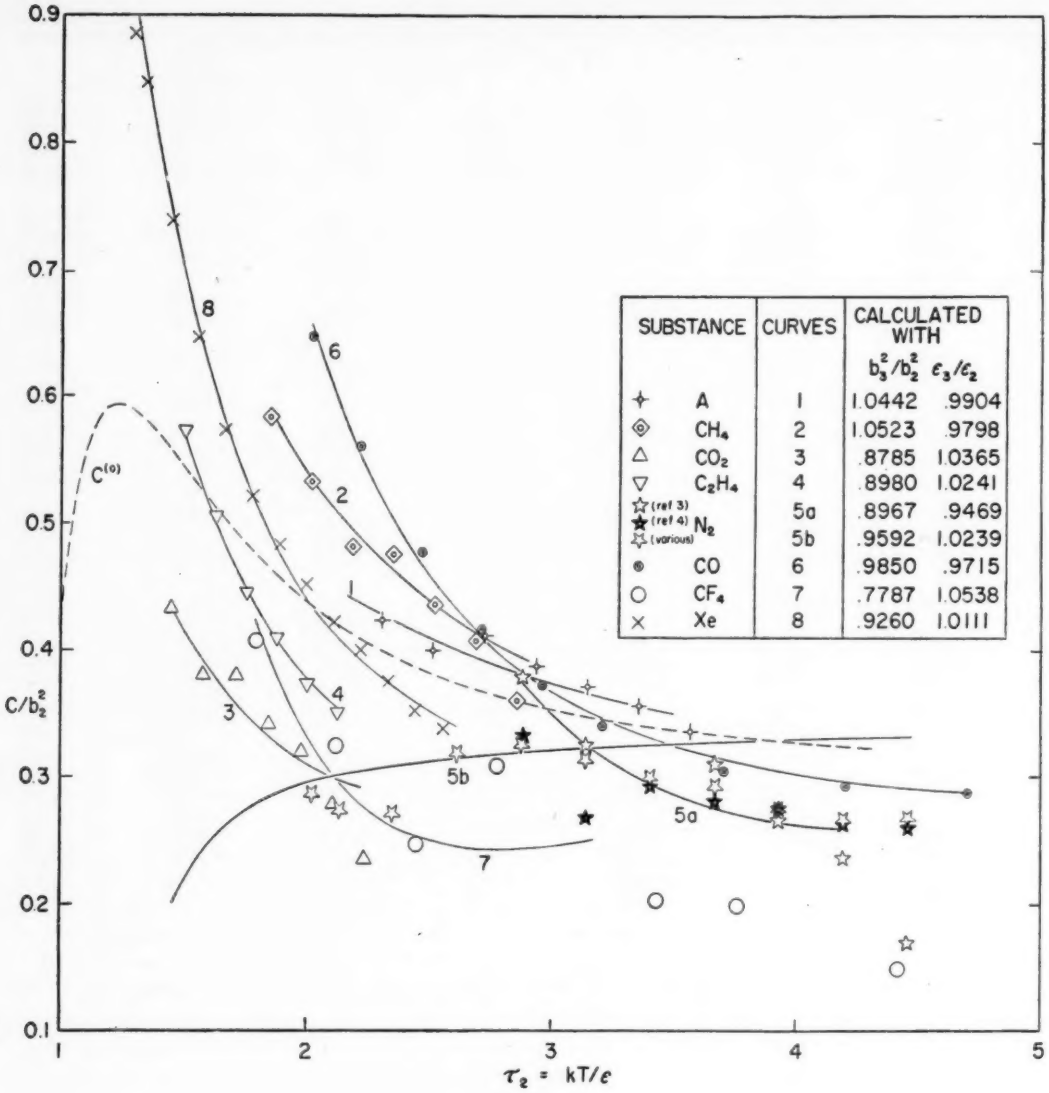

FIG. 3. Third virial coefficients.

for the third virial is markedly improved over that reported in reference 3. It is presumed that the detailed law of interaction is considerably more complicated than is indicated by the mere substitution of the differing effective Lennard-Jones parameters in regard to clusters of more than two in place of the parameters for single isolated pairs. Nevertheless, the cluster as a whole can have a natural size differing somewhat from that which would be calculated on the basis of the separation parameter for isolated pairs and the binding energy of the cluster may differ from that which would be estimated on the basis of compound pairs. The independent choice of parameters for clusters of more than two permits a closer representation of *PVT* data for gases which are not strictly of the Lennard-Jones type in regard to independence of pair energies.

The process might be extended to higher order clusters including more properties if theoretically calculated higher order virial coefficients and their derivatives were available based on the 6–12 potential. In principle, the process likewise is applicable to cases other than the 6–12 potential when the fundamental calculations have been made.

Figures 1 and 2 show, respectively, the course of theoretical values for observed quantities for clusters of two and of three Lennard-Jones type molecules having a 6–12 potential function and can be used in the determination of the parameters ϵ/k and b. Table I gives numerical values which may be plotted to obtain large scale graphs of Figs. 1 and 2 for the actual curve fitting. In Fig. 1, curve (d) is for a gas with $\gamma^0=1.40$.

Using b_3 and $\tau_3=kT/\epsilon_3$ for the cluster of three obtained in this way and b_2 and $\tau_2=kT/\epsilon_2$ for the cluster of two, the third virial coefficient by Eq. (12) is given in the notation of Bird, Spotz, and Hirschfelder as

$$C=b_3^2\{C^{(0)}(\tau_3)-4[B^{(0)}(\tau_3)]^2\}+4b_2^2[B^{(0)}(\tau_2)]^2. \quad (15)$$

The ability of this equation to represent actual third virial coefficients for nonpolar gases is shown by Fig. 3, which includes a dashed curve for the ordinary theo-

retical $C^{(0)}$ or C/b_0^2 and, for comparison, points for the experimental values of third virial coefficients for several gases, divided in each case by the square of b_2 or of the b_0 obtained for the second virial coefficient for the gas. This is similar to an illustration in the paper by Bird, Spotz, and Hirschfelder.[3] In addition, curves are also shown similarly representing the third virial coefficients as given by the preceding equation of this paper, with the parameters b_3 and ϵ_3 for the cluster of three selected for each gas by the method of Fig. 2, using the experimental values of the third virial coefficient. In the legend on the figure, the name of each gas is followed by the number of the corresponding curve, and the ratios b_3^2/b_2^2 and ϵ_3/ϵ_2 used for these curves. The values b_2 and ϵ_2/k as accepted for the present use will be found in Table II. It seems clear that the explanation for the shift of parameters for most molecules is to be found largely in their lack of spherical shape, as indicated by Bird, Spotz, and Hirschfelder.

In the case of N_2, values of the third virial coefficient as revised recently by Michels, Lunbeck, and Wolkers[4] are also shown in Fig. 3, together with values from the same and other sources as obtained in a graphical treatment by the present author. On the basis of the earlier data of Michels as used in reference 3, curve 5*a* was at first regarded as an appropriate representation. However, curve 5*b* was later used by the author[5] on the basis of these data and data at lower temperatures. More recent data by White[6] for the lower temperatures suggest that the best curve would be approximately in the position of curve 7.

Values of third virial coefficient for CO as obtained in a graphical analysis by Touloukian[7] using the PVT data in the literature are also shown. As in the case of N_2, the values obtained are somewhat affected by the choice made for the second virial coefficient. The dipole moment for CO is small enough to allow treatment as a nonpolar gas for the temperatures covered.

Figure 3 also shows values for CF_4 based on the work of MacCormack and Schneider[8,9] and for Xe based on the work of Beattie, Barriault, and Brierley.[10,11]†

It may be seen that Eq. (15) is fairly well adapted to the representation of third virial coefficients, as it is very sensitive to the adjustment of the effective parameters for the cluster of three molecules.

It is also evident that the curves obtained do not have so characteristic a shape as to determine values exactly by extrapolation far outside the range of actual experimental data, particularly in cases of molecules differing markedly from the monatomic, with appreciable deviations between experimental and theoretical values. In cases with poor representation of the data, a still more adjustable empirical representation might be tried. If one observes that the equilibrium constant for cluster formation may depend on more than two parameters, namely binding energy and the extent of phase space in which there is significant binding energy, one may include as a third parameter a measure of the extent of phase space from which cluster configurations are effectively excluded. Recognizing that this third quantity has some degree of independence of the other parameters, it may be permissible to allow for it as an additive constant both for clusters of three (with $K_3(RT)^2$ or $2B^2-C/2$) and also for pairs (with K_2RT or B).

TABLE II. Data concerning Lennard-Jones parameters for several gases.

Substance		b_2 (cm³/mole)	ϵ_2/k (°K)	b_3^2/b_2^2	ϵ_3/ϵ_2
A		49.804	119.75	1.0442	0.9904
CH_4		70.16	148.2	1.0523	0.9798
CO_2		113.9	189	0.8785	1.0365
C_2H_4		115.5	199.2	0.8980	1.0241
N_2	(a)	63.78	95.05	0.8967	0.9469
	(b)	63	95.42	0.9592	1.0239
	(c)	(63.78)	(95.05)	(0.7787)	(1.0538)
CO		69.22	100.78	0.9850	0.9715
CF_4		131.0	152.5	0.7787	1.0538
Xe		84.65	224.5	0.9260	1.0111

[4] Michels, Lunbeck, and Wolkers, Physica **17**, 801 (1951).
[5] H. W. Woolley, Table 11.20, "The NBS–NACA Thermal Tables Project," Ref. W-5358.
[6] D. White, private communication.
[7] Y. S. Touloukian, Table 14.20, "The NBS–NACA Tables of Thermal Properties of Gases," National Bureau of Standards, September, 1950.
[8] K. E. MacCormack and W. G. Schneider, J. Chem. Phys. **19**, 849 (1951).
[9] K. E. MacCormack and W. G. Schneider, J. Chem. Phys. **19**, 845 (1951).
[10] Beattie, Barriault, and Brierley, J. Chem. Phys. **19**, 1219 (1951).
[11] Beattie, Barriault, and Brierley, J. Chem. Phys. **19**, 1222 (1951).

† *Note added in proof.*—Similarly for krypton, 99 percent pure, $\epsilon_2/k=169$°K, $b_2=61$ cm³/mole, $\epsilon_3/\epsilon_2=0.9704$ and $b_3^2/b_2^2=1.0836$, based on their data in J. Chem. Phys. **20**, 1615 (1952), omitting their four highest temperatures.

Substituted Methanes. X.* Infrared Spectral Data, Assignments, Potential Constants, and Calculated Thermodynamic Properties for CF_3Br and CF_3I†

PAUL R. MCGEE,‡ FORREST F. CLEVELAND, ARNOLD G. MEISTER, AND CHARLOTTE E. DECKER,
Spectroscopy Laboratory, Department of Physics

AND

SIDNEY I. MILLER, *Department of Chemistry, Illinois Institute of Technology, Chicago 16, Illinois*
(Received August 19, 1952)

Infrared wave numbers, relative intensities, and percent transmission curves have been obtained for CF_3Br and CF_3I in the region 400–2200 cm^{-1}. Assignments are given for the observed bands, in which the assignments of Plyler and Acquista for ν_2 and ν_3 are interchanged. Potential constants were calculated for both molecules by the Wilson *FG* matrix method. And, finally, the heat content, free energy, entropy, and heat capacity for the ideal gaseous state at 1 atmos pressure were calculated for 12 temperatures from 100°to 1000°K, using a rigid rotator, harmonic oscillator approximation.

INFRARED spectral curves[1] or numerical data[2–4] have been obtained in four investigations, but no normal coordinate treatment has been reported. The present paper contains a comparison of the various sets of infrared data, a list of probable values, a revised assignment, and the results of normal coordinate treatments for the two molecules.

EXPERIMENTAL

The method of preparation of the samples was given previously.[2] The infrared spectra were obtained with the sample in the gaseous state, using a Beckman IR-2 spectrophotometer with KBr optics. The cell length was 10 cm and several records for various pressures were obtained. Bands were found in the region 400–2200 cm^{-1}. The percent transmission curves are shown in Figs. 1 and 2.

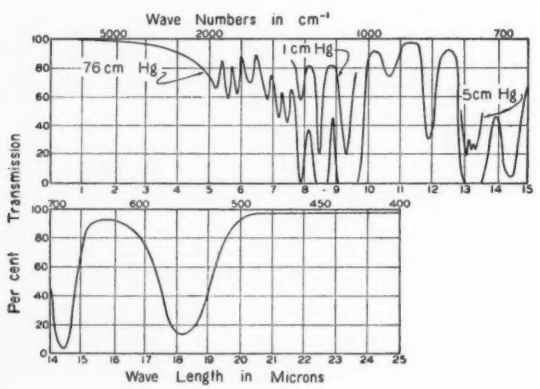

FIG. 1. Percent transmission curve for CF_3Br.

INFRARED SPECTRAL DATA

CF_3Br

The present infrared spectral data are compared with those of the previous workers in Table I, and probable values are adopted. In our work, bands observed at 731, 721, 649, and 616 cm^{-1} were later shown to originate from CO_2, a by-product trapped in the sample during the preparation process. Reference to Table I shows that Polo and Wilson reported a band at 649, which was not observed in the other two investigations, and that both Plyler and Acquista, and Polo and Wilson, reported a band near 734 cm^{-1}. It is possible, therefore, that these two bands belong to CO_2 rather than to CF_3Br.

The values of the two lowest fundamentals, ν_3 and ν_6, were obtained, in our work, indirectly from binary combinations or first overtones. For ν_3, five of these gave 350±6 cm^{-1}, while for ν_6 seven binary combinations gave 297±3 cm^{-1}. It is interesting to note that these values are identical with those obtained by Polo and Wilson, also by use of combination frequencies. In

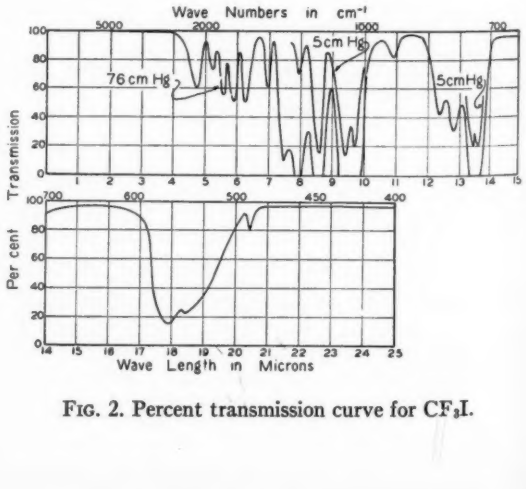

FIG. 2. Percent transmission curve for CF_3I.

* For previous papers in this series see J. Chem. Phys. **18**, 346, 1073, 1076, 1081 (1950); **19**, 119, 784, 1561 (1951); **20**, 454, 1949 (1952).

† Part of a research program aided by a grant from the American Academy of Arts and Sciences, and by a contract (DA-11-022-ORD-464) with the Office of Ordnance Research.

‡ An investigation completed in partial fulfillment of the requirements for the Master of Science degree. Present address: Magnolia Petroleum Company, Dallas, Texas.

[1] Hauptschein, Nodiff, and Grosse, J. Am. Chem. Soc. **74**, 1347 (1952).

[2] McGee, Cleveland, and Miller, J. Chem. Phys. **20**, 1044 (1952).

[3] E. K. Plyler and N. Acquista, J. Research Natl. Bur. Standards **48**, 92 (1952).

[4] S. R. Polo and M. K. Wilson, J. Chem. Phys. **20**, 1183 (1952).

TABLE I. Infrared spectral data, assignments, and calculated wave numbers for gaseous CF_3Br.[a]

Plyler and Acquista ν	I	Polo and Wilson ν	Present results ν	I	Probable values ν	ν_c	Theoretical Assignment	Type
180[b]	...	297[c]	297[c]	...	**297**	**300**	ν_6	e^g
348	vw	350[c]	350[c]	...	**348**	**348**	ν_3	a_1
470	vw	...	...	...	*470*[e]	*465*	$\nu_2-\nu_6$	E
550	w	548	547	m	**548**	**547**	ν_5	e
...	...	649	...	...	*649*[e]	*645*	$\nu_3+\nu_6$	E
689	m	...	692	s	*694*	*696*	$2\nu_3$	A_1
700	m	700						
735	m	733	...	...	*734*[e]	*739*	$\nu_1-\nu_3$	A_1
754	s	764	754	vs	**762**	**761**	ν_2	a_1
761			760					
767			768					
826	w	...	...	...	*830*[e]	*833*[f]	$(\nu_1+\nu_6)-\nu_5$	A_1+A_2+E
830								
833								
849	w	848	848	m	*848*	*845*	$\nu_5+\nu_6$	A_1+A_2+E
915	vw	910	...	...	*912*	*910*	$\nu_4-\nu_6$	A_1+A_2+E
949	vw	...	950	w	*949*	*942*	$\nu_3+2\nu_6$	A_1+E
1085	s	1087	1089	vs	**1087**	**1089**	ν_1	a_1
1121	m	1120	...	...	*1120*	*1110*	$\nu_2+\nu_3$	A_1
1173	m	...	...	...	*1173*[e]	*1176*	$2\nu_2-\nu_3$	A_1
1206	vs	1206	1210	vs	**1207**	**1210**	ν_4	e
1305	m	1304	1308	s	*1305*	*1310*	$\nu_2+\nu_5$	E
1383	w	1381	1379	w	*1381*	*1384*	$\nu_1+\nu_6$	E
1426	w	1429	1424	w	*1426*	*1435*	$\nu_1+\nu_3$	A_1
1470	w	1470	...	...	*1470*	*1456*	$\nu_2+2\nu_3$	A_1
1507	w	1503	1501	w	*1504*	*1504*	$\nu_4+\nu_6$	A_1+A_2+E
1626	w	1625	1622	w	*1624*	*1635*	$\nu_1+\nu_5$	E
1754	w	1755	1747	w	*1754*	*1755*	$\nu_4+\nu_5$	A_1+A_2+E
1844	w	1843	1839	w	*1843*	*1849*	$\nu_1+\nu_2$	A_1
...	...	1863	...	...	*1863*	*1865*	$(2\nu_1)-\nu_6$	E
1886	w	1882	...	...	*1884*	*1901*	$(2\nu_3)+\nu_4$	E
1960	w	1962	1961	w	*1961*	*1969*	$\nu_2+\nu_4$	E
2164	vw	2160	...	...	*2162*	*2174*	$2\nu_1$	A_1
...	...	2177	...	...	*2177*	*2183*	$\nu_1+2\nu_5$	A_1+E
...	...	2198	...	...	*2198*	*2191*	$(\nu_1+\nu_2)+\nu_3$	A_1
2282	m	2281	...	...	*2281*	*2294*	$\nu_1+\nu_4$	E
...	...	2315	...	...	*2315*	*2327*	$(\nu_2+\nu_3)+\nu_4$	E
2392	m	2399	...	...	*2395*	*2414*	$2\nu_4$	A_1+E
...	...	2510	...	...	*2510*	*2509*	$(\nu_2+\nu_4)+\nu_5$	A_1+A_2+E
...	...	2830	...	...	*2830*	*2829*	$(\nu_1+\nu_4)+\nu_5$	A_1+A_2+E
...	...	2935	...	...	*2935*	*2943*	$(2\nu_4)+\nu_5$	A_1+A_2+2E
...	...	3360[d]	...	...	*3360*[d]	*3369*	$(2\nu_1)+\nu_4$	E
...	...	3475[d]	...	...	*3475*[d]	*3482*	$\nu_1+(2\nu_4)$	A_1+E
...	...	3590[d]	...	...	*3590*[d]	*3602*	$3\nu_4$	A_1+A_2+E

[a] ν = wave number in cm^{-1}; I = relative intensity (w = weak, m = medium, s = strong, v = very); and ν_c = calculated wave number.
[b] Stepanov's calculated value. (B. I. Stepanov, Compt. rend. acad. sci. U.R.S.S. **45**, 56 (1944).
[c] Determined from overtone and combination bands.
[d] Approximate values.
[e] These bands may be caused by impurities.
[f] The *observed* values of the combinations and overtones—given within the parentheses—were used in calculating the wave numbers of the higher combination bands.
[g] In line with the recent proposal of R. S. Mulliken (private communication, July 31, 1952) and the practice of G. Herzberg, *Infrared and Raman Spectra* (D. van Nostrand Company, 1945), first edition, Chapter III, the fundamentals are designated by lower case letters.

our work, the region below 400 cm^{-1} was beyond the range of the KBr instrument. However, both Plyler and Acquista, and Polo and Wilson, used prisms which permitted them to cover this region, and at first glance it seems strange that neither investigation yielded a direct value for ν_3. However, Plyler and Acquista state that they could not observe weak bands in the region 275–400 cm^{-1} (the region of the broken lines in their absorption curve) because of atmospheric bands, so if ν_3 is a weak band it could have been overlooked; and Polo and Wilson not only did not observe ν_3, but also did not record the 348 band obtained by Plyler and Acquista. So it still appears probable that ν_3 is near 297 cm^{-1}, despite the failure to observe it directly in the two investigations. Stepanov's calculated value of 180 cm^{-1} for ν_6, listed by Plyler and Acquista, seems definitely to be too low.

CF_3I

The present and previous infrared spectral data for CF_3I are compared in Table II. Again, the fundamentals ν_3 and ν_6 were obtained indirectly by us, using only first overtones and binary combinations; the results were $\nu_3 = 286 \pm 3$ (observed value 284) and $\nu_6 = 260 \pm 3$ cm^{-1}. Polo and Wilson also obtained these two wave numbers from combinations and overtones; their values were 290 and 265 cm^{-1}, slightly different from ours. Plyler and Acquista observed ν_3 directly, but from overtone and

combinations predicted a value of 163 cm^{-1} for ν_6. This seems certainly to be too low.

ASSIGNMENTS

The assignments for CF_3Br, included in Table I, agree with those given very recently by Polo and Wilson,[4] except for a few relatively unimportant bands. The assignments of Plyler and Acquista do not agree as well. This is in part the result of the low value adopted by them for the lowest fundamental ν_6. Besides this, they considered the 762 band to correspond to the C—Br stretching vibration, and the 348 band to correspond to a CF_3 deformation. Our normal coordinate treatment shows clearly, however, that these assignments must be reversed.

The probable values of the wave numbers corresponding to the fundamental vibrational frequencies of CF_3Br are compared with those for other substituted methanes containing three or more *F* atoms in Table III.

For CF_3I, also, our assignment of the fundamentals and of most of the combination and overtone bands was in agreement with that of Polo and Wilson. Comparing with the assignments of Plyler and Acquista, however, one sees that again their value of ν_6 is too low; and that the 743 band should correspond to a CF_3 deformation, the 284 band to a C—I stretching vibration—rather than the reverse, as in their assignment.

The probable values of the fundamentals for CF_3I also are listed in Table III, in comparison with other CF_3X compounds.

TABLE II. Infrared spectral data, assignments, and calculated wave numbers for gaseous CF_3I.[a]

Plyler and Acquista ν	Plyler and Acquista I	Polo and Wilson ν	Present results ν	Present results I	Probable values ν	ν_6	Theoretical Assignment	Type
163[b]	...	265[b]	260[b]	...	**260**[b]	**261**	ν_6	e
284	w	290[b]	286[b]	...	**284**	**280**	ν_3	a_1
448	w	457	...	...	*453*	*459*	$\nu_2-\nu_3$	A_1
...	...	...	518	vw	*518*	*520*	$2\nu_6$	A_1+E
		540	537	m	**539**	**537**	ν_5	e
550	m							
		563[c]	560	m	*561*	*558*	$\nu_1-(2\nu_6)$	A_1+E
...	...	575[c]	...	...	*575*	*568*	$2\nu_3$	A_1
711	vw	...	...	...	*711*[d]	*734*	$(\nu_2+\nu_5)-\nu_5$	A_1+A_2+E
735			737					
740	s	746	742	vs	**743**	**742**	ν_2	a_1
746			747					
776	vw	782	777	m	*778*	*778*	$3\nu_6$	A_1+A_2+E
820	w	813	811	m	*812*[e]	*816*	$\nu_1-\nu_6$	E
916	vw	920	924	w	*920*	*925*	$\nu_4-\nu_6$	A_1+A_2+E
...	...	949	...	...	*949*[d]	*947*	$2\nu_2-\nu_5$	E
1020	m							
1025	m	1027	1030	s	*1027*	*1027*	$\nu_2+\nu_3$	A_1
1031								
1068								
1073	vs	1076	1080	vs	**1076**	**1080**	ν_1	a_1
1080								
1114	w	...	...	...	*1114*[d]	*1114*	$(2\nu_3)+\nu_5$	E
...	...	1173	...	...	*1173*[d]	*1182*	$(\nu_4+\nu_5)-\nu_5$	A_1+A_2+3E
1186	vs	1183	1187	vs	**1185**	**1187**	ν_4	e
1246	m	1273	1274	s	*1273*	*1282*	$\nu_2+\nu_5$	E
1329	w	1336	1334	w	*1333*	*1336*	$\nu_1+\nu_6$	E
...	...	1359	...	...	*1359*	*1360*	$\nu_1+\nu_3$	A_1
1443	vw	1444	1441	w	*1443*	*1445*	$\nu_4+\nu_6$	A_1+A_2+E
1605	w	1609	1611	w	*1608*	*1615*	$\nu_1+\nu_5$	E
1721	w	1722	1714	w	*1721*	*1724*	$\nu_4+\nu_5$	A_1+A_2+E
...	...	1775	...	...	*1775*	*1770*	$2\nu_2+\nu_3$	A_1
1818	vw	1816	1814	w	*1816*	*1819*	$\nu_1+\nu_2$	A_1
1915	w	1921	1910	w	*1915*	*1928*	$\nu_2+\nu_4$	E
2100	vw	2100	...	...	*2100*	*2100*	$(\nu_1+\nu_2)+\nu_3$	A_1
2141	w	2142	2132	vw	*2141*	*2152*	$2\nu_1$	A_1
2197	vw	2202	...	...	*2200*	*2212*	$(\nu_2+\nu_3)+\nu_4$	E
2246	m	2250	...	...	*2248*	*2261*	$\nu_1+\nu_4$	E
2336	w	2354	...	...	*2348*	*2370*	$2\nu_4$	A_1+E
2438	vw	2459	...	...	*2452*	*2454*	$(\nu_2+\nu_4)+\nu_5$	A_1+A_2+E
...	...	2776	...	...	*2776*	*2787*	$(\nu_1+\nu_4)+\nu_5$	A_1+A_2+E
2898	vw	2890	...	...	*2893*	*2887*	$(2\nu_4)+\nu_5$	A_1+A_2+2E
...	...	3315[c]	...	...	*3315*	*3326*	$(2\nu_1)+\nu_4$	E
3400	vw	3420[c]	...	...	*3410*	*3424*	$\nu_1+(2\nu_4)$	A_1+E
3495	vw	3530[c]	...	...	*3510*	*3533*	$3\nu_4$	A_1+A_2+E

[a] Symbols have same meaning as in Table I.
[b] Determined from overtone and combination bands.
[c] Approximate values.
[d] These bands may be caused by impurities.
[e] Can also be assigned as $\nu_5+\nu_6=799$ or $\nu_3+\nu_5=823$. The mean of these two values is 811; observed 812.

TABLE III. Probable values of the wave numbers and degeneracies corresponding to the fundamental vibrational frequencies of tetrafluoromethane and the trifluoromethanes.

Description	Type	Degeneracy	CF_3H	CF_3D[a]	CF_3Cl	CF_3Br	CF_3I	CF_4	Degeneracy	Type
CF_3 deformation	e	2	*508*[b]	*496*	560[c]	548[c]	539[c]	*437*	2	e
CF_3 deformation	a_1	1	*697*	*687*	783[c]	762[c]	743[c]	630[c]	3	f_2
C–F stretching	a_1	1	*1117*	*1080*	1102[c]	1087[c]	1076[c]	*904*	1	a_1
C–F stretching	e	2	*1160*	*988*	1210[c]	1207[c]	1185[c]	1265[c]	3	f_2
C–X bending	e	2	*1376*	*1210*	*356*	297[c,d]	260[c,d]			
C–X stretching	a_1	1	*3062*	*2288*	*478*	348[c,d]	284[c,d]			

[a] Calculated values.
[b] Wave numbers in cm^{-1}.
[c] Values for the gaseous state.
[d] Obtained from binary combinations and 1st overtones.

NORMAL COORDINATE TREATMENTS

As a check on the assignments, as well as to obtain information about the potential functions for the two molecules, normal coordinate treatments were carried out, using the Wilson *FG* matrix method and a quadratic potential energy expression containing as many terms as possible (see Paper I,[5] p. 352). The symmetry coordinates and the *G* matrices for the CY_3X type molecule have been given previously.[6] Also, the *F* matrices are somewhat the same as those obtained previously[6] and will not be repeated here, for once the form of the potential energy function and symmetry coordinates are known, they can be found very simply by the method already described.[6]

The notation for the potential constants is the same as that introduced in paper VIII.[7] Some of the potential constants (f_δ, $f_\delta{}'$, $f_\delta{}''$, and $f_{\delta\delta}$) were transferred from other CF_2X molecules.[8] Others were evaluated from the observed values of the fundamentals. The final set of constants, which yields the calculated wave numbers included in Tables I and II, is given in Table IV.

During the investigation, it was found that changing the C–X (X=Br or I) stretching constant f_x produced a definite change in the 348 wave number for CF_3Br (or 284 for CF_3I), and not in the 762 (or 743), as should have been the case if the latter corresponds to the C–X stretching frequency as previously assigned. Consequently, the 348 and 284 cm^{-1} bands are now assigned to the C–Br and the C–I stretching frequencies in CF_3Br and CF_3I, respectively, while the 762 and 743 bands are assigned to CF_3 deformation frequencies in the two molecules. The assignments of the 478 and 783 cm^{-1} bands in CF_3Cl (previously investigated) have now been interchanged (Table III) for the same reason.

It was also found that, in order to obtain a value for ν_6 as low as that given by Plyler and Acquista (who followed Stepanov for CF_3Br), it would be necessary to make the F–C–X (X=Br or I) bending constant $f_{x\delta}$ much smaller than seems possible. Furthermore, Stepanov's calculated values (see reference given under Table I) for CF_3Br do not agree well with observed values for any of the other fundamentals, except ν_3, so there is no reason to expect that his value of ν_6 is any more accurate. The potential energy function used by him was not as general as that used in the present work, so his calculated values could not be expected to be as reliable. The normal coordinate treatment thus supports the values previously given for ν_6 for the two molecules.

THERMODYNAMIC PROPERTIES

Using the probable values of the fundamentals given in Table III, the heat content, free energy, entropy, and heat capacity for the ideal gaseous state at 1 atmos pressure were calculated for both molecules for 12 temperatures from 100 to 1000°K, assuming a rigid rotator, harmonic oscillator approximation. The moment of inertia $I_{xx}=I_{yy}$ was taken as 242.1 awu A^2 for CF_3Br and 331.9 for CF_3I, from the microwave work of Sheridan and Gordy.[9] Using their C–F bond distance, 1.326A, I_{zz} was calculated to be 89.08 awu A^2. Birge's 1941 values of the physical constants, and a symmetry number of 3, were used. The calculated values are given in Tables V and VI.

TABLE IV. Potential constants for CF_3Br and CF_3I.[a]

Type[b]	CF_3Br	CF_3I
f_r	6.2460	6.2460
f_x	3.0352	2.2890
$f_r{}'$	0.87900	0.87900
$f_x{}'$	0.71247	0.63250
$f_r{}''$	0.41770	0.41770
$f_r{}''{}'$	−0.22339	−0.22339
$f_r{}^{x\prime}$	0.24665	0.29545
$f_r{}^{x\prime\prime}$	−0.09272	−0.11430
$f_\alpha{}'' - f_\alpha{}^{x\prime}$	−0.46499	−0.3640
$f_{x\delta}$	0.73841	0.51360
$f_{\delta\delta}$	2.1329	2.1329
$f_{x\delta}{}^{x\prime}$	−0.23225	−0.28590
$f_{\delta\delta}{}''$	0.57700	0.6392
$f_{x\delta}{}''$	0.0500	0.0300
$f_{x\delta}{}''{}'$	0.0000	0.0000

[a] Bond stretching constants are in md/A; bond-angle interaction constants are in md/rad; and angle-angle interaction, or angle bending constants, are in md A/rad^2.
[b] $x=b$ for CF_3Br and i for CF_3I.

[5] Meister, Rosser, and Cleveland, J. Chem. Phys. 18, 346 (1950).
[6] A. G. Meister and F. F. Cleveland, Am. J. Phys. 14, 13 (1946).
[7] Davis, Cleveland, and Meister, J. Chem. Phys. 20, 454 (1952).
[8] Decker, Meister, and Cleveland, J. Chem. Phys. 19, 784 (1952).
[9] J. Sheridan and W. Gordy, Phys. Rev. 77, 292 (1950).

TABLE V. Heat content, free energy, entropy, and heat capacity of CF_3Br for the ideal gaseous state at 1 atmos pressure.[a]

T	$(H^0-E_0^0)/T$	$-(F^0-E_0^0)/T$	S^0	C_p^0
100	8.27	49.11	57.37	9.42
200	9.89	55.30	65.20	13.51
273.16	11.19	58.58	69.77	15.88
298.16	11.61	59.58	71.19	16.58
300	11.64	59.65	71.30	16.63
400	13.20	63.22	76.42	18.95
500	14.52	66.31	80.83	20.63
600	15.65	69.06	84.71	21.82
700	16.59	71.55	88.14	22.68
800	17.39	73.81	91.21	23.30
900	18.08	75.88	93.96	23.76
1000	18.66	77.84	96.51	24.12

[a] In this and the following table, T is in °K, and the other quantities are in cal deg^{-1} mole^{-1}.

TABLE VI. Heat content, free energy, entropy, and heat capacity of CF_3I for the ideal gaseous state at 1 atmos pressure.

T	$(H^0-E_0^0)/T$	$-(F^0-E_0^0)/T$	S^0	C_p^0
100	8.46	50.61	59.07	10.02
200	10.30	57.02	67.32	14.03
273.16	11.61	60.43	72.04	16.29
298.16	12.03	61.47	73.50	16.95
300	12.06	61.54	73.60	17.00
400	13.59	65.23	78.81	19.22
500	14.88	68.40	82.28	20.84
600	15.98	71.21	87.19	21.99
700	16.90	73.75	90.65	22.81
800	17.68	76.06	93.73	23.41
900	18.34	78.18	96.52	23.86
1000	18.91	80.13	99.04	24.19

ACKNOWLEDGMENT

Trifluoroacetic acid, a starting material in the preparation of CF_3Br and CF_3I, was kindly supplied by the Minnesota Mining and Manufacturing Company.

Note added in proof:—W. F. Edgell and C. E. May [J. Chem. Phys. **20**, 1822 (1952)] have very recently reported both Raman and infrared spectral data for both CF_3Br and CF_3I. Their results and assignments are in essential agreement with ours. It is especially interesting to note that their lowest Raman fundamental ν_6 for the liquid appeared at 305 for CF_3Br and at 265 for CF_3I, as compared with our values of 297 and 260 cm^{-1} deduced from combinations and overtones for the gas, neglecting effects arising from the anharmonicity.

THE JOURNAL OF CHEMICAL PHYSICS VOLUME 21, NUMBER 2 FEBRUARY, 1953

On Drickamer's Modification of the Theory of the Thermal Diffusion Column

KOZO HIROTA AND YASUSHI KOBAYASHI

Research Institute of Applied Electricity, Hokkaido University, Sapporo, Japan

(Received July 1, 1952)

By use of thermal diffusion columns, the N_2-H_2 system has been separated continuously and its thermal diffusion ratio α has been determined with a method of least ambiguity under a pressure range of 1∼12.6 atmos. The α-values thus obtained, based on the Furry-Jones theory of the apparatus, have been found to be not constant and also to differ very much in most cases from those hitherto reported. However, the values corrected according to the theory modified by Drickamer *et al.* have been shown to be reasonable, supporting their modified theory.

I. INTRODUCTION

ATTEMPTS have often been made to determine[1] thermal diffusion factor α from the concentrations at the top (c_t) and at the bottom (c_b) of the thermal diffusion column. Because the constant is related to the separation factor q_e, i.e., $c_t(1-c_b)/c_b(1-c_t)$, c's being expressed in mole fraction, q_e for the diffusion column of length L is theoretically given by the following formula:

$$\ln q_e = 2LH/(K_c+K_d), \qquad (1)$$

where K_c, K_d, and H which is proportional to α, are, respectively, the factors of vertical convection, of vertical diffusion, and that concerned with horizontal diffusion and thermal diffusion. These factors are functions of several variables, concerning the system to be separated, operating conditions, and size of apparatus, as will be defined by Eq. (3).

It is generally accepted that this relation can be applied qualitatively when the above variables are changed, but also that it is quantitatively not justified in some cases. Among the cases of discrepancy, the most important example is that experimental points measured at several pressures cannot be fitted by Eq. (1)[2] if some numerical constants are not multiplied into the terms K_c, K_d, and H. A similar conclusion is drawn from the experiments of other researchers. Considering the situation, it seems natural to modify the theory as did Simon,[3] or Drickamer *et al*,[4] who took into considera-

[1] For example, R. C. Jones and W. H. Furry, Revs. Modern Phys. **18**, 151 (1946); Furry, Jones, and Onsager, Phys. Rev. **55**, 1083 (1940).

[2] A. O. Nier, Phys. Rev. **56**, 1009 (1940).

[3] R. Simon, Phys. Rev. **69**, 596 (1946).

[4] Drickamer, Mellow, and Tung, J. Chem. Phys. **18**, 945 (1950).

tion the effect of turbulence on the laminar flow in the column. However, there is opposition to the theory modified by Drickamer, although it seems to be supported by their separate reports published in succession;[5] for example, according to Becker[6] the discrepancy can be explained by the introduction of pressure variation of α, while Darenport and Winter[7] consider it to be brought about by the parasitic effect of the apparatus.

As such a divergence of the theory of the column is an important problem in studying the thermal diffusion under high pressure, it is the object of the present report to settle the matter in question. To meet the requirement, thermal diffusion in the H_2-N_2 system, the α of which does not change markedly with the pressure according to Becker, was studied over a pressure range of 1∼12.6 atmos.

II. METHOD OF DETERMINATION OF α

As shown by the schematic diagram (Fig. 1), the original gas to be separated is introduced from the top and the bottom, making the flow velocity of the bottom outlet small as compared with that of the top one.

According to the theory of the column, net transport τ of the heavy component in grams per second to the downward direction z will be given, provided that the laminar flow is preserved in the column, by the algebraic sum of terms including H, K_c, and K_d, i.e.,

$$\tau \equiv vdc = Hc(1-c)+(K_c+K_d)/(-dc/dz), \qquad (2)$$

where dc denotes the concentration increase of the heavy component between two positions of interval dz; v is the flow velocity (in grams per second) of the gas flowing out from the bottom outlet; and H, K_c, and K_d are given by*

$$H=\frac{\alpha\rho\rho_0 w^3 gB}{90\eta}\left(\frac{\Delta T}{T}\right)^2, \quad K_c=\frac{\rho_0\rho^2 g^2 w^7 B}{2835\eta^2 D}\left(\frac{\Delta T}{T}\right)^2,$$

$$K_d=2wB\rho_0 D, \qquad (3)$$

where ρ_0 = density of the original gas, ρ, η = density, viscosity of the gas in the column, g = acceleration of the gravity, $2w$ = wall distance, T = mean temperature, ΔT = temperature difference, and B = horizontal wall length. The numerical constants (90 and 2835) adopted in the terms H and K_c are those for the case when ΔT is small (see Eqs. (70), (71), and (72) of Jones and Furry[1]), so as to be applicable to the data in the present report. The introduction of a new constant ρ_0 is necessary when difference of molecular weights of the components is large. However, it can be made equal to ρ in such a case of isotopic gases.

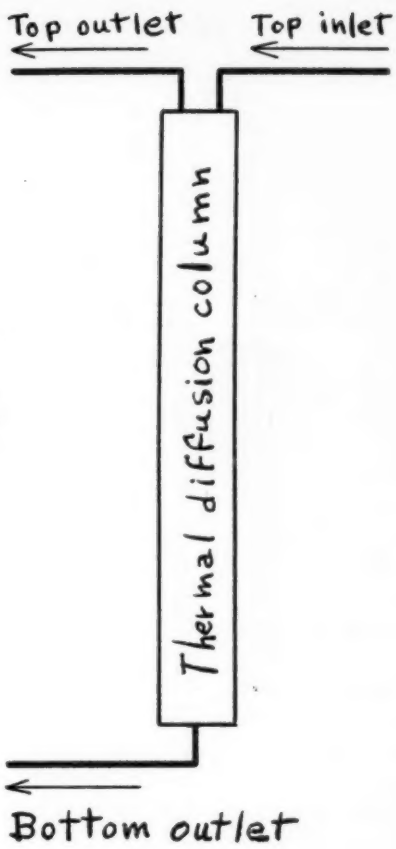

FIG. 1. Schematic diagram of operating the thermal diffusion column.

If we assume that dc/dz is constant and that $c(1-c)$, ρ, and η can be replaced by their mean values of the gas in the column, Eq. (2) can be transformed by integration into

$$v'=\frac{H}{\rho_0}\cdot\frac{c(1-c)}{c_b-c_t}-\frac{(K_c+K_d)}{\rho_0 L}, \qquad (4)$$

where v' is the flow velocity in cc per sec. Equation (4) will, therefore, be applied provided that c_b-c_t is small.

If η/ρ does not vary with composition, as is realized in cases of isotopic gases, H/ρ_0 and $(K_c+K_d)/\rho_0$ can be regarded to be constant in the vertical direction of the column. Then a linear relation may exist between v' and $c(1-c)/(c_b-c_t)$. Actually, it was found that as far as v' is small the relation holds in the systems H_2-O_2[8] and H_2-N_2,[9] even if c_b-c_t is fairly large. This is because η/ρ_0 included in H/ρ_0 and $(K_c+K_d)/\rho_0$ changes in parallel with c in those systems. Then if v' is plotted against $c(1-c)/(c_b-c_t)$, H and K_c+K_d can be given independently by the slope of the straight line here obtained and the ordinate at which the line intersects. Hence, considering that the thermal diffusion factor is

[5] Pierce, Duffield, and Drickamer, J. Chem. Phys. **18**, 950 (1951); Giller, Duffield, and Drickamer, J. Chem. Phys. **18**, 1027 (1951).

[6] E. W. Becker, J. Chem. Phys. **19**, 131 (1951).

[7] A. N. Darenport and E. R. S. Winter, Trans. Faraday Soc. **47**, 1160 (1951).

* In the present report, notations of the apparatus, operation, etc., are the same as those of the theory cited in reference 1.

[8] K. Hirota and K. Oguro, J. Chem. Soc. (Japan) **64**, 450 (1943).

[9] K. Hirota and Y. Kobayashi, Hokkaido Meeting of Chem. Soc., Japan, November, 1950.

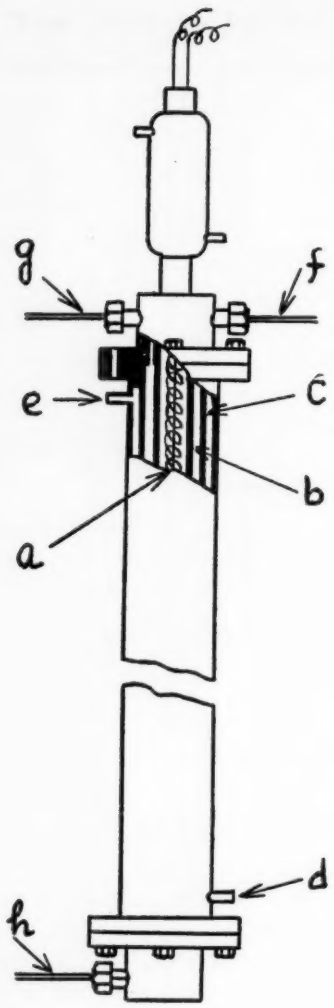

FIG. 2. Thermal diffusion column. (a) Heater. (b) Working space. (c) Cooling mantle. (d) Cooling water inlet. (e) Cooling water outlet. (f) Top inlet. (g) Top outlet. (h) Bottom outlet.

related to H as shown in Eq. (3), it can be determined by obtaining H/ρ_0, and similarly, the ordinary diffusion coefficient by obtaining $(K_c+K_d)/\rho_0$.

Now, the separation factor q_e can be given as follows: By putting v equal to zero in Eq. (2) and by integrating it with respect to z,

$$\ln q_e=\frac{63}{2}L\alpha\frac{D\eta}{\rho g w^4[1+5670(D\eta T/w^3\rho g\Delta T)^2]}. \quad (5)$$

Experimentally, q_e can be determined exactly by the point of intersection of the line at the abscissa in the figure made in the first method of determination of α. Thus α is obtainable by use of Eq. (5), provided that the magnitude of D is known already. This second method of determination will be used in the present research in the case when c_b-c_t is so large that application of the first method is not reasonable. However, it is rather favorable for the purpose of examining Drickamer's modification of the theory to utilize both methods, because the theory can be checked more fundamentally than they themselves did, as will be understood in Sec. IV.

TABLE I. The size of the columns.

Apparatus	Inner diameter of the outer tube (cm)	Outer diameter of the inner tube (cm)	Annular distance $2w$ (cm)	Effective length L (cm)
V	3.88	1.28	1.30	84
VI	3.88	2.86	0.51	84

III. EXPERIMENTAL

The thermal diffusion columns used consisted of concentric tubes, or belonged to the type of the nearly plane case,[10] and their main part was made of brass and copper. Their construction was similar to that of the previous reports (see Fig. 2),[8,9] their size is shown in Table I. The higher temperature (111°C) was kept constant by boiling toluene electrically, while the lower temperature (20°C) was maintained by adjusting the velocity of the cooling water in the mantle. The ratio of the flow velocity of the bottom outlet to that of the top one was kept constant at nearly 1:5. The original gas was prepared by the catalytic decomposition of ammonia in the laboratory of Professor Okamoto of Technology Faculty of Hokkaido University. The initial composition (c_0), therefore, was $H_2:N_2=3:1$, but as the composition at the top outlet changed because of the separating action of the column, the mean concentration of c_0 and that flown from the top outlet was taken as c_t.

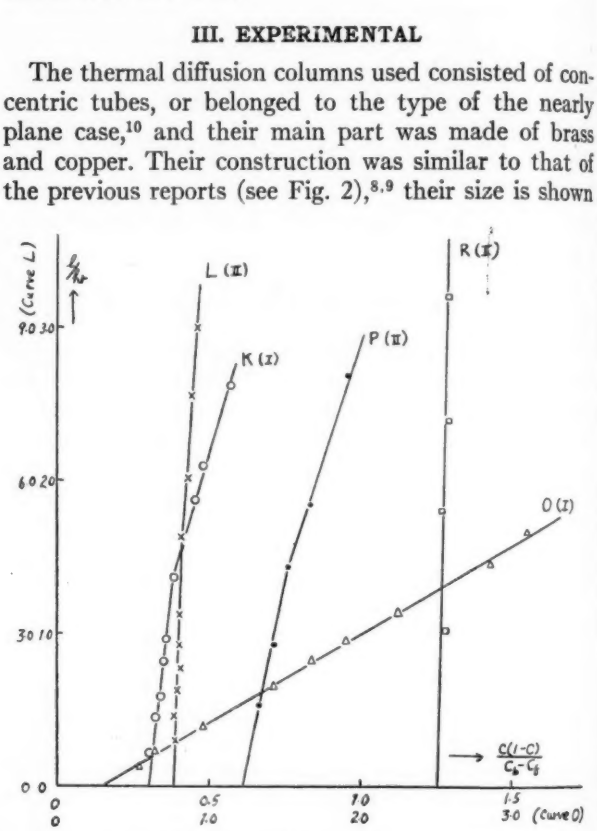

FIG. 3. The data arranged by making use of Eq. (4).

IV. RESULTS AND DISCUSSION

The data concerning five runs were arranged according to the procedure explained in Sec. II and are shown diagrammatically in Fig. 3, where v' is plotted in

[10] W. H. Furry and C. Jones, Phys. Rev. 69, 459 (1946).

liter/hour. It is shown that the linear relation holds between v and $c(1-c)/(c_b-c_t)$ in the region of small flow velocity, as ought to be expected.† Thus it was possible to determine α by the two methods described above. Latin number I or II, attached in parentheses to run numbers denotes the method adopted in each run. The diffusion coefficient at 61°C, which was necessary in the case of the second method of determination, was estimated to be 0.835 cm²/sec from that at 25°C (0.674 cm²/sec) and the relation $D\alpha T^{1.75}$.[11] The α's obtained are summarized in the fourth column of Table II.

All α-values of the mean H_2 concentration 0.54∼0.70 in mole fraction are found not to be constant, ranging from 0.38∼0.95; and most of them are somewhat larger than that of Becker (0.35), who adopted the two-bulb method of measurement over the pressure range in question. This discrepancy cannot be diminished, even if a correction factor 0.975 due to the cylindrical shape of the annular space is taken into consideration.[10] It seems also unreasonable to ascribe the disagreement to difference of the temperature or mean concentration

TABLE II. Thermal diffusion factor α of various pressures.[a]

No. of run	No. of appar.	Press. in atmos	Uncorrec. α'	Method of det.	Corr. α	Mean H_2 conc. (%)
P	V	1.0	0.38	II	0.34	0.62
O	VI	1.0	0.54	I	0.35	0.70
K	VI	3.9	0.945	I	0.37	0.54
L	VI	9.7	0.58	II	0.35	0.64
R	VI	12.6	0.77	II	0.37	0.69

[a] α' and α are values determined without and with the Drickamer's correction factors.

of the present data from those of other researchers. Because, in spite of the lack of agreement of these experimental conditions, the data of the others coincided among themselves, as shown in the remarks described in Fig. 4, in which α's of the present system published hitherto are plotted against composition.

However, the above difference can be eliminated if the correction terms proposed by Drickamer *et al.* are taken into consideration. According to them, only fractions of the gap space, φ and φ', are available, respectively, for horizontal diffusion and thermal diffusion and for convection due to the inevitable entrainment between the streams. Thus the terms H, K_c, and K_d given by Eq. (3) can become correct, if they are multiplied by factors $\varphi^{\frac{1}{3}}(\varphi')^3$, $\varphi^{\frac{1}{3}}(\varphi')^6$, and $\varphi^{\frac{1}{3}}$, respectively. Equation (5) will then be transformed into

$$\ln q_e = \frac{63}{2} L\alpha \frac{D\eta}{\rho g w^4 (\varphi')^3 \varphi \left[1+\frac{5670}{\varphi(\varphi')^6}\left(\frac{D\eta T}{w^3 \rho g \Delta T}\right)^2\right]}. \quad (6)$$

† Numerical values will be shown and discussed in detail by the separate report in which the relation between separation velocity and pressure will be discussed.

[11] Chapman and Cowling, *Theory of Non-Uniform Gases* (Cambridge University Press, Cambridge, 1939), p. 252.

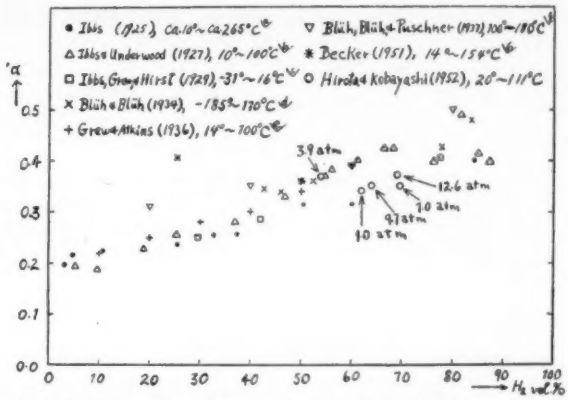

[a] T. L. Ibbs, Proc. Roy. Soc. (London) **A107**, 470 (1925).
[b] T. L. Ibbs and L. Underwood, Proc. Phys. Soc. (London) **39**, 227 (1927).
[c] Ibbs, Grew, Hirst, Proc. Phys. Soc. (London) **41**, 456 (1929).
[d] O. Blüh and G. Blüh, Z. Physik **90**, 12 (1934).
[e] K. E. Grew and B. E. Atkins, Proc. Phys. Soc. (London) **48**, 415 (1936).
[f] Blüh, Blüh, and Puschner, Phil. Mag. **24**, 1103 (1937).

FIG. 4. Thermal diffusion factor of N_2-H_2 system hitherto reported.

The correction factors φ and φ' are shown in diagrams as well as in formulas in their original paper.

In the fifth column of Table II, the α's thus corrected are shown and they give reasonable values; i.e., at the same pressure they are equal to each other (0.34 and 0.35), even if the columns are of different size (see runs *P* and *O*), and the correction factors are widely different in magnitude. The agreement will, moreover, be made more conspicuous by Fig. 4; i.e., it is clear that generally the uncorrected values take positions completely outside of the curve formed by the ones hitherto reported, while the corrected ones practically fall on the curve. Such being the situation, introduction of the Drickamer's correction terms φ and φ' are indispensable in the determination of α from the data of the thermal diffusion column, because the percentage deviation reached more than 150 percent in such a run as *K*.

Besides, as the data collected in the figure (except that of Becker), are measured at or below ordinary pressure, the result obtained above seems to support the result of Becker that α of the present system is independent of pressure below 10 atmos.[5] This, in turn, makes clear that his opposition, which is based on the pressure variation of α, has no connection with the occurrence of turbulence and that it is quite a different problem, worthy of study.

Concluding the discussion, it might be added that the diffusion coefficient at 61°C was calculated to be 0.78 cm²/sec from K_c+K_d determined by the experiment of number 0. Although it is slightly smaller than that of the estimated value 0.835 cm²/sec mentioned above, the agreement is satisfactory, considering the accuracy of the method of determination.

The authors wish to express their thanks to the Ministry of Education of Japan for the financial grant.

Quasi-Chemical Treatment of Mixtures of Oriented Molecules*

H. TOMPA
Courtaulds Limited, Maidenhead, Berkshire, England
(Received July 8, 1952)

A simple model of a solution is constructed, assuming that the interaction energies of the molecules depend on their mutual orientation. The thermodynamic properties of the model are calculated by the combinatory method of the strictly regular solution. Graphs of the excess free energy, entropy, and heat of mixing are obtained numerically for a number of typical cases.

1. INTRODUCTION

IN the current quantitative statistical treatments of mixtures of roughly equal-sized, uncharged molecules, such as Hildebrand's regular solutions[1] or Guggenheim's strictly regular solutions[2] the assumption is always made that the force fields around the molecules have spherical symmetry and that the intramolecular rotations and vibrations are not affected by the nature of the neighboring molecules. One of the consequences of this is that the free energy, heat, and entropy of mixing are symmetrical about the mole fraction of either component. Moreover, the excess entropy of mixing is either taken to be zero by Hildebrand or, as in Guggenheim's original treatment, turns out to be quite small, even for critical mixing, though Guggenheim[3,4] has later shown how larger values of the excess entropy of mixing can be made consistent with the theory.

Experimental evidence has been accumulating for some time that there are cases of binary mixtures in which the thermodynamic functions are not symmetrical about the mole fraction; this asymmetry is especially marked for the entropy. This is usually so when the assumption of a spherical force field is particularly unsatisfactory, either because of the asymmetry of one of the components, e.g., benzene or methyl alcohol, or because of specific interactions between the molecules, e.g., hydrogen bonding as for the system chloroform-acetone. In many of these cases it may be assumed that the molecules tend to be oriented in some preferential directions. The effect of orientation on the thermodynamic properties of solutions has been dealt with qualitatively by several authors[5,6] and quantitatively by Münster;[7,8] as a result of his very cumbersome mathematical technique, Münster could only derive formulas for a very limited number of cases.

It seemed to be worth while therefore to construct an appropriate model of a mixture of two components and to investigate its thermodynamic properties. The model chosen is an extension of the model used by Guggenheim for strictly regular solutions; the molecules are taken as occupying sites on a quasi lattice, but while the molecules of the first component are assumed to have spherical symmetry, those of the second kind are assumed to have rotational symmetry around an axis and a plane of symmetry at right-angles to it (point group $D_{\infty h}$). We shall further assume that the molecules of the second kind can take up any one of a number of well-defined orientations on each site and that the interaction energies with nearest neighbors depend on the orientation. In other words, we assume that there are potential barriers large enough to prevent free rotation, so that the molecules can only vibrate about any one of a number of equilibrium positions; we shall assume that these vibrations are independent of the nature of the neighboring molecules, so that they can be left out of consideration when considering processes of mixing only. At the same time we do not regard the potential barrier as so large that the molecules can never change their orientation. Apart from this, we make the usual assumptions of the strictly regular solution.

The method of treatment is the combinatory method, based on the assumption of non-interference of pairs,[9] in which the configurational partition function can be written down immediately in terms of the numbers of nearest neighbor pairs; this method has been fully described by Guggenheim and McGlashan,[10,11] and the reader is referred to this paper for full details.

In the next section the thermodynamic functions of this model are derived, taking the orientations as non-cooperative, i.e., as being independent of each other; in Sec. 3 the true interdependence of the orientations is taken into account for the case of the plane square lattice and the simple cubic lattice, and in Sec. 4 we show how to evaluate the formulas obtained in Sec. 3

* Substantially as presented before the XII International Congress of Pure and Applied Chemistry, New York, September 1951.

[1] J. H. Hildebrand and R. L. Scott, *Solubility of Non-Electrolytes* (Reinhold Publishing Corporation, New York, 1950) third edition.

[2] R. H. Fowler and E. A. Guggenheim, *Statistical Thermodynamics* (Cambridge University Press, Cambridge, 1939).

[3] E. A. Guggenheim, Trans. Faraday Soc. **44**, 1007 (1948).

[4] E. A. Guggenheim, Nuovo Cimento **6** (Suppl.), 181 (1949).

[5] S. E. Wood, J. Chem. Phys. **15**, 358 (1947).

[6] H. Goller and E. Wicke, Angew. Chem. **B19**, 117 (1947).

[7] A. Münster, Trans. Faraday Soc. **46**, 165 (1950).

[8] A. Münster, Z. physik Chem. **196**, 106 (1950).

[9] R. H. Fowler and E. A. Guggenheim, Proc. Roy. Soc. (London) **A174**, 189 (1940).

[10] E. A. Guggenheim and M. L. McGlashan, Proc. Roy. Soc. (London) **A206**, 335 (1951).

[11] The author is indebted to Professor Guggenheim and Dr. McGlashan for a copy of their manuscript before publication.

numerically. In the last section the results of the calculation are given in the form of graphs for a number of special cases, and the results are discussed in general.

2. ORIENTATIONS INDEPENDENT OF EACH OTHER

Let there be n_1 molecules of kind 1 and n_2 of kind 2. Let n_a of the latter be in orientation a and n_b in orientation b so that

$$n_a+n_b=n_2. \tag{2.1}$$

We assume here that it is physically sensible to speak of "a molecule in orientation a" and "a molecule in orientation b." Let zX_{11} denote the number of 1−1 nearest neighbor pairs and let zX_{1a}, zX_{1b}, zX_{aa}, zX_{ab}, and zX_{bb} be defined similarly, where z is the coordination number of the lattice. Let also zX_{12}, zX_{22} denote the total number of 1−2 and 2−2 pairs, respectively, so that

$$X_{1a}+X_{1b}=X_{12}, \tag{2.2}$$

$$X_{aa}+X_{ab}+X_{bb}=X_{22}. \tag{2.3}$$

Finally, let w_{11} denote the energy of a 1−1 pair, taken from any convenient zero, and let w_{1a}, etc., be defined similarly.

We can write down at once an expression for the configurational partition function Q (see reference 10)

$$Q=\frac{(n_1+n_2)!}{n_1!(\frac{1}{2}n_2)!^2}\frac{(zX_{11}^*)!(\frac{1}{2}zX_{1a}^*)!^2(\frac{1}{2}zX_{1b}^*)!^2(zX_{aa}^*)!(\frac{1}{2}zX_{ab}^*)!^2(zX_{bb}^*)!}{(zX_{11})!(\frac{1}{2}zX_{1a})!^2(\frac{1}{2}zX_{1b})!^2(zX_{aa})!(\frac{1}{2}zX_{ab})!^2(zX_{bb})!}$$
$$\times\exp[-z(X_{11}w_{11}+X_{1a}w_{1a}+X_{1b}w_{1b}+X_{aa}w_{aa}+X_{ab}w_{ab}+X_{bb}w_{bb})/kT]. \tag{2.4}$$

The asterisk denotes the values for the athermal case (all w's equal). The exponential is the Boltzmann factor and the factors before it are the number of configurations, and we have already replaced the sum of a number of similar terms by the largest term, so that the X's denote the equilibrium values. The six X's are not independent, but are connected by the two relations

$$2X_{11}+X_{1a}+X_{1b}=n_1, \tag{2.5}$$

$$X_{1a}+X_{1b}+2X_{aa}+2X_{ab}+2X_{bb}=n_2. \tag{2.6}$$

We eliminate two of the X's—X_{11} and X_{ab} for convenience—from (2.4) with the help of these two equations, and express the fact that the right-hand side of (2.4) is in fact the largest term by equating to zero its derivatives with respect to the other four X's; the resulting equations are of the usual quasi-chemical form:

$$X_{1a}^2/2X_{11}X_{ab}=\exp[-(2w_{1a}-w_{11}-w_{ab})/kT], \tag{2.7}$$

$$X_{1b}^2/2X_{11}X_{ab}=\exp[-(2w_{1b}-w_{11}-w_{ab})/kT], \tag{2.8}$$

$$2X_{aa}/X_{ab}=\exp[-(w_{aa}-w_{ab})/kT], \tag{2.9}$$

$$2X_{bb}/X_{ab}=\exp[-(w_{bb}-w_{ab})/kT]. \tag{2.10}$$

From the last two of these equations, we get

$$X_{22}=\tfrac{1}{2}X_{ab}[\exp(-w_{aa}/kT)+2\exp(-w_{ab}/kT)+\exp(-w_{bb}/kT)]/\exp(-w_{ab}/kT)$$
$$=\tfrac{1}{2}X_{ab}Q_{22}/\exp(-w_{ab}/kT), \tag{2.11}$$

and from the first two,

$$X_{12}=(2X_{11}X_{ab})^{\frac{1}{2}}[\exp(-w_{1a}/kT)+\exp(-w_{1b}/kT)]/\exp[-\tfrac{1}{2}(w_{11}+w_{ab})/kT]$$
$$=(2X_{11}X_{ab})^{\frac{1}{2}}Q_{12}/\exp[-\tfrac{1}{2}(w_{11}+w_{ab})/kT]. \tag{2.12}$$

We can combine (2.11) and (2.12) and get, writing Q_{11} for $\exp(-w_{11}/kT)$,

$$X_{12}^2/4X_{11}X_{22}=Q_{12}^2/Q_{11}Q_{22}. \tag{2.13}$$

This equation is formally identical with the usual quasi-chemical equation of the theory of the strictly regular solution, if we replace in it each factor $\exp(-w_{ij}/kT)$ by Q_{ij}; in fact, (2.13) might have been written down at once by carefully considering the meaning of the quantities occurring in it.

We obtain the chemical potentials by differentiating $-kT\ln Q$ with respect to n_1 and n_2, and though the X's and X^*'s are functions of n_1 and n_2, we can disregard the partial derivatives with respect to them on account of the maximizing conditions (see Guggenheim and McGlashan[10]). Apart from the first factor in Q, n_1 only occurs where X_{11} and X_{11}^* have been eliminated, and n_2 where X_{ab} and X_{ab}^* have been eliminated. Therefore,

$$\mu_1/RT=\ln x_1+\tfrac{1}{2}z\ln(X_{11}/X_{11}^*)+\tfrac{1}{2}zw_{11}/kT, \tag{2.14}$$

$$\mu_2/RT=\ln(\tfrac{1}{2}x_2)+\tfrac{1}{2}z\ln(X_{ab}/X_{ab}^*)+\tfrac{1}{2}zw_{ab}/kT,$$
$$=\ln(\tfrac{1}{2}x_2)+\tfrac{1}{2}z\ln(X_{22}/X_{22}^*)-\tfrac{1}{2}z\ln Q_{22}. \tag{2.15}$$

Here x_1 and x_2 denote mole fractions. Subtracting the chemical potentials of the pure components, obtained by putting $x_1=1$ in μ_1, and $x_2=1$ in μ_2, we have for the chemical potentials of mixing

$$\Delta\mu_1/RT=\ln x_1+\tfrac{1}{2}z\ln(X_{11}/X_{11}^*), \tag{2.16}$$

$$\Delta\mu_2/RT=\ln x_2+\tfrac{1}{2}z\ln(X_{22}/X_{22}^*). \tag{2.17}$$

These expressions are identical with the ones for the strictly regular solution and expressions for the chemical potentials and the free energy of mixing as functions of the mole fractions can be obtained in exactly the same way, e.g., by introducing a quantity κ defined as the root lying between 0 and 2 of the equation

$$1-\kappa=\kappa^2x_1x_2[(Q_{11}Q_{22}/Q_{12}^2)-1] \tag{2.18}$$

(see Tompa[12,13]). The expression for the excess molar

[12] H. Tompa, J. Chem. Phys. **16**, 292 (1948).
[13] H. Tompa, Trans. Faraday Soc. **45**, 101 (1949).

free energy of mixing ΔG^E is then

$$\Delta G^E/RT=\tfrac{1}{2}zx_1\ln[(1-\kappa x_2)/x_1]+\tfrac{1}{2}zx_2\ln[(1-\kappa x_1)/x_2]. \quad (2.19)$$

The molar heat of mixing ΔH is

$$\Delta H/RT=z\kappa x_1x_2(w-Tdw/dT)/kT \quad (2.20)$$

[see Eq. (6.6) of reference 3], if we define an average interaction energy w by

$$\exp(-2w/kT)=Q_{12}^2/Q_{11}Q_{22}. \quad (2.21)$$

In the original quasi-chemical treatment w was tacitly assumed to be independent of temperature. It is easily seen that here the quantity w is temperature dependent, even if all the constituent w's are not; in consequence the excess entropy of mixing can have values comparable to those of the heat and free energy of mixing. This case provides one of the possible interpretations of the physical significance of the temperature dependence of w.

The above treatment can be easily extended to the case where the molecules of the second kind can take up any one of p different orientations. The only difference in the result is that the definitions of Q_{12} and Q_{22} have to be replaced by

$$Q_{12}=\sum_{j=a}^{p}\exp(-w_{1j}/kT), \quad (2.22)$$

$$Q_{22}=\sum_{i=a}^{p}\sum_{j=a}^{p}\exp(-w_{ij}/kT). \quad (2.23)$$

It is easily verified that the formulas given here reduce to those given by Münster[7] for the special case treated by him, *viz.*, no orientation in the pure component 2, all $w_{ij}=w_{22}$, and all $w_{1j}=w_{12}$ except w_{1p}, so that

$$\frac{X_{12}^2}{4X_{11}X_{22}}=\exp\left(-\frac{2w'}{kT}\right)\times\left[\frac{p-1+\exp(-w''/kT)}{p}\right]^2 \quad (2.24)$$

with appropriate meanings for w' and w''. Münster's formulas are recovered on expanding ΔG^E and ΔH in a series of powers of x_1 and neglecting all terms after x_1^2; his W equals $-2w'$, and his W_{or} is $-w''$.

In fact, the case treated by Münster[7] is one of the few cases in which the model of this section is physically sensible, when there is no preferential orientation in the pure components, though the molecules 2 are oriented with respect to molecules 1, and there are relatively few of the orienting molecules 1 present; it is then possible to speak of the orientation of a molecule of kind 2, and to regard this orientation as noncooperative. To give an example of a case, where our model is physically obviously nonsensical, let us consider molecules like those of benzene, and let us assume that the energy of a pair is much lower if the two molecules are "face to face" than for any other relative orientation. Then our model would predict that nearly all the pairs of benzene molecules are face to face. But it is obviously impossible to arrange a number of benzene molecules in such a way that nearly all pairs are face to face, and any arrangement containing a large number of face to face pairs must also contain a large number of "edge to edge" pairs. We will examine in the next section how to take this interdependence of the orientations into proper consideration.

3. INTERDEPENDENCE OF ORIENTATIONS

We consider n_1 spherical molecules and n_2 molecules of symmetry $D_{\infty h}$ arranged on the $N=n_1+n_2$ sites of a plane square lattice ($z=4$), and we take the sides of the square for directions x and y. We assume that the axes of symmetry of the molecules 2 are parallel either to x or to y, and denote the numbers of molecules with axes in the x or y directions by n_x and n_y, respectively,

$$n_x+n_y=n_2. \quad (3.1)$$

We also denote by n_{11}, n_{1x}, n_{1y}, n_{xx}, n_{xy}, and n_{yy} the numbers of nearest neighbor pairs of molecules, indicated by the subscripts, which are next to each other in the x direction, and we use similarly $n_1{}^1$, $n_1{}^x$, $n_1{}^y$, $n_x{}^x$, $n_x{}^y$, and $n_y{}^y$ for the numbers of pairs of molecules next to each other in the y direction.

The following relations are self-evident:

$$2n_1=2n_{11}+n_{1x}+n_{1y}=2n_1{}^1+n_1{}^x+n_1{}^y, \quad (3.2a, b)$$
$$2n_x=2n_{xx}+n_{1x}+n_{xy}=2n_x{}^x+n_1{}^x+n_x{}^y, \quad (3.3a, b)$$
$$2n_y=2n_{yy}+n_{1y}+n_{xy}=2n_y{}^y+n_1{}^y+n_x{}^y. \quad (3.4a, b)$$

Now n_{xx} and $n_y{}^y$ are pairs of the same type, the axes of the molecules lying in one straight line; similarly, n_{1y} and $n_1{}^x$ are of the same type, the axis of the molecule 2 being at right angles to the line joining the molecules. Altogether there are six different types of pairs, whose numbers we denote by zNA, zNB, zNC, zNU, zNV, and zNW, so that

$$zNA=n_{xy}+n_x{}^y,\ zNB=n_{1y}+n_1{}^x,\ zNC=n_{1x}+n_1{}^y,$$
$$zNU=n_{11}+n_1{}^1,\ zNV=n_{xx}+n_y{}^y,\ zNW=n_{yy}+n_x{}^x. \quad (3.5)$$

For easier reference we show the types of pairs associated with zNA, etc., using the symbol (0) for a molecule of the first kind, and $(-)$ or $(|)$ for a molecule of the second kind, according to orientation:

$$A:(-|),\ B:(0|),\ C:(0-),\ U:(00),\ V:(--),\ W:(||).$$

There are three relations between the numbers of pairs and the mole fractions x_1 and x_2, obtained by adding (3.2a) and (3.2b), (3.3a) and (3.4b), (3.3b) and (3.4a), and dividing by $4N$:

$$2U+B+C=x_1, \quad (3.6)$$
$$2V+C+A=\tfrac{1}{2}x_2, \quad (3.7)$$
$$2W+A+B=\tfrac{1}{2}x_2. \quad (3.8)$$

The configurational partition function can be written down at once in terms of the numbers of pairs, as before:

$$Q=\frac{(n_1+n_2)!}{n_1!(\frac{1}{2}n_2)!^2}\frac{(zNU^*)!(\frac{1}{2}zNB^*)!^2(\frac{1}{2}zNC^*)!^2(zNV^*)!(\frac{1}{2}zNA^*)!^2(zNW^*)!}{(zNU)!(\frac{1}{2}zNB)!^2(\frac{1}{2}zNC)!^2(zNV)!(\frac{1}{2}zNA)!^2(zNW)!}$$
$$\times\exp[-zN(Uw_U+Bw_B+Cw_C+Vw_V+Aw_A+Ww_W)/kT], \quad (3.9)$$

where the w's denote the energies of the pairs indicated. We eliminate U, V, and W with the help of (3.6), (3.7), and (3.8), and equate the derivatives of Q with respect to A, B, and C to zero, to show that the term written down is in fact the largest term; we thus get the equations of the quasi-chemical form

$$A^2/4VW=\exp[-(2w_A-w_V-w_W)/kT], \quad (3.10)$$

$$B^2/4WU=\exp[-(2w_B-w_W-w_U)/kT], \quad (3.11)$$

$$C^2/4UV=\exp[-(2w_C-w_U-w_V)/kT], \quad (3.12)$$

which we write simply

$$a^2A^2=4VW,\ b^2B^2=4WU,\ c^2C^2=4UV \quad (3.13a, b, c)$$

with obvious meanings for a, b and c. It seems worth while to point out that these equations are the conditions of quasi-chemical equilibrium for simple, physically realizable processes: (3.10) for the interchange $(n_xn_yn_xn_y)=(n_xn_xn_yn_y)$, (3.11) for $(n_1n_yn_1n_y)=(n_1n_1n_yn_y)$, and (3.12) similarly, if all the neighboring sites are occupied in an identical manner; (3.10) is also the equilibrium condition for a change of orientation of the type

$$\begin{matrix} n_x & n_x \\ (n_xn_xn_x)=(n_xn_yn_x), \\ n_x & n_x \end{matrix}$$

and it can be verified that the condition of equilibrium for any simple process of interchanging molecules or changing orientations is given by an appropriate product of (3.10), (3.11), and (3.12). This is a check that we have obtained neither too many nor too few quasi-chemical equations.

The chemical potentials are obtained by differentiating the substituted expression for $-kT\ln Q$ with respect to $n_1=Nx_1$ and $n_2=Nx_2$:

$$\mu_1/RT=\ln x_1+\tfrac{1}{2}z\ln(U/U^*)+\tfrac{1}{2}zw_U/kT, \quad (3.14)$$

$$\mu_2/RT=\ln(\tfrac{1}{2}x_2)+\tfrac{1}{4}z\ln(VW/V^*W^*)+\tfrac{1}{4}z(w_V+w_W)/kT; \quad (3.15)$$

and by subtracting the values for the pure components we get

$$\Delta\mu_1/RT=\ln x_1+\tfrac{1}{2}z\ln(U/U^*), \quad (3.16)$$

$$\Delta\mu_2/RT=\ln x_2+\tfrac{1}{4}z\ln(VW/V^*W^*)-\tfrac{1}{4}z\ln(V^0W^0/V^{0*}W^{0*}). \quad (3.17)$$

V^0, W^0, and, for later reference, A^0 are the values of V, W, and A in the pure component 2 and are obtained from (3.6)–(3.8) and (3.13) on putting $x_2=1$, $x_1=0$, so that $U=B=C=0$:

$$V^0=W^0=a/[4(1+a)], \quad A^0=1/[2(1+a)]; \quad (3.18)$$

and V^{0*}, W^{0*}, and A^{0*} are the corresponding athermal values ($a=1$). Then

$$\Delta\mu_2/RT=\ln x_2+\tfrac{1}{4}z\ln[(VW/V^*W^*)(1+a)^2/4a^2]=\ln x_2+\tfrac{1}{2}z\ln[\tfrac{1}{2}(A/A^*)(1+a)]. \quad (3.19)$$

It is interesting to note that $V^0=W^0$ here, which means that if benzene molecules are arranged on a plane square lattice with their axes parallel to x or y, the number of "face to face" pairs equals the number of "edge to edge" pairs, which is relevant to the remark at the end of the preceding section.

Equations (3.6)–(3.8) and (3.13a, b, c) are solved easily with $a=b=c=1$ to give

$$U^*=\tfrac{1}{2}x_1^2, \quad A^*=\tfrac{1}{4}x_2^2; \quad (3.20a, b)$$

and with these values and with $z=4$, we get for the excess free energy of mixing

$$\Delta G^E/RT=2x_1\ln(2U/x_1^2)+2x_2\ln[2A(1+a)/x_2^2]. \quad (3.21)$$

It is not possible to reduce this expression further, except in special cases; it will be shown in the next section that (3.6)–(3.8) and (3.13a, b, c), from which the numbers of pairs can be calculated, give in general quartic equations for any one of them, and values have been obtained numerically for a number of specified systems (given a, b, and c) at three concentrations.

To get the heat of mixing we can use the Gibbs-Helmholtz equation in the form

$$\frac{\Delta H}{RT}=\frac{1}{kT}\frac{\partial(\Delta G^E/RT)}{\partial(1/kT)}=2x_1\frac{\dot U}{U}+2x_2\frac{\dot A}{A}+2x_2\frac{\dot a}{1+a}, \quad (3.22)$$

where a dot denotes $(1/kT)\partial/\partial(1/kT)$. With the help of the equations which are obtained by applying this operator to (3.6)–(3.8) and the logarithms of (3.13a, b, c), and with $\dot a=a\ln a$ which follows from the definition of a on the assumption that the constituent w's are temperature independent, (3.22) can be transformed into

$$\Delta H/RT=4[A-\tfrac{1}{2}x_2/(1+a)]\ln a+4B\ln b+4C\ln c. \quad (3.23)$$

It is a matter of simple algebra to verify that the same expression is obtained from the physically obvious

$$\Delta H/RT=z[Uw_U+Bw_B+Cw_C+Vw_V+Aw_A+Ww_W-x_1U^0w_U-x_2(V^0w_V+A^0w_A+W^0w_W)]/kT, \quad (3.24)$$

which provides a useful check on the self-consistency of the formulas. ΔH has also been calculated in the next section for the same systems as ΔG^E.

Another check on the formulas is provided by putting $a=1$ and $b=c$, in which case the formulas for the strictly regular solution are recovered easily.

We can further test the self-consistency of the formulas obtained by calculating from them an approximation which in the theory of the strictly regular solution is called the zeroth approximation; this is of some interest in itself. This approximation is equivalent to putting the entropy of mixing equal to the athermal entropy of mixing, i.e., to neglecting the effect on the entropy of the heat of mixing and of the corresponding changes in the numbers of the different types of nearest neighbor pairs. We get this approximation for the strictly regular solution by taking w/kT to be small, expanding in terms of w/kT, and neglecting all but the first terms of the expansions. Both the excess free energy and the heat of mixing come out to be equal to what the heat of mixing would be if the numbers of the nearest neighbor pairs were those of the athermal solution, and the excess entropy of mixing is thus zero. The same result can be obtained formally by letting z tend to infinity. This last method of obtaining the zeroth approximation is obviously not applicable to our case, but if we calculate A, B, C, U, V, and W from (3.6)–(3.8) and (3.13) with the assumption that all w/kT's are small and substitute the values obtained into (3.21) and (3.23), expressions are obtained which are both identical with the expressions obtained directly from (3.23) if A, B, and C are replaced by A^*, B^*, and C^*. Denoting the zeroth approximation by a superscript 0 in brackets, we get for these expressions

$$\frac{\Delta H^{(0)}}{RT}=\frac{\Delta G^{(0)E}}{RT}=x_1x_2\ln\frac{b^2c^2}{a}$$
$$=4x_1x_2\left[\frac{w_B+w_C}{2}-\frac{1}{2}w_U-\frac{1}{2}\frac{2w_A+w_V+w_W}{4}\right]\Big/kT. \tag{3.25}$$

These expressions would also be obtained as the zeroth approximation of a strictly regular solution, in which the interaction energies of the 1−1, 1−2, and 2−2 pairs have values which are equal to the average values of these energies in our solution.

An analysis on very similar lines can be carried out for the simple cubic lattice $z=6$. In addition to n_x and n_y we have n_z molecules with their axes in the z direction, at right angles to both x and y. In addition to n_{xz}, etc., we also have pairs of neighbors next to each other in the z direction, and in addition to the six previous types of pairs there is a new type, for which n_{yz} is a typical representative, and in which the axes of the two molecules are not in the same plane but are skew; the number of pairs of this type is denoted by zND. Furthermore, symmetry considerations show that the types A, B, and W must each be split into two types of equal numbers.

Omitting all details of algebra, we get as before

$$2U+B+C=x_1,\quad 2V+C+A=\tfrac{1}{3}x_2,$$
$$2W'+A+B=\tfrac{2}{3}x_2, \tag{3.26a, b, c}$$
$$a'^2A^2=4VW',\quad b'^2B^2=4W'U,$$
$$c^2C^2=4UV,\quad d^2D^2=W^2, \tag{3.27a, b, c, d}$$

where we have used the abbreviations

$$W(1+d)/d=W',\quad a^2(1+d)/2d=a'^2,$$
$$b^2(1+d)/2d=b'^2 \tag{3.28a, b, c}$$

and with obvious meaning for d. Further, we get

$$\Delta G^E/RT=3x_1\ln(2U/x_1^2)$$
$$+x_2\ln[27VW^2(e+3)^3(e-1)/32x_2^6a^4]/kT, \tag{3.29}$$

$$\Delta H/RT=6[A-4x_2/3(e+3)]\ln a+6B\ln b+6C\ln c$$
$$+6[D-x_2(e+1)/3(e+3)(d+1)]\ln d, \tag{3.30}$$

where e stands for $(1+8a'^2)^{\frac{1}{2}}$.

Equations (3.26) and (3.27) again yield quartics for any one of the unknowns and further calculation was carried out numerically for a number of sets of a, b, c, and d at three concentrations. These results are given in the next sections.

The zeroth approximation can be obtained exactly as for $z=4$; the expression obtained is

$$\frac{\Delta H^{(0)}}{RT}=\frac{\Delta G^{(0)E}}{RT}=x_1x_2\ln\frac{b^4c^2}{a^{4/3}d^{2/3}}=6x_1x_2\left[\frac{2w_B+w_C}{3}\right.$$
$$\left.-\frac{1}{2}w_U-\frac{1}{2}\frac{4w_A+2w_D+w_V+2w_W}{9}\right]\Big/kT \tag{3.31}$$

and can be interpreted as before.

It is interesting to note that the admission of the three directions x, y, and z for the axis of the molecules of kind 2 on the plane square lattice leads to the strictly regular solution, with a temperature dependent w: omitting all pairs, in which the line joining the molecules is parallel to z, we get only two equations to replace (3.26):

$$2U+B+C=x_1,\ 2V+2W+2A+B+C+2D=x_2, \tag{3.32}$$

but five quasi-chemical equations

$$b^2B^2=16UV,\quad c^2C^2=4UV,\quad aA=4V,$$
$$dD=2V,\quad \omega W=2V, \tag{3.33}$$

where ω is appropriately defined and is used instead of w to avoid confusion. It can be shown that all these quasi-chemical equations correspond to physically realizable processes. Equations (3.32) and (3.33) reduce to quadratic equations for any one of the unknowns, and may be solved most easily by reintroducing the quantities

X_{11}, X_{12}, and X_{22}, used in Sec. 2:

$$X_{11}=NU,\quad X_{12}=N(B+C),\qquad X_{22}=N(V+W+A+D). \tag{3.34}$$

Elimination of A, B, C, D, U, V, and W from (3.33) and (3.34) gives

$$\frac{X_{12}^2}{X_{11}X_{22}}=\frac{(2/b+1/c)^2}{(1+4/a+2/d+2/\omega)}, \tag{3.35}$$

which is indeed the usual quasi-chemical equation of the strictly regular solution with a temperature dependent w, putting the right-hand side equal to $\exp(-2w/kT)$ as definition of w. This case will not be considered any further.

4. NUMERICAL EVALUATION

Values of A, B, C, U, V, and W were calculated for $z=4$ from Eqs. (3.6), (3.7), (3.8), and (3.13) in the following manner. Dividing the product of (3.13a) and (3.13b) by (3.13c) gives

$$bcBC=2aAU, \tag{4.1}$$

and substituting for U from (3.6) gives

$$bcBC=aA(x_1-B-C). \tag{4.2}$$

Similarly,

$$acAC=bB(\tfrac{1}{2}x_2-A-C), \tag{4.3}$$

$$abAB=cC(\tfrac{1}{2}x_2-A-B). \tag{4.4}$$

Substituting for BC its value from (4.2) transforms (4.3) and (4.4) into two equations, which are linear in B and C, regarded as functions of A, and can be solved. Substituting the expressions obtained into (4.2) gives an equation of the fourth degree in A, which for greater convenience in computation has been simplified by putting

$$A=\tfrac{1}{2}x_2y. \tag{4.5}$$

The equation is

$$[(1-y)^2-a^2y^2]\left[(1-y)^2+2\frac{a}{bc}y(1-y)+a^2\left(\frac{1}{b^2}+\frac{1}{c^2}-1\right)y^2\right]=2\frac{x_1}{x_2}\frac{a}{bc}y\left(1-y+\frac{ab}{c}y\right)\left(1-y+\frac{ac}{b}y\right), \tag{4.6}$$

and can be solved for y for given values of a, b, c, and the mole fractions. It was found most convenient to obtain y by a method of trial and error, using the equation in its above factorized form. Of the four possible solutions the physically significant one is that which on continuously changing the parameters a, b, and c toward unity goes over into the solution for the athermal case $y^*=\frac{1}{2}x_2$. This was always taken as the first trial value. From y, A, B, and C were calculated from (4.5) and (4.7):

$$B=\tfrac{1}{2}x_2\frac{(1-y)^2-a^2y^2}{1-y+(ab/c)y},\quad C=\tfrac{1}{2}x_2\frac{(1-y)^2-a^2y^2}{1-y+(ac/b)y}. \tag{4.7a, b}$$

U, V, and W were calculated from (4.1) and the two analogous equations, and (3.6)–(3.8) used as a check.

Values of A, B, C, U, V, and W were thus calculated for a number of systems (given a, b, and c) at mole fractions $\frac{1}{4}$, $\frac{1}{2}$, and $\frac{3}{4}$; from these, ΔG^E and ΔH were calculated from (3.21) and (3.23) and are shown in the next section plotted against the mole fractions, together with $T\Delta S^E$, the excess molar entropy of mixing. In order to be able to draw curves through the points with reasonable accuracy, the tangents at $x_1=0$ (and $x_2=0$) were calculated by regarding x_1 (or x_2) as small, expanding in terms of x_1 (or x_2) and neglecting higher powers. The result is for $x_1\ll 1$

$$\frac{\Delta G^E}{RT}=2x_1\ln\left[\frac{4b^2c^2}{(b+c)^2}\frac{1+a}{2a}\right], \tag{4.8}$$

$$\frac{\Delta H}{RT}=2x_1\left[-\frac{\ln a}{1+a}+2\frac{c\ln b+b\ln c}{b+c}\right]; \tag{4.9}$$

and for $x_2\ll 1$

$$\Delta G^E/RT=2x_2\ln[bc(1+a)/2a], \tag{4.10}$$

$$\Delta H/RT=2x_2[-(\ln a)/(1+a)+\ln(bc)]. \tag{4.11}$$

These values have some interest in themselves, since they are the partial molar excess free energy and heat of mixing of either component in infinitely dilute solutions.

The calculation for the simple cubic lattice $z=6$ is entirely analogous. From (3.26) and (3.27) we obtain with

$$A=\tfrac{1}{3}x_2y, \tag{4.12}$$

an equation of the fourth degree for y:

$$[(1-y)(2-y)-a'^2y^2]\left[(1-y)(2-y)+2\frac{a'}{b'c}y(1-y)+a'^2\left(\frac{1}{b'^2}+\frac{1}{c^2}-1\right)y^2\right]=3\frac{x_1}{x_2}\frac{a'}{b'c}y\left(1-y+\frac{a'b'}{c}y\right)\left(1-y+\frac{a'c}{b'}y\right). \tag{4.13}$$

The equations for B and C are

$$B=\tfrac{1}{3}x_2\frac{(1-y)(2-y)-a'^2y^2}{1-y+(a'b'/c)y},$$

$$C=\tfrac{1}{3}x_2\frac{(1-y)(2-y)-a'^2y^2}{2-y+(a'c/b')y}. \tag{4.14}$$

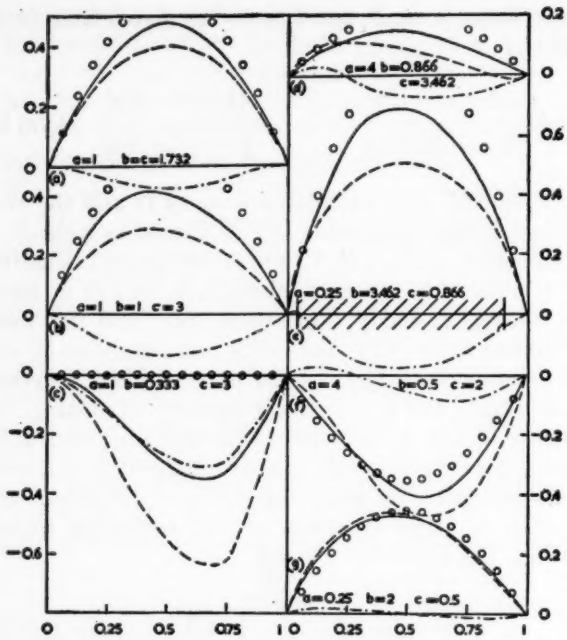

FIG. 1. Excess molar free energy, heat, and entropy of mixing, in units of RT, *vs* mole fraction x_2, $z=4$. ———— ΔG^E, — — — ΔH, —·—·— $T\Delta S^E$, ○○○○ $\Delta G^{(0)E}=\Delta H^{(0)}$. The shaded range of concentration is a two-phase region.

D, U, V, and W' are obtained as before, using (3.26) as a check, and W is calculated from (3.28a). Values of ΔG^E and ΔH can then be obtained from (3.29) and (3.30); the slopes of the tangents at the two ends are given by expressions which we shall give only for the two special cases used, $a=d=1$, and $ab=c$, $d=1$; for $x_1 \ll 1$

$$\frac{\Delta G^E}{RT}=6x_1\ln\frac{3bc}{b+2c} \quad \text{or} \quad 3x_1\ln\frac{3b^2(e+1)}{2(e+3)}, \tag{4.15 a, b}$$

$$\frac{\Delta H}{RT}=6x_1\frac{2c\ln b+b\ln c}{b+2c} \quad \text{or} \quad 6x_1\left[\frac{e-1}{e(e+3)}\ln a+\ln b\right]; \tag{4.16 a, b}$$

and for $x_2 \ll 1$

$$\frac{\Delta G^E}{RT}=2x_2\ln(b^2c) \quad \text{or} \quad x_2\ln\frac{b^6(e+3)^3}{54(e+1)}, \tag{4.17 a, b}$$

$$\frac{\Delta H}{RT}=2x_2\ln(b^2c) \quad \text{or} \quad 6x_2\left[\frac{e-1}{3(e+3)}\ln a+\ln b\right]. \tag{4.18 a, b}$$

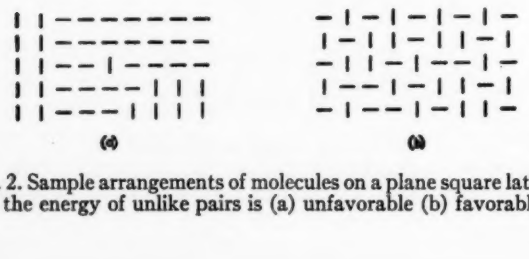

FIG. 2. Sample arrangements of molecules on a plane square lattice, if the energy of unlike pairs is (a) unfavorable (b) favorable.

Numerical values were calculated for a number of systems and are shown and discussed in the next section.

5. RESULTS IN DISCUSSION

All the systems chosen for numerical calculation belong to one of two limiting cases, which might be described as "orientation in solution only" and "orientation in the pure component only." In the first case all 2−2 pairs have the same energy $w_V=w_A=w_W=w_D$, and therefore $a=1$, $d=1$, but the energy of a 1−2 pair depends on the orientation of the molecule 2, $w_B \neq w_C$ and $b \neq c$; in the second case all 1−2 pairs have the same energy $w_B=w_C$, but the energy of a 2−2 pair depends on orientation. For the sake of simplicity in calculation it is assumed that all types of 2−2 pairs have the same energy with the exception of one; to resemble the case of benzene, where the "face to face" position is known to have a lower energy, it is w_V which is assumed different from $w_A=w_W=w_D$; this leads to $ab=c$, $d=1$. The references to d and w_D apply only for $z=6$.

Figure 1 shows plots of ΔG^E, ΔH, and $T\Delta S^E$ against mole fraction for $z=4$. For the sake of comparison, one case of a strictly regular solution is also included in Fig. 1(a), with $b=c=1.732$, which is near the critical value 2. To show the effect of orientation on the thermodynamic functions for orientation in solution only, systems with the same average 1−2 interaction energy should be compared. The total interaction of a molecule of kind 2, surrounded by molecules of kind 1, with all its neighbors is $2w_B+2w_C$, and thus equality of the product bc is the required criterion for equality of the average 1−2 interaction. Accordingly, the system chosen for Fig. 1(b) has $bc=3$, like the strictly regular system of Fig. 1(a), and the effect of orientation is shown by the asymmetry of the curves. The system of Fig. 1(c) has $bc=1$ and should be compared with the ideal solution, $\Delta G^E=\Delta H=T\Delta S^E=0$; the asymmetry of the curves is much more marked here. Figures 1(d) to 1(g) show systems with orientation in the pure component only. In Fig. 1(d) and 1(f) $a=4$, which means that w_A is much larger than $\frac{1}{2}(w_V+w_W)$, so that like pairs will predominate in the pure liquid 2, as indicated in Fig. 2(a). On the other hand, in the systems of Fig. 1(e) and 1(g), w_A is much smaller than $\frac{1}{2}(w_V+w_W)$, so that A will be the preferred type of 2−2 pair, as indicated in Fig. 2(b). Two of these systems have $bc=3$, the other two $bc=1$, but no such simple significance can be attached to these products here as for orientation in solution only.

It should be noted that for the systems with orientation in the pure component only $T\Delta S^E$ has an S-shaped form, resembling the curves found experimentally by Scatchard and co-workers (see Wood[14] for a summary of these results) for mixtures containing methanol; as a matter of fact the slopes of the tangents to the curves at the two ends are equal and of opposite sign.

[14] S. E. Wood, J. Am. Chem. Soc. **68**, 1963 (1946).

Figures 3 and 4 show graphs for the simple cubic lattice, $z=6$. Figure 3(a) is again a strictly regular solution, with an interaction constant near the critical value, which is 1.5. Figures 3(b) and 3(c) show two cases of orientation in solution only, with the same values of b^2c—which is relevant here for equality of the average 1–2 interaction—as the strictly regular solution of Fig. 3(a). Figures 3(d) and 3(e) are also systems with orientation in solution only, with $b^2c=1$; there is a strange proportionality here between ΔG^E, ΔH, and $T\Delta S^E$. Figure 3(f) is an extreme case, where ΔG^E is S-shaped, while Fig. 4(e) shows a system—on twice the scale of all the other graphs—where the heat of mixing is S-shaped; this latter behavior has also been observed experimentally. Finally, Figs. 4(a) to 4(d) represent the behavior of systems analogous to those of Figs. 1(d) to 1(g). The large variety of shapes obtainable with different values of the parameters a, b, and c is noteworthy.

It must be added here that the calculation of the conditions for the appearance of critical phases has so far proved too involved algebraically and the possibility must be considered that some of the systems shown on the diagrams might show phase separation. Values of $\Delta\mu_1/kT$ were therefore calculated for the plane square lattice from (3.16) for $x_2=\frac{1}{4}$, $\frac{1}{2}$, and $\frac{3}{4}$ and plotted against x_2. Systems in which $\Delta\mu_1/kT$ appears to be a monotonic function of the mole fraction are above the critical temperature and mix in all proportions; systems in which $\Delta\mu_1$ appears to have a maximum and a minimum have solubility gaps and the compositions of the coexisting phases were determined by calculating $\Delta\mu_1$ and $\Delta\mu_2$ from (3.16) and (3.19) for a number of points in the appropriate concentration range. To reduce the arithmetical labor involved, values of x_2 were calculated from (4.6) for arbitrary values of y instead of calculating y from x_2. The values of the chemical potentials were plotted, and the mole fractions of the coexisting phases estimated from the requirement that the chemical potentials of both components must have the same values in both phases. The cubic lattice was treated similarly. The mole fractions of the coexisting phases are shown on the diagrams where applicable, and the heterogeneous region is indicated by cross-hatching.

Values obtained for the zeroth approximation from (3.25) and (3.31) are marked on the diagrams by circles.

It is interesting to compare the results obtained in Sec. 2, insofar as they are physically significant, with those of Sec. 3. Taking the case of orientation in solution only ($a=1$) and a solution dilute with respect to the orienting molecules ($x_1 \ll 1$), we obtain, on expanding in powers of x_1 and keeping only the first two terms, the expression already obtained by Münster[7] for $z=4$

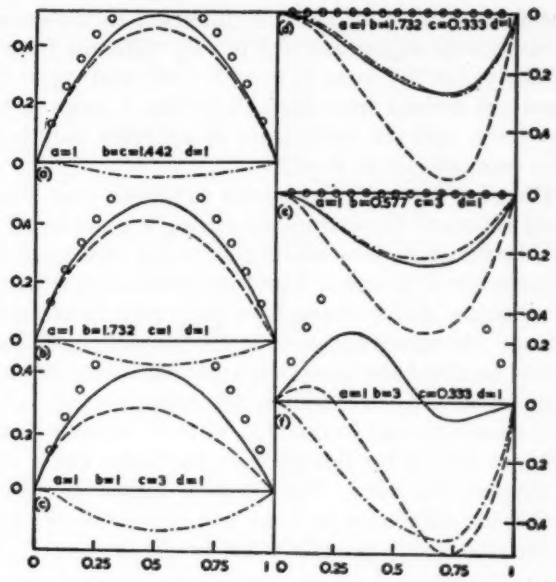

FIG. 3. Excess molar free energy, heat, and entropy of mixing, in units of RT, *vs* mole fraction x_2, $z=6$. ——— ΔG^E, — — — — ΔH, —·—·— $T\Delta S^E$, ○○○○ $\Delta G^{(0)E}=\Delta H^{(0)}$.

and $p=2$, using the notation of this section:

$$\frac{\Delta G^E}{RT}=zx_1\ln\frac{2bc}{b+c}-\tfrac{1}{2}zx_1^2\left[\frac{4b^2c^2}{(b+c)^2}-1\right], \qquad (5.1)$$

while keeping second-order terms in the calculation leading to (4.8), with $a=1$, gives

$$\frac{\Delta G^E}{RT}=4x_1\ln\frac{2bc}{b+c}-2x_1^2\left[\frac{4b^2c^2}{(b+c)^2}-1-\frac{(b-c)^2}{(b+c)^2}\right]. \qquad (5.2)$$

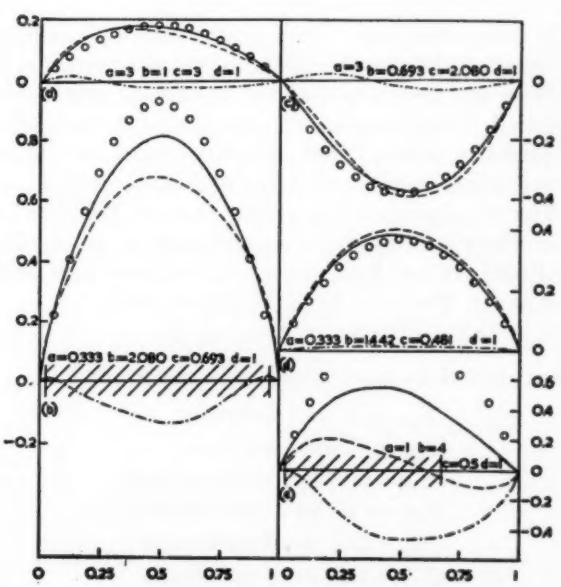

FIG. 4. Excess molar free energy, heat, and entropy of mixing, in units of RT, *vs* mole fraction x_2, $z=6$. ——— ΔG^E, — — — — ΔH, —·—·— $T\Delta S^E$, ○○○○ $\Delta G^{(0)E}=\Delta H^{(0)}$. The shaded ranges of concentration are two-phase regions.

The first terms agree and the difference in the second terms is only significant if b is very different from c. Similarly, for the same case with $z=6$, and $p=3$, the equations derived from Sec. 2 and Sec. 3 agree in the first term, and the coefficients of x_1^2 differ only by a term proportional to $(b-c)^2$.

The view has sometimes been expressed that if unusual values of the entropy of mixing are the result of orientation in a pure component being destroyed by solution, then, if such a liquid be mixed with either of two liquids, which themselves mix with little excess entropy, the excess entropies in the two systems formed should be about the same, the argument being that the same amount of orientation is destroyed, corresponding to the same change in entropy. There is nothing in the different curves for liquids with the same value of a to support this view. The intuitive reason for this is that if the differences between the interaction energies of the different types of nearest neighbor pairs in the pure component 2 are so large that they give rise to considerable degrees of orientation, and therefore to considerable entropy values, then these large interaction energies will greatly influence the numbers of configurations in solution too and will thus produce entropies of mixing which are different in each case.

No attempt has been made to obtain quantitative agreement between experimental data and any of the curves of Figs. 1, 3, and 4; many good fits could no doubt be produced by a proper choice of the parameters a, b, c, and d, but in view of the nature of the model, it is uncertain how much physical significance could be attached to values so obtained. Further, it must be remembered that orientation effects are not the only possible reason for lack of agreement of experimental results with the theory of the strictly regular solutions, e.g., the influence of the changing environment on the molecular vibrations also contributes to the excess entropy of mixing (see reference 15), and all these effects will have to be taken into consideration when making comparisons between experiment and theory.

[15] I. Prigogine and V. Mathot, J. Chem. Phys. **20**, 49 (1952).

THE JOURNAL OF CHEMICAL PHYSICS VOLUME 21, NUMBER 2 FEBRUARY, 1953

Some Overlap Integrals Involving d Orbitals

H. H. JAFFÉ
Venereal Disease Experimental Laboratory, U. S. Public Health Service, School of Public Health, University of North Carolina, Chapel Hill, North Carolina

(Received July 7, 1952)

Formulas are presented for overlap integrals for overlap of $d\pi$ with $p\pi$ and $d\pi$ orbitals, and for $d\delta$ with $d\delta$ orbitals. Slater AO's were used throughout. Numerical tables for these integrals for a variety of values of the parameters ρ and τ are given.

IN connection with some work concerning multiple bonds involving d orbitals,[1] overlap integrals of $d\pi$ with $p\pi$ and $d\pi$ orbitals, and of $d\delta$ with $d\delta$ orbitals were required. These integrals were calculated by the method of Mulliken, Rieke, Orloff, and Orloff,[2] and are reported in this paper together with the necessary formulas.

The calculations follow closely those of Mulliken and co-workers;[2] the notation of these authors, as modified by Roothaan and Rüdenberg,[3] was followed throughout this paper. The AO's have the general form

$$\chi^{nl\lambda}=R_{nl}(r)S_{l\lambda}(\theta,\phi). \tag{1}$$

The S functions considered in this paper are

$$\begin{aligned}
S_{p\pi}&=(3/4\pi)^{\frac{1}{2}}\sin\theta\cos\phi;\\
S_{p\pi'}&=(3/4\pi)^{\frac{1}{2}}\sin\theta\sin\phi;\\
S_{d\pi}&=(15/4\pi)^{\frac{1}{2}}\sin\theta\cos\theta\cos\phi;\\
S_{d\pi'}&=(15/4\pi)^{\frac{1}{2}}\sin\theta\cos\theta\sin\phi;\\
S_{d\delta}&=(15/16\pi)^{\frac{1}{2}}\sin^2\theta\cos2\phi;\\
S_{d\delta'}&=(15/16\pi)^{\frac{1}{2}}\sin^2\theta\sin2\phi.
\end{aligned} \tag{2}$$

For the R functions we have used Slater's approximation[4]

$$R_{nl}(r)=N_{nl}r^{n-1-\delta}\exp(-\zeta r/a_{\mathrm{H}}), \tag{3}$$

where $\delta=0$ for $n=1$ to 3, $\delta=0.7$ for $n=4$, and $\delta=1$ for $n=5$,

$$\zeta=Z_{\mathrm{eff}}/(n-\delta),$$

$$1/N_{nl}^2=\int^{\infty} r^{2(n-\delta)}\exp(-2\zeta_{nl}r/a_{\mathrm{H}})dr.$$

Z_{eff} is found in accordance with Slater's formula.[4]

For integration, the polar coordinates of the two atoms were transformed into spheroidal coordinates:

$$\xi=(r_a+r_b)/R;\quad \eta=(r_a-r_b)/R;\quad \phi=\phi_a=\phi_b. \tag{4}$$

The integration over ξ ranges from 1 to ∞, over η from -1 to 1 and over ϕ from 0 to 2π. The element of volume is $(\xi^2-\eta^2)d\eta d\xi d\phi$. Again following Mulliken and coworkers,[2,3] the following parameters were used:

$$\rho\equiv\tfrac{1}{2}(\zeta_a+\zeta_b)R/a_{\mathrm{H}};\quad \tau\equiv(\zeta_a-\zeta_b)/(\zeta_a+\zeta_b);\quad m\equiv n-\delta. \tag{5}$$

[1] H. H. Jaffé (to be published).
[2] Mulliken, Rieke, Orloff, and Orloff, J. Chem. Phys. **17**, 1248 (1949).
[3] C. C. J. Roothaan and K. Rüdenberg, J. Chem. Phys. **19**, 1445, 1459 (1951).
[4] J. C. Slater, Phys. Rev. **36**, 57 (1930).

TABLE I. $S(2p\pi, 3d\pi)$.

ρ	$\tau=-0.75$	$\tau=-0.5$	$\tau=-0.25$	$\tau=-0.125$	$\tau=0.0$	$\tau=0.125$	$\tau=0.25$	$\tau=0.5$	$\tau=0.75$
0.0	0.000	0.000	0.000	0.000	0.000	0.000	0.000	0.000	0.000
0.5		0.073			0.199			0.073	
1.0	0.021	0.136	0.295	0.350	0.370	0.353	0.299	0.140	0.022
1.5		0.183			0.495			0.194	
2.0	0.034	0.212	0.450	0.533	0.567	0.547	0.472	0.233	0.039
2.5		0.224			0.590			0.257	
3.0	0.039	0.223	0.453	0.535	0.573	0.563	0.499	0.268	0.051
3.5		0.211			0.529			0.267	
4.0	0.038	0.193	0.368	0.432	0.465	0.466	0.418	0.256	0.057
4.5		0.173			0.402			0.243	
5.0	0.034	0.151	0.268	0.309	0.335	0.344	0.329	0.223	0.058
5.5		0.130			0.272			0.201	
6.0	0.029	0.110	0.176	0.200	0.217	0.229	0.230	0.180	0.057
6.5		0.092			0.170			0.159	
7.0	0.024	0.077	0.109	0.120	0.132	0.143	0.151	0.138	0.053
7.5		0.063			0.100			0.119	
8.0	0.020	0.052	0.064	0.069	0.075	0.084	0.094	0.101	0.048
9.0	0.016	0.034	0.036		0.041		0.057	0.074	0.043
10.0	0.013	0.022	0.020	0.020	0.022	0.026	0.033	0.052	0.038
12.0	0.008	0.009	0.006	0.005	0.006	0.007	0.011	0.025	0.028
14.0	0.005	0.004	0.002	0.001	0.001	0.002	0.003	0.011	0.020
16.0	0.003	0.001	0.000	0.000	0.000	0.000	0.001	0.005	0.014

TABLE II. $S(2p\pi, 5d\pi)$.

ρ	$\tau=-0.75$	$\tau=-0.5$	$\tau=-0.25$	$\tau=-0.125$	$\tau=0.0$	$\tau=0.125$	$\tau=0.25$	$\tau=0.5$	$\tau=0.75$
0.0	0.000	0.000	0.000	0.000	0.000	0.000	0.000	0.000	0.000
0.5		0.088			0.161			0.030	
1.0	0.030	0.168	0.305	0.326	0.308	0.257	0.187	0.059	0.005
1.5		0.232			0.428			0.083	
2.0	0.051	0.277	0.499	0.537	0.513	0.437	0.326	0.109	0.009
2.5		0.303			0.562			0.129	
3.0	0.061	0.311	0.549	0.594	0.577	0.504	0.390	0.144	0.014
3.5		0.306			0.563			0.155	
4.0	0.062	0.288	0.490	0.533	0.527	0.476	0.385	0.161	0.019
4.5		0.265			0.477			0.163	
5.0	0.057	0.237	0.383	0.416	0.419	0.392	0.334	0.161	0.022
5.5		0.209			0.359			0.156	
6.0	0.050	0.181	0.271	0.294	0.301	0.293	0.264	0.148	0.025
6.5		0.154			0.248			0.139	
7.0	0.043	0.130	0.179	0.192	0.200	0.203	0.194	0.129	0.026
7.5		0.109			0.160			0.118	
8.0	0.035	0.090	0.112	0.118	0.125	0.133	0.135	0.107	0.027
9.0	0.029	0.061	0.067		0.075		0.090	0.086	0.027
10.0	0.023	0.041	0.038	0.039	0.043	0.049	0.058	0.067	0.026
12.0	0.015	0.017	0.012	0.011	0.013	0.016	0.022	0.038	0.024
14.0	0.009	0.007	0.003	0.003	0.005	0.005	0.008	0.020	0.019
16.0	0.006	0.003	0.001	0.001	0.001	0.001	0.003	0.010	0.015

With these definitions and Mulliken's conventions concerning the order of assignment of atoms a and b, the master formulas for the overlap integrals, after integration over ϕ, are as follows:

$$S(n_a p\pi, n_b d\pi) = (3/4)(5)^{\frac{1}{2}} N_a N_b \left(\frac{R}{2}\right)^{m_a+m_b+1} \times \int_1^\infty \int_{-1}^1 (\xi^2-1)(1-\eta^2)(1-\xi\eta) \times (\xi+\eta)^{m_a-2}(\xi-\eta)^{m_b-3} \times (\xi^2-\eta^2) e^{-\rho(\xi+\eta\tau)} d\eta d\xi,$$

$$S(n_a d\pi, n_b p\pi) = (3/4)(5)^{\frac{1}{2}} N_a N_b \left(\frac{R}{2}\right)^{m_a+m_b+1} \times \int_1^\infty \int_{-1}^1 (\xi^2-1)(1-\eta^2)(1+\xi\eta) \times (\xi+\eta)^{m_a-3}(\xi-\eta)^{m_b-2} \times (\xi^2-\eta^2) e^{-\rho(\xi+\eta\tau)} d\eta d\xi,$$

$$S(n_a d\pi, n_b d\pi) = (15/4) N_a N_b \left(\frac{R}{2}\right)^{m_a+m_b+1} \times \int_1^\infty \int_{-1}^1 (\xi^2-1)(1-\eta^2)(1-\xi^2\eta^2) \times (\xi+\eta)^{m_a-3}(\xi-\eta)^{m_b-3} \times (\xi^2-\eta^2) e^{-\rho(\xi+\eta\tau)} d\eta d\xi, \quad (6)$$

$$S(n_a d\delta, n_b d\delta) = (15/16) N_a N_b \left(\frac{R}{2}\right)^{m_a+m_b+1} \times \int_1^\infty \int_{-1}^1 (\xi^2-1)^2(1-\eta^2)^2 \times (\xi+\eta)^{m_a-3}(\xi-\eta)^{m_b-3} \times (\xi^2-\eta^2) e^{-\rho(\xi+\eta\tau)} d\eta d\xi.$$

The integrals in Eqs. (6) may be evaluated in terms of the integrals

$$A_n(\alpha) = \int_1^\infty x^n e^{-\alpha x} dx, \tag{7}$$

$$B_n(\alpha) = \int_{-1}^1 x^n e^{-\alpha x} dx. \tag{8}$$

The N in Eq. (3) and (6) may be evaluated by means of the integral

$$C_n(\alpha) = \int_0^\infty x^n e^{-\alpha x} dx = \frac{n!}{\alpha^{n+1}}. \tag{9}$$

Values of the integrals $A_n(\alpha)$ and $B_n(\alpha)$ were taken from the extensive tabulations of Kotani, Ameniya, and Simose.[5] A few values not listed by these authors were computed, using recursion formulas.[5] In Eqs. (10) to (21) below, the desired overlap integrals are expressed in terms of the integrals A and B. No special formulas for $\tau=0$ are given, since they foilow immediately from Eqs. (10) to (21) by substituting $B_n(0)=0$ for n odd, and $B_n(0)=2/(n+1)$ for n even.

TABLE III.

	$S(3d\pi, 3p\pi)$			$S(3p\pi, 3d\pi)$				
ρ	$\tau=0.5$	$\tau=0.25$	$\tau=0.125$	$\tau=0.0$	$\tau=0.125$	$\tau=0.25$	$\tau=0.5$	$\tau=0.75$
0.0	0.000	0.000	0.000	0.000	0.000	0.000	0.000	0.000
0.5	0.014			0.151			0.097	
1.0	0.029	0.147	0.224	0.289	0.324	0.317	0.169	0.035
1.5	0.043			0.404			0.263	
2.0	0.058	0.258	0.383	0.487	0.543	0.533	0.324	0.064
2.5	0.070			0.537			0.366	
3.0	0.080	0.308	0.442	0.553	0.616	0.610	0.390	0.085
3.5	0.087			0.543			0.398	
4.0	0.091	0.300	0.415	0.510	0.567	0.570	0.393	0.097
4.5	0.091			0.464			0.377	
5.0	0.089	0.255	0.339	0.409	0.456	0.468	0.354	0.101
5.5	0.085			0.352			0.326	
6.0	0.080	0.196	0.251	0.297	0.333	0.350	0.296	0.100
6.5	0.073			0.233			0.264	
7.0	0.065	0.139	0.171	0.199	0.224	0.244	0.234	0.094
7.5	0.059			0.159			0.204	
8.0	0.053	0.094	0.108	0.125	0.141	0.161	0.177	0.087
9.0	0.040	0.060		0.075		0.102	0.130	0.078
10.0	0.029	0.037	0.039	0.043	0.050	0.062	0.093	0.069
12.0	0.015	0.013	0.012	0.013	0.015	0.021	0.045	0.052
14.0	0.007	0.004	0.003	0.003	0.004	0.007	0.021	0.038
16.0	0.003	0.001	0.001	0.001	0.001	0.002	0.009	0.027

TABLE IV. $S(3p\pi, 5d\pi)$.

ρ	$\tau=-0.5$	$\tau=-0.25$	$\tau=-0.125$	$\tau=0.0$	$\tau=0.125$	$\tau=0.25$	$\tau=0.5$	$\tau=0.75$
0.0	0.000	0.000	0.000	0.000	0.000	0.000	0.000	0.000
0.5	0.025			0.148			0.046	
1.0	0.049	0.186		0.285		0.232	0.091	0.009
1.5	0.072			0.404			0.132	
2.0	0.093	0.329	0.439	0.497	0.487	0.412	0.169	0.017
2.5	0.111			0.562			0.200	
3.0	0.125	0.404	0.528	0.597	0.591	0.509	0.224	0.024
3.5	0.132			0.605			0.241	
4.0	0.141	0.409	0.523	0.589	0.590	0.523	0.253	00.33
4.5	0.143			0.556			0.258	
5.0	0.141	0.363	0.452	0.509	0.516	0.475	0.257	0.039
5.5	0.136			0.455			0.251	
6.0	0.128	0.292	0.355	0.398	0.411	0.393	0.241	0.043
6.5	0.119			0.341			0.228	
7.0	0.109	0.219	0.257	0.287	0.305	0.302	0.213	0.046
7.5	0.099			0.238			0.197	
8.0	0.088	0.153	0.174	0.194	0.211	0.220	0.180	0.047
9.0	0.068	0.102		0.125		0.152	0.146	0.047
10.0	0.051	0.066	0.070	0.076	0.087	0.101	0.115	0.046
12.0	0.027	0.024	0.024	0.026	0.031	0.041	0.066	0.041
14.0	0.013	0.008	0.007	0.008	0.010	0.015	0.036	0.034
16.0	0.006	0.003	0.002	0.002	0.003	0.005	0.018	0.027

[5] Kotani, Ameniya and Simose, Proc. Phys.-Math. Soc. Japan **20**, Extra No. 1, 1 (1938); **22**, Extra No., 1 (1940).

TABLE V. $S(3d\pi, 3d\pi)$.

ρ	$\tau=0.0$	$\tau=0.125$	$\tau=0.25$	$\tau=0.5$	$\tau=0.75$
0.0	−1.000	−0.946	−0.798	−0.365	−0.055
0.5	−0.948			−0.353	
1.0	−0.802	−0.762	−0.650	−0.311	−0.050
1.5	−0.595			−0.252	
2.0	−0.365	−0.353	−0.249	−0.183	−0.038
2.5	−0.144			−0.114	
3.0	+0.044	+0.032	+0.002	−0.051	−0.024
3.5	0.187			+0.003	
4.0	0.282	0.260	0.200	0.046	−0.011
4.5	0.335			0.077	
5.0	0.353	0.331	0.271	0.098	−0.001
5.5	0.344			0.109	
6.0	0.319	0.304	0.260	0.114	+0.006
6.5	0.284			0.113	
7.0	0.245	0.236	0.210	0.109	0.010
7.5	0.206			0.102	
8.0	0.169	0.166	0.153	0.093	0.013
9.0	0.109		0.104	0.074	0.014
10.0	0.065	0.066	0.067	0.057	0.014
12.0	0.021	0.022	0.025	0.030	0.012
14.0	0.006	0.006	0.008	0.010	0.009
16.0	0.001	0.002	0.003	0.004	0.007

TABLE VI. $S(3d\pi, 5p\pi)$.

ρ	$\tau=-0.75$	$\tau=-0.5$	$\tau=-0.25$	$\tau=-0.125$	$\tau=0.0$	$\tau=0.125$	$\tau=0.25$
0.0	0.000	0.000	0.000	0.000	0.000	0.000	0.000
0.5		0.105			0.089		
1.0	0.047	0.205	0.272		0.175		0.046
1.5		0.294			0.253		
2.0	0.087	0.368	0.494	0.427	0.321	0.200	0.090
2.5		0.424			0.373		
3.0	0.117	0.461	0.592	0.528	0.408	0.268	0.142
3.5		0.481			0.425		
4.0	0.136	0.485	0.598	0.536	0.425	0.293	0.170
4.5		0.476			0.410		
5.0	0.144	0.455	0.530	0.474	0.384	0.277	0.173
5.5		0.428			0.350		
6.0	0.144	0.395	0.425	0.374	0.311	0.232	0.157
6.5		0.359			0.271		
7.0	0.138	0.322	0.316	0.277	0.232	0.181	0.130
7.5		0.285			0.194		
8.0	0.128	0.251	0.221	0.191	0.161	0.131	0.100
9.0	0.116	0.189	0.147		0.105		0.073
10.0	0.103	0.138	0.094	0.077	0.066	0.058	0.046
12.0	0.076	0.070	0.035	0.027	0.023	0.021	0.021
14.0	0.057	0.034	0.011	0.008	0.007	0.007	0.008
16.0	0.041	0.015	0.004	0.002	0.002	0.002	0.003

TABLE VII. $S(3d\pi, 5d\pi)$.

ρ	$\tau=-0.75$	$\tau=-0.5$	$\tau=-0.25$	$\tau=-0.125$	$\tau=0.0$	$\tau=0.125$	$\tau=0.25$	$\tau=0.5$
0.0	−0.091	−0.513	−0.933	−0.996	−0.935	−0.775	−0.560	−0.171
0.5		−0.496			−0.913			−0.168
1.0	−0.084	−0.449	−0.795		−0.799		−0.493	−0.159
1.5		−0.378			−0.647			−0.145
2.0	−0.066	−0.292	−0.463	−0.485	−0.465	−0.406	−0.320	−0.126
2.5		−0.201			−0.273			−0.103
3.0	−0.044	−0.112	−0.097	−0.088	−0.092	−0.105	−0.113	−0.078
3.5		−0.033			+0.064			−0.052
4.0	−0.023	+0.034	+0.174	+0.204	0.186	+0.131	+0.061	−0.024
4.5		0.087			0.273			−0.005
5.0	−0.005	0.125	0.311	0.403	0.326	0.214	0.168	+0.015
5.5		0.151			0.337			0.033
6.0	+0.007	0.165	0.341	0.370	0.352	0.294	0.209	0.044
6.5		0.170			0.332			0.053
7.0	0.016	0.168	0.298	0.316	0.304	0.263	0.201	0.059
7.5		0.160			0.269			0.062
8.0	0.021	0.150	0.234	0.242	0.233	0.209	0.170	0.063
9.0	0.023	0.124	0.168		0.163		0.131	0.060
10.0	0.024	0.097	0.114	0.111	0.107	0.102	0.094	0.053
12.0	0.021	0.054	0.046	0.041	0.040	0.041	0.042	0.036
14.0	0.017	0.027	0.016	0.013	0.014	0.014	0.017	0.021
16.0	0.013	0.013	0.005	0.004	0.004	0.004	0.006	0.011

Special formulas are needed for $\rho=0$, and these are given in Eqs. (22) to (25).

(a) For $\rho\neq 0$:

$$S(2p\pi, 3d\pi) = (3/4)(5)^{\frac{1}{2}}\mathfrak{N}_{2,3}[-A_5(B_1-B_3)+A_4(B_0-B_2) +A_3(B_1-B_5)-A_2(B_0-B_4) -A_1(B_3-B_5)+A_0(B_2-B_4)], \quad (10)$$

$$S(2p\pi, 5d\pi) = (3/4)(5)^{\frac{1}{2}}\mathfrak{N}_{2,5}[-(A_6-A_2)(B_1-B_3) +(A_5-A_3)(B_0-B_4)+(A_4-A_0)(B_3-B_5) -(A_3-A_1)(B_2-B_6)], \quad (11)$$

$$S(3p\pi, 3d\pi) = (3/4)(5)^{\frac{1}{2}}\mathfrak{N}_{3,3}[-(A_6-A_4)(B_1-B_3) +(A_5-A_3)(B_0-B_2)-(A_5-A_1)(B_2-B_4) +(A_4-A_2)(B_1-B_5)+(A_3-A_1)(B_4-B_6) -(A_2-A_0)(B_3-B_5)], \quad (12)$$

$S(3d\pi, 3p\pi)$: same as $S(3p\pi, 3d\pi)$ except each $B_n(\alpha)$ replaced by $B_n(-\alpha)$,

$$S(3p\pi, 5d\pi) = (3/4)(5)^{\frac{1}{2}}\mathfrak{N}_{3,5}[-A_7(B_1-B_3)+A_6(B_0-B_2) +A_5(B_1+B_3-2B_5)-A_4(B_0+B_2-2B_4) -A_3(2B_3-B_5-B_7)+A_2(2B_2-B_4-B_6) +A_1(B_5-B_7)-A_0(B_4-B_6)], \quad (13)$$

TABLE VIII. $S(3d\delta, 3d\delta)$.

ρ	$\tau=0.0$	$\tau=0.125$	$\tau=0.25$	$\tau=0.5$	$\tau=0.75$
0.0	1.000	0.946	0.798	0.365	0.055
0.5	0.982			0.361	
1.0	0.932	0.883	0.747	0.347	0.054
1.5	0.856			0.325	
2.0	0.762	0.724	0.606	0.298	0.049
2.5	0.660			0.268	
3.0	0.558	0.533	0.461	0.237	0.043
3.5	0.461			0.207	
4.0	0.374	0.359	0.319	0.178	0.037
4.5	0.298			0.151	
5.0	0.233	0.226	0.206	0.127	0.031
5.5	0.180			0.106	
6.0	0.137	0.132	0.127	0.088	0.025
6.5	0.103			0.072	
7.0	0.077	0.077	0.075	0.059	0.020
7.5	0.057			0.048	
8.0	0.042	0.042	0.043	0.039	0.016
9.0	0.022		0.024	0.026	0.013
10.0	0.011	0.012	0.013	0.016	0.010
12.0	0.002	0.003	0.004	0.007	0.006
14.0	0.001	0.001	0.001	0.002	0.004

$$S(3d\pi, 3d\pi) = (15/4)\mathfrak{N}_{3,3}[-(A_6-A_0)(B_2-B_4) + (A_4-A_2)(B_0-B_6)], \quad (14)$$

$$S(3d\pi, 5p\pi) = (3/4)(5)^{\frac{1}{2}}\mathfrak{N}_{3,5}[(A_7-3A_5)(B_1-B_3) + A_6(B_0-3B_2+2B_4) - A_4(B_0-3B_2+2B_6) + A_3(2B_1-3B_5+B_7) - (3A_2-A_0)(B_4-B_6) - A_1(2B_3-3B_5+B_7)], \quad (15)$$

$$S(3d\pi, 5d\pi) = (15/4)\mathfrak{N}_{3,5}[-(A_7-A_1)(B_2-B_4) + (A_6-A_0)(B_3-B_5)+(A_5-A_3)(B_0-B_6) - (A_4-A_2)(B_1-B_7), \quad (16)$$

$$S(5p\pi, 5d\pi) = (3/4)(5)^{\frac{1}{2}}\mathfrak{N}_{5,5}[-(A_8-A_4)(B_1-B_3) + A_7(B_0-2B_2+B_4)+2A_6(B_1-B_5) - A_5(B_0-3B_4+2B_6)+A_3(2B_2-3B_4+B_8) + 2A_2(B_3-B_7)-A_1(B_4-2B_6+B_8) + (A_4-A_0)(B_5-B_7)], \quad (17)$$

$S(5d\pi, 5p\pi)$: same as $S(5p\pi, 5d\pi)$ except each $B_n(\alpha)$ replaced by $B_n(-\alpha)$,

$$S(5d\pi, 5d\pi) = (15/4)\mathfrak{N}_{5,5}[-(A_8-A_2)(B_2-B_4) + (A_6-A_4)(B_0-B_6)+(A_6-A_0)(B_4-B_6) - (A_4-A_2)(B_2-B_8)], \quad (18)$$

$$S(3d\delta, 3d\delta) = (15/8)\mathfrak{N}_{3,3}[A_6(B_0-2B_2+B_4) - A_4(2B_0-3B_2+B_6)+A_2(B_0-3B_4+2B_6) - A_0(B_2-2B_4+B_6)], \quad (19)$$

$$S(3d\delta, 5d\delta) = (15/8)\mathfrak{N}_{3,5}[A_7(B_0-2B_2+B_4) - A_6(B_1-2B_3+B_5) - A_5(2B_0-3B_2+B_6) + A_4(2B_1-3B_3+B_7)+A_3(B_0-3B_4+2B_6) - A_2(B_1-3B_5+2B_7) - A_1(B_2-2B_4+B_6) + A_0(B_3-2B_5+B_7)], \quad (20)$$

$$S(5d\delta, 5d\delta) = (15/8)\mathfrak{N}_{5,5}[A_8(B_0-2B_2+B_4) - 2A_6(B_0-B_2-B_4+B_6)+A_4(B_0+2B_2-6B_4 + 2B_6+B_8)-2A_2(B_2-B_4-B_6+B_8) + A_0(B_4-2B_6+B_8)]. \quad (21)$$

(b) For $\rho=0$:

$$S(n_a p\pi, n_b d\pi) = S(n_a d\pi, n_b p\pi) = 0, \quad (22)$$

$$S(3d\pi, 3d\pi) = -S(3d\delta, 3d\delta) = -(1-\tau^2)^{7/2}, \quad (23)$$

$$S(3d\pi, 5d\pi) = -S(3d\delta, 5d\delta) = -[(49/56)(1+\tau)^7(1-\tau)^9]^{\frac{1}{2}}, \quad (24)$$

TABLE IX. $S(3d\delta, 5d\delta)$.

ρ	$\tau=-0.75$	$\tau=-0.5$	$\tau=-0.25$	$\tau=-0.125$	$\tau=0.0$	$\tau=0.125$	$\tau=0.25$	$\tau=0.5$
0.0	0.091	0.513	0.933	0.996	0.935	0.775	0.560	0.171
0.5		0.507			0.924			0.170
1.0	0.088	0.491	0.886		0.889		0.537	0.167
1.5		0.466			0.835			0.162
2.0	0.082	0.433	0.765	0.811	0.772	0.641	0.474	0.156
2.5		0.396			0.686			0.147
3.0	0.073	0.356	0.604	0.629	0.602	0.509	0.385	0.138
3.5		0.316			0.518			0.127
4.0	0.063	0.267	0.438	0.464	0.437	0.375	0.297	0.119
4.5		0.238			0.363			0.105
5.0	0.053	0.204	0.300	0.338	0.296	0.240	0.214	0.094
5.5		0.173			0.238			0.083
6.0	0.045	0.145	0.194	0.208	0.189	0.159	0.146	0.073
6.5		0.121			0.148			0.064
7.0	0.036	0.100	0.121	0.120	0.115	0.107	0.096	0.055
7.5		0.083			0.088			0.048
8.0	0.029	0.068	0.072	0.070	0.067	0.064	0.060	0.041
9.0	0.023	0.047	0.042		0.038		0.037	0.030
10.0	0.019	0.029	0.024	0.021	0.020	0.021	0.022	0.021
12.0	0.012	0.012	0.007	0.006	0.006	0.006	0.007	0.010
14.0	0.007	0.004	0.002	0.002	0.001	0.002	0.002	0.004

$$S(5d\pi, 5d\pi) = -S(5d\delta, 5d\delta) = -(1-\tau^2)^{9/2}. \quad (25)$$

The factors $\mathfrak{N}_{n_a,n_b}$ in Eqs. (10) to (21) have the following values:

$$\mathfrak{N}_{2,3} = (24)^{-1}(30)^{-\frac{1}{2}}\rho^6(1+\tau)^{5/2}(1-\tau)^{7/2}, \quad (26)$$

$$\mathfrak{N}_{2,5} = (96)^{-1}(105)^{-\frac{1}{2}}\rho^7(1+\tau)^{5/2}(1-\tau)^{9/2}, \quad (27)$$

$$\mathfrak{N}_{3,3} = (720)^{-1}\rho^7(1-\tau^2)^{7/2}, \quad (28)$$

$$\mathfrak{N}_{3,5} = (1440)^{-1}(14)^{-\frac{1}{2}}\rho^8(1+\tau)^{7/2}(1-\tau)^{9/2}, \quad (29)$$

$$\mathfrak{N}_{5,5} = (401\,320)^{-1}\rho^9(1-\tau^2)^{9/2}. \quad (30)$$

The integrals were evaluated numerically for a variety of values of the parameters ρ and τ, and the values are tabulated in Tables I to X.

Of the five d orbitals, four are equivalent, having the form given in Eq. (2) [the orbitals $d\pi$ and $d\delta$ of Eq. (2) are identical except for orientation in the coordinate system]. However, a fifth orbital ($d\sigma$) has a different form:

$$S_{d\sigma} = (5/16\pi)^{\frac{1}{2}}(3\cos^2\theta - 1). \quad (31)$$

This orbital has nodal surfaces $\cos^2\theta = \frac{1}{3}$, which can comprise the four tetrahedral bonds from the central atom. Accordingly, this orbital may be involved in formation of multiple bonds resembling π-bonds,[1] and the corresponding overlap integrals are of interest.

Evaluation of these overlap integrals requires rotation of the coordinate system of $d\sigma$ until its nodal surface $\cos^2\theta = \frac{1}{3}$ comprises the z axis of the interacting $p\pi$ or $d\pi$ orbital and is tangential to the nodal plane of the interacting orbital. This rotation can be achieved by rotating the coordinate system of $d\sigma$ around the y axis. Under this transformation r and ϕ are transformed into themselves; $\cos\theta'$ is transformed into $\cos\alpha\cos\theta + \sin\alpha\sin\theta\cos\phi$, where θ' the polar angle in the original, θ in the final coordinate system, and α the angle of rotation. $S_{d\sigma}$ then becomes

$$S_{d\sigma} = (5/16\pi)^{\frac{1}{2}}[3\cos^2\alpha\cos^2\theta + 3\sin^2\alpha\sin^2\theta\cos^2\phi + 6\sin\alpha\cos\alpha\sin\theta\cos\theta\cos\phi - 1]. \quad (32)$$

On multiplying $\chi_{nd\sigma}$, with $S_{d\sigma}$ in this form, by $p\pi$ or $d\pi$ it is seen that the first, second, and last terms in the bracket in Eq. (32) lead to odd powers of $\cos\phi$ and hence the integrals of these terms over ϕ vanish. The third term, however, leads to an overlap integral of the exact form, except for the normalization factor, of the $S(np\pi, nd\pi)$ and $S(nd\pi, nd\pi)$ evaluated above.

If α is given by $\cos^2\alpha = \frac{1}{3}$, i.e., for overlap of an orbital having its nodal plane tangential to the nodal surface of the orbital $d\sigma$, the term $6(5/16\pi)^{\frac{1}{2}}\sin\alpha\cos\alpha$ becomes $(5/2\pi)^{\frac{1}{2}}$. Consequently, the overlap integral

$$S(\chi_a{}^{nl\tau}, n_b d\pi^*) = (2/3)^{\frac{1}{2}}S(\chi_a{}^{nl\tau}, n_b d\pi), \quad (33)$$

where $d\pi^*$ stands for the $d\sigma$ orbital involved in the overlap described above, and the asterisk on the π is used to indicate that the orbital is not a true π orbital, but has some similar properties.

Mulliken, Rieke, Orloff, and Orloff,[2] have shown how overlap integrals of the type tabulated in this paper can be used to evaluate similar overlap integrals based on othogonalized Slater AO's, SCF–AO's, and hybrid AO's. Therefore, no discussion of such calculations is necessary here.

TABLE X.

ρ	$S(5p\pi, 5d\pi)$ $\tau=0.0$	$S(5d\pi, 5d\pi)$ $\tau=0.0$	$S(5d\delta, 5d\delta)$ $\tau=0.0$
0.0	0.000	−1.000	1.000
0.5	0.111	−0.970	0.990
1.0	0.217	−0.882	0.960
1.5	0.313	−0.748	0.913
2.0	0.395	−0.580	0.851
2.5	0.460	−0.396	0.779
3.0	0.507	−0.212	0.699
3.5	0.533	−0.042	0.617
4.0	0.541	+0.104	0.536
4.5	0.532	0.210	0.458
5.0	0.509	0.304	0.386
5.5	0.475	0.358	0.320
6.0	0.433	0.428	0.263
6.5	0.388	0.387	0.213
7.0	0.342	0.373	0.170
7.5	0.294	0.347	0.135
8.0	0.250	0.314	0.106
9.0	0.173	0.239	0.063
10.0	0.114	0.169	0.039
12.0	0.044	0.072	0.011
14.0	0.015	0.026	0.003
16.0	0.005	0.008	0.001

A Semi-Empirical Equation for the Vapor Pressure of Liquids as a Function of Temperature*

ARTHUR A. FROST AND DONALD R. KALKWARF†
Chemical Laboratory of Northwestern University, Evanston, Illinois
(Received August 27, 1952)

The slight reverse curvature in the plot of log$P$ *versus* $1/T$ (P, vapor pressure; T, absolute temperature) may be explained on the basis of the nonideal behavior of the vapor together with the change in heat of vaporization with temperature. If it is assumed that ΔH is linear with T and that the van der Waals a/V^2 term is a first approximation to the deviation from the ideal, the following equation may be obtained by integration of the Clapeyron equation:

$$\log P = A + \frac{B}{T} + C \log T + D\frac{P}{T^2}.$$

The last term is the nonideal gas correction with constant $D = a/2.303R^2$. With constants A, B, and C determined empirically, the equation reproduces experimental vapor pressures from the triple point to the critical point with an average deviation of 0.3 percent.

NUMEROUS equations, both empirical and theoretical have been given relating vapor pressure P with absolute temperature T.[1] The simplest theoretical relation is the familiar Clausius-Clapeyron equation:

$$\log P = A - (B/T), \tag{1}$$

where A and B are empirical constants. This equation is derived from the thermodynamically exact Clapeyron equation:

$$dP/dT = \Delta H/T\Delta V, \tag{2}$$

where ΔH is the heat of vaporization and ΔV the corresponding increase in volume on converting liquid to vapor. The derivation of (1) assumes: (a) constant ΔH independent of T, (b) that the vapor is an ideal gas, and (c) that the liquid volume is negligible. Equation (1) predicts linearity in a plot of log$P$ *versus* $1/T$.

Thodos,[2] in a careful survey of empirical vapor pressures of saturated hydrocarbons, has shown that the plot of log$P$ *versus* $1/T$ is not quite linear but really S shaped with a reversal of curvature between the boiling point and the critical point. This is illustrated by Fig. 1 in which data for n heptane as selected by Thodos have been graphed. The extra curve in the figure shows in exaggerated fashion the nature of the curvature which may just be seen in the actual plot by careful inspection.

The S shaped form is inherent in the empirical equation of Cox[3] which is as follows:

$$\log P = A[1 - (T_b/T)], \tag{3}$$

where P is the vapor pressure in atmospheres, T_b is the absolute boiling point and

$$A = A_c 10^{E(1-T_r)(F-T_r)}.$$

Here T_r is the reduced temperature T/T_{crit} and A_c, E, and F are constants. The quantity A was found to go through a minimum at a reduced temperature of about 0.92. A graphical interpretation of Cox's A can be obtained by solving Eq. (3) for A in the following form:

$$A = \frac{1}{T_b}\frac{\log P}{[(1/T_b) - (1/T)]}, \tag{4}$$

showing that A is proportional to the negative slope of the chord joining the points on the log$P$ *versus* $1/T$ plot corresponding to the boiling point ($\log P = 0$, $1/T = 1/T_b$) and an arbitrary point ($\log P$, $1/T$). It is seen that the reverse curvature of the log$P$ *versus* $1/T$ plot then corresponds to Cox's A going through a minimum.

DERIVATION OF THE EQUATION

Over the greater part of the temperature range (lower temperatures) the log$P$ *versus* $1/T$ plot is convex upwards. This has been explained quite well as due to a decrease in ΔH as T increases. In particular, if it is assumed that ΔH falls linearly as T increases but that the other assumptions of the Clausius-Clapeyron equation are satisfied, the Rankine equation results:[1]

$$\log P = A - (B/T) + C \log T. \tag{5}$$

Now the reversal in curvature being discussed in this paper occurs at higher temperatures, between the boiling point and the critical point. This is a region of high vapor pressure where deviations of the vapor from the ideal gas law would be most noticeable. It is only logical, then, to consider the effect of such deviations. Being unable to integrate the equation in complete generality, an approximate solution will be obtained which contains

* Presented at the Cleveland meeting of the American Chemical Society, April, 1951.

† Abstracted from the Ph.D thesis of Donald R. Kalkwarf. Present address: General Electric Company, Hanford Works, Richland, Washington.

[1] For a review see G. W. Thomson, Chem. Revs. **38**, 1 (1946), also A. Weissberger, *Physical Methods of Organic Chemistry* (Interscience Publishers, Inc., New York, 1949), second edition, Vol. I, Part 1, Chap. V by G. W. Thomson.

[2] G. Thodos, Ind. Eng. Chem. **42**, 1514 (1950).

[3] E. R. Cox, Ind. Eng. Chem. **28**, 613 (1936).

a first-order correction for the nonideal gas behavior such that the resulting equation should be good up to a reduced temperature of perhaps 0.8 or more.

Van der Waals' equation,

$$[P+(a/V^2)](V-b)=RT, \tag{6}$$

a and b being van der Waals' constants, may be put in the form:

$$V=b+\frac{RT}{P+(a/V^2)}. \tag{7}$$

If V in the correction term a/V^2 is approximated by RT/P, and it is realized that the liquid volume is to a first approximation equal to b, then the change in volume on vaporization is approximately

$$V=\frac{RT}{P[1+(aP/R^2T^2)]}. \tag{8}$$

As in the Rankine Eq. (5), it will be assumed that ΔH is linear in T; specifically,

$$\Delta H=\Delta H_0-C'T, \tag{9}$$

where ΔH_0 and C' are considered empirical constants. Substitution of (8) and (9) in the Clapeyron Eq. (2) yields

$$\frac{dP}{dT}=\frac{P(\Delta H_0-C'T)\left(1+\frac{aP}{R^2T^2}\right)}{RT^2}$$

or

$$\frac{d\ln P}{dT}=\frac{\Delta H_0}{RT^2}\left(1-\frac{C'}{\Delta H_0}T\right)\left(1+\frac{aP}{R^2T^2}\right) \tag{11}$$

or

$$d\ln P=\left(\frac{\Delta H_0}{RT^2}-\frac{C'}{RT}+\frac{aP\Delta H}{R^3T^4}\right)dT. \tag{12}$$

Equation (12) may be integrated if P in the small last term is given as a function of T. To a sufficient approximation, consistent with our previous assumptions, this P may be represented by

$$P=P_0e^{-\Delta H/RT}, \tag{13}$$

which is equivalent to the Clausius-Clapeyron equation. With this substitution, the last term in (12) integrates as follows:

$$\int\frac{aP\Delta H}{R^3T^4}dT=\frac{a\Delta HP_0}{R^3}\int\frac{e^{-\Delta H/RT}}{T^4}dT$$

$$=\frac{aP}{R^2T^2}\left[1+\frac{2RT}{\Delta H}+\frac{2R^2T^2}{(\Delta H)^2}\right]+\text{const}, \tag{14}$$

where it has been assumed that the ΔH of Eqs. (14), (13), and the last term of (12) is constant, this being permissible because this is a first-order correction. In the integrated result in (14), P has been reintroduced using (13). $RT/\Delta H$ is of the order of magnitude of 0.1; therefore, the last two terms of (14) will be neglected. Integration of the complete Eq. (12) then results in

$$\ln P=A'-\frac{\Delta H_0}{RT}-\frac{C'}{R}\ln T+\frac{aP}{R^2T^2} \tag{15}$$

or

$$\log P=A+\frac{B}{T}+C\log T+\frac{DP}{T^2}, \tag{16}$$

where A, B, and C are empirical constants, B and C being negative, and D is related to van der Waals' a by

$$D=a/2.303R^2. \tag{17}$$

Alternatively, all four constants may be evaluated empirically.[4]

Although Eq. (15) has been derived using only first-order corrections for the deviation of the vapor from an ideal gas and for the temperature variation of ΔH, and, therefore, presumably limited to temperatures not too near the critical, it is found as shown in the next section that the equation quite accurately reproduces vapor pressure data right up to the critical point. This situation may be partially understood by the following

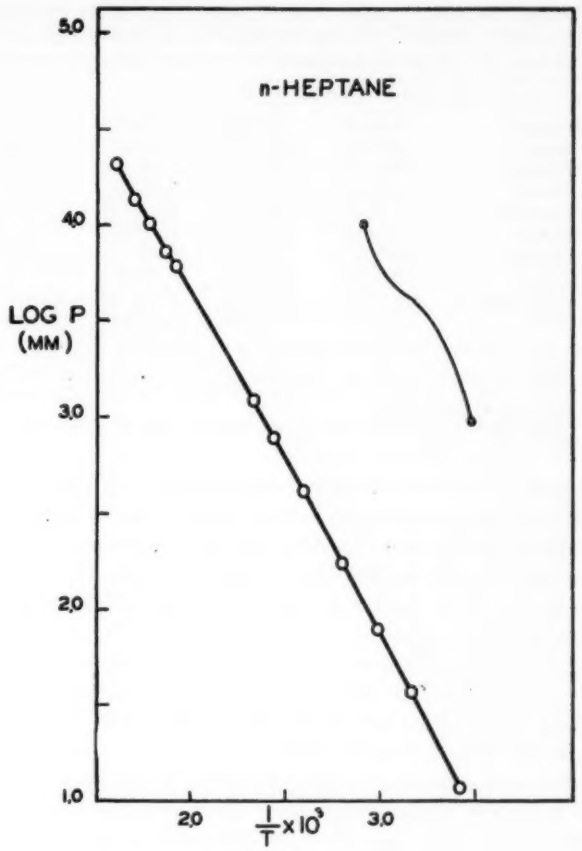

FIG. 1. Vapor pressure of n-heptane.

[4] R. E. Perry and G. Thodos, Ind. Eng. Chem. 44, 1649 (1952).

TABLE I. Numerical values of the constants used in the equation $\log P = A + (B/T) + C \log T + (DP/T^2)$ (P in mm Hg)

	A	$-B$	$-C$	D
Methane[a]	13.44740	567.5868	2.681065	0.191423
Ethane	16.74451	1068.273	3.566685	0.457881
Propane	19.05446	1429.728	4.227769	0.736275
n-Butane	21.68560	1793.194	5.024486	1.22954
n-Pentane	22.92307	2098.332	5.328139	1.61495
n-Hexane	25.08480	2436.187	5.955353	2.07240
n-Heptane	26.86378	2750.888	6.458216	2.67736
n-Octane	29.02343	3087.966	7.080892	3.17191
Carbon dioxide[b]	23.06810	1374.064	5.634143	0.305254
Water[c]	22.75017	2908.894	4.695517	0.424676

[a] Experimental data for hydrocarbons as selected by Thodos (reference 2).
[b] Data from C. H. Meyers and M. S. van Dusen, Natl. Bur. Standards J. Research **10**, 381 (1933).
[c] Data from N. S. Osborne and C. H. Meyers, Natl. Bur. Standards J. Research **13**, 1 (1934).

argument: As the critical temperature is approached, ΔV actually approaches zero rather than the finite value given by Eq. (8). Also ΔH approaches zero at an increasing rate rather than linearly as Eq. (9) would indicate. More explicitly, both ΔV and ΔH have as a limiting form near the critical point $(T_c - T)^n$, where T is the critical temperature and the exponent n is approximately 0.3 to 0.4.[5] If n is not the same in expressions for ΔV and ΔH for the same substance, the ratio $\Delta H/\Delta V$ would become zero or infinite at the critical point and result, according to the Clapeyron Eq. (2), in a zero or infinite slope in a vapor pressure-temperature plot. This latter is not observed; therefore, the same n must apply to both ΔV and ΔH, and as a result $\Delta H/\Delta V$ is to this approximation independent of temperature. This argument shows that the first-order corrections used in deriving (15) are better than first expected owing to a cancellation of higher-order corrections as the critical temperature is approached.[6]

EVALUATION OF THE CONSTANTS AND TEST OF THE EQUATION

Use of the equation $\log P = A + (B/T) + C \log T + (DP/T^2)$ requires the determination of the constants A, B, and C for the substance involved. As was shown in the preceding section, the constant D is simply related to the van der Waals constant a which in turn is derived from data at the critical point of the substance. The method used to determine the other constants is as follows: A reference point (P_f, T_f) is taken where the experimental data are felt to be particularly accurate. These data may be put into the equation to give $\log P_f = A + (B/T_f) + C \log T_f + (DP_f/T_f^2)$. Subtracting this expression from the general equation for $\log P$ eliminates the constant A and leaves

$$\log \frac{P}{P_f} = B\left(\frac{1}{T} - \frac{1}{T_f}\right) + C \log \frac{T}{T_f} + D\left(\frac{P}{T^2} - \frac{P_f}{T_f^2}\right).$$

[5] ΔV is related to the orthobaric density difference. For this latter see S. Sugden, J. Chem. Soc. **1927**, 1780. For ΔH see K. M. Watson, Ind. Eng. Chem. **35**, 398 (1943).
[6] For other qualitative considerations see O. L. I. Brown, J. Chem. Educ. **28**, 428 (1951).

If the proposed equation is correct, a plot of the quantity

$$\alpha = \frac{\log(P/P_f) - D[(P/T^2) - (P_f/T_f^2)]}{(1/T) - (1/T_f)}$$

$$versus \quad \frac{\log(T/T_f)}{(1/T) - (1/T_f)} = \beta$$

should be a straight line of slope C and intercept B.

As an example, the data for *n*-heptane are plotted in Fig. 2 using the critical point as the reference point (P_f, T_f). A straight line is determined by the data when the value 2.67 for D is used as calculated from van der Waals' constant a for *n*-heptane. When other values of D such as zero or one are used, the other curves shown in Fig. 2 are obtained. Thus, it is seen that data plotted in this way are very sensitive to changes in the value of D and that the correct value is that obtained from the van der Waals' constant a.

By visual inspection of the plot with $D = 2.67$ it is possible to pick two points which lie on the "best" straight line through the experimental data, and from them determine the slope C and intercept B. Knowing B, C, and D, the constant A may be evaluated by substituting in the general equation for any of the three points thus far used.

Although evaluation of the constants A, B, and C

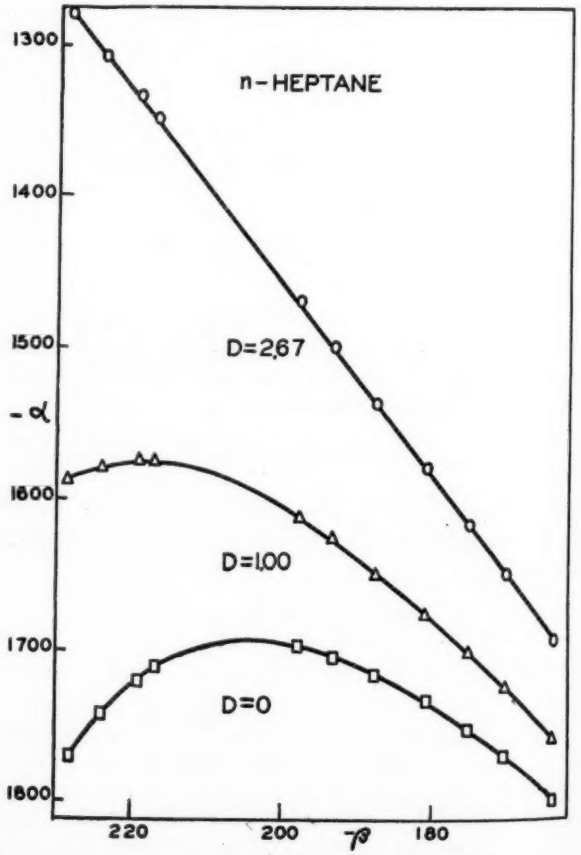

FIG. 2. Evaluation of constants of Eq. 16 for *n*-heptane.

by the method of least squares would undoubtedly improve the fit of the equation to the experimental data, it was felt that this simpler procedure was sufficient to indicate the accuracy of an equation of this type.

Table I shows the constants as evaluated for eight hydrocarbons together with carbon dioxide and water. For the hydrocarbons the reference point was the critical point; for carbon dioxide, the triple point; for water, the normal boiling point.

A summary of the average deviations between vapor pressures calculated from various equations and experimental values, utilizing data over the complete liquid range, is shown in Table II. Although the Thodos equation shows an average deviation of only 0.17 percent, somewhat less than the 0.31 percent of the present equation, it should be realized that the former has six empirical constants as compared with only three here.

The presence of P on both sides of the equation would make it difficult to solve for P as a function of T if it were not for the fact that the last term DP/T^2 is a small correction. It suffices to carry out a calculation by successive approximation, placing successively better values of P in the last term to obtain still better values of P from log$P$. Even in the most unfavorable case, at temperatures near the critical point, not more than three or four cycles are necessary to obtain a value of P accurate within half a percent.

TABLE II. Average deviation.[a]

	Eq. 1	Eq. 2	Eq. 3	Eq. 4
Methane	0.44 percent	1.43 percent	0.15 percent	... percent
Ethane	0.20	1.00	0.08	...
Propane	0.36	9.33	0.10	2.08
n-Butane	0.38	1.26	0.17	1.61
n-Pentane	0.25	1.13	0.42	1.15
n-Hexane	0.25	0.67	0.24	0.60
n-Heptane	0.34	1.35	0.07	0.51
n-Octane	0.31	0.85	0.14	0.89
Carbon dioxide	0.05	...	...	...
Water	0.41	...	...	...
Average	0.31	2.11	0.17	1.16

[a] Data for Eqs. 2, 3, and 4 as calculated by Thodos (see reference 2).
[b] Equation 1: This paper.
[c] Equation 2: Gamson and Watson (see reference 2).
[d] Equation 3: Thodos (see reference 2).
[e] Equation 4: Cox (see reference 3).

THE JOURNAL OF CHEMICAL PHYSICS VOLUME 21, NUMBER 2 FEBRUARY, 1953

The Effect of Pressure on Self-Diffusion in Carbon Disulfide*

R. C. KOELLER AND H. G. DRICKAMER
Department of Chemistry, University of Illinois, Urbana Illinois
(Received September 3, 1952)

A method has been developed for measuring diffusion coefficients in liquids to 10 000 atmospheres pressure. Measurements have been made over this pressure range at 0°, 20°, and 40°C for the system CS_2-CSS^{35}. The results are interpreted in terms of the enthalpy, entropy, and volume of activation as a function of temperature and pressure.

INTRODUCTION

IT is evident that one of the most important distinguishing characteristics of liquids is their molecular motion. The difference between a liquid and an isotropic solid lies in the immensely shorter residence time in the liquid phase. This comes about as a result of the free volume in liquids (about 10 percent of the molal volume) which considerably reduces cohesive forces and permits increased molecular motion. It is clear then that any understanding of this motion must be obtained through a comparison of diffusivity with free volume. When one realizes that many organic liquids may lose 20 to 30 percent of their molal volume in being compressed to 10 000 atmos, it is obvious that a study of diffusion over this pressure range will give information about the nature of motion in liquids which is not obtainable from any other approach.

A suitable cell was developed so that it was possible to determine diffusion coefficients in liquids under pressures up to 10 000 atmos. Radioactive tracers were used in the diffusing component and a scintillation counting technique was employed to give a continuous account of the concentration of tracer element at one end of the diffusion cell. Knowing the concentration at one end of the cell to be a function of time, it was possible to calculate the diffusion coefficient.

Results are presented in this paper for self-diffusion in carbon disulfide at 0°, 20°, and 40°C to 10 000 atmospheres pressure. The S^{35} tagged CS_2 was obtained from Tracerlab.

Further results on organic mixtures, on water, and on aqueous solutions will be reported in the near future.

THEORY

Various approaches to a kinetic theory for liquids have been made by Frenkel,[1] Eyring,[2] Wirtz,[3] Prigogine,[4] and others. While the methods differ, they all

* This work was supported in part by the AEC.

[1] J. Frenkel, Z. Physik **35**, 652 (1926).
[2] Eyring, Laidler, and Glasstone, *Theory of Rate Processes* (McGraw-Hill Book Company, Inc., New York, 1941).
[3] Wirtz, Physik Z. **44**, 221, 309 (1944).
[4] Prigogine, de Broukere, and Amand, Physica **16**, 577 (1950).

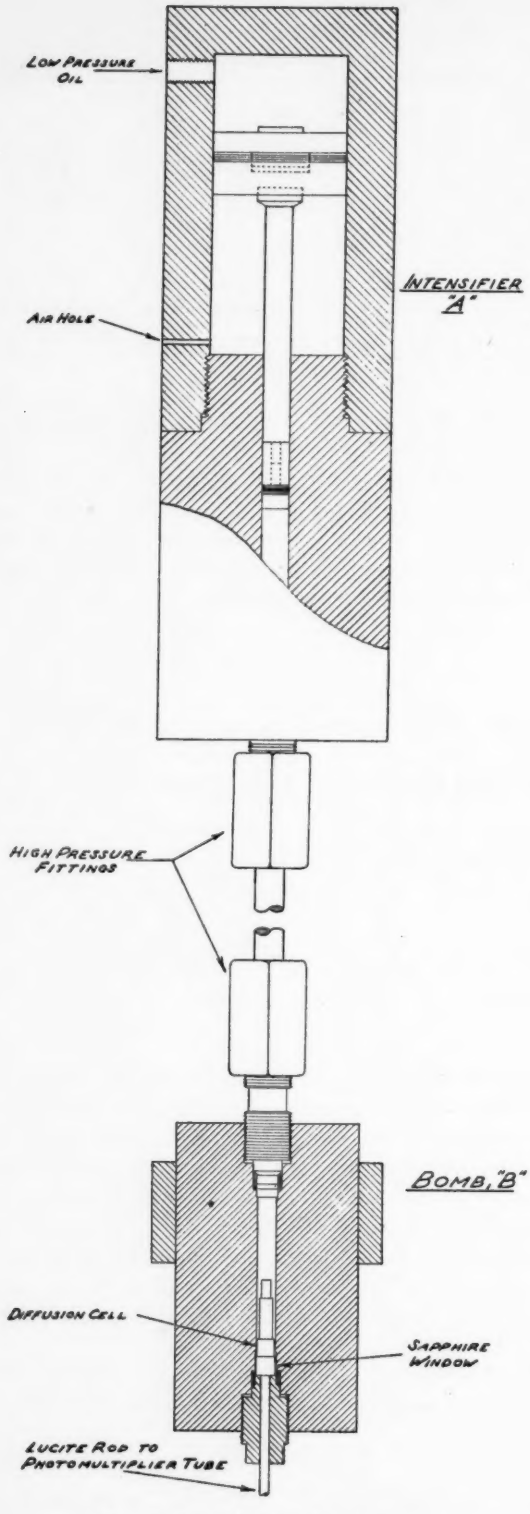

FIG. 1. General view of apparatus.

arrive at an equation of the form

$$D=\lambda^2 j_0 \exp\left(-\frac{\Delta F^\ddagger}{RT}\right), \tag{1}$$

where D=diffusion coefficient, λ=a characteristic distance, j_0=a characteristic frequency, $\Delta F^\ddagger$=free energy of activation, T=absolute temperature, and R=gas constant. Equation (1) can be written

$$D=\lambda^2 j_0 \exp\left(\frac{\Delta S^\ddagger}{R}\right)\exp\left(-\frac{\Delta H^\ddagger}{RT}\right), \tag{2}$$

introducing the entropy and enthalpy of activation.

Assuming negligible temperature dependence of λ, j_0 and $\Delta S^\ddagger$ over short ranges, $\Delta H^\ddagger$ can be evaluated from a plot of $\ln D$ *versus* $1/T$ either at constant pressure or at constant density.

Assuming λ^2 is proportional to $V^{\frac{2}{3}}$ and j_0 is independent of pressure, or varies slowly with pressure, one can write

$$\frac{\partial \ln D}{\partial p}=-\frac{2}{3}\frac{1}{V}\frac{\partial V}{\partial p}-\frac{1}{RT}\frac{\partial \Delta F^\ddagger}{\partial p}, \tag{3}$$

or

$$\frac{\partial \ln D}{\partial p}=-\frac{2}{3}\frac{1}{V}\frac{\partial V}{\partial p}-\frac{1}{RT}\Delta V^\ddagger, \tag{4}$$

where a new entity, the activation volume $\Delta V^\ddagger$ is introduced. This may be interpreted as the local volume change associated with motion, and is very useful in interpretation of the data.

It is not possible to evaluate $\Delta S^\ddagger$ from our data, but the change in $\Delta S^\ddagger$ above the value at atmospheric pressure ($\Delta S_0^\ddagger$) can be obtained from the relationship

$$(\Delta S_p^\ddagger-\Delta S_0^\ddagger)=R\ln\frac{D_p}{D_0}+\frac{2}{3}R\ln\frac{V_0}{V_p}+\frac{(\Delta H_p^\ddagger-\Delta H_0^\ddagger)}{T}. \tag{5}$$

Two equations commonly used to predict diffusion coefficients are the Stokes-Einstein equation and Arnold's[5] equation. Insofar as their pressure dependence is concerned the former may be written

$$D_p/D_0=\eta_0/\eta_p(V_0/V_p)^{\frac{1}{3}}, \tag{6}$$

where the η's are viscosities. The Arnold relationship becomes

$$D_p/D_0=(\eta_0/\eta_p)^{\frac{1}{3}}(V_0/V_p)^{\frac{1}{3}}. \tag{7}$$

As will be shown later, neither equation holds even approximately.

EQUIPMENT AND PROCEDURE

The diffusion coefficients were measured in a cell which fit in a high pressure bomb as described below. Pressures below 2000 atmospheres were obtained by the use of a Blackhawk hand pump and measured directly by means of a Bourdon gauge calibrated against a dead weight gauge. Above 2000 atmospheres an intensifier was used. The standard of pressure used in this range was a Manganin gauge calibrated at 2000 atmospheres

[5] J. H. Arnold, J. Am. Chem. Soc. **52**, 3937 (1930).

against a dead weight gauge and at the freezing point of mercury at 0°C. Because rapid changes in pressure, which were frequent in this work, damaged the Manganin gauge, it was not left in the circuit during actual runs. A Bourdon gauge on the low pressure end of the intensifier was calibrated against the Manganin gauge and used to measure the pressure. The low pressure gauge was recalibrated against the Manganin gauge at frequent intervals. It never varied more than 3–4 percent, and this much only when a piston was repacked. The pressure measurements should be accurate within 1 percent.

A general view of the setup is shown in Fig. 1. The intensifier is connected to a lower bomb. At the bottom of this bomb is a plug with a synthetic sapphire window. The windows used were $\frac{1}{2}$ in.$\times\frac{1}{2}$ in. cylinders with axis perpendicular to the c axis of the crystal. They were made by the Linde Air Products Company. The seal was a Poulter[6] type sapphire to metal seal. The surface supporting the window was first prepared by surface grinding and then by hand-lapping with 3/0 and 4/0 emery paper. The flatness of the surface could be checked through the use of an optically flat quartz block with monochromatic light. However, the final test was whether or not the window would hold to the dry surface while held in an inverted position. The plug was lapped until this condition was achieved.

The bomb was located in a temperature bath controlled to ± 0.1°C.

The cell is shown in Fig. 2. First, it was necessary to prepare the scintillation crystal which was sealed to the top of the quartz window in the cylinder C. Because of solubility considerations it was necessary to use a cadmium tungstate crystal, sealed in with water glass. The crystal was made in the shape of a flat disk with a maximum thickness of 1/64 in. and of a diameter sufficient to completely cover the window (0.35 in.). After allowing time for the adhesive holding the crystal to dry, a special mandrel was used to screw the insert ring R down firmly against the crystal; this was done, of course, with the fritted glass G-2 removed from the ring. G-2 was then inserted into the end of a small cylinder fitted with a lapped piston. This pump was then immersed in a nonradioactive portion of the liquid to be studied, and the piston pumped until the fritted glass was filled with liquid to the exclusion of air. After having been pushed out of the pumping cylinder, G-2 was lifted out of the liquid with fine tweezers and dropped into the insert ring in the cylinder C to rest against the crystal. The next step was to fill the radioactive end of the cell.

The fritted glass G-1 was sealed tightly into the sleeve S using litharge cement. The sleeve was set into a small glass reservoir and, with the piston removed, it was filled to the top with radioactive liquid. The piston was then inserted and slowly depressed until it touched the fritted glass. Keeping the bottom of the sleeve immersed in the liquid, the piston was pumped with very short strokes until all the air had been displaced from the fritted glass. The piston was then set to allow for a predetermined gap between the top of G-1 and the bottom of the piston and locked in this position with the set screw M to prevent it from moving during the next operation. The significance of this gap will be discussed below. After locking the piston, Duco cement was applied around the piston at the top of the sleeve. The purpose of the Duco, a rather viscous, quick-drying acetate cement, was to prevent leakage of either radioactive liquid out of or pressure transmitting liquid into the cell during application of pressure. The sleeve assembly was then lifted from the liquid in the reservoir, the threads were wiped dry, and it was immediately screwed into the cylinder C firmly against the lower fritted glass G-2. The set screw N was in a loosened position during this operation to allow for the escape of air. N was then locked tight and Duco applied around the sleeve at the top of the cylinder. The final step prior to placing the cell into the bomb was to remove the set screw M from the sleeve.

Time was of the essence throughout the entire operation described above. It was generally the case that the bomb was sealed and pressure applied within 50 seconds of the time that the sleeve and cylinder were screwed together.

Though not dimensioned, the cell shown in Fig. 2 is drawn to scale. The outside diameters of the cylinder, sleeve and piston were 0.470 in., 0.350 in., and 0.2500 in. ± 0.0001 in., respectively. The piston and sleeve were hand-lapped together. The final fit was such that it was

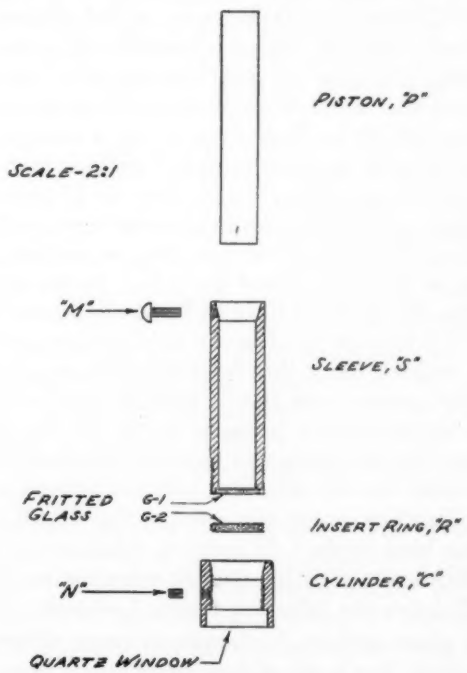

FIG. 2. Details of diffusion cell.

[6] T. C. Poulter, Phys. Rev. 35, 297 (1930).

TABLE I. Measured diffusion coefficients for $CS^{35}S$ in CS_2.

Temp °K	Pressure atmos	Effective cell length cm	Observed $D\times10^5$ cm²/sec	ρ g/cc
293	3500	0.557	2.36	1.483
293	6500	0.611	1.57	1.580
293	1500	0.504	3.00	1.389
293	5000	0.611	2.07	1.537
293	9100	0.665	0.70	1.646
293	7500	0.665	1.45	1.606
293	800	0.504	3.49	1.340
293	200	0.504	3.29	1.284
273	7000	0.611	0.75	1.618
273	5000	0.611	1.25	1.562
273	3500	0.557	1.50	1.51
293	2000	0.504	2.40	1.417
273	2500	0.557	1.70	1.467
273	1500	0.504	2.46	1.414
273	800	0.504	2.18	1.366
273	200	0.504	2.44	1.312
273	2000	0.504	1.80	1.442
273	10 000	0.665	0.164	1.691
313	7000	0.611	2.76	1.569
313	3500	0.557	5.60	1.461
313	5000	0.611	3.58	1.513
313	1000	0.504	4.2	1.323
313	2000	0.557	4.05	1.389
313	200	0.504	4.67	1.250
313	10 000	0.665	1.72	1.642
313	2900	0.557	3.52	1.435
293	2500	0.557	2.78	1.44
293	1000	0.504	3.49	1.356

possible to draw acetone into the sleeve and then hold the assembly in mid-air without losing any liquid. The cell was made of stainless steel. A fine thread, 48 TPI, was used to screw the cylinder and sleeve together. Both *M* and *N* were 2–56 stainless screws.

The quartz windows used in the bottom of the cylinder were approximately 0.10 in. thick with a diameter of 0.390 in. to 0.400 in. Some of the windows used were purchased from Hanovia Chemical Manufacturing Company, but most of them were made in this laboratory from quartz rod. Both pieces of fritted glass had a diameter of 0.300 in. They were cut out of the filter plate from a 100-mm Buchner funnel of medium porosity.

It was assumed that plug-like flow would prevail and thus upon compression the interface between active and nonactive liquid would be in a plane somewhere below the top of the lower fritted glass, *G*-2. It was apparent that the sleeve would have to be filled to some height above *G*-1 in order to allow for this compression. Also, it was desired that a thin layer of liquid remain above *G*-1 after pressure had been applied in order to be sure of having hydrostatic pressure in the cell. In order to facilitate the calculation of the diffusion coefficient, it is desirable that the interface between active and nonactive liquid be at the mid-point of the cell after pressure has been applied. In order to calculate the necessary thicknesses of fritted glass for this situation to exist, we will define the following terms: l_1=length of upper fritted glass (active), l_2=length of lower fritted glass (nonactive), l_3=depth of free liquid above upper glass after pressure has been applied, f=ratio of effective to apparent path length in fritted glass, and $\sigma=V_p/V_0$ for the liquid concerned at any given temperature. The maximum amount of nonactive liquid available is that contained in the lower fritted glass at 1 atmos. Upon the application of pressure we assume that there will be "plug-flow" and thus the upper surface of this liquid will be depressed to some distance below the top of the fritted glass. The thickness of this compressed layer of liquid is the half-cell length. Thus, after compression the total effective cell length is equal to $2fl_2\sigma$. It then follows that

$$2fl_2\sigma=f(l_1+l_2)+l_3;$$

solving for l_2, we have

$$l_2=\frac{l_1+(l_3/f)}{2\sigma-1}.$$

f was found to be 2.1, l_3 was arbitrarily set at 0.051 cm, and l_1 was fixed at 0.089 cm. This fixed value for l_1 was found to give the most satisfactory over-all cell length. Thus, it is now possible to calculate l_2 as a function of σ for each liquid used. Values of l_2 found were rounded off to the nearest (0.025 cm) and thicknesses of 0.127, 0.153, 0.178, and 0.203 cm were found satisfactory to cover the entire pressure range.

Before each run, it was necessary to calculate the proper clearance between the piston and the upper fritted glass so that we would have l_3=0.051 cm after pressure had been applied. Knowing the void fraction of the fritted glass, (determined by weighing to be 0.35), the total volume of liquid in the cell under pressure was calculated. This was then divided by σ to give the volume of the same amount of liquid at one atmosphere. The necessary clearance to be set when filling the cell was then the sum of l_3 and a length of piston stroke equivalent to the volume loss on compression.

The compressibility data of Bridgman[7] were used.

The effective path length for diffusion through the fritted glass is not the same as the apparent path length.

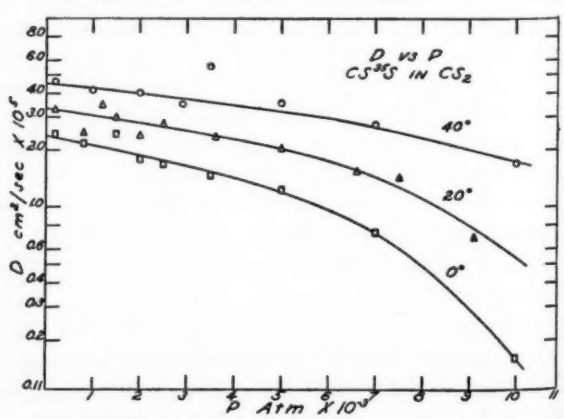

FIG. 3. Diffusion coefficient *versus* pressure CSS^{35} in CS_2.

[7] P. W. Bridgman, *The Physics of High Pressure* (The Macmillan Company, New York, 1931).

Therefore, it was necessary to calibrate the fritted glass. To do this, several atmospheric pressure runs were made with water and the effective path length was calculated by using values for the diffusion coefficient of D_2O in H_2O as reported by Orr and Butler.[8] For the purpose of calibration, tritiated water was used. These results will be discussed in detail in a further paper. The effective path length for the fritted glass used in this experiment was 2.1 times the apparent length. It has been our experience in this laboratory that the path length does not vary with the fluid used, for a given piece of glass.

A scintillation counting technique was employed to provide a means of continuously following the approach to equilibrium in the diffusion cell. After the start of a run, tagged molecules diffuse from the upper to the lower fritted glass at a rate indicative of the diffusion coefficient. As the concentration of the radioactive tracer builds up at the surface of the crystal the frequency of light pulses given off by the crystal increases proportionately. The light pulses pass out of the cell through the quartz window and then through the sapphire window out of the bomb and down a Lucite rod to the photomultiplier tube. Water-white petroleum ether was used as pressure transmitting fluid to allow for the passage of the maximum amount of light between the quartz and sapphire window. A Lucite rod conducted the light from the sapphire window to the photomultiplier tube.

RESULTS

From the plot of counts *versus* time a diffusion coefficient could be calculated as has been described in detail in previous publications.[9,10] An advantage of the continuous analysis is that any effect of convection at the beginning of the run could be detected and eliminated as described by Robb.[10]

The diffusion coefficients are shown in Table I.

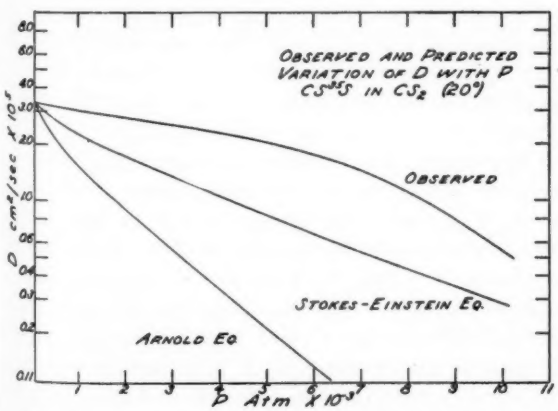

FIG. 4. Observed and predicted variation of diffusion coefficient with pressure.

[8] W. J. C. Orr, and J. A. V. Butler, J. Chem. Soc. **1935**, 1273.
[9] K. D. Timmerhaus and H. G. Drickamer, J. Chem. Phys. **19**, 1242 (1951).
[10] W. L. Robb and H. G. Drickamer, J. Chem. Phys. **19**, 1504 (1951).

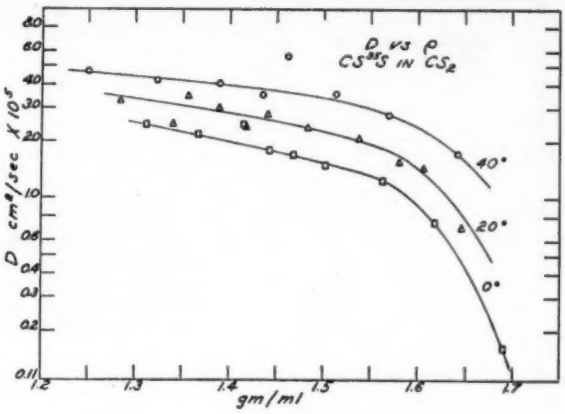

FIG. 5. Diffusion coefficient *versus* density CSS^{35} in CS_2.

The graph in Fig. 3 of ln$D$ plotted as a function of P illustrates that the self-diffusion coefficient for carbon disulfide is a monotonically decreasing function of pressure along the three isotherms studied, 0, 20, and 40°C. The decrease in D over the 10 000-atmos range in pressure is not nearly so great as that predicted by the Stokes-Einstein and Arnold[5] equations. This is clearly seen in Fig. 4 where the 20° isotherm of ln$D$ *vs* P is plotted along with the curves predicted by these two equations. At a pressure of 6000 atmos the actual decrease in D from atmospheric pressure is 46 percent; the Stokes-Einstein equation predicts a decrease of 80 percent and using Arnold's equation the decrease would be 96 percent. Bridgman's[7] viscosity data were used.

In comparing the three isotherms, a plot of ln$D$ as a function of density is also informative. Such a graph is shown in Fig. 5. The effect of using density rather than pressure as abscissa is to move the isotherms closer together and to make them more symmetrical. This is particularly noticeable at the high density end of the scale.

In general it appears that the three isotherms have the same shape and are merely displaced upwards as temperature is increased. The similarity of the three isotherms further indicates that the molecular geometry and mechanism of motion must be primarily a function of density. If this is the case, the displacement between isotherms is then merely the result of a higher frequency of migration at the higher temperature because of an increased degree of thermal excitation in the individual molecules. It can also be inferred from the curves in Fig. 5 that beyond a density of 1.55 (P about 5000 atmos) the molecular packing rapidly "closes in" to inhibit diffusion.

Activation enthalpies were calculated and are shown plotted as a function of pressure in Fig. 6. Two calculations were made. The first, based on the curves in Fig. 3, was for $\Delta H^{\ddagger}$ at constant pressure and in the second case, $\Delta H_{\rho}^{\ddagger}$ was obtained at constant density, using the curves in Fig. 5. Qualitatively, both $\Delta H^{\ddagger}$ and $\Delta H_{\rho}^{\ddagger}$ show the same trend of increasing as the pressure is

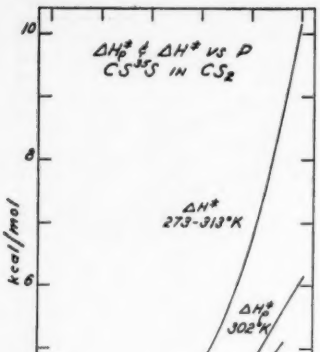

FIG. 6. Enthalpies of activation (at constant pressure and at constant density) as a function of pressure.

increased. Over the entire pressure range the activation enthalpy at constant pressure is independent of temperature for the interval 273 to 313°K. At constant density, however, $\Delta H_\rho^\ddagger$ varies with the temperature, being in general higher at the higher temperature. Curves of $\Delta H_\rho^\ddagger$ are therefore shown for 283 and 302°K. At constant pressure the heat of activation increases from 2.7 kcal/mole at atmospheric pressure to 10.1 kcal/mol at 10 000 atmos. Over the same pressure range, $\Delta H_\rho^\ddagger$ goes from about 2.3 to 6.1 kcal/mol at 302°K.

Although the heat of activation at constant density varies more erratically with pressure than does that at constant pressure, the former is probably of more physical significance. $\Delta H_\rho^\ddagger$ is a heat of activation for a definite molecular configuration while $\Delta H^\ddagger$ is an average between two different packings. Normally, one would expect the enthalpy of activation at constant density to remain constant with temperature. Since $\Delta H_\rho^\ddagger$ varies with temperature it is apparent that density is not the only measure of configuration.

In accordance with Levi's[11] observation, we should expect to find a positive entropy of activation associated with the high values of $\Delta H^\ddagger$ calculated. An absolute value of $\Delta S^\ddagger$ cannot be ascertained; however, the change in $\Delta S^\ddagger$ has been calculated. These data are plotted as $\Delta S^\ddagger - \Delta S_0^\ddagger$ *vs* P in Fig. 7, where it is seen that the activation entropy increases pressure. The total increase is 22 cal/°K/mol in 10 000 atmos.

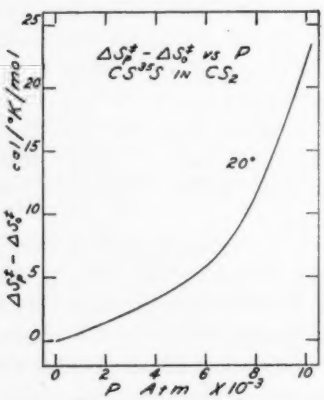

FIG. 7. Entropy of activation (above the atmospheric pressure value) as a function of pressure.

[11] D. L. Levi, Trans. Faraday Soc. **42a**, 152 (1946).

The increasing activation entropy with increasing pressure indicates that the structure, i.e., the normal structure, not the activated, becomes more ordered as the density is increased. Interpreted in other terms, the increasing entropy of activation indicates that the process of activation prior to migration of a molecule involves an increasing degree of disruption in the structure of the liquid. That is, the necessary shifting of neighbors becomes more of a complicated process as density is increased. Levi's interpretation is that a positive $\Delta S^\ddagger$ indicates an increase in the degrees of freedom in the activated state over those in the initial state. We might say that a certain minimum number of dgrees of freedom are necessary for a molecule to be in the activated state. As density is increased, the degrees of freedom of a molecule in the initial state are decreased and therefor the span between initial and activated states is increased. Such a picture as this also serves to explain the increase in heat of activation with increasing pressure. It is reasonable to assume a higher energy requisite for a molecule to convert over the increasing span from initial to activated state.

TABLE II. $\Delta F^\ddagger - \Delta F_0^\ddagger$ for self-diffusion in CS_2 at 20°C.

P (atmos)	$\Delta F^\ddagger - \Delta F_0^\ddagger$ (cal/mol)
1000	15
2000	40
3000	81
6000	268
10 000	930

The observation that a high value for the heat of activation for diffusion will have associated with it a large activation entropy has been verified by the data discussed above. Considering this in view of the thermodynamic relationship: $\Delta F - \Delta H - T\Delta S$, it appears that the free energy of activation must remain substantially constant with pressure. For this reason it was of interest to calculate the change in $\Delta F^\ddagger$ at any pressure from that at atmospheric pressure. The values obtained are shown in Table II. Eyring[2] has estimated the activation entropy to be essentially zero for atmospheric pressure diffusion in several organic solutions and for diffusion of bromine in CS_2. It is reasonable to assume the same is true for self-diffusion in CS_2. Then $\Delta F_0^\ddagger = \Delta H_0^\ddagger = 2680$ cal/mole. Thus we see from the above table that over a 6000-atmos range the free energy of activation increases by only 10 percent. The increase in 10 000 atmos is 35 percent.

Activation volumes were calculated for the three isotherms. Compressibility data given by Bridgman[7]

were used. The results of the calculations are shown plotted as the ratio $\Delta V^\ddagger$ to $\bar{V}$, the molal volume, as a function of pressure in Fig. 8 and as a function of density in Fig. 8. Here again it is seen that using density as abscissa rather than pressure has the effect of moving the isotherms closer together. It was observed above in the curves of $\ln D$ *vs* ρ (Fig. 4) that beyond $\rho=1.55$ the diffusion coefficient decreases rapidly. From Fig. 8 it is seen that the activation volume increases rapidly in the same range. In the lower density range up to $\rho=1.55$, the ratio $\Delta V^\ddagger/\bar{V}$ appears to increase linearly with density.

One might expect that as density is increased and free volume decreased it should also follow that the activation volume would decrease; and furthermore, that $\Delta V^\ddagger$ would be higher at a higher temperature. A contrary effect is observed in the data in that the highest activation volumes occur at the lowest temperature for a given density, and $\Delta V^\ddagger/V$ increases with density.

A reasonable explanation is based upon the deduction made above that the sharp rise of activation entropy with density is indicative of an increase in the orderliness of the liquid structure. Assuming this to be the case, it is then reasonable to assume further that as free volume is decreased and the degree of order increased, the number of "effective" neighbors to a molecule, for purposes of determining local expansion during activation for diffusion, is also increased. In other words, as the degree of order in the liquid is increased the local expansion necessary for a single molecule to diffuse becomes less local and is felt throughout a greater portion of the liquid surrounding the molecule. The free volume associated with any molecular configuration in a liquid is a function of the configuration and is at a minimum value in the initial or equilibrium state, such that a slight distortion will cause an increase in the free volume. Thus we see that as density increases the complexity of the liquid structure increases, the local expansion necessary for a single molecule to diffuse effects the orientation of a greater number of surrounding molecules causing an increase in the free volume change associated with the distortion. We measure, indirectly, an apparent activation volume which is the sum of the actual volume necessary for the activation of a molecule plus the free volume increase associated with the local expansion of the structure.

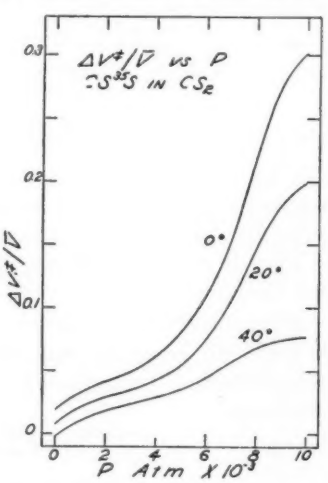

FIG. 8. Activation volume as a function of pressure.

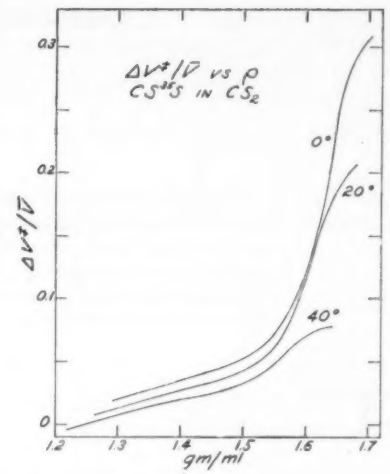

FIG. 9. Activation volume as a function of density.

Insofar as order of magnitude is concerned, it is seen in Fig. 8 that the activation volume per mole increases from zero at atmospheric pressure to 7.8 percent at 10 000 atmos at 40°C; at 20° the increase over the same range is from 0.8 to 20 percent and at 0° the activation volume rises from 1.9 to 30 percent of the molal volume.

The maximum value observed for the activation enthalpy at constant density $\Delta H_\rho^\ddagger$ is 6.1 kcal/mole at 10 000 atmos. There are no data available for diffusion in solid CS_2 or in solid organic compounds, but Barrer[12] lists activation enthalpies for diffusion in solid salts and metals. For salts the average $\Delta H^\ddagger$ is about 15 kcal/mol and for metals it is about 40 kcal/mole. Both of these values are greater than the maximum observed for CS_2 at 10 000 atmos. Thus it appears that diffusion in carbon disulfide retains the characteristics of the phenomenon in the liquid phase even though the liquid is compressed to a density exceeding that of the solid at atmospheric pressure.

H. G. Drickamer would like to acknowledge the assistance received from visits to the laboratories of A. W. Lawson at the University of Chicago and P. W. Bridgman at Harvard University. R. C. Koeller would like to acknowledge the financial assistance from the Pan-American Refining Corporation and from the U. S. Atomic Energy Commission.

[12] R. M. Barrer, *Diffusion in and through solids* (The Macmillan Company, New York, 1941).

A Quantum-Mechanical Treatment of Virial Coefficients*

JOHN E. KILPATRICK
Department of Chemistry, The Rice Institute, Houston, Texas, and The Los Alamos Scientific Laboratory, University of California, Los Alamos, New Mexico

(Received September 22, 1952)

The virial equation of state for gases has been developed with the quantum-mechanical grand partition function as a basis, instead of with the usual Slater sum or the density matrix. Attention is thereby focused on the energy levels of systems of one, two, three, etc., molecules rather than on their wave functions. An explicit, closed solution has been found for the nth virial coefficient in terms of the first n cluster integrals which is valid either classically or quantum mechanically. A simple generating function for the virial coefficients has been proposed.

THE partition function for an assembly of N molecules† is given by

$$Z_N=\sum \exp(-E/kT). \tag{1}$$

The summation is over all possible quantum states of the N molecules. E is a running symbol for the energy of these states. Alternatively we may write

$$Z_N=\sum_E \Omega \exp(-E/kT), \tag{2}$$

where Ω is the degeneracy of the state with energy E and the summation is over all energy states.

The grand partition function is given by

$$(GPF)=\sum_N Z_N z^N, \tag{3}$$

where $z=\exp(\mu/kT)$. z is the absolute activity and μ is the usual partial molecular Gibbs free energy or chemical potential. (GPF) is a function of the absolute activity z (or the chemical potential μ), the volume V and the temperature T of the assembly. It is related to the internal energy E, the number of molecules N and the pressure-volume product PV by the equations

$$E=kT^2(\partial/\partial T)\ln(GPF), \tag{4}$$

$$N=z(\partial/\partial z)\ln(GPF), \tag{5}$$

$$PV=kT\ln(GPF). \tag{6}$$

The physical meaning of Eqs. (4) and (5) can be seen from their expansions:

$$E=\frac{\sum_E \sum_N E\Omega \exp(-E/kT)z^N}{\sum_E \sum_N \Omega \exp(-E/kT)z^N}, \tag{7}$$

$$N=\frac{\sum_E \sum_N N\Omega \exp(-E/kT)z^N}{\sum_E \sum_N \Omega \exp(-E/kT)z^N}. \tag{8}$$

For an assembly with given values for z, V, and T, the observed values of the internal energy and the number of molecules present will be the average of all possible values of E and N, each with the relative probability of its occurrence as a weighting factor.

We now expand $\ln(GPF)$ as a power series in z:

$$\ln \sum_{N=0}^{\infty} Z_N z^N=\sum_{j=1}^{\infty} Vg_j z^j. \tag{9}$$

The coefficients, Vg_j, are obtained by comparing corresponding powers of z:

$$Vg_1=Z_1, \tag{10a}$$

$$Vg_2=Z_2-\tfrac{1}{2}Z_1^2, \tag{10b}$$

$$Vg_3=Z_3-\tfrac{1}{2}(Z_2Z_1+Z_1Z_2)+\tfrac{1}{3}Z_1^3, \tag{10c}$$

$$Vg_m=Z_m-\tfrac{1}{2}\sum_{\substack{i\\ i+j=m}}\sum_{j} Z_iZ_j+\tfrac{1}{3}\sum_{\substack{i\\ i+j+k=m}}\sum_{j}\sum_{k} Z_iZ_jZ_k-\cdots. \tag{11}$$

The general relation between the Vg_j and the Z_N can be expressed in the more compact notation:

$$Vg_j=\sum_{i=1}(-)^{i-1}(i-1)!\sum_{(k_m)}\prod_{m=1}\frac{Z_m{}^{k_m}}{k_m!}. \tag{12}$$

$$\begin{cases}\sum k_m=i\\ \sum mk_m=j\end{cases}$$

The second summation symbol is to be interpreted as: sum over all sets of positive or zero integers consistent with the restrictive conditions given below.

The g's may now be considered known functions of the Z_N's.

If we substitute the right-hand member of Eq. (9) for $\ln(GPF)$ in Eqs. (5) and (6), perform the indicated differentiation, introduce $x=N/V$ and clear out V, we obtain

$$P=kT\sum g_j z^j, \tag{13}$$

$$x=\sum jg_j z^j. \tag{14}$$

In order to eliminate z between these two equations, we invert the latter:

$$z=\sum C_k x^k. \tag{15}$$

* Work done under the auspices of the AEC.

† Our symbol Z_N is taken from the notation used by Hirschfelder, de Boer, *et al.* in their forthcoming book *The Properties of Gases*. Z_1 and Z_N are the same as (pf) and (PF) as used by G. S. Rushbrooke, *Statistical Mechanics* (Oxford University Press, London, 1949).

The C_k's may be obtained as functions of the g_j's by introducing Eq. (15) into Eq. (14) and matching coefficients:

$$C_1=1/g_1, \tag{16a}$$

$$C_2=-2g_2/g_1^3, \tag{16b}$$

$$C_3=(8g_2^2-3g_1g_3)/g_1^5 \text{ etc.} \tag{16c}$$

With these values for the C_k's, Eq. (15) may be substituted into Eq. (13) and z eliminated:

$$P=kT\left(x-\frac{g_2}{g_1^2}x^2-\frac{2g_3g_1-4g_2^2}{g_1^4}x^3-\cdots\right). \tag{17}$$

The coefficient of x^n in Eq. (17) is the nth molecular virial coefficient.

The elimination of z between Eqs. (13) and (14) just outlined is purely algebraic. The same result may be achieved with considerably less effort by the use of complex variable theory. Equation (13) is written in the form

$$P=kT\sum_1 g_jz^j=kT\sum_1 \alpha_kx^k, \tag{18}$$

and therefore

$$\sum_1 g_jz^j=\sum_1 \alpha_kx^N. \tag{19}$$

We eliminate x by means of Eq. (14), multiply by $z^{-n-1}dz$ and integrate around the origin:

$$g_n=\frac{1}{2\pi i}\oint z^{-n-1}\sum\alpha_k(\sum jg_jz^j)^kdz. \tag{20}$$

Therefore g_n is equal to the coefficient of z^n in the expansion of $\sum\alpha_k(\sum jg_jz^j)^k$. It is advantageous to replace jg_j by the new symbol p_j. We obtain the family of equations

$$p_1=p_1\alpha_1, \tag{21a}$$

$$\tfrac{1}{2}p_2=p_2\alpha_1+p_1^2\alpha_2, \tag{21b}$$

$$\tfrac{1}{3}p_3=p_3\alpha_1+2p_2p_1\alpha_2+p_1^3\alpha_3, \tag{21c}$$

or in general,

$$\frac{p_n}{n}=\sum_{i=1} i!\alpha_i\sum_{(r_s)}\prod_{s=1}\frac{p_s^{r_s}}{r_s!}, \tag{22}$$

$$\begin{cases}\sum_1 r_s=i\\ \sum_1 sr_s=n.\end{cases}$$

These equations can be solved for α_1, α_2, α_3, in turn:

$$\alpha_1=1, \tag{23a}$$

$$\alpha_2=(-\tfrac{1}{2}p_2)/p_1^2, \tag{23b}$$

$$\alpha_3=(-\tfrac{2}{3}p_3p_1+p_2^2)/p_1^4, \tag{23c}$$

$$\alpha_4=(-\tfrac{3}{4}p_4p_1^2+3p_3p_2p_1-5/2p_2^3)/p_1^6, \tag{23d}$$

$$\alpha_5=(-\tfrac{4}{5}p_5p_1^3+4p_4p_2p_1^2+2p_3^2p_1^2-12p_3p_2^2p_1+7p_2^4)/p_1^8. \tag{23e}$$

These equations give α_n, the nth molecular virial coefficient, in terms of the p_j and therefore of the g_j. The g_j are known functions of the partition functions for n molecules, $n-1$ molecules, $\cdots$, two molecules and one molecule. The physical significance of the g_j will be discussed later.

A more complicated treatment of Eqs. (13) and (14) leads to an explicit solution for the nth virial coefficient:

$$\alpha_n=\sum_{(k_j)}\frac{(-)^{n-k_1-1}(n-1)(2n-k_1-3)!}{n!p_1^{2n-2}}p_1^{k_1}\prod_{j=2}\frac{p_j^{k_j}}{k_j!}. \tag{24}$$

$$\begin{cases}\sum_1 k_j=n-1\\ \sum_1 jk_j=2n-2\end{cases}\qquad(n>1)$$

The sets of k_j, the powers of the various p_j products, are merely the various ways (independent of order) that $2n-2$ can be partitioned into $n-1$ parts. The proof of this expression will be found in the appendix.

As an example of the use of Eq. (24) we shall calculate one of the terms of α_8. The step by step solution of Eq. (22) as far as α_8 is tedious, and the direct algebraic solution would be very laborious.

All of the ways that 14 can be partitioned into 7 parts are given below:

8 1 1 1 1 1 1	5 2 2 2 1 1 1
	4 3 2 2 1 1 1
7 2 1 1 1 1 1	3 3 3 2 1 1 1
6 3 1 1 1 1 1	
5 4 1 1 1 1 1	4 2 2 2 2 1 1
	3 3 2 2 2 1 1
6 2 2 1 1 1 1	
5 3 2 1 1 1 1	3 2 2 2 2 2 1
4 4 2 1 1 1 1	
4 3 3 1 1 1 1	2 2 2 2 2 2 2

It is evident there are 15 terms in α_8. The partition 5 2 2 2 1 1 1 corresponds to the p_k product $p_5p_2^3p_1^3$. The complete term is

$$\frac{(-)^{8-3-1}(7)(10!)}{8!p_1^{14}}\frac{p_5p_2^3p_1^3}{1!3!}=\frac{105p_5p_2^3p_1^3}{p_1^{14}}.$$

Written directly as a function of the g_j's, this term becomes

$$105(5)(2^3)g_5g_2^3g_1^3/g_1^{14}.$$

CLASSICAL FORM OF EQUATIONS

It is evident upon comparing Eqs. (13) and (14) with those of Rushbrooke[1] and of Mayer and Mayer[2] that our g_j is the quantum-mechanical equivalent of Rushbrooke's g_j, and that $g_j=g_1^jb_j$, where b_j is the cluster integral introduced by Mayer. If the classical partition

[1] See reference †.

[2] J. E. Mayer and M. G. Mayer, *Statistical Mechanics* (John Wiley and Sons, Inc., New York, 1940).

function is introduced by Z_N

$$Z_N=\frac{\lambda^{-3N}}{N!}\int\cdots\int_{(V)}\exp(-U(r)/kT)d(r), \quad (25)$$

where $\lambda^2=h^2/2\pi mkT$, (r) is the set of N position vectors, and $U(r)$ is the potential energy of the N molecules, our set of equations (10), (11), and (12) at once reduces to the Ursell-Kahn[3] expressions for the cluster integrals. If the assumption of additivity of potential energy between pairs of molecules is introduced, we get Mayer's expressions for the cluster integrals.

The substitutions necessary to obtain the second virial coefficient in classical form are quite easy. Upon substituting Eq. (25) in Eqs. (10a) and (10b) we have

$$Vg_1=\lambda^{-3}\int d(r)=\lambda^{-3}V, \quad (26)$$

$$Vg_2=\frac{\lambda^{-6}}{2!}\int\int\exp(-U(r)/kT)d(r)-\tfrac{1}{2}\lambda^{-6}V^2. \quad (27)$$

If the relative potential energy of two molecules depends only upon their separation, we can perform five of the indicated six integrations and write

$$Vg_2=2\pi\lambda^{-6}V\int_{r=0}^{\infty}(e^{-U(r)/kT}-1)r^2dr. \quad (28)$$

Now, since $g_1=p_1$ and $2g_2=p_2$, Eq. (23b) yields

$$\alpha_2=2\pi\int_0^{\infty}(1-e^{-U(r)/kT})r^2dr \quad (29)$$

in the usual classical form.

Expressing Eq. (24) in terms of the classical cluster integrals b_j introduces no complications. Since $p_j=jb_jp_1^j$, b_1 cancels out identically, even though its value were not unity:

$$\alpha_n=\sum_{(k_j)}\frac{(-)^{n-k_1-1}(n-1)(2n-k_1-3)!}{n!}\prod_{j=2}\frac{(jb_j)^{k_j}}{k_j!}, \quad (30)$$

$$\begin{cases}\sum_1 k_j = n-1\\ \sum_1 jk_j=2n-2.\end{cases}$$

THE SECOND VIRIAL COEFFICIENT IN QUANTUM-MECHANICAL FORM

The partition function for one molecule of a monoatomic gas (with nuclear spin s) can easily be evaluated by summing over the translational energy states of a free particle in a container of volume V:

$$Z_1=(2s+1)\sum_{r=1}^{\infty}\sum_{s=1}^{\infty}\sum_{t=1}^{\infty}\exp(r^2+s^2+t^2)\left(-\frac{h^2}{8mkTV^{\frac{2}{3}}}\right)$$

$$=(2s+1)\lambda^{-3}V. \quad (31)$$

The last expression is of course identical with the corresponding classical partition function except for the nuclear spin degeneracy factor. It is a very accurate representation of the triple sum except for very high gas densities and for temperatures far below 1°K. We have then for g_1 (or p_1)

$$g_1(2s+1)\lambda^{-3}. \quad (32)$$

It is advantageous to replace the denominators of Eqs. (23b), etc., with this expression but not to replace the Z_1's that will appear in the numerators. For the second virial coefficient, we get

$$\alpha_2=-\frac{\lambda^6(Z_2-\frac{1}{2}Z_1^2)}{V(2s+1)^2}. \quad (33)$$

This expression has been given by de Boer[4] for gases with zero nuclear spin.

The precise way in which the nuclear spin of any gas, real or ideal, affects its second virial coefficient can easily be deduced from Eq. (33). We need to introduce several symbols: Z_1^s, $Z^s{}_{2(BE)}$, and $Z^s{}_{2(FD)}$. The superscript refers to the nuclear spin, and the parenthetical BE or FD refers to whether the summation is over even or odd states (with respect to exchange of identical atoms). Naturally no such subscript is necessary for Z_1 since the states of only one atom are involved. Every state of one atom is degenerate by the factor $2s+1$ resulting from the nuclear spin. Therefore, $Z_1^s=(2s+1)Z_1^0$, everything else being the same. A state for two (identical) atoms may be even or odd, aside from the symmetry resulting from nuclear spin. For a spin of s, there are $(s+1)(2s+1)$ even and $s(2s+1)$ odd nuclear spin wave functions. It follows that

$$Z^s{}_{2(BE)}=(s+1)(2s+1)Z^0{}_{2(BE)}+s(2s+1)Z^0{}_{2(FD)}, \quad (34a)$$

$$Z^s{}_{2(FD)}=(s+1)(2s+1)Z^0{}_{2(FD)}+s(2s+1)Z^0{}_{2(BE)}. \quad (34b)$$

When these relations are inserted into Eq. (33), we get

$$(\alpha_2)^s{}_{(BE)}=\frac{s+1}{2s+1}\left[-\frac{\lambda^6(Z^0{}_{2(BE)}-\frac{1}{2}Z^0{}_1{}^2)}{V}\right]$$

$$+\frac{s}{2s+1}\left[-\frac{\lambda^6(Z^0{}_{2(FD)}-\frac{1}{2}Z^0{}_1{}^2)}{V}\right], \quad (35a)$$

[3] Boris Kahn, thesis, Utrecht, 1938.

[4] de Boer, Van Kranendonk, and Compaan, Physica XVI, 545 (1950).

and

$$(\alpha_2)^s{}_{(FD)}=\frac{s+1}{2s+1}\left[-\frac{\lambda^6(Z^0{}_{2(FD)}-\frac{1}{2}Z^0{}_1{}^2)}{V}\right]$$

$$+\frac{s}{2s+1}\left[-\frac{\lambda^6(Z^0{}_{2(BE)}-\frac{1}{2}Z^0{}_1{}^2)}{V}\right]. \quad (35b)$$

The physical interpretation of these two equations is

$$(\alpha_2)^s{}_{(BE)}=\frac{s+1}{2s+1}(\alpha_2)^0{}_{(BE)}+\frac{s}{2s+1}(\alpha_2)^0{}_{(FD)}, \quad (36a)$$

$$(\alpha_2)^s{}_{(FD)}=\frac{s+1}{2s+1}(\alpha_2)^0{}_{(FD)}+\frac{s}{2s+1}(\alpha_2)^0{}_{(BE)}. \quad (36b)$$

These two equations have been previously derived but by a different argument. So far as we are aware, this direct deduction from Eq. (33) is new. $(\alpha_2)^0{}_{(FD)}$ probably is not the second virial coefficient of any actual gas, since zero spin and Fermi-Dirac statistics are inconsistent. It is really only a convenient abbreviation for a certain sum.

The relations between the second virial coefficients of ideal Bose-Einstein, Fermi-Dirac, and (corrected) Maxwell-Boltzman gases also follow readily from Eq. (33). We have evaluated α_2 in these three cases directly (including nuclear spin), but the argument is greatly shortened if use is made of the general relation of Eqs. (36a) and (36b). We need only then to consider the case of zero spin.

The argument is perhaps most readily visualized as follows. We arrange the energies of all of the possible translational energy states of one atom in a row, reading from left to right, and in a column, reading from top to bottom, in the same (and completely arbitrary) order in both cases. The energy of every state of two atoms will be found by taking every possible sum of one number from the row and one from the column. We form a square table (infinite in extent to the right and downward) by entering the Boltzman factors for all of these energies in the appropriate places. Z_2 for an ideal *MB* (distinguishable atoms) gas is the sum of all of the entries in the table, i.e., $Z_2=Z_1{}^2$. For a *CMB* gas, $Z_2=(1/2!)Z_1{}^2$ or the sum of all terms above the diagonal plus half the sum of the diagonal terms. It follows at once that $Z_2-\frac{1}{2}Z_1{}^2=0$ and $\alpha_2=0$. For a *BE* gas, Z_2 is the sum of all the terms above the diagonal and all those on the diagonal. $Z_2-\frac{1}{2}Z_1{}^2$, is not zero; it is exactly half the sum of these diagonal terms:

$$Z_2-\tfrac{1}{2}Z_1{}^2=\tfrac{1}{2}\left(\sum_{n=1}^{\infty}\exp-\frac{2h^2}{8mkTV^{\frac{2}{3}}}n^2\right)^3=2^{-5/2}\lambda^{-3}V. \quad (37)$$

Therefore, the second virial coefficient of an ideal zero spin, *BE* gas is

$$\alpha_2=-2^{-5/2}\lambda^3. \quad (38)$$

Z_2 for a *FD* gas is just the terms above the diagonal and none of those on the diagonal. The second virial coefficient is equal and opposite to that of the *BE* gas.

Including nuclear spin, according to Eqs. (36a) and (36b), we have

$$(\alpha_2)^s{}_{\substack{(BE)\\(FD)}}=\mp\frac{2^{-5/2}\lambda^3}{2s+1}. \quad (39)$$

As usual, the presence of a spin greater than zero serves to reduce the quantum deviation from classical statistics. It is sometimes stated that ideal *BE* and *FD* gases have equal and opposite second virial coefficients. This is of course true if the two gases have the same nuclear spin, but apparently *FD* statistics are always associated with half integral spin and *BE* statistics with integral spin.

APPENDIX

We multiply Eq. (19) by $x^{-n-1}dx$, eliminate x from the left-hand member by Eq. (14) and integrate around the common origin of x and z:

$$\alpha_n=\frac{1}{2\pi i}\oint(\sum_1 lg_l z^l)^{-n-1}(\sum_1 g_j z^j)(\sum_1 l^2 g_l z^{l-1})dz$$

$$=\frac{1}{2\pi i}\oint(g_1 z)^{-n-1}\left(1+\sum_2\frac{lg_l z^{l-1}}{g_1}\right)^{-n-1}$$

$$\times(\sum_1 g_j z^j)(\sum_1 l^2 g_l z^{l-1})dz.$$

Therefore, α_n is just the coefficient of z^n in the expansion of

$$g_1{}^{-n-1}\left(1+\sum_2\frac{lg_l z^{l-1}}{g_1}\right)^{-n-1}(\sum_1 g_j z^j)(\sum_1 l^2 g_l z^{l-1}).$$

Upon replacing jg_j by p_j, as before, and performing the indicated operations, we obtain

$$\sum_{i=0}^{\infty}\sum_{j=1}^{\infty}\sum_{k=1}^{\infty}\frac{(-)^i(n+i)!}{n!p_1{}^{n+1+i}}\frac{kp_jp_k}{j}z^{j+k-1}\sum_{(r)}\prod_{s=2}\frac{p_s{}^{r_s}z^{(s-1)r_s}}{r_s!},$$

$$\left\{\sum_{s=2} r_s=i.\right.$$

The coefficient of z^n is

$$\alpha_n=\sum_{i=0}\sum_{j=1}\sum_{k=1}\frac{(-)^i(n+i)!}{n!p_1{}^{n+1+i}}\frac{kp_jp_k}{j}\sum_{(r_s)}\prod_{s=2}\frac{p_s{}^{r_s}}{r_s!},$$

$$\begin{cases}\sum_2 r_s=i\\ \sum_2 sr_s=n+i+1-j-k.\end{cases}$$

This expression is one form of the general solution but is unduly complicated. Its principal disadvantages are that it has about three too many summation signs and that a given p_s product arises in several ways. We can group all p_s products of the same sort together in the following way. Let $k_s'=r_s$ for $s\geq 2$; $k_s''=\delta_{sj}$ and $k_s'''=\delta_{sk}$. Both k_s'' and k_s''' are defined for all s including $s=1$. In addition, let $k_s=k_s'+k_s''+k_s'''$ for all s. We have not as yet defined k_1'. The product

$$\prod_{s=2} p_s^{k_s}$$

is the form of the general term except for the factor in p_1. From the first restrictive condition we have

$$\sum_2 k_s=i+2-k_1''-k_1''',$$

and from the second,

$$\sum_2 sk_s=n+i+1-k_1''-k_1'''.$$

We now consider the factor in p_1. The largest value of i possible is $n-1$, since for no larger i is it possible to divide $n-1+i$ into i parts, each two or larger. We will therefore write the general term with the denominator p_1^{2n-2} and write the remaining factor (if any) in p_1 in the numerator in the form $p_1^{k_1}$. This statement defines k_1 (and therefore k_1'). It follows then that

$$-n-1-i+k_1''+k_1'''=k_1-(2n-2),$$
$$i=n-3-k_1'.$$

The two restrictive conditions now simplify:

$$\sum_{s=1} k_s = n-1,$$

$$\sum_{s=1} sk_s=2n-2.$$

The last remaining task is to determine the numerical coefficient of the general term. A close inspection shows that this coefficient is

$$\frac{(-)^{n-3-k_1}(2n-k_1-3)!}{n!}\left\{\prod_{s=2}\frac{1}{k_s!}\right\}$$
$$\times\left\{(2n-k_1-1)(2n-k_1-2)\right.$$
$$-(2n-k_1-2)\sum_{s=2}\left(s+\frac{1}{s}\right)k_s$$
$$\left.+\sum_{s=2}\sum_{t>s}\left(\frac{s}{t}+\frac{t}{s}\right)k_sk_t+\sum_{s=2}k_s(k_s-1)\right\},$$

Of the four terms in the braces, the first represents all terms in which $j=k=1$, that is, $k_1''=k_1'''=1$ and all other k_s'' and $k_s'''=0$. In that case, the r_s are just the k_s. The second term represents all terms with either j or k equal to unity. One of the r_s is then just one less than the corresponding k_s. The third term represents the case when $j\neq 1$, $k\neq 1$ and $j\neq k$. The fourth term is similar, except that $j=k$. In the last two terms, $k_1''=k_1'''=0$ so $k_1'=k_1$. In the first and second terms, $k_1=k_1'+1$ and $k_1=k_1'+2$, respectively. The index i, of course, is replaced by $n-3-k_1'$.

With the aid of the two restrictive equations the complicated expression in the braces reduces to just $n-1$. The general expression for α_n is therefore

$$\alpha_n=\sum_{(k_s)}\frac{(-)^{n-3-k_1}(n-1)(2n-k_1-3)!}{n!p_1^{2n-2}}p_1^{k_1}\prod_{s=2}\frac{p_s^{k_s}}{k_s!},$$
$$\begin{cases}\sum_1 k_s = n-1\\ \sum_1 sk_s=2n-2\end{cases}\qquad(n>1).$$

After completing this proof, we observed that this final expression for α_n is obtained directly as the coefficient of z^{2n} in the expansion of

$$(\sum_1 p_jz^j)^{-n+1}/n.$$

This expression can probably be obtained directly from Eqs. (14) and (19), but we have not pursued the matter. In any event, this expression may prove useful as a generating function for the virial coefficients.

Nuclear Magnetic Resonance Multiplets in Liquids*

H. S. GUTOWSKY AND D. W. MCCALL
Noyes Chemical Laboratory, University of Illinois, Urbana, Illinois

AND

C. P. SLICHTER
Department of Physics, University of Illinois, Urbana, Illinois

(Received June 16, 1952)

Multiple magnetic resonance lines have been observed for H^1, F^{19}, and P^{31} nuclei in compounds such as PH_3, PF_3, $F_2PO(OH)$, and BrF_5, in the liquid state. The multiplets consisted of two to seven equally spaced narrow components, symmetrically placed about a central frequency, and with splittings from 0.02 to 0.8 gauss. These multiplets arise from a new variety of interaction among the nuclear moments in a molecule. Resonance lines were found to be multiple either when a nucleus interacted with a different species of nucleus or when there was interaction between nuclei of the same species with resonance frequencies separated by a chemical shift. No compounds exhibited multiplets attributable to interactions among structurally equivalent nuclei. Nor were multiplets caused by nuclei whose electric quadrupole moments were coupled to a direction fixed in the molecule.

The number and relative intensities of the components of a multiplet were determined by the number and statistical weights of the various nuclear spin orientations of the nuclei causing the splitting. In a given molecule, the ratio of the multiplet splittings of the two different resonance lines was inversely proportional to the ratio of the gyromagnetic ratios of the interacting nuclei. The splittings were independent of applied magnetic field at 4180 and 6365 gauss; they were independent of temperature over ranges from 55°C to −130°C. In PF_5, the one gas examined, the splitting of the doublet fluorine resonance was the same in the gas and liquid phases; also, the doublet was demonstrated to arise from coupling with the phosphorus nucleus, rather than from a chemical shift between the resonances from the apex and meridian fluorines in the bipyramidal structure, as proposed earlier.

All of the above characteristics are accounted for theoretically by assuming the magnetic nuclei interact via magnetic fields inside the molecule. The qualitative aspects are predicted by coupling of the form $A_{12}\boldsymbol{\mu}_1\cdot\boldsymbol{\mu}_2$ between the nuclear moments $\boldsymbol{\mu}_1$ and $\boldsymbol{\mu}_2$. The coupling constant A_{12} depends upon the detailed mechanism, which must involve the molecular electrons. Second-order perturbation theory was used to calculate the relative magnitudes of coupling via the electron orbital and the electron spin magnetic moments. The electron spin mechanism was found to give splittings ten to twenty times the orbital. Approximate calculation of the electron spin mechanism in several simpler cases gave good agreement with experiment. The influence upon the splittings of electric quadrupole coupling and spin-lattice relaxation was considered and is discussed briefly.

INTRODUCTION

In earlier observations of nuclear magnetic resonance,[1] the absorption lines in liquids were found to be single. This agreed with the fact that the direct magnetic interaction between two nuclear spins would average to zero over all the orientations possible in the liquid state.[2] The width of the resultant single, narrow resonance line is determined usually by inhomogeneities in the applied magnetic field[3] or else by the relaxation processes.[2] If the nuclear spin is greater than $\frac{1}{2}$, an electric quadrupole moment exists and can interact with electric field gradients at the nucleus; however, the resultant splitting of the resonance line in single crystals[4] is averaged also in the liquid state to a more or less broadened single line.

The discovery of chemical shifts[5] in the magnetic shielding of nuclei led to the observation[6,7] of complex resonance lines in liquids with structurally nonequivalent nuclei of the given species. In such cases, the number and relative intensities of the component lines are given usually[8] by the number and population of nonequivalent sets of the nucleus observed. For example, the fluorine resonance in liquid *para*-fluorobenzotrifluoride, $CF_3-C_6H_4-F$, has two narrow components with an intensity ratio of 3 to 1. The separation of the components is directly proportional[5,9] to the applied magnetic field because the nuclear magnetic shielding results from the interaction between the applied field and the molecular electrons. The relative magnitudes of the chemical shifts are determined by the differences in electron distribution about the nuclei.

In this paper, the principle concern is another new type of complex resonance line in liquids. The fluorine resonance in PF_3 was found[10] to be a doublet, with narrow components of equal intensity separated by 0.35 gauss. The structural equivalence of the fluorines and the preparation and purification of samples by different methods eliminated chemical shifts and impurities as possible causes of the doublet. Similar multiple fluorine and phosphorus resonance lines[11] were observed later in $POCl_2F$, $POClF_2$, and CH_3OPF_2, the

* Supported in part by the ONR.

[1] Purcell, Torrey, and Pound, Phys. Rev. **69**, 37 (1946); Bloch, Hansen, and Packard, Phys. Rev. **69**, 127 (1946). See also G. E. Pake, Am. J. Phys. **18**, 438, 473 (1950) for a general review and bibliography.

[2] Bloembergen, Purcell, and Pound, Phys. Rev. **71**, 466 (1947).

[3] R. M. Brown, Phys. Rev. **78**, 530 (1950).

[4] R. V. Pound, Phys. Rev. **79**, 685 (1950).

[5] W. D. Knight, Phys. Rev. **76**, 1259 (1949); W. C. Dickinson, Phys. Rev. **77**, 736 (1950); W. G. Proctor and F. C. Yu, Phys. Rev. **77**, 717 (1950).

[6] H. S. Gutowsky and C. J. Hoffman, Phys. Rev. **80**, 110 (1950).

[7] E. L. Hahn, Phys. Rev. **80**, 580 (1950).

[8] Gutowsky, McCall, McGarvey, and Meyer, J. Am. Chem. Soc., **74**, 4809 (1952).

[9] N. F. Ramsey, Phys. Rev. **78**, 699 (1950).

[10] Gutowsky, Hoffman, and McClure, Phys. Rev. **81**, 305(A) (1951).

[11] H. S. Gutowsky and D. W. McCall, Phys. Rev. **82**, 748 (1951).

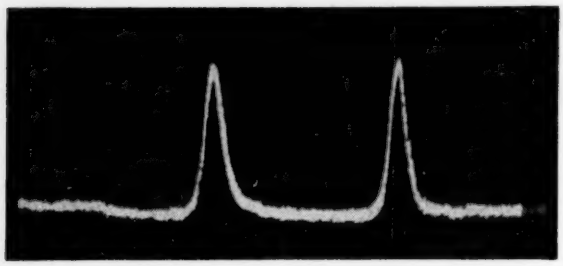

FIG. 1. Oscilloscope photograph of the doublet fluorine magnetic resonance in $POCl_2F$, using a slow-sweep modulation of the applied magnetic field. The applied field is about 6365 gauss; the modulation about 0.8 gauss; and the splitting is 0.294 gauss.

details of which suggested magnetic interaction between the fluorine and phosphorus nuclei. Since then, other examples have been found, and investigations made of the influence upon the multiplets of factors such as temperature, applied magnetic field, nuclear species, and molecular structure. A brief general account of the results has been published elsewhere,[12] with the proposal that the multiplets arise from an indirect magnetic interaction of the nuclei by a second-order process involving the molecular electrons. Herein are presented the details of the experiments and the theoretical analysis.

Several other results related to this discussion have been published. Proctor and Yu[13] reported the Sb^{121} and Sb^{123} resonances in an aqueous HF solution of $NaSbF_6$ to be symmetrical multiplets, with splittings of 1.90 gauss, and at least five, probably seven, and perhaps nine components, with intensities decreasing from the central line. A qualitative interpretation[13] on the basis of rotational hindrance was extended in detail by Andrew[14] who suggested hydrogen bonding could constrain the octahedral SbF_6^- ion to rotate about a tetrad axis. In this event, the direct magnetic interactions between the antimony and fluorine nuclei would not average to zero and a symmetrical fine structure is predicted similar to that observed in rigid lattice solids[15] or in several cases of restricted rotation in solids.[16] Andrew's ingenious analysis is in good agreement with Proctor and Yu's initial observations; however, rotational hindrance is unable to account for the multiplets[12] observed in the other compounds. Recently, Dharmatti[17] and Weaver re-examined the SbF_6^- case experimentally in detail, and showed it to be similar in nature to the multiplets observed here. They found seven components in the antimony resonances with intensities going as the binomial coefficients, in accord with the rules[11,12] for the multiplets.

[12] Gutowsky, McCall, and Slichter, Phys. Rev. **84**, 589 (1951).
[13] W. G. Proctor and F. C. Yu, Phys. Rev. **81**, 20 (1951).
[14] E. R. Andrew, Phys. Rev. **82**, 443 (1951).
[15] G. E. Pake, J. Chem. Phys. **16**, 327 (1948).
[16] H. S. Gutowsky and G. E. Pake, J. Chem. Phys. **18**, 162 (1950).
[17] S. S. Dharmatti, and H. E. Weaver, Jr., Phys. Rev. **87**, 675 (1952). We are grateful to them for sending us their results prior to publication.

It often happens that two independent and apparently different lines of research are found to be related. The steady-state multiplet studies reported here and the "slow-beat" effects[7] in spin echoes are an interesting example. Much parallel work was done by Hahn and Maxwell[18] at Stanford and by these laboratories before it became clear that both groups were dealing with the same physical phenomena. The parallel was obscured by large differences in the types of compounds and the magnitudes of the effects observed by the two groups. In our case, a combination of chemical shifts and small multiplet splitting was observed[19] in the fluorine resonances of BrF_5 and IF_5, and later it was found[20] that these compounds exhibited the "slow-beat" spin-echo effects. On the other hand, Hahn discovered the "slow-beats" in the proton spin echoes of ethanol,[7] and later the steady state resonance was resolved[21] into a combination of chemical shifts and multiplet splittings similar to those in BrF_5 and IF_5, but much smaller. The phenomena found with the different methods and compounds appear to arise from the same cause; however, the theoretical analyses and the observables are quite different in the two experiments. Many of the conclusions reported in this paper concerning the nature of the nuclear interactions have been reached independently by Hahn and Maxwell.[18] Although there has been considerable duplication of thinking, we feel that the independent and originally unrelated approaches have led to a deeper understanding of the phenomena. It is a pleasure to acknowledge several interesting exchanges of information with the Stanford group.

EXPERIMENTAL

Most of the equipment and procedures have been described in detail previously.[19] The resonance lines were displayed on an oscilloscope, using 30 cycle per second modulation[2] of the applied magnetic field, or else a slow-sweep saw-tooth[19,21] at about one cycle per second. The choice of modulation depended on the splittings, interference between the relaxation wiggles,[2] and line widths. Chemical shifts and multiplet splittings were observed as differences in the applied magnetic field at a fixed resonance frequency. The chemical shifts are defined as $(H_c-H_r)/H_r$ where H_r and H_c are the fields applied for the resonance in the reference and for the center of any multiplet line structure in the compound; the differences were found by interchanging the sample and reference. Trifluoroacetic acid, CF_3CO_2H, was used as the reference[22] for the fluorine shifts, aque-

[18] E. L. Hahn and D. E. Maxwell, Phys. Rev. **84**, 1246 (1951).
[19] H. S. Gutowsky and C. J. Hoffman, J. Chem. Phys. **19**, 1259 (1951).
[20] McNeil, Slichter, and Gutowsky, Phys. Rev. **84**, 1245 (1951).
[21] M. E. Packard and J. T. Arnold, Phys. Rev. **83**, 210(A) (1951); Arnold, Dharmatti, and Packard, J. Chem. Phys. **19**, 507 (1951).
[22] The chemical shifts given here can be converted to the F_2 scale used in reference 19 by adding 50.76×10^{-6}, which is the chemical shift of trifluoroacetic acid on the F_2 scale.

ous phosphoric acid for phosphorus, while the hydrogen data have been reduced to the unshielded proton.[19] In most cases, a series of ten measurements was made giving probable statistical errors, for the splittings, of about ± 0.001, ± 0.002, and ± 0.003 gauss for the H^1, F^{19}, and P^{31} resonances, respectively, and about twice as much for the chemical shifts and for lower fields. In addition, there are possible systematic errors of ± 1.0 percent of the measured values.[19]

The effect of applied magnetic field was investigated by using permanent magnets of 4180 and 6365 gauss. The design and operation of the smaller magnet is generally similar to that of the larger.[19] Earlier field dependence observations[12] were made with the assistance of T. R. Carver, using an electromagnet. A cryostat[19] was used to investigate the influence of temperature on the splittings and also to condense PH_3, PF_3, PF_5, and POF_3 to the liquids for observation at about $-90°C$. Otherwise, most experiments were on the liquids or aqueous solutions at room temperature. The higher boiling compounds were sealed in Pyrex, polyethylene, or Kel-F polymer[23] tubes.

The samples of PH_3, PF_3, and PF_5 were synthesized, and purified by bulb to bulb distillation. The POF_3 was formed by the moisture catalyzed reaction of PF_5 with the SiO_2 in Pyrex.[24] The fluorine resonance from the SiF_4 also produced in the reaction was identified from its chemical shift observed previously[19] in the pure compound. The BrF_5 and IF_5 were commercial samples from Harshaw Chemical Company; the PBr_3 from Dow Chemical Company; the PCl_3, $P_4(y)$, and H_2SiF_6 from J. T. Baker and Company; the NH_4ZrF_6 from Delta Chemical Company; and the HBF_4 from General Chemical Division. The inorganic fluosilicates were obtained from Dr. Glenn C. Finger of the Illionis State Geological Survey. The CH_3OPF_2, $POCl_2F$, $POClF_2$, $PSCl_3$, $POCl_3$, PI_3, and P_2I_4 were supplied by Dr. D. R. Martin, then at this university. The K-25 laboratories of Carbide and Carbon Chemicals Division at Oak Ridge furnished the MoF_6, WF_6, and UF_6. The phosphorous acid, $HPO(OH)_2$ (70 percent), and hypophosphorous acid, $H_2PO(OH)$ (50 percent), were donated by the Oldbury Electrochemical Company. Samples of $FPO(OH)_2$, $F_2PO(OH)$, HPF_6 (65 percent), KPF_6, Na_2PO_3F, and NH_4VF_6 were donated by Dr. Wayne E. White of Ozark-Mahoning Company.

RESULTS AND DISCUSSION

The Fluorine Magnetic Resonance

Phosphorus Compounds

Figure 1 is an oscilloscope photograph of the doublet fluorine resonance in $POCl_2F$, at an applied magnetic field of 6365 gauss; this resonance is typical of the fluorine doublets observed in the eleven fluorine containing phosphorus compounds investigated. The total field sweep in the picture is 0.8 gauss; the splitting is 0.294 gauss. It is seen that the components are of equal intensity and narrow compared to the splitting; in fact, the widths of the components were determined by inhomogeneities in the applied field, which were about 0.03 gauss over the sample volume used in this case. Table I summarizes the splittings and chemical shifts. In HPF_6 several weak lines were found besides the strong doublet given in Table I; the weak lines occurred at applied fields corresponding to $F_2PO(OH)$, $FPO(OH)_2$, and $SiF_6^=$, with an unassigned single line at a chemical shift of 6.90×10^{-6}. In the samples of $F_2PO(OH)$ and $FPO(OH)_2$ weak lines were obtained from the hydrolysis products.

The fluorine resonance in PF_5 was reported earlier to be a doublet with components of unequal intensity interpreted[19] as arising from a chemical shift between the apex and meridian plane fluorines in the trigonal bipyramid structure. However, the subsequent observation of fluorine doublets in all other compounds with only structurally identical fluorines bound to phosphorus called for a re-investigation of PF_5. No additional fine structure was found in the two components, with resolution at least 0.03 gauss. Moreover, the two components were found[25] to be of equal intensity within an experimental error of less than ± 3 percent, upon observation with a sensitive spectrometer, narrow-band amplifier, and recording potentiometer. Finally, the splitting was found to be the same at 4180 and 6365 gauss, eliminating conclusively the field-dependent[5,9] chemical shift. The absence of even a small chemical shift suggests that the electron distribution must be very nearly the same about the structurally distinguishable apex and meridian fluorines in PF_5, at least when averaged over the lifetime of the nuclear magnetic states.

TABLE I. The fluorine multiplets and chemical shifts in several phosphorus compounds.[a]

Compound	Line structure[b]	Splitting	Chemical shifts[c]
PF_3	(1–1)	0.350 gauss	-4.34×10^{-6}
CH_3OPF_2	(1–1)	0.320	−2.50
$POCl_2F$	(1–1)	0.294	−6.90
$POClF_2$	(1–1)	0.280	−3.04
POF_3	(1–1)	0.264	+1.58
$F_2PO(OH)$	(1–1)	0.244	+0.90
$FPO(OH)_2$	(1–1)	0.238	−0.25
PF_5	(1–1)	0.232	−0.50
Na_2PO_3F (aq.)	(1–1)	0.195	+2.68
HPF_6	(1–1)	0.178	−0.55
KPF_6 (aq.)	(1–1)	0.176	−0.77

[a] Measurements were made at an applied field of 6365 gauss.
[b] The numbers are the relative intensities of the components observed in the resonance for each compound.
[c] Referred to CF_3CO_2H.

[23] Available from Plax Corporation, Hartford, Connecticut. Threaded joints were sealed with a fluorocarbon polymer wax.

[24] A. B. Burg, "Volatile Inorganic Fluorides" in *Fluorine Chemistry* (Academic Press, Inc., New York, 1950), p. 98.

[25] These observations were made on the gas in a sealed tube at room temperature at a pressure of five atmospheres.

TABLE II. The fluorine multiplets and chemical shifts in BrF_5 and IF_5 at different magnetic fields.

Compound and line structure[a]	Splitting at 6365 gauss	Splitting at 4180 gauss	Chemical shifts External[b]	Chemical shifts Internal[c] at 6365 gauss	Chemical shifts Internal[c] at 4180 gauss	R
BrF_5	gauss	gauss		gauss	gauss	
(a) (32–32)	0.019	0.020	-21.71×10^{-5}	0.876	0.576	1.521
(b) (1–4–6–4–1)	0.019		−35.47			
IF_5						
(a) (32–32)	0.021	0.021	− 8.94	0.314	0.205	1.531
(b) (1–4–6–4–1)	0.021		−13.87			

[a] (a) and (b) are chemically shifted components; numbers are relative intensities of various components observed in the resonance for each compound.
[b] Referred to CF_3CO_2H; values taken from reference 19.
[c] These values are the separations in gauss of the chemically shifted sets of multiplets. R, the ratio of the internal shifts, should equal 1.523, the ratio of the applied fields.

BrF_5 and IF_5

The fluorine resonance in each of these compounds was complex, consisting of two multiplets with the same small splittings of about 0.02 gauss, the stronger one a doublet and the weaker a quintuplet. The data in Table II show the splittings to be field independent, while in each case the separation in gauss between the two multiplets was proportional to the field and thus a chemical shift. This confirms the assignment[19] of the stronger multiplet to the four coplanar fluorines and the weaker multiplet to the apex fluorine in a tetragonal pyramid molecule. It is only in compounds such as these, with a combination of chemical shifts and multiplets for a given resonance, that the "slow beats" have been observed[7,18,20] in the spin-echo experiments.[26]

Other Fluorides

The fluorine resonances were examined in a number of other compounds with structures pertinent to the origin of the multiplets. Single sharp lines were found in liquid MoF_6, WF_6, and UF_6 as well as in aqueous solutions of a number of fluosilicate salts, $MSiF_6$ (M= Cu, Mg, Co, and Zn), and also of NH_4ZrF_6. In these compounds the central atoms, to which the fluorines are bound, have zero or very small magnetic moments, at least in the case of isotopes present in appreciable abundance. Moreover, the molecules and ions have octahedral or very nearly octahedral[27] symmetry, with equivalent or essentially equivalent fluorines. So in these compounds there should be neither multiplet splitting nor chemically shifted components, in agreement with observations.

Aqueous H_2SiF_6 is similar to the HF solution of $NaSbF_6$ in which Proctor and Yu[13] found the antimony multiplets. Extensive hydrogen bonding or lack of dissociation of the H_2SiF_6 was indicated by the observation of two proton resonances of unequal intensity in the solution, one probably from the H_2O and the other from protons bound to $SiF_6^{=}$. Thus the restricted rotation mechanism of Andrew[14] might be expected to give a complex or broadened fluorine resonance; on the other hand, Si^{28} has a zero magnetic moment so there could be no multiplet type splitting. Actually, a single sharp fluorine resonance was found, confirming the conclusion of Dharmatti and Weaver[17] that the antimony multiplets do not arise from restricted rotation.

Multiplets might be expected in aqueous NH_4VF_6 and HBF_4, since B^{11} and V^{51} have relatively large magnetic moments and are present in high abundance. However, only somewhat broadened resonance lines were found. In HBF_4, the widths of the proton and fluorine resonances appeared to be determined by field inhomogeneities of about 0.01 gauss, with the B^{11} resonance slightly but definitely broader, about 0.02 gauss. In the NH_4VF_6 solution, the fluorine resonance was broadened to about 0.05 gauss, while the V^{51} resonance was about 0.15 gauss.

The Proton Magnetic Resonance

Multiple proton lines were observed in the three phosphorus containing compounds PH_3, $H_2PO(OH)$, and $HPO(OH)_2$. In PH_3 the proton resonance was a doublet but with a much smaller splitting than that of the fluorine in PF_3. The proton resonances in both $H_2PO(OH)$ and $HPO(OH)_2$ were complex, with a partially resolved line displaced by several milligauss from the mid-point of a rather weak doublet. The central line is assigned to the protons in the water and in the OH groups attached to phosphorus, and the doublet to the protons bound directly to the phosphorus. The splittings and chemical shifts of the doublets are given in Table III.

The Phosphorus Magnetic Resonance

In contrast to the fluorine and hydrogen doublet resonances observed in the phosphorus compounds, the phosphorus resonances in the same compounds had

TABLE III. The proton multiplets and chemical shifts in some phosphorus compounds.[a]

Compound	Line structure[b]	Splitting	Chemical shifts[c]
PH_3[d]	(1–1)	0.043 gauss	2.93×10^{-5}
$HPO(OH)_2$	(1–1)	0.166	2.83
$H_2PO(OH)$	(1–1)	0.137	2.64

[a] Measurements were made at an applied field of 6365 gauss.
[b] The numbers are the relative intensities of the components observed in the resonance for each compound.
[c] Referred to the unshielded proton.
[d] The chemical shift for PH_3 agrees with the trends reported in reference 19 for other hydrides.

[26] The "slow beats" have not been found in compounds such as $POCl_2F$ where the multiplet splitting results from interaction between different nuclear species. In these compounds an rf pulse at say the fluorine resonance frequency would leave the phosphorus nuclei virtually unaffected. Hence the phosphorus spin would merely act like a magnetic field inhomogeneity in shifting the resonance, and would not affect the echo.
[27] This applies to MoF_6, WF_6, and UF_6; Burke, Smith, and Nielsen, J. Chem. Phys. **20**, 447 (1952).

from two to seven components. In these multiplets, as as well as all others observed, the number of components was $(2M_I+1)$, where M_I is the maximum value of the total nuclear spin quantum number of the nuclei responsible for the splitting. The relative intensities of the components agreed with the statistical weights of the associated M_I values, the weights being given ordinarily by the binomial coefficients.

Figure 2 is an oscilloscope photograph of the triplet phosphorus resonance in CH_3OPF_2. Similar triplets were observed in $POClF_2$, $F_2PO(OH)$, and $H_2PO(OH)$. The total range in applied field in Fig. 2 is 2.0 gauss; the observed splitting is 0.740 gauss. It is seen that the components have relative intensities of 1:2:1 and are very narrow in comparison to their separation. The line widths, as in the case of the proton and fluorine multiplets, were determined usually by field inhomogeneities. In the $FPO(OH)_2$ sample the phosphorus resonance was partially obscured by the presence of H_3PO_4 and $F_2PO(OH)$; in addition the doublet components may have been somewhat broader than field inhomogeneities. In any event, no good phosphorus measurements could be obtained on it nor on the PF_5, POF_3, aqueous KPF_6 and Na_2PO_3F samples in which the resonances were too weak for accurate measurement. The line structures, splittings, and chemical shifts found in the other nine compounds are given in Table IV.

Single phosphorus resonance lines were observed in several compounds where the only other magnetic nuclei attached directly to phosphorus have electric quadrupole moments. These include PCl_3, PBr_3, PI_3, $POCl_3$, and $PSCl_3$. Single lines were found also in yellow phosphorus (P_4) and in I_2P-PI_2 in both of which the phosphorus nuclei are in structurally equivalent positions.

Temperature Experiments

The influence of temperature on the splittings was checked for the fluorine resonances in CH_3OPF_2 and HPF_6, and for the fluorine and phosphorus resonances in $POCl_2F$. In all cases, the splittings were independent of temperature, within experimental error, over the observed range. Observations on $POCl_2F$ extended from

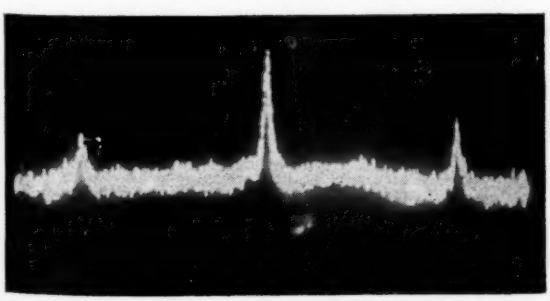

FIG. 2. Oscilloscope photograph of the triplet phosphorus magnetic resonance in CH_3OPF_2, using a slow-sweep modulation of the applied magnetic field. The applied field is about 6365 gauss, the modulation about 2.0 gauss; and the splitting is 0.740 gauss.

TABLE IV. The phosphorus multiplets and chemical shifts in some compounds with fluorine or hydrogen.*

Compound	Line structure†	Splitting	Chemical shift‡
PF_3	(1–3–3–1)	0.818 gauss	-9.7×10^{-6}
CH_3OPF_2	(1–2–1)	0.740	−11.1
$POCl_2F$	(1–1)	0.684	0.0
$POClF_2$	(1–2–1)	0.659	+1.5
$F_2PO(OH)$	(1–2–1)	0.570	+2.1
HPF_6	(1–6–15–20–15–6–1)§	0.41	+14.8
$HPO(OH)_2$	(1–1)	0.410	−0.4
$H_2PO(OH)$	(1–2–1)	0.344	−1.4
PH_3	(1–3–3–1)	0.104	+24.1

* Measurements were made at an applied field of 6365 gauss.
† The numbers are the relative intensities of the components observed in the resonance for each compound.
‡ Referred to aqueous phosphoric acid, H_3PO_4.
§ Resonance too weak for oscilloscope display; intensities estimated from output of narrow-band amplifier.

55°C to −90°C, and on CH_3OPF_2 and HPF_6 from room temperature to −130°C and −80°C, respectively. Experimental error was ±0.01 gauss for the phosphorus resonance in $POCl_2F$ and ±0.003 gauss for the fluorine resonances in the three compounds. At the lower temperatures the intensities of the multiplet lines decreased as a broad-line back-ground developed; however, the the splittings remained constant as the sharp components disappeared into the broad line resulting from the freezing out of the molecular reorientations.[2,16] The fluorine splittings in PF_5 were observed in the liquid phase[19] at −75°C and in the gas at five atmospheres at room temperature.[25] The change in state did not change the splittings, demonstrating conclusively that restricted rotation in the liquid phase is not the origin of the splittings, at least in PF_5.

Different Applied Magnetic Fields

Proctor and Yu[13] found the splittings of the Sb^{121} and Sb^{123} resonances in aqueous $NaSbF_6$ to be independent of applied magnetic field. Also, indirect confirmation of the field independence of the multiplet splittings has been provided in several cases[7,18,20] by the related "slow-beats" in spin echo experiments. In addition, we have made a number of direct measurements of the H^1, F^{19}, and P^{31} splittings in several compounds at applied fields of 4180 and 6365 gauss. It is seen from the results summarized in Table V that the splittings are field independent. Similar data have been given above in Table II for BrF_5 and IF_5, in which the fluorine chemical shifts are directly proportional to the applied field while the splittings are field independent.

Relation of Splittings to Nuclear Magnetic Moments

The nuclear origin of the splittings is demonstrated by the interdependence of the splittings and the magnetic moments of the different nuclear species in the same molecules.[11] Table VI lists the ratios of the splittings observed for two different resonance lines in

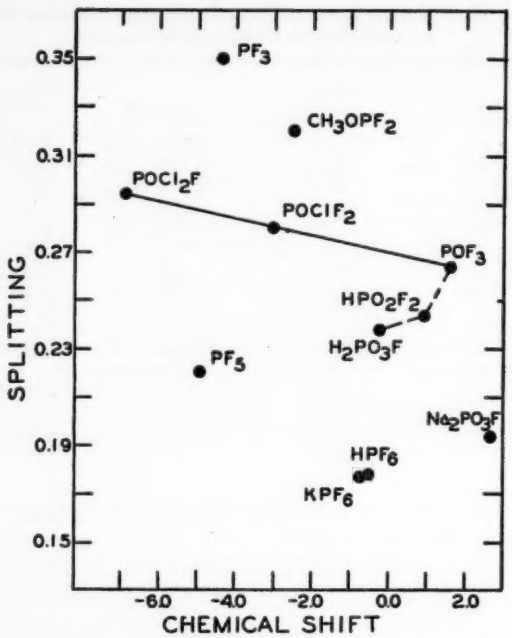

FIG. 3. The multiplet splittings in gauss, of the fluorine magnetic resonance plotted against the chemical shifts, in units of $10^6\times(H_c-H_r)/H_r$, where H_c and H_r are the applied fields required for resonance in the compound and in the CH_3CO_2H reference, respectively. The data were obtained at 6365 gauss.

several compounds. It is seen that $(\delta H_A/\delta H_B)=\mu_B/\mu_A$, within experimental error, where δH is the splitting and μ the magnetic moment of the nucleus. Strictly speaking, this rule holds only for nuclei of the same spin; the general relation is given in the theoretical discussion.

General Results and Conclusions

The existence and size of multiplet splitting in a particular resonance depends upon several factors. Splittings have *not* been found which can be assigned to interaction between structurally equivalent nuclei. Special searches were made in a number of compounds such as $F_2PO(OH)$, where interaction between the equivalent fluorines might lead to further splitting of the fluorine doublet produced by the phosphorus. However, negative results were always obtained, even under conditions where resolution approached a milligauss. Moreover, the resonance lines observed in all other compounds containing only equivalent magnetic nuclei have been single. This includes not only the compounds mentioned in the preceding sections, but also a very large number of others.[6,8,19] On the other hand, structurally nonequivalent nuclei of the same species, whose resonances are separated by a chemical shift within a molecule, *can interact* to give birth to multiplets. However, the splitting is less than a tenth of that produced by different nuclear species. For example, the proton and fluorine splittings assigned to the phosphorus in PH_3 and PF_3 are 0.043 and 0.350 gauss, respectively, while the proton-proton splitting in ethanol is about 0.001 gauss[21] and the fluorine-fluorine splitting in BrF_5 and IF_5 is 0.020 gauss. Except for size, the two classes of splitting appear identical.[28]

Cases in which nonequivalent magnetic nuclei in a molecule do *not* interact to give observed multiplets are of several types. In compounds such as CH_3OPF_2 and $F_2PO(OH)$, the fluorine and phosphorus multiplets may be explained without reference to the protons even though the proton magnetic moment is large. But the protons are separated from the fluorine and phosphorus nuclei by one or two other nuclei which must attenuate any interactions to something less than the experimental resolution.[29] In ethanol,[21] CH_3CH_2OH, the proton lines corresponding to CH_3 and CH_2 are multiple, while that from the OH is single with a temperature and concentration dependent chemical shift. Liddel and Ramsey[30] have suggested that since the hydroxyl protons are hydrogen bonded in association complexes, the chemical shift must be averaged over the temperature and concentration dependent dynamic equilibrium state. A similar averaging of the nuclear interactions between the CH_2 and OH groups would wash out the multiplet structure in the latter; this mechanism could account for the nonmultiplet proton resonances in liquid[19] HF and in the HPF_6 and HBF_4 described above.

Magnetic nuclei with electric quadrupole moments usually do not produce multiplets. Thus, in PCl_3, PBr_3, and PI_3, the phosphorus resonances are single even though the chlorine, bromine, and iodine nuclei have appreciable magnetic moments. However, in these compounds the strong coupling of the electric quardupole moments of the halogen nuclei with the electrostatic field gradients fixed in the molecule provides a mech-

TABLE V. Multiplet splittings at different applied magnetic fields.

Fluorine compounds	F^{19} resonance at 4180 gauss	F^{19} resonance at 6365 gauss	P^{31} resonance at 4180 gauss	P^{31} resonance at 6365 gauss
CH_3OPF_2	0.328 gauss	0.320 gauss	0.751 gauss	0.740 gauss
$F_2PO(OH)$	0.242	0.244	...	0.570
$FPO(OH)_2$	0.241	0.238	...	...
HPF_6	0.179	0.178	...	0.41
Hydrogen compounds	**H^1 resonance**		**P^{31} resonance**	
$HPO(OH)_2$	0.166	0.166	0.407	0.410
$H_2PO(OH)$	0.136	0.137	...	0.344

[28] Experiments in progress, with equipment giving milligauss resolution or better, indicate multiplet splitting of chemically shifted components of the proton resonances is the rule rather than the exception in most organic compounds.

[29] This fact can be used as the basis for molecular structure determination. Phosphorous acid, H_2PO_3, is known to be dibasic so it is generally supposed that one of the three protons is bonded directly to phosphorus. [See, e.g., D. M. Yost and H. Russell, Jr., *Systematic Inorganic Chemistry* (Prentice-Hall, Inc., New York, 1944), Chapter 6.] The phosphorus doublet observed in H_3PO_2 indicates that indeed one and only one proton is bonded directly to the phosphorus. Similarly, the phosphorus triplet in H_3PO_2 confirms that two protons in it are bonded to phosphorus; and in $FPO(OH)_2$ and $F_2PO(OH)$ the fluorines are also attached directly to the phosphorus.

[30] U. Liddel and N. F. Ramsey, J. Chem. Phys. **19**, 1608 (1951).

anism whereby the magnetic interactions may be averaged over all *relative* orientations of the nuclear moments, giving single phosphorus resonances.[31] The antimony, boron, and vanadium resonances in SbF_6^-, BF_4^-, and VF_6^- are special cases of this type, since the nuclei have quadrupole moments, while the ionic symmetry prevents electric field gradients at the nuclei. In spite of the apparently similar nature of these ions, the B^{11} and V^{51} resonances were only slightly broadened, while the antimony was multiplet. The association-dissociation mechanism might be responsible for the difference, as could spin-relaxation effects. In the concluding theoretical section, a discussion is given of some the conditions under which the multiplet-type interactions may average to zero.

The values of the splittings in different compounds are related to the chemical shifts. This may be seen in Fig. 3 where the fluorine splittings are plotted against the chemical shifts, and more clearly in Fig. 4 where the phosphorus splittings and chemical shifts are shown. In general, the correlations between splittings and chemical shifts are too extensive to be accidental. However, different classes of compounds differ in the relation between splittings and chemical shifts. Thus, in Fig. 3, the data for the fluorine resonances in the homologous series $POCl_2F$, $POClF_2$, and POF_3 fall upon a good straight line of negative slope while the related series $FPO(OH)_2$, $F_2PO(OH)$, and POF_3 has a positive slope. Similarly, the phosphorus resonance data for the hydrogen compounds, PH_3, H_3PO_3, and H_3PO_2, in Fig. 4 fall upon a line separate from that for the fluorine compounds.[32] It seems likely, therefore, that the connection between chemical shifts and splittings is an indirect one, both effects being related to the molecular electronic distribution but in somewhat different ways. This question is considered also, in more detail, in one of the following theoretical sections.

TABLE VI. The splittings of different multiplets in the same compound.

Compound	F^{19} or H^1 splitting[a] / P^{31} splitting	$\mu(P^{31})$ / $\mu(F^{19}$ or $H^1)$
PF_2	0.428	0.430
CH_3OPF_2	0.434	
$POCl_2F$	0.430	
$POClF_2$	0.425	
$F_2PO(OH)$	0.429	
HPF_6	0.434	
$HPO(OH)_2$	0.402	0.405
$H_2PO(OH)$	0.405	
PH_3	0.413	

[a] From data obtained at an applied field of 6365 gauss.

[31] Jeffries, Loeliger, and Staub, Phys. Rev. 85, 478 (1952), have reported a very broad titanium triplet resonance line in liquid $TiCl_4$. In this case, it seems likely that the quadrupolar effects would prevent a multiplet of the sort described in the present article.

[32] A discussion of the dependence of the phosphorus chemical shifts upon molecular structure is planned for publication at some future date.

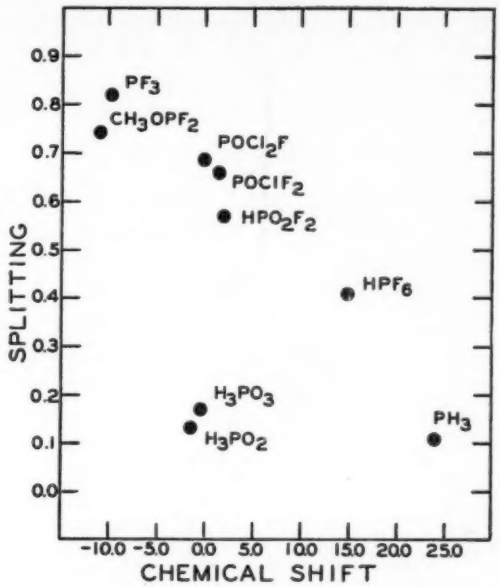

FIG. 4. The multiplet splittings, in gauss, of the phosphorus resonance plotted against the chemical shifts, in units of $10^6 \times (H_c - H_r)/H_r$, where H_c and H_r are the applied fields required for resonance in the compound and in the aqueous phosphoric acid reference, respectively. The data were obtained at 6365 gauss.

THEORETICAL

The experimental results described above show that the multiplets occur despite rapid molecular reorientation and are not produced by interactions between equivalent nuclei, eliminating a direct magnetic dipole-dipole interaction as their cause. Also, the multiplets are independent of applied magnetic field, eliminating a direct second-order interaction.[12] And, finally, their dependence upon the nuclear magnetic moments and the electronic structure of the molecule suggests a second-order process in which one nucleus induces a magnetic moment in the electron distribution in the molecule, the induced moment interacting with the second nucleus.

The Dot Product $\mu_1 \cdot \mu_2$

Without inquiring too deeply into the coupling mechanism, one can show that an interaction of the form $A_{12}\mu_1 \cdot \mu_2$ leads to the essential qualitative aspects of the observed multiplets. A_{12} is a coupling constant independent of temperature and applied magnetic field, but related to the electronic structure of the system. This form for the interaction can be deduced in the following way. If the nuclei interact by some sort of induced magnetization, the field induced at one nucleus should be proportional to the magnetic moment of the other, and the interaction energy is then proportional to the product of the nuclear moments. Also, since the multiplets persist during rapid molecular reorientations, the interaction must depend on the *relative* orientation of the nuclear moments. The interaction is therefore of the form $A_{12}\mu_1 \cdot \mu_2$. Moreover, since the

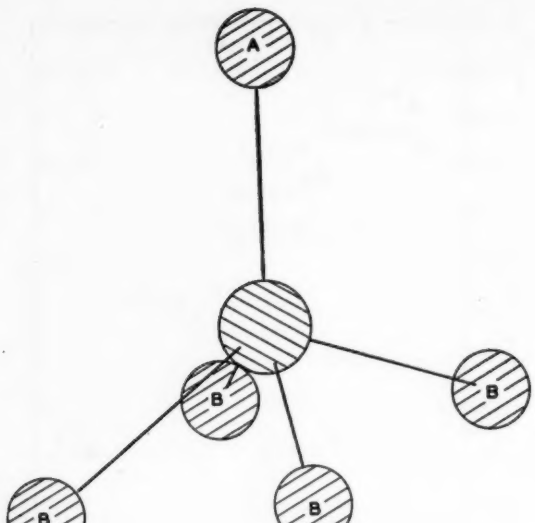

FIG. 5. Molecular model of BrF_5.

interactions of the electrons with the applied magnetic field and with thermal jostlings are small compared to the electronic energies associated with the multiplet interaction, the coupling constant A_{12} should be unaffected by applied field and temperature.

The Hamiltonian for the dot product coupling may be determined by considering a typical molecule, such as BrF_5. As shown in Fig. 5, the five fluorines are divided into two groups; group A is the single fluorine at the apex of a tetragonal pyramid, while group B contains the four equivalent nuclei at the corners of the square base. The bromine nucleus can be ignored because of the effects of quadrupole coupling. Now, interactions can occur between groups A and B, and also among the nuclei in B. The structural equivalence of the B requires that each B has the same interaction with A, even though different pairs of B may differ in their interactions, e.g., adjacent pairs contrasted with opposite pairs. In many cases, such as PF_3, groups A and B represent different nuclear species, not merely chemically nonequivalent nuclei of the same species as in BrF_5. The results are generalized readily to more than two groups of nuclei.

The required Hamiltonian is

$$\mathcal{H}=\gamma_A\hbar F_{Az}H_A+\gamma_B\hbar F_{Bz}H_B+a\mathbf{F}_A\cdot\mathbf{F}_B + \sum_{i,j=A \text{ and } i,j=B} b_{ij}\mathbf{I}_i\cdot\mathbf{I}_j, \quad (1)$$

where $\mathbf{F}_A=\sum_{i=A}\mathbf{I}_i$ is the total spin angular momentum of group A, $\mathbf{F}_B=\sum_{i=B}\mathbf{I}_i$, and F_{Az} and F_{Bz} are the components along the static fields H_A and H_B at nuclei A and B. H_A and H_B are different, of course, because of chemical shifts in the nuclear magnetic shielding. The solution of Eq. (1) is complicated by the last term, which involves the interactions within each given group. However, this term does not represent observable effects and hence may be omitted from the Hamiltonian, as we will now show by a direct calculation of the observable measured in our experiments.

Interactions between Equivalent Nuclei

The sample is placed in an rf coil whose axis, the x axis, is transverse to the static field. The component of total nuclear magnetization along the coil axis is measured, that is the equipment responds to the expectation value $(\Psi, M_x\Psi)$ of the operator M_x, where

$$M_x=\gamma_A\hbar F_{Ax}+\gamma_B\hbar F_{Bx}. \quad (2)$$

$(\Psi, M_x\Psi)$ varies with time, inducing voltages in the coil at the nuclear resonance frequencies. The time dependent Schrodinger equation for the system may be written as [1]

$$-\frac{\hbar}{i}\frac{\partial\Psi}{\partial t}=(\mathcal{H}_0+\mathcal{H}_1)\Psi, \quad (3)$$

where

$$\mathcal{H}_0=\gamma_A\hbar F_{Az}H_A+\gamma_B\hbar F_{Bz}H_B+a\mathbf{F}_A\cdot\mathbf{F}_B + \gamma_A\hbar F_{Ax}H_{Ax}\sin\omega t+\gamma_B\hbar F_{Bz}H_{Bz}\sin\omega t \quad (4)$$

and

$$\mathcal{H}_1=\sum_{i,j=A \text{ and } i,j=B} b_{ij}\mathbf{I}_i\cdot\mathbf{I}_j. \quad (5)$$

The terms in H_{Ax} and H_{Bx} are from the alternating magnetic field produced in the coil by the external oscillator of angular frequency ω. We need to show that $(\Psi, M_x\Psi)$ is not influenced by $\mathcal{H}_1$, the interactions among the equivalent nuclei.

$\mathcal{H}_1$ does not depend explicitly on time. A canonical transformation is performed to a new wave function:

$$\Phi=\exp(i\mathcal{H}_1t/\hbar)\Psi \quad (6)$$

obeying the equation

$$\mathcal{H}_0'\Phi=-\frac{\hbar}{i}\frac{\partial\Phi}{\partial t}, \quad (7)$$

where

$$\mathcal{H}_0'=\exp(i\mathcal{H}_1t/\hbar)\mathcal{H}_0\exp(-i\mathcal{H}_1t/\hbar), \quad (8)$$

and since $\mathcal{H}_0$ and $\mathcal{H}_1$ commute,

$$\mathcal{H}_0\Phi=-\frac{\hbar}{i}\frac{\partial\Phi}{\partial t}. \quad (9)$$

Therefore, Φ unfolds in time as if $\mathcal{H}_1$ were not present, and represents the solution of the simplified problem in which there is zero interaction among nuclear spins in the same group. The observed quantity $(\Psi, M_x\Psi)$ can be expressed in terms of Φ,

$$(\Psi, M_x\Psi)=[\exp(-i\mathcal{H}_1t/\hbar)\Phi, M_x\exp(-i\mathcal{H}_1t/\hbar)\Phi] =[\Phi, \exp(i\mathcal{H}_1t/\hbar)M_x\exp(-i\mathcal{H}_1t/\hbar)\Phi], \quad (10)$$

and since $\mathfrak{H}_1$ and M_z commute,

$$(\Psi, M_z\Psi)=(\Phi, M_z\Phi). \tag{11}$$

This is the desired result, as it says the behavior of M_z as a function of time is the same as it would be if there were no interactions among spins in the same group. Note that this proof makes no statement about stationary states, for the problem is a dynamical one.[33] Moreover, the proof is exact and does not require the interaction constants b_{ij} in Eq. (5) to be small. The physical significance of this result is that while the apparatus detects the combined effects of all the nuclear moments, the coupling among the spins of a given group causes them to precess about one another in some complicated way, but leaves the resultant total nuclear magnetization unchanged. It is essential that any theoretical model for the coupling have this property, otherwise the coupling among equivalent nuclei would predict multiplets where none have been found experimentally.

Solution of the Simplified Hamiltonian

The Hamiltonian, simplified by omission of the coupling between equivalent nuclei, is

$$\mathfrak{H}=\gamma_A\hbar F_{Az}H_A+\gamma_B\hbar F_{Bz}H_B+a\mathbf{F}_A\cdot\mathbf{F}_B. \tag{12}$$

In solving this equation, the last term $a\mathbf{F}_A\cdot\mathbf{F}_B$ may be approximated by $aF_{Az}F_{Bz}$.[34] This is a first-order perturbation calculation, which is valid providing

$$|\gamma_A\hbar H_A-\gamma_B\hbar H_B|\gg a, \tag{13}$$

a condition satisfied in our experiments. With this approximation, the simplified Hamiltonian, Eq. (12), becomes

$$\mathfrak{H}=\gamma_A\hbar F_{Az}H_A+\gamma_B\hbar F_{Bz}H_B+aF_{Az}F_{Bz}. \tag{14}$$

Clearly, the operators $\mathbf{F}_A^2$, $\mathbf{F}_B^2$, F_{Az}, and F_{Bz} commute with the Hamiltonian and with one another, so they may be used to describe the system. If there are n_A nuclei of spin I_A in group A and n_B nuclei of spin I_B in group B, the appropriate quantum numbers are F_A, M_A, F_B, and M_B, where $F_A=n_AI_A$, n_AI_A-1, $\cdots 0$ or $\frac{1}{2}$, and $M_A=F_A$, F_A-1, $\cdots -F_A$, with similar expressions for F_B and M_B. The energy levels are then

$$E=\gamma_A\hbar M_AH_A+\gamma_B\hbar M_BH_B+aM_AM_B. \tag{15}$$

In the approximation of the perturbation treatment used, the selection rules for transitions are $\Delta F_A=\Delta F_B=0$; $\Delta M_A=\pm 1$, $\Delta M_B=0$, or $\Delta M_A=0$, $\Delta M_B=\pm 1$. Resonance absorption lines for nuclei A and B occur at angular frequencies

$$\omega_A=\gamma_AH_A+\frac{a}{\hbar}M_B$$

and (16)

$$\omega_B=\gamma_BH_B+\frac{a}{\hbar}M_A.$$

For instance, ω_A consists of a family of components, with spacing $a/\hbar$, centered at γ_AH_A. The number of components and their relative intensities are given by the number and relative probabilities of the various values of M_B, in agreement with the experimental facts.

Our original conclusions about the form of the internuclear coupling enables us to write the constant a as

$$a=c\gamma_A\gamma_B, \tag{17}$$

where c is a constant. By combining this with Eq. (16), it is seen that transitions occur at

$$\omega_A=\gamma_A\left(H_A+\frac{c}{\hbar}\gamma_BM_B\right)$$

and (18)

$$\omega_B=\gamma_B\left(H_B+\frac{c}{\hbar}\gamma_AM_A\right).$$

The multiplet splitting of A, expressed in terms of an equivalent static field, δH_A is $c\gamma_B/\hbar$, while δH_B is $c\gamma_A/\hbar$. And as a final result

$$\delta H_A/\delta H_B=\gamma_B/\gamma_A. \tag{19}$$

If both nuclei have the same spin, this ratio is the same as the ratio of the magnetic moments, in further agreement with the experiments on H^1, F^{19}, and P^{31}. The only case reported in which splittings have been observed for nuclei with different spins is SbF_6^-, where the data are in qualitative agreement[17] with Eq. (19).

The Coupling Mechanism

The dot product coupling discussed above has the desired qualitative characteristics and accounts for effects unexplained by other hypotheses. The next major question concerns the magnetization induced in the molecule by the magnetic nuclei. This magnetization is the basic mechanism for the coupling, and could involve either the electron orbital or the electron spin magnetic moments, or both. Second-order perturbation

[33] This result is directly applicable, therefore, to the spin echo experiment, where the Hamiltonian is the same except that H_{Az} and H_{Bz} are zero most of the time. The switching on and off of the rf field does not affect the time dependence of $\mathfrak{H}_1$ or the commutability of $\mathfrak{H}_1$ with $\mathfrak{H}_0$ and M_z.

[34] It is not justifiable to make a similar approximation to the complete Hamiltonian, Eq. (1), by replacing the last term, Eq. (5), with the product of the z components; this gives the erroneous result that coupling among equivalent nuclei would produce multiplets. A simple physical argument will serve to show the difference between the two situations. It is possible, if two spins are in group A, for example, to find a rotating reference frame in which the effect of the external field is transformed to zero at *both* spins. In this frame, the dot product coupling would cause the two spins to precess about one another, their vector resultant remaining constant. On the other hand, if the spins are in different groups, a rotating reference frame transforming the external field at A to zero will not transform H_B to zero. The motion of B will then be predominantly precession about that fraction of H_B remaining. The additional field due to coupling with species A will add vectorially to this residual of H_B, with only the component of A's field along H_B important to first order.

theory is required to estimate the relative magnitudes of such magnetization, since to first order there is zero electron orbital and spin magnetization in any direction.

Orbital Effects

$M_A^{(i)}$, the orbital moment induced by a nuclear moment A, is of order of magnitude

$$M_A^{(i)} \sim \frac{\mu_A \beta^2}{\Delta E} \langle 1/r_A^3 \rangle_{Av}, \tag{20}$$

where β is the Bohr magneton; ΔE, the energy to an excited electronic orbital; and $\langle 1/r_A^3 \rangle_{Av}$ is the average inverse cube of the distance from a valence electron to nucleus A. If R is the internuclear distance between A and B, the induced electron orbital moment will interact with the nuclear moment of B with an energy of order

$$\frac{M_A^{(i)} \mu_B}{R^3} = \frac{\mu_A \mu_B \beta^2}{R^3 \Delta E} \langle 1/r_A^3 \rangle_{Av}. \tag{21}$$

This calculation assumes the induced orbital moment does not average to zero over the molecular tumbling, hence requires anisotropic polarizability.

Electron Spin Effects

Naively, one might suppose the electron spin moments could be neglected, as is allowed in Ramsey's treatment[9] of chemical shifts in nuclear magnetic shielding in molecules, or that at most the spin effects would be the same order of magnitude as the orbital, except for orbital S states. However, Ramsey and Purcell[35] have pointed out that a more careful analysis is required. In a covalent bond, the electron spins of the two shared electrons are paired. The spin magnetization induced by the interaction of nucleus A with its electron is

$$M_A^{(i)} \sim \frac{\mu_A \beta^2}{\Delta E} \langle 1/r_A^3 \rangle_{Av}, \tag{22}$$

where ΔE is now the energy to an excited electronic spin state. But when the electron spin is up for the electron on one atom, it is down for the other electron on the second atom, so there must be an identical spin magnetization, $M_B^{(i)}$ in the opposite direction transmitted to B's electron. The interaction energy of this moment with nucleus B is

$$M_B^{(i)} \mu_B \langle 1/r_B^3 \rangle_{Av} = \frac{\mu_A \mu_B \beta^2}{\Delta E} \langle 1/r_A^3 \rangle_{Av} \langle 1/r_B^3 \rangle_{Av}. \tag{23}$$

This energy is larger than the orbital interaction, Eq. (21), in the ratio $R^3 \langle 1/r_B^3 \rangle_{Av}$, a factor of ten to twenty in many cases, assuming the spin and orbital ΔE's to be comparable. Detailed calculations given below show that the electron spin terms give an order of magnitude comparable to the experimental results.

[35] N. F. Ramsey and E. M. Purcell, Phys. Rev. **85**, 143 (1952).

Calculation of the Electron Spin Coupling

The complete Hamiltonian for the electron-nuclear spin interactions in a molecule has been given previously.[35,36] The required second-order interaction energy of the nuclear magnetic moments with the electron spin moments is given by

$$\Delta E_{AB} = A v_\lambda \sum_n^{} \frac{(0|\mathfrak{H}_A|n)(n|\mathfrak{H}_B'|0) + (0|\mathfrak{H}_B'|n)(n|\mathfrak{H}_A|0)}{E_n - E_0}, \tag{24}$$

where $\mathfrak{H}_A$ is the interaction between nucleus A and the electrons, and $\mathfrak{H}_B$ is that between nucleus B and the electrons. The Hamiltonian contains two types of terms representing nucleus-electron interaction, $\mathfrak{H}_2$ and $\mathfrak{H}_3$ in the notation of Ramsey and Purcell,[35] one representing S orbital electronic states, the other non-S states. The prime on $\mathfrak{H}_B$ in Eq. (24) indicates that cross terms between $\mathfrak{H}_2$ and $\mathfrak{H}_3$ may have to be computed. "Av_λ" signifies an average over all spatial molecular orientations "λ." E_0 is the energy of the ground electronic state whereas E_n is that of the nth excited electronic state. An approximation to ΔE_{AB} is obtained by replacing $E_n - E_0$ by an average energy difference ΔE, and making use of the diagonal sum property to eliminate the excited states. This gives

$$\Delta E_{AB} = A v_\lambda \frac{(0|\mathfrak{H}_A \mathfrak{H}_B'|0) + (0|\mathfrak{H}_B' \mathfrak{H}_A|0)}{\Delta E}. \tag{25}$$

The magnitude of ΔE depends upon the type of excited state to which $\mathfrak{H}_A$ and $\mathfrak{H}_B$ couple. The excited states may involve a change in the orbital part of the wave function, the spin part, or both. When coupling occurs, the excited state mixed in corresponds to a more favorable electron spin alignment, that is, the perturbed wave function has a net spin polarization. Such states are formed by mixing the electron spin triplet states in with the singlet ground state. Addition of other singlet states will not produce a net polarization of the electron spins. So the appropriate energy ΔE is that needed to unpair the electron spins.

Before attempting numerical calculations with Eq. (25), two useful theorems will be proved. (1) To a good approximation the electron-nuclear spin interaction can be calculated for each atom separately. (2) Only the two electrons involved directly in the covalent bond need be considered.

[36] A. Abragam and M. H. L. Pryce, Proc. Roy. Soc. (London) **A205**, 136 (1951).

Proof of Theorems

The ground-state molecular electronic wave function is needed to evaluate integrals of the type in Eq. (25). A Heitler-London product of atomic orbitals should be a good approximation for our purpose, since the radial dependence of the coupling is $(1/r^3)$, which is most important close to the nucleus where the atomic orbitals are most accurate. The angular dependence is important principally in averaging over molecular orientations; this may be accomplished by hybridizing the atomic orbitals to give the required molecular symmetry.

Accordingly, ψ, the ground-state wave function for a molecule with N electrons, is taken to be a linear combination of functions

$$\phi_k=\frac{1}{\sqrt{N!}}\sum_P(-1)^P Pa(\alpha)_1 b(\beta)_2 c(\alpha)_3 d(\beta)_4\cdots)_\nu, \quad (26)$$

where a, b, $c\cdots$ represent the spatial dependence of the individual hybridized orbitals; subscripts, 1, $2\cdots\nu$ label the N electrons; P is the permutation operator; and α and β are the spin up and spin down functions. The other ϕ's included in ψ differ only in interchanges of spin functions. In practice, the closed shell orbitals are omitted, and the N electrons are simply the valence electrons. ψ may be written as the product of ψ_0, the orbital part, and ψ_s, the spin part, with the permutation operator applied to satisfy the Pauli principle, so that

$$\psi=\frac{1}{\sqrt{N!}}\sum_P(-1)^P P\psi_0\psi_s. \quad (27)$$

With this function, we must calculate integrals such as

$$\int\psi^*\sum_{i,j}\mathfrak{H}_{Ai}\mathfrak{H}_{Bj}'\psi d\tau, \quad (28)$$

where the integration is over all electron spatial and spin coordinates, and $\mathfrak{H}_{Ai}$ is the interaction between nulecus A and electron i, etc. Introducing ψ from Eq. (27), the integral equals

$$\frac{1}{N!}\int\sum_P(-1)^P P\psi_0^*\psi_s^*\times\sum_{i,j}\mathfrak{H}_{Ai}\mathfrak{H}_{Bj}'\sum_P(-1)^P P\psi_0\psi_s d\tau$$

$$=\int\psi_0^*\psi_s^*\sum_{i,j}\mathfrak{H}_{Ai}\mathfrak{H}_{Bj}'\sum_P(-1)^P P\psi_0\psi_s d\tau. \quad (29)$$

The function ψ_0 is $a(1)b(2)\cdots n(\nu)$, where $a(1)$ means electron 1 is in orbital a, etc. For ψ_0, the permutation P gives contributions to Eq. (29) that are small unless electron i is in an orbital on atom A and electron j is in an orbital on B. Other terms are small because $\mathfrak{H}_{Ai}$ and $\mathfrak{H}_{Bj}$ depend strongly on the distance from the nucleus; the only permutations that are not small for this reason involve exchange of electrons on a given atom. But these terms are likewise negligible if $\int a(1)^*b(1)d\tau_1$ and similar integrals are small; in many cases they are zero since a and b are orthogonal functions, and, in general, they can be ignored. With these reductions, Eq. (29) becomes simply

$$\int\psi_0^*\psi_s^*\sum_{i,j}\mathfrak{H}_{Ai}\mathfrak{H}_{Bj}'\psi_0\psi_s d\tau. \quad (30)$$

The next step is to integrate over either the spin or spatial coordinates. The spatial integrations are over each atom separately; this proves theorem (1). After such integration the problem is reduced to the electron spin manifold.

For further progress, ψ_s is required, and is assumed to have the form

$$\psi_s=\frac{1}{\sqrt{2}}\{\alpha(1)\beta(2)-\beta(1)\alpha(2)\}\times\frac{1}{\sqrt{2}}\{\alpha(3)\beta(4)-\beta(3)\alpha(4)\}\cdots \quad (31)$$

where electrons 1 and 2 share a bond, 3 and 4 another, etc. In effect, this implies that the covalent bonds completely dominate the spin coupling. The various terms $\mathfrak{H}_{Ai}\mathfrak{H}_{Bj}'$ involve products such as $S_{zi}S_{yj}$ between the different electron spin operators. This is a sort of correlation between the spins, which we expect for electrons in the same bond since when one spin is up the other is down. However, the ψ_s chosen does not correspond to any correlation between electron spins not in the same bond, as can be shown by explicit calculation. Therefore, if Eq. (31) is used as the spin function, we need consider only terms arising from the orbitals bonding atom A to atom B. This is theorem (2). This approximation greatly simplifies the calculations.

Numerical Results

In the case of PF_3, we assume p bonds for both the fluorine and phosphorus. Taking the z axis along one bond, the phosphorus-fluorine interaction is proportional to

$$I_{Px}I_{Fx}+I_{Py}I_{Fy}+4I_{Pz}I_{Fz}, \quad (32)$$

where I_{Px} is the x component of the phosphorus spin.[37] The bond is assumed to have cylindrical symmetry so the x and y components are symmetrical. The axes we have chosen tumble with the molecule. We must therefore express the spin components in terms of axes fixed in space, and perform an average over molecular orientations, since the tumbling frequency in the liquid is extremely high. When this is done for PF_3, the inter-

[37] The calculation giving Eq. (32) is very similar to that involved in the anisotropic nucleus-electron interaction treated by Abragam and Pryce, reference 36.

action energy is found to be

$$(1/\Delta E)\left(\frac{16}{25}\beta^2\langle 1/r_F^3\rangle_{Av}\langle 1/r_P^3\rangle_{Av}\gamma_F\gamma_P\hbar^2\mathbf{I}_F\cdot\mathbf{I}_P\right). \quad (33)$$

Values for $(1/r_P^3)_{Av}$ and $(1/r_F^3)_{Av}$ may be obtained from Sternheimer's paper,[38] and when substituted in Eq. (33), give a splitting $\Delta H_P=3.0/\Delta E$ gauss, where ΔE, the energy to unpair the bonding electron spins, is in electron volts. Reasonable values for ΔE are of the order of an electron volt or so, which gives satisfactory agreement with the experimental ΔH_P of 0.82 gauss.

For PH_3, assuming pure s and p orbitals for the hydrogen and phosphorus, respectively, the molecular tumbling makes the interaction vanish. However, the bond angles in PH_3 are greater than 90°, indicating some s character in the phosphorus orbitals, which can account for the small splittings observed. For $H_2PO(OH)$ and $HPO(OH)_2$, the phosphorus orbitals used in the P—H bonds should contain a fair amount of s character since the orbitals available are sp^3d. The larger proton splittings in these compounds, compared to PH_3, are therefore to be expected; the phosphorus d orbital does not add to the splitting since its interaction with the hydrogen s orbital averages to zero over the molecular tumbling.

The general trends among the fluorine compounds are explained in a similar manner. The P—F splitting in a compound is determined primarily by the amount of p character in the phosphorus orbital, since the s does not couple to the fluorine p electron when averaged over molecular tumbling. The d terms are neglected because of the smallness of the d functions near the origin. Actually, cross terms between s and d orbitals on the phosphorus can couple, but their effect is rather small compared to that of a p orbital. The estimated ratios of the phosphorus splittings, PF_3 to $POCl_2F$ to PF_6^- is 0.82 to 0.62 to 0.49; the experimental values are 0.82 to 0.68 to 0.41. In these estimates, the same value of ΔE was assumed and also that there was about as much p-character in the $POCl_2F$ bond as in an sp^3 hybrid. In the case of PF_5, the bond orbitals are not known. Duffy[39] lists a possible set, those for a trigonal bipyramid. These predict a splitting of the F^{19} resonance of about 0.17 gauss relative to 0.35 gauss in PF_3. The experimental value is 0.23. It is interesting to note that both the chemical shift and multiplet data imply that all bonds in PF_5 are equivalent.

Cases such as BrF_5 and IF_5 are more difficult to analyze since the interacting nuclei are not bonded directly to one another. The coupling might occur via the weak spin-spin interactions of the electrons in the separate X—F bonds; however, this mechanism cannot be estimated directly by the procedure developed above since it requires the terms discarded by assuming Eq. (31) for ψ_s. Another way to describe the situation is in terms of an electron spin moment induced by one fluorine nucleus on the intervening X atom, which then couples with a second fluorine. This mechanism gives significant coupling only if the moment induced on X varies with the orientation of the fluorine moment relative to the X—F bond direction, otherwise the coupling averages to zero over the molecular tumbling. Such anisotropy is present in BrF_5 and IF_5, and the corresponding F—F splitting has been estimated to be a few per cent of the P—F in PF_3. This result compares favorably with the respective experimental values of 0.02 and 0.82 gauss.

The preceding numerical calculations are approximate at best. Besides the approximations inherent in the method, in evaluating the $\langle 1/r^3\rangle_{Av}$ terms, and in ΔE, most bonds have an appreciable amount of ionic character, which may vary in different compounds. For instance, the P—F bond is probably only about 40 percent covalent; and the 60 percent ionic character would not participate in the splitting. However, the approximate results do provide simple explanations for the observed general trends, and the values are certainly of the right order of magnitude. More refined calculations of this sort are of potential interest and value for investigating the dependence of bond hybridization upon molecular structure.

Spin Relaxation Effects

In the experimental work, multiplets were not found in a number of cases where the interactions described above could occur. This is reasonable, for even though nuclei A and B are coupled together, rapid random transitions of the spin of A among its various spatial orientations can smear out the multiplet structure of B's resonance. In fact, if A's transitions become rapid enough, the resonances of both A and B will be unaffected by the coupling and B will be a single narrow line. Processes inducing transitions include spin-lattice and spin-spin relaxation; also, a similar effect would be produced by an actual chemical exchange of atoms between two molecular species. In these processes, and others of a similar nature, there is some time, τ, which characterizes the flipping or rate process of say nucleus A. If the multiplet splitting in frequency units is $\delta\omega$, then when τ is $1/\delta\omega$, the multiplet structure starts to disappear. We will derive this result by considering the particular case of spin-lattice relaxation.

To study the relaxation effects, we shall make use of the Bloch equations,[40] including an extra term to represent the nuclear coupling field. The modified Bloch

[38] R. Sternheimer, Phys. Rev. 84, 244 (1951).
[39] G. H. Duffy, J. Chem. Phys. 17, 196 (1949).
[40] F. Bloch, Phys. Rev. 70, 460 (1946).

equations then become

$$\frac{du}{dt}+\left(\Delta\omega+\frac{\delta\omega}{2}\right)v=-\frac{u}{T_2},$$
$$\frac{dv}{dt}-\left(\Delta\omega+\frac{\delta\omega}{2}\right)u=-\frac{v}{T_2}-\omega_1 M_z, \qquad (34)$$
$$\frac{dM_z}{dt}-\omega_1 v=-\frac{(M_z-M_0)}{T_1}.$$

The quantities u, v, and M_z are the three components of nuclear magnetization along a set of axes rotating with angular frequency γH_0 in the static field H_0. $\omega_1=\gamma H_1$, where H_1 is the strength of the rotating magnetic field (that is, one of the two rotating components into which the linearly polarized field may be decomposed). H_1 is taken as parallel to u. $\Delta\omega$ is $\gamma H_0-\omega$, where ω is the angular frequency of the alternating magnetic field.

If, for concreteness, we consider the P−F case, u, v, and M_z can be the fluorine nuclear magnetization, and $\delta\omega/2$ then represents the local field due to the phosphorus. There are three more equations similar to Eq. (34) except for replacement of $\delta\omega$ with $-\delta\omega$. These latter equations correspond to the other orientation of the phosphorus spin. (If the spin is greater than $\frac{1}{2}$, correspondingly more equations are needed). Our treatment is then a mixture of the classical (the Bloch equations) and the quantum (the discrete local field correction.) This mixture provides a simple way of taking into account the internuclear coupling. The modified Bloch equations are readily solved if one assumes ω_1 is small (no saturation) since then $M_z\cong M_0$. If we call $u+iv=G$, an equation for G is obtained by adding the first equation to i times the second. G obeys the equations

$$\frac{dG_+}{dt}+\left[\frac{1}{T_2}-i\left(\Delta\omega+\frac{\delta\omega}{2}\right)\right]G_+=-i\omega_1 M_0$$
and
$$\frac{dG_-}{dt}+\left[\frac{1}{T_2}-i\left(\Delta\omega-\frac{\delta\omega}{2}\right)\right]G_-=-i\omega_1 M_0, \qquad (35)$$

where G_+ and G_- denote G for the two phosphorus spin orientations. To follow G in time we consider these two equations. While $+\delta\omega$ applies, G obeys the G_+ equation. When the phosphorus spin flips, G obeys the G_- equation. The solutions join on with the boundary condition that G is continuous, since the fluorine magnetization does not change when the phosphorus spin flips.

The problem is to find the behavior of G for a given fluorine as its phosphorus spin is alternately up and down, and then to perform the appropriate average over the various phosphorus life histories of different molecules to give the average fluorine magnetization at any time. We begin by considering one particular fluorine nucleus. We shall start studying the behavior of G at the time the phosphorus spin flips to the up position; that is, from the time the G_+ equation holds. For convenience, let us define α_+ and α_- as

$$\alpha_+\equiv\frac{1}{T_2}-i\left(\Delta\omega+\frac{\delta\omega}{2}\right),$$
$$\alpha_-\equiv\frac{1}{T_2}-i\left(\Delta\omega-\frac{\delta\omega}{2}\right). \qquad (36)$$

Then if $t=0$ is the time of the phosphorus spin transition, we find

$$G_+=-\frac{i\omega_1 M_0}{\alpha_+}(1-e^{-\alpha_+ t})+G_{0+}e^{-\alpha_+ t}, \qquad (37)$$

where G_{0+} is the value of G at $t=0$.

At any time there is a group of fluorine spins which had an initial value G_{0+}, and which were "formed" a time t earlier. The probability that a phosphorus spin orientation will have lasted a time between t and $t+dt$ is $(1/\tau)e^{-t/\tau}dt$ where τ is the mean life of phosphorus in a given spin state. We can therefore compute $\bar{G}_+$, the average value at any given time of those G_+'s formed with $G=G_{+0}$ initially. $\bar{G}_+$ is given by the equation

$$\bar{G}_+=\int_0^\infty \frac{e^{-t/\tau}}{\tau}G_+(t)dt=-\frac{i\omega_1 M_0\tau}{1+\alpha_+\tau}+\frac{G_{0+}}{1+\alpha_+\tau}. \qquad (38)$$

Different fluorine nuclei will have different values of G_{0+}. So far we have considered only those with a given value of G_{0+}. We must now average over all the possible values of G_{0+} to get $\langle\bar{G}_+\rangle_{Av}$, the average value of G_+ we would find at any time.

What is the average value of G_{0+}? This question is easy to answer if we remember that G does not change when the phosphorus spin flips. Therefore the average value of G_{0+} is merely the average value of G_- at the time of a flip. However, a phosphorus spin is as likely to flip at any one time as at any other. The average value of G_- at the time of a spin flip is therefore the average value of G_- at any time, namely $\langle\bar{G}_-\rangle_{Av}$. Thus we get the equation

$$\langle\bar{G}_+\rangle_{Av}=\frac{\langle\bar{G}_-\rangle_{Av}}{1+\alpha_+\tau}-\frac{i\omega_1 M_0\tau}{1+\alpha_+\tau}, \qquad (39)$$

and a corresponding equation, by symmetry,

$$\langle\bar{G}_-\rangle_{Av}=\frac{\langle\bar{G}_+\rangle_{Av}}{1+\alpha_-\tau}-\frac{i\omega_1 M_0\tau}{1+\alpha_-\tau}. \qquad (40)$$

Since at any time half the phosphorus nuclei will be in each spin orientation, the average value of G, $\langle\bar{G}\rangle_{Av}$, will

be given by

$$\langle \bar{G} \rangle_{Av} = \tfrac{1}{2}(\langle \bar{G}_+ \rangle_{Av} + \langle \bar{G}_- \rangle_{Av}) = \frac{-\omega_1 M_0 \tau\{2+[(1/T_2)-i\Delta\omega]\tau\}}{(1+\alpha_+\tau)(1+\alpha_-\tau)-1}. \quad (41)$$

When τ is very large we have

$$\langle \bar{G} \rangle_{Av} = \frac{-\omega_1 M_0}{2}\left\{\frac{1}{(1/T_2)-i[\Delta\omega+(\delta\omega/2)]} + \frac{1}{(1/T_2)-i[\Delta\omega-(\delta\omega/2)]}\right\} \quad (42)$$

a double resonance of total splitting $\delta\omega$.

When τ is very small we get

$$\langle \bar{G} \rangle_{Av} = \frac{i\omega_1 M_0}{(1/T_2)-i\Delta\omega} \quad (43)$$

which represents a single resonance of twice the intensity of the double ones above. The single line for small τ results from the averaging of the phosphorus spin. The transition from long to short τ occurs when $\tau\delta\omega \sim 1$, as can be shown form Eq. (41). For typical cases, this relation shows that splittings would disappear for τ a few tenths of a millisecond.

Examples of the lack of multiplet structure probably explained by relaxation effects are the apparent absence of an interaction between Br and F in BrF_5, or between P and Cl in $POClF_2$. In both cases we are dealing with an atom (Br or Cl) whose nucleus possesses an electric quadrupole moment, situated at a site in a molecule at which there is an electric field gradient. The Br (or Cl) spin-lattice relaxation time is probably very short, since the quadrupolar coupling provides a potent relaxation mechanism. Even when there is no static electric field gradient, a quadrupole moment may still provide the dominant relaxation process. We may well fail to observe splittings even when there is no quadrupole "splitting" present.

We should mention one other point related to electric quadrupole interactions, but not a relaxation process, however. If we have a molecule in which the quadrupole coupling frequency is greater than the molecular tumbling frequency, another effect may arise. The nuclear spin is then dragged around by the molecular tumbling. No splitting would be observed in this case either.

ACKNOWLEDGMENT

We wish to express our appreciation to Dr. E. L. Hahn for several interesting and valuable discussions and communications, including advance notification of the significant spin-echo experiments at Stanford. We thank Dr. Wayne E. White of Ozark-Mahoning Company, Mr. R. Mattair of Oldbury Electro-Chemical Company, and Professor D. R. Martin for their generosity in supplying many of the compounds. The equipment was provided mainly by grants-in-aid from Research Corporation. Mr. R. E. McClure assisted in a number of the measurements; Mr. T. R. Carver assisted in the early field dependence measurements.

Announcement

Volume 1 (1933) of *The Journal of Chemical Physics* is being reprinted by the

Johnson Reprinting Corporation
125 East 23 Street
New York 10, New York.

This reprinting is being undertaken with the permission of the American Institute of Physics and copies will be available in the spring of 1953. The format of the reprinted volume will be 6⅛ in. × 9¼ in. The volume will be offered for sale at $20. Orders should be sent directly to the Johnson Reprinting Corporation.

Field Emission from Nickel Surfaces*

ROBERT GOMER
Institute for the Study of Metals, The University of Chicago, Chicago, Illinois
(Received September 19, 1952)

An account of field emission experiments on clean and contaminated nickel surfaces is presented. It is concluded that the equilibrium shapes of Ni single crystals are close to spheroidal with flat regions at low index directions. Evidence for the formation of surface phases of carbon, silicon, and oxygen on Ni is presented. A method for studying the diffusion of Si in Ni is described. Chemisorption of O_2 on Ni is briefly described. A method for studying grain boundary migration is given.

THE development of the field emission microscope by Müller[1] has opened the way for studies of single crystal metal surfaces under much cleaner conditions and with more resolution than is possible with other methods. Most field emission work has been confined to tungsten and molybdenum, probably because of the great ease of preparation of emission points with these high melting and mechanically strong metals. A great deal of very interesting information is being gathered from these sources; from the purely chemical point of view, somewhat greater interest attaches to the transition metals with their *d* bands and consequent high catalytic activity. For this reason a study of the emission characteristics of Ni was undertaken. The present report is a qualitative summary of some of the phenomena encountered and will not attempt very detailed explanations.

EXPERIMENTAL

Microscopes, electrical apparatus, and vacuum techniques have been described previously.[1] Experiments requiring vacua not better than 10^{-8} mm Hg were carried out without sealing off or gettering the tubes. For the maintenance of lower pressures, gettered[1] and sealed-off tubes were used. With the latter procedure, pressures of the order of 10^{-15} mm Hg could be obtained.[2]

Nickel wire (12 mil) was drawn from various samples. For highest purity "five nine" Ni obtained from Jarrell-Ash and Company was used. Spectroscopic analysis showed no impurities present in concentrations over 0.001 percent. Silicon contaminated wires were prepared accidentally by wet hydrogen annealing at 1250°C in a silica tube.

Emission tips were prepared by electrolytic etching in a 30 percent HCl solution, saturated with $KClO_4$, at 1–20 volts ac, until smooth points could no longer be resolved in a light microscope at 500-fold magnification. The points were then rinsed carefully in distilled H_2O, and the cathode assembly was sealed into the microscope bulb.

When pressures of $\sim 10^{-7}$ are reached, the tip assembly is heated electrically to 950°C (as determined with a Leeds and Northrup Optical Pyrometer). Considerable outgassing takes place. It is necessary to heat the tip to nearly 1000°C before applying high voltage to the anode. If this is not done, the tip is generally pulled off by the very high electrostatic forces developed. Before heating, the tip is undoubtedly extremely sharp and only assumes hemispherical form after heating. It is necessary not to overheat. At 1000°C the tip will often become enlarged beyond usefulness in as little as 60 seconds, because the high surface and bulk mobility of Ni make possible a rapid increase in the radius of curvature. The enlargement is slowed considerably when the radius of the tip hemisphere approaches that of the cylindrical wire forming the support, since a further decrease in surface free energy can now be achieved only by the formation of a ball at the end of the cylinder.† It is therefore possible by

* This work was supported in part by Contract AF 33(038)-6534 with the United States Air Force.

[1] For reference to the work of Müller, Becker, and the author, see R. Gomer and D. Speer, J. Chem. Phys. 21, 73 (1953).

[2] This estimate applies only to strongly chemisorbed gases, e.g., N_2, O_2, etc., and is based on the time of monolayer formation, assuming a sticking coefficient of unity.

† It can be shown from simple geometric arguments and expressions for the flux of diffusing atoms, based on the gradients of the chemical potentials involved [taken from C. Herring, "Surface Tension as a Motivation for Sintering," in *Physics of Powder Metallurgy* (McGraw-Hill Book Company, Inc., New York, 1951), p. 149], that the following equations roughly govern the rate of transport of material and the rate of enlargement of the tip:

(a) Hemisphere of radius r on frustum of cone: For bulk diffusion,

$$dV/dt = D\sigma v\pi/kT \text{ cm}^3/\text{sec}, \quad (1)$$
$$dr/dt = D\sigma v/kTr^2 \text{ cm/sec}, \quad (2)$$

and for surface diffusion,

$$dV/dt = 4\pi^2\theta D_s\sigma v^2/kTr \text{ cm}^3/\text{sec}, \quad (3)$$
$$dr/dt = 4\pi\theta D_s\sigma v^2/kTr^3 \text{ cm/sec}. \quad (4)$$

(b) Sphere of radius r on cylinder of radius h: For bulk diffusion,

$$dV/dt = D\sigma v\pi h^4/kTr^2(4r^2-h^2) \text{ cm}^3/\text{sec}, \quad (5)$$
$$dr/dt = 2D\sigma vh^4/kTr^2(4r^2-h^2)^2 \text{ cm/sec}, \quad (6)$$

and for surface diffusion,

$$dV/dt = 8\pi^2\theta D_s\sigma v^2h^3/kTr^2(4r^2-h^2) \text{ cm}^3/\text{sec}, \quad (7)$$
$$dr/dt = 8\pi\theta h^3D_s\sigma v^2/kTr^2(4r^2-h^2)^2, \quad (8)$$

where D and D_s are bulk and surface diffusion tensors (cm²/sec), σ is the specific surface free energy (ergs/cm²), v the molecular volume (cm³/molecule), θ the number of molecules per cm² of surface, T the absolute temperature and k Boltzmann's constant.

It can easily be seen that the rates for the second geometry are smaller by a factor of *ca* 10^2 than the corresponding ones for the first. This results from two causes. First, dV/dr and dz/dr are greater for the second geometry. dz/dr represents the rate of

FIG. 1. Device for obtaining temperature gradients of desired sign.

careful etching to obtain tips which can stand a great deal of heating.

In some experiments it was desirable to know whether the temperature gradient existing at the tip as a result of the heating arrangement used was of importance. A device, shown in Fig. 1, was therefore constructed to provide zero, positive, and negative gradients at the tip. It consisted of a thin piece of Ta foil bent into a cylinder of 2-mm diameter with a very thin slit along the longitudinal axis (for pyrometer sighting). This was so arranged that a Ni wire could be pushed into the Ta tube to any desired depth by means of a magnetically operated sled. The two main support rods on which both the Ta tube and the sled rested were also used as electrical leads so that the Ta cylinder served as furnace. By using a piece of thin capillary with further constricted ends as guide, it was possible to line up the assembly so that the Ni wire could be pushed into and out of the furnace without touching it. Thus, the section of wire in the furnace is heated by radiation only. If the tip is placed in the center, there will be practically no temperature gradient over the region of importance. If the tip is made to project beyond the furnace, a section of wire behind the tip will be hottest and the normal negative gradient results. If only the tip is allowed to stick into the furnace, it will be the hottest part of the Ni wire, and a positive gradient will exist.

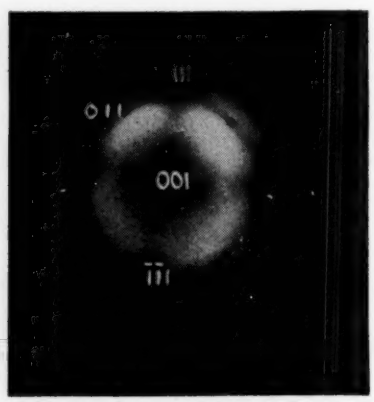

FIG. 2. 111 oriented tip, clean Ni surface. 110 and 100 directions indicated in white ink. 1 μa, 16 800 volts.

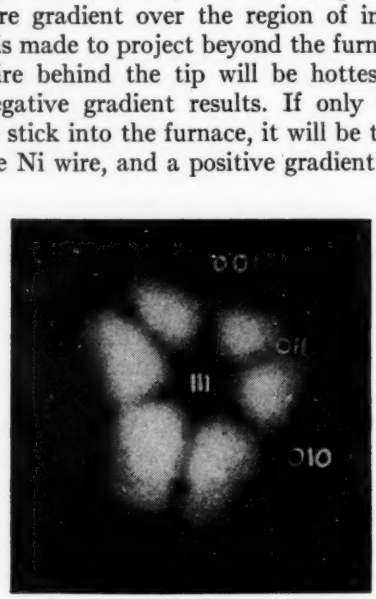

FIG. 3. 100 oriented tip, clean Ni surface. 110 and 111 directions marked. 1 μa, 16 000 volts.

It was found necessary to outgas the Ta at 2000°C, with the Ni wire completely withdrawn.

Crystallographic indexing of the main directions, (111) and (100), is possible from symmetry alone in the case of fcc metals. A knowledge of the theoretical angles between these directions, their actual separation on the screen, and the tip to screen distance, then makes it possible to calculate the factor by which the pattern is compressed because of the residual support wire.[1] This is equivalent to calculating the virtual tip to screen distance so that all other crystallographic directions can now be identified by cross-checking the angles of the various directions.

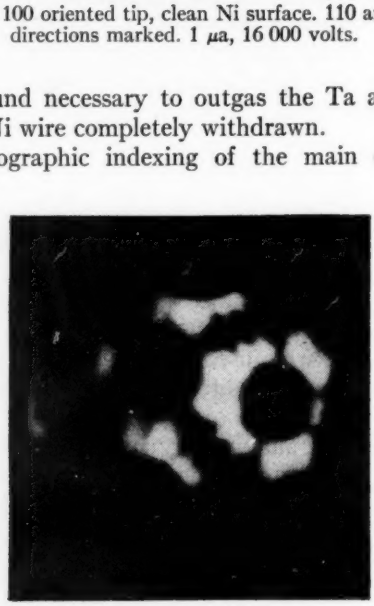

FIG. 4. Pattern from tip at *ca* 400°C, 2 μa, 10 000 volts.

contraction in the direction of the wire axis relative to the rate of change of the tip radius. Since all the material being put into the ball at the end of the cylinder must eventually come from a cylindrical section of smaller radius, this is reasonable. The second reason is that in the first case the cross-sectional area, *viz.*, the length of circumference for surface transport, keeps increasing with increasing r, but stays constant for the second geometry. The method used in deriving these formulas is due to Herring and is illustrated in his paper at the National Research Council Conference on the Structure and Properties of Solid Surfaces, Lake Geneva, Wisconsin, October 1952 (to be published).

For accurate goniometry, and also to have a record enabling one to find angles from photographs, the following device proved very useful. A transparent plastic hemisphere, fitting accurately over the microscope bulb, was ruled with latitude circles. A hemisphere of the same external radius as the microscope bulb was painted with glossy white paint. For a series of measurements on one tip and for one camera position, a reference photograph was now taken with the plastic cap over the microscope. It was then possible to put this

FIG. 5. 100 oriented tip after evaporation of Ni from auxiliary filament for 270 seconds. Evaporator at 1000°C, tip at 25°C. 1 μa, 16 000 volts.

negative in a photographic enlarger and to project onto the white hemisphere, on which the plastic cap was fitted. It was only necessary to adjust the image on the white hemisphere until the latitude lines from the

FIG. 6. Tip of Fig. 5 after additional 120 seconds of evaporation. 1 μa, 15 200 volts.

negative coincided with those of the plastic cap to have a true projection of the image. It was then possible to make measurements at leisure, without danger of high voltage, x-rays, and so on.

RESULTS

1. Clean Ni Surfaces

Figures 2 and 3 show clean Ni patterns of single crystal tips oriented with the (111) and (100) directions

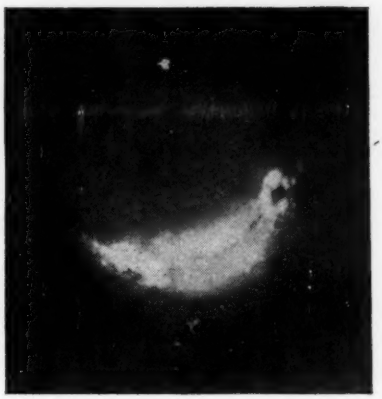

FIG. 7. Tip of Fig. 6 after additional 180 seconds of evaporation. 1 μa, 14 000 volts.

parallel to the wire axis. It is known that these orientations are preferred and occur about equally in drawn Ni wire. It may be mentioned that these patterns can never be obtained directly, even by most prolonged heating. It is always found that carbon contamination takes place, even in all mercury systems. It is therefore necessary to admit *ca* 10^{-6} mm of O_2 into the system and to oxidize the surface carbon by careful heating to 800°C. This is a rather tricky operation in that too high a pressure of O_2 or too hot a filament temperature will result in bulk oxidation of the tip. No amount of heating can restore an oxidized tip.

When high voltage is applied, the tip must be at room temperature. The mobility of Ni atoms on the surface is so high that at temperatures of only 100°C or so the tip becomes deformed by the electrostatic forces. It is possible to heat a tip carefully with the field applied and to watch the surface migration leading to a pattern like that of Fig. 4.[3] If the temperature is too high or the field increased, loss of the tip results. If the tip is cooled with the field on, the pattern of Fig. 4 can be "frozen in." If the tip is now heated without field,

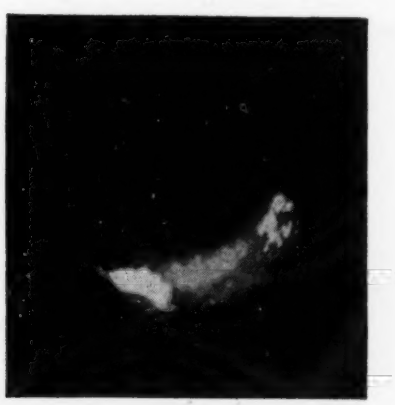

FIG. 8. Tip of Fig. 7 after additional 250 seconds. 0.8 μa, 12 000 volts. On heating to 500°C for a few seconds this pattern changed to that of Fig. 3 (1 μa, 15 600 volts).

[3] This is the pattern reported by M. Benjamin and R. O. Jenkins, Proc. Roy. Soc. (London) 176A, 262 (1940).

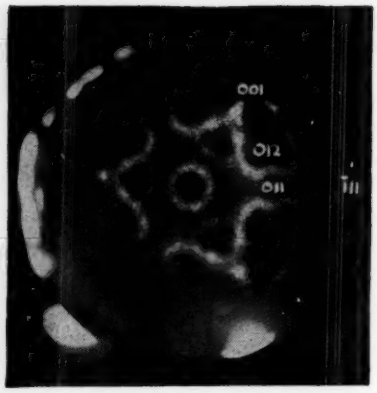

FIG. 9. Carbon contaminated tip, 111 oriented, after heating to 950°C. 1.5 μa, 9000 volts.

the original pattern results. Emission from patterns like that of Fig. 4 is greatly increased over that of smooth patterns, because of field enhancement.[1]

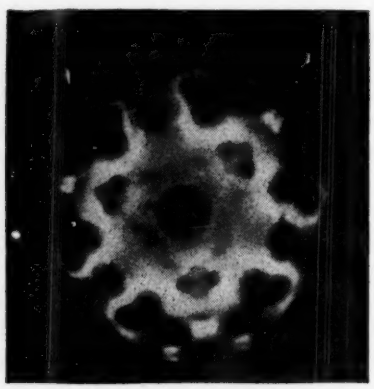

FIG. 10. Carbon contaminated tip, 111 oriented, after heating at 900°C. 1 μa, 20 000 volts.

Figures 5 to 8 show the results of evaporating Ni from an auxiliary filament onto the tip. In these experiments the tip was at 30°C and the evaporator at 1000°C.

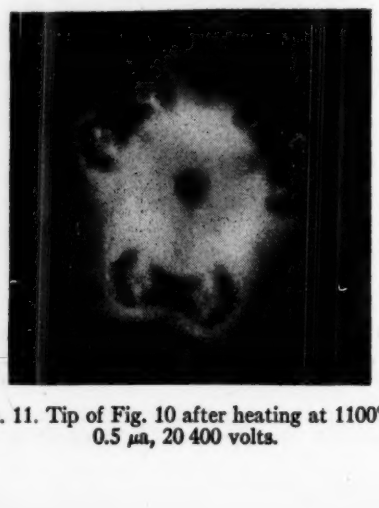

FIG. 11. Tip of Fig. 10 after heating at 1100°C. 0.5 μa, 20 400 volts.

2. Carbon Contamination

When a clean tip is allowed to remain in a tube still connected to an oil diffusion pump and the level of liquid nitrogen is allowed to drop, the pattern first becomes generally obscured because of adsorption of various gases. If the tip is now heated to 500–600°C, patterns like those in Fig. 9 result. On prolonged heating at 1000°C this pattern changes to that of Fig. 10 and finally, via Fig. 11, to that of Fig. 12. Treatment with O_2 results in a cleaning up of the tip. With care, inter-

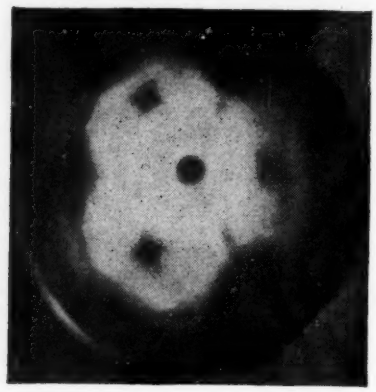

FIG. 12. 111 oriented tip, carbon contaminated after prolonged heating at 1100°C. 1 μa, 18 000 volts.

mediate stages of the process such as those shown in Fig. 13 can be seen. The patterns here ascribed to carbon contamination will also result if the tip is allowed to come in contact with a few mm of CO at

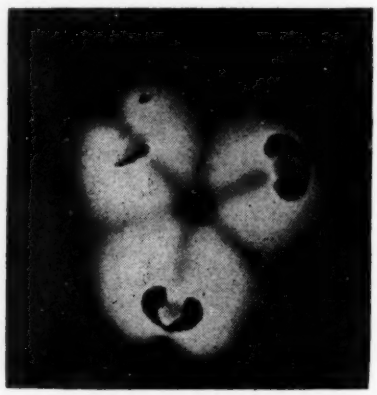

FIG. 13. Carbon contaminated tip after partial clean-up with O_2. 0.5 μa, 20 800 volts.

400–500°C. These facts support the proposed explanation very strongly.

3. Silicon Contamination

Tips were prepared from wires containing 0.3 percent Si and 0.5 percent Al as principal impurities. Figures 14 through 24 show the resulting patterns as a function of tip temperature. The photographs were obtained with

the tip at room temperature, after additional heating at a given temperature produced no further changes. These patterns are remarkable in that they are equilibrium patterns. It is possible to approach a given pattern from above or below in a completely reversible manner. The time it takes for a given pattern to emerge without further changes is governed by the temperature and by the initial pattern. Furthermore, a pattern will approach its final form via the intermediate patterns between the initial and final ones. Thus a tip heated to

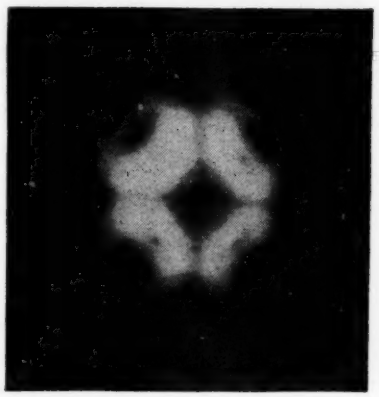

FIG. 14. Si contaminated (0.3 percent) 100 oriented tip after heating to 1160°C. 1 μa, 15 500 volts.

1100°C and then kept at 700°C will approach the 700°C pattern by going through the forms of the 1050, 1000°C, etc., patterns, much in the manner of a human embryo experiencing the evolution of the race. It will

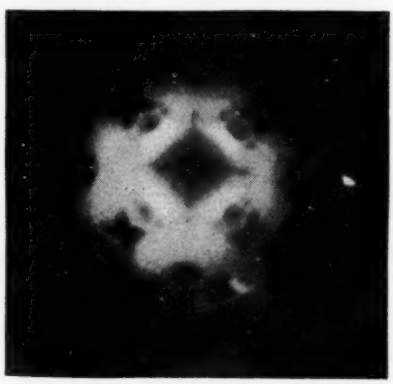

FIG. 15. Tip of Fig. 14 after 1100°C. 1 μa, 15 000 volts.

be noted that the silicon patterns resemble the carbon patterns markedly. In one instance it proved possible to get rid of Si by prolonged treatment in 20 mm H_2 at *ca* 500°C. In most experiments with H_2, the tip was lost before significant results could be found, most likely because of hydrogen embrittlement of the metal.

The patterns shown are not caused by temperature gradients at the tip; this was shown with the device discussed previously.

FIG. 16. Tip of Fig. 14 after 1075°C.

4. Oxygen Contamination

Two types must be distinguished. At temperatures below 400°C only adsorption takes place. This is an irreversible phenomenon. Figures 25 to 27 show the

FIG. 17. Tip of Fig. 14 after 1045°C. 1 μa, 16 800 volts. Tip has been enlarged from previous over-heating.

patterns resulting when O_2 at pressures from 10^{-7} to 10^{-4} is admitted to tubes containing a clean Ni tip at 25°C. The patterns seem to appear almost instantly

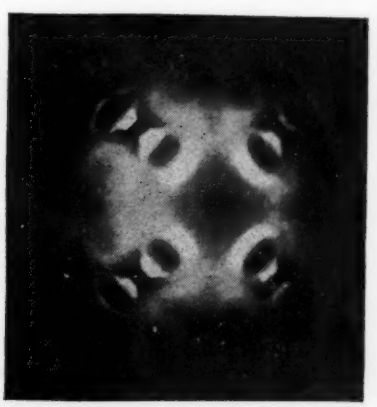

FIG. 18. Tip of Fig. 17 after 1015°C. 1 μa, 16 600 volts. Rings around 210 faces developed bridge on 110 faces incipient.

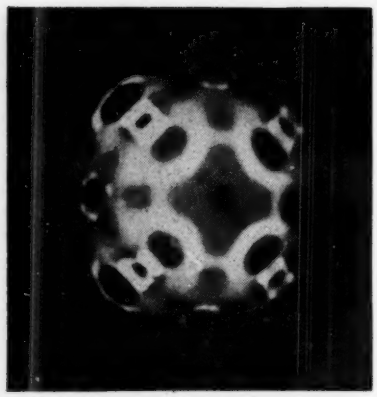

FIG. 19. Same tip after 975°C. 1 μa, 16 400 volts. Bridge over 110 faces closing, rings on 111 incipient.

without subsequent changes. If a high pressure pattern is kept at very low pressure, no appreciable change takes place in 24 hours. On the other hand, the pattern resulting at pressures of 10^{-6} does not seem to change

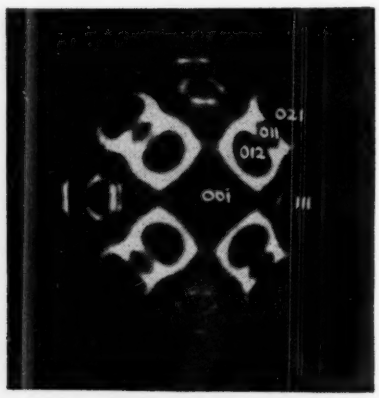

FIG. 20. Same tip after 950°C. Steps in 111 apparent, rings around 110 enlarged.

over periods of minutes. On heating to 400°C at 10^{-7} the pattern of Fig. 27 (10^{-4} mm) changes to that of Fig. 28. Further heating produces small oxide patches, distinguishable by the fact that emission is confined to

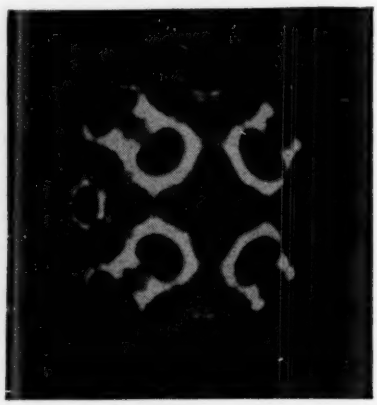

FIG. 21. Same tip after 925°C. 1 μa, 15 400 volts.

spots which seem due to very sharp small prominences. At pressures of $\sim 10^{-7}$ mm, molecular movement can be observed on these points. On heating to 800°C, randomly placed rings appear, as in Fig. 29. On further heating at 800–900°C these give rise to a pattern like that of Fig. 30. This photograph was obtained with a different tip than the one shown in the preceding oxygen patterns, oriented with the 111 direction along the wire axis. Although it was not possible to record the fact on

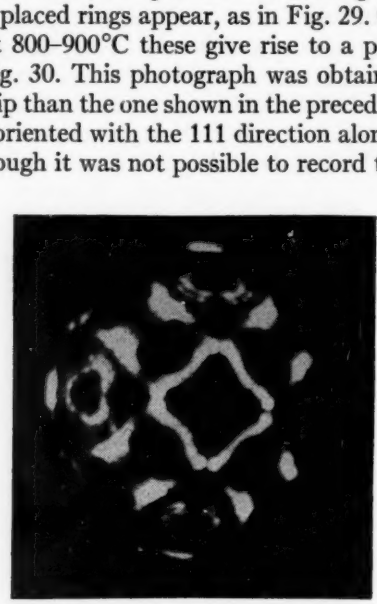

FIG. 22. Same tip after 880°C. 1 μa, 13 000 volts. Build-up of corners near 110 beginning.

film, the underlying pattern of clean Ni could be faintly discerned by eye under the bright line pattern of Fig. 30. On continued heating at 1000°C, this pattern disappears to produce once more the clean Ni pattern.

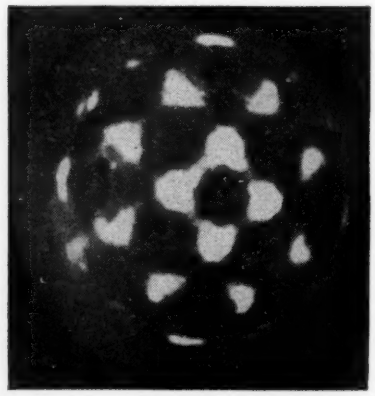

FIG. 23. Same tip after 850°C. 1 μa, 11 200 volts. Build-up of corners becoming general.

5. Twin Boundaries

It is often possible to observe grain and twin boundaries and to watch their apparent migration with time and temperature. The orientations of the boundaries may be found easily by means of the plastic cap and white projection globe. The image is projected onto the latter, and it is attempted to make the boundary line coincide with a latitude circle on the plastic cap by sliding it over the globe. If this can be done, it is proved

that the boundary was caused by a plane surface, whose pole is now in coincidence with that of the plastic cap. It is thus possible to show that the boundary lines in Figs. 31 to 35 are the intersection of a 111 plane with the crystal surface, i.e., that they are twin boundaries. Figure 35, obtained with a Si-contaminated tip is especially striking as it shows the mirror symmetry and the common 110 and 112 planes of the twins. Figures 31 to 34 were obtained with an originally carbon contaminated tip (Fig. 31) cleaned up with O_2 (Figs.

FIG. 24. Same tip after 760°C. 1 μa, 10 000 volts. Corners built up to point where emission from these predominates.

32–33) which is beginning to show a little carbon contamination again in Fig. 34. The found angles between the twinning plane and the various other directions agree to within 1° with theoretical ones. The apparent

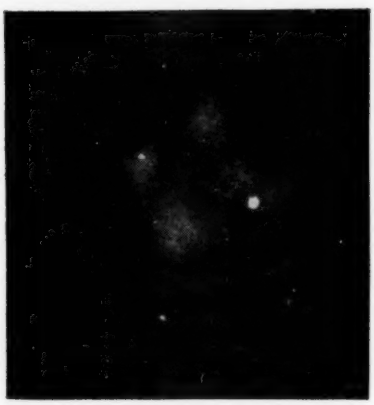

FIG. 25. 100 oriented tip, at $2 \cdot 10^{-6}$ mm O_2. 0.25 μa, 20 000 volts.

shift from 111 to 100 orientation along the wire axis by tip growth is typical of the observed behavior of Ni tips. In fact, it is sometimes possible to make a series of desired measurements on a 111 oriented tip and then to heat to 800°C or so, with a high probability of obtaining 100 orientation. Occasionally more than one boundary is observed. In one instance a tip was pulled off. On heating, a new tip with a boundary emerged. This suggests that only part of one grain was pulled off; this must have been a sufficiently small portion of the

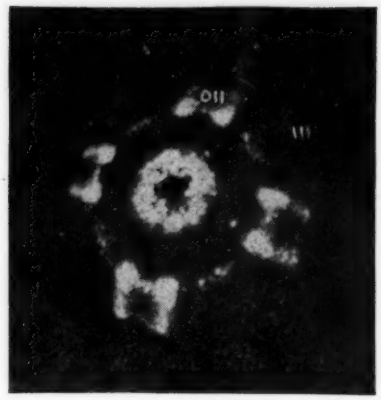

FIG. 26. Tip of Fig. 25 at 10^{-5} mm O_2. 0.1 μa, 20 000 volts.

tip region to permit the remainder to constitute a still usable tip.

DISCUSSION

1. Clean Ni Patterns

All the patterns shown for clean and contaminated Ni surfaces were obtained with tips ranging in radius

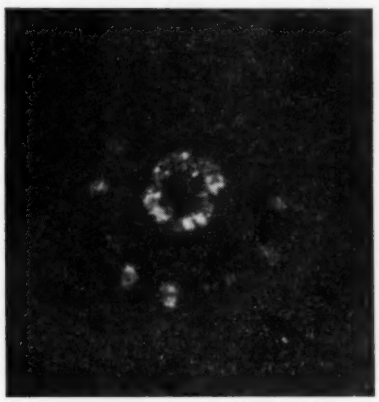

FIG. 27. Tip of Fig. 26 at 10^{-3} mm O_2. 0.05 μa, 20 000 volts.

from 10^{-5} to 10^{-4} cm as computed from the emission at known voltage and the Fowler Nordheim equation.[1] The magnifications obtained are therefore of the order

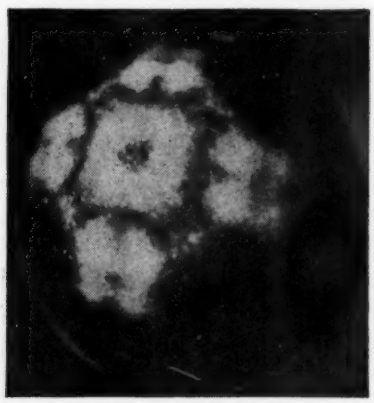

FIG. 28. Tip of Fig. 27 after heating to 400°C at 10^{-7} mm O_2. 3.6 μa, 16 000 volts.

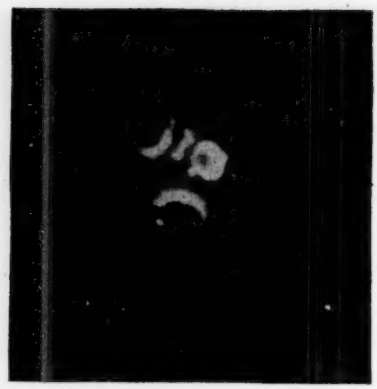

FIG. 29. 111 oriented tip, O_2 contaminated, after heating to 850°C for 350 seconds.

of 10^5. Resolution has been estimated[1] at 30A under these conditions. The most prominent feature of the patterns for clean Ni surfaces is the close analogy to the patterns of W, Mo, and so on. Here, as there, the closest packed planes appear as the least emitting regions. Thus, (111), (100), and (110) appear darkest and the regions intermediate to these principal directions, corresponding to high index planes, appear as the most strongly emitting regions. The dark bands connecting adjacent (111) regions are quite likely to be due to last remnants of chemisorbed oxygen. Similar bands have been seen by the author on almost clean W tips. Since it is not possible to heat Ni tips above 1200°C at the most, these bands can never be removed by ordinary heating.

The question remains whether the tip is completely spheroidal or whether it consists of spheroidal regions flattened into planes of low index corresponding to part or all of the dark regions of low emission. Both high work function or decrease in surface field, caused by decreased curvature, could account for the observed decreases in emission. The evaporation of Ni onto Ni tips answers this question. When Ni, or other metals, are evaporated onto a tip, the resulting layer is not smooth, but consists of small crystallites. This is seen

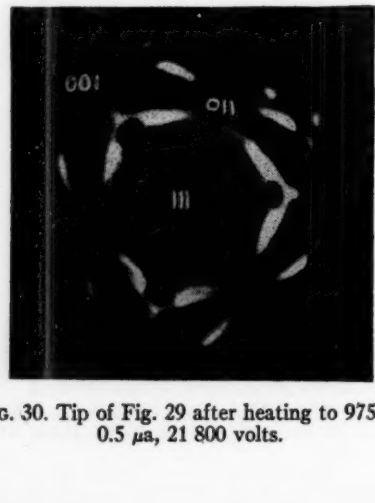

FIG. 30. Tip of Fig. 29 after heating to 975°C. 0.5 μa, 21 800 volts.

FIG. 31. Carbon contaminated tip showing twin boundary.

readily from the small isolated spots of light at first produced. Since these crystallites project from the smooth substrate surface, field enhancement in their vicinity occurs, resulting in increased emission. Thus,

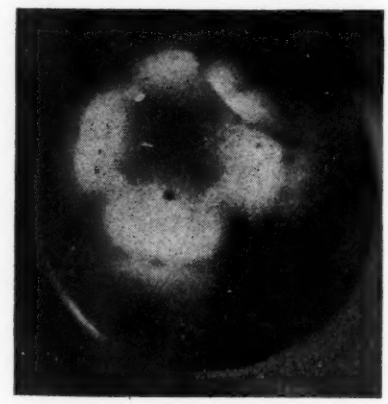

FIG. 32. Tip of Fig. 31 after O_2 treatment at 500° and 1000°C. 0.4 μa, 16 400 volts.

the region of deposit is clearly visible in Figs. 5 to 8. Emission has increased so much from the covered region in Figs. 7 and 8 that the field had to be reduced to the point where the uncovered portion of the tip hardly

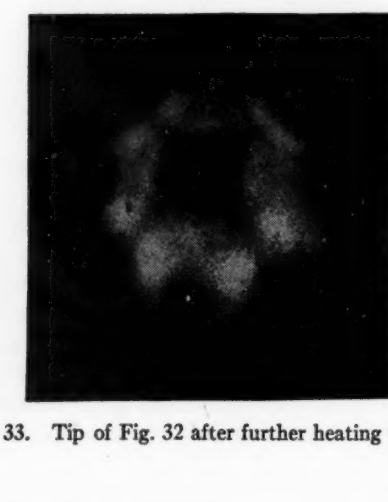

FIG. 33. Tip of Fig. 32 after further heating to 800°C.

emitted. It will be seen from the patterns of Figs. 5 to 8 that the general region of evaporation is bounded by two circular arcs; a slight "penumbra" is observable, corresponding to the fact that the emitter is not quite a point or line source. The clearly discernible circular shape of this zone shows that the tip must be spheroidal over most of its extent. Similar arcs bounded by circular regions were found by Müller [Z. Physik **108**, 668 (1938)], when he evaporated Ba onto W tips from the

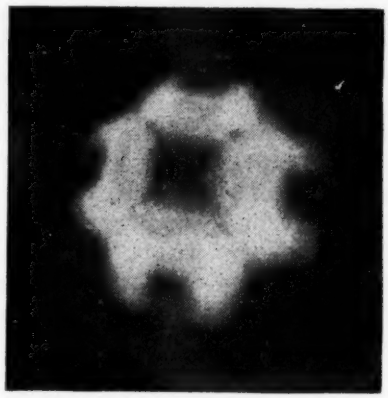

FIG. 34. Tip of Fig. 33 after heating for 1 hour at 800°C.

side. His interpretation is the same as mine in the case of Ni tips. Figure 36 shows the evaporation onto a (100) oriented tip with the emitter at a slightly different angle than before, so that about half of the large dark region corresponding to the 100 face of the

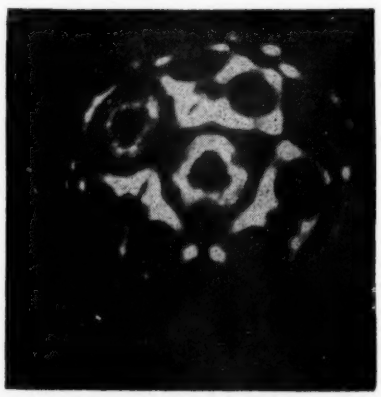

FIG. 35. 111 oriented, Si contaminated tip showing twin boundary, mirror symmetry and common 110 and 112 planes. 1 μa, 18 000 volts.

tip is covered. It is seen that even in this large dark region the shape of the "umbra" is circular, showing that most of it is also curved. It will be noticed in these figures that bright rings appear around the two 111 faces exposed to the impinging beam of Ni atoms. This suggests very strongly that the small regions enclosed by the bright rings are actually planar. If this is the case, a ring of small crystallites would stand out above the plane surface, leading to field enhancement

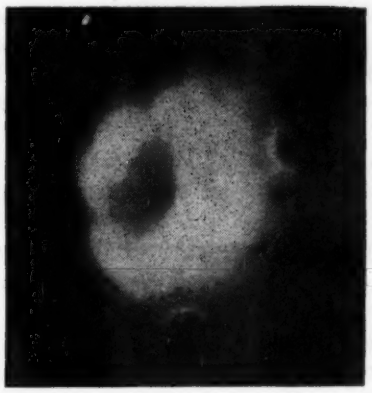

FIG. 36. 100 oriented tip showing evaporated Ni from auxiliary filament. Note rings around 111 faces, exposed to impinging beam. 0.75 μa, 14 000 volts.

and hence vastly increased emission. No bright spots appear in the regions enclosed by the bright rings. The assumption that on a plane substrate there is sufficient decrease in field to make even protuberances unnoticeable is not tenable. It has been shown that protuberances as small as single molecules of phthalocyanine still produce normal images even when found at the center of dark regions.[1]

The most likely explanation is that the rate of migration of the impinging Ni atoms is so high on the close-packed 111 planes that they skitter over these regions and come to rest only at the peripheries. If the tips of Figs. 5 to 8 are heated to 450°C, the ordinary Ni pattern is restored in a time too short to be measured conveniently. This supports the above explanation.

From the foregoing it appears as if the tip consists of small flat regions at the lowest index directions, merging without sharp edges into spheroidal regions of continually varying indices. It has been suggested by Stranski and co-workers,[4] in the case of W, Ta, and Mo tips, that the spheroidal shape of tips found with these metals is a steady-state condition resulting from the

FIG. 37. 111 oriented tip after 6 hours at 450°C in 10^{-6} mm of residual gases. 0.5 μa, 16 000 volts.

[4] Honigman, Müller, and Stranski, Z. physik. Chem. **196**, 6 (1950). These authors have observed bright rings around the close-packed planes of a W tip on evaporating W onto the latter.

tendency toward larger radius of curvature and should not be considered to be an equilibrium shape. Herring[5] has recently pointed out, however, that edgeless and nonplanar shapes of crystals can be equilibrium forms subject to the classical Wulff conditions. In order to test this point, a tip was kept at 450°C for a month. No change in shape and very little enlargement occurred, as shown by the appearance and current voltage relation of the pattern. Heating to various higher temperatures for periods of hours gave similarly negative results. Since tips were so shaped that their radius of curvature must have been equal or bigger than the cylinder radius of the support wire immediately adjoining the tip (i.e., hemispheres resting on cylindrical rather than conical sections) net rates of diffusion away from the tip probably were small compared to possible rates of diffusion on the tip surface itself. Under these conditions the steady state produced should not differ appreciably from equilibrium, and one must conclude that the equilibrium shapes of Ni crystals are spheroidal without sharp edges, even at temperatures as low as 450°C or that the free energy difference between the observed and true equilibrium shape is very small. Adsorbed impurities can modify this behavior. Thus, Fig. 37 shows an originally clean Ni tip heated for 10 hours at 450°C in a poor vacuum. The appearance of the pattern suggests the formation of crystal planes and edges rather than changes in work function due to adsorbate.

2. Carbon Contamination

The patterns found suggest a surface phase of nickel carbide. The increased emission from the bright areas could be caused by protuberances no higher than one or two atom distances. The location of the lines suggests that one is dealing with a form of epitaxy; by assuming preferred orientations on the substrate, free energy is minimized. At the same time self-adhesion (further lowering the energy) leads to the filar structures found. On heating of tips not containing equilibrium amounts of dissolved carbon, these carbides disappear by diffusion, leaving only the dark crosses in the 110 regions. These probably correspond to some sort of smooth surface layer of graphitic carbon, although the spacing of the substrate in this region is not that of graphite. Little more can be said about this phenomenon at present. Very similar patterns have been observed by the author and others[6] in the case of tungsten.

3. Silicon Contamination

The general nature of these patterns is probably similar to those with carbon. The shape of the rings seems to depend on fit with the substrate and also on lateral self-cohesion. Thus, the regions of best fit with the substrate are first occupied. At lower temperatures the equilibrium concentration of Si in the surface phase is higher. This leads, at first, to enlargement of rings already present, at the expense of fit with the substrate, but preserving self-cohesion. At still lower temperatures (~950°), a point is reached where the misfit for further enlargement of rings already present becomes too great, resulting in the formation of new regions of epitaxy, i.e., the rings around the 111 regions. At still lower temperatures further increases in the surface concentration lead merely to vertical build-up of regions already present, resulting in the great field enhancement and correspondingly high emission from built-up points noticeable in Figs. 22 to 24. The embryo-like mode of development of the patterns previously mentioned suggests that the amount of Si actually present on the surface at a given instant controls the pattern. Temperature is effective only in determining the final, or equilibrium, amount of Si on the surface. This suggests a simple method for determining activation energies for bulk diffusion of Si in Ni. The tip is heated to a high temperature and then heated at a lower temperature T_1, but only for a time t_1 short enough to produce a pattern still far from equilibrium. The tip is then reheated to the original condition and now heated at some different temperature T_2 for a length of time t_2 just sufficient to produce the exact state of the pattern resulting from heating for a length of time t_1 at T_1. The patterns can be easily compared by their emission characteristics. From a knowledge of various temperatures and times, the activation energy may then be found to be 42 ± 6 kcal. This most likely corresponds to bulk diffusion which should be the rate-determining step.

It should be mentioned that the solid solubility of Si in Ni in the temperature region here dealt with is assumed by most authorities[7] to be of the order of several percent; spectroscopic analysis of the present samples showed 0.3 percent Si. This means that the formation of a surface phase, containing, of course, only a small fraction of the total Si content, leads to a sufficient decrease in free energy to account for the present phenomena, or that the patterns are due to some other impurity, or a compound of Si with the latter. This is unlikely, but experiments to check this point are in progress.

4. Oxygen Contamination

The surface oxides, formed at temperatures above 500°C shown in Fig. 30 show the general behavior of the C and Si patterns discussed. It seems (from Fig. 29) that the oxidation of a totally covered tip proceeds more or less randomly. During this process apparently some of the initially chemisorbed oxygen is bound as oxide, while part of it evaporates. On prolonged heating at 800° to 1000°C the bound oxygen seems able to migrate and to form the epitaxed oxide pattern of Fig. 30. Undoubtedly more oxygen is lost during this process,

[5] C. Herring, Phys. Rev. **82**, 87 (1951).
[6] E. W. Müller, private communication.
[7] M. Hansen, *Der Aufbau der Zweistofflegierungen* (Julius Springer, Berlin, 1936), pp. 947–51.

since further heating eventually leads to a clean tip. Little can be said at present about the exact nature of the steady states involved which are governed by the rates of diffusion, evaporation, and oxide formation.

The patterns at room temperature (Figs. 25 to 27) show first of all that chemisorption does not proceed uniformly over the entire surface, but seems to be preferential at various definite crystallographic regions. Thus, the brightest areas appear as rings around the 100 and 110 planes. It is possible that these bright regions correspond to the formation of a partially filled layer (not necessarily the first) giving rise to field enhancement. This idea gains support from Fig. 28, which shows that heating to 400°C results in increases of the bright areas. This could be due to partial evaporation from previously dark regions. If the tentative observation is correct that the rate of formation of these patterns is not a linear function of pressure, some sort of cooperative mechanism would be required. Since these observations were not carried out with a thin wire type of ion gauge, they cannot be regarded as reliable at present. A detailed investigation is planned.

5. Twin Boundaries

The patterns shown in Figs. 31 to 35 indicate that the boundary layer at the surface must be over one atom diameter deep and of a width not less than the resolution obtainable,[1] i.e., 30A. Under these circumstances it can be expected that the reduction in field resulting from the concave boundary will show up as a dark line. The observed migration of the boundaries outward from the center of the tip is probably to be attributed to the growth of the tip, giving rise to an apparent migration, since the activation energy for real twin boundary migration is practically infinite. For the real migration of boundaries, the effect can be distinguished from the above by computing the radius of the tip before and after migration. Thus, there is the possibility of obtaining the rates of this process and the activation energies involved. The pattern of Fig. 35 shows that the surface phase of Si can be sufficiently high to fill and extend above the grain boundary. This follows from the appearance of the bright Si lines at the junction of the 210 faces coinciding with the boundary.

CONCLUSIONS

While many of the above findings cannot yet be explained in detail, certain general features seem established. Thus, there seems no doubt that cusps exist in the surface energy plot of Ni[5] and that electron emission is least from close-packed regions where the unfavorable electric double layer is strongest. Adsorption of an electronegative gas like O_2 modifies the work functions in a very complicated manner, although definite relations between crystallographic direction and adsorption seem to exist. It seems certain that relatively small amounts of impurities form surface phases of definite orientation. It is quite possible that catalyst poisoning often consists of the formation of these phases on normally active regions of the catalyst surface. The exact orientation of these phases and, indeed, their composition is probably not to be explained by extrapolating from structures and compositions of macrophases. Very likely minimum free energy can be achieved on this scale by the formation of new structures and quasi compounds. It is probable that these phenomena also resemble those taking place at the interfaces between solid phases. The detailed elucidation of the various phenomena discussed will require considerable effort.

THE JOURNAL OF CHEMICAL PHYSICS VOLUME 21, NUMBER 2 FEBRUARY, 1953

Streaming Potentials across Glass Capillaries for Sinusoidal Pressure

ROBERT GAY PACKARD*
Defense Research Laboratory, The University of Texas, Austin, Texas
(Received June 16, 1952)

A mathematical expression for the streaming potentials developed across capillaries for sinusoidal pressure variations is derived. Glass capillaries are used to check the theory experimentally, and good agreement is obtained for all samples tested.

THE theory for the streaming potentials developed across capillaries for unidirectional flow has undergone considerable modification since it was first postulated by Helmholtz.[1] The Helmholtz expression did not take into account either the effects due to surface conductance or those due to the diffuse arrangement of the ions in the solution. Rutgers,[2] among others, modified the Helmholtz expression to take into account the effects of surface conductance on the streaming potentials, and Neale[3] accounted for the diffuse arrangement of ions. The extensive measure-

* This paper is part of a dissertation submitted to the Graduate School of The University of Texas in partial fulfillment of the degree of Doctor of Philosophy, resulting from research done under Bureau of Ordnance Research and Development Contract NOrd-10639 between the Department of the Navy and The University of Texas.

[1] Helmholtz, Wied. Ann. 7, 337 (1879).

[2] A. J. Rutgers, Trans. Faraday Soc. 36, 69 (1940).

[3] S. M. Neale, Trans. Faraday Soc. 42, 473 (1946).

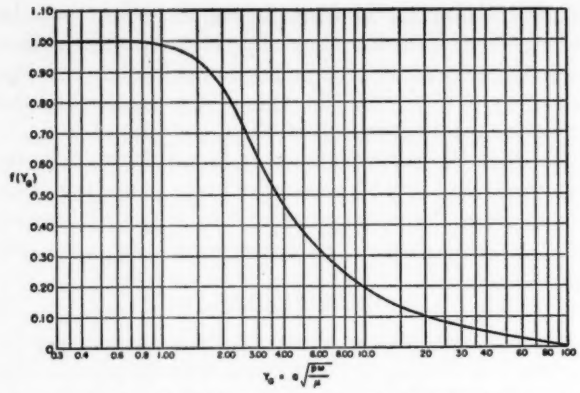

FIG. 1. A plot of $f(Y_a)$ *versus* Y_a (symbols defined in text).

ments which have been made on the streaming potentials developed across capillaries and porous diaphragms for steady flow have given impetus to further modifications.

Until 1948 no attention, apparently, had been given to the streaming potentials developed across capillaries for sinusoidal flow. In that year, Williams[4] described an electrokinetic transducer which responded to sinusoidal variations in oil pressures but did not include any mathematical treatment of the phenomena. A search of the literature did not reveal any other work on streaming potentials for sinusoidal flow. There was needed a mathematical treatment of the streaming potentials developed across capillaries for sinusoidal pressures, as well as experimental verification of the theory.

I. THEORY

Mathematically, the problem of extending the theory for steady flow to the case for sinusoidal flow presented no difficulties. The classical approach was followed, neglecting surface conductance and the diffuse ion distribution of the double layer. This was done because the experiments performed on glass capillaries to check the theory seemingly obeyed the expression derived from classical considerations.[5] It is left to the experimenter to extend the theory as Rutgers and Neale have done when the experimental conditions warrant.

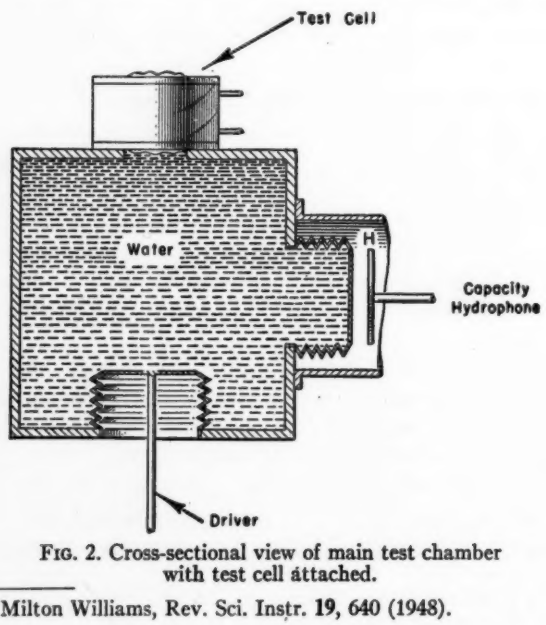

FIG. 2. Cross-sectional view of main test chamber with test cell attached.

The differential equation for laminar flow in a cylinder of length l, of circular cross section with a radius a, containing a fluid of viscosity μ and density p subjected to a uniform driving pressure $Pe^{-i\omega t}$ at one end is given by

$$\frac{l\mu}{r}\frac{\partial}{\partial r}\left(r\frac{\partial^2 x}{\partial r\partial t}\right)-lp\frac{\partial^2 x}{\partial l^2}=Pe^{-i\omega t},$$

where x is measured along the axis of the cylinder and r is measured radially. The equation is written for the assumption that the motion of the fluid is angularly independent.

Following the analysis given by Crandall,[6] the particle velocity of the fluid in the tube for the boundary condition $v_r=0$ when $r=a$ is given by

$$v_r=\frac{iP}{lp\omega}\left[\frac{J_0(kr)}{J_0(ka)}-1\right]e^{-i\omega t}, \qquad (1)$$

$$k^2=ip\omega/\mu.$$

For an electrolyte flowing in the cylinder, the transport of charge I_1, by the fluid per unit time along the tube is given by

$$I_1=\int_0^s 2\pi r\cdot\rho\cdot v_r dr, \qquad (2)$$

where s is the radius of the surface of shear (boundary of the Helmholtz rigid double layer in the liquid[7]), and ρ is the electric charge density. Poisson's equation of electrostatics, relating the charge density ρ to the electrical potential ψ at a point r in the tube, assuming ψ depends only on r, is

$$\frac{1}{r}\frac{d}{dr}\left(r\frac{d\psi}{dr}\right)=-\frac{4\pi\rho}{D}, \qquad (3)$$

where D is the dielectric constant of the solvent. Combining Eq. (3) and Eq. (1) in Eq. (2),

$$I_1=\int_0^s 2\pi r\left[\frac{iP}{lp\omega}\left(\frac{J_0(kr)}{J_0(ka)}-1\right)\right]\times e^{-i\omega t}\left[-\frac{D}{4\pi}\frac{1}{r}\frac{d}{dr}\left(r\frac{d\psi}{dr}\right)\right]dr.$$

[4] Milton Williams, Rev. Sci. Instr. **19**, 640 (1948).

[5] Booth [Nature **161**, 84 (1948)] expressed the opinion that the use of the Helmholtz theory of the rigid double layer is not serious in the case of streaming potentials.

[6] I. B. Crandall, *Theory of Vibrating Systems and Sound* (D. Van Nostrand Company, Inc., New York, 1926), p. 233.

[7] The separation of the electrical charge on the solid phase and that of the charge on the liquid phase is between 0.5Å and 5Å (see reference 2, pp. 75–76). Consequently, when the radius of the tube is large compared to the thickness of the double layer, the boundary of the double layer can be considered to be the radius of the capillary, i.e., $s\doteq a$.

Integrating by parts,

$$I_1=\frac{-iDPe^{-i\omega t}}{2lp\omega}\left[\frac{1}{J_0(ka)}\left\{J_0(kr)r\frac{d\psi}{dr}\Big|_0^s+\int_0^s krJ_1(kr)\frac{d\psi}{dr}dr\right\}-r\frac{d\psi}{dr}\Big|_0^s\right].$$

The first term in the brackets cancels with the last term. Upon integrating the remaining integral by parts, there results upon applying the boundary conditions $\psi=\zeta$ at $r=s$ by definition of the zeta-potential[8]

$$I_1=\frac{-iDPe^{-i\omega t}}{2lp\omega J_0(ka)}[krJ_1(kr)\psi(r)|_0^s],$$

where the integral remaining after this second integration by parts has been neglected since it is negligible if the diameter of the capillary is large compared to the thickness of the double layer. Since $s\doteq a$,

$$I_1=\frac{-iDP\zeta akJ_1(ka)}{2lp\omega J_0(ka)}e^{-i\omega t},$$

TABLE I. Dimensions of the glass capillaries used as test elements.

Symbol	Diameter (inches)	Length (inches)
G1	0.0820	0.7950
G2	0.0661	0.8409
G3	0.0357	0.7570
G4	0.0576	0.8467
G5	0.0232	0.7652
G6	0.0384	0.7667
G7	0.0429	0.8002

where

$$k^2=ip\omega/\mu.$$

I_1 can be simplified to obtain

$$I_1=\frac{DP\zeta aJ_1(ka)}{2l\mu kJ_0(ka)}e^{-i\omega t}. \quad (4)$$

I_1 gives rise to a potential difference E_s at the ends of the capillary causing a current of conduction I_2, given by

$$I_2=E_s\pi a^2\sigma/l. \quad (5)$$

For steady state conditions $I_1=I_2$. Hence

$$E_s=\left[\frac{\zeta DP}{4\pi\sigma\mu}\right]\left[\frac{2}{ka}\frac{J_1(ka)}{J_0(ka)}e^{-i\omega t}\right]. \quad (6)$$

When $\omega\rightarrow 0$ and P becomes the hydrostatic differential pressure across the ends of the capillary, Eq. (6) reduces to the well-known steady flow case for the streaming potential. This can be shown by applying the recursion relation for the Bessel functions,

$$\frac{2n}{z}J_n(z)=J_{n-1}(z)+J_{n+1}(z).$$

For $n=1$ and $z=ka$

$$\frac{2}{ka}J_1(ka)=J_0(ka)+J_2(ka),$$

and since $k\rightarrow 0$ as $\omega\rightarrow 0$ and $J_0(0)=1$ and $J_2(0)=0$,

$$\lim_{k\to 0}\left(\frac{2}{ka}\frac{J_1(ka)}{J_0(ka)}\right)=\lim_{k\to 0}\left(1+\frac{J_2(ka)}{J_0(ka)}\right)=1.$$

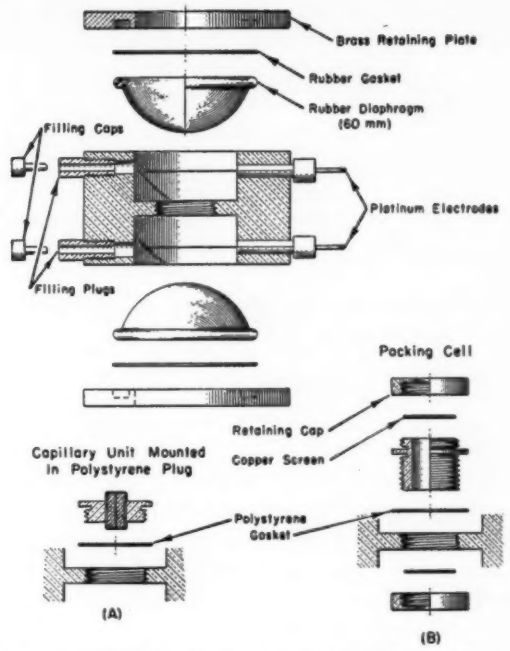

FIG. 3. Diagrammatic view of test cell, showing capillary unit. Dimensions of test cell: internal diameter: 1.75 in.; outer diameter: 3.00 in.; height polystyrene body: $1\frac{7}{8}$ in.; distance between electrodes: $1\frac{1}{4}$ in.; length platinum electrodes: $1\frac{1}{2}$ in.; diameter platinum electrodes: 0.016 in.; thickness threaded section: $\frac{3}{8}$ in.; diameter threaded section: $\frac{7}{8}$ in.

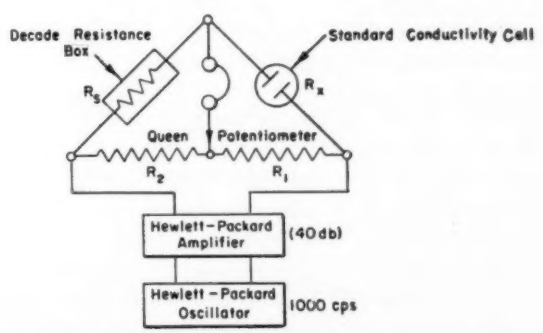

FIG. 4. Conductivity bridge used to determine conductivity of distilled water. Reproduced from Daniels, Mathews, and Williams, *Experimental Physical Chemistry* (McGraw-Hill Book Company, Inc., New York, 1941), third edition, pp. 177–180.

[8] To quote Bulter (*Electrical Phenomena at Interfaces* (Methuen and Company Ltd., London, 1951), p. 76. "The zeta-potential is defined as the potential at the surface of shear due to the combined effect of charges of one sign on the surface of a solid, for instance, and the equal and opposite ionic atmosphere in the liquid."

TABLE II. Summary of data obtained for four glass capillaries.

Unit	$\mu=0.920\times10^{-2}$ poise frequency = 30 cps Y_a	$f(Y_a)$	E_s/P volt/(dyne/cm²)	$\rho=0.996$ gm/cm³ temp = 25°C σ ohm⁻¹ cm⁻¹	σ esu	$\left[\frac{E_s}{P}\frac{\sigma}{f(Y_a)}\right]\left(\frac{\text{volt}}{\text{dyne}}\frac{\text{cm}^3}{\text{ohm}}\right)$
G5	4.4	0.42	0.34×10^{-6}	3.550×10^{-6}	3.195×10^{6}	0.29×10^{-11}
G7	8.1	0.23	0.21×10^{-6}	3.550×10^{-6}	2.929×10^{6}	0.30×10^{-11}
G2	12	0.14	0.04×10^{-6}	10.17×10^{-6}	9.156×10^{6}	0.30×10^{-11}
G1	15	0.12	0.14×10^{-6}	2.550×10^{-6}	2.295×10^{6}	0.31×10^{-11}

A theoretical plot of $f(Y_a)$, i.e., $f(Y_a)$ equal to the absolute magnitude of

$$\left[\frac{-2}{Y_a}\frac{ii^{\frac{1}{2}}J_1(i^{\frac{1}{2}}Y_a)}{J_0(i^{\frac{1}{2}}Y_a)}e^{-i\omega t}\right],$$

against $Y_a(Y_a=a(j\omega/\mu)^{\frac{1}{2}}, ak=i^{\frac{1}{2}}Y_a)$ is given in Fig. 1. The values for the Bessel functions for Y_a in the range from 1 to 10 have been made from the tables given in *Tables of Functions* by Jahnke and Emde. For the range 10 to 100, the following asymptotic relations are used to calculate the functions:

$$J_0(z)\sim(2/\pi z)^{\frac{1}{2}}\cos(z-\pi/4),$$
$$J_1(z)\sim(2/\pi z)^{\frac{1}{2}}\cos(z-3\pi/4).$$

For Y_a greater than 100, $f(Y_a)$ is approximately equal to $2/Y_a$.

II. EXPERIMENTAL RESULTS

A hydrodynamical test system designed by G. B. Thurston at the Defense Research Laboratory, The University of Texas, was used to provide the sinusoidal pressure variations.[9] Figure 2 is a cross-sectional view of the main test chamber. Sinusoidal motion in the main chamber is delivered by the sylphon bellows which is driven by a geophone-type push-pull driver. The pressure is detected by a capacitive hydrophone (labeled H in the figure). With the system, pressure amplitudes of 0 to 20 000 dynes/cm² over a frequency range of 20 to 200 cps can easily be achieved.

Soda glass capillaries were used for the test elements. A polystyrene test cell was constructred into which the various glass samples could be fitted. Figure 3 represents a diagrammatic view of the test cell used for the streaming potential measurements. Referring to the figure, the test cell is seen to consist of a polystyrene body into which are fitted two platinum electrodes and two vacuum filling plugs. The cell body contains an upper and lower chamber connected by a threaded section into which the capillary elements fit. Brass retaining plates with circular depressions to hold the rubber diaphragms are fastened to the main body by means of six brass screws. The entire assembly is attached to the hydrodynamical test system by means of six more brass screws which penetrate the outer rim of the plastic body and brass retaining plates. Appropriate polystyrene and rubber washers are used wherever necessary to insure a tight connection. After the glass

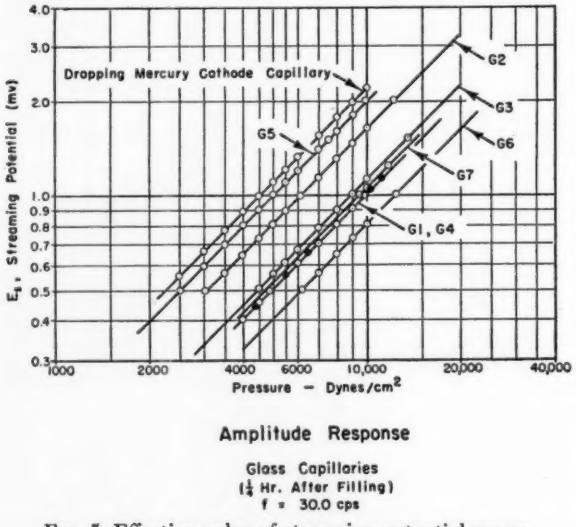

FIG. 5. Effective value of streaming potential *versus* effective value of the pressure amplitude.

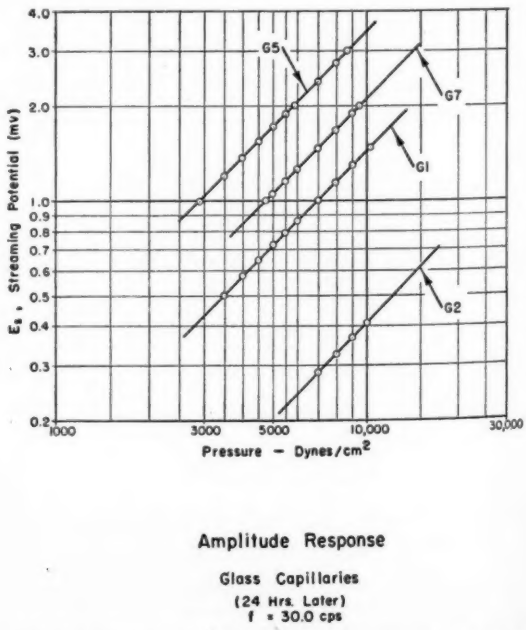

FIG. 6. Effective value of streaming potential *versus* effective value of pressure amplitude after equilibrium had been reached between polystyrene test cell and "equilibrium water."

[9] A complete description of the hydrodynamical test equipment together with the electronic equipment used for measurements is given in a paper by George B. Thurston, "Apparatus for absolute measurement of analogous impedance of acoustic elements," J. Acoust. Soc. Am. (to be published).

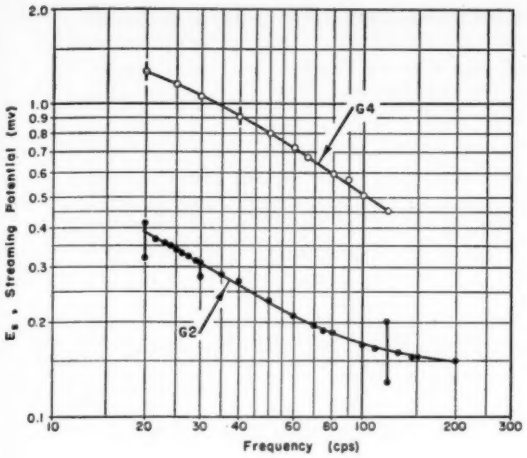

FIG. 7. Effective value of streaming potential *versus* frequency for a constant pressure amplitude.

capillaries had been sealed in the test cell (the usual precaution having been made to insure clean surfaces), the cell was vacuum filled with "equilibrium water".[10] The conductivity of this distilled water with which the cell was filled was measured on a standard conductivity bridge as shown in Fig. 4. The conductivity cell had a "cell constant" of 2.168×10^{-1}, this having been determined with standard 0.05M $AgNO_3$. A Hewlett-Packard oscillator Model 201B fed into a Hewlett-Packard amplifier (40 db gain) Model 450A provided the 1000 cps signal. A new cell is being designed which will provide for the measurement of the conductivity at the same time the streaming potential is being measured.

The glass was commercial stock soda glass with uniform bore size ranging from 0.020 inch to 0.080 inch. The dimensions of the glass capillaries used are given in Table I.

The first experimental check on Eq. (6) was made by taking pressure amplitude responses. The frequency of the geophone driver was held constant, and the pressure amplitude was varied. This pressure variation produced a streaming potential voltage of the same frequency. The results, shown in Fig. 5 and Fig. 6, show a linear relation between the effective value of the streaming potential and the effective value of the pressure amplitude. Since the conductivity of distilled water changes when it comes into contact with the polystyrene test cell body, four of the glass capillaries were mounted in the cell for 24 hours. At the end of this time,

[10] "Equilibrium water" is distilled water in equilibrium with air and soda glass. This distilled water was procured from the Chemistry Department, The University of Texas, in small quantities from time to time during the experiments and accounts for the variations in conductivity.

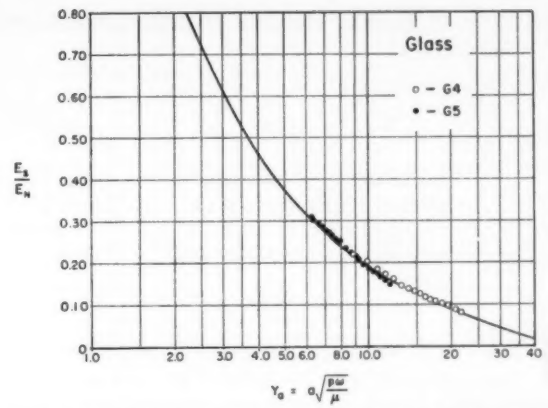

FIG. 8. Comparison of experimental values of streaming potential (E_N defined in text) *versus* frequency with theory [solid curve is part of $f(Y_a)$ given in Fig. 1].

the conductivity of the distilled water was constant with time for all practical purposes. The streaming potential measurements made on these four glass capillaries are given in Table II. Equation (6) can be written in the following form:

$$E_s=\frac{k''}{\sigma}Pf(Y_a),$$

where k'' = constant for the same solid-liquid contacts, σ = conductivity of the "equilibrium water" in bulk, P = effective value of the pressure amplitude in dynes/cm², and $f(Y_a)$ = defined previously.

In Table II, $[E_s\sigma/Pf(Y_a)]$ is seen to be essentially constant which is in agreement with the theory.

A second check on Eq. (6) is provided by making a frequency response run on the glass samples. The pressure amplitude was held constant and the frequency varied from 20 to 200 cps. The frequency response of two glass samples is shown in Fig. 7. Since Y_a for a particular glass capillary increases with an increase in frequency, the streaming potential E_s should decrease with frequency (one $f(Y_a)$ exceeds unity). This is seen to be the case. In Fig. 6, the solid vertical lines represent "beats" in the hydrodynamical system. Figure 8 shows a plot of the theoretical values with those obtained experimentally, where E_N is the value of the streaming potential that would be recorded for $f(Y_a)$ equal to unity. E_N is computed by dividing the experimentally obtained value of the streaming potential at 20 cps by the calculated value of $f(Y_a)$ for the capillary being tested. The theoretical curve shown in Fig. 8 is a portion of $f(Y_a)$ shown in Fig. 1. The agreement between theory and experiment for all glass samples tested was good. Additional work on sulphur, paraffin, beeswax, and plastic capillaries will be reported in a later paper.

The author wishes to express his appreciation to Dr. S. LeRoy Brown for his help and advice and to Dr. Norman Hackerman for his many suggestions throughout the work.

Electric Dipole Moments of Several Molecules from the Stark Effect*

S. N. GHOSH,† RALPH TRAMBARULO,‡ AND WALTER GORDY
Department of Physics, Duke University, Durham, North Carolina
(Received October 6, 1952)

The following molecular electric dipole moments, in Debye units, have been obtained from the Stark effect of pure rotational spectra observed in the microwave region: 0.234±0.004 for NF_3; 1.03±0.01 for PF_3; 1.77±0.02 for POF_3; 3.00±0.02 for HCN; 3.92±0.06 for CH_3CN; 3.83±0.06 for CH_3NC; 1.79±0.02 for CH_3F; 0.75±0.01 for CH_3CCH; 1.26±0.01 for SiF_3H. All values apply to the ground vibrational state.

THE Stark effect in microwave rotational spectra is now a well-known method for measurement of molecular dipole moments. Unlike that of other gaseous methods the accuracy obtainable is not affected by impurities in the sample. The limiting factor upon the accuracy is either the precision with which the electrode spacing can be maintained and measured, or the accuracy with which the Stark splitting of the lines can be measured. If the molecule exhibits a first-order Stark effect, as do symmetric-top molecules when $K \neq 0$, a relatively large Stark splitting can be obtained with moderate field strengths. The electrode spacing then becomes the limiting factor in the accuracy. If a second-order Stark effect must be employed, as is always the case with linear molecules in the ground vibrational state, and if in addition the dipole moment is small, as it is in N_2O and CO, it is not possible to produce a wide splitting with a reasonable voltage, and the line separation becomes the limiting factor on the accuracy. Frequently dipole moment determinations are complicated by nuclear quadrupole hyperfine structure.

In the present work the dipole moments of nine molecules have been evaluated from the Stark splitting of their rotational lines. Six of these have been previously measured, either with the Stark effect or with other methods.

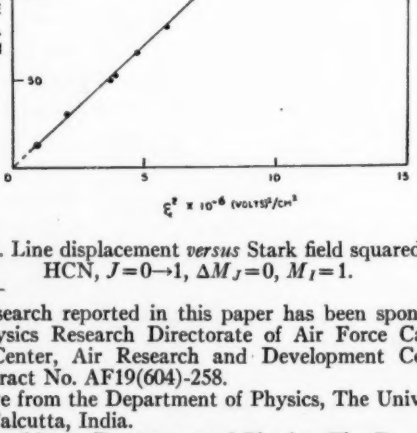

FIG. 1. Line displacement *versus* Stark field squared for HCN, $J=0\rightarrow1$, $\Delta M_J=0$, $M_I=1$.

EXPERIMENTAL METHOD

Our measurements were made with a K-band waveguide Stark cell with a plane electrode supported across the center of the guide by Teflon[1] so that the conducting surfaces were perpendicular to the $\mathcal{E}$-lines of the microwave radiation.

A 100-kc square wave modulation method was used for all measurements except that for HCN. For the HCN line, 4-kc square wave modulation was employed. All line splittings were measured by standard frequency markers in the usual manner.

The electrode spacing as well as the over-all spectrometer was calibrated with OCS. Because OCS has a moderately large dipole moment, a rotational spectrum which is devoid of fine or hyperfine structure, and low J lines which fall in the centimeter wave region, this molecule provides a convenient standard for calibration. The dipole moment of OCS has been carefully measured by several workers.[2] The value obtained by Shulman and Townes[2c] is 0.7085±0.004 debye units. Since this is an accuracy equal to or greater than that to which the electrode spacing in our cell could be directly measured, we have used OCS to calibrate the spectrometer for each measurement.

RESULTS

For all symmetric-top molecules investigated we have used only rotational lines with $K=0$. The $K=0$ lines of symmetric-top molecules have only a second-order Stark effect, which makes them similar in the present measurements to linear molecules.

In CH_3NC the nuclear quadrupole coupling is too small to produce an observable hyperfine structure, and hence it can be ignored in the present considerations. In HCN and CH_3CN the N^{14} coupling eqQ is of the order of 4 Mc and produces an observable splitting of the line. Nevertheless, the large dipole moments of these molecules make it easy to impose a field of sufficient

* The research reported in this paper has been sponsored by the Geophysics Research Directorate of Air Force Cambridge Research Center, Air Research and Development Command, under Contract No. AF19(604)-258.

† On leave from the Department of Physics, The University of Calcutta, Calcutta, India.

‡ Present address: Department of Physics, The Pennsylvania State College, State College, Pennsylvania.

[1] McAfee, Hughes, and Wilson, Rev. Sci. Instr. **20**, 821 (1949).

[2] (a) Dakin, Good, and Coles, Phys. Rev. **71**, 640 (1947); (b) Strandberg, Wentink, and Kyhl, Phys. Rev. **75**, 270 (1949); (c) R. G. Shulman and C. H. Townes, Phys. Rev. **77**, 500 (1950); (d) J. N. Shoolery and A. H. Sharbaugh, Phys. Rev. **82**, 95 (1951).

TABLE I. Transitions and B values used.

Molecule	Transition employed	ν (Mc/sec)	B_0 (Mc/sec)	Reference
NF_3	$J=0\rightarrow1$	21 361.92	10 680.96	a
PF_3	$J=1\rightarrow2$	31 279.60	7 819.90	b
POF_3	$J=1\rightarrow2$	18 377.0	4 594.25	c
HCN	$J=0\rightarrow1$	88 631.94	44 315.97	d
CH_3CN	$J=1\rightarrow2$	36 793.64	9 198.83	e
CH_3NC	$J=0\rightarrow1$	20 105.80	10 052.90	e
CH_3F	$J=0\rightarrow1$	51 071.69	24 862.37	f
CH_3CCH	$J=1\rightarrow2$	34 183.37	8 545.84	g
SiF_3H	$J=1\rightarrow2$	28 831.90	7 207.98	h

[a] J. Sheridan and W. Gordy, Phys. Rev. **79**, 513 (1950).
[b] Gilliam, Edwards, and Gordy, Phys. Rev. **75**, 1014 (1949).
[c] Williams, Sheridan, and Gordy, J. Chem. Phys. **20**, 164 (1952).
[d] Simmons, Anderson, and Gordy, Phys. Rev. **77**, 77 (1950); **86**, 1055 (1952).
[e] Kessler, Ring, Trambarulo, and Gordy, Phys. Rev. **79**, 54 (1950).
[f] Gilliam, Edwards, and Gordy, Phys. Rev. **75**, 1014 (1949).
[g] R. Trambarulo and W. Gordy, J. Chem. Phys. **18**, 1613 (1950).
[h] See reference 4.

magnitude to break down the nuclear coupling and to produce the simple strong-field case.

The usual second-order formulas,

$$E_{\substack{JM_J \\ J\neq0}}^{(2)}=-\frac{\mu^2\mathcal{E}^2}{2hB}\frac{[3M_J^2-J(J+1)]}{J(J+1)(2J-1)(2J+1)}$$
$$E_{00}^{(2)}=-\frac{\mu^2\mathcal{E}^2}{6hB}, \tag{1}$$

for linear molecules (or the symmetric-top formula with $K=0$) without nuclear coupling apply to the strong field case, but a small correction given by

$$E_Q^{(1)}=-eqQ\left\{\frac{[3M_J^2-J(J+1)][3M_I^2-I(I+1)]}{4I(2I-1)(2J-1)(2J+3)}\right\} \tag{2}$$

must be added[3] to the energies to correct for the nuclear perturbations. In our experiments with the electrode placed so that the Stark field $\mathcal{E}$ was parallel to the electric vector of the microwave radiation, only the $M\rightarrow M$ transitions are allowed.

The strong-field displacement observed for the $J=0\rightarrow1$, $M_J=0$ line is then

$$\Delta\nu_{\substack{(J=0\rightarrow1) \\ M_J=0}}=\frac{4}{15}\frac{\mu^2\mathcal{E}^2}{h^2B}+\text{term independent of }\mathcal{E}. \tag{3}$$

It is readily seen that $\Delta\nu$ plotted as a function of $\mathcal{E}^2$ is a straight line in the strong field region with slope S:

$$S_{\substack{(J=0\rightarrow1) \\ M_J=0}}=\frac{d(\Delta\nu)}{d(\mathcal{E}^2)}=\frac{4}{15}\frac{\mu^2}{h^2B}. \tag{4}$$

The nuclear effects do not influence the slope in the strong-field region but only the projected intercepts. The dipole moment can then be found readily if the line displacements are plotted against $\mathcal{E}^2$ (or V^2 since the electrode spacing is held constant) for both the standard OCS molecule and the molecule X being investigated, and if the ratios of the two slopes are then taken.

For the $J=1\rightarrow2$ transition of linear molecules (or of symmetric tops with $K=0$) there are two $\Delta M_J=0$ Stark components corresponding to $M_J=0$ and $M_J=1$. The strong-field $\Delta\nu$ *versus* $\mathcal{E}^2$ plots of these have slopes,

$$S_{\substack{(J=1\rightarrow2) \\ M_J=0}}=\frac{d(\Delta\nu)}{d(\mathcal{E}^2)}=-\frac{8}{105}\frac{\mu^2}{h^2B}, \tag{5}$$

and

$$S_{\substack{(J=1\rightarrow2) \\ M=1}}=\frac{d(\Delta\nu)}{d(\mathcal{E}^2)}=\frac{13}{210}\frac{\mu^2}{h^2B}. \tag{6}$$

It was found most convenient to employ the $J=1\rightarrow2$ transition of OCS for all calibrations. However, the $J=0\rightarrow1$ transition was used for some of the molecules under investigation. For the $J=0\rightarrow1$, $K=0$, $\Delta M=0$, transition of the molecule X (symmetric top or linear) used with the $J=1\rightarrow2$, $M_J=0$, line of OCS, Eqs. (4) and (5) are combined to give the unknown moment,

$$\mu_X=\mu_{OCS}\left(\frac{2}{7}\frac{B_X}{B_{OCS}}\frac{|S_X|}{|S_{OCS}|}\right)^{\frac{1}{2}} \begin{cases} J=0\rightarrow1 \text{ for } X \\ J=1\rightarrow2,\ M_J=0 \text{ for OCS.} \end{cases} \tag{7}$$

When the same rotational transition with the same second-order Stark component is measured for both the unknown molecule X and for OCS, the formula for the unknown moment in terms of the measured parameters becomes

$$\mu_X=\mu_{OCS}\left(\frac{B_X}{B_{OCS}}\frac{|S_X|}{|S_{OCS}|}\right)^{\frac{1}{2}} \begin{cases} J=1\rightarrow2 \text{ and same second-} \\ \text{order Stark component} \\ \text{for } X \text{ and OCS.} \end{cases} \tag{8}$$

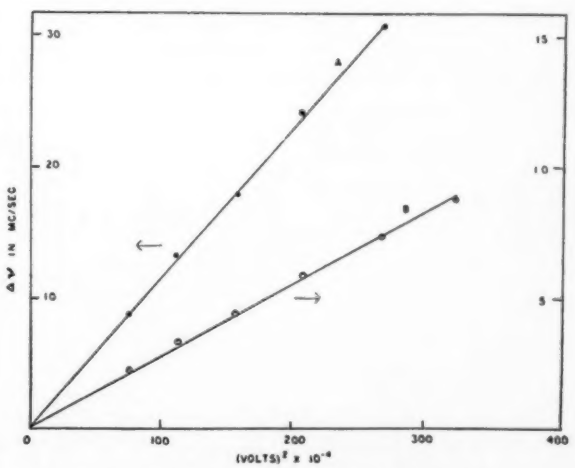

FIG. 2. Line displacement *versus* Stark voltage squared:
A. OCS, $J=1\rightarrow2$, $M_J=0\rightarrow0$
B. $N^{15}F_3$, $J=0\rightarrow1$, $M_J=0\rightarrow0$.

[3] U. Fano, J. Research Natl. Bur. Standards **40**, 215 (1948).

TABLE II. Electric dipole moments.

Molecule	Moment in debye units: Present study	Previous value and method
NF_3	0.234±0.004	0.21–0.25 (Dielectric const)[a]
PF_3	1.03 ±0.01	1.03±0.01 (Stark)[b]
POF_3	1.77 ±0.02	1.74±0.04 (Stark)[c]
HCN	3.00 ±0.02 (Ground vib. state)	2.957 (Stark)[d] (Excited bending vib. state)
CH_3CN	3.92 ±0.06	3.97 (Stark)[e]
CH_3NC	3.83 ±0.06 (Ground vib. state)	
	3.78 ±0.06 (Excited bending vib. state)	
CH_3F	1.79 ±0.02	1.81–1.84 (Dielectric const)[f]
CH_3CCH	0.75 ±0.01	
SiF_3H	1.26 ±0.01	

[a] K. L. Ramaswamy, Proc. Indian Acad. Sci. **2A**, 364 (1934).
[b] Shulman, Dailey, and Townes, Phys. Rev. **78**, 145 (1950).
[c] S. J. Senatore, Phys. Rev. **78**, 293 (1950).
[d] R. G. Shulman and C. H. Townes, Phys. Rev. **77**, 421 (1950).
[e] Coles, Good, and Hughes, Phys. Rev. **79**, 224 (1950).
[f] C. P. Smyth and K. B. Alpine, J. Chem. Phys. **2**, 449 (1934); R. L. Ramaswamy, Proc. Indian Acad. Sci. **4A**, 108 (1936).

The B_0 values for all the molecules included in the present study have been previously measured by means of microwave spectroscopy. The values used, with the references, are listed in Table I.

Although the Stark effect of HCN in an excited bending vibrational state has been measured earlier, that of the normal or ground vibrational state has not. For HCN we have used the OCS data to calibrate the electrode separation and have plotted in Fig. 1 the Stark displacement against the square of the field, in volts^2/cm^2. For other molecules, the splitting is plotted simply as a function of the voltage squared along with a similar plot of the OCS data. Figure 2 shows the plot for $N^{15}F_3$. Plots for the other molecules are similar and are not given. A few moments, namely, those for POF_3, PF_3, and CH_3CN already measured with the Stark method in other laboratories, were remeasured as a check. In all instances the agreement with the previous values was within the estimated experimental error. Because of the exceptionally small dipole moment of NF_3 it did not prove easy to obtain the necessary field strength to breakdown completely the N^{14} nuclear quadrupole coupling even though the coupling constant, eqQ, is only -7.07 Mc/sec.[4] Rather than solve the complex intermediate case we chose the easier course of measuring the splitting for $N^{15}F_3$, which has no nuclear hyperfine structure.

The electric dipole moments obtained for the different molecules in the present study are listed in Table II with earlier values from the literature. The moment of CH_3NC was measured for both the ground state and the lowest excited bending vibrational state. The moment was found to be less for the bending state by about 1.5 percent than for the ground state. Although the combined absolute errors are greater than this amount, the possible error in the relative value is slightly less. Hence, the difference appears to be significant. Also the value obtained for the HCN ground vibrational state is correspondingly larger than that of the first excited bending mode.

The interpretation of molecular dipole moment in terms of the electronic structures of the molecules is a formidable task on which but little progress has been made, even for simple diatomic molecules. It is to be hoped that the dependable moment-values now being obtained from the microwave Stark effect in many different laboratories will stimulate new theoretical efforts to understand them. The very small dipole moment of NF_3 provides strong evidence for the importance of the atomic hybridization moments predicted quantum mechanically by Coulson.[5] Both the N^{14} nuclear coupling and the bond angles[4] in this molecule suggest a large amount, about 17 percent of s-hybridization of the bonding orbitals of N. The two electrons in the nonbonding orbital (which has complementary hybridization of about 50 percent p character) produce a large N atomic moment which is opposed to, and almost cancels, the primary moment expected from the high ionic character of the NF bonds.

We wish to thank Dr. John Sheridan who prepared some of the chemicals used, Mr. W. C. King who helped with the measurements on HCN, and Dr. M. Mizushima for helpful discussion of theory.

[4] J. Sheridan and W. Gordy, Phys. Rev. **77**, 719 (1950).
[5] C. A. Coulson, Trans. Faraday Soc. **38**, 433 (1942).

The Far Ultraviolet Absorption Spectra of Simple Alkyl Amines*

EILEEN TANNENBAUM,†‡ ESTHER M. COFFIN,§ AND ANNA J. HARRISON
Department of Chemistry, Mount Holyoke College, South Hadley, Massachusetts

(Received September 4, 1952)

A quantitative study of the absorption spectra of ammonia, the three methyl and the three ethyl amines, has been made in the region 39 000 to 63 000 cm^{-1}. Three electronic transitions have been observed in most cases. The first is of low intensity particularly in the secondary amines, the second is of higher intensity and increases from the primary to the tertiary compound, and the third, which is only partially covered by these measurements, is of intermediate intensity. The positions of all transitions, particularly the second, are influenced by alkyl substitution. These transitions are discussed in relation to the spectrum of ammonia. Vibrational structure, present in ethyl amine, methyl amine, and dimethyl amine, has been analyzed in part.

INTRODUCTION

THE investigation of the far ultraviolet spectra of the simple aliphatic amines was undertaken to obtain fundamental information concerning the electronic transitions that occur in these molecules and, if possible, to correlate the spectra with the chemical reactivity of the compounds. Thompson and Duncan,[1] who reported oscillator strengths and positions of bands for the spectrum of ammonia, the parent compound of these series, were able to measure four electronic transitions in the range of 45 000 cm^{-1} to 120 000 cm^{-1}. These four transitions were assigned as being transitions of one electron of the unshared pair: $2p_z-3s$, $2p_z-3d_z$, $2p_z-4s$, and $2p_z-5s$. The assignment of the second transition was, however, tentative, and it was pointed out that another possibility involved an NH bonding electron; a $N-V$, bonding to antibonding, or a $(\pi e)-(\pi e)'$, bonding to bonding, transition being consistent with the position and intensity of the observed band. These possible assignments were based on an electron configuration proposed by Mulliken.[2]

EXPERIMENTAL

Purification of Compounds

Methods of purification of amine samples obtained from Eastman Kodak Company are summarized as follows: (1) direct distillation of the free amine: ethyl and triethyl amine; (2) direct distillation of an aqueous solution of the amine: methyl and dimethyl amine; (3) fractional crystallization of the hydrochloride from absolute alcohol or ether followed by treatment with base and distillation: ethyl, methyl, diethyl, and dimethyl amine; (4) free amine refluxed with acetic anhydride and distilled: triethyl and trimethyl amine; (5) treatment with Hinsberg reagent followed by distillation: trimethyl amine. All distillations were carried out in an atmosphere of nitrogen. Compounds whose boiling points are above room temperature were refluxed with a drying agent and fractionally distilled through a modified Fenske column. Fractions boiling within a 0.1°C range were used for the measurements. More volatile compounds were distilled over a long column of soda lime or other drying agent.

Diethyl amine was also prepared by the acid hydrolysis of a purified sample of diethyl cyanamide which was prepared in this laboratory.

Ammonia was prepared from Baker's cp ammonium sulfate by heating in a nitrogen atmosphere and passing the vapor over potassium hydroxide pellets.

The flowing vapor method used for intensity measurements provides a criterion of purity more sensitive than any available chemical method. The impurity will become more or less concentrated in the course of a series of measurements depending on the relative vapor pressures of compound and contaminant, and can be detected by noting any drift in the values of the extinction coefficient obtained. The agreement between measurements on different samples provided an additional assurance of purity.

TABLE I. Summary of experimental details.

	Vacuum Spectrograph	Quartz Spectrograph	Beckman Spectrophotometer
Region	2300–1600A	3000–2100A	3000–2100A
Source	flowing hydrogen lamp	standard hydrogen lamp	standard hydrogen lamp
Exposure time	3 and 4 min	2 and 3 min	
Cell length	32.5 cm 31.0 cm	5.0 cm 12.5 cm 15.5 cm	1.00 cm 10.00 cm
Pressure of the amine vapor	0.01–1.8 mm	5–500 mm	1.5–120 mm
State of sample	flowing vapor	static vapor	static vapor
Measurements made	extinction coefficient and band position	band position	extinction coefficient
Plates	Ilford Q1	Eastman No. 50	

* Supported in part by the ONR.
† Presented in partial fulfillment of the degree of Master of Arts, 1952.
‡ Present address: University of California, Berkeley, California.
§ Presented in partial fulfillment of the degree of Master of Arts, 1949.
[1] R. J. Thompson and A. B. F. Duncan, J. Chem. Phys. 14, 573 (1946).
[2] R. S. Mulliken, J. Chem. Phys. 3, 506 (1935).

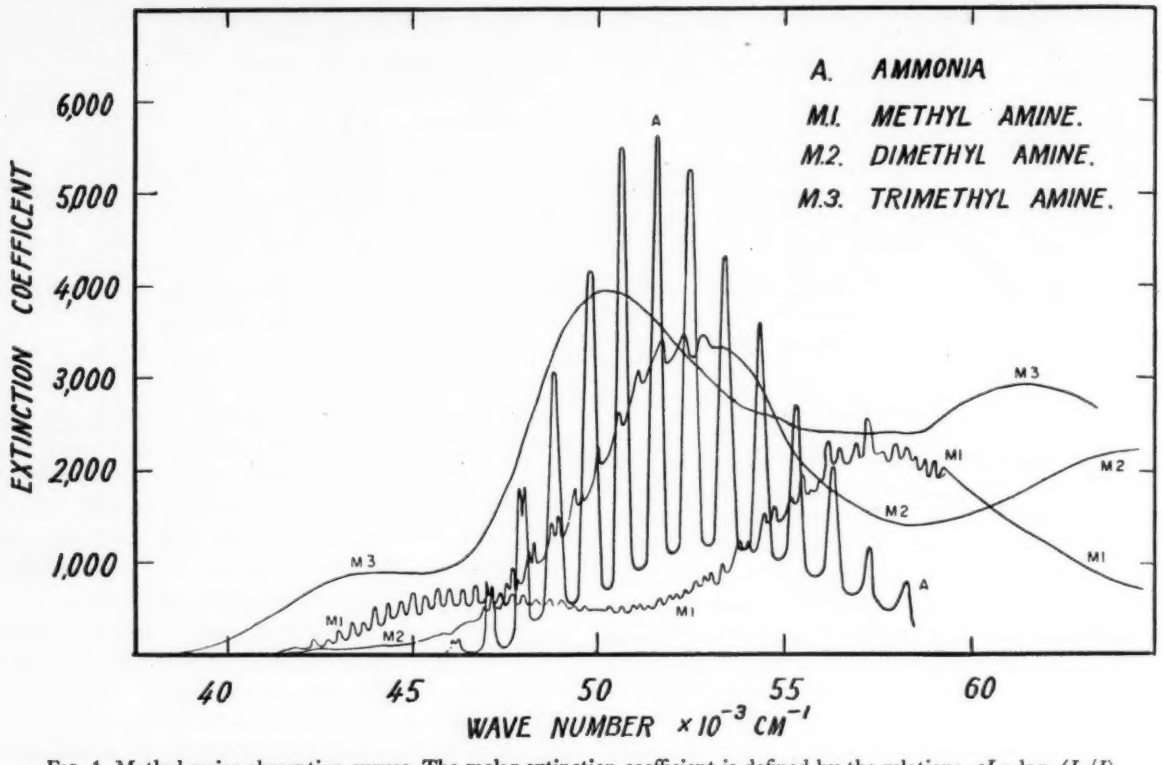

FIG. 1. Methyl series absorption curves. The molar extinction coefficient is defined by the relation: $\epsilon cL = \log_{10}(I_0/I)$ where c is concentration in moles per liter, L is path length in cm.

Spectrographic Measurements

The experimental details of measurement are summarized in Table I. The apparatus and flowing vapor method for intensity measurements have been previously described.[3] Modification of the apparatus for low temperature studies involved the adaptation of a condenser for use as an absorption tube. The method used for intensity measurements is based on time calibration. The data for ammonia, the least extensively studied compound of the group, were determined from 8 plates. For each of the other compounds, the curves are based on data taken from between ten and sixteen plates.

With the exception of ammonia, the precision of the measurements of log epsilon on both the Beckman spectrophotometer and the vacuum spectrograph was usually not greater than 0.02 with an occasional average deviation of 0.05. In the region in which two instruments overlapped, from 42 500–47 500 cm^{-1}, intensity measurements determined on the two instruments checked within 0.02. The band positions, as measured on a Hilger comparator and from microphotometer tracings of plates taken at low temperatures, were determined with a precision of 20 cm^{-1}. A superimposed copper-silver spark and the mercury absorption line were used as the wavelength standards. The hydrogen emission lines were used in the region from 59 700 cm^{-1} to 65 000 cm^{-1}. For this reason, any fine structure that the spectra of these compounds may have in this region could not be determined.

The measurement of the spectrum of ammonia was not originally considered as a part of this problem since band positions and oscillator strengths had been reported previously. However, a plot of the spectrum was desirable for comparison with the other curves and a series of measurements were made. The unusual height of vibrational band structure made measurements more difficult and accentuated experimental errors. For example, measurements with the Beckman spectrophotometer indicated that slit width and scattered light were both too large a factor in the region from 220 mμ to 210 mμ to make reliable intensity measurements on this compound. The results of measurements with the vacuum spectrograph showed only a slightly greater average deviation than those of other compounds. However, the height of the bands is so great that only two or three values of epsilon were obtained at most of the maxima and minima with the eight plates which were taken. Since in this case, the width of the band becomes an appreciable factor in determining the area under the curves, the width of each band was measured at two or three points between each maximum and minimum.

The positions of the vibrational bands have been extensively studied by Duncan[4] using a grating instrument of high dispersion. Our band positions which are necessarily less precise are in substantial agreement with

[3] Harrison, Gaddis, and Coffin, J. Chem. Phys. **18**, 221 (1950).

[4] A. B. F. Duncan, Phys. Rev. **47**, 822 (1935); **50**, 700 (1936).

his reported values. However, our value of the oscillator strength of the first band was found to be 0.079 as compared with 0.13 reported by Thompson and Duncan. In both cases, the estimated precision was of the order of ten percent. The methods of measurement are so different that it is difficult to account satisfactorily for the discrepancy between the two f values. Under the conditions of their experiments (carried out on static samples at a pressure of 0.4–0.5 mm Hg, a cell length of 17.2 cm, and an exposure time of 40–60 minutes), they obtained a smooth curve[5] with no evidence of vibrational structure between 50 000–60 000 cm^{-1}. Our measurements were made at comparable pressures on flowing vapor samples and exposure times of four minutes.

DISCUSSION OF THE ABSORPTION CURVES

The absorption curves of corresponding members of the ethyl and methyl series show striking similarities (see Figs. 1 and 2). Ethyl and methyl amine both have a shallow band extending from about 40 000 cm^{-1} to about 50 000 cm^{-1} followed by a second broad band of more intense absorption. In each of these spectra both bands are rich in vibrational structure. A third band is beginning to appear in the spectrum of ethyl amine between 57 000 and 60 000 cm^{-1}.

Dimethyl and diethyl amine have an extremely shallow region of absorption beginning at about 46 000 cm^{-1}, and another region of intense absorption beginning at about 57 000 cm^{-1}. The maximum of the third band is beyond the range of the spectral measurements.

The spectrum of trimethyl amine consists of three bands, the first beginning at about 39 000 cm^{-1}, the second at about 46 000 cm^{-1}, and the third at about 56 000 cm^{-1}. The spectrum of triethyl amine consists of two well-defined bands, the first of which is probably composed of two overlapping bands corresponding to the first two bands in trimethyl amine. There is a suggestion of this in the slope of the curve in the region from about 40 000 cm^{-1} to about 45 000 cm^{-1}. The band with a maximum at about 57 000 cm^{-1} corresponds to the third transition in trimethyl amine.

The essential characteristics of the first two bands are summarized in Table II. Data on the third band are not sufficiently complete to warrant inclusion in the table. Values in parentheses are somewhat uncertain due to overlapping of two bands. In the case of triethyl amine, the first band is so completely obscured by the second that the characteristics of the first band could not be determined. The values of oscillator strength are based on the assumption that one band ends and the next begins at a minimum in the absorption curves. The exact values selected are given in the table. By dividing the curves of the amines into these three general regions of absorption, they are found to form an ordered pattern, each region exhibiting a characteristic behavior towards alkyl substitution through each series from

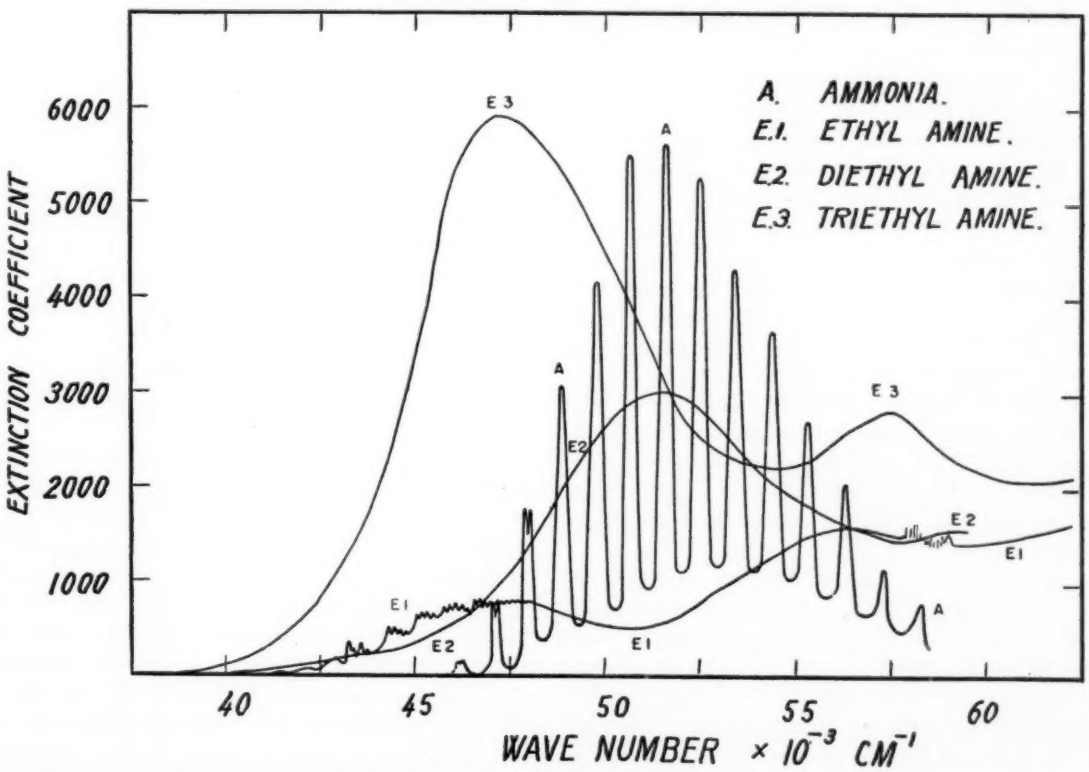

FIG. 2. Ethyl series absorption curves. The diffuse structure of the ethyl amine curve out to 55 000 cm^{-1} is not shown. The sharp bands at about 58 000 cm^{-1} has been indicated by vertical lines drawn at the band positions.

[5] A. B. F. Duncan, private communication.

TABLE II.

	Ammonia	Methyl amine	Dimethyl amine	Trimethyl amine	Ethyl amine	Diethyl amine	Triethyl amine
Pressure range mm Hg	0.0676–0.501	0.0895–1.53	0.0925–0.630	0.0799–0.311	0.190–0.805		
Wave number extrapolated $\log\epsilon=1.0$	45 700	40 800	40 500	37 800	41 300	39 700	37 700
FIRST BAND							
(1) Position of max cm^{-1}	51 500	46 500	(45 000)	44 000	47 000	(45 000)	...
(2) Maximum ϵ	5600	600	(100)	900	800	(300)	...
(3) Oscillator strength	0.079	0.017	(0.0017)	0.016	0.019	(0.0028)	...
(4) Wave number range	46 000–60 000	41 000–50 500	40 000–46 000	38 000–45 500	41 000–50 500	40 000–45 000	
(5) Position of 0—0	46 140	41 690			42 870		
SECOND BAND							
(1) Position of max cm^{-1}	66 000[a]	57 500	52 500	50 250	56 500	51 500	(47 250)
(2) Maximum ϵ		2200	3300	3950	1600	3000	(5900)
(3) Oscillator strength	0.0095[a]	0.084	0.10	0.13	0.050	0.10	(0.18)
(4) Wave number range		50 500–65 000	46 000–58 500	45 500–56 500	50 500–60 000	45 000–57 500	38 500–54 000
(5) Position of 0—0	60 135[a]	(50 360)	45 870				
Difference between maxima of first and seconds bands in cm^{-1}	14 500	11 000	7500	6250	9500	6500	...

[a] See reference 3.

primary to tertiary amine. The first band in all of the amines is of low intensity and is shifted only slightly with alkyl substitution. All the amines begin absorption between 38 000 cm^{-1} and 41 000 cm^{-1}, that is, within a range of only 3000 cm^{-1}, which is also the separation between the first maximum of methyl and trimethyl amine. Comparing either the beginning of absorption or the maximum of the first band, the shift from ammonia to ethyl or methyl amine is about 5000 cm^{-1}. The second band, on the other hand, is strikingly influenced by alkyl substitution, ethyl substitution being more effective than methyl substitution. The total spread in position of maxima is about 9000 cm^{-1} in contrast to the 3000 cm^{-1} of the first band. The shift in position of the second maximum towards the visible through the series from primary to tertiary amine is accompanied by an increase in intensity. The fact that the second band shifts by large increments while the first band shifts only about 1000 cm^{-1} from one member of the series to the next makes reasonable the assumption that the first and second bands of triethyl amine almost completely overlap.

Generalizations about the characteristics of the third band are less certain since it extends, in most cases, beyond the limit of the spectral measurements. However, the band appears to shift to the visible and increase in intensity from primary to tertiary amine, and probably has an oscillator strength of value between that of the first and second transitions. Inspection of the curves indicates that the pattern formed by this band is more nearly like that of the second band than the first.

VIBRATIONAL ANALYSES

Methyl Amine

The near ultraviolet spectrum of methyl amine and its deuterated forms was determined by Förster and Jungers[6] who analyzed the structure in terms of two frequencies, 650 cm^{-1} and 1000 cm^{-1}, with the 0—0 transition at 41 680 cm^{-1}. The 650 cm^{-1} frequency was associated with the amino group and the 1000 cm^{-1} was found to be influenced more by substitution of deuterium on the methyl group. The results of this investigation are in essential agreement with the above and extend the measurements out to 65000 cm^{-1}. All the bands to about 50000 cm^{-1} were accounted for by the following equation:

$$\nu=41\,690\ cm^{-1}+660v_1'+1000v_2',$$
$$v_1'=0, 1, \cdots 6;\quad v_2'=0, 1, 2, \cdots 8.$$

The frequency assignments of the individual bands are listed in Table III. One weak band was found 770 cm^{-1} on the long wave side of the 0—0 transition. This frequency is in good agreement with the value of 783 cm^{-1} as determined by a number of investigators[7] from infrared data corresponding to a ground state NH bending vibration, and is most probably the same type of vibration as the 660 cm^{-1} of the excited state. Similarly, it is reasonable to correlate the 1000 cm^{-1} of the excited state with the strong CN vibration (1045 cm^{-1}) of the

[6] T. Förster and J. C. Jungers, Z. physik. Chem. **B36**, 387 (1937).

[7] A. P. Cleaves and E. K. Plyler, J. Chem. Phys. **7**, 563 (1939); Bailey, Carson, and Daly, Proc. Roy. Soc. (London) **A173**, 339 (1939); R. G. Owens and E. F. Barker, J. Chem. Phys. **8**, 229 (1940).

ground electronic state found in the infrared. The structure in the region from about 50 000 cm^{-1} to about 60 000 cm^{-1} forms a pattern different in appearance from that below 50 000 cm^{-1} and is probably associated with a different electronic transition. The structure may actually continue beyond 60 000 cm^{-1}, but intensity measurements in the hydrogen line region of the spectrum are not sufficiently sensitive to detect it. From inspection of the microphotometer records, the 0—0 of the second transition appears to be a band at 50 360 cm^{-1}. However, no attempt has been made, to analyze the structure in this region, and the appearance of the microphotometer record can often be misleading.

Ethyl Amine

The spectrum of ethyl amine is very much like that of methyl amine in many respects. The general shape of the two curves is the same and both have a marked amount of structure. The structure of ethyl amine consists of very narrow bands which become somewhat diffuse at about 45 000 cm^{-1} and gradually go over into a continuum. At about 58 000 cm^{-1} another short series of very sharp narrow bands begins unlike the first series. The bands very probably mark the beginning of a third electronic transition. The details of the structure cannot be shown on a plot the size of Fig. 2, which indicates only the most prominent bands. Figure 3 shows a microphotometer tracing of part of the spectrum indicating clearly the details of the structure. In Fig. 4 the structure has been schematically represented by vertical lines drawn above the curve where the maxima occur.

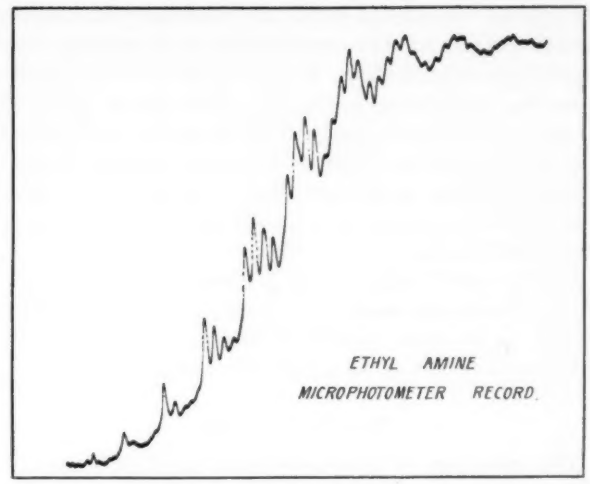

FIG. 3. Microphotometer tracing of ethyl amine in the region from 42 500 cm^{-1} to 48 000 cm^{-1} showing the details of the structure.

TABLE III. Methyl amine—vibrational analysis.

Wave no. Exptl	Wave no. Calc	ν_1' 660 cm^{-1}	ν_2' 1000 cm^{-1}	ν_1'' 770 cm^{-1}
40 920	40 920	0	0	1
41 690	41 690	0	0	0
42 350	42 350	1	0	0
42 710	42 690	0	1	0
43 000	43 010	2	0	0
43 350	43 350	1	1	0
43 680	43 690	0	2	0
	43 670	3	0	0
44 000	44 010	2	1	0
44 350	44 330	4	0	0
	44 350	1	2	0
44 680	44 690	0	3	0
	44 670	3	1	0
45 015	45 010	2	2	0
	44 990	5	0	0
45 350	45 350	1	3	0
	45 330	4	1	0
45 690	45 690	0	5	0
	45 670	3	2	0
45 980	45 990	5	1	0
46 370	46 350	1	4	0
47 700	47 690	0	6	0
	47 670	3	4	0
48 010	48 010	2	5	0
	47 990	5	3	0
48 370	48 330	4	4	0
48 670	48 690	0	7	0
	48 670	3	5	0
	48 650	6	3	0
49 010	49 010	2	6	0
	48 990	5	4	0
49 340	49 350	1	7	0
	49 330	4	5	0
49 640	49 650	6	3	0
	49 690	0	8	0

The vibrational structure was analyzed by determining the temperature dependence of the intensity of the bands. The method consisted of confining a constant amount of sample in the absorption tube by means of a stopcock situated at the entrance to the tube, and taking successive photographic exposures as the temperature was changed from −35° to 70°.[8] At low temperatures, the bands became sharper and their relative intensities were altered. The peak at 42 870 cm^{-1} increased whereas the bands on either side of it were lowered. Figure 5 illustrates this effect, showing two superimposed microphotometer tracings of the portion of the spectrum at the two indicated temperatures. This peak was identified as the 0—0. All the most prominent bands were accounted for by the equation

$$\nu = 42\,870\ cm^{-1} - 620v_1'' + 740v_1' - 1500v_2'' + 1620v_2',$$

$v_1''=0,1,2,3$; $v_1'=0,1,\cdots 8$; $v_2''=0,1$; $v_2'=0,1,2,3$. Although this equation accounts both for the position and expected relative insensities of the bands (see Table IV), it is a questionable assignment since it lacks corroborative evidence from other sources. First of all, one would expect the vibrational frequencies of ethyl amine to be analogous to those of methyl amine, where the vibrations in the excited electronic state so clearly parallel the skeletal vibrations of the molecule found in the infrared, but this is not the case. Furthermore, the methyl amine frequencies originate almost entirely from

[8] Photodecomposition was not a factor here since the wavelength region was restricted by the use of quartz equipment. The lower limit of temperature is determined by the vapor pressure of the compound and the length of the tube.

the ground vibrational level, whereas many of the frequencies of ethyl amine are assigned as originating from excited vibrational states of the ground electronic state. Also, the frequencies on the long wave side of the 0—0 do not check convincingly those found in the infrared and Raman spectra.[9] Despite repeated attempts to find another pattern more consistent with the other data, none could be found to account for all of the most prominent bands.

Earlier work[10] reported on the near ultraviolet spectrum of this compound was done on smaller spectrographs which were unable to resolve as much of the fine structure as has been here determined.

Dimethyl Amine

The spectrum of dimethyl amine is characterized by a sharp series of vibrational bands beginning at 45 130 cm^{-1}. It is notable that the region of absorption from 41 000 cm^{-1} to about 45 000 cm^{-1} is of low intensity and completely devoid of structure in contrast to the two primary amines which have such pronounced structure from the very beginning of absorption.

The vibrational bands were analyzed by exactly the same method as was the structure of ethyl amine. The peak at 45 870 cm^{-1} was, in this way, identified as the 0—0 transition. Most of the bands were described by a formula involving one ground frequency and one upper state frequency as follows:

$$45\,870\ cm^{-1}-750v''+605v',$$
$$v''=0,1;\quad v'=0,1,2,\cdots 6.$$

Listed in Table V are the individual frequency assignments.

No information could be found in the literature on the infrared spectrum of dimethyl amine to check the 750 cm^{-1} frequency. A frequency of 794 cm^{-1} is reported in the Raman spectrum,[11] but the difference between these values is beyond experimental error.

INTERPRETATION OF RESULTS

It is reasonable to assume that the observed transitions of the alkyl amines are analogous to those of ammonia. The first transition, a $2p_z-3s$, is progressively

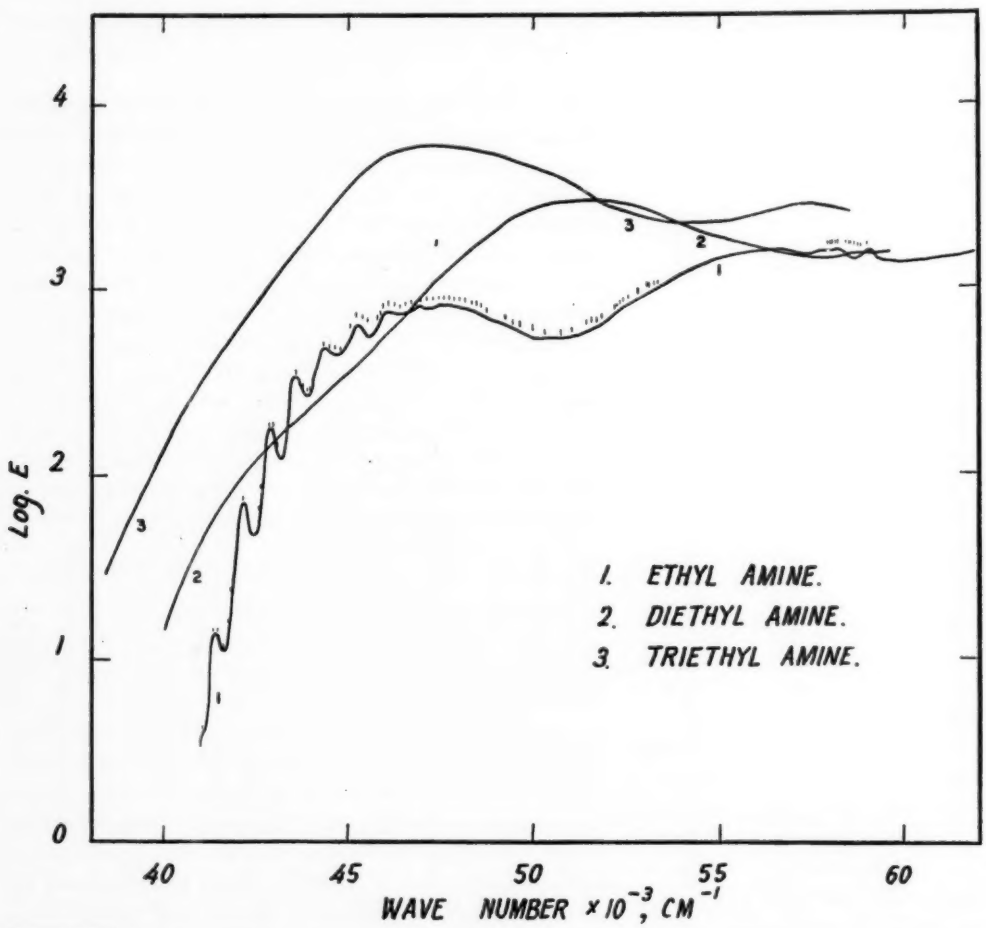

FIG. 4. Log epsilon plot of the ethyl amine series of absorption curves. All of the ethyl amine vibrational structure has been schematically represented by vertical lines drawn above the band positions.

[9] E. Frolich, Calco Division, American Cyanamid Corporation, private communication; J. T. Edsall, J. Chem. Phys. 5, 225 (1937); K. W. F. Kohlrausch, *Der Smekal-Raman Effekt* (J. Springer, Berlin, 1931), p. 312.
[10] H. J. Emeleus and L. J. Jolley, J. Chem. Soc. 1612 (1935); S. Vencov, Bull. sect. sci. acad. Roumaine 26, 89 (1943).
[11] J. S. Kirby-Smith and L. G. Bonner, Phys. Rev. 55, 1113 (1939).

TABLE IV. Ethyl amine—vibrational analysis.

Wave no. Exptl		Wave no. Calc	ν_1'' 620	ν_1' 740	ν_2'' 1500	ν_2' 1620
40 760	vw[a]	40 750	1	0	1	0
41 070	vw	41 010	3	0	0	0
41 370	w	41 370	0	0	1	0
41 490	w	41 490	1	1	1	0
41 640	vw	41 630	2	0	0	0
41 770	vw	41 750	3	1	0	0
41 860	vw					
42 180	w	42 110	0	1	1	0
42 265	w	42 250	1	0	0	0
		42 230	1	2	1	0
42 610	vw					
42 660	vw					
42 870	s	42 870	0	0	0	0
		42 850	0	2	1	0
42 995	m	42 990	0	0	1	1
		42 990	1	1	0	0
43 100	w	43 110	1	1	1	1
		43 110	2	2	0	0
43 610	s	43 610	0	1	0	0
		43 590	0	3	1	0
43 785	m	43 730	1	2	0	0
43 920	w	43 870	1	0	0	1
43 970	vw	43 990	2	1	0	1
44 345	s	44 330	0	4	1	0
		44 350	0	2	0	0
44 510	s	44 490	0	0	0	1
		44 470	1	3	0	0
		44 470	0	2	1	1
44 660	m	44 610	0	0	1	2
		44 610	1	1	0	1
44 810	w					
45 070	m	45 070	0	5	1	0
		45 090	0	3	0	0
45 220	s	45 230	0	1	0	1
		41 210	1	4	0	0
		45 210	0	3	1	1
45 380	s	45 350	1	2	0	1
45 530	m					
45 805	m	45 810	0	6	1	0
		45 830	0	4	0	0
45 945	s	45 970	0	2	0	1
		45 950	0	5	0	1
		45 950	0	4	1	1
46 120	s	46 090	1	3	0	1
46 270	s	46 230	1	1	0	2
46 410	w					
46 575	m	46 550	0	7	1	0
		46 570	0	5	0	0
46 720	s	46 690	0	5	1	1
		46 710	0	3	0	1
		46 690	1	6	0	0
46 840	s	46 830	1	4	0	1
		46 850	0	1	0	2
46 990	s	46 970	1	2	0	2
		46 970	0	1	1	3
47 160	w	47 110	1	0	0	3
47 320	m	47 310	0	6	0	0
47 440	s	47 450	0	4	0	1
		47 430	1	7	0	0
		47 430	0	6	1	1
47 590	s	47 570	1	5	0	1
		47 570	0	2	0	2
47 730	s	47 730	0	0	0	3
		47 700	1	3	0	2
47 870	m	47 850	1	1	0	3
48 030	w	48 050	0	7	0	0
48 165	w	48 170	0	7	1	1
48 350	m	48 330	0	3	0	2
48 485	s	48 450	1	4	0	2
		48 490	0	1	0	3
48 600	m	48 590	1	2	0	3
48 770	w	48 790	0	8	0	0
48 290						
49 445						
49 655						
49 990						
50 305						
50 760						
51 050						
51 440						
51 580						
51 720						
etc.						

[a] Relative vibrations are indicated as: strong, s; medium, m; weak, w; and very weak, vw.

displaced to smaller wave numbers by alkyl substitution as measured by the beginning of absorption; the first alkyl group giving a displacement of about 5000 cm^{-1} and each additional group a displacement of about 1000 cm^{-1}. Methyl and ethyl groups seem to be about equally effective. The low oscillator strength of the dimethyl and diethyl amine seems to be an anomaly. However, the first band of dipropyl amine,[12] of piperidine,[13] and pyrrolidine[15] is very similar in both position and intensity and seems to be characteristic of secondary amines. It seems possible that these low oscillator strengths may be related to the high base strength of these compounds: The greater the probability that the pair of electrons may enter into a chemical reaction, the lower the probability that one of the electrons be excited to a higher energy level.

The second transition is more sensitive to alkyl substitution. The displacement to smaller wave numbers is 18 500, 5000, and 2250 cm^{-1} for 1, 2, and 3 methyl groups, respectively, and 19 500, 5500, and 4250 cm^{-1} for the corresponding ethyl groups. Throughout both series there is a marked increase in oscillator strength, the increase being most pronounced in the ethyl series. These characteristics strongly indicate that this transition is closely related to the alkyl group and might be either a charge transfer of an unshared electron or a transition involving a CN bonding electron. The latter interpretation would support Thompson and Duncan's suggestion that the second transition in ammonia might involve a bonding electron. In an attempt to distinguish between these two interpretations, the effect of protons on this band was investigated. A few exploratory plates made with the quartz spectrograph indicated that although the spectrum of an aqueous solution of trimethyl amine exhibited two regions of absorption (one of low intensity beginning about 44 000 cm^{-1} and another more intense region beginning about

[12] Preliminary determination in this laboratory.
[13] L. W. Pickett, *et al.*, final Report, ONR, Contract N8onr-74100, Project NR-055-160, 37 (1950).

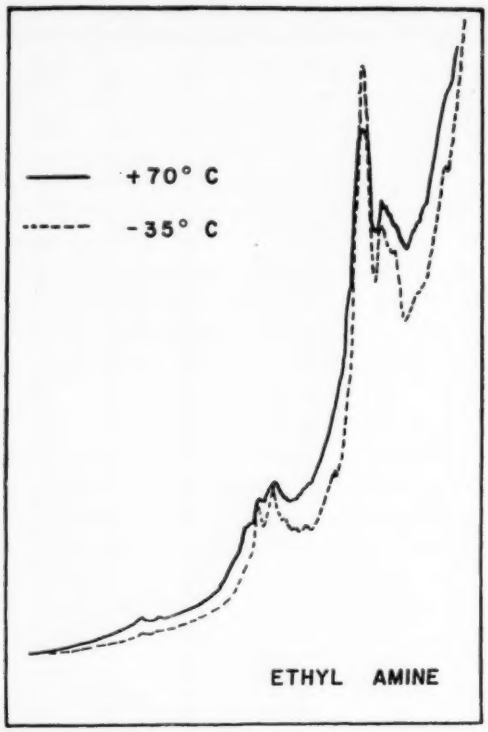

FIG. 5. Two superimposed microphotometer tracings showing the temperature dependence of the intensity of the band at 42 870 cm^{-1}. The exposure was made on a nonflowing sample using the Hilger Quartz Spectrograph.

46 500 cm^{-1}) an acid solution of the same concentration is practically transparent to the limit of the instrument (48 000 cm^{-1}). These results strongly indicate that both transitions involve an unshared electron. However, the evidence is not conclusive since it is possible that the presence of a proton might stabilize the CN bonding electrons to such a degree that the transition would not occur below 48 000 cm^{-1}.

Although the third transition is incompletely covered by these measurements, some characteristics seem to be apparent, and the effect of alkyl substitution does not

TABLE V. Vibrational analysis—dimethyl amine.

Wave no. Exptl		Wave no. Calc	ν_1'' (750)	ν_1' (605)
45 130	m[a]	45 120	1	0
45 290	w			
45 720	m	45 725	1	1
45 870	s	45 870	0	0
46 300	m	46 330	1	2
46 480	s	46 475	0	1
46 590	w			
46 920	m	46 935	1	3
47 080	s	47 080	0	2
47 200	w			
47 550	m	47 540	1	4
47 680	s	47 685	0	3
48 160	m	48 145	1	5
48 290	s	48 290	0	4
48 780	m	48 750	1	6
48 890	s	48 895	0	5
49 420				
49 560		49 500	0	6
50 030				
50 610				
51 120				
51 700				

[a] See reference a, Table IV.

parallel exactly that on either the first or the second transition. Again, alkyl substitution gives progressive displacement to smaller wave numbers. The magnitude of the displacement is greater than that of the first band but less than that of the second and is greater for ethyl substitution than for methyl substitution. The intensity of the transition seems to be greater than that of the first and less than that of the second. Oscillator strengths may have little meaning here since the shape of the curves indicate that this transition may be superimposed upon a broad continuum. Saturated hydrocarbons begin to absorb in this region and other transitions might be expected. There is sufficient pattern indicated by even these incomplete data to suggest that the same transition is involved in all the amines studied. The very sharp bands occurring at 57 500–58 500 cm^{-1} in ethyl amine strongly suggest a Rydberg transition and lends support to the analogy with the $2p_z-4s$ assignment in ammonia.

On the Ultraviolet Absorption Spectra of Uninegative Ions*

HAROLD L. FRIEDMAN
Department of Chemistry, University of Southern California, Los Angeles, California
(Received August 11, 1952)

New spectral data are reported for NO_2^-, ClO_2^-, and ClO^- in aqueous solution.

The theory of the electron transfer spectra of aqueous halide ions is extended to uninegative polyatomic ions by allowing for the greater excitation energy of the polyatomic radicals produced in the act of absorption, as compared with the excitation energy of the atoms produced from halide ions. This additional excitation energy arises from the operation of the Franck-Condon principle in determining the internuclear distances in the radical. Tri-iodide ion is the only one of the uninegative ions for which the required data are available and for which these data are not consistent with the assignment of the intense ultraviolet bands to transitions involving transfer of an electron to the solvent.

It is found that the low intensity absorption bands of NO_2^- and ClO_2^- coincide with the bands predicted by R. S. Mulliken for triatomic oxide molecules (AO_2), with the same numbers of valence electrons.

AQUEOUS solutions of many ions are characterized by very intense absorption of light in the ultraviolet region. The evidence for the assignment of these absorption bands to transitions involving the change in location of a single electron from one atom or group of atoms to another has been reviewed by E. Rabinowitch.[1] In the case of uninegative ions, it is possible to relate the energy of this electron transfer transition to the hydration energy and ionization potential of the gaseous ion in a simple way, as pointed out by Franck and Scheibe,[2] Franck and Haber,[3] Farkas and Farkas,[4] and Farkas and Klein.[5]

The regularities observed by these authors suggested that data on electron transfer spectra of this kind might be employed to estimate the solvation energy of the electron in water and also to estimate solvation energies in other solvents. On this account it seemed worth while to obtain spectral data for the few other uninegative ions for which the thermal data required in the calculations were available.

EXPERIMENTAL

All spectral data were obtained with a Beckman Model DU quartz spectrophotometer, calibrated with the Hg 2537 line. The region below 2000A seemed of interest in several cases, and after a number of unsuccessful attempts to record absorption spectra photographically in this region with a small Hilger quartz spectrograph, the Beckman instrument was adapted for use in this region by taking the following steps: (a) The Littrow mirror was moved in until the Hg 2537 line fell at 661 on the Beckman scale. (b) An RCA 1P21 photomultiplier tube, sensitized with oil and connected to a sensitive galvanometer was substituted for the Beckman photocell. (c) The instrument was flushed with nitrogen during use to remove oxygen which absorbs in this region. (d) The wavelength scale was calibrated in this region using the Hg 1849 line and the NO_2^- and I^- absorption maxima. (e) A filter of 1 cm thickness of $0.002M$ KBr solution was employed to allow a correction for the considerable amount of stray light of wavelength longer than 2100A. The intensity of the light passing this filter at each wavelength was subtracted from the I and I_0 readings. Extinction coefficients ϵ reported in this paper are defined by the equation $\log_{10}(I_0/I)=\epsilon cd$; c in moles/l and d in cm.

Hypochlorite ion spectra were obtained both from commercial reagent grade sodium hypochlorite, suitably diluted, and from specially prepared and distilled hypochlorous acid made basic with sodium hydroxide solution. Only a single solution of pure HOCl, adjusted to a pH of 10, was examined below 2000A, but at longer wavelengths Beers' law was obeyed within a few percent in the concentration range investigated, $0.0002M$ to $0.004M$; and no differences were observed between hypochlorite solutions from the two sources. The absorption maximum at 2900A has been previously reported by Schafer.[6]

As a further check upon the identity of the absorbing species the 2910A maximum was investigated as a function of pH, giving a pK of about 7.5 for the acid ionization of HOCl, in satisfactory agreement with the accepted value of 7.5.[7] The spectrum of HOCl (aq) was obtained in the course of the study of the effect of changing acidity on the OCl^- spectrum, which showed that the hump at 2900A is not due to OCl^- in equilibrium with HOCl. This spectrum is in quantitative agreement with that reported for HOCl (aq) by Fergusson, Slotin, and Style.[8]

The chlorite ion spectrum was obtained both from solutions made directly from Mathieson reagent sodium chlorite, and from purified potassium chlorite made by

* It is a pleasure to acknowledge the financial support of this research by the U. S. Atomic Energy Commission.

[1] E. Rabinowitch, Revs. Modern Phys. **14**, 112 (1942).
[2] J. Franck and G. Scheibe, Z. physik. Chem. **139A**, 22 (1928).
[3] J. Franck and F. Haber, Sitzber. preus. Akad. Wiss., Physik-math. Kl. **1931**, 250.
[4] A. Farkas and L. Farkas, Trans. Faraday Soc. **34**, 1113 (1938).
[5] L. Farkas and F. Klein, J. Chem. Phys. **16**, 886 (1948).
[6] K. Schafer, Z. physik. Chem. **93**, 312 (1919).
[7] W. M. Latimer, *Oxidation Potentials* (Prentice-Hall, Inc., New York, 1952), second edition.
[8] Fergusson, Slotin, and Style, Trans. Faraday Soc. **32**, 956 (1936).

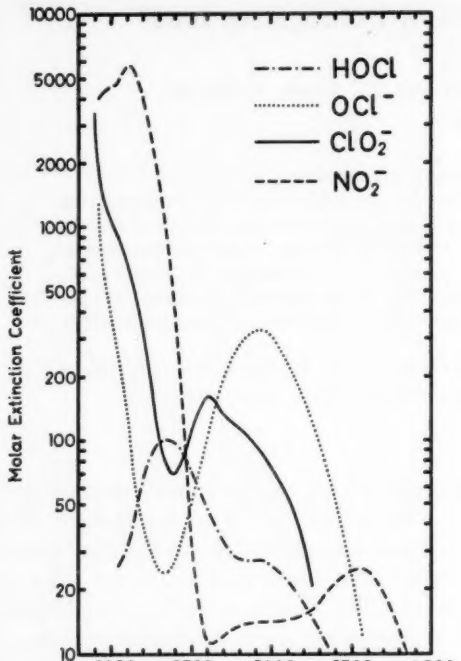

FIG. 1. Ultraviolet absorption spectra.

metathesizing freshly precipitated silver chlorite with potassium chloride. The observations from 1900 to 2000A were made with a solution of the purified chlorite. At longer wavelengths Beers' law was found to be obeyed from $0.0002M$ to $0.004M$, and no differences were observed between solutions of different origin. Added OH^- had no effect upon the absorption at 2900A, indicating that the asymmetry of the 2610A peak is not due to OCl^- ion impurity. The solutions were not stable when acidified, but a search for peaks due to $HClO_2$ (aq) indicated that this species had a considerable absorption in the region from 3000A to 2100A [$50<\epsilon<800$], but no absorption maxima in this region. A similar conclusion regarding $HClO_2$ was reached by Schafer,[6] but he reported that ClO_2^- does not absorb in the region 2300–4000A.

The nitrite ion spectrum was obtained from solutions made by dissolving reagent grade KNO_2. The results in the range 2500–4000A agree with those of Körtum.[9] The 2110A peak had the same extinction coefficient in solutions $0.00007M$ and $0.006M$ in nitrite ion.

The observations of Farkas and Klein[5] on the spectrum of chlorate ion were checked using solutions made from reagent grade $NaClO_3$. Agreement was satisfactory from 2300A to 2100A, but at shorter wavelengths higher extinction coefficients were observed in the present work than reported by Farkas and Klein. They report $\epsilon_{2000}=65$; according to the present work $\epsilon_{2000}=100$.

The cyanide ion spectrum was investigated using freshly prepared solutions of reagent grade KCN. It was found that the spectrum changed with time in a manner indicating that either cyanide ion or an impurity in the solution was reacting to give a species which absorbs more strongly than CN^-, especially at wavelengths longer than 2100A. This complication was not investigated in more detail, but it was concluded from the observations that for CN^-, $\epsilon_{2000A}<90$, and the absorption falls off sharply at longer wavelengths.

[9] G. Körtum, Z. physik. Chem. **B43**, 418 (1939).

RESULTS AND CALCULATIONS

The very intense, short wavelength absorption bands characteristic of the spectra of negative ions such as those in Fig. 1 will be discussed in terms of the energy diagram of Fig. 2. The process of absorption of a light quantum in one of these bands by a negative ion is here assumed to be accompanied by the transfer of an electron from the ion (X^-) to the solvent. The hypothetical process in which the products of such a transition, designated as X^* and e^{-*}, pass to the species X(aq) and e^-(aq), is assigned the enthalpy change $-\Delta H^*$. It will be assumed that ΔH^* is positive; for the rest, the formal treatment employed here requires no detailed knowledge of the state, X^*+e^{-*}. X(aq) is defined as the radical in equilibrium with respect to solvation by the water, and with respect to internal configuration if X is not monatomic. e^-(aq) is defined as the electron in equilibrium with respect to solvation by the water, it being assumed that such an equilibrium is possible because the reaction $e^-+H_2O=H+OH^-$ is slow compared with the rate of orientation of water molecules about an ion. It will be shown later that this assumption is not necessary to the conclusions to be drawn, but it is made here to make the picture as definite as possible.

The rest of the steps in the cycle of Fig. 2 are self-explanatory except for the symbols for the energy quantities. ΔH_f^0 has its usual meaning, the standard states being those defined by the National Bureau of Standards tables for 25°.[10] $\Delta H_s(Y)$, the solvation energy of Y, is defined as ΔH^0 for the process, $Y(aq)\rightarrow Y(g)$.

Hydrogen is carried around the cycle of Fig. 2 in appropriate form in order to demonstrate that the

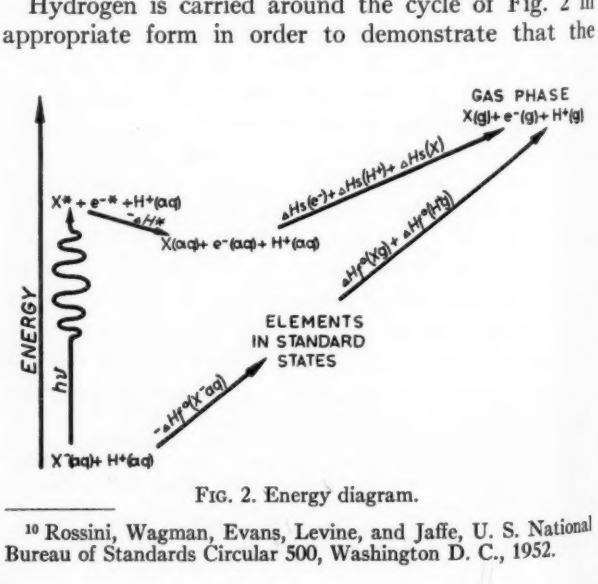

FIG. 2. Energy diagram.

[10] Rossini, Wagman, Evans, Levine, and Jaffe, U. S. National Bureau of Standards Circular 500, Washington D. C., 1952.

conclusions to be drawn are quantitatively independent of the controversial division of the solvation energies of pairs of ions into absolute values for positive and negative ions separately. Another apparent difference between the cycle of Fig. 2 and the cycles employed by earlier workers may be resolved by noting that

$$-\Delta H_f^0(X^-, \text{aq})+\Delta H_f^0(X, \text{g})+\Delta H_f^0(H^+, \text{g}) = \Delta H_s(X^-)+E(X)+\Delta H_s(H^+),$$

where $E(X)$ is the electron affinity of X in the gas phase. The separate terms in the right-hand member of this equality are in no case known as well as their sum, and therefore, it seems more direct to tabulate the thermodynamic data of the left-hand member, which may be found in standard tabulations.

One other question which must be considered before proceeding to a discussion of the data is the choice of the wavelength characteristic of the electron transfer transition. The intense absorption band of nitrite ion around 2110A (Fig. 1) has the characteristic appearance of an electron transfer band and differs from the halide ion bands only in having a series of weak bands on the long wavelength side of the main band. If an electron transfer band has a clearly defined onset on the low energy side, the energy of this onset provides an experimental threshold energy for the transition, representing the transition to products with the smallest possible excitation energy, or in the present nomenclature, with the smallest possible ΔH^*. However, even for the halide ions the experimental data themselves do not clearly define the onset, and Farkas and Farkas[4] rather arbitrarily defined the wavelength at which $\epsilon=1$ as the onset of the band and chose this as the characteristic wavelength. Another possible choice of a characteristic wavelength is the wavelength of the band maximum, corresponding, according to the Franck-Condon principle, to a transition to an upper state in which the internuclear distances are the same as the equilibrium distances in the ground state. Although ΔH^* for such a transition may be relatively large, this choice is made here because it more readily allows the quantitative extension of the electron-transfer concept to appropriate spectra of polyatomic ions. The primary reason is that the wavelength of the band maximum ($\epsilon\sim 10\,000$) is less likely to be shifted by neighboring weak absorption bands of the same species or by absorption by impurities in the solution, than the wavelength of the onset of the band, defined as above. It is noteworthy that in the absence of such complications, the choice is not important. For the ions Cl^-, Br^-, I^-, OH^-, and SH^- the average difference in energy between the onset of the band and the band maximum is 22 kcal, and the maximum deviation from this value is 2 kcal. Therefore, in this series, making one choice or the other only gives rise to a 22 kcal difference in ΔH^* and does not obscure any regularities.[2]

Table I presents the quantities for a cycle according to Fig. 2 for each of the ions for which the required thermal data are available. The variation in the term in the last column of the table must be ascribed entirely to variation in ΔH^*, the negative of the enthalpy change of the reaction

$$X^*+e^{-*}\rightarrow X(\text{aq})+e^-(\text{aq}).$$

For the discussion we may divide ΔH^* into two parts: ΔH_a^* arising from rearrangement of the water molecules about X and about e^-; and ΔH_b^* arising from change in the internuclear distances within the X radical.

For monatomic ions, $\Delta H_b^*=0$ and the constancy of ΔH^* in the series Cl^-, Br^-, I^- indicates that ΔH_a^* is not sensitive to the solvation energy of the original ion. Assuming that this constancy of ΔH_a^* extends to polyatomic ions, we ascribe the considerable spread in ΔH^* for polyatomic ions to ΔH_b^*. It is gratifying that this term is never negative, showing that the interpretation of these absorption bands of polyatomic ions as electron transfer bands is consistent, although complicated by the appearance of the term ΔH_b^*. It is noteworthy that the present set of data only requires ΔH_b^* to be larger than 10 kcal in the case of the ions ClO_2^- and NO_2^-, where it is possible for X^- and X to have different bond angles as well as bond lengths.

The halide ion spectra indicate that 276 kcal is a lower limit for $\Delta H_s(e^-)+\Delta H_s(H^+)$. Roughly the same result may be obtained from the cycle employed by Farkas and Klein,[5] noting that the term they designate as E_{H_2O} is the energy of solvation of an electron in water to the activated state produced in the phototransition, that their cycle employed the energy of band origin rather than that of band maximum, and that they assumed a value of 277 kcal for the hydration energy

TABLE I. Energy quantities of Fig. 2 for various anions.[a]

Ion X^-	λ_{max}[f] A	$h\nu_{max}$	$-\Delta H_f^0(X_{aq}^-)$	$\Delta H_f^0(X_g)$	$\Delta H_s(X)$[b]	$\Delta H_s(H^+)+\Delta H_s(e^-)-\Delta H^*$
Cl^-	1810	158	40.0	29.0	2.7	275
Br^-	2000	143	28.9	26.7	3.6	276
I^-	2260	126	13.4	25.5	4.5	276
OH^-	1870	153	55.0	10.1	12	267
SH^-	2270	126	4.2	35±4[e,d]	6	274±4
OCl^-	<1900	>150	25.9[g]	25[d]	3	<265
CN^-	<1900	>150	−36.1	94.3±6[e]	4	<277
ClO_2^-	<1900	>150	17.2[b]	24.7	7	<252
NO_2^-	2110	136	25.4	8.1	7	258
ClO_3^-	<1900	>150	23.5	37.0	7	<271
NO_3^-	1936	148	49.4	13	7	275

[a] All thermodynamic data from the N.B.S. Tables, reference 10, unless otherwise indicated. All energies in kcal/mole.
[b] B. Fontana and W. Latimer, J. Am. Chem. Soc. **69**, 2598 (1947).
[c] H. L. Friedman, J. Chem. Phys. **20**, 1046 (1952).
[d] G. Porter, Disc. Faraday Soc. **9**, 60 (1950).
[e] Brewer, Templeton, and Jenkins, J. Am. Chem. Soc. **73**, 1462 (1951).
[f] Spectral data from this paper or from Rabinowitch, reference 1.
[g] Bichowsky and Rossini, *Thermochemistry of Chemical Substances* (Reinhold Publishing Corporation, New York, 1936).
[h] Hydration energies of radicals estimated as follows, using hydration energies of gases summarized by H. S. Frank, J. Chem. Phys. **13**, 518 (1945):
Cl, Br, I: like adjacent noble gases. (Note lack of effect of unpaired electron in series N_2, NO, O_2).
OH: like HF in 1*M* aqueous HF.
ClO: like NO.
CN: like CO.
ClO_2: N.B.S. Tables.
SH, ClO_3, NO_3: guessed.

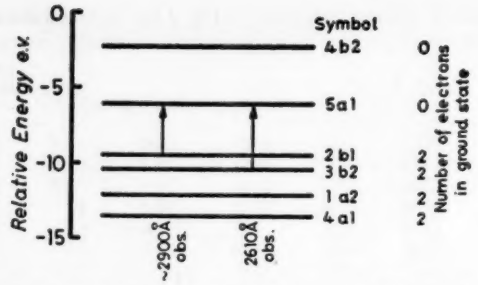

FIG. 3. Molecular orbitals for AO_2 with 20 valence electrons. Orbitals and approximate energies from Mulliken, reference 12, Fig. 6. Six MO's of lower energy are not shown. Allowed transitions at wavelengths longer than 2000A are represented by arrows.

of H^+. A third cycle which may be shown to yield the same result is

$$X^-(aq)+H^+(aq)\rightarrow X^*+e^{-*}+H^+(aq)\rightarrow X(aq)+H(aq)\rightarrow X(g)+H(g)\rightarrow (\text{elements in standard states})\rightarrow X^-(aq)+H^+(aq).$$

Calculation for the halide ions yields $\Delta H'=-40$ kcal for the second step. Employing the additional cycle, $H^+(g)+e^-(g)\rightarrow H(g)\rightarrow H(aq)\rightarrow H^+(aq)+e^-(aq)\rightarrow H^+(g)+e^-(g)$, and taking $-\Delta H'$ as an upper limit for the ΔH of the third reaction in this cycle, we can calculate the lower limit for ΔH of the fourth reaction, again 276 kcal. Assuming that $-\Delta H'$ is the ΔH of ionization of H(aq) in this case is perfectly analogous to the assumption that $\Delta H^*=0$ in reaching the limit for $\Delta H_s(e^-)+\Delta H_s(H^+)$ in the original cycle. It is proposed that the advantage of the cycle of Fig. 2 over the others lies in the fact that the uncertain energy quantities arising from the operation of the Franck-Condon principle are clearly separated from the other more definite energy terms.

If the onset of the electron transfer band, as defined by Farkas and Farkas corresponds to the relatively improbable transition from X^- in its ground state to $X(aq)+e^-(aq)$ with all nuclei in this final state at their equilibrium distances, then the difference in energy between the onset of the band and the band maximum, 20 kcal, would equal ΔH^*. In this case, we would have $\Delta H_s(H^+)+\Delta H_s(e^-)=296$ kcal. For iodide, bromide, and chloride ions, the corresponding sums are, respectively, 330.3, 340.7, and 348.8 kcal. Evidently, a spherical ion with as low a solvation energy as the electron should have according to this calculation, would have to have a very large radius (about 3.5A). Unfortunately, there does not seem to be any better way to estimate ΔH^* at the present time.

Although tri-iodide ion has very strong ($\epsilon_{max}>10\,000$) absorption maxima at 3530A and 2875A,[11] these do not seem to be analagous in origin to the bands discussed above. This conclusion may be reached by assuming that the tri-iodide ion bands do arise from transitions in which an electron is transferred from the ion to the solvent. Then, employing Fig. 2, and estimating $\Delta H_s(I_3)=10$ kcal and $\Delta H_b^*=0$, we calculate $\Delta H_f^0(I_3, g)=5$ kcal for the 2900A peak and -14 kcal for the 3500A peak. Even the more positive of these values requires $S_{293}^0(I_3, g)<32$ eu for $\Delta F>0$ for the reaction $3I_2(g)\rightarrow 2I_3(g)$ at room temperature, and therefore the assumption tested is not consistent with the observation that iodine gas is diatomic at room temperature. Assumption of $\Delta H_b^*>0$ would make this inconsistency worse. Another possibility is that these bands correspond essentially to the reaction $I_3^-(aq)\rightarrow I_2^-(aq)+I(aq)$. The separation of the two peaks (18.6 kcal) is roughly the difference in energy (21.1 kcal) of the two lowest electronic states of iodine atom.

[11] A. D. Autrey and R. E. Connick, J. Am. Chem. Soc. **73**, 1842 (1951).

The Low Intensity Maxima of NO_2^- and ClO_2^-

Mulliken[12] has succeeded in correlating the electronic spectra of gaseous triatomic oxide (AO_2) molecules in a relatively simple way by employing a single variable, the total number of valence electrons in the molecule. These fill the available molecular orbitals in order of stability and play a primary role in determining the shape, stability, and spectrum of the molecule, indicating that the orbitals are relatively independent of the nature of the A atom.

It is interesting to note that the aqueous ions NO_2^- and ClO_2^- fit Mulliken's correlation very well, a fact which if not due to chance indicates that there is no strong solvent effect on these spectra and that the spacing of the energies of the orbitals of an AO_2^- ion are relatively the same as in the neutral molecules with the same number of electrons, although of course the ionization potential will be shifted.

SO_2, like NO_2^-, has 18 valence electrons. SO_2 has weak absorption bands with maxima at 3700A and at 2940A and a strong band at just below 2000A. $NO_2^-(aq)$ has weak bands at 3500A and at 2900A, a remarkable correspondence. A calculation according to the cycle of Fig. 2, employing the lower limit for $\Delta H_s(H^+)+\Delta H_s(e^-)$ established above, indicates that the ionization potential of nitrite ion in water solution is only 118 kcal, so that any bands corresponding to the 2000A SO_2 band would be above the ionization limit. For this reason it seems likely that the 2110 band is an electron transfer band, as assumed above.

There is no stable AO_2 molecule with twenty valence electrons with which to compare ClO_2^-, but Fig. 6 of Mulliken's paper[12] provides a prediction of the nature and energy of the molecular orbitals for such a molecule. Figure 3 illustrates the predicted orbitals and the observed transitions. The $1a_2\rightarrow 5a_1$ and $3b_2\rightarrow 2b_1$ transitions are forbidden and the other possible transitions lie outside of the spectral range accessible here.

[12] R. S. Mulliken, Revs. Modern Phys. **14**, 204 (1942).

F Bands in Some Mixed Crystals of the Alkali Halides

ROBERT J. GNAEDINGER, JR.*†
Department of Chemistry, University of Chicago, Chicago 37, Illinois
(Received November 10, 1952)

X-ray induced *F* bands in melt-grown mixed crystals of KCl and RbCl were studied. Though no resolution of "component" *F* bands was obtained at liquid nitrogen temperature, the behavior of the *F* band parameters as a function of concentration of RbCl in KCl and as a function of temperature is shown to be explainable by postulating the existence of a set of "component" *F* bands, each arising from an *F* center with a given composition of positive ions immediately surrounding it. Some studies of other mixed crystals are also mentioned.

I. INTRODUCTION

AN *F* center in an alkali halide crystal is, at present, conceived to be an electron that is trapped at a vacant negative ion lattice site. The most obvious characteristic of *F* centers is that they absorb light in or very near the visible spectrum, thus causing the crystal in which they occur to appear colored when observed in ordinary light. In view of this characteristic it is readily evident that these centers of absorption are not present in the normally colorless alkali halides. They can be produced in normal crystals by bombardment with high energy radiation, by heating the crystals below their melting points in the vapor of the alkali metal component of the salt, and by electrolysis of the crystals at high temperatures. X-rays, cathode rays, pile radiation, and irradiation in the long wave tail of the characteristic ultraviolet absorption of the crystal have all been used to color these crystals.

Though numerous investigations have been made of these *F* centers in more or less pure alkali halides,[1] no studies of them in mixed salt crystals have been reported. The pursuance of such a study offered the added inducement of possibly finding indications of several types of *F* centers in contrast to the one type postulated for pure crystals. Since at normal pressures most of the alkali halides have the NaCl type crystal structure, an *F* center in these lattices consists, diagrammatically, of an electron immediately surrounded by six positive ions at the apices of a regular octahedron. This molecule-like picture suggested that different "iso-structured" *F* centers could be induced in mixed crystals. For example, in a mixed crystal of RbCl and KCl, there could occur seven different combinations of K^+ and Rb^+ ions in the six positive ion positions about the trapped electron (i.e., $6K^+$, $5K^+-1Rb^+$, etc.). (Indeed, the structure "$4K^+-2Rb^+$ electron" should have two "stereoisomeric" forms, comparable in a sense to $[Co(NH_3)_4Cl_2]^+$, for example.) It would appear reasonable that each of these iso-structures should have a somewhat different *F* band (i.e., graph of absorption coefficient *versus* frequency of absorbed light), that is, the optical transition energy should at least in part depend upon the natures of the immediately surrounding ions. If the differences among these iso-structured *F* bands were large enough, then mixed crystal *F* bands might be expected to indicate their presence.

In this work certain postulates were made as to the nature and intensities of these iso-structured *F* bands by reasoning from the known characteristics of the *F* bands in pure crystals. These calculated "component" bands were then summed to give expected "composite," mixed crystal *F* bands, and these latter were compared with the experimentally determined mixed crystal bands. Attention was primarily centered on the KCl—RbCl mixtures because these salts are mutually soluble in all proportions in the solid phase at room temperature. In addition, the *F* bands of these pure salts are almost identical when plotted as reduced absorption coefficient *versus* reduced frequency (see Sec. IV).

Perhaps it should be noted here that the above molecule-like model is certainly a simplified one. Even in $MX-M'X$ mixtures (e.g., KCl—RbCl), it can be expected that the composition of the third nearest neighbor sphere will influence the energy levels of the *F* center, especially the excited levels. In $MX-MX'$ and $MX-M'X'$ mixtures even more varieties of *F* centers can occur. In all of these cases the energy levels of a center of a given type can also be expected to depend to some extent upon the gross composition of the mixed crystal.

II. EXPERIMENTAL PART

The salts used in this work were: RbCl No. 2, 99.9 percent, less than 0.1 percent K, trace Cs and RbCl No. 1, 98 percent, A. D. Mackay; KCl, A. R., Mallinckrodt; NaCl and NaBr, Reagent, Merck; KBr, cp, Bakers' Analyzed. A spectroscopic analysis of RbCl No. 2 revealed the presence of 0.07 percent KCl and traces of Na, Cs, Ca, and Fe. These chemicals were used without further purification. All crystals were prepared in air as follows: The desired salt or salt mixture was melted in a platinum crucible with an electric furnace. Crystallization was allowed to occur on a platinum wire that was slowly withdrawn from the melt surface. The resultant crystal was cooled to room temperature over a period of

* Present address: Department of Physics, University of Illinois, Urbana, Illinois.
† Atomic Energy Commission Predoctoral Fellow, 1950–1951.
[1] For reviews of this subject see: F. Seitz, Revs. Modern Phys. **18**, 384 (1946); R. W. Pohl, Proc. Phys. Soc. (London) **49** (extra part), 3 (1937); N. F. Mott and R. W. Gurney, *Electronic Processes in Ionic Crystals* (Oxford University Press, New York, 1940), Chapter IV.

two hours. This crystal was cleaved into platelets with the approximate dimensions, $1\times7\times10$ mm^3, which were then used for the F band measurements.

The compositions of the KCl—RbCl mixed crystals were determined by chemical analysis. This consisted of weighing a sample of the mixed crystal and then determining the amount of chloride present by titration with $AgNO_3$ solution using the absorption indicator, dichlorofluorescein. The average error in these measurements was less than one mole percent RbCl. Only the original melt compositions of the other mixtures (NaCl—NaBr, KCl—KBr, NaCl—KCl, and RbCl—KBr) were ascertained. These composition values are included in Tables II and V.

F centers were produced in the crystals by x-irradiations (10 to 20 min duration) with a Machlett type A-2 molybdenum target diffraction tube (50 kv, 20 ma) with beryllium windows. This produced optical densities of 0.5 to 0.9 at the F band maximum in the KCl—RbCl crystals. In all irradiations the crystals were approximately one centimeter away from the x-ray tube window. Both the x-irradiation and the transfer to the spectrophotometer were done without exposure of the crystals to room light. Examination of the crystals after the absorption measurements had been made revealed a fairly uniform color intensity over the portion of the crystal surface that was exposed to the monochromatic measuring beam. When viewed through an edge, there was color apparent throughout the thickness of the crystal, although the intensity was highest near the irradiated surface.

The absorption coefficients of the crystals were measured as a function of wavelength with a Beckman (model DU) photoelectric quartz spectrophotometer using a tungsten filament lamp as light source. Crystal mounts for both low temperature (liquid nitrogen coolant) and room temperature measurements were constructed to fit the cell holder of the Beckman that was ordinarily used for the one square centimeter cross-sectional liquid absorption cells. The low temperature mount was similar to that described by Casler, Pringsheim, and Yuster;[2] however, all x-irradiations were made at room temperature.

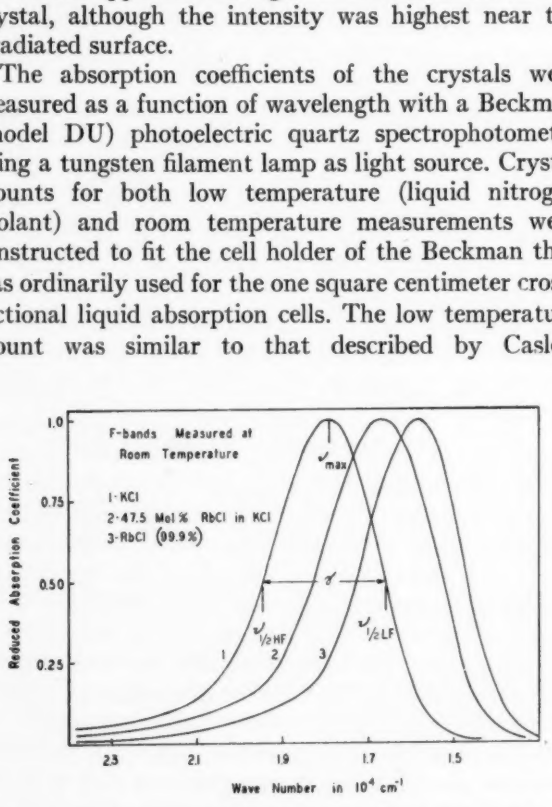

FIG. 1. X-ray induced F bands produced and measured at room temperature.

Measurements were made on each crystal sample every 50A over the whole range of appreciable absorption. Slit widths were those required for use of the instrument with maximum accuracy in transmission measurements. The maximum spectral band width was about 40A and occurred at 6250A.[3] The apparent optical density spectrum ($\log I_0/I$ *versus* frequency) of each colored crystal was corrected by subtracting a blank, apparent optical density spectrum that was determined on the same sample immediately preceding the x-irradiation. The corrected optical density spectrum obtained in this manner is proportional to the linear absorption coefficient (constant is crystal thickness).

Figure 1 shows the F bands for pure KCl, pure RbCl, and 47.5 mole percent RbCl in KCl as determined at room temperature. The ordinate in this plot is the reduced absorption coefficient, i.e., the absorption coefficient divided by the maximum absorption coefficient (occurring at ν_{max}). The parameter, $\gamma(=\nu_{\frac{1}{2}}HF-\nu_{\frac{1}{2}}LF)$, is the width of the band at one-half the maximum absorption.

The half-maximum width limits were rather easily determinable since they occurred on steep portions of the curve. The frequency at which the maximum occurred was somewhat more difficult to determine, especially at room temperature where the bands had comparatively broad peaks. The assumption was made that near the band peak the curve was symmetrical about the ν_{max}. The frequency values of points with the same absorption coefficients on either side of the peak were then determined from the graph and averaged. Two or three such averages were obtained at different distances below the peak. These usually agreed within $\pm0.002\cdot10^4$ cm^{-1} ($\pm$7A at 6000A).

At room temperature the F band was partially bleached by each exposure to the incident beam. (A rather smaller amount of bleaching was observed at liquid nitrogen temperatures.) To partially compensate for errors produced in F band parameters from this source, two absorption curves were generally determined at room temperature, one with successive points of measurement lying in the direction of increasing wavelength and the other in the direction of decreasing wavelength. (No backlash was found in the wavelength adjustment of the instrument.) The curves shown in Fig. 1 are averages of pairs of curves obtained in the above fashion.

Both the red-sensitive and the ultraviolet-sensitive phototubes (used above and below 6250A, respectively) were employed since most of the bands extended in part beyond 6250A. At high absorption, identical transmis-

[2] Casler, Pringsheim, and Yuster, J. Chem. Phys. 18, 887 (1950).

[3] Dispersion data from Bulletin 91-C, Beckman National Technical Laboratories, South Pasadena, California, February, 1947.

sion readings from both tubes at this wavelength were not usually obtained. (Percent transmission scale could be read to ±0.1 percent.) Presumably this divergence was due to the fact that the two phototubes had different responses to wavelengths predominating in the scattered radiation. The effect of this source of error was important only where *F* bands had maxima around 6250A (crystals with high RbCl content). Estimates, based on the results of Gibson and Balcom,[4] indicated that the observed values of ν_{max} and γ might be in error by $0.003 \cdot 10^4$ cm^{-1}. However, the use of values corrected for this error would only serve to accentuate the effects discussed in the next section.

The wavelength scale of the instrument (readable to ±5A in the region of 6000A) was calibrated with the Balmer lines of hydrogen. The maximum correction in this region was $+0.007 \cdot 10^4$ cm^{-1}.

In this work room temperature was 25±2°C. Corresponding to this 2°C uncertainty in temperature is an uncertainty of $0.0006 \cdot 10^4$ cm^{-1} in ν_{max} and one of $0.001 \cdot 10^4$ cm^{-1} in γ.[5] The temperatures of the crystals in the low temperature cell were not measured, but were undoubtedly somewhat higher than that of the liquid nitrogen coolant (−196°C). If it is assumed that each crystal, when in this cell, was at a certain temperature to ±10°C, then (again for the purpose of intercomparison of parameters) the corresponding uncertainty in ν_{max} would be $0.003 \cdot 10^4$ cm^{-1} and that in γ, $0.005 \cdot 10^4$ cm^{-1}.

Though the chemical analyses showed no evidence of extensive fractionation within the KCl−RbCl crystal growths, the presence within a given crystal platelet of a concentration gradient as large as 5 mole percent per centimeter would not appreciably affect the position of the maximum in relation to the analyzed composition and would affect the half-maximum width by less than $0.0003 \cdot 10^4$ cm^{-1}.

In determining the *F* band parameters from the observed absorption curves it was assumed that there was no appreciable absorption in this region arising from unknown induced color centers. The *R* bands were considered to be absent since the long wave sides of the absorption curves dropped off smoothly to zero. Likewise, at the low temperature there was no evidence that any *F'* centers were present. The small hump occurring on the short-wave side of the main band has been tentatively assigned to transitions of the *F* center into higher excited states (presumably unbound states). It can be seen that at low temperatures this band does not have a large slope at any point and is rather well displaced from the main band; thus, its effect on the true position of the *F* band maximum will be negligible. Since it is about the same height in all cases, its effect on the relative values of the half-maximum widths will be quite small. Its absolute effect might be sufficient to cause an apparent broadening of the *F* band of $0.005 \cdot 10^4$ cm^{-1}.

In several cases the blank absorptions were redetermined after complete bleaching of color with white light. (This was not always possible. Some specimens still showed a surface coloration after prolonged illumination. Why this was true of only some samples is not clear.) The blank absorption was found to have increased by about 3 percent of its pre-x-irradiation value. If this latter were the correct blank, the true γ would be about $0.001 \cdot 10^4$ cm^{-1} smaller than that determined by using the initial blank.

The length of the unit cell edges of the KCl−RbCl mixed crystals were determined using a G-E (XRD) x-ray diffraction unit with a molybdenum target tube ($K_{\alpha 1}$=0.70926A). A sample of each mixed crystal (except 21.5 mole percent RbCl) was ground together with an equal amount of pure KCl in an agate mortar. The relative positions of the reflection maxima (first order, $d_{100}=\frac{1}{2}$ unit cell edge) of the two crystalline powders were determined using the Brentano parafocusing, divergent beam technique. No attempt was made to correct for errors due to absorption, refraction, alignment, and inhomogeneities in the samples. Some of these were inherently compensated for in the method.

The pure KCl was assumed to have a unit cell edge length, *a*, of 6.292A[6] at 25°C. The edge lengths for the various mixtures are listed in Table I. They agree quite well with a linear relation between mole percent RbCl and lattice constant. Three measurements were made on each sample. The probable error in each of these measurements was about 0.002A. Only one sample from each mixture was measured. Graphical interpolation of these results yielded a value of 6.441A for the 50 mole percent mixture. This can be compared with two other results for the 50 mole percent RbCl in KCl found in the literature, namely, 6.431[7] and 6.445A.[8] These two values have been corrected for the difference between the grating and the Siegbahn scales of wavelength by multiplication of the given values by 1.002.[9] These same

TABLE I. Lattice constants of mixed crystals of KCl and RbCl at room temperature.

Mole percent RbCl	*a* in A
0	6.292
8.7	6.322
47.5	6.431
66.2	6.491
99.9	6.592

[4] K. S. Gibson and M. M. Balcom, J. Opt. Soc. Am. **37**, 593 (1947).

[5] Estimated from pure crystal data of E. Mollwo, Z. Physik **85**, 56 (1933).

[6] Calculated from the density measurements of D. A. Hutchison, Phys. Rev. **66**, 144 (1944) using the 1949 International Atomic Weights for K and Cl and the value of Avogadro's number given in reference 9.

[7] E. B. Thomas and L. J. Wood, J. Am. Chem. Soc. **57**, 822 (1935).

[8] Havighurst, Mack, and Blake, J. Am. Chem. Soc. **47**, 29 (1925).

[9] J. W. M. DuMond and E. R. Cohen, Revs. Modern Phys. **20**, 82 (1948).

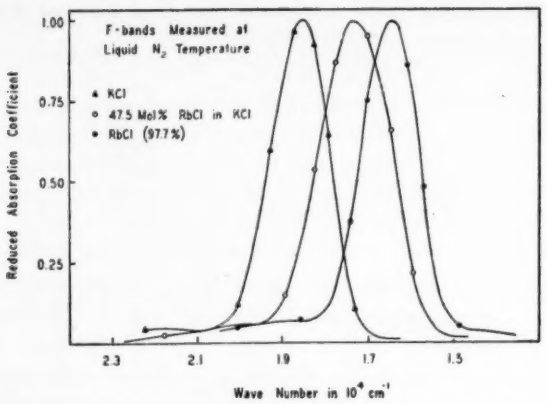

FIG. 2. X-ray induced F bands produced at room temperature and measured at liquid nitrogen temperature.

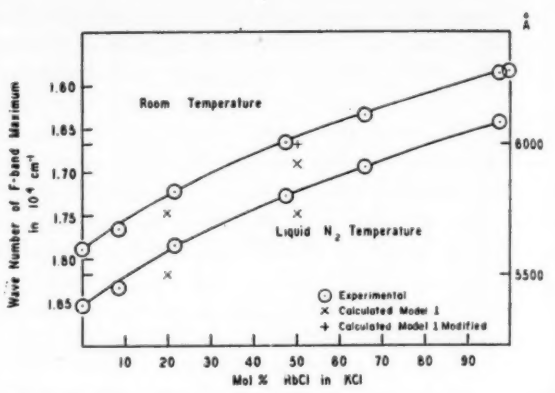

FIG. 3. Position of F band maximum *versus* mole percent RbCl in KCl. Ordinate diameter of experimental-result circles is $0.015 \cdot 10^4$ cm^{-1}.

sources give corrected values of 6.293A for a (KCl) and 6.583 and 6.584A for a (RbCl), respectively.

X-ray investigation of the KCl—RbCl mixtures and of the NaCl—NaBr mixtures also showed that if a second phase were present, it amounted to less than 10 percent of the major phase.

III. RESULTS

Figures 1 and 2 illustrate typical F bands obtained from pure KCl, pure RbCl and 47.5 mole percent RbCl in KCl. Compiled in Table II are the observed F band parameters. The agreement of the results at a given composition and temperature (as indicated by the average errors) was characteristic of all regions of the band. Table III contains F band parameters of pure KCl and RbCl as obtained by Mollwo and by the author. The agreement between the room temperature values of γ is good. The intercomparison of the low temperature results is limited by uncertainties in the temperatures of measurement.[10]

TABLE II. Parameters of F bands in KCl—RbCl mixed crystals.

Crystal	Mole percent RbCl	ν_{max}	Av error ν_{max}	$\nu_{\frac{1}{2}}HF$	$\nu_{\frac{1}{2}}LF$	γ	Av error γ	γ/ν_{max}
				10^4 cm^{-1}				
(A) Room temperature								
KCl	0	1.789	0.000	1.949	1.658	0.291	0.001	0.163
KCl—RbCl No. 1	8.7	1.766	0.001	1.929	1.629	0.300	0.000	0.170
KCl—RbCl No. 3	21.5	1.723	0.001	1.889	1.584	0.305	0.000	0.177
KCl—RbCl No. 2	47.5	1.666	0.001	1.831	1.525	0.306	0.002	0.184
KCl—RbCl No. 4	66.2	1.634	0.002	1.793	1.500	0.293	0.000	0.179
RbCl No. 1	97.7	1.586	0.002	1.736	1.464	0.272	0.004	0.172
RbCl No. 2	99.9	1.583	0.001	1.731	1.468	0.263	0.001	0.166
(B) Liquid nitrogen temperature								
KCl	0	1.854	0.001	1.946	1.776	0.170	0.007	0.092
KCl—RbCl No. 1	8.7	1.834	···	1.929	1.750	0.179	···	0.098
KCl—RbCl No. 3	21.5	1.785	···	1.890	1.694	0.196	···	0.110
KCl—RbCl No. 2	47.5	1.728	0.001	1.830	1.627	0.203	0.003	0.118
KCl—RbCl No. 4	66.2	1.694	0.003	1.789	1.602	0.187	0.004	0.110
RbCl No. 1	97.7	1.643	···	1.729	1.573	0.156	···	0.095

[10] It might be noted that the presence of a smaller amount of KCl in the authors pure RbCl than in the specimens of the others would account equally for the disagreement in the frequency of the F band maximum at room temperature and also the disagreement in lattice constant as indicated in the preceding section.

Figures 3, 4, and 5 are plots of the data in Table II. In each of these graphs the experimental points are drawn as circles. All results, including those for both increasing and decreasing wavelength measurements fall within these circles.

IV. DISCUSSION

The striking fact is that the half-maximum width of the F band, as a function of concentration, goes through a maximum at about 40 mole percent RbCl in KCl (Fig. 4). This effect is most simply explained by assuming the presence of several unresolved components, that is, precisely the iso-structured, component F bands postulated in the introduction.

In an attempt to account for the observed F bands on the above basis it was found that two composite band models appeared reasonable and simple. In the first model it was assumed that there were seven different component F bands, each associated with one of the seven iso-structured F centers. In the second model it was assumed that there were three different component F bands in these mixed crystals, corresponding to the electronic transitions that occur in the one-dimensional

TABLE III. Parameters of F bands in KCl and RbCl.

	λ_{max} A	ν_{max}	γ	γ/ν_m
		10^4 cm^{-1}		
KCl				
Mollwo[a] 20°C	5630	1.776	0.289	0.163
Authors 25°C	5590	1.789	0.291	0.163
Mollwo −186°C	5480	1.825	0.191	0.105
Authors[b] liq. N_2	5390	1.854	0.170	0.092
RbCl				
Mollwo 20°C	6240	1.603	0.258	0.161
Authors 25°C	6320	1.583	0.263	0.166
Mollwo −160°C	6050	1.653	0.179	0.108
Authors liq. N_2	6090	1.643	0.156	0.095

[a] Reference 5 in text.
[b] Temperature somewhat higher than −196°C, but was not measured.

models, $K^+-e^-K^+$, $K^+-e^-Rb^+$, $Rb^+-e^-Rb^+$. The difference between these two composite band models can be seen more clearly as follows: Consider for simplicity that an *F* center in a pure KCl crystal is an electron that is trapped in a cubical box (i.e., the unit crystallographic cell) whose walls are at infinite potential. Model 1 postulates that the substitution of a Rb^+ for a K^+ in one of the unit cell faces will change the size of the box, but will leave its cubic symmetry intact. There is only one *F* band associated with a given type of center. There are, in all, seven possible component *F* bands. Model 2, on the other hand, assumes that the substitution of a Rb^+ for a K^+ will change only one of the dimensions of the box. In this model there can be one, two, or three *F* bands associated with a given type of center. There are, in all, three possible component *F* bands. If the other assumptions that are necessary to carry out these composite band constructions are valid, then it is reasonable to suppose that the proper composite *F* band to be compared with experiment should lie somewhere in between those calculated by models 1 and 2.

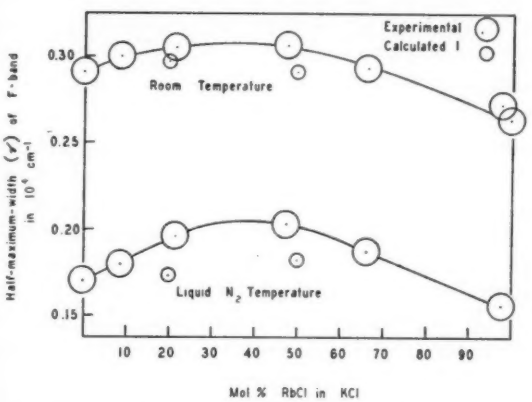

FIG. 4. Half-maximum width of *F* band *versus* mole percent RbCl in KCl. Large circles (ordinate diameter $0.015\cdot10^4$ cm^{-1}) are experimental results. Small circles are results calculated by composite band model 1.

Composite bands were constructed for 20 and 50 mole percent RbCl in KCl under the following assumptions:

1. Model 1: The component bands, if plotted in reduced coordinates (i.e., $\log(I_0/I)/\log(I_0/I)_{\max}$ *versus* $\nu/\nu_{\max}$) are identical with the reduced plot of the pure KCl band. This assumption about the component band shape arises from the fact that the *F* bands of all the pure alkali halides approximately superimpose upon one another when plotted in this fashion and, in addition, agree fairly well with that predicted by dispersion theory[11] (Fig. 6).

Model 2: The same.

2. Model 1: The frequency of the maximum, $\nu_m(X)$, of a component band arising from centers with *X* Rb^+ ions in the nearest neighbor sphere is

$$\nu_m(X)=\nu_m(\mathrm{KCl})-\tfrac{1}{6}X[\nu_m(\mathrm{KCl})-\nu_m(\mathrm{RbCl})]$$

[11] A. Smakula, Z. Physik **59**, 603 (1930).

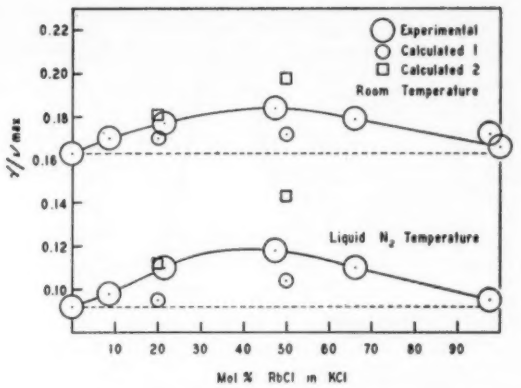

FIG. 5. Ratio of half-maximum width to frequency of maximum of *F* band *versus* mole percent RbCl in KCl. Large circles (ordinate diameter 0.01) are experimental results. Small circles and squares are results calculated by composite band models 1 and 2, respectively.

and is thus assumed to be independent of the gross concentration of RbCl in the KCl.

Model 2: The ν_m's of the *F* bands corresponding to the electronic transitions of $K^+-e^-K^+$, $Rb^+-e^-Rb^+$, and $K^+-e^-Rb^+$ are equal to $\nu_m(\mathrm{KCl})$, $\nu_m(\mathrm{RbCl})$, and $[\nu_m(\mathrm{KCl})+\nu_m(\mathrm{RbCl})]/2$, respectively. These ν_m's are thus assumed to be independent of the composition of both the remainder of the nearest neighbor sphere and the gross crystal.

3. Model 1: The distribution of the different types of *F* centers actually present is random (the energies of formation of the different types of vacancies are the same, and each type has trapped electrons in proportion to its concentration); that is, the concentration of a given type, $N(X)$, is proportional to $6!/X!(6-X)!\cdot(N_{\mathrm{KCl}})^{6-X}(N_{\mathrm{RbCl}})^X$, where N_{KCl} is the mole fraction of KCl in the crystal and N_{RbCl} that of RbCl.

Model 2: The distribution of the three types of oscillators is likewise assumed to be random, that is, the concentration of a given type, $N(X)$, is proportional to $2!/X!(2-X)!\cdot(N_{\mathrm{KCl}})^{2-X}(N_{\mathrm{RbCl}})^X$.

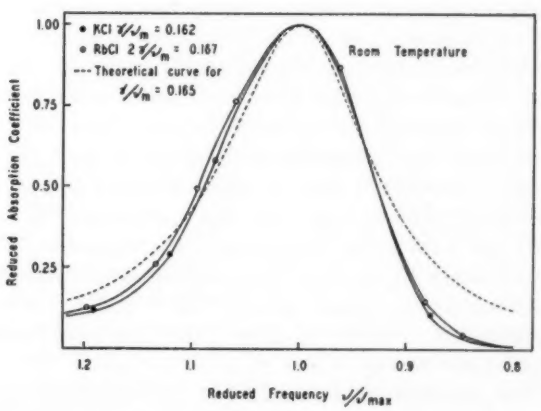

FIG. 6. *F* bands at room temperature in terms of reduced frequency. Dashed curve is calculated from dispersion treatment of Smakula (reference 11).

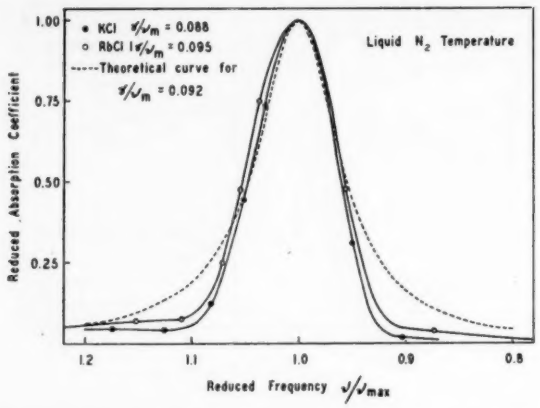

FIG. 7. *F* bands at liquid nitrogen temperature in terms of reduced frequency. Dashed curve is calculated from dispersion treatment of Smakula (reference 11).

4. Model 1: The absorption coefficient, $\alpha_m(X)$, equals $KN(X)/\gamma(X)$, where K is a constant with a value that is the same for the different types of centers. This relation arises from dispersion theory[11] with the additional assumption that the oscillator strengths are the same for all types.

Model 2: The same.

The method thus consisted of summing the contributions of the component *F* bands to the total absorption coefficient at a given frequency. After assignment of the $\nu_m(X)$'s using assumption 2, a reduced frequency was calculated for each component at the given frequency. The reduced absorption coefficients corresponding to these reduced frequencies were then obtained from the KCl plot (Figs. 6 and 7). These reduced absorption coefficients were multiplied by the concentration weighting factors appropriate to assumptions 3 and 4 and then summed. A number of such summations were made at different frequencies over the range of appreciable absorption in order to get the parameters and the shape of the composite band.

F bands were constructed for 20 and 50 mole percent RbCl based upon the KCl reduced *F* bands at both room and liquid nitrogen temperatures. The room temperature value of $\nu_m(\mathrm{KCl})-\nu_m(\mathrm{RbCl})$ was used also for the low temperature computations, though the experimental value at the low temperature exceeded that at room temperature by $0.005\cdot10^4$ cm^{-1}. The values of ν_m, γ, and γ/ν_m as calculated are contained in Table IV. These values (with the exception of model 2 ν_m and γ) are also plotted in Figs. 3, 4, and 5, respectively.

Figure 8 shows the 50 mole percent composite bands as calculated by models 1 and 2 together with the band observed for 47.5 mole percent RbCl in KCl at room temperature. Figure 9 shows the low temperature counterpart of Fig. 8.

The presence of a maximum in the calculated results of γ *versus* mole percent RbCl and the increased prominence of this maximum at the lower temperature are in agreement with experiment. The supposition that the observed results should lie somewhere in between the two models is likewise upheld in the case of γ and γ/ν_m. However, the position of these computed bands does not show as good an agreement with experiment. The calculated *F* band maxima are consistently at higher frequencies than those observed (Figs. 3, 8, and 9).

A possible reason for this discrepancy is as follows. A Rb^+ ion is larger than a K^+ ion. Conceivably, then, the energy of formation of a negative ion vacancy might be smaller if Rb^+ ions rather than K^+ ions were present in the nearest neighbor sphere. If the other assumptions remain unchanged, this effect will increase the relative concentrations of those negative ion vacancies with neighboring Rb^+ ions and consequently shift the composite band maxima towards lower frequencies.

Composite bands were computed for 50 mole percent RbCl in KCl using models 1 and 2, assumption 3 being modified to include such energy differences. It was assumed that the energy of formation decreased linearly with the number of Rb^+ ions surrounding the vacancy, that is, $\epsilon(X)=\epsilon(6K^+)-X\Delta\epsilon$. A plausible order of magnitude estimate for $\Delta\epsilon$ was taken to be the heat of solid solution of RbCl in KCl. This value has been determined to be $+203$ cal/mole of solution.[12] The concentrations of the iso-structured vacancies as obtained from model 1 were consequently weighted by the factors, $\exp(X\Delta\epsilon/kT)$, $X=0$ to 6, assuming room temperature equilibrium. In the case of model 2 the concentrations of the three one-dimensional oscillators were weighted similarly by the factors, $\exp(X\Delta\epsilon/kT)$, $X=0$ to 2. (Note that under the postulates that have been made above, this simple form of the model 2 weighting is valid only for 50 mole percent mixtures.)

TABLE IV. Calculated composite band parameters.

	Mole percent RbCl	ν_m	$\nu_{\frac{1}{2}}$HF	$\nu_{\frac{1}{2}}$LF	γ	γ/ν_m
			10^4 cm^{-1}			
Room temperature						
Model 1	50.0	1.689	1.846	1.555	0.291	0.172
Model 2	50.0	1.689	1.868	1.534	0.334	0.198
Model 1, energy-modified	50.0	1.667	1.822	1.535	0.287	0.172
Model 2, energy-modified	50.0	1.660	1.843	1.515	0.328	0.198
Observed	47.5	1.666	1.831	1.525	0.306	0.184
Model 1	20.0	1.747	1.913	1.616	0.297	0.170
Model 2	20.0	1.752	1.926	1.609	0.317	0.181
Observed	21.5	1.723	1.889	1.584	0.305	0.177
Liquid nitrogen temperature						
Model 1	50.0	1.749	1.848	1.666	0.182	0.104
Model 2	50.0	1.749	1.884	1.634	0.250	0.143
Observed	47.5	1.728	1.830	1.627	0.203	0.118
Model 1	20.0	1.813	1.907	1.734	0.173	0.095
Model 2	20.0	1.819	1.930	1.726	0.204	0.112
Observed	21.5	1.785	1.890	1.694	0.196	0.110

[12] Value from compilation in article by W. E. Wallace, J. Chem. Phys. **17**, 1095 (1949).

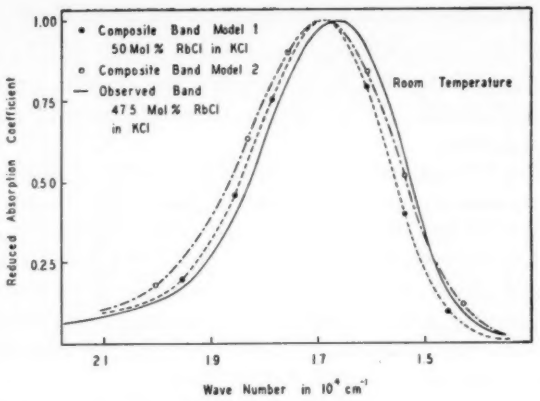

FIG. 8. Experimental and calculated *F* bands at room temperature.

The composite band parameters as computed in this manner are shown in Table IV. The agreement between the calculated and observed ν_m's is greatly improved. Also the half-maximum width limits as well as γ and γ/ν_m are now bracketed by the results of models 1 and 2.

V. FURTHER KCl–RbCl EXPERIMENTS

Experimentally it has been found that under a diversity of conditions of preparation and observation, the *F* band parameters of a pure crystal at a given temperature are fixed, as would be predicted by the present concept of an *F* center. From the preceding discussion it is apparent that this should not necessarily be so for the *F* band in a mixed crystal with a specified composition. That is, the *F* band parameters should change if the distribution of the iso-structured *F* centers is changed.

Several experiments were carried out to try and observe such an effect. First, an attempt was made to change the distribution of the iso-structured negative ion vacancies (before x-irradiation) by heat treatment of the crystals. Second, an attempt was made to change the distribution of the iso-structured *F* centers after x-irradiation by bleaching them differentially with monochromatic light.

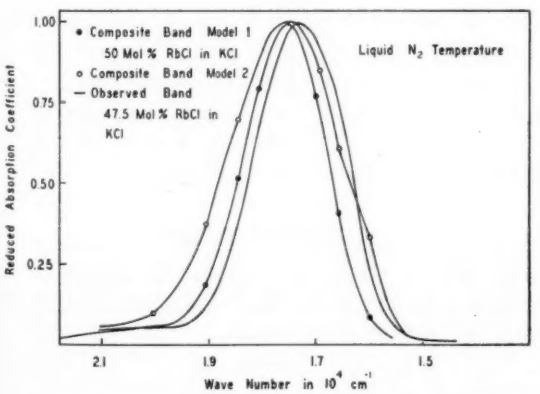

FIG. 9. Experimental and calculated *F* bands at liquid nitrogen temperature.

In the first method the intention was to "anneal" several crystals at several different high temperatures, following this with a quench to room temperature. This treatment could produce an appreciable change in the iso-structured vacancy distribution providing that (among other things): 1. The magnitudes of the differences among the energies of formation of the vacancies were sufficiently large. 2. The magnitudes of the differences among the true, quenched in temperatures were sufficiently large.

Only two experiments of this type were carried out. Two crystals (47.5 mole percent RbCl) were heated in air, one at 500°C, the other at 600°C, for about one day and then cooled to room temperature. The subsequently induced *F* bands showed some distinct differences from the untreated crystals, but the presence of several new bands in the ultraviolet (3500A and 2950A) indicated that the results could not be trusted.[13]

Ten monochromatic bleaching experiments were performed at room temperature using 47.5 mole percent RbCl in KCl crystals. Seven different wavelengths were used, and the amount bleached ranged from 15 to 60 percent. The results were generally inconclusive, prominent *F* band parameter changes occurring only when a relatively high percentage of the band was bleached, in which cases there was evident quite extensive *R* band formation. The parameter changes to be expected from both models 1 and 2 were in any case rather small, even with optimum experimental conditions.

One 65°C thermal bleach (in the dark) was done without resultant changes in the *F* band parameters.

VI. *F* BANDS IN OTHER MIXED CRYSTALS

F bands of several other mixed crystals were measured to determine whether or not they exhibit a behavior similar to that of the *F* bands in KCl–RbCl mixed crystals. They were not investigated as fully as the latter, however.

A. Fifty Mole Percent KBr in KCl

A mixed crystal was grown from a melt whose composition was 50 mole percent KBr in KCl. This mixture was selected as the anionic counterpart of the cationic mixture, RbCl in KCl; KCl and KBr are also completely mutually soluble in the solid crystalline state. The *F* band parameters obtained from this mixed crystal are compared in Table V(A) with those obtained from the pure components. As in the case of the 50 mole percent KCl–RbCl *F* band, the ν_m of the mixture is seen to be situated about halfway between the ν_m's of the pure components. Also similar is the fact that the γ of the mixture is larger than the γ's of the pure components. Though the γ/ν_m for this mixed crystal lies between the γ/ν_m's of the pure components, it appears that it would

[13] These new bands may be associated with oxygen impurity. See P. Pringsheim, *Fluorescence and Phosphorescence* (Interscience Publishers, Inc., New York, 1949), pp. 624–627 and references given there.

TABLE V. *F* band parameters of other mixed crystals.

Crystal	ν_m	$\nu_{\frac{1}{2}}$HF	$\nu_{\frac{1}{2}}$LF	γ	γ/ν_m
		10^4 cm^{-1}			
	(A)				
KCl	1.789	1.949	1.658	0.291	0.163
KBr in KCl, 50 mole percent	1.681	1.850	1.544	0.306	0.182
KBr	1.600	1.765	1.468	0.297	0.186
	(B)				
KCl	1.789	1.949	1.658	0.291	0.163
NaCl in KCl, 10 mole percent	1.774	1.989	1.572	0.417	0.235
33 percent bleached with 6750A light	1.788	1.992	1.595	0.397	0.222
NaCl[a]	2.146	2.358	1.976	0.382	0.178
	(C)				
NaCl[a]	2.146	2.358	1.976	0.382	0.178
NaBr in NaCl, 17 mole percent					
At room temp	2.088	2.345	1.883	0.462	0.221
At liq. N_2 temp	2.156	2.334	2.007	0.327	0.152
NaBr[b]	1.852	2.083	1.667	0.416	0.225

[a] Reference 5 in text.
[b] Values estimated from R. Ottmer, Z. Physik 46, 798 (1928).

probably reach a maximum value at a composition of about 75 mole percent KBr in KCl.

B. Ten Mole Percent NaCl in KCl

A mixed crystal was grown from a melt whose composition was 10 mole percent NaCl in KCl. These components were selected because they are only partially miscible in the solid crystalline state, thus providing an example of the effect of appreciably different ions upon the *F* band parameters. The parameters obtained from this mixed crystal are shown in Table V(B). It is rather striking that the ν_m occurs on the low frequency side of the ν_m in pure KCl and not between those of the pure components. Also the increase in γ over that of pure KCl is amazingly large in view of the presence of less than 10 mole percent NaCl in the crystal.

The crystal specimens used in these measurements were clear. If two phases were present at the time of these determinations, one must have occurred only in very small amounts in the gross crystal. Some time after the measurements were made there was some evidence of slight surface clouding. Since the most intense coloration is obtained at the irradiated surface, it is possible that two phases did contribute to the observed absorption. Their presence could, in part, account for the width of the observed band, but not its position. Bleaching of the *F* band with 6750A light produced large changes in the long wave region of the band as shown in Table V(B).

C. Seventeen Mole Percent NaBr in NaCl

A mixed crystal was grown from a melt of 17 mole percent NaBr in NaCl. These components are reportedly mutually soluble in all proportions at room temperature.

The *F* band parameters, determined after x-irradiation of specimens of this mixed crystal, are shown in Table V(C). The ν_m is seen to be reasonably positioned between the maxima of the pure NaCl and pure NaBr *F* bands. Again, γ is much larger than that of either pure component. No component band resolution was effected by measurement at low temperature; the high frequency side of this curve was quite large, however.

If it were assuredly true that the absorption bands measured in these last two mixed crystals were only *F* bands and were in only one solid phase, then these mixtures would seem to present a much better opportunity for successful differential bleaching studies than was offered by the KCl–RbCl mixed crystals. In such a case, however, the assumptions used in the KCl–RbCl composite band constructions could not explain the position of the peak in the KCl–NaCl mixed crystal. Conjecture should best await further experimentation.

D. Fifty Mole Percent KBr in RbCl

A mixed crystal was grown from a melt of composition 50 mole percent KBr in RbCl. This mixture was of interest since the lattice constants and the positions of the *F* band maxima of the components are very similar. However, specimens of this mixed crystal colored much too weakly to make reasonable measurements of the *F* band parameters.

A second mixed crystal was grown from the remainder of the same melt with about 0.3 mole percent KOH added. Though the intensity of color was about doubled by this means, it was still less than that induced in crystals of either pure component and again too weak to give much better parameters than obtainable from the first specimens. It would appear that the density of vacancies is rather lower than in the pure components, but the reason is not clear.

E. *M* Bands in KCl–RbCl Mixed Crystals

A weak *M* band was produced along with the *F* band in the KCl–RbCl mixed crystals. Though it was not studied carefully, its ν_m was observed to shift towards lower frequencies with increasing RbCl concentrations as in the case of the *F* band maximum.

ACKNOWLEDGMENT

The author wishes to express his appreciation to Professor J. E. Mayer for his encouragement and advice during the pursuit of this work.

An Infrared Spectroscopic Study of the Carbonyl Stretching Frequency in a Group of *Ortho* and *Para* Quinones*

MARIE-LOUISE JOSIEN, NELSON FUSON, JEANNE-MARIE LEBAS, AND THOMAS M. GREGORY
Fisk University, Nashville, Tennessee

(Received July 16, 1952)

This paper reports on an experimental study of the C=O stretching vibration frequency in a large number of quinonoid compounds, both substituted and unsubstituted. For nonsubstituted *ortho* and *para* quinones, relationships between the carbonyl frequency and (a) the number of fused rings, (b) the oxidation-reduction potential, and (c) the index of free valence on the parent hydrocarbon are pointed out and discussed. It is shown that for a six-atom quinonoid ring the C=O frequency is, to a first approximation, a function of the C=O bond order. For substituted quinones, the variation in the carbonyl frequency is related to the induction effect of the substituent in the same way as is the variation in oxidation-reduction potential. Certain hydroxy-substituted quinones show spectral anomalies which do not seem to fit into the usual category of hydrogen bonded compounds.

I. INTRODUCTION

SEVERAL theoretical and experimental papers appearing during the last few years have discussed the variation of the C=O stretching frequency with changes in the molecular environment. A recent paper from this laboratory,[1] which includes a detailed bibliography on this subject, considers, among others, the following two questions: (a) the influence upon the carbonyl frequency of the addition of fused benzene rings to nonsubstituted *ortho* and *para* quinones; and (b) the influence of substituents upon the carbonyl frequency in quinones. This investigation has been continued through the study of additional polycyclic quinones in order to give a basis for drawing more definite conclusions. The results are here summarized for the *ca* 130 quinones reported not only in this paper but in previous ones[1,2,3] as well.

II. EXPERIMENTAL

The spectrometer used for this study was a single beam automatic recorder equipped with a large rock salt prism.[4] The calibration of the "double bond region" was based on the well-known six-micron water vapor band profile present as a background on each spectrum made. Reproducibility was such that sharp bands between 1600 cm^{-1} and 1800 cm^{-1} could be measured to within ± 1 cm^{-1} or ± 2 cm^{-1}.

All the spectra were obtained with samples in solution, in a nonpolar solvent if possible. Carbon tetrachloride was the standard solvent, although carbon disulfide was more satisfactory in a few cases. In one case chloroform was used as the solvent because of poor solubility in either of the less polar solvents.

The C=O frequencies of a number of compounds studied previously in CS_2 solution[1] have been remeasured for inclusion in this paper using CCl_4 as the solvent. The only difference observable between the two sets of results was a tendency for the CCl_4 solution values to be one or two reciprocal centimeters higher than the corresponding CS_2 solution values.

III. REMARKS ON ASSIGNMENT OF BANDS TO THE C=O VIBRATION

In the majority of compounds studied the band to be assigned to the carbonyl vibration frequency is easy to locate because of its intensity and because of the absence of other bands in the 1600–1800 cm^{-1} region. All the symmetrical nonsubstituted quinones as well as all of the symmetrically substituted quinones exhibited only one band in that region. This is also true of unsymmetrical nonsubstituted quinones. The spectra of unsymmetrically substituted quinones (see Table IV), however, showed two distinct bands in a few cases as follows: 2-chloro-1,4-naphthoquinone (1672 cm^{-1} and 1684 cm^{-1}), 2-bromo-1,4-naphthoquinone (1670 cm^{-1} and 1686 cm^{-1}), and 2-methyl-3-bromo-1,4-naphthoquinone (1669 cm^{-1} and 1681 cm^{-1}). It is conceivable that in the other cases of unsymmetrical quinones two close bands are also present but are not far enough apart to be resolved.

Each of the following compounds has an additional band (see figures in parentheses in Table IV), *ca* 1700 cm^{-1}, which is not yet understood: 3-cyano-9,10-phenanthraquinone (1722 cm^{-1} in solid state), 1-hydroxy-9,10-phenanthraquinone (1684 cm^{-1} in solid state), 2-acetylamino-1,4-naphthoquinone (1725 cm^{-1} in solution), β-lapachone (1703 cm^{-1} in solution), and 2-methoxy-1,4-naphthoquinone (1690 cm^{-1} in solution). The spectrum of 2-acetylamino-1,4-naphthoquinone showed in addition to the quinone C=O band (1636 cm^{-1} in the solid state, and 1666 cm^{-1} in solution) two additional bands (1590 cm^{-1} and 1672 cm^{-1} in the solid state) which were assigned as characteristic of the CONH group.

In the case of 3-benzoyl-9,10-phenanthraquinone two

* This paper has been reported in part at the Annual Meeting of the Southeastern Section of the American Physical Society, Raleigh, North Carolina, April 10–12, 1952, and at the Spring Meeting of the American Physical Society, Washington, D. C., May 1–3, 1952.

[1] M. L. Josien and N. Fuson, Bull. soc. chim. France **19**, 389 (1952).
[2] M. L. Josien and N. Fuson, J. Am. Chem. Soc. **73**, 478 (1951).
[3] M. L. Josien and N. Fuson, Compt. rend. **234**, 1680 (1952).
[4] Josien, Fuson, and Cary, J. Am. Chem. Soc. **73**, 4445 (1951).

TABLE I. Carbonyl frequencies, oxidation-reduction potentials and indices of free valence for unsubstituted *ortho* and *para* quinones.

Structure number[a]	Compound	Source[b]	Frequency[c] (cm^{-1})	Oxidation-reduction potential[d] (volts)	Index of free valence[e]
I	1,2-Benzoquinone	5, 7	1669	0.81	0.398
II	1,2-Naphthoquinone	5	1678[f]	0.58	0.428
III	9,10-Phenanthraquinone	6	1684	0.46	0.451
IV	1,2-Phenanthraquinone	4	1677	0.66	0.428
V	3.4-Phenanthraquinone	4	1668	0.62	0.424
VII	1,2-Benzanthra-3,4-quinone	3	1685	0.43	0.456
VIII	1,2-Chrysenequinone	2	1679	0.47	0.449
IX	Picenequinone	4	1680	0.46	0.450
X	1,4-Benzoquinone	6	1667	0.71	0.398
XI	1,4-Naphthoquinone	5	1675	0.48	0.452
XII	Anthraquinone	6	1678	0.15	0.520
XV	Naphthacenequinone	4	1682		0.530
XVI	1,2-Benzanthra-9,10-quinone	3	1670	0.23	0.508
XVII	2,3,6,7-Dibenzanthraquinone	4	1680		0.540
XVIII	1,2,3,4-Dibenzanthraquinone	1	1668		0.499
XIX	1,2,5,6-Dibenzanthraquinone	1	1660	0.27	0.498

[a] Structure diagrams keyed to these Roman numerals are given in Figs. 1, 2, 3, and 4.

[b] 1. Dr. Ernst D. Bergmann, Weizmann Institute, Rehovoth, Israel. 2. Dr. St. Elmo Brady, Fisk University, Nashville, Tennessee. 3. Dr. J. W. Cook, Glasgow University, Glasgow, Scotland. 4. Dr. Louis F. Fieser, Harvard University, Cambridge, Massachusetts. 5. Mr. and Mrs. Clay M. Greer, Vanderbilt University, Nashville, Tennessee. 6. Purified from commercial product by Mrs. (Clay) Frances Greer, Vanderbilt University, Nashville, Tennessee. 7. Dr. Carl M. Hill, Tennessee A & I State University, Nashville, Tennessee.

[c] All compounds were studied in CCl_4 solution.

[d] All potential values were obtained from reference 13, except for compound IX which is given by Fieser, J. Am. Chem. Soc. **53**, 1128 (1931). No potentials were found in the literature for compounds XV, XVII, and XVIII.

[e] Index of free valence on the carbon atom of the hydrocarbon which corresponds to the carbonyl carbon of the corresponding quinone. Values obtained from reference 8.

[f] This value of the carbonyl frequency differs radically from that previously reported by us (see reference 1) for 1,2-naphthoquinone, the earlier sample studied having been impure.

C=O bands have been found in the solid state sample spectrum. We have assigned the higher frequency band (1680 cm^{-1}) to the quinone C=O and the lower (1660 cm^{-1}) to the benzoyl C=O. Because this latter carbonyl group is located between two benzene rings, its frequency can be compared with that of benzophenone (XXI) (1664 cm^{-1}).

IV. NONSUBSTITUTED *ORTHO* AND *PARA* QUINONES

Table I summarizes the results obtained from nonsubstituted *ortho* and *para* quinones. Two preliminary remarks may be made before discussing the findings in more detail. In the first place the results found for *ortho* and *para* quinones are in sharp contrast with the C=O frequencies measured for very highly condensed quinones[1] such as the pyrenequinones. As has been previously mentioned,[1] the C=O frequency is lower for the latter set of quinones. In the second place the carbonyl frequencies of *ortho* quinones tend to be slightly higher than those of the corresponding *para* quinones. Compare, for example, the frequencies of *ortho* (I) and *para* benzoquinone (X) (1669 cm^{-1} and 1667 cm^{-1}); *ortho* (II) and *para* naphthoquinone (XI) (1678 cm^{-1} and 1675 cm^{-1}); and 9,10-phenanthraquinone (III) and anthraquinone (XII) (1684 cm^{-1} and 1678 cm^{-1}).

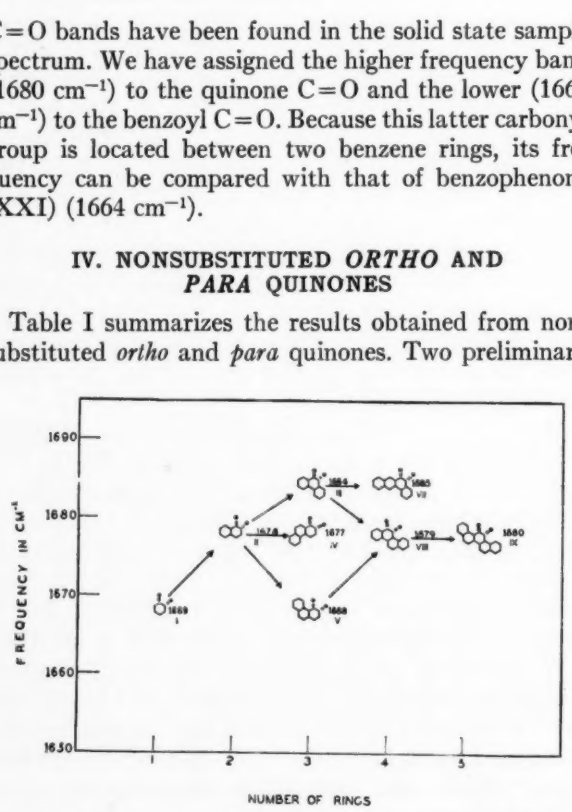

FIG. 1. Carbonyl bond vibration frequency *versus* number of fused rings for *ortho* quinones.

A. Influence of the Number of Rings

Figures 1 and 2 use the data from Table I to show how the quinone frequency varies with the number of rings in *ortho* and *para* quinones, respectively.

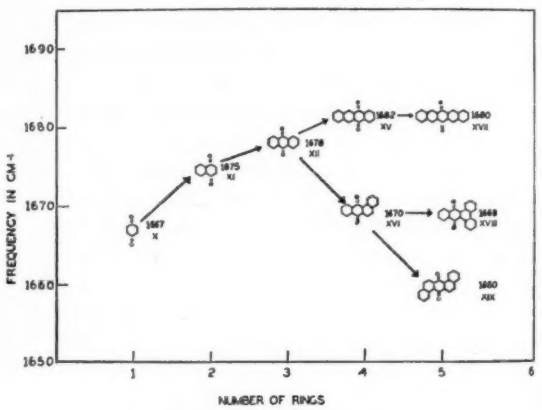

FIG. 2. Carbonyl bond vibration frequency *versus* number of fused rings for *para* quinones.

The addition of fused rings to a quinonoid compound increases the carbonyl frequency as long as none of the added rings makes an angle concave to the carbonyl group. In such cases if the added ring is fused to a ring adjacent to the quinonoid ring the effect is much less pronounced than if the ring is fused to the quinonoid ring itself. This results in a "plateau effect" which is clearly seen in the figures for both *ortho* and *para* quinones. For example, 1,2-phenanthraquinone (IV) (1677 cm^{-1}) differs almost not at all from 1,2-naphthoquinone (II) (1678 cm^{-1}). This is also true of 1,2-benzanthra-3,4-quinone (VII) (1685 cm^{-1}) and 9,10-phenanthraquinone (III) (1684 cm^{-1}). Likewise, to use a *para* quinone example, the naphthacenequinone (XV) (1682 cm^{-1}) and 2,3,6,7-dibenzanthraquinone (XVII) (1680 cm^{-1}) carbonyl frequencies agree within the limits of experimental error.

In contrast to the effect just discussed, the addition of fused benzene rings in such a way that they make a concave angle with one of the quinonoid ring carbonyl

groups markedly decreases the C=O vibration frequency. This "angle effect" influence upon the frequency may be seen in Figs. 1 and 2 if one compares 3,4-phenanthraquinone (V) (1668 cm^{-1}) with 1,2-naphthoquinone (II) (1678 cm^{-1}), chrysenequinone (VIII) (1679 cm^{-1}) with 9,10-phenanthraquinone (III) (1684 cm^{-1}), and 1,2,5,6-dibenzanthra-9,10-quinone (XIX) (1660 cm^{-1}) with 1,2-benzanthra-9,10-quinone (XVI) (1670 cm^{-1}) and with anthraquinone (XII) (1678 cm^{-1}).

While the size of the conjugated molecule influences the magnitude of the carbonyl frequency,[5] it has already been pointed out[1] that size is not the only factor. The preceding discussion confirms that the C=O vibration frequency in cyclic quinones is not a single-valued function of the number of rings. Perhaps the most striking illustration (see Fig. 1) is given by the addition of a benzene ring to 1,2-naphthoquinone (II) (1678 cm^{-1}). One can obtain either the same frequency, as in 1,2-phenanthraquinone (IV) (1677 cm^{-1}), a higher frequency, as in 9,10-phenanthraquinone (III) (1684 cm^{-1}), or a lower frequency, as in 3,4-phenanthraquinone (V) (1668 cm^{-1}), depending on the place of attachment of the added ring.

B. Carbonyl Vibration Frequency *versus* Oxidation-Reduction Potential

A relationship has already been indicated[1] between the carbonyl vibration frequency of a compound and its corresponding oxidation-reduction potential.[6] Figure 3 uses the data in Table I to illustrate this relationship for all the compounds we have studied spectroscopically and for which the potential is known. The C=O frequency is a multiple-valued function of oxidation-reduction potential just as it is of the number of rings. Nevertheless, it is of interest to mention that all the *ortho* quinones which do not involve the "angle effect" give points on a straight line. The points of those which do exhibit the "angle effect" are grouped so that they lie on portions of straight lines bearing off from the main graph line. The same is true of the *para* quinones. As shown in Fig. 3 the C=O frequency for these compounds decreases with increase in oxidation-reduction potential. This is consistent with our previous findings.[1] However, as will be noted in more detail later on, the C=O frequency is, in contrast, an *increasing* function of oxidation-reduction potential for compounds which differ only in the substituent on a given parent quinone.

C. Carbonyl Vibration Frequency *versus* Index of Free Valence on the Parent Hydrocarbon

It has been suggested[1] that the negative slope of the graph of carbonyl frequency *vs* oxidation-reduction potential (Fig. 3) may be related to the effect of resonance in these quinone molecules. On the basis of this hypothesis it becomes of interest to see if any relationship can be found between the C=O frequency and the index of free valence[7] on the corresponding carbon atom in the parent hydrocarbon. The results of this study, using the index values calculated by means of the method of molecular orbitals,[8] are presented in Fig. 4. In those cases where the free valence indices on the two carbonyl carbon atoms involved were not identical, the arithmetical average of the two values was used. The curves in Fig. 4, which is taken from the data in Table I, appear to be almost the mirror image of the curves in Fig. 3, the difference between them being largely in the reversal of slope.

In Fig. 4 the slope of the *ortho* quinone family line is

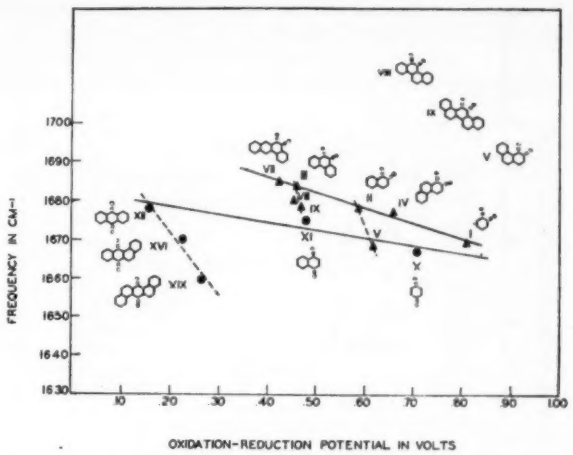

FIG. 3. Carbonyl bond vibration frequency *versus* oxidation-reduction potential for *ortho* quinones (triangles) and *para* quinones (circles).

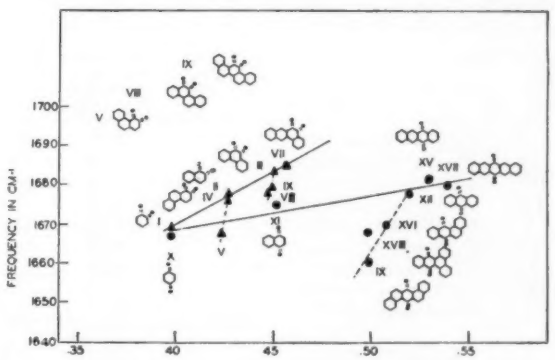

FIG. 4. Carbonyl bond vibration frequency for *ortho* quinones (triangles) and *para* quinones (circles) *versus* index of free valence on the corresponding parent hydrocarbons.

[5] C. A. Coulson, Trans. Faraday Soc. **42**, 106 (1946).

[6] The oxidation-reduction potential under "normal" conditions is proportional to the drop in free energy in going from the quinone plus hydrogen form to the hydroquinone form and can be thought of as a measure of the oxidizing power of the quinone (see reference 13).

[7] This index, computed for each carbon atom, is the concentration of unpaired electrons in the neighborhood of each atom and is a measure of the reactivity of the hydrocarbon at each atom (see reference 8).

[8] B. Pullman and A. Pullman, *Les Theories Electronique de la Chimie Organique* (Masson et cie, Paris, 1952), pp. 588–591.

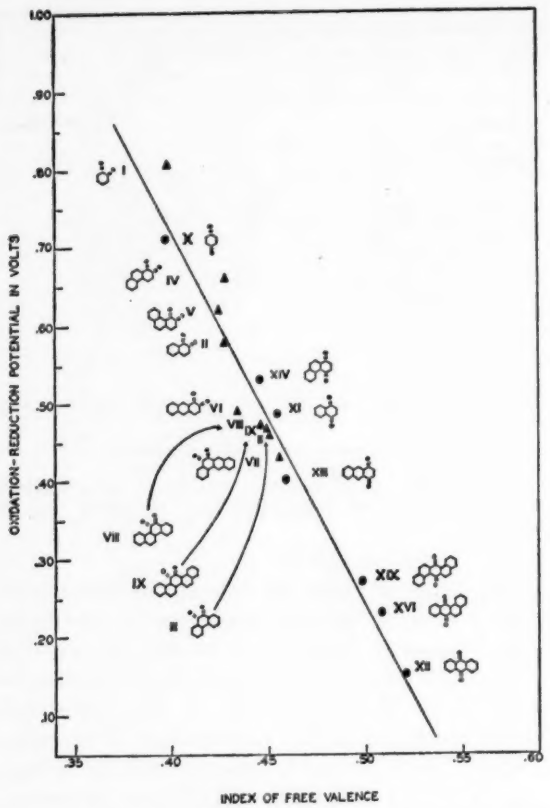

FIG. 5. Oxidation-reduction potential for *ortho* quinones (triangles) and *para* quinones (circles) *versus* index of free valence on the corresponding parent hydrocarbons.

greater than that for the *para* quinone family. The quinones which present an "angle effect" give points on the graph which lie below the two corresponding lines. It seems probable that the smaller frequencies of these quinones are related to some induction effect resulting from the presence of the added benzene ring close to one of the carbonyl groups. Such an explanation has already been considered to account for the presence of the two different OH frequencies in benzyl alcohol.[9] Some kind of hydrogen bonding might also be possible.[10,11,12]

TABLE II. Comparison of index of free valence and oxidation-reduction potential for unsubstituted *ortho* and *para* quinones.

Structure number[a]	Compound[b]	Oxidation-reduction potential[b] (volts)	Index of free valence[c]
I	1,2-Benzoquinone	0.81	0.398
II	1,2-Naphthoquinone	0.58	0.428
III	9,10-Phenanthraquinone	0.46	0.451
IV	1,2-Phenanthraquinone	0.66	0.428
V	3.4-Phenanthraquinone	0.62	0.424
VI	1,2-Anthraquinone	0.49	0.434
VII	1,2-Benzanthra-3,4-quinone	0.43	0.456
VIII	1,2-Chrysenequinone	0.47	0.449
IX	Picenequinone	0.47	0.450
X	1,4-Benzoquinone	0.71	0.398
XI	1,4-Naphthoquinone	0.48	0.452
XII	9,10-Anthraquinone	0.15	0.520
XIII	1,4-Anthraquinone	0.40	0.459
XIV	1,4-Phenanthraquinone	0.53	0.446
XVI	1,2-Benzanthra-9,10-quinone	0.23	0.508
XIX	1,2,5,6-Dibenzanthra-9,10-quinone	0.27	0.498

[a] Structure diagrams keyed to these Roman numerals are given in Figs. 1 to 4 and 7a.
[b] This particular list of compounds includes all those whose potentials are compiled by Branch and Calvin. (See reference 13, pages 311–313.)
[c] Index of free valence on the carbon atom of the hydrocarbon which corresponds to the carbonyl carbon of the corresponding quinone. Values obtained from reference 8.

D. Oxidation-Reduction Potential *versus* Index of Free Valence

The similarity between Figs. 3 and 4 is not accidental as is shown by Table II, in which the oxidation-reduction potential of a group of quinones is tabulated along with the index of free valence of the corresponding carbonyl carbon atoms in the parent hydrocarbon. The list in Table II is composed of those compounds whose oxidation-reduction potentials are given by Branch and Calvin.[13] The corresponding indices of free valence are taken from the compilation made by the Pullmans.[8] It should be noted that Table II includes most of the compounds listed in Table I but also others (see Fig. 7 for structures) for which no carbonyl vibration frequencies are published and which we have not as yet been able to obtain for study in this laboratory.

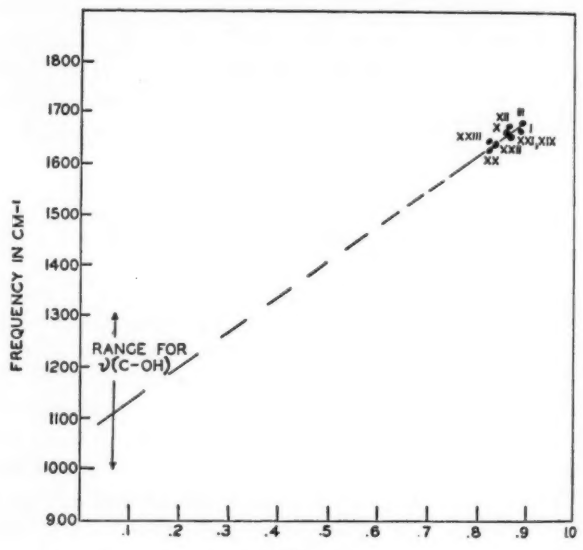

FIG. 6. Carbonyl bond order *versus* carbonyl bond vibration frequency for unsubstituted quinones, benzophenone, and benzonaphthenone.

Figure 5, the graph of the data given in Table II, shows that the oxidation-reduction potential is a de-

[9] J. J. Fox and A. E. Martin, Trans. Faraday Soc. **36**, 902 (1940).
[10] Buswell, Rodebush, and Roy, J. Am. Chem. Soc. **60**, 2528 (1938).
[11] W. Gordy, J. Am. Chem. Soc. **60**, 605 (1938).
[12] L. H. Jones and R. M. Badger, J. Am. Chem. Soc. **73**, 3132 (1951).
[13] G. E. K. Branch and M. Calvin, *The Theory of Organic Chemistry* (Prentice-Hall, Inc., New York, 1941), p. 303*ff*.

creasing linear function of the index of free valence on the carbon atoms in the parent hydrocarbon. This seems to be true even though the electronic distribution in the hydrocarbon is certainly disturbed by the introduction of the carbonyl groups in the quinone so that the relation can only be expected to hold on a first approximation. The frequencies of the two benzoquinones, *ortho* (I) and *para* (X) are a case in point, both of these compounds having been derived from benzene, in which, because of symmetry, each carbon atom has the same index of free valence.

The interest of Fig. 5 will be more apparent when it is pointed out that the past decade has seen several attempts to relate the oxidation-reduction potentials of quinones to their structures. One method of attack, first utilized by Branch and Calvin[13] in 1941, is to relate the potential to the resonance energy of the quinone. More recently, several authors[14] have computed the change in resonance energy, $R_{HQ}-R_Q$, for the reduction of a quinone: quinone $(Q)+H_2=$hydroquinone (HQ).[6] The graphs of observed potential *vs* calculated resonance energy change were found[14] to consist of two nearly parallel and approximately rectilinear curves, one for the family of *ortho* quinones and the other for that of *para* quinones. These curves, as well as those shown in Figs. 3 and 4, thus present a sharp contrast to the single-valued curve of Fig. 5.

E. Carbonyl Vibration Frequency and Bond Order

In a previous paper[1] a relationship was suggested between the bond order[15] and the vibration frequency of the carbonyl group. Recent theoretical studies made by Bonino, Chiorboli, and Scrocco[16] and by Berthier, Pullman, and Pontis[17] have shown that this hypothesis is sound. Table III indicates the relation between frequency and bond order for benzophenone (XXI), benzonaphthenone (XXIII), and for the several quinonoid compounds for which bond order values have been calculated. If the data in Table III are graphed as in Fig. 6, it may be seen that there is an approximately linear relationship between frequency and bond order. Furthermore, it is interesting to note that if the straight line is extrapolated to a bond order of zero, it intercepts the frequency axis at a point well within the experimental range (1000 to 1300 cm^{-1}) found for the single bond C—OH stretching vibration.

F. Carbonyl Vibration Frequency and Ring Strain

Another important factor influencing the magnitude of the carbonyl stretching frequency is the amount of strain in the ring.[17,18,19] When the formation of a ring does not introduce appreciable strain, however, as is true when the ring has six atoms, one observes that the C=O frequency remains constant. For example, the carbonyl frequencies of xanthone (XXVI) (1666 cm^{-1}) and anthrone (XXVII) (1667 cm^{-1}), both of which com-

TABLE III. Carbonyl bond order *vs* carbonyl frequency for unsubstituted quinones, benzophenone, benzonaphthenone, xanthone, and anthrone.

Structure number[a]	Compound	Frequency[b] (cm^{-1})	Bond[c] order
I	1,2-Benzoquinone	1669	0.879
III	9,10-Phenanthraquinone	1684	0.885
X	1,4-Benzoquinone	1667	0.856
XII	Anthraquinone	1678	0.860
XIX	1,2,5,6-Dibenzanthra-9,10-quinone	1660	0.858
XX	Diphenoquinone	1634	0.819
XXI	Benzophenone	1664	0.857
XXII	Pyrene-3,10-quinone	1645	0.833
XXIII	Perinaphthenone (Benzonaphthenone)	1649	0.820
XXVI	Xanthone	1666	···
XXVII	Anthrone	1667	···

[a] Structure diagrams keyed to these Roman numerals are given in Figs. 1 and 7b.
[b] All compounds were studied in CCl_4 solution except diphenoquinone for which the solvent was $CHCl_3$.
[c] Values calculated by Berthier, B. Pullman, and Pontis (see reference 17).

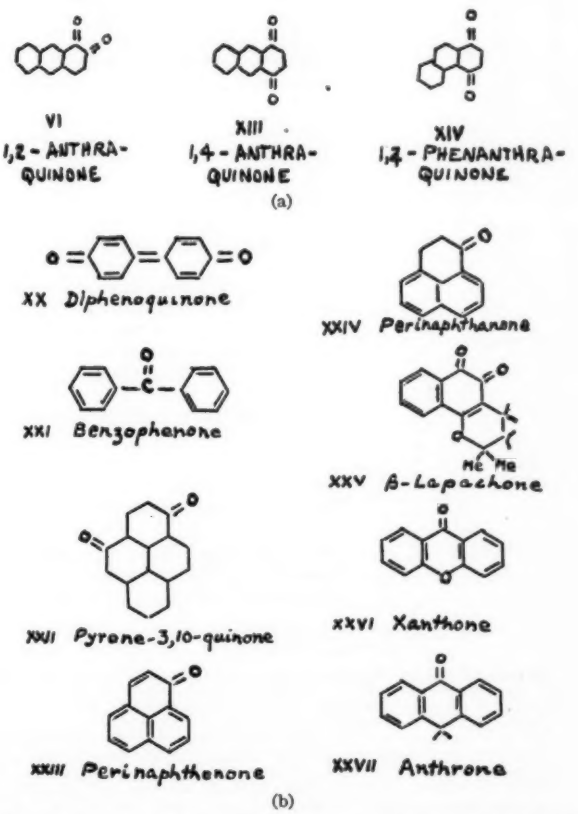

FIG. 7. Structure diagrams of (a) compounds VI, XIII, XIV, and (b) compounds XX through XXVII. (Structures of other compounds are shown in Figs. 1 through 5.)

[13] B. Pullman and A. Pullman, see reference 8, p. 266.
[15] Bond order as used here is defined to be the number of pairs of pi electrons which are localized between two atoms to form a particular bond (see reference 8).
[16] G. B. Bonino and E. Scrocco, Rend. Acc. Line. **6**, 421 (1949 VIII); **8**, 183 (1950 VIII); E. Scrocco and P. Chiorboli, Rend. Acc. Line. **8**, 248 (1950 VIII).
[17] Berthier, Pullman, and Pontis, J. chim. phys. (to be published).
[18] J. Lecomte, J. Phys. **6**, 257 (1945).
[19] Chabbal, Diplome d'études supérieures, Paris, 1949.

TABLE IV. Carbonyl frequency and oxidation-reduction potential for substituted quinones.

Structure number[a]	Compound	Source[b]	Frequency[c] (cm^{-1}) Sol'n[d]	Solid[e]	Oxidation-reduction potential[f]
XI	1,4-Naphthoquinone	3	1675		0.48
	2-Methyl-1,4-naphthoquinone	2	1670		0.42*
	2,3-Dimethyl-1,4-naphthoquinone	2	1660		0.34
	2,6-Dimethyl-1,4-naphthoquinone	2	1668		0.41
	2,7-Dimethyl-1,4-naphthoquinone	2	1673		0.41
	2-Methyl-3(β,β-diphenyl) ethyl-1,4-naphthoquinone	1	1663		...[i]
	2-Phenyl-1,4-naphthoquinone	2	1667		0.45
	2-Methoxy-1,4-naphthoquinone	2	1660 (1690)		0.35
	2-Hydroxy-1,4-naphthoquinone	2	1663	1660[g]	0.36*
	2,3-Dihydroxy-1,4-naphthoquinone (Isonaphthazarin)	2	1649		0.29*
	5,8-Dihydroxy-1,4-naphthoquinone (Naphthazarin)	2	1623		0.38*
	3-Hydroxy-2-methyl-1,4-naphthoquinone (Phthiocol)	2	1660		0.30
	2-Amino-1,4-naphthoquinone	2	1640		0.27
	2-Chloro-1,4-naphthoquinone	2	1672 1684		0.51
	2,3-Dichloro-1,4-naphthoquinone	2	1687		0.50
	2-Bromo-1,4-naphthoquinone	2	1670 1686		0.51
	2,3-Dibromo-1,4-naphthoquinone	2	1685		0.50[j]
	2-Methyl-3-bromo-1,4-naphthoquinone	2	1669 1681		...[i]
	2-Ethoxy-3-bromo-1,4-naphthoquinone	2	1676		...[i]
	2-Acetylamino-1,4-naphthoquinone	2	1666 (1725)	1590[h] 1636 1672[h]	0.42
II	1,2-Naphthoquinone	3	1678		0.58*
	3,7-Dimethyl-1,2-naphthoquinone	2	1667		0.54
	6-Hydroxy-1,2-naphthoquinone	2	...	1660	...[i]
	4-Amino-1,2-naphthoquinone	2	1686[g]		0.32
	3-Bromo-1,2-naphthoquinone	2	1692		...[i]
	Potassium-1,2-naphthoquinone-sulfonate	2	...	1662	0.64
XXV	β-Lapachone	2	1662 (1703)		0.40
III	9,10-Phenanthraquinone	4	1684		0.46
	1-Methyl-7-isopropyl-9,10-phenanthraquinone	1	1681		0.42
	1-Hydroxy-9,10-phenanthraquinone	2	1639	(1684) 1634	0.41
	2-Hydroxy-9,10-phenanthraquinone	2	...	1660	0.46
	3,4-Dihydroxy-9,10-phenanthraquinone	2	...	1644[g]	0.39
	2-Amino-9,10-phenanthraquinone	2	...	1672	0.44
	3-Bromo-9,10-phenanthraquinone	2	1691		0.50
	3-Cyano-9,10-phenanthraquinone	2	1671	1660 (1722)	0.55
	3-Benzoyl-9,10-phenanthraquinone	2	1680[g]	1680 1660[k]	0.52
X	1,4-Benzoquinone	4	1667		0.69*
	Tetrachloro-1,4-benzoquinone	4	1695		0.71*
XXIII	Perinaphthenone (Benzonaphthenone)	2	1649[l]		
	2-Bromo-4-methoxy-1-benzonaphthenone	5	1647		
	4-Methoxy-1-benzonaphthenone	5	1643		

[a] Structure diagrams keyed to these Roman numerals are given in Figs. 1 and 7.

[b] 1. Dr. Ernst D. Bergmann, Weizmann Institute, Rehovoth, Israel. 2. Dr. Louis F. Fieser, Harvard University, Cambridge, Massachusetts. 3. Mr. and Mrs. Clay M. Greer, Vanderbilt University, Nashville, Tennessee. 4. Purified from commercial product by Mrs. (Clay M.) Frances Greer, Vanderbilt University, Nashville, Tennessee. 5. General Aniline and Film Corporation, New York, New York.

[c] Numbers in parentheses have not been assigned, as is pointed out early in the paper.

[d] The compounds were studied in CCl_4 solution, the one exception being 1-methyl-7-isopropyl-9,10-phenanthraquinone for which the solvent was CS_2. (Dots in this column mean that the compound was too insoluble in nonpolar solvents to obtain its solution spectrum.)

[e] Compounds were studied in solid state only when no solution values could be obtained or when some particular reason arose for seeking a comparison.

[f] All the oxidation-reduction potentials are taken from the work of Louis F. Fieser (see reference 21). The only exceptions are the seven starred (*) values which are taken from the work of K. Wallenfels and W. Mohle, Ber. deut. chem. Ges. **76B**, 924 (1943).

[g] Broad absorption band.

[h] Assigned to CONH group.

[i] Potential not found in the literature.

[j] This potential was not found in the literature; however, it was assumed to be the same as for 2,3-dichloro-1,4-naphthoquinone.

[k] Assigned to benzoyl C=O.

[l] Note the contrast of this carbonyl frequency with that of perinaphthanone (1-benzonaphthanone) (XXIV) (1696 cm^{-1} in CCl_4 solution) which has the same structure except that the ring to which the carbonyl group is attached is saturated.

pounds are obtained from benzophenone (XXI) by ring closure without conjugation, are practically the same as the frequency of benzophenone itself (1664 cm^{-1}).[19a] The structures of these compounds is given in Fig. 7.

V. SUBSTITUTED QUINONES

In addition to the investigation of unsubstituted *ortho* and *para* quinones, a further study was made of the carbonyl frequency for substituted quinones. The data are to be found in Table IV. A few of the substituted quinones proved to be insoluble in any transparent solvent. For these compounds the carbonyl frequency was obtained from the spectrum of the compound in solid form suspended in a nujol mull, thus enabling one to gain a rough idea of the position of the "free" carbonyl frequency's absorption. The term "rough" is used since it has been observed[1] that, presumably because intermolecular forces exert an appreciable effect in the solid state, the frequency of the carbonyl vibration of quinones in this state has a value lower than that found in the state of dilute solution in a nonpolar solvent. The magnitude of this shift is, as yet, unpredictable for a given quinone, but it may range anywhere from 0 cm^{-1} to 30 cm^{-1}.[1]

Figure 8 is a graph of the solution data taken from Table IV. Previously published values[1] for anthraquinones and fluorenones[19b] have also been included in Fig. 8 for comparison purposes. Figure 9 is a detailed study of substituted 1,4-naphthoquinones. An examination of Table IV and Figs. 8 and 9 leads to several remarks.

A. Carbonyl Frequency *versus* the Induction Effect and the Oxidation-Reduction Potential

The number of quinones studied is large enough to establish the generality of the fact already pointed out[1,20] that, with respect to the unsubstituted quinone, electronegative substituents like Cl, Br, and CN increase the frequency of the carbonyl group vibration, while electropositive substituents like CH_3, C_6H_5, and OCH_3 decrease the frequency, i.e., the induction effect. Exactly parallel conclusions were reached some years ago by Fieser[21] concerning the effect of substituents on the oxidation-reduction potential of quinones.

There were four groups of compounds for which we had three or more samples with known values of the oxidation-reduction potentials. For these four series[22] the frequency *vs* potential curves are straight lines

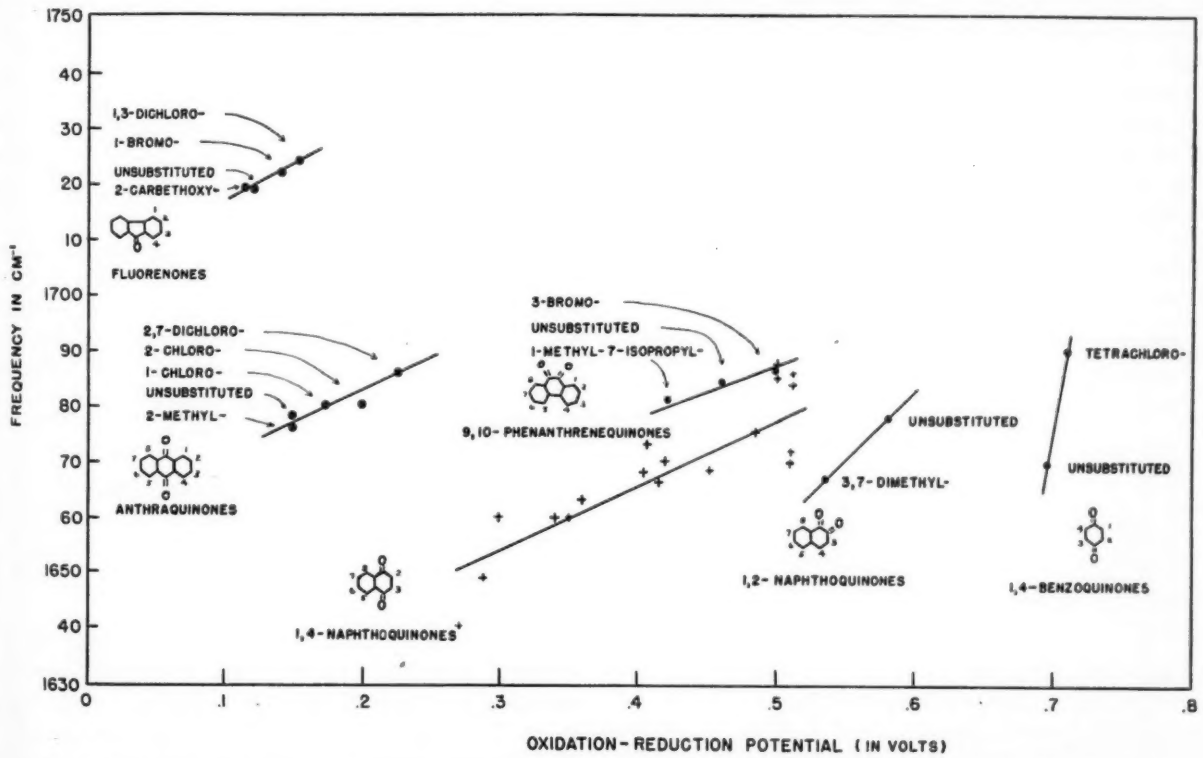

FIG. 8. Carbonyl bond vibration frequency *versus* oxidation-reduction potential for substituted quinones and fluorenones.

[19a] (*Note added in proof*).—We have recently run a sample of thioxanthone in CCl_4 solution and have found the carbonyl frequency at 1649 cm^{-1}. The explanation for this lower value when sulfur replaces oxygen in xanthone is still under discussion.

[19b] In the previous report, reference 1, p. 390, Fig. 2, a typographical error was made in numbering the carbons in fluorenone, the intended numbering being the standard one.

[20] M. St. C. Flett, J. Chem. Soc. **1948**, 1441.

[21] Louis F. Fieser, J. Am. Chem. Soc. **44**, 2480 (1922); **45**, 2194 (1923); **46**, 1868 (1924); **49**, 2604 (1927); **50**, 437 (1928); **51**, 3101 (1929); **52**, 5204 (1930); **53**, 802 and 4120 (1931); **56**, 1565 (1934); **57**, 491 (1935).

[22] The curves for the other two groups of compounds were not based on enough points for their slopes to be significant.

having *positive* slopes which are all of the same order of magnitude (1 cm^{-1} per centivolt).[1] This behavior is, of course, implicit in the conclusions cited above, and can furthermore be directly correlated with the degree of ionic character of the carbon-oxygen double bond.[1] It is postulated that the inductive effect of electronegative groups is to decrease the ionic character of this bond and that of electropositive groups is to increase it. It then follows that frequency and potential both vary inversely with the degree of ionic character of the bond.

B. Effect of Position of Substituent

The addition of substituents on the quinonoid ring itself is more effective in changing both the oxidation-reduction potential[21] and the C=O frequency[1] than is the addition of substituents on rings adjacent to the quinonoid ring.

C. Compounds not Fitting Well on the Frequency *versus* Potential Curves

As is particularly evident from the 1,4-naphthoquinones (see Fig. 9), some of the graph points lie far from the average line. Thus, the induction factor is not the only one influencing the carbonyl frequency of substituted quinones. Perturbing factors, such as mesomerism, or mechanical resonance with other vibrations in the molecule, are presumably present.

If chlorine or bromine atoms are substituted into the quinonoid ring the elevation of the C=O frequency is more marked than the corresponding effect for the oxidation-reduction potential, with the result that compounds such as 2,3-dichloro-1,4-naphthoquinone give points which fall above the average position of the curves.

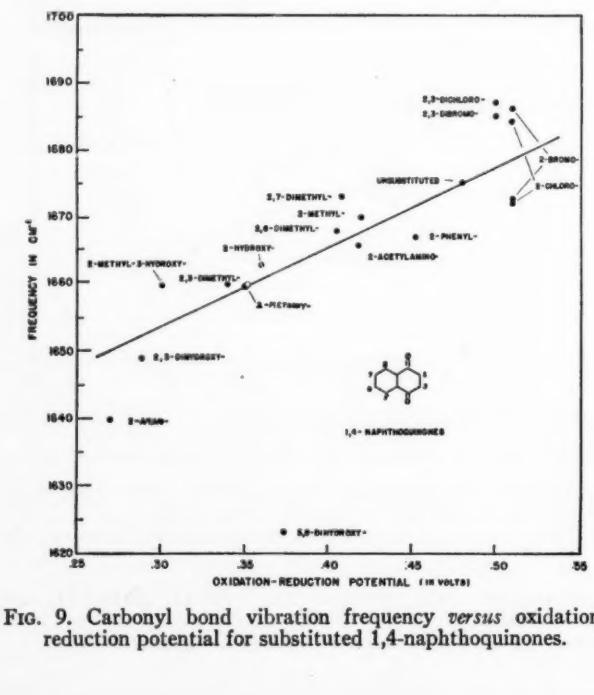

FIG. 9. Carbonyl bond vibration frequency *versus* oxidation-reduction potential for substituted 1,4-naphthoquinones.

Six compounds for which both solution frequency and oxidation-reduction potential are known (see Table IV) have not had their frequency-potential points included in Fig. 8, usually because of their large deviation from the region in which such points usually lie. Of these 1-hydroxy-9,10-phenanthraquinone and 5,8-dihydroxy-1,4-naphthoquinone are discussed in detail later. β-lapachone (XXV) fits fairly well onto an extrapolation of the 1,2-naphthoquinone curve if the slope of the latter, drawn before the β-lapachone spectrum had been obtained, is modified to equal approximately that of the four others. Points for 3-cyano-9,10-phenanthraquinone and 2-amino-1,4-naphthoquinone fall far below what would be predicted for them. The sample of 4-amino-1,2-naphthoquinone we studied has its main six-micron region absorption at 1686 cm^{-1}, whereas one would expect under ordinary circumstances to find it 20 to 30 cm^{-1} below the 1678-cm^{-1} position of 1,2-naphthoquinone. The interpretation of this 1686 cm^{-1} band as a carbonyl vibration of the compound is under question and is being restudied.

D. Hydroxy-Substituted Quinones

In the presence of an hydroxyl substituent the lowering of the carbonyl frequency is sometimes all out of proportion to the similar effect upon the oxidation-reduction potential. This occurs for 5,8-dihydroxy-1,4-naphthoquinone and for 1-hydroxy-9,10-phenanthraquinone but not for any of the other hydroxy-substituted compounds studied.[23] An analysis of possible perturbing factors in these compounds is presented in the following paragraphs.

The OH and C=O frequencies of all these hydroxy-substituted compounds are compiled in Table V. Solid state values are given where necessary to supplement solution work or where the compound is insoluble in a nonpolar solvent. Simultaneously with the abnormal displacement of the carbonyl frequency the O–H stretching vibration band disappears from the 3600–3000 cm^{-1} region where the free and associated O–H bands are usually found. Furthermore, the CH vibration band region does not appear to have any strong band superimposed upon it, and no other strong unassigned band appears in the region between 3000 cm^{-1} and 1500 cm^{-1}.

Flett[20] has noticed this marked lowering of the carbonyl frequency in hydroxyl substituted anthraquinones when the OH group is "adjacent" to the C=O group. This has also been reported by Johnson *et al.*[24] for other hydroxyquinones. A similar phenomenon has been

[23] The six-micron region absorption of dihydroxynaphthacenequinone (1792 cm^{-1}) previously reported and assigned to the carbonyl vibration (see footnote 1) is anomalous. This frequency would be expected to lie far below that of naphthacenequinone (XV) (1682 cm^{-1}) (see Table IV). This compound and its band interpretation are thus in question and are being restudied.

[24] Johnson, Quayle, Robinson, Sheppard, and Todd, J. Chem. Soc. **1951**, 2633.

TABLE V. Carbonyl frequencies of several hydroxyquinones.

Structure number[a]	Compound	ν(OH)[b,c] (cm^{-1}) Sol'n	Solid	ν(C=O)[c] (cm^{-1}) Sol'n	Solid	$\Delta\nu$(C=O)[d]
XI	1,4-Naphthoquinone	...	...	1675		0
	2-Hydroxy-1,4-naphthoquinone	3410		1663		12
	2,3-Dihydroxy-1,4-naphthoquinone	3420	3342	1649		26
	5,8-Dihydroxy-1,4-naphthoquinone	no band	no band	1623		52
	3-Hydroxy-2-methyl-1,4-naphthoquinone	3410	3347	1660		15
II	1,2-Naphthoquinone	...	...	1678		0
	6-Hydroxy-1,2-naphthoquinone	insol	3300	insol	1660	(18)
III	9,10-Phenanthraquinone	...	...	1684		0
	1-Hydroxy-9,10-phenanthraquinone	no band	no band	1639		45
	2-Hydroxy-9,10-phenanthraquinone	insol	3250	insol	1660	(24)
	3,4-Dihydroxy-9,10-phenanthraquinone	insol	3482 3230	insol	1644	(40)
XV	Naphthacenequinone	...	...	1682		0
	Dihydroxynaphthacenequinone	no band	no band	1792[e]		−110[e]

[a] Structure diagrams keyed to these Roman numerals are given in Figs. 1 and 2.
[b] The dots in the spaces below indicate that no bands are expected because the compound has no hydroxyl group.
[c] Blank spaces indicate that no study of the compound in solid form was made.
[d] $\Delta\nu(C=O) = \nu(C=O)_{\text{nonsubstituted}} - \nu(C=O)_{\text{substituted}}$. Numbers in parentheses are $\Delta\nu$ values obtained from solid state spectra and thus are not significant.
[e] This figure is in question; see footnote 23.

observed by Hunsberger for hydroxynaphthaldehydes and hydroxyacetonaphthones.[25] Flett suggests that the explanation for this is hydrogen bonding along with some resonance contribution. The strength of the hydrogen bridge bond is usually obtained from the difference, $[\nu(OH)_{\text{free}} - \nu(OH)_{\text{associated}}]$. In this case, however, the ν(OH) has disappeared, and Flett proposes, therefore, to estimate the strength of the hydrogen bridge bond from the difference $[\nu(C=O)_{\text{free}} - \nu(C=O)_{\text{associated}}]$, which is of the order of 40 cm^{-1}.[20]

We are reluctant to apply the term hydrogen bonding in the ordinary sense to this phenomenon because, in contrast to the disappearance (or abnormally large shift?) of ν(O−H), the shift of ν(C=O) is not excessive when a comparison is drawn between these hydroxy-substituted compounds and the carboxylic acid dimers. The shift in the position of the carbonyl vibration for the acid dimers as compared to that of the corresponding monomers has been found to be as great as 60 to 70 cm^{-1} [26,27] [which is larger than the $\Delta\nu$(C=O) observed for the hydroxyl substituted quinones (see Table V)], while $\nu(O-H)_{\text{associated}}$ appears only about 400 cm^{-1} below the usual location of $\nu(O-H)_{\text{free}}$. It is known from electron diffraction studies[28] that in the case of these acid dimers the carbon-oxygen distances are not the same, one being more consistent with a single bond character, the other with double bond character.

Examination of these new results and of Flett's and Johnson's data on hydroxy-substituted anthraquinones[20] leads us to conclude that this effect occurs when and only when the O−H group is able to form with the C=O group a six atom ring system,

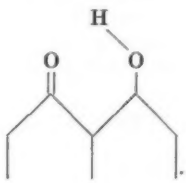

This makes possible a complete symmetry of the ring system if we assume the carbon-oxygen separation is the same in both cases. We propose, therefore, that in contrast with ordinary hydrogen bonding,[8] this phenomenon is due, in the main, to resonance[29] between the two hybrid forms,

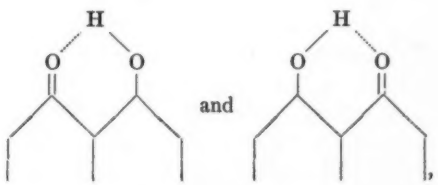

with the hydrogen atom being bound equally to the two oxygen atoms.[30] Similar hypotheses were made recently in order to explain peculiarities of the spectra of acetylacetone and of metallic acetylacetonates.[31] In

[25] I. M. Hunsberger, J. Am. Chem. Soc. **72**, 5626 (1950).
[26] Fuson, Josien, Jones, and Lawson, J. Chem. Phys. **20**, 1627 (1952).
[27] Josien, Fuson, Lawson, and Jones, Compt. rend. **234**, 1163 (1952).
[28] J. Karle and L. O. Brockway, J. Am. Chem. Soc. **66**, 574 (1944).
[29] L. Pauling, J. chim. phys. **46**, 435 (1949).
[30] Ultraviolet spectroscopic data [M. Pestemer, Disc. Faraday Soc. **9**, 213 (1950); Merkel and Wiegand, Naturwiss. **34**, 122 (1947); Morton and Earlam, J. Chem. Soc. **1941**, 159] appear to support this hypothesis as will be discussed in a later paper.
[31] Duval, Freymann, and Lecomte, Bull. soc. chim. France **19**, 106 (1952); Rasmussen, Tunnicliff, and Brattain, J. Am. Chem. Soc. **71**, 1068 (1949).

order to confirm this hypothesis it would be desirable to make an electron diffraction or x-ray diffraction study of these compounds to see if the two carbon-oxygen bonds are, in fact, of equal length. Another approach would be to search the spectrum of these compounds for the location of the band which might be specifically assigned to the hydrogen stretching vibration of a symmetrical $-O..H..O-$ group. This band would probably lie in the skeletal vibration region and would require a deuterization study to isolate it from other vibrations.

VI. ACKNOWLEDGMENT

We should like to express our appreciation to Dr. Ernst D. Bergmann, Dr. St. Elmo Brady, Dr. J. W. Cook, Dr. Louis F. Fieser, Mr. and Mrs. Clay M. Greer, Dr. Carl M. Hill, and the General Aniline and Film Corporation for supplying us with compounds for this study. We want to thank Dr. Bernard Pullman and his collaborators for making available to us a manuscript copy of their most recent paper on the carbonyl vibration prior to publication. This investigation has been supported by a grant from the National Cancer Institute, United States Public Health Service.

THE JOURNAL OF CHEMICAL PHYSICS VOLUME 21, NUMBER 2 FEBRUARY, 1953

Rotational and Vibrational "Temperatures" of CH in Flames at Atmospheric Pressure*

HERBERT P. BROIDA
National Bureau of Standards, Washington 25, D. C.
(Received August 28, 1952)

Spectra of the R branch of the $^2\Delta-^2\Pi$ transition of CH have been obtained from flames of acetylene, propane, and methane premixed with oxygen burning at atmospheric pressure. The distributions of rotational and vibrational intensities have been measured and compared with those expected from thermal excitation. Although in some flames the distributions are close to thermal, the majority of distributions indicate that the excited CH is formed by a nonthermal process and is unreliable as a temperature indicator. The suppression of predissociation of CH in rich hydrogen flames with added acetylene has also been investigated. A continuous emission reaching a maximum near 4000A has been measured.

I. INTRODUCTION

BEFORE the rotational and vibrational distributions in the electronic emission bands of the short-lived radicals OH, CH, and C_2 can be used for measurements of temperature and radical concentrations in flames, it is necessary to know what conditions of mixture, pressure, and position with respect to the reaction zone give adiabatic or anomalous "temperatures." In addition, studies of mechanisms of combustion using flame spectra are dependent upon knowledge of methods of excitation of the radicals.

In the last few years several detailed studies of emission of these radicals from flames have been reported. It has been observed that the radiation of the $^2\Sigma-^2\Pi$ transition of OH near 3100A from hydrocarbon flames at low pressure[1-3] appears to be of chemiluminescent origin. Evidence also has been presented which indicates that at least part of the OH radiation from the reaction zone of hydrocarbon flames at atmospheric pressure[4] is due to chemiluminescence. While somewhat less work has been reported for CH and C_2 radiation from flames, Gaydon and Wolfhard[5] have observed that "rotational temperatures" of the $^2\Sigma-^2\Pi$ (3889A) and $^2\Delta-^2\Pi$ (4315A) bands of CH from both low and atmospheric pressure flames are close to the theoretical maximum flame temperatures. However, the $^2\Sigma^+-^2\Pi$ (3143A) CH band gives an effective rotational "temperature" much higher than theoretical. C_2 also gives

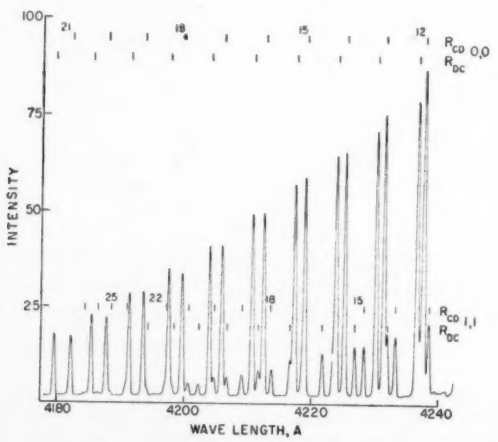

FIG. 1. Recorded spectrum of the R branches of the $^2\Delta-^2\Pi$ transition of CH in a flame with a stoichiometric mixture of acetylene and oxygen diluted with 50 percent argon.

* Supported in part by the U. S. Office of Naval Research.

[1] A. G. Gaydon and H. G. Wolfhard, Proc. Roy. Soc. (London) **A194**, 169 (1948).
[2] A. G. Gaydon and H. G. Wolfhard, Rev. Inst. Frac. Petrole **4**, 405 (1949).
[3] Penner, Gilbert, and Weber, J. Chem. Phys. **20**, 522 (1952).
[4] (a) H. P. Broida and G. Lalos, J. Chem. Phys. **20**, 1466 (1952). (b) W. R. Kane and H. P. Broida, **21**, 347 (1953).
[5] A. G. Gaydon and H. G. Wolfhard, Proc. Roy. Soc. (London) **A199**, 89 (1949).

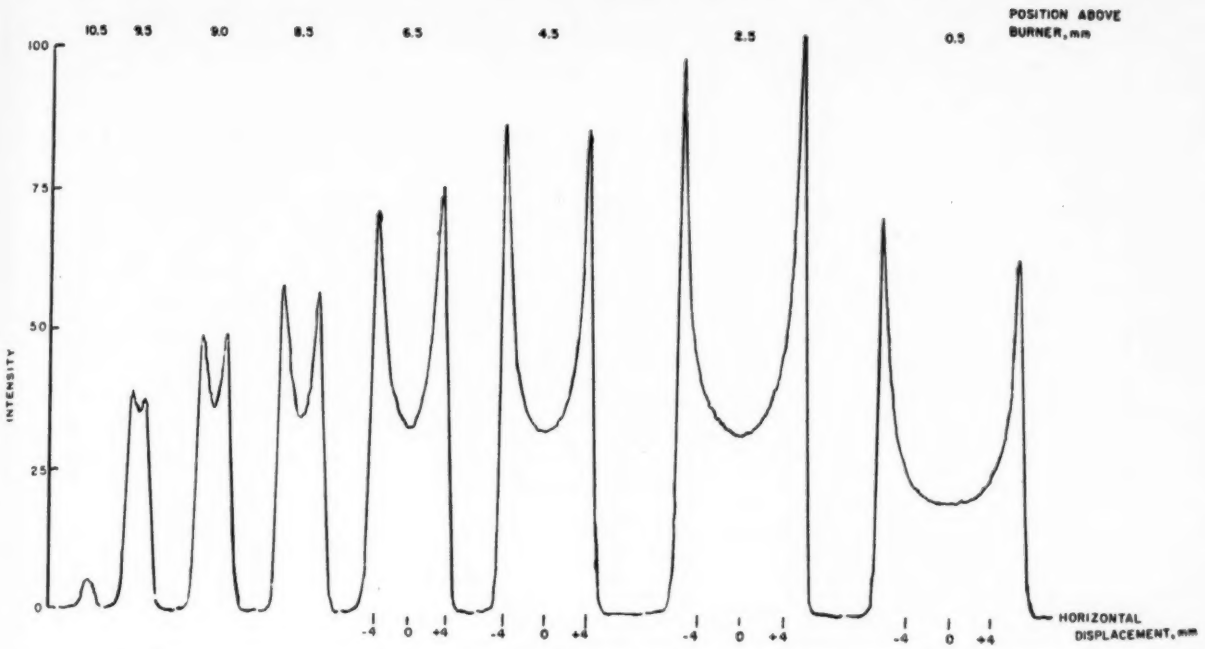

FIG. 2. Horizontal intensity scans at various distances above the base of the flame. The position of the inner cone (reaction zone) is clearly indicated by the maximum intensity at each side of the flame.

an effective rotational temperature somewhat above theoretical.[6] As yet no detailed mechanism exists to explain these observations and, in fact, even the reactions forming excited CH are unknown.

This paper reports the relative intensity measurements of lines of the R_{cd} branches in the 0, 0 and 1, 1 transitions of the $^2\Delta-^2\Pi$ bands of CH in the region of 4300A from the reaction zones of flames of various compositions at atmospheric pressure. Away from the band head, the doubling of the R branches of the 4300A band is easily resolved and predissociation is not evident below the twenty-first rotational level. The spin splitting is quite small and a fairly wide monochromator slit was used to superimpose the two spin components. Lines below $R(12)$ are unusable because of overlapping lines. In addition to the 4300A band, two other CH bands, which are less suitable for rotational intensity measurements, are prominent in hydrocarbon flames. The $^2\Sigma^+-^2\Pi$ transition at 3143A is partially masked by overlapping lines of OH. The $^2\Sigma^--^2\Pi$ transition at 3889A shows a pronounced predissociation[7] at rotational levels greater than 15 and in addition large resolving power is needed to separate overlapping lines.

Although many of the measured rotational and vibrational "temperatures" of the $^2\Delta-^2\Pi$ band are consistent with the calculated adiabatic temperatures, on the whole this radiation is unreliable as a temperature indicator. In particular, too high "temperatures" are measured from flames with an excess of acetylene and "temperatures" in flames with diluents do not decrease as rapidly as the adiabatic temperatures. CH "temperatures" in hydrogen flames with added hydrocarbon increase with increased concentration of hydrocarbon.

A continuous emission from the reaction zone which reaches a maximum near 4000A was observed to increase relative to the CH line emission in fuel-lean flames as well as in rich flames. This continuum is also present in hydrogen flames with small quantities of hydrocarbon but the intensity is greatly reduced when excess hydrogen is added.

II. EXPERIMENTAL

The main details of the apparatus and arrangement have been described previously in more detail.[8] A tube burner of 1.5-mm inner diameter was used. The burner could be positioned to ± 0.1-mm both vertically and horizontally with sets of racks and pinions. Commercial grade tank gases were used with flow controlled by needle valves and measured by floating ball type meters to an accuracy of ± 5 percent. An image of the flame was focused by a quartz lens with an $f/10$ aperture upon the slit of a high resolution, grating monochromator[9] with photoelectric detection and direct intensity recording. The monochromator has a 3×3 inch, 91 440-line grating with a usable resolving power ($\lambda/\Delta\lambda$) of 55 000.

For the rotation and vibration intensity measurements of CH, a portion of the spectrum from 4180 to

[6] A. G. Gaydon and H. G. Wolfhard, Proc. Roy. Soc. (London) A201, 561 (1950).
[7] T. Shidei, Japan. J. Phys. 11, 23 (1936).

[8] H. P. Broida and K. E. Shuler, J. Chem. Phys. 20, 168 (1952).
[9] This equipment was constructed by the Research Department of Leeds and Northrup Company and loaned to the National Bureau of Standards on a field trial arrangement. See W. Fastie, J. Opt. Soc. Am. 40, 800 (1950).

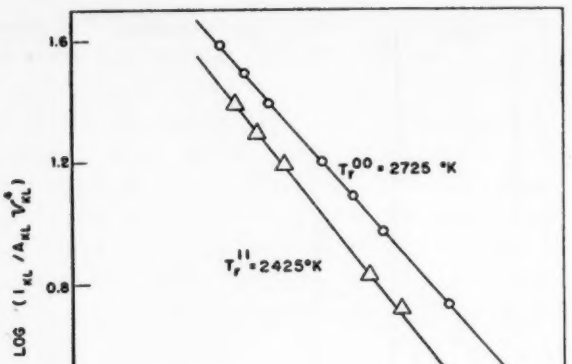

FIG. 3. Logarithmic plots for rotational "temperature" measurements using the intensities of the spectrum in Fig. 1.

4240A was recorded. The recorder trace in Fig. 1 is an example of the spectra obtained. A 0.035-mm (which corresponds to 0.35A) slit was used; this is large enough so that the spin components are not resolved but yet small enough to give adequate separation of the doublets. In this region most of the lines of the R branches are resolved in both the 0, 0 and 1, 1 transitions and can be used for intensity measurements. At longer wavelengths the decreasing Λ separation causes overlapping lines and at shorter wavelengths lines are weakened because of predissociation.

CH "temperatures" at various parts of the reaction zone were measured to determine whether any gradients could be found either through the reaction zone or as a function of the distance above the burner. Within the experimental reproducibility of ± 100°K, no differences in temperatures were observed. Since the reaction zone of flames at atmospheric pressure is quite thin being of the order 0.1 mm, it is difficult to measure differences from one part of the zone to the other. Since the spatial resolution obtained was approximately the same as the thickness of the reaction zone, only a large difference in "temperature" would have been detected. However, it was possible to position the flame so that the CH intensity of the reaction zone when viewed along the edge was two to three times that at the center. Figure 2 shows tracings obtained by setting the monochromator on a single CH line with an entrance slit of 0.035 by 0.3 mm and driving the flame at a constant speed perpendicular to the optic axis. This horizontal scan was made at several vertical positions. At the base of the flame the sides of the inner cone were approximately 2 mm apart, with increasing distance above the base the cone narrows and the intensity of the sides decreases due to the decreasing diameter of the circle of the cone. The intensity at the center is constant except at the top and the bottom where the flame is only partially exposed to the slit. In the resulting plot of intensity *versus* position, the half-widths of the peak intensity above that of the center is of the order of 0.15 mm.

A. Rotational "Temperature"

The effective rotational "temperature" of CH was obtained in the usual manner from the plot of the logarithm of the intensity distribution divided by the rotational transition probability *versus* the energy in the excited state. When the emissivity of the flame is small and there is thermal equilibrium, the intensity I_{KL} of a transition from an excited electronic state with an energy E_K to a lower electronic state is given by the expression

$$I_{KL}=C\frac{N}{Q_r}A_{KL}\nu_{KL}^4\exp(-E_K/kT), \qquad (1)$$

where K and L are, respectively, the quantum numbers of the rotational levels in the upper and lower electronic states, N is the total population of CH radicals, Q_r the rotational state sum, A_{KL} the transition probability including the statistical weight factor, ν_{KL} the frequency of the emitted radiation, T the absolute temperature, k the Boltzmann constant, and C a constant depending upon the electronic transition and upon the instrumental factors. Since it is not known whether the rotational and vibrational distributions are in thermal equilibrium, the temperature as measured with the use of Eq. (1) or similar equations will be referred to as "temperature." The quotation marks are to emphasize that the "temperature" is a measure of the distribution of observed intensities and cannot be used as a measure of the thermal equilibrium temperature without additional confirming evidence.

For a fixed vibrational transition, E_K is the rotational energy and T is the rotational "temperature," T_r. It is convenient to put Eq. (1) in another form:

$$\log_{10}(I_{KL}/A_{KL}\nu_{KL}^4)=\text{constant}-(E_K/kT_r)\log_{10}e. \qquad (2)$$

Values of E_K and ν_{KL} listed in Table I were taken from

TABLE I. Wavelengths λ_{KL}, rotational energy of the initial excited state E_K, and the superimposed transition probabilities A_{KL} of R_{ed} branches of $CH(^2\Delta-^2\pi)$.

L	ν_{KL}^{00} cm^{-1}	λ_{KL}^{00} A	$E_K^{(v'=0)}$ cm^{-1}	ν_{KL}^{11} cm^{-1}	λ_{KL}^{11} A	$E_K^{(v'=1)}$ cm^{-1}	A_{KL}
12	23593.9	4237.2	2419.6	23560.5	4243.2	2305.6	16.13
13	628.4	31.0	2798.1	589.3	38.0	2665.5	17.12
14	662.9	24.8	3202.0	617.8	32.9	3049.4	18.11
15	697.2	18.7	3631.1	645.6	27.9	3457.2	19.11
16	731.4	12.7	4084.7	672.8	23.1	3887.3	20.10
17	765.5	06.6	4562.0	699.1	18.4	4340.0	21.09
18	799.1	00.7	5062.7	724.1	13.9	4814.5	22.09
19	832.4	4194.8	5586.1	748.7	09.6	5310.0	23.09
20	865.4	89.0	6131.4	771.8	05.5	5825.7	24.08
21	897.3	83.4	6698.3	793.4	01.7	6361.3	25.08

Fagerholm,[10] and A_{KL} values have been calculated from the equation of Mulliken[11] as the sum of the transition probabilities of the two spin states of the R branches. Thus a plot of $\log_{10}(I_{KL}/A_{KL}\nu_{KL}^4)$ *versus* E_K can be made from the measured intensities and, for thermal equilibrium, this gives a straight line whose slope is inversely proportional to the temperature. However, the existence of a straight line plot is not sufficient information for deciding that there is thermal equilibrium and a "temperature" measured from the rotational intensity distribution is not necessarily the adiabatic temperature of the flame. In particular, the CH radiation is from the reaction zone of the flame where neither chemical nor thermal equilibrium exists and measured rotational "temperature" can be used only as an indication of the physical and chemical processes which are taking place during combustion. Rotational "temperatures" have been obtained from both the 0, 0 and 1,1 transitions. Figure 3 shows the logarithmic plots for both transitions from the same acetylene-oxygen-argon flame used to obtain Fig. 1; only lines of the R_{cd} branches without any superimposed lines have been plotted. The *cd* lines are more easily used than the *dc* lines since the spin splitting is less for smaller K values. It will be noticed that the points lie on striaght lines but that the slope of the 1, 1 transition is steeper than that of the 0, 0 transition. This difference is characteristic of CH radiation from all the flames observed.

B. Vibrational "Temperature"

Since the relative vibration transition probabilities of CH are not known, it was not possible to obtain an independent vibrational "temperature." However, it was possible to obtain relative "temperatures" by measuring relative intensities of lines from the 0, 0 and the 1, 1 transitions. For a fixed rotational transition the intensity of the line $I^{v'v''}$ from the v'th vibration level is obtained from Eq. (1),

$$I^{v'v''}=C'A_{v'v''}\nu_{v'v''}e^{-E_{v'}/kT_{vib}}, \qquad (3)$$

where C' is a constant which includes the concentration of CH as well as rotation and electronic transition probabilities and instrumental factors and the other symbols are defined similarly to those in Eq. (1). Intensities of lines of the 1, 1 band relative to those of the same rotational transition of the 0, 0 band I^{11}/I^{00} are given by

$$I^{11}/I^{00}=(A_{11}/A_{00})e^{-(E_{11}-E_{00})/kT_{vib}}. \qquad (4)$$

In order to obtain the vibrational temperature T_{vib} it is necessary to know the relative transition probability A_{11}/A_{00}. The latter quantity was estimated by assuming that T_{vib} was equal to the measured T_r^{00} for several flames in which the rotational "temperature" was close to the adiabatic temperature. Since the A_{11}/A_{00} measured in this manner was of the order of unity, being a few percent higher for propane flames and a few percent lower for acetylene flames, a value of one was arbitrarily assigned to the relative transition probability. Although on an absolute basis the measured vibrational "temperatures" are not independent measurements, they are useful for comparison of vibrational intensities.

[10] E. Fagerholm, Ark. Mat., Astro. Fys. **27A** No. 19 (1940).
[11] R. S. Mulliken, Phys. Rev. **30**, 785 (1927).

III. RESULTS

A. Hydrocarbons and Oxygen

The measured rotational and vibrational "temperatures" in acetylene flames are summarized in Fig. 4. All measurements were obtained at the center of the inner cone using a monochromator slit of 0.035 by 1 mm. The rotational "temperatures", T_r^{00} and T_r^{11}, which correspond to the 0 and 1 vibrational levels of the $^2\Delta$ state were obtained from the slopes of graphs like those illustrated in Fig. 3. For "temperatures" greater than 3000°K the scatter in points gives a maximum error of any single determination of ±50°C. However, the limit to the accuracy of a "temperature" determination is in reproducing burning conditions and the measured values for the same flames conditions were reproducible only to ±100°C. All graphs were straight lines, over the range of flame conditions measured, indicating a Maxwell-Boltzmann distribution of rotational energy in the $^2\Delta$ state. Vibrational "temperatures" were obtained by using Eq. (4) with A_{11}/A_{00} equal to one.

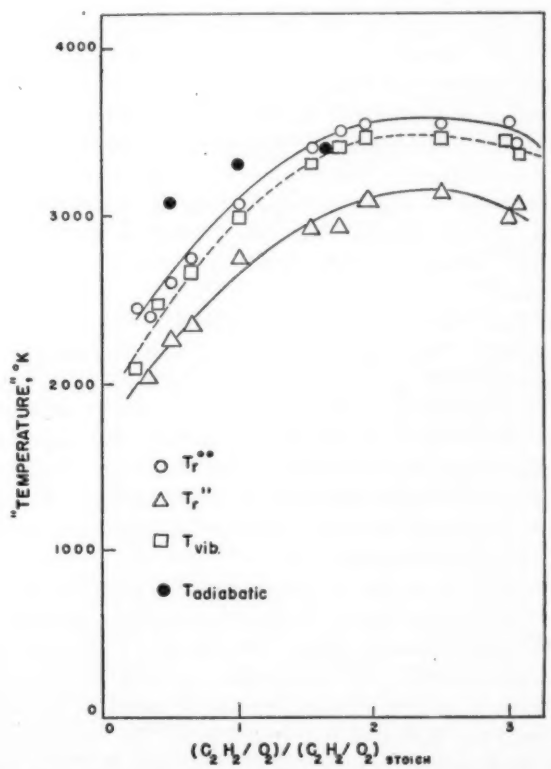

FIG. 4. Measured rotational and vibrational "temperatures" of CH($^2\Delta$—$^2\Pi$) in acetylene-oxygen flames as a function of the ratio of acetylene/oxygen used to the stoichiometric acetylene/oxygen. Adiabatic temperatures were taken from reference 1.

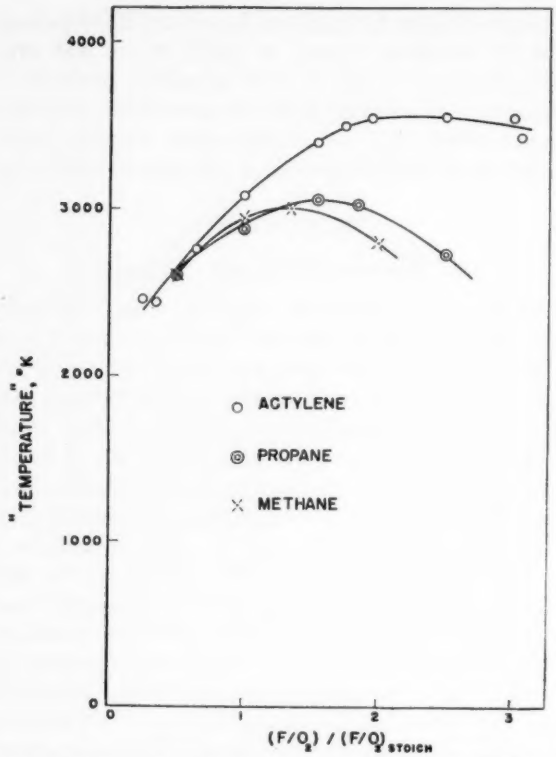

FIG. 5. Measured rotational "temperatures", T_r^{00}, CH($^2\Delta-{}^2\Pi$) in acetylene, propane, and methane flames as a function of the ratio of fuel/oxygen to stoichiometric fuel/oxygen.

It will be noticed that rotational "temperatures" in the $v=1$ vibration state are consistently lower than those in the $v=0$ vibration state by about 10 percent and that the difference increases with decreasing temperature. Vibrational "temperatures" follow as close to the rotational "temperatures" in the zero vibration state as can be expected considering the approximation used for the relative vibration transition probability. Similar differences were observed with methane and propane.

Figure 5 shows the different behavior of the measured rotational "temperatures" in acetylene, methane, and propane flames as a function of the ratio of fuel/oxygen to stoichiometric fuel/oxygen. Note that the "temperature" of the acetylene flame reaches a flat maximum at mixtures between two and three times stoichiometric whereas the "temperatures" of propane and methane flames decrease before the mixture is twice that necessary for stoichiometric.

Figure 6 is a plot of the measured intensities of the R_{cd} (14) lines of the 0, 0 transition and the continuum in the same spectral region. The intensity of the $R_{cd}(14)$ line was selected for comparison of relative intensity because it occurs without blends or overlapping lines in both the 0, 0 and 1, 1 transitions. The intensity of the background between $R_{dc}^{00}(12)$ and $R_{cd}^{11}(14)$ was taken as the continuum intensity in this region; the effect of scattered light in the monochromator is negligible. The peak intensity of CH occurs near twice the fuel-to-oxygen ratio needed for a stoichiometric mixture and even though the "temperatures" of the acetylene flames remain constant for mixtures richer in fuel the intensities decrease. While the intensity of the continuum increases with increasing acetylene concentration, in propane and methane flames the continuum reaches a maximum near stoichiometric and then decreases in richer mixtures. The change of continuum relative to line emission has a completely different behavior. Figure 7 shows that with all fuels, the intensity of the continuum relative to $R_{cd}^{00}(14)$ reaches a minimum at a fuel-rich mixture and increases rapidly on both sides of the minimum. Also the continuum as compared to CH line emission is greater in methane than in acetylene or propane. Separate measurements have shown that the continuum in acetylene flames has a broad maximum in the vicinity of 4000A.

B. Diluents

The effects of nitrogen and argon added to a stoichiometric acetylene-oxygen mixture also were measured. The vibrational "temperature" is somewhat below that with no diluent but remains relatively constant for mixtures up to 80 percent diluent. Rotational "temperatures" also are relatively constant as compared to the 400 to 500°C decrease of the adiabatic temperature over this same range of diluent. There is more effect of argon than of nitrogen on the relative intensity of the continuum compared to CH emission and with both diluents the relative intensity remains constant with increasing diluent.

A small amount of acetylene added to hydrogen-oxygen flames is known to produce very abnormal OH($^2\Sigma$) rotational distributions.[2,4(b)] To see if there also is some anomalous distribution of rotation in CH in similar flames, small quantities of acetylene and of propane were added to stoichiometric hydrogen-oxygen mixtures, making them slightly lean in oxygen. CH intensities with small amounts of added methane were too weak for measurements. Rotational "temperatures" of CH are several hundred degrees less than the adiabatic temperature of 3000°K and the "temperature" increases with increasing hydrocarbon concentration. The vibrational "temperature" is higher than the rotational "temperature" and appears to be constant for a given hydrocarbon.

C. Predissociation of CH

Recently Durie[12] has found hydrogen-hydrocarbon flame conditions in which the predissociation in the $^2\Sigma^-{}^2\Pi$ bands of CH are suppressed and in which there is an enchancement of the 1, 0 and 1, 1 bands. This is best observed in rich hydrogen mixtures (of the order of twice stoichiometric) with one to two percent of added organic material. These are extremely interesting observations, and therefore the 0, 0 and 1, 1

[12] R. A. Durie, Proc. Phys. Soc. (London) **65**, 125 (1952).

bands of this transition in hydrogen-oxygen flames at stoichiometric and twice and three times stoichiometric with 2.5 percent acetylene have been observed. In agreement with Durie, for those mixtures rich in hydrogen, lines in the P and R branches up to $K'=20$ of the zero vibration level of the upper state were observed. In the stoichiometric hydrogen flame and in acetylene flames no lines from levels beyond $K'=18$ are found. Although these observations show at least a partial suppression of the predissociation in rich hydrogen flames, the decrease in intensity for the high K values is still so rapid that thermal equilibrium of the CH rotational intensity distribution does not appear to have been reached. A twofold enhancement of the 1, 1 band relative to the 0, 0 band was observed in the hydrogen flames as compared to acetylene flames. Although the intensity of the 1, 1 band remains relatively constant compared to the 0,0 band with increasing hydrogen-oxygen ratio, the continuous background greatly decreases so that the intensity of the 1, 1 band relative to the continuum increases approximately fourfold between a 2/1 and a 6/1 hydrogen-oxygen ratio.

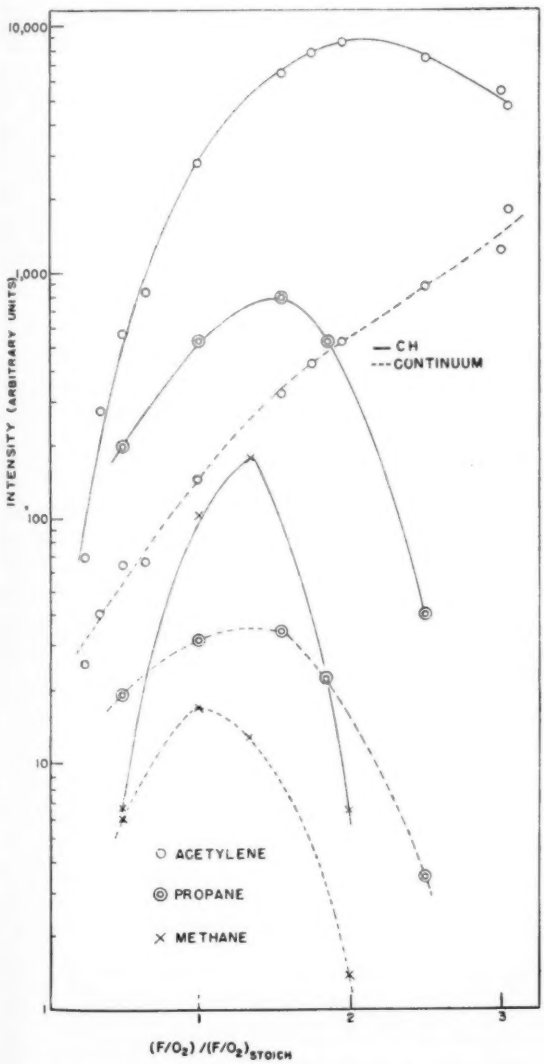

FIG. 6. Measured intensities of CH and the continuum in the same spectral region (4235A).

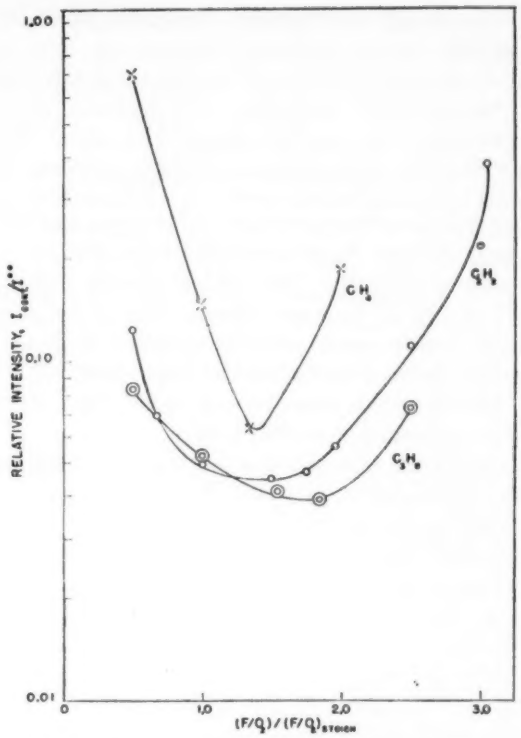

FIG. 7. The intensity of the continuum at 4235A relative to the CH($^2\Delta-^2\Pi$) intensity.

IV. CONCLUSIONS

The rotational "temperatures" of the $v=1$ vibrational state and the vibrational "temperatures" are closely related to the adiabatic flame temperature and the measured rotational "temperatures" for many of the hydrocarbon flames. For example, the rotational "temperature" of CH for a $\frac{4}{5}$ ratio of acetylene-to-oxygen (twice stoichiometric) is 3550°K and the vibrational temperature is 3450°K, whereas the adiabatic temperature is 3400°K and the OH rotational "temperature" is 3200°K.[4(a)] Gaydon and Wolfhard[5] quote a value of 3600°K for the measured CH "temperature" in an "oxyacetylene welding flame" at atmospheric pressure. No figures are given on the relative concentrations, but for agreement with the results presented in this paper, their flame must have been rich in acetylene. For stoichiometric mixtures of acetylene, propane, and methane with oxygen the CH rotational and vibrational "temperatures" are within 10 percent of the measured OH "temperatures" and adiabatic temperatures.[4(b)] This apparent agreement of "temperatures" of excited CH with the flame temperatures would seem to indicate that there is a thermal distribution of rotational energy.

However, in contradiction to the apparent agreement between CH and other flame temperatures are the observations that (1) the rotational distribution of the

$v=1$ vibrational level gives a temperature which is consistently several hundred degrees less than that in the $v=0$ level, (2) very rich acetylene flames have a CH "temperature" in excess of adiabatic, (3) CH "temperatures" of acetylene flames with added diluent do not decrease as rapidly as adiabatic temperatures, (4) rotational "temperatures" of CH in hydrogen-oxygen flames with small amounts of hydrocarbon are considerably less than adiabatic and increase with increased hydrocarbon, and (5) vibrational "temperatures" of CH in hydrogen flames with added hydrocarbons depend upon the hydrocarbon and do not follow the trend of the rotational "temperature." These facts indicate that some process other than thermal collision is producing excited CH.

The difficulty of finding a satisfactory mechanism for the formation of excited CH has led Gaydon and Wolfhard[5] to the favoring for this process of collisions of unexcited CH with other excited species rather than a true chemiluminescent formation. The present evidence does not lend definite support to either general view. Unless there are particular reactions to choose between, it appears hopeless to attempt to say more than that under certain conditions the formation of excited CH is not a thermal process.

Measurements[13] and calculations[14] of OH intensity distributions have shown that for flames with large emissivities it is possible to obtain "anomalous" distributions of rotational intensity that are caused by self-absorption. Such effects increase with increased emissivity of the source. The CH emission has been observed along the edge of the flame as well as at the center, this resulting in three times the intensity. If self-absorption were causing any abnormality in the rotational distribution, the measured "temperature" would be different in the two positions. Since no measurable difference was found, it is reasonable to assume that self-absorption was not a source of error.

The weak continuum in the region of 4000A should not be confused with the strong continuum in hydrocarbon flames burning with a large excess of fuel which gives the brightly luminous appearance to such flames. Such continua are apparently due to incandescent carbon particles formed in the combustion process; they have been used for temperature indications of rich flames.[15] Intensity measurements of the weak continuum observed in the present study of these hydrocarbon flames have not been previously reported.

In carbon monoxide-oxygen flames an ultraviolet continuum is well known.[16] It extends throughout the visible and near ultraviolet and is strongest in the region between 3500 and 4500A. The continuum has been attributed to the association reaction

$$CO+O=CO_2+h\nu,$$

which has sufficient energy to extend the continuum to 2300A.

The occurrence of the weak continuum in hydrocarbon flames in the same region as that in carbon monoxide flames is an indication of the possibility of a similar process for its formation. In addition, the increase of the continuum intensity relative to the line intensity with increasing oxygen is in agreement with a similar result reported by Hornbeck[17] in carbon monoxide-oxygen flames. For flames very rich with fuel the relative increase of continuum is probably caused by the formation of incandescent carbon particles. The decrease of the continuum intensity with added hydrogen indicates that the continuum in hydrocarbon flames is not the same as that observed in hydrogen flames, but rather that the hydrogen competes with the carbon monoxide for the atomic oxygen.

It is a pleasure to acknowledge the aid of Mr. W. R. Kane and to thank him for his assistance in obtaining some of the spectra and for discussions concerning possible mechanisms.

[13] G. H. Dieke and H. M. Crosswhite, "The Ultra-Violet Bands of OH", Bumblebee Series, Report No. 87 (Bur. Ord., U. S. Navy, 1948).

[14] S. S. Penner, Technical Report No. 5, U. S. Office of Naval Research (April, 1952).

[15] E. K. Plyler and C. J. Humphreys, J. Research Natl. Bur. Srandards 47, 456 (1951).

[16] A. G. Gaydon, *Spectroscopy and Combustion Theory* (Chapman and Hall, Ltd., London, 1948), second edition.

[17] G. A. Hornbeck, J. Chem. Phys. 16, 845 (1948).

Rotational "Temperatures" of OH in Diluted Flames*

W. R. KANE† AND H. P. BROIDA
National Bureau of Standards, Washington 25, D. C.
(Received May 12, 1952)

The effects of gaseous diluents upon the distribution of rotational energies of the electronically excited OH($^2\Sigma^+$) radical in flames at atmospheric pressure have been studied. Helium, argon, nitrogen, and oxygen have been added to stoichiometric mixtures of fuel and oxygen in amounts up to 90 percent of the total volume. In the reaction zones of the acetylene and methane flame diluted with helium, argon, or nitrogen, a departure from rotational equilibrium is found which increases with increasing dilution. This effect is absent in the hydrogen flame and in flames with excess oxygen. Vibrational and electronic nonequilibria are also indicated. These results are consistent with the hypothesis proposed in connection with low pressure studies (see references 2 and 4) that excited OH is formed in an exothermic reaction imparting high rotational energy to the products. Persistence of this rotational energy throughout the radiative lifetime, 10^{-6} sec, or 10^4 collisions, is indicated.

I. INTRODUCTION

RECENT spectroscopic studies[1–3] of OH in flames have revealed that under certain conditions an apparent nonequilibrium exists among rotational energy levels in the electronically excited ($^2\Sigma^+$) state. This nonequilibrium takes the form of an excess of intensity of lines from states with high rotational energy compared with the intensities determined for those states by an equilibrium thermal distribution. The effect is significant because of the information it may furnish concerning energy transfer and the mechanism of combustion and for the reason that the relative intensities of rotational lines in the ultraviolet spectrum of OH provide a convenient means for determining the temperatures of hot gasses which are in thermal equilibrium.

This nonthermal rotational distribution occurs in the primary reaction zone of many hydrocarbon flames. In the hot gases beyond the reaction zone, in which combustion has been completed, thermal equilibrium apparently exists, and the effect is not observed. For this reason nonthermal rotation is thought to be closely associated with reactions taking place during the combustion process.

While the electronically excited OH radical possesses nonthermal rotation in the reaction zones of certain flames, the ($^2\Pi$) ground state of OH has been found, from absorption spectra, to be in rotational equilibrium in the methane-air flame,[1] and in the present studies, in the acetylene-oxygen flame diluted with argon.

The nonthermal distribution of energy among various rotational levels of the excited state, although observed to a small extent at atmospheric pressure in the acetylene-oxygen flame,[2,3] is more pronounced in flames burning at low pressures. Gaydon and Wolfhard,[2,4] who have made extensive studies of low pressure flames, have proposed that this rotational nonequilibrium may arise from a highly exothermic reaction in which excited OH ($^2\Sigma^+$) radicals are formed with excess rotational energy, and that the effect of lowered pressures is to decrease the number of collisions that an excited OH radical will suffer during its radiative lifetime and thus retard the equipartition of this excess energy among the various rotational levels. Radiation from molecules excited in such a manner is said to be of chemiluminescent origin. Recently Penner has suggested that these nonthermal distributions at low pressure are caused by self-absorption.[5]

In the present studies it was found that the appearance of nonthermal rotation is enhanced by the addition of inert diluents to the flame. It is most likely that this is due primarily to a lowering of the average temperature, causing a decrease in both the equilibrium concentration of OH radicals and in the amount of radiation due to purely thermal excitation, thus allowing the chemiluminescent radiation from radicals with excess rotational energy to form a greater share of the total radiation observed. This explanation is borne out by the fact that as increasing amounts of diluent are added to a flame, radiation from the hot gases surrounding the inner cone becomes weak much more rapidly than radiation from the inner cone or reaction zone.

The work described here is a systematic survey of the effects of gaseous diluents upon the distribution of energy among the rotational levels of the excited OH radical in flames at atmospheric pressure. For this purpose the relative intensities of emission lines in the (0, 0) band of the $^2\Sigma^+ - ^2\Pi$ transition of OH in the vicinity of 3100A were measured in spectra of various regions of Bunsen flames in which stoichiometric mixtures of hydrogen, acetylene, or methane with

* This work was supported in part by the U. S. Office of Naval Research.
† Now at Los Alamos Scientific Laboratory, Los Alamos, New Mexico.
[1] H. P. Broida, J. Chem. Phys. **19**, 1383 (1951).
[2] A. G. Gaydon and H. G. Wolfhard, Proc. Roy. Soc. (London) A194, 169 (1948).
[3] H. P. Broida and K. E. Shuler, J. Chem. Phys. **20**, 168 (1952); **20**, 1383 (1952).
[4] A. G. Gaydon and H. G. Wolfhard, *Third Symposium on Combustion, Flame, and Explosion Phenomena* (Williams & Wilkins Company, Baltimore, Maryland, 1949), pp. 504–508.
[5] S. S. Penner, Tech. Report No. 5 ONR (April, 1952) and J. Chem. Phys. **20**, 507 (1952).

TABLE I.

Gas	Purity	Impurities
Hydrogen	99.8 percent	Oxygen
Methane	99.6 percent	
Acetylene	98 (estimate) percent	Acetone
Oxygen	99.7 percent	
Nitrogen	99.2–99.4 percent	Argon
Argon	99.4 percent	Nitrogen
Helium	99.99 percent	Air, hydrogen

oxygen were burned diluted with varying amounts of nitrogen, argon, helium, or oxygen. A flame in which 5 percent acetylene was added to a hydrogen-oxygen mixture diluted with argon was also studied. The three fuel gases were chosen because previous work had indicated that in the hydrogen flame there is rotational equilibrium,[3] while in the latter two there are departures from rotational equilibrium.[1,2,4] Small amounts of acetylene added to a hydrogen flame at low pressure are known to produce an abnormal rotational distribution of excited OH.[4] The diluent gases were chosen so as to provide a comparison of the influence of gases of different molecular structure, specific heats, and masses on the OH rotational energy distribution. The amount of diluent added was varied from zero to approximately 90 percent for each mixture of gases. For purposes of comparison, sodium line reversal "temperatures" were also measured.

The measurements can be conveniently discussed in terms of a rotational temperature.[6] When there is thermal equilibrium the populations of excited radicals in various rotational levels of a given electronic and vibrational state are proportional to

$$(2J+1)e^{-E_K/kT},$$

where E_K is the energy of a level with rotational quantum number K and the factor $2J+1$ is the statistical weight. J is the total angular momentum of the molecule, equal to $K+\frac{1}{2}$ and $K-\frac{1}{2}$, respectively, for the two orientations of the electron spin. The intensities I_{KL} of lines arising from the same electronic and vibrational transition and from transitions between various rotational levels K and L will be given by the expression

$$I_{KL}=CNA_{KL}\nu_{KL}e^{-E_K/kT},$$

where K is the rotational quantum number of the excited state, N the population in the ground state, A_{KL} a factor which is a product of the transition probability and statistical weight $2J+1$ of the excited state, ν_{KL} the frequency of the emitted radiation, and C a constant for a given electronic and vibrational transition.

A plot of $\log(I_{KL}/A_{KL}\nu_{KL}^4)$ *versus* E_K will be a straight line, the slope of which is proportional to the reciprocal of the temperature. The limitations on the use of this method for measurement of temperature should be clearly understood. If there is nonequilibrium, such a plot will probably not be linear, or if linear, will indicate a spurious value for the temperature. Strictly speaking, the temperature is not defined if the system is not in equilibrium, but even in such cases it is sometimes convenient to designate the value obtained for T as the "rotational temperature," and to regard it as a parameter describing the distribution of energy among the various rotational levels. Similar procedures may be applied to vibrational and electronic levels, resulting in vibrational and electronic "temperatures," which, for nonequilibrium, may not be equal to one another nor to the rotational "temperature."

Still another effect which may give rise to spurious results when this method is used is the absorption‡ of radiation within the flame.[7] Since the absorption is proportional to the intensity, intense lines are absorbed more strongly than weak ones, resulting in a lower apparent intensity for the stronger lines, which leads to a higher apparent temperature. This difficulty may be avoided by selecting lines of equal intensity and nearly the same frequency, where the absorption, at least in the first order, is the same, and computing the temperature from the transition probabilities and rotational energies. The temperature obtained by this method is designated as the "iso-intensity" temperature.[7] Successive pairs of lines will indicate the same temperature when the rotational energies follow a Boltzmann distribution.

Rotational temperatures were obtained by both of these methods in and above the inner cones of the flames described.

II. EXPERIMENTAL ARRANGEMENT

The flames studied were obtained by burning premixed gases in two burners, one an acetylene welding torch of 1.5-mm throat diameter, the other a 1-meter steel tube of 38-mm diameter with a nozzle of 12.7-mm throat diameter designed so as to provide a uniform flow velocity profile.

Commercial tank gases were used. Their composition, as specified by the supplier, is tabulated in Table I.

The flow of gas was controlled by needle valves and measured by floating ball type flow meters which had previously been calibrated against standard orifices. The accuracy of flow measurement is estimated to be between 5 and 10 percent. Total flow of gas through the burner ranged from 50 to 400 cm³/sec.

A Hilger, Littrow type spectrograph of aperture $f/30$, with quartz optics and a dispersion of 5.5A/mm, was employed to obtain the spectra. With a slit width of

[6] G. Herzberg, *Molecular Spectra and Molecular Structure I* (D. Van Nostrand Company, Inc., New York, 1950), second edition, pp. 124, 204.

‡ As a result of detailed calculations, Penner (see reference 17) concludes that all measured nonthermal distributions may be the result of self-absorption. A careful comparison between calculated and experimental distributions will be made in a forthcoming paper.

[7] G. H. Dieke and H. M. Crosswhite, "The Ultraviolet Bands of OH," Bumblebee Series, Report No. 87 (Bur. Ord. USN, 1948).

0.012 mm the resolving power of the instrument was approximately 10 000. The range of intensities in the ultraviolet was such that exposure times ranged from 5 seconds to 6 hours. Intensities of well-resolved rotational lines in the P_1 and R_2 branches of the (0, 0) band at 3064A, which are unaffected by satellite lines, were measured using a recording densitometer. An intensity calibration was carried out over the wavelength region of interest using a standard tungsten strip filament lamp with a quartz window and a rotating sector wheel. Temperatures computed from these data were reproducible to within ±3 percent for flames with no diluent. The accuracy diminished with the longer exposure times required for more dilute flames. It should be emphasized that these measurements were intended primarily for a comparison of large-scale effects over a wide range of conditions rather than for accurate determinations of flame temperatures.

A second spectrometer, a photoelectric, automatic recording grating monochromator§[3,8] with a resolving power of 55 000 was employed to verify results obtained with the prism instrument. The resolving power of this instrument was sufficiently high to permit spectral absorption measurements to be made.

Line reversal temperature measurements[9] at points 3 to 5 mm above the inner cone were carried out by the standard technique of introducing sodium into the flame and matching the brightness of a standard tungsten lamp to that of the D lines. Measurements were made throughout the range of temperatures allowed by the brightness of the tungsten strip lamp used as a comparison source.

III. RESULTS

A. The Hydrogen-Oxygen Flame

No evidence was found for rotational nonequilibrium in any region of the hydrogen-oxygen flame. Unfortunately, in the case of hydrogen certain errors caused some gas mixtures to be slightly lean in fuel, so that a constant, stoichiometric fuel-oxygen ratio was not maintained for varying amounts of diluent. The OH rotational 'temperatures" obtained are in fair agreement with the measured sodium line reversal "temperatures" and with the adiabatic temperatures calculated from thermodynamic data.[10] In Fig. 1 measured OH rotational "temperatures" in the inner cone and above the inner cone, measured sodium line reversal "temperatures," and calculated adiabatic temperatures are plotted as functions of the percentage of the total mixture of argon added as diluent to a stoichiometric mixture of hydrogen and oxygen. Similar results were found with nitrogen and with helium as diluents. As might be expected, taking into consideration heat losses and temperature gradients, the temperature above the inner cone lies below that of the inner cone itself, which in turn lies below the calculated adiabatic flame temperature. The trends of both the OH and line reversal "temperatures" follow those of the calculated temperatures.

B. The Acetylene-Oxygen and Methane-Oxygen Flames

Rotational nonequilibrium was observed in the reaction zones of the acetylene, methane, and hydrogen-acetylene flames diluted with nitrogen, helium, and argon. Stoichiometric proportions of fuel and oxygen were maintained in these flames. The hot gases above the reaction zone were found to possess a normal distribution.

The nature of the nonequilibrium observed is best described by referring to the logarithmic intensity plot whose slope, under equilibrium conditions, gives the rotational temperature. In cases of nonequilibrium this plot consists of two intersecting straight line segments, one through points arising from low-lying rotational levels and the other through points arising from higher levels. The lower levels indicate a relatively normal temperature and the upper levels an abnormally high "temperature." Figure 2 is such a logarithmic plot of the intensities in an acetylene-oxygen flame with 90 percent argon, showing the two distinct line segments with the intensity distribution of the higher levels giving an apparent "temperature" of 5500°K, and the lower levels 1360°K. The calculated adiabatic temperature is 1860°K. Similar curves were obtained for all hydrocarbon flames studied, when diluted with large amounts of inert gases.

It is convenient, in discussing the results, to take the rotational "temperature" indicated by the group of

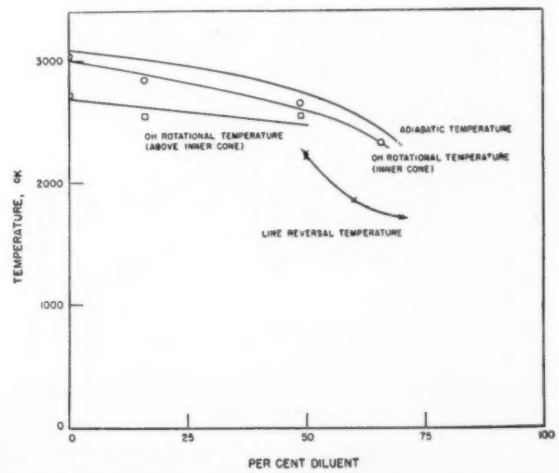

FIG. 1. Measured "temperatures" plotted *vs* percent diluent in the hydrogen-oxygen flame diluted with argon. The calculated adiabatic temperature is added for comparison.

§ This instrument was constructed by the Research Department of the Leeds and Northrup Company and is on loan to the National Bureau of Standards on a field trial basis.

[8] W. Fastie, J. Opt. Soc. Am. **40**, 800 (A) (1950).

[9] E. Griffith and J. H. Awberry, Proc. Roy. Soc. (London) A123, 401 (1929).

[10] Hottel, Williams, and Satterfield, *Thermodynamic Charts for Combustion Processes* (John Wiley & Sons, Inc., New York 1949).

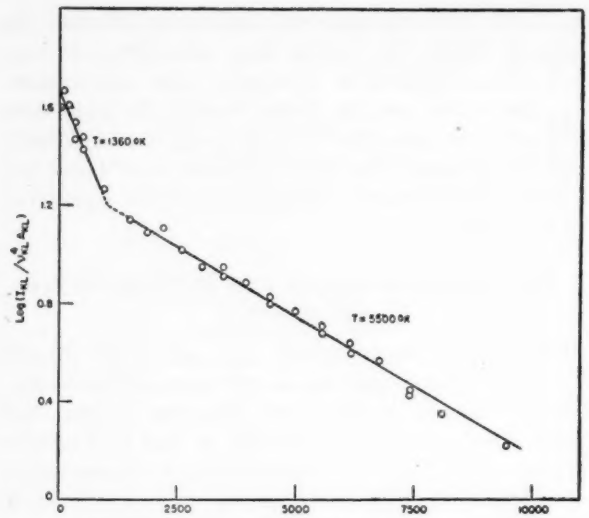

FIG. 2. Abnormal rotational distribution in the inner cone of the acetylene-oxygen flame diluted with 90 percent argon. Log($I_{KL}/\nu_{KL}{}^4 A_{KL}$) is plotted *vs* E_K for resolved lines in the P_1, R_1, and Q_1 branches of the (0, 0) band of the $^2\Sigma^+ - {}^2\Pi$ transition of OH.

higher rotational levels as a measure of the degree of nonequilibrium. In Figs. 3 to 5 this quantity is plotted against the percentage of added diluent for the acetylene, hydrogen-acetylene, and methane flames. Sodium line reversal temperatures, and, for flames with added nitrogen, adiabatic temperatures, are included for comparison. The most important property of these curves is the steady increase of the rotational "temperature" in the inner cone with increasing dilution, approaching values of the order of 10 000°K in the hydrogen-acetylene flame diluted with 90 percent argon. This flame exhibits the effect to the greatest degree, followed closely by acetylene, while for methane it is somewhat less pronounced. Although rotational temperatures differ little for the various diluents, the value is highest for helium and lowest for argon.

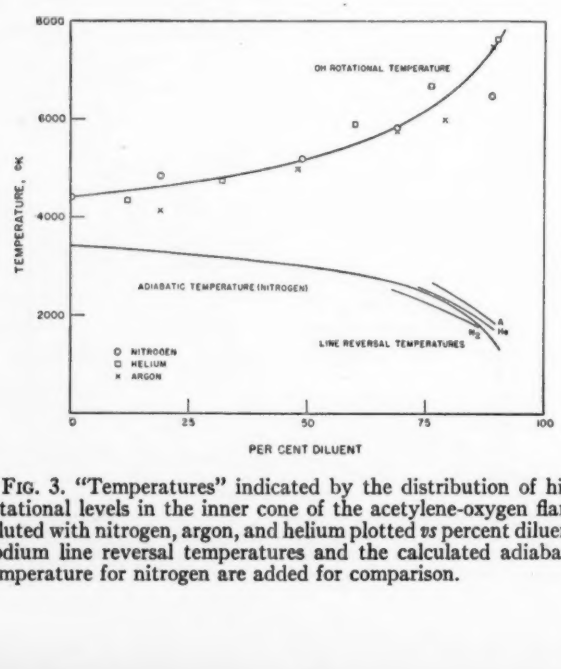

FIG. 3. "Temperatures" indicated by the distribution of high rotational levels in the inner cone of the acetylene-oxygen flame diluted with nitrogen, argon, and helium plotted *vs* percent diluent. Sodium line reversal temperatures and the calculated adiabatic temperature for nitrogen are added for comparison.

The reaction zone of the acetylene flame diluted with excess oxygen exhibits a radically different rotational distribution from the flames with added nitrogen, helium, or argon. The logarithmic plot consists of a single straight line, indicating a Boltzmann distribution. The rotational "temperature" decreases with increasing dilution, but more slowly than the adiabatic flame temperature. In Fig. 6 rotational "temperatures" obtained both from the logarithmic plot and by the iso-intensity method in the reaction zone and the adiabatic flame temperatures are plotted *versus* the amount of added diluent. The distribution of well-resolved lines made it necessary to use lines from the R_2 branch for iso-intensity measurements and lines chiefly from the P_1 branch for the logarithmic plot. Although there are fewer well-resolved lines in the R_2 branch, both high and low K lines lie in a narrow wavelength region, which

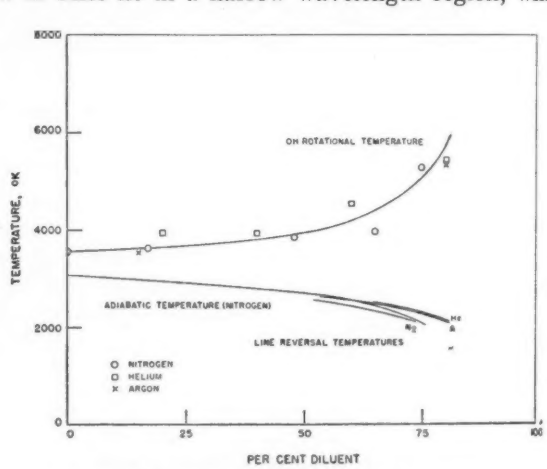

FIG. 4. "Temperatures" in the methane-oxygen flame with inert diluents.

tends to eliminate possible errors in the iso-intensity measurements. The difference between the "temperatures" measured by the two methods is not clearly understood. However, the important feature of the curves in Fig. 6 is that the general trends are markedly different from those observed with other diluents. The amount of oxygen in excess of that required for a stoichiometric mixture is considered to be diluent.

The effect of the fuel-oxygen ratio upon the rotational distribution was also investigated. In the acetylene-oxygen flame diluted with 60 percent nitrogen, "temperatures" were obtained for fuel-oxygen ratios twice stoichiometric, stoichiometric, and half-stoichiometric. The values obtained were 5000°K, 4810°K, and 4170°K, respectively.

The acetylene flame diluted with excess oxygen is also characterized by the appearance of the hydrocarbon flame bands, as previously reported by Hornbeck and Herman.[11] These bands were not observed in

[11] G. A. Hornbeck and R. C. Herman, Ind. Eng. Chem. 43, 2739 (1951).

flames with diluents other than oxygen even though the adiabatic temperatures were approximately the same.

Rotational temperatures obtained from the region 2 mm above the inner cone disclosed no abnormality in any of the flames. Their accuracy was so seriously limited by the low intensities in that region that their numerical values are not presented.

In order to make certain that poor resolution of individual lines or other instrumental effects were not responsible for the results observed, spectra were taken in several representative flames with the high resolution, grating monochromator described previously. This instrument could not be used for all the measurements because intensities from many flames were too weak for photoelectric detection. The results obtained agree to within 15 percent with those obtained at lower resolution and show clearly the presence of the nonthermal rotational distribution.

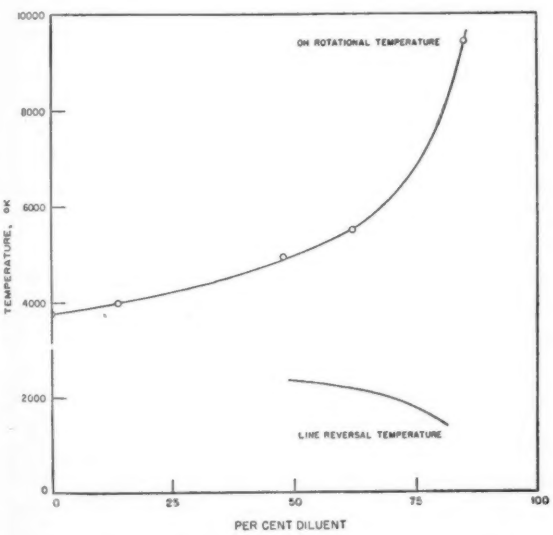

FIG. 5. "Temperatures" in the hydrogen 5 percent acetylene-oxygen flame diluted with argon.

C. Intensities

In addition to the comparison of the intensities of individual lines, a study was made of the manner in which the over-all intensity of the (0, 0) band of OH in the reaction zone varied with the nature and quantity of the added diluent. In the hydrocarbon flames a significant trend occurs in the relative total intensities of the (0, 0) band in the inner cone and in the hot gases above it as increasing amounts of diluent are added. With no diluent the intensities of individual lines, and hence the total intensities, are practically identical in both regions. With the introduction of diluent the intensity emitted from each region decreases, but that emitted from above the inner cone decreases much more rapidly than that from the inner cone itself. The effect is more pronounced for acetylene than for

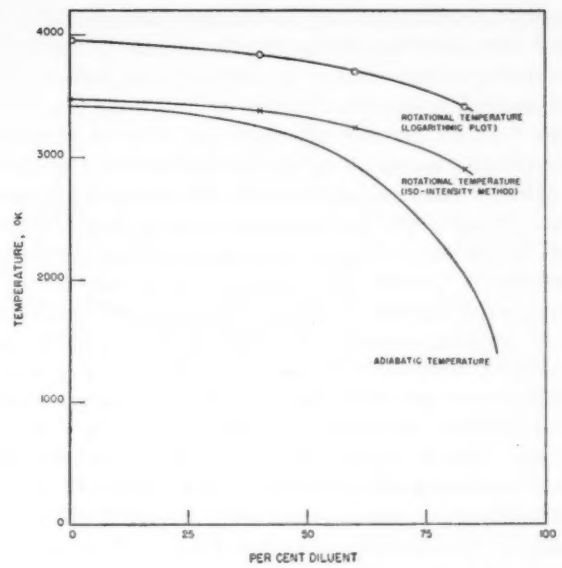

FIG. 6. Measured rotational "temperatures" in the acetylene-oxygen flame diluted with excess oxygen. The calculated adiabatic temperature is added for comparison.

methane. Examination of spectra of methane flames shows that intensities of lines arising from low-lying rotational levels remain sensibly the same in the two regions, but that lines from higher levels are progressively enhanced in the inner cone, causing the difference in total intensity. This may be seen in Fig. 7, in which spectra of the methane-oxygen flame diluted with varying amounts of nitrogen are shown. In acetylene flames all rotational lines are weakened relatively in the region above the reaction zone.

For several flames, the observed inner cone intensity was compared with that predicted from the temperature and equilibrium concentration of OH for ordinary thermal radiation. The values for the calculated in-

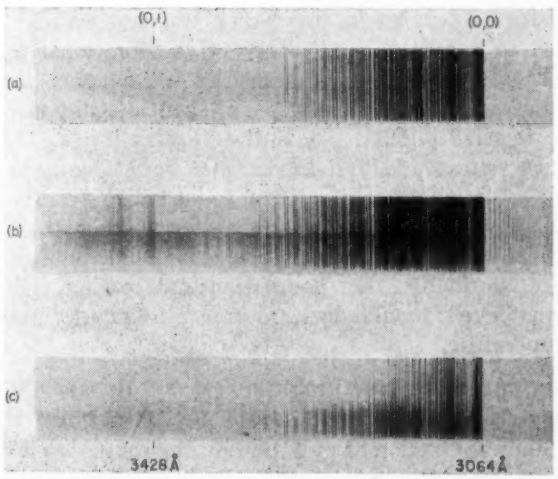

FIG. 7. The (0, 0) band of the $^2\Sigma^+ - ^2\Pi$ transition of OH in a methane-oxygen flame diluted with nitrogen. The inner cone occupies the lower half of each spectrum; (a) 0 percent nitrogen, (b) 30 percent nitrogen, (c) 70 percent nitrogen.

tensity are accurate only to within a factor of 2 or 3, since the thickness of the emitting zone in the flame had to be estimated and the temperature gradients are not accurately known. For the hydrogen-oxygen flame with 0 to 60 percent nitrogen, the ratio of observed intensities was 4×10^{-4}, while the predicted value is 1×10^{-4}. This is considered to be fair agreement. In contrast to this, for the acetylene-oxygen flame with 0 and 85 percent nitrogen the observed intensity ratio was 4×10^{-4}, while the predicted ratio was 6×10^{-8}. Thus, with 85 percent nitrogen there are apparently 10^4 times as many excited OH radicals as would be produced by thermal excitation, provided that they are in equilibrium concentration in the undiluted flame. Furthermore between the acetylene-oxygen flames diluted with 80 percent argon and 80 percent nitrogen there is a difference in adiabatic temperatures of 420°K, giving rise to a predicted intensity ratio of 7×10^{-3}. The ratio of observed intensities is 5×10^{-1}. For methane the magnitudes of such differences were much smaller. However, the methane flame covered a much smaller temperature range than did the acetylene flame, so that the effect would be expected to be less pronounced. The intensity observed in the acetylene-oxygen flame diluted with oxygen is somewhat weaker than for the inert diluents, but still greatly in excess of that predicted for thermal radiation.

D. Relative Vibrational Populations

Although the spectra taken in these studies were intended primarily for a comparison of intensities in the (0, 0) band, it was considered desirable, upon discovering the high degree of rotational nonequilibrium, to examine the relative intensities of different vibrational bands. The acetylene flame with added argon was chosen for study, and the intensities of well-resolved, low-lying rotational lines from the (0, 0), (1, 0), and (2, 1) bands were measured and compared. The intensity calibration in this region was not sufficiently good to permit the calculation of a vibrational temperature, so the ratios of intensities in the higher bands to those in the (0, 0) band were taken as a measure of the relative populations in the various levels. These ratios were found first to decrease very slightly with increasing dilution, and then to increase steadily to a final value roughly twice that for no diluent. This indicates a pronounced vibrational nonequilibrium, since normally the populations in higher vibrational levels should decrease rapidly with decreasing temperature.

E. Absorption Measurements

Since absorption of radiation by the source itself can give a spuriously high value for the measured rotational temperature, a study was made of absorption in an acetylene flame diluted with argon in order to enable an estimate to be made of the importance of this effect. For this purpose the high resolution grating monochromator and hydrogen discharge source, giving a continuum in the region of 3000A, were used. In a flame diluted with 85 percent argon absorption in the inner cone was negligible. Above the inner cone, where the optical path through the hot gases is several times as long, the absorption amounted to approximately 20 percent for the strongest lines. In the same flame diluted with 90 percent argon, the absorption in all regions of the flame was too weak to be measured. These absorption spectra were also used to obtain the rotational "temperature" of the ground state, which was found to be close to the adiabatic temperature.

Since the experimental slit width of the monochromator was approximately the same as the half-width of the OH lines in the flame, it is to be expected that the measured peak absorption from a continuous source would be somewhat less than the true peak absorption. This was checked by using the OH emission from a high frequency electrodless discharge (150 megacycles) through a mixture of argon and water vapor, with a partial pressure of water of 0.2 mm Hg and a total pressure of 3 mm Hg. Emission lines from this source are narrow and much more intense than corresponding lines in the flame, so that absorption in the flame is independent of the monochromator resolution. The apparent absorption of the discharge lines in the flame was nearly three times that of the peak absorption of the continuum.

Penner[5] has recently calculated rotational intensity distributions for various emissivities. These results show that the curvature of the logarithmic plots due to self-absorption within the flame (e.g., Fig. 4) is negligible for emissivities of the $P_1(1)$ line less than 0.3. For acetylene flames with 85 percent argon through the $\frac{1}{2}$-inch burner the line absorption measurements indicate an emissivity of 0.4 for the $P_1(1)$ line. With 88 percent argon the emissivity is 0.17. This trend in emissivity is to be expected due to the rapid decrease in temperature and in the concentration of OH. In addition, since the emissivity is decreasing while the abnormality increases, it appears safe to conclude that measured nonthermal rotational distributions in highly diluted flames are not caused by self-absorption.

In flames with a smaller amount of diluent, however, there was certainly higher absorption. An estimate of the magnitude of its effect upon measured rotational "temperatures" was obtained by comparing temperatures obtained by the iso-intensity method with those given by the logarithmic intensity plot for the region above the inner cone, in which there is rotational equilibrium. It was found that while for flames with small quantities of added diluent the "temperatures" obtained from the logarithmic plot are somewhat high due to self-absorption, this error decreases rapidly with increasing dilution, and the observed rotational nonequilibrium cannot be attributed to this effect. The inner cone rotational "temperatures" have been com-

puted from the logarithmic plot, since it is not possible to apply the iso-intensity method to cases of non-equilibrium.

IV. DISCUSSION

The principal result of this work is that the addition of inert diluents to the acetylene-oxygen and methane-oxygen flames reveals a phenomenon that has previously been found to appear in low pressure flames[2,4] and in electrical discharges through water vapor,[12] that is, the existence of two distinct groups of electronically excited OH radicals, one exhibiting a relatively normal distribution of rotational energies, and the other consisting of particles possessing abnormally high rotational energies. The interpretation of Gaydon and Wolfhard,[1] proposed in connection with flames at low pressure, that electronically excited OH is formed with a high rotational energy in an exothermic reaction, appears to be equally valid here. Further evidence in support of this hypothesis is furnished by the nonthermal nature of the radiation from the inner cone. For example, as shown earlier, the intensity of the radiation from an acetylene-oxygen flame diluted with 85 percent nitrogen is 10^4 times greater than that predicted for thermal radiation. However, the explanation for the appearance of nonthermal rotation at low pressures, that the collision frequency is reduced in consequence of the low total pressure, retarding equipartition of rotational energy, is not entirely applicable to the present results at atmospheric pressure.

As stated earlier, probably the most important function of inert diluents is the lowering of the equilibrium temperature of the flame, causing a rapid decrease in radiation of thermal origin. The large amount of radiation originating from OH radicals in thermal equilibrium in undiluted flames could mask the radiation from radicals with abnormally high rotational energy. Thus radiation from excited radicals with abnormally high rotational energy may be present at all times, but is observed only when the background of thermal radiation is reduced to a sufficiently low level. This also is suggested by the results of temperature scans through similar flames,[13] which show that the rotational temperature is highest at the base of the inner cone, where the layer of hot gases surrounding the inner cone is thinnest, and decreases with increasing height in the flame, as the contribution from an increasingly thicker mantle of hot gases is superimposed on the radiation from the reaction zone.

Another possible function of inert diluents is to influence exchange of rotational energy between excited OH radicals and other particles present in the gas during the radiative lifetime of the excited state. It appears unlikely that high rotational energies of the $^2\Sigma^+$ state of OH are produced through collisions, since both the ground state of OH, as determined from absorption measurements, and the excited state of the CH radical[14] exhibit normal rotational temperatures. If no such process exists, then the high rotational energy possessed by the excited OH radical must persist throughout its radiative lifetime. The transition to the ground state is half-forbidden, so that the lifetime is longer than for most electronic transitions, having been measured by Oldenberg and Rieke[15] to be 3.8×10^{-6} sec. This corresponds to 10^4 collisions at atmospheric pressure. That the OH radical is able to retain its rotational energy through this many collisions is of interest, since the times required for other diatomic molecules to reach equilibrium with the translational degrees of freedom are of the order of 10^{-9} to 10^{-8} sec, corresponding to 10^1 to 10^2 collisions.[16]

The combined effects of dilution and the lowering of the equilibrium temperature possibly could influence the transfer of rotational energy in collisions by reducing greatly the concentrations of particles that might be especially effective in removing rotational energy from the excited OH radical, such as OH in the ground state, hydrogen atoms, or other species. In particular the concentration of OH is reduced by greater than a factor of ten over the range of dilution used in these experiments. In addition to this effect, the introduction of inert diluents causes the reaction zone rapidly to become thicker, probably reducing the concentrations of some such species in this region, since many of them may be present in the narrow reaction zone in concentrations far in excess of those for thermal equilibrium.

The fact that rotational temperatures in the inner cone were practically identical for all three inert diluents suggests that the diluent gas molecules themselves have little effect in collisions with the excited OH radical, since otherwise the three types of particles at different mass and molecular structure would be expected to be different in their effectiveness in removing rotational energy. In contrast to this, Oldenberg, in studying the abnormal rotational distribution of excited OH produced in an electrical discharge, found that the introduction of a small amount of helium caused the disappearance of high rotational levels, and he attributed this to the effectiveness of the light helium atom in removing rotational energy from the OH radical. Lyman[17] was unable to confirm this in similar experiments.

The partial disappearance of the nonthermal rotation in the acetylene flame in the presence of a large excess of oxygen indicates that particles efficient in removing rotational energy from the radical are present. The appearance of the hydrocarbon flame bands suggests the first alternative, since it indicates that certain

[12] O. Oldenberg, Phys. Rev. **46**, 210 (1934).
[13] H. P. Broida and G. T. Lalos, J. Chem. Phys. **20**, 1466 (1952).
[14] A. G. Gaydon and H. G. Wolfhard, Proc. Roy. Soc. (London) **A199**, 89 (1949).
[15] O. Oldenberg and F. F. Rieke, J. Chem. Phys. **6**, 439, 779 (1938).
[16] A. J. Zmuda, J. Acoust. Soc. Am. **23**, 472 (1951).
[17] E. R. Lyman, Phys. Rev. **53**, 379 (1938).

reactions taking place in the oxygen diluted flame are different from those taking place in the inert gas diluted flames. Evidence for the second alternative, however, is furnished by the high intensity of the radiation emitted from the inner cone, which, although somewhat weaker than that from flames with inert diluents, is still many times thermal intensity, indicating chemiluminiscence. In addition, while in the inner cone there exists a single Boltzmann distribution of rotational energies, the rotational "temperatures" obtained are higher than the calculated adiabatic temperatures, the discrepancy between the two increasing with increasing dilution. For comparison in the hydrogen flame, where there is apparent rotational equilibrium, the opposite is true; inner cone rotational "temperatures" are several hundred degrees lower than adiabatic temperatures. This suggests that while the gross abnormality seen in flames with inert diluents is removed by excess oxygen, complete equipartition of rotational energy is not achieved during the radiative lifetime.

The principal results of these studies are as follows:

(1) The hydrogen flame diluted with inert gases exhibits rotational equilibrium.

(2) The acetylene and methane flames diluted with inert gases exhibit a rotational nonequilibrium which is characterized by the presence of two groups of excited OH radicals, each in a Boltzmann distribution. A vibrational nonequilibrium is also observed.

(3) OH radiation from the hydrogen flame is apparently of thermal origin, while that from the hydrocarbon flames is largely due to chemiluminescence.

(4) An excess of oxygen causes the partial disappearance of the rotational abnormality seen in flames diluted with inert gases and the simultaneous appearance of the hydrocarbon flame bands.

It is a pleasure to acknowledge the assistance of Mr. G. H. Morgan in obtaining sodium line-reversal temperatures; these measurements and flame speed data will be presented in more detail elsewhere.

THE JOURNAL OF CHEMICAL PHYSICS VOLUME 21, NUMBER 2 FEBRUARY, 1953

Some Thermal Reactions of the Higher Iron Carbides*

ERNST M. COHN† AND L. J. E. HOFER†
Fuels Technology Division, Bureau of Mines, Pittsburgh, Pennsylvania
(Received August 11, 1952)

One of the undesirable side reactions of the Fischer-Tropsch synthesis is deposition of carbon. To ascertain whether thermal reactions of iron carbides might cause this deposition and to learn more about the nature of iron carbides, the transition from hexagonal close-packed (h.c.p.) iron carbide to Hägg iron carbide and the reaction of higher iron carbide with metallic iron to form cementite have been studied in a copper- and alkali-promoted iron catalyst by means of a magnetic balance.

The transition from h.c.p. to Hägg iron carbide is heterogeneous, with no apparent change of the compositions of both carbides, nor any detectable solubility of one carbide in the other. The data confirm the narrow range of composition of Hägg carbide and the fact that it contains somewhat more iron than corresponds to the formula Fe_2C.

The synthesis of cementite from metallic iron and higher iron carbide proceeds via Hägg carbide and only above about 320°C. It does not go to completion up to 440°C; above that temperature, decomposition of Hägg carbide into cementite and free carbon is sufficiently rapid to prevent completion of the synthesis.

The data show that deposition of carbon on iron catalysts during the Fischer-Tropsch synthesis is not caused by thermal reactions of iron carbides, unless h.c.p. iron carbide should contain more carbon than Hägg iron carbide. A possible explanation of the apparent stabilizing effect of copper on h.c.p. iron carbide is given.

INTRODUCTION

AMONG the metastable interstitial alloys of transition metals, the carbides of iron occupy an important position because of their dual role in catalytic chemistry and in metallurgy. Their preparation by carburization of iron oxide, iron nitride, or finely divided iron[1–5] and their formation in the course of the Fischer-Tropsch synthesis[2,5–8] have been described. Table I presents a summary of their structural and magnetic characteristics.

This study is concerned with two thermal reactions of the higher iron carbides: the transformation from hexagonal close-packed (h.c.p.) to Hägg iron carbide, and the synthesis of cementite from higher iron carbide and metallic iron. It was made to show the effect of

* Part of a thesis submitted to the University of Pittsburgh by Ernst M. Cohn in partial fulfillment of the requirements for the degree of Master of Science.

† Physical Chemist, Synthetic Fuels Research Branch, Bureau of Mines, Region VIII, Bruceton, Pennsylvania.

[1] K. H. Jack, Proc. Roy. Soc. (London) **A195**, 34 (1948).

[2] H. Pichler and H. Merkel, Bureau of Mines Tech. Paper 718 (1949).

[3] Hofer, Cohn, and Peebles, J. Am. Chem. Soc. **71**, 189 (1949).

[4] L. J. E. Hofer and E. M. Cohn, J. Chem. Phys. **18**, 766 (1950); U. S. Patent 2,535,042 (1950).

[5] H. Merkel and F. Weinrotter, Brennstoff-Chem. **32**, 289 (1951).

[6] H. Lefebvre and G. LeClerc, Compt. rend. **203**, 1378 (1936); Congr. Chim. Ind. Compt. rend., 18th Congr. Nancy, 725 (1938).

[7] H. C. Eckstrom and W. A. Adcock, J. Am. Chem. Soc. **72**, 1042 (1950).

[8] Anderson, Hofer, Cohn, and Seligman, J. Am. Chem. Soc. **73**, 944 (1951).

TABLE I. Structural and magnetic characteristics of iron carbides.

Name	Composition	Crystal structure	Unit-cell dimensions, kx	Curie point, °C	Specific magnetization at room temperature, cgs/g
[a]	"FeC"	···	···	247±3	···
Hexagonal close-packed or ε-iron carbide	$Fe_{2+}C$[b]	Hexagonal close-packed	$a=2.749$ $c=4.340$	380	~139
Hägg or χ-iron carbide	$Fe_{2+}C$	[c]	[c]	247±3	128[d]
Cementite	Fe_3C	Orthorhombic	$a=4.517$ $b=5.079$ $c=6.730$	212±3	139

[a] This carbide has only been found in catalysts used in the fluidized Fischer-Tropsch process (reference 7).
[b] $Fe_{2+}C$ is used in this paper to indicate that the carbide contains more iron than corresponds to Fe_2C.
[c] Doubtful, as stated by K. H. Jack. Discussion and papers presented at the Ninth Annual Pittsburgh Conference on X-Ray and Electron Diffraction, Mellon Institute, Pittsburgh, Pennsylvania, November 29 and 30, 1951.
[d] See J. Crangle and W. Sucksmith, J. Iron Steel Inst. **168**, 141 (1951).

reactions in the iron-carbon system on an undesirable side reaction in the Fischer-Tropsch synthesis, namely, deposition of free carbon on the catalyst surface, and to learn more about the nature and reactivities of higher iron carbides.[9]

EXPERIMENTAL

The reactions were studied by means of a magnetic balance;[10] this instrument permits continuous measurements of reactions of solids[11] as well as qualitative and quantitative analyses of ferromagnetic mixtures.[12] The analyses were substantiated by x-ray diffraction diagrams.[3]

A precipitated, doubly promoted iron catalyst (Bureau of Mines catalyst P-3003.1,[3] Fe:Cu:K_2O::100:10:0.32) was used because its activity had been studied extensively and because higher iron carbide can be prepared quantitatively with such doubly promoted catalysts in a reasonable time.[2] The catalyst was reduced to virtually constant weight with hydrogen at 208°C for 1164 hours and then carburized with carbon monoxide at 170°C for 464 hours to a carbon-iron weight ratio of 0.1075 (the theoretical ratio for Fe_2C is 0.1076). X-ray analysis showed that all the iron had been converted to h.c.p. iron carbide, while thermomagnetic analysis revealed the presence of a barely detectable amount of Hägg carbide. Samples of this material were used to study the mode of transition from h.c.p. to Hägg carbide, and from Hägg carbide to cementite.[13]

Another batch of the same catalyst was reduced to virtually constant weight with hydrogen at 220°C for 327 hours and then carburized with carbon monoxide at 188°C for 24¾ hours to a carbon-iron ratio of 0.06966 (the stoichiometric ratio for cementite is 0.07163). X-ray analysis showed the presence of metallic iron and h.c.p. iron carbide. The absence of Hägg carbide was substantiated by magnetic analysis, which gave a point of inflection of 340°C. This was undoubtedly due to kinetic effects and not a true Curie point; as will be shown, the preparation underwent chemical changes as low as 100°C below the point of inflection. (A true Curie point is the characteristic temperature at which the ferromagnetism of a substance disappears while no phase change occurs. Phase changes usually entail changes of magnetic moments and give rise to points of inflection on thermomagnetic curves. Unlike true Curie points, such points of inflection are not characteristic temperatures but may be shifted at will by varying the rate of heating of the substance.[3,12]) This preparation was used to follow the transition from h.c.p. to Hägg carbide, to study the kinetics of that reaction, and to investigate the synthesis of cementite from Hägg carbide and metallic iron.[4]

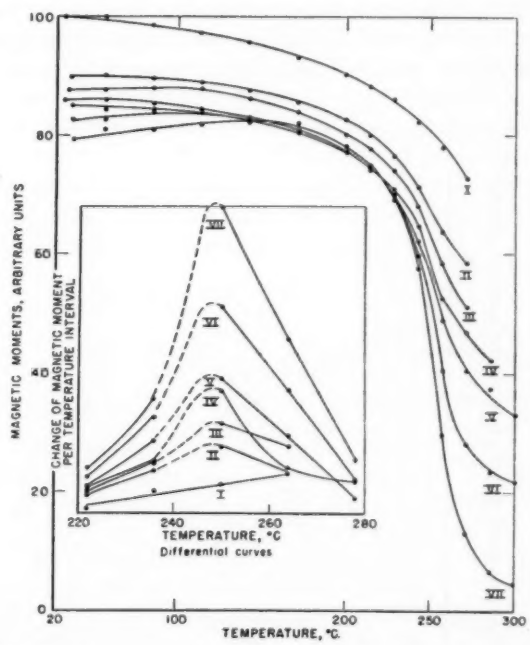

FIG. 1. Thermomagnetic curves showing the discontinuous transition from hexagonal to Hägg iron carbide (fully carburized sample).

[9] The compositions of the h.c.p. and Hägg carbides were originally thought to correspond to the formula Fe_2C (see reference 3 and R. Brill, FIAT Reel R-19, Frames 7136–7147). Later, Jack expressed the opinion that h.c.p. iron carbide may have a range of composition from Fe_3C to Fe_2C, corresponding to the h.c.p. nitride of iron [K. H. Jack, J. Iron Steel Inst. **169**, 26 (1951)]; he also showed that the formula for Hägg carbide is circa $Fe_{20}C_9$ (see reference 1). More recent, as yet unpublished data indicate that h.c.p. iron carbide (obtained by M. Cohen and E. C. Roberts upon tempering of martensite) and Hägg carbide (obtained by H. C. Eckstrom and W. A. Adcock upon carburization of finely divided iron) have the same composition, namely, $Fe_{2.4}C$ (reference c of Table I). The assumption of equal composition for both higher carbides of iron is immaterial for the determination of the mode of transition from one to the other, but it is quite important for evaluation of the kinetic data.

[10] Storch, Anderson, Hofer, Hawk, Anderson, and Golumbic, Bureau of Mines Tech. Paper 709, 132 (1948).

[11] Hofer, Cohn, and Peebles, J. Phys. Colloid Chem. **53**, 661 (1949); **54**, 1161 (1950).

[12] L. J. E. Hofer and E. M. Cohn, Anal. Chem. **22**, 907 (1950).

[13] E. M. Cohn and L. J. E. Hofer, J. Am. Chem. Soc. **72**, 4662 (1950).

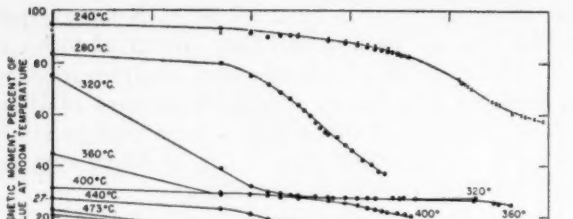

FIG. 2. Isothermal decomposition of a partly carburized, precipitated iron Fischer-Tropsch catalyst.

RESULTS

Mode of Transition from h.c.p. to Hägg Iron Carbide

Figure 1 represents magnetic analyses, obtained by slow heating and simultaneous measurement of the magnetic moments at about 550 gauss, of fully carburized h.c.p. iron carbide after each heat treatment according to the schedule of Table II. At the end of the heat treatments, the magnetic moment at 300°C had dropped to less than 5 percent of its original value at room temperature, showing that the reaction was essentially complete. The insert in Fig. 1 clearly shows the development of the invariant Curie point of Hägg carbide during the treatment. The reaction was therefore heterogeneous, and the composition of Hägg carbide remained constant throughout. To determine what changes, if any, occurred in the h.c.p. carbide, another sample of the same preparation was heated for two hours at 287°C and then subjected to magnetic analysis. Curie points at 250° and 380°C showed that some transformation had taken place but that the composition of the remaining h.c.p. iron carbide had not changed.

The same results were obtained with the partly carburized sample. An analysis of the h.c.p. iron carbide in that specimen was impossible, because the synthesis of cementite from Hägg carbide and metallic iron would have introduced spurious effects into the thermomagnetic curve. The heating schedule of this sample is shown in Table III. The kinetic data obtained with this preparation indicate that h.c.p. iron carbide had been essentially completely converted to Hägg carbide by heating at 260° to 274°C for 24 hours, while heating to about 340°C was necessary to complete the same transformation in a fully carburized sample (Table II). Although the heating schedules cannot be compared directly, it is obvious that the transformation was faster in the partly carburized sample. This difference in rates of reaction may be explained by assuming that strains are present in the partly carburized crystallites (carburization occurs by nucleation[14]) because of the difference in structure and dimensions of the two phases, carbide and iron. Such strains would increase the free energy of the crystallites and supply part of the energy necessary for rearrangement of the carbide from the h.c.p. to the Hägg structure.

TABLE II. Heating schedule for conversion of h.c.p. to Hägg carbide (fully carburized sample).

Heating period	Reaction temp, °C	Time at temp, hours
I	...	...
II	274	1
III	274	1
IV	274	3
V	287	2
VI	300	1
	314	1
VII	342	1

FIG. 3. Arrhenius plot to determine the activation energy for the transition from hexagonal to Hägg iron carbide.

Kinetic Studies

Isothermal reactions of several samples of partly carburized catalyst are shown in Fig. 2, where the magnetic moments are plotted as a function of time, with temperature as the parameter. For convenience, the time scale is logarithmic. The magnetic moment is expressed as percent of the moment at room temperature, so that all runs are directly comparable, regardless of the masses of the individual samples. A plateau is observed at 27 percent, marking the end of the transition from h.c.p. to Hägg carbide and the beginning of the synthesis of cementite from Hägg carbide and iron, as established by thermomagnetic and x-ray analyses. This arrest of the magnetic moment occurred because the reaction rates differed markedly. A clear distinction

[14] Podgurski, Kummer, DeWitt, and Emmett, J. Am. Chem. Soc. 72, 5382 (1950).

between both reactions was thus possible. Furthermore, the magnetic moment of iron changes only very little in the range of temperatures studied, so that no perceptible change was noticeable in the position of the plateau as a function of temperature.

After 10 000 minutes of heating at 240°C, the temperature of that sample was raised to 320°C to hasten completion of the rearrangement. No change of magnetic moment occurred after two hours' heating at that temperature, and subsequent magnetic analysis proved that cementite had not been formed in detectable quantity. A linear relationship exists between the magnetic moment and the extent of reaction (see appendix), so that the amount of h.c.p. iron carbide could be calculated from the data. A plot of the percentage of remaining h.c.p. iron carbide as a function of time at 240°C showed the absence of an induction period. An empirical rate law was found by plotting the logarithm of the rate (interpolated from the data) as a function of the logarithm of the percentage of remaining h.c.p. iron carbide. The slope of the line, 5/3, was the apparent order of the reaction and fitted the data from

TABLE III. Heating schedule for conversion of h.c.p. to Hägg carbide (partly carburized sample).

Heating period	Reaction temp, °C	Time at temp, hours
I	...	...
II	260	1
III	260	1
IV	274	1
V	274	1
VI	274	2.5
VII	274	17.5

100 to 3 percent of h.c.p. iron carbide. The same rate law, of which no physical interpretation can be made at present, correlated the measurements at 240°, 280°, and 320°C and yielded reaction rate constants of 0.315, 7.02, and 247×10^{-4} (minute)$^{-1}$ (percent ϵ-carbide)$^{-\frac{2}{3}}$, respectively. The apparent energy of activation was 50 kcal/mole, and the "frequency factor" was 1×10^{15} (second)$^{-1}$ (percent ϵ-carbide)$^{-\frac{2}{3}}$ (see Fig. 3). The activation energies of the thermal reactions of iron carbides are compared in Table IV with those measured for the decomposition of the cobalt and nickel carbides.

A complete mathematical evaluation of the synthesis of cementite was not possible for the following reasons: (a) The synthesis stopped before it went to completion. (b) The extent of reaction depended on the temperature. (c) The decomposition of Hägg carbide into cementite and free carbon became appreciable above about 440°C, so that the synthesis could not be completed by raising the temperature.

The last-mentioned effect is noticeable from the experiments made at 473° and 480°C, in which all of the Hägg carbide was destroyed. While more iron was present initially at 473°C, the synthesis was more

TABLE IV. Activation energies and "frequency factors" for the isothermal decomposition of iron, nickel, and cobalt carbides.

Reaction[a]	Activation energy, kcal/mole	Frequency factor
ϵ-iron carbide to χ-iron carbide	50	1×10^{15} (sec)$^{-1}$ (percent-ϵ)$^{-\frac{2}{3}}$
χ-iron carbide + α-iron to cementite	~80	...
Cobalt carbide to elements (zero-order range)	54.3	3.9×10^{15} sec^{-1}
Fully carburized nickel carbide to elements,		
Induction period	55	3×10^{15} sec^{-1}
Decomposition period (zero-order range)	61	1×10^{16} sec^{-1}
"95 percent" carburized nickel carbide to elements,		
Induction period	36	4×10^{9} sec^{-1}
Decomposition period (zero-order range)	71	1×10^{21} sec^{-1}

[a] The data for cobalt and nickel carbides are from reference 11, Table 5.

complete at that temperature than at 480°C, because the final magnetic moment was lower. This can only be explained by the fact that more Hägg carbide decomposed into cementite and free carbon at the higher temperature, thus leaving a larger amount of iron unreacted. An estimate (see appendix) shows that at 480°C about 30 percent of the Hägg carbide decomposed and only 70 percent reacted with iron. It appears likely that copper retarded the reaction and prevented more complete synthesis by impeding the necessary diffusion, since data obtained with a copper-free, fused catalyst showed more complete reaction at 450°C[4] than was obtained at 440° and 480°C in this study.

As no rate law could be found for the synthesis of cementite, an estimate of the activation energy of the reaction was made on the basis of the treatment of Parkins, Dienes, and Brown.[15] They showed that if (1) a physical property p is a single-valued function of the extent of reaction, (2) the mechanism is the same throughout the temperature range studied, and (3) the initial value p_0 is the same for all isothermal experiments, then, for a particular value p,

$$\log(t_1/t_2)=0.2186E(T_1^{-1}-T_2^{-1}),$$

TABLE V. Estimation of the activation energy of the synthesis of cementite.

Temperatures, °C	p/p_0[a]	Activation energy, kcal/mole
360 and 400	0.280	(negative)
	0.254	75
400 and 440	0.233	80
	0.207	80
440 and 473	0.141	(120)
440 and 480	0.141	80

[a] Values of the relative magnetic moments chosen for the time ratios.

[15] Parkins, Dienes, and Brown, J. Appl. Phys. 22, 1012 (1951).

where t is the time, T the temperature in °K, and E the activation energy in cal/mole. Values of relative magnetic moments were chosen for pairs of temperatures (Table V), and activation energies near 80 kcal/mole were obtained.

DISCUSSION

If the composition of the h.c.p. iron carbide were variable, it should have been possible to homogenize the partly carburized preparation to h.c.p. Fe_3C. Two attempts to do this, by heating a sample at 180°C for 18.5 hours and another one at 190°C for 3 days, failed; the slight observed change of the magnetic moment of the sample heated at 190°C corresponded to the formation of a small amount of Hägg carbide. The copper promoter in the catalyst may have presented a barrier to the homogenization. However, in view of the data cited in footnote 9 and for economy of hypothesis, it may be assumed that the composition of both higher carbides of iron is the same and that the transition from one to the other is simply a structural rearrangement. The fully carburized specimen thus must have contained some free carbon.

The plateau at 27 percent of the magnetic moment (Fig. 2) provides support for the formula $Fe_{2+}C$ for Hägg carbide. Knowing the carbon-iron ratio of the sample and the specific magnetizations of Hägg carbide and iron under the experimental conditions, one finds that the position of the plateau should be 40 percent for Fe_2C. The difference between the observed and calculated values must arise from the fact that the amount of iron contained in the carbide was more than corresponds to Fe_2C. Accord between calculation (28 to 29.5 percent) and observation (27 percent) was attained by ascribing the formula $Fe_{2.4}C$ to Hägg carbide, but this good agreement with Eckstrom and Adcock's result[16] must be considered purely fortuitous in view of the relatively low field strength and the uncertainty of the numerical value of the specific magnetization of the carbide under these conditions.

Magnetic and x-ray analyses of the samples treated at 240° and 280°C showed the presence of Hägg carbide and the absence of cementite. After heating at 320°C, another sample contained a small amount of cementite, barely detectable by magnetic analysis but not observed on the x-ray diffraction pattern. These observations and other known facts[17] make it unlikely that cementite is a precursor of Hägg carbide, as postulated in one of Trillat's reaction mechanisms.[18] As concerns the carburization and thermal reactions of iron powders, at least, Hägg carbide may precede but not follow the formation of cementite.

[16] H. C. Eckstrom and W. A. Adcock, "The Formation of Iron Compounds in the Hydrocarbon Synthesis," presented at the Ninth Annual Pittsburgh Conference on X-Ray and Electron Diffraction, Mellon Institute, Pittsburgh, Pennsylvania, November 29 and 30, 1952.

[17] Manes, Damick, Mentser, Cohn, and Hofer, J. Am. Chem. Soc. **74**, 6207 (1952).

[18] J. J. Trillat and S. Oketani, Compt. rend. **232**, 1116 (1951).

Extrapolation of the rate data to higher temperatures shows that the transition from h.c.p. to Hägg carbide was completed in 2.1 minutes at 360°C, 0.20 minute at 400°C, 0.02 minute at 440°C, and 0.00 minute at 480°C. The synthesis of cementite, therefore, probably never takes place directly from h.c.p. iron carbide and iron; instead, h.c.p. iron carbide is converted to Hägg carbide prior to its reaction with iron.

Iron Carbides in the Fischer-Tropsch Synthesis

Brill and co-workers made an x-ray diffraction study of the thermal stability of the h.c.p. iron carbide found in used Fischer-Tropsch catalysts (see Brill, reference 9). They heated these catalysts, containing between zero and 25 parts of copper per 100 parts of iron, for three hours at various temperatures to determine the onset and the completion of the transformation of h.c.p. iron carbide. With no copper present, no transformation was noted at 275°C, some at 290°, more at 300°, and complete transformation at 330°C. The data for the catalyst containing ten parts of copper are not so detailed; it is noted, however, that the x-ray pattern of the h.c.p. iron carbide has disappeared after heating at 350°C. With 25 parts of copper, the transformation started at 350°C and was completed at 430° to 450°C. It was concluded that the maximum synthesis temperature for preserving h.c.p. iron carbide is 250° to 275°C for copper-free catalysts, about 50°C higher for those containing 10 parts of copper, and about 100°C higher for those containing 25 parts of copper per 100 parts of iron.

The conclusion that h.c.p. iron carbide is stabilized by copper is questionable in the light of the present study. Brill's observations are best explained by the facts that copper facilitates reduction and carburization of iron catalyst[2,5] and that the stability of the carbide increases with increasing extent of carburization.

None of the known reactions of iron carbides, involving only solid phases, produces free carbon in the temperature range of the Fischer-Tropsch synthesis (about 200° to 350°C), assuming h.c.p. and Hägg carbide to have the same composition.

APPENDIX. CONVERSION OF MAGNETIC MOMENT TO PERCENTAGE OF CONSTITUENTS

Transition from Hexagonal Close-Packed to Hägg Iron Carbide

The magnetic moment M of a ferromagnetic substance is defined as the product of its mass m and its specific magnetization σ:

$$M = \sigma m.$$

Experimentally, M is measured by the movement D of the substance in the magnetic field:

$$M = D/k,$$

where k is the sensitivity constant of the magnetic balance. (In this case, k is the angle per unit of specific magnetization through which the suspension must be twisted to move the sample to the arbitrary null position.[12])

When "i" ferromagnetic phases are present, the moments are simply additive,

$$M=\sum\sigma_i m_i=\sum D_i/k=D/k.$$

In the case of three ferromagnetic phases having σ_1, σ_2, and σ_3 as their specific magnetizations and m_1, $m_2(=m_1)$, and m_3 as their masses, respectively,

$$\sigma_1 m_1+\sigma_3 m_3=D_0/k, \quad \text{(at time } t=0)$$

$$\sigma_1(m_1-x)+\sigma_2 x+\sigma_3 m_3=D_t/k, \quad \text{(at any time)}$$

and

$$\sigma_2 m_1+\sigma_3 m_3=D_\infty/k, \quad \text{(at time } t=\infty)$$

where x is the amount of m_1 that has been transformed into m_2 at time t. Upon rearrangement, the second of these equations becomes

$$(\sigma_2-\sigma_1)x+(\sigma_1 m_1+\sigma_3 m_3)=D_t/k.$$

Since only x and D_t are variable, this is the equation of a straight line and shows the linear dependence of the magnetic moment on the amount of transformation. At any temperature, therefore, D_0 corresponds to 100, D_∞ to 0, and D_t to $100[(D_t-D_\infty)/(D_0-D_\infty)]$ percent of m_1. Hence, the absolute amounts of material, specific magnetizations, and the sensitivity of the magnetic balance need not be known for this type of analysis.

Formation of Cementite

When a mixture of Hägg carbide and iron is heated, two reactions are possible (the formula $Fe_{2.4}C$ is here assumed for Hägg carbide): $Fe_{2.4}C+0.6Fe\rightarrow Fe_3C$, and $1.25Fe_{2.4}C\rightarrow Fe_3C+0.25C$. Hence, x grams of Hägg carbide react with $(33.5/146.1)x$ grams of iron to form $(179.6/146.1)x$ grams of cementite; and y grams of Hägg carbide decompose into $(179.6/182.6)y$ grams of cementite and $(3/182.6)y$ grams of (magnetically non-detectable) free carbon. Letting the subscripts 1, 2, and 3 stand for Hägg carbide, cementite, and iron, respectively, one finds

$$\sigma_1(m_1-x-y)+\sigma_2\left(\frac{179.6x}{146.1}+\frac{179.6y}{182.6}\right)+\sigma_3\left(m_3-\frac{33.5x}{146.1}\right)=D_t/k. \quad (1)$$

Since σ_1 and σ_2 are zero at the temperatures at which all of the Hägg carbide is destroyed,

$$x=\frac{146.1}{33.5}\left(1-\frac{D_\infty}{D_0}\right)m_3, \quad (2)$$

where D_0 is the initial and D_∞ is the final movement of the sample. Because of the reactivity of the system, the magnetic moment at zero time at the reaction temperature cannot be measured directly but must be calculated from the initial contribution of iron to the magnetic moment at room temperature. Since Eq. (2) contains a ratio of magnetic moments, only the relative magnetic moments, the D's, need be known; also, fractions of the total mass may be used instead of the absolute masses of x and m_3. Thus, since the carbon-iron weight ratio was 0.06966 for the catalyst but is 0.08955 for $Fe_{2.4}C$, the preparation contained 0.7779 gram of Hägg carbide and 0.2221 gram of iron per gram of sample, after the transition from h.c.p. to Hägg carbide was completed. Under the experimental conditions, the magnetic moment at room temperature of Hägg carbide is about 140 cgs/g and that of iron about 218 cgs/g; the magnetic moment of the mixture was thus 157.3 cgs/g, to which iron contributed 0.3078. Again under the experimental conditions, the magnetic moment of iron at 480°C is 0.918 of its magnetic moment at room temperature. Hence, $D_0=0.2825$; $D_\infty=0.119$ was determined experimentally. Substitution into Eq. (2) shows that 72 percent of the Hägg carbide present reacted with iron to form cementite, while 28 percent of the carbide decomposed into cementite and free carbon. These values are approximate, especially because of the uncertainty of the composition of Hägg carbide.

ACKNOWLEDGMENT

Thanks are due Mrs. W. C. Peebles for x-ray diffraction analyses.

The Infrared and Raman Spectra of SiH_2Cl_2

JANET A. HAWKINS AND M. KENT WILSON
Mallinckrodt Chemical Laboratory, Harvard University, Cambridge, Massachusetts
(Received August 20, 1952)

An investigation of the infrared spectrum of gaseous SiH_2Cl_2 and the Raman spectrum of liquid SiH_2Cl_2 results in the following fundamental assignment:

$\nu_1(a_1)=2200\ cm^{-1}$, $\nu_2(a_1)=953\ cm^{-1}$, $\nu_3(a_1)=531\ cm^{-1}$,
$\nu_4(a_1)=188\ cm^{-1}$, $\nu_5(a_2)=710\ cm^{-1}$, $\nu_6(b_1)=2200\ cm^{-1}$,
$\nu_7(b_1)=810\ cm^{-1}$, $\nu_8(b_2)=877\ cm^{-1}$, $\nu_9(b_2)=592\ cm^{-1}$.

Thermodynamic functions for SiH_2Cl_2 were calculated with the usual assumptions. The infrared spectrum of gaseous CH_2Cl_2 and the infrared and Raman spectrum of liquid CH_2Cl_2 were remeasured.

INTRODUCTION

THIS paper is the first of a series of investigations concerning the spectra and molecular structure of simple silicon compounds. Although the infrared and Raman spectra of SiH_4 and the Raman spectra of $SiHCl_3$ and $SiCl_4$ have been known for some time[1] and the infrared spectra of $SiHCl_3$[2] and SiH_3Cl have recently been published,[3] to the authors' knowledge, no information concerning the vibration spectrum of SiH_2Cl_2 has been reported. Since the fundamental frequencies of this molecule would be useful in a general force constant treatment of the silane derivatives, the present paper is a report on the infrared and Raman spectra of dichlorosilane.

TABLE I. The infrared spectrum and band assignments of gaseous SiH_2Cl_2.

ν cm^{-1}	Relative intensity[a]	Assignment
531	0.57	$\nu_3(a_1)$
592	0.10	$\nu_9(b_2)$
776	0.05	$\nu_4+\nu_9(B_2)$
810	0.73	$\nu_7(b_1)$
877	18.4	$\nu_8(b_2)$
953	9.2	$\nu_2(a_1)$
1063	0.03	$2\nu_3(A_1)$
1075	0.03	$\nu_4+\nu_8(B_2)$
1118	0.07	$\nu_3+\nu_9(B_2)$
1198	0.04	$2\nu_9(A_1)$
1312	0.03	$\nu_5+\nu_9(B_1)$
1422	0.03	$\nu_3+\nu_8(B_2)$
1438	0.03	$\nu_8+\nu_9(A_1)$
1560	0.03	$\nu_2+\nu_9(B_2)$
1605	0.03	$2\nu_7(A_1)$
1755	0.02	$2\nu_8(A_1)$
2200	1.6[b]	$\nu_1(a_1)$, $\nu_6(b_1)$
2920	0.02	$\nu_5+\nu_6(B_2)$
3090	0.03	$\nu_8+\nu_1(B_2)$
3170	0.03	$\nu_2+\nu_1(A_1)$

[a] The values given are the apparent absorption coefficient at the peak of the band and are evaluated from $a=1/PL\ \log_{10}T_0/T$. The path length is in units of cm atmos at 0°C.
[b] Not resolved into two bands.

[1] G. Herzberg, *Infrared and Raman Spectra of Polyatomic Molecules* (D. Van Nostrand Company, Inc., New York, 1945), p. 322.
[2] T. G. Gibian and D. S. McKinney, J. Am. Chem. Soc. 73, 1431 (1951).
[3] A. Monfils, J. Chem. Phys. 19, 138 (1951).

EXPERIMENTAL

Measurements of the infrared spectrum of gaseous SiH_2Cl_2 were made on a Baird Associates spectrophotometer equipped with NaCl optics and a Perkin-Elmer Model 12C spectrograph equipped with CaF_2 and KBr prisms. A 5-cm gas cell with KBr windows was used with both instruments.

The grating spectrograph used to obtain the Raman spectrum has been described by Brown.[4] The qualitative depolarization of the lines was obtained by the method of Edsall and Wilson.[5] The Raman data refer to liquid SiH_2Cl_2 and were obtained with an exciting mercury line of 4358.4A; a Wratten 2A filter was used as a short wavelength filter.

The sample of SiH_2Cl_2 was obtained through the courtesy of the Linde Air Products Corporation. As no

TABLE II. The infrared spectrum of gaseous and liquid CH_2Cl_2.

ν cm^{-1} (liquid)	ν cm^{-1} (gas)	Relative intensity[a]	Assignment
707[b]	706	0.63	$\nu_3(a_1)$
743[b]	762	58.4	$\nu_9(b_2)$
897	898	0.05	$\nu_7(b_1)$
984			$\nu_4+\nu_3(A_1)$
1020			$\nu_4+\nu_9(B_2)$
1158			$\nu_5(a_2)$
1265	1270	10.2	$\nu_8(b_2)$
1432	1480	0.08	$\nu_2(a_1)$
1559			$2\nu_9(A_1)$
1620			$\nu_3+\nu_7(B_1)$
2040			$\nu_5+\nu_7(B_2)$
2110			$\nu_2+\nu_9(B_2)$
2302			$\nu_2+\nu_7(B_1)$
2408			$\nu_5+\nu_8(B_1)$
2670			$\nu_2+\nu_8(B_2)$
2970	2980[c]	0.10	$\nu_1(a_1)$, $\nu_6(b_1)$
3020			
3710			$\nu_1+\nu_3(A_1)$
4000			$\nu_6+\nu_7(A_1)$
4320			$\nu_1+\nu_8(B_2)$
4660			$\nu_2+\nu_6(B_1)$

[a] The values given are the apparent absorption coefficient for the gas at the peak of the band and are evaluated from $a=1/PL\ \log_{10}T_0/T$. The path length is in units of cm atmos at 0°C.
[b] Observed in CS_2 solution.
[c] Unresolved for the gas.

[4] W. E. Brown, Ph.D. thesis, Harvard University (1948).
[5] J. T. Edsall and E. B. Wilson, Jr., J. Chem. Phys. 6, 124 (1938).

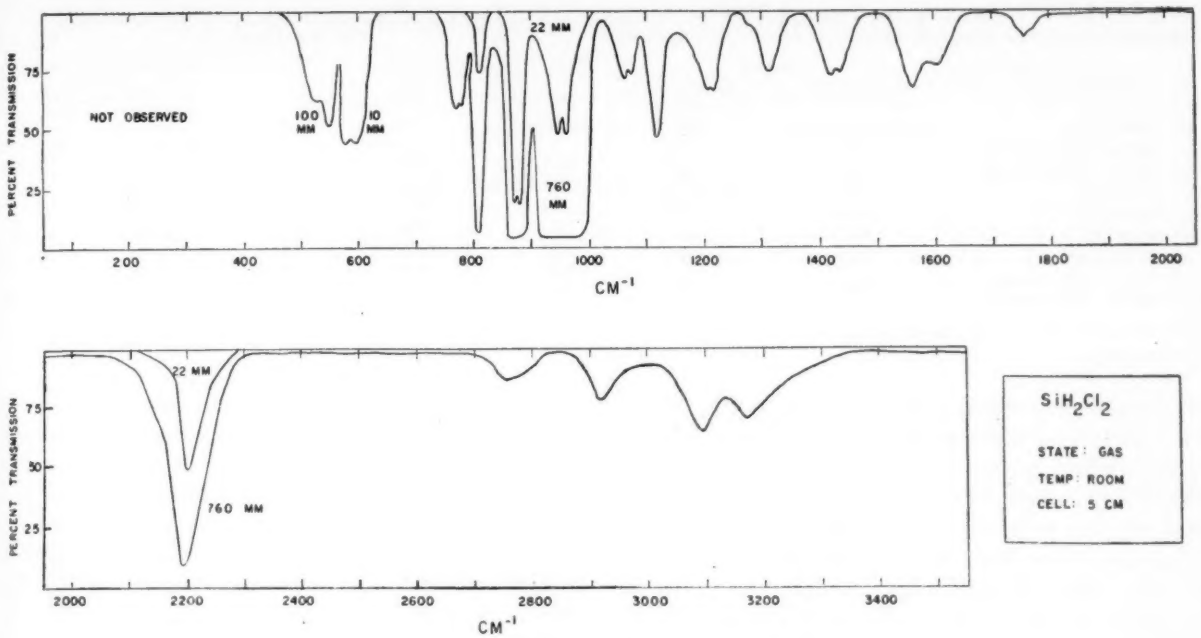

FIG. 1. Infrared absorption spectrum of gaseous SiH_2Cl_2.

infrared bands were observed which coincided with the known frequencies of silane or the other chlorosilanes and the only extraneous band in the Raman effect was encountered only on the longest exposure, the material was used without further purification.

Dichlorosilane reacts so vigorously with moisture that when admitted to a system evacuated only by a mechanical oil pump it combines with the adsorbed water on the glass surface to form a white, opaque deposit. It was found that this precipitation could be prevented by previously treating the system with methylchlorosilane vapor. Accordingly, a mixture of methylchlorosilane vapors* was admitted to the evacuated apparatus and allowed to remain for several minutes. When the system was re-evacuated and SiH_2Cl_2 passed in, no detectable hydrolysis occurred.

Because there has been some question as to the depolarization data for the corresponding carbon compound CH_2Cl_2,[6] the Raman spectrum of this compound in the liquid state and the infrared spectrum of both the liquid and the vapor were re-examined. Eastman White Label methylene chloride was used after distillation through a 150-cm packed column.

EXPERIMENTAL RESULTS

The observed frequencies, band assignments, and relative intensities of the infrared bands of SiH_2Cl_2 and CH_2Cl_2 are given in Tables I and II, while the Raman data for both molecules are contained in Table III. The values given for the apparent absorption coefficients are included only to indicate the approximate relative intensities of the bands.

The observed spectrum of SiH_2Cl_2 replotted on a linear frequency scale is illustrated in Fig. 1. Although the spectrum was investigated to 5000 cm^{-1} at a pressure of 760 mm in a 5-cm cell, no bands were observed beyond 3170 cm^{-1}.

DISCUSSION

SiH_2Cl_2 has been shown to have the expected C_{2v} symmetry as a result of the electron diffraction investigation of Brockway and Coop.[7] The nine fundamentals of a molecule of this symmetry consist of four totally symmetric (a_1) vibrations which may loosely be described as bending and stretching motions involving the SiH_2 and $SiCl_2$ subgroups. The torsional vibration is alone in the species a_2. This vibration is forbidden in the infrared and is the only vibration of SiH_2Cl_2 which is not

TABLE III. The Raman spectra of liquid SiH_2Cl_2 and CH_2Cl_2.

Assignment	SiH_2Cl_2 $\Delta\nu$ (cm^{-1})	CH_2Cl_2 $\Delta\nu$ (cm^{-1}) Present work	CH_2Cl_2 $\Delta\nu$ (cm^{-1}) Herzberg (reference 1)
$\nu_4(a_1)$	188 (m. depol.)	287 (s. pol.)	283 (pol.)
	451[a]	650[a]	
$\nu_3(a_1)$	514 (s. pol.)	707 (s. pol.)	700 (pol.)
$\nu_9(b_2)$	566 (v. w. depol.)	740 (w. depol.)	736 (depol.)
$\nu_7(b_1)$[b]			898 (depol.)
$\nu_5(a_2)$	710 (w. depol.)	1152 (v. w. depol.)	1148 (depol.)
$\nu_8(b_2)$	868 (v. w. depol.)	1219 (v. w.)	1255 (v. w.)
$\nu_2(a_1)$	942 (w. depol.)	1426 (w. depol.)	1417 (depol.)
$\nu_1(a_1)$	2221 (s. pol.)[c]	2987 (s. pol.)	2985 (pol.)
$\nu_6(b_1)$		3048 (w. depol.)	3045 (depol.)

[a] Found only with very long exposures and may be the result of impurities.
[b] No line is observed even with long exposures.
[c] Broad and diffuse line which cannot be resolved.

* General Electric Company, Dri-Film SC-77.

[6] G. Herzberg, reference 1, p. 319.

[7] L. O. Brockway and I. E. Coop, Trans. Faraday Soc. **34**, 1429 (1938).

TABLE IV. Fundamental frequencies of SiH_2Cl_2.

Assignment	ν (cm^{-1}) Infrared (gas)	Raman (liq.)
$\nu_4(a_1)$—$SiCl_2$ bend	(not investigated)	188
$\nu_3(a_1)$—sym. $SiCl_2$ stretch	531	514
$\nu_9(b_2)$—asym. $SiCl_2$ stretch	592	566
$\nu_7(b_1)$—rocking	810	(not observed)
$\nu_5(a_2)$—torsion	(inactive)	710
$\nu_8(b_2)$—rocking	877	868
$\nu_2(a_1)$—SiH_2 bend	953	942
$\nu_1(a_1)$—sym. SiH_2 stretch $\nu_6(b_1)$—asym. SiH_2 stretch	2200[a]	2221[a]

[a] Not resolved.

TABLE V. Thermodynamic functions for SiH_2Cl_2 (cal deg^{-1} mole^{-1}).

T (°K)	Cp^0	S^0	$\frac{(H^0-H_0^0)}{T}$	$-\frac{(F^0-H_0^0)}{T}$
273.15	13.79	66.58	10.23	56.35
298.15	14.45	67.83	10.56	57.27
400	16.75	72.41	11.87	60.54
600	19.63	79.79	13.97	65.82
800	21.40	85.71	15.61	70.10
1000	22.56	90.67	16.89	73.78
1200	23.35	94.76	17.86	76.90
1500	24.23	100.13	19.10	81.03

both infrared and Raman active. The b_1 and b_2 species each contain an asymmetrical stretch and a rocking motion. All first overtones are infrared active, while only those binary combinations arising from $b_1 \times b_2 = A_2$ and $a_1 \times a_2 = A_2$ are forbidden in the infrared.

As indicated in Table III only two polarized Raman lines were observed for SiH_2Cl_2 although there should be four totally symmetric modes. These two polarized lines at 514 cm^{-1} and 2221 cm^{-1} may be assigned with confidence to the symmetric Si—Cl stretch $\nu_3(a_1)$ and the symmetric Si—H stretch $\nu_1(a_1)$, respectively. The fairly intense line at 188 cm^{-1} cannot be due to an impurity and is in the general region one would expect to find a $SiCl_2$ bending vibration. The low bending frequency in $SiCl_4$ and $SiHCl_3$ occurs at 149 cm^{-1} and 179 cm^{-1}, respectively.[8] Therefore, this line is assigned as $\nu_4(a_1)$ even though it appears to be depolarized. The corresponding band in CH_2Cl_2 is observed to be polarized. As the fourth symmetric mode, we assign the weak, depolarized line at 942 cm^{-1} as the SiH_2 bend, $\nu_2(a_1)$. Again the observed polarization is unsatisfactory, but here a similar situation exists for CH_2Cl_2. In this molecule, we observe a weak depolarized line at 1426 cm^{-1} which agrees moderately well with the value of 1417 cm^{-1} for the weak depolarized line assigned by Herzberg[5] as $\nu_2(a_1)$. This apparent discrepancy may be due to rather large depolarization factors, as Wolkenstein and Eliashevich[9] calculated depolarization factors of 0.77 and 0.75 for ν_4 and ν_2, respectively, of CH_2Cl_2.

The rest of the assignment follows in a straightforward manner. The torsional mode $\nu_5(a_2)$ is not observed in the infrared spectrum of the vapor for both molecules and appears in the liquid spectrum of CH_2Cl_2, presumably because of the breakdown of the selection rules in the condensed phase.

With two exceptions the agreement between the Raman shifts in the liquid and the infrared frequencies in the vapor phase is quite acceptable. It is observed that $\nu_2(a_1)$ of CH_2Cl_2 appears in the infrared absorption of the gas at 1480 cm^{-1} and at 1426 cm^{-1} in the Raman spectrum of the liquid. This discrepancy can be ascribed to the change of state since this band occurs at 1432 cm^{-1} in the absorption spectrum of liquid CH_2Cl_2. In both CH_2Cl_2 and SiH_2Cl_2, $\nu_9(b_2)$ is found to decrease 20–30 cm^{-1} in going from the vapor to the liquid. The over-all similarity between the carbon and silicon analogs may be emphasized by noting that for both compounds the rocking motions $\nu_7(b_1)$ and $\nu_8(b_2)$ are quite weak in the Raman effect. The fundamental frequencies of SiH_2Cl_2 are collected in Table IV.

THERMODYNAMIC FUNCTIONS

Thermodynamic functions for SiH_2Cl_2 over a convenient temperature range are listed in Table V. Calculations were made using a rigid-rotor, harmonic oscillator approximation for the ideal gas at 1-atmos pressure. The bond distances used were Si—H = 1.50A and Si—Cl = 2.048A. These were taken from the microwave investigation of SiH_3Cl [10] and fall within the experimental limits of error quoted in the electron diffraction investigation of SiH_2Cl_2.[6] The bond angles were assumed to be tetrahedral. Except for $\nu_4(a_1)$ and $\nu_5(a_2)$, which were observed only in the Raman spectrum of the liquid, the infrared frequencies of the vapor were used in this calculation.

It seems worthwhile to postpone a force constant calculation for the chlorosilanes until the concurrent investigation of the deutero and fluorosilanes is completed.

ACKNOWLEDGMENTS

The authors wish to thank Dr. J. M. Gaines of the Linde Air Products Corporation for the sample of SiH_2Cl_2 used in this investigation. We wish to thank the Radcliffe Graduate School for a predoctoral fellowship. We also wish to thank the Mallinckrodt Chemical Works for financial assistance covering a portion of this investigation and the American Academy of Arts and Sciences for a grant-in-aid.

[8] K. W. F. Kohlrausch, *Der Smekal-Raman Effekt* (Verlag Julius Springer, Berlin, 1931).

[9] M. Wolkenstein and M. Eliashevich, Acta Physicochim. U.R.S.S. **20**, 525 (1945).

[10] Dailey, Mays, and Townes, Phys. Rev. **76**, 136 (1949).

The Microwave Spectrum of $C_8H_{13}Br$ and $C_8H_{13}Cl$†

A. H. NETHERCOT, JR.,* AND A. JAVAN
Department of Physics, Columbia University, New York, New York
(Received August 28, 1952)

The spectrum and structure of the molecules $C_8H_{13}Br$ and $C_8H_{13}Cl$ have been determined. Despite the large size of these molecules, the spectra can be analyzed with the exception of the quadrupole hyperfine splittings which cannot be resolved. The B values are 1090.9 Mc for Cl^{35}, 1065.9 for Cl^{37}, 725.9 for Br^{79}, and 718.5 for Br^{81}. The value of the normal single bond carbon-carbon distance is found to be $d_{c-c}=1.545 \pm 0.004$A. The angle of twist about the symmetry axis is $\phi=0°\pm4°$, and the angle between the carbon-carbon and carbon-halide bonds is $\theta=109°50'\pm10'$.

THE molecules 1-bromo and 1-chloro bicyclo [2,2,2] octane have been synthesized by Professor W. V. Doering and Dr. A. Sayigh, Department of Chemistry, Columbia University, who kindly made samples of them available for this investigation. The structure of these molecules is shown in Fig. 1. The strongest of chemical evidence indicated that they are symmetric tops, and it was thought to be of interest to determine how great the complications in the spectra due to their large size would be. These complications arise from the sixty normal vibrations, some of which would lie at low frequencies and would therefore be well populated at room temperature, from the many K states of different energies available at high J values, and from the four quadrupole hyperfine structure levels for each of the above levels. For example, for an initial J value of 17, these factors lead to 162 transitions of different frequencies for each vibrational state.

Typical traces of the absorption lines of these two molecules at room temperature are shown in Fig. 2. The chloride band is resolved into some vibrational levels, but the bromide band is only slightly resolved even at −30°C. A rough calculation of the half-width of the chloride lines for a given vibrational state agrees well with the experimentally observed width of approximately 4 Mc: Assuming the same eqQ as for methyl chloride, the forty-four strong $F\rightarrow F+1$ lines were summed over a reasonable frequency separation (which gave the observed dependence of absorption and line width with pressure); this sum led to a half-width of about 5 Mc. The many hyperfine lines are less separated than the 200 kc resolving power of the Stark modulation spectrometer. In the case of the bromide, the much larger eqQ would merge the various vibrational states. This accounts for the difference in appearance of the two spectra. The amount of absorption increases up to the highest pressures and Stark voltages available.

The frequencies of the observed transitions are given in Table I. The frequencies listed for the chloride are for the most intense vibrational lines, while for the bromide they are for the center of the room temperature bands, which are fairly symmetrical about this frequency. Centrifugal distortion is absent within the experimental error.

Various molecular constants derived from these frequencies are given in Table II. ΔB is the difference between the B_0's for the two isotopes. The B_0's for Br derived from the tabulated frequencies are 726.2 and 718.85 but have been decreased by 0.3 Mc, since the spectrum at −30°C indicated that the low frequency side of the band becomes relatively more intense.

The first error given is the experimental error, and the second error, in parentheses, is the first plus the maximum possible error involved when it is assumed that B_e is the same as B_0 for the low frequency vibrations. Later calculations are made under the assumption that low frequency vibrations (such as torsional vibrations about the symmetry axis) do not occur; this parenthesized error, therefore, gives the maximum possible error in such calculations. This maximum error can be found as follows: Since these vibrations are low frequency ones, their excited energy levels should be well populated at room temperature, leading to intense satellite lines about the ground-state line; since B_n equals $[B_e+(n+\frac{1}{2})\alpha]$, (B_1-B_0) is equal to $2(B_0-B_e)$; therefore, assignment of the most separated intense satellite line to the first excited torsional vibration state gives, for the maximum error possible when B_e and B_0 for this vibration are assumed to be identical, a value $(B_1-B_0)/2$, or one-half of the separation of the satellite and ground-state rotational constants. This

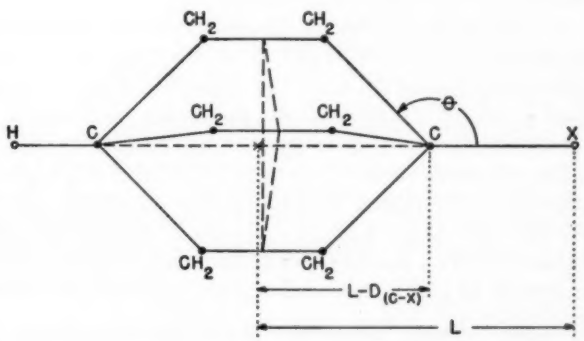

FIG. 1. The structure of $C_8H_{13}X$.

* Carbide and Carbon Chemical Corporation Postdoctora Fellow, 1950–1951.
† Work supported in part by the Signal Corps and the U. S. Office of Naval Research.

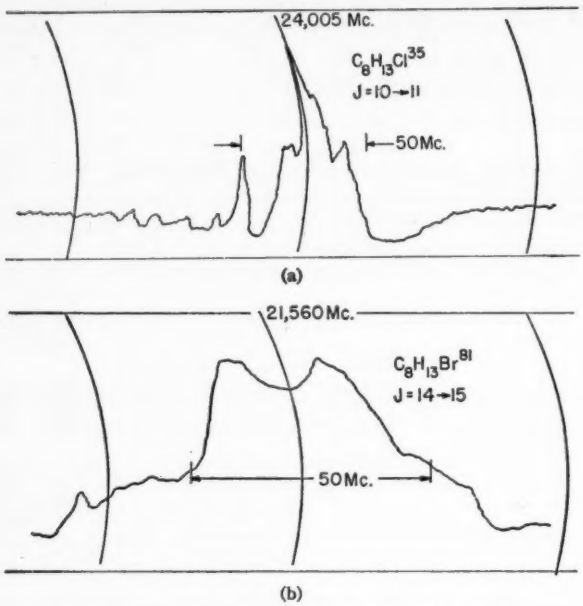

FIG. 2. Typical absorption traces for the two halides.

value is approximately $\frac{1}{2}\cdot 25$ Mc/$(2J+1)\simeq 0.5$ Mc, where the 25 Mc value is taken from Fig. 2.

The L appearing in Table II is a convenient molecular parameter, the distance between the halide and the center of mass of the radical, and is given directly in terms of measured quantities. From the theorem of parallel axes

$$L^2M_{\text{rad}}[m_{x'}/(M_{\text{rad}}+m_{x'})-m_{x''}/(M_{\text{rad}}+m_{x''})] = 505\,488\Delta B/B_{x'}B_{x''},$$

where M_{rad} is the mass of the molecule less the mass of the halide isotope, $m_{x'}$ and $m_{x''}$ are the masses of the two halide isotopes, $B_{x'}$ and $B_{x''}$ are the rotational constants of the two isotopic molecules in Mc, and ΔB is their difference; L is then given in A. The bond distances taken from the corresponding methyl halides[1] as $d_{C-Cl}=1.781$, $d_{C-Br}=1.939$, and $d_{C-H}=1.10$A give the tabulated values of $L-d_{C-X}$. The agreement between the two values is excellent, the tabulated error being primarily that from the error in measurement of ΔB. Geometrically, $L-d_{C-X}$ is determined only by d_{C-C} and the various angles in the molecule.

Various values of d_{C-C} are possible if θ, the nominally tetrahedral C−C−X angle, or φ, the angle of torsion about the symmetry axis, are changed in such a way that $L-d_{C-X}$ is held constant at 1.319A. Various combinations of these parameters can be checked by calculation of the B values and comparison with the experimentally determined B values. For example, $\varphi=0$, $\theta=109°\,30'$, $d_{C-C}=1.557$($L-d_{C-X}=1.319$A) yields a B value of 1059.4 for Cl^{37}, while the experimental value is 1065.9. If φ is increased from zero and d_{C-C} is correspondingly increased, the agreement of B values is even worse. However, it is to be expected that φ is very small. φ could only be large if the potential well for φ were very shallow (possibly having a double minimum). If this were the case, higher vibrational states would be well populated at room temperature and could be allowed for. As has been previously explained, the B values cannot be changed by more than about 0.5 Mc from their values for $\varphi=0$ if $\varphi\neq 0$ (since this is the maximum possible difference between B_0 and B_e for such vibrations). Therefore, the calculations were made assuming $\varphi=0$, allowing a 0.5 Mc error to compensate for this assumption. This error corresponds to $\varphi=0°\pm 4°$.

[1] Miller, Aamodt, Dousmanis, Townes, and Kraitchman, J. Chem. Phys. **20**, 1112 (1952). There exist differences in the chemical reactivity of carbon-halide bonds when the carbon is or is not bonded to three other carbons. However, this would not be expected to change the carbon-halide distance markedly.

TABLE I. Frequencies of observed transitions.

	$J=5\to 6$	$15\to 16$	$16\to 17$	$17\to 18$
$C_8H_{13}Br^{81}$	8627.5	22 997	24 441	25 882
$C_8H_{13}Br^{79}$	8716.5	23 231	24 691	26 146
	$J=10\to 11$		$J=11\to 12$	
$C_8H_{13}Cl^{37}$	23 449.6		25 582.7	
$C_8H_{13}Cl^{35}$	23 999.8		26 182.0	

Four calculations were made of the B values for the chlorides for various choices of the parameters d_{C-C} and θ which maintain $L-d_{C-X}$ equal to 1.319A, namely, $d_{C-C}=1.540$, 1.543, 1.544, and 1.557A and corresponding values of θ. These calculated B values lay on a straight line when plotted against d_{C-C}, and this line yielded for the experimental B value a value of d_{C-C} equal to 1.543 ± 0.003A. For the bromides, a similar calculation yielded d_{C-C} equal to 1.548 ± 0.004A. These errors allow for the errors in L and in the experimental measurements, as well as those arising from the assumption that $\varphi=0$. The weighted average gives $d_{C-C}=1.545\pm 0.004$A and $\theta=109°\,50'\pm 10'$. Since the low frequency zero-point vibrations are accounted for in the error, this value of d_{C-C} should hold for the smaller single bonded organic molecules as well.

TABLE II. Molecular constants of $C_8H_{13}X$.

$C_8H_{13}Cl^{35}$	$B_0=1090.90\pm 0.02(\pm 0.6)$ Mc
$C_8H_{13}Cl^{37}$	$B_0=1065.91\pm 0.02(\pm 0.6)$ Mc
$\Delta B=24.99\pm 0.01$ Mc	$L-d_{C-Cl}=1.319\pm 0.0015$A
$C_8H_{13}Br^{79}$	$B_0=725.9\pm 0.2(\pm 0.6)$ Mc
$C_8H_{13}Br^{81}$	$B_0=718.55\pm 0.2(\pm 0.6)$ Mc
$\Delta B=7.30\pm 0.015$ Mc	$L-d_{C-Br}=1.320\pm 0.003$A

This work has benefited from the aid of many members of the Columbia Radiation Laboratory. In particular, Mr. George Dousmanis performed most of the calculations, Mr. W. A. Hardy made his spectrometer and time available for some of the measurements, and Professor C. H. Townes contributed many valuable suggestions. One of the authors wishes to acknowledge his great appreciation to the Carbide and Carbon Chemical Corporation for the fellowship which made this work possible.

Letters to the Editor

THIS section will accept reports of new work, provided these are terse and contain few figures, and especially few half-tone cuts. The Editorial Board will not hold itself responsible for opinions expressed by the correspondents. Contributions to this section should not exceed 600 words in length and must reach the office of the Editor not later than the 15th of the second month preceding that of the issue in which the Letter is to appear. No proof will be sent to the authors. A publication charge of $10.00 per Letter is made which, when honored, will entitle the Institution to 100 free reprints.

Photoionization as an Important Secondary Process in a Low Frequency Electrodeless Discharge

A. P. SAXENA, *Holkar College, Indore, India*
AND
M. G. BHATAWDEKAR* AND N. A. RAMAIAH, *Chemistry Department, Delhi University, Delhi, India*
(Received November 25, 1952)

IT has been reported previously[1] that when a low frequency electrodeless discharge in H_2O or I_2 vapor is investigated by a cathode-ray oscillograph, two types of pulses are noticed: (a) longer pulses resulting from avalanches formed by electrons released from the (temporary) cathode c by well-known γ- and $\eta\theta g$ mechanisms, and (b) shorter pulses produced by "primary" electrons created in the neighborhood of c by other β-processes[2,3] (see Fig. 1). In this communication are reported a few important observations regarding the behavior of the shorter pulses (b), which indicate the primary role of one of the β-processes in the maintenance of the discharge. The shorter pulses (b) were detected only at potentials V above the starting voltage (V_m) of the self-maintained discharge (at V_m, however, longer pulses only could be noticed[4]). At much larger V, the entire current trace was almost completely superimposed by (b), i.e., the rms value of the current was contributed chiefly by (b); these were roughly of the same height. Further, external irradiation initiated (at $V \leqslant V_m$) or enhanced the number of (b).[1,5] These results suggest that of the secondary processes occurring in gas phase and responsible for (b),[1] photoionization is the significant mechanism for maintenance of a low frequency electrodeless discharge in nonheterogeneous gases; it predominates at $V > V_m$. This points out, for the first time in this field of research, a distinction between alternate and direct current discharges: it has been emphasized that in dc discharges the above process is unimportant.[3] Furthermore, the avalanche-formation leading to (b), commences from a point r away from c by a fixed distance. That is, the photoelectrons produced in the gas phase between c and r acquire energy under fields and start ionizing gas particles by inelastic collisions chiefly from r. This point r, therefore, might correspond to the beginning of plasma region. It may be mentioned that ionization is not excluded between c and r, but is caused by the fast electrons liberated from c to give pulses of longer heights under favorable conditions (see the foregoing).

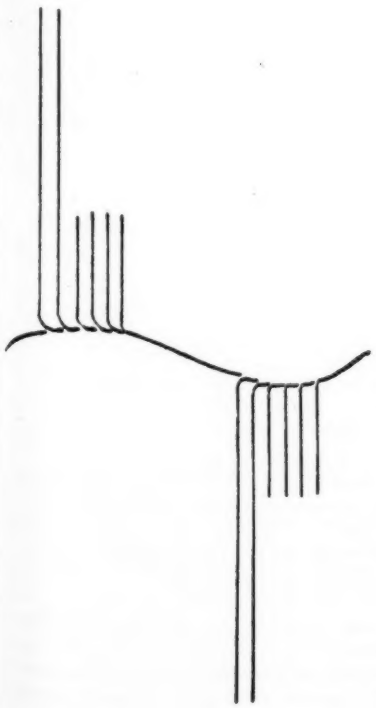

FIG. 1. Current structure at 2.1 kv (p_{12} =0.47 mm Hg, V_m =1.9 kv (50 cycles/sec).

* Present address: Maharajah's College, Jaipur, India.
[1] A. P. Saxena and N. A. Ramaiah, J. Chem. Phys. **20**, 1342 (1952).
[2] L. B. Loeb, *Fundamental Processes of Electrical Discharge in Gases* (John Wiley & Sons, Inc., New York, 1939).
[3] L. B. Loeb, Revs. Modern Phys. **8**, 267 (1936).
[4] The importance of the differential production of pulses (a) and (b) at varied fields will be discussed elsewhere.
[5] N. A. Ramaiah, J. Sci. Ind. Research (India) **10A**, 182 (1951).

Statistical Mechanics of Polymer Adsorption

H. L. FRISCH,* ROBERT SIMHA, AND F. R. EIRICH
Polytechnic Institute of Brooklyn and New York University, New York, New York
(Received December 9, 1952)

WE have considered the formation of a monolayer on a substrate from dilute solution. Because of chain flexibility, deposition of whole chains is unlikely to occur. Instead we shall have short sequences of adsorbed segments, interrupted by "bridges" extending into the solution. This conclusion was also reached by Jenckel and Rumbach[1] on the basis of their experimental results. Hence the problem has two aspects. First, the statistics of deposition of a coiling molecule on a surface, and second, the thermodynamics of the mixture consisting of empty sites, adsorbed segments, bridges, and solution.

If we take as a model the random coil consisting of t segments, the adsorbed molecule is statistically characterized by p, the probability averaged over all t segments, that an arbitrary segment is trapped on the surface, provided one of the chain termini is there. For p one finds:

$$p = 2\alpha(\pi f \cdot t)^{-\frac{1}{2}} - 0(1/t), \tag{1}$$

$\alpha \leqq 1$ is the probability that a segment is adsorbed on hitting an active site of the substrate, and

$$6f = (1+\cos\xi_1)\cdot(1+\langle\cos\xi_2\rangle)/(1-\cos\xi_1)\cdot(1-\langle\cos\xi_2\rangle). \tag{2}$$

$\pi - \xi_1$ is the valence angle and the second cos-terms measure in the usual manner the effect of a rotation barrier on the average extension of the chain in solution. Consequently f is of the order of unity. The average number $\langle\nu\rangle$ of adhering segments per chain equals pt and increases therefore for a given molecular weight with increasing flexibility (small f) of the chain. A poor solvent effectively reduces f and acts in the same direction. In any case, the fraction of segments adsorbed is small, as anticipated. The parameter p determines the size distribution of adsorbed sequences and bridges. Since $p \ll 1$, the former are preponderantly small.

In order to obtain the thermodynamic functions, let N_0 chains be (partially) adsorbed and $N - N_0$ molecules in the solution. The partition function of the whole system, omitting the solvent, is

$$Z_f = Z_{\text{mix}}(\lambda) Z_{\text{mix}}(\epsilon) \times \exp(N_0\langle\nu\rangle x/kT)\Big[\prod_{i=1}^{t} j_i(T)\Big]^N j_{tr}{}^{N-N_0} Z_{\text{mix}}(N-N_0, \epsilon). \tag{3}$$

The first factor accounts for the mixing of sequences of all lengths

$\lambda \geqq 1$ with active sites, the second for the mixing of bridges of all lengths $\epsilon \geqq 1$ with the solution, and x in the Boltzmann factor is the work necessary to remove one segment from the surface. The next two factors are the result of the internal and translational degrees of freedom. The last factor arises from the mixing of $N-N_0$ chains with the solvent containing the bridges. Prior to the adsorption:

$$Z=[\prod_{i=1}^{t} j_i(T)]^N j_{tr}{}^N Z_{\mathrm{mix}}(N), \tag{4}$$

with $Z_{\mathrm{mix}}(N)$ being the mixing term for the solution containing N polymer molecules.

In the evaluation of Eqs. (3) and (4), we assume the original solution to be infinitely dilute. This eliminates interference between the dissolved polymer and the bridges. Calculation of all mixing terms was based essentially on the Flory-Huggins treatment of polymer solutions. We mention here only the results for the adsorption isotherm and ΔH_{ads}, the integral heat of adsorption. Thus,

$$\{\theta/1-\theta e^{2\kappa_1\theta}[p(1-\theta)/\theta e^{-1/1-\theta}]^p\}^{\langle\nu\rangle}=K(T, t, x, \kappa_2)c. \tag{5}$$

$$\Delta H_{\mathrm{ads}}/kT=-N_0\langle\nu\rangle(x/kT+\kappa_2')+\kappa_2' N_0{}^2/N_s(\langle\nu\rangle)^2. \tag{6}$$

Theta is the fraction of the total number N_s of active sites occupied, κ_1[1] a measure of the interaction energy of the adsorbed segments, κ_1 the corresponding term in the free energy of mixing, containing an additional entropy contribution. κ_2' and κ_2 are the analogous quantities for the polymer-solvent system. c is the polymer concentration in the solution. The function K_1 containing among others the chemical potential of the pure polymer, can be formulated explicitly.

The following conclusions may be drawn from Eqs. (5) and (6). In the limit $p\to 0$, attained for $t\to\infty$, all sequences consist of single adsorbed segments. The isotherm assumes the form expected for $\langle\nu\rangle$-mers, which dissociate completely on the surface. Since $\langle\nu\rangle \gg 1$, no simple Langmuir isotherm is obtained, even for $p\to 0$, and θ depends only slightly on c after an initial steep rise. For small θ, ΔH_{ads} is proportional to the square root of the molecular weight. For higher degrees of occupancy of the surface, a term proportional to the molecular weight and the cohesive energy density of the polymer is added.

* Present address: Department of Physics, Syracuse University, Syracuse, New York.

[1] E. Jenckel and B. Rumbach, Z. Elektrochem. 55, 612 (1951).

Neutron Diffraction Study of the NaCl-type Modification of ND_4Br and ND_4I*

HENRI A. LEVY AND S. W. PETERSON
Chemistry Division, Oak Ridge National Laboratory, Oak Ridge, Tennessee

(Received October 14, 1952)

AMMONIUM bromide above 137.8°, deutero-ammonium bromide above ~125°, and ammonium iodide above −17.6° crystallize in the face-centered cubic system with ion centers in the NaCl-type arrangement. We have made powder neutron diffraction studies of ND_4Br at 250°C and ND_4I at 23°C in order to obtain information on the ammonium ion orientation in these materials.

Previous neutron studies[1,2] of the lower temperature phases of ND_4Br and of ND_4Cl all disclose structures in which a close approach between hydrogen and anion is achieved. In the NaCl type structure there is no way in which four tetrahedrally arranged hydrogen atoms can achieve a close approach to the octahedrally distributed anions simultaneously. This fact suggests that either the attractive interaction between H and anion is overcome in these phases, so that the ion undergoes free or nearly free rotation, or that fewer than four close approaches are achieved, the cubic symmetry being satisfied statistically by randomness among several equivalent orientations.

We have accordingly compared observed structure factors for 10 bromide and 8 iodide reflections with those calculated from the following models, in each of which N is placed in positions 4(*a*) and Br in 4(*b*) of space group $O_h{}^5$.

Model	Hydrogen positions[3] (space group $O_h{}^5$)
Freely rotating	16*D* uniformly on 4 spheres around *N*.
Single approach	4*D* in 24(*e*), $x=b$, 12*D* uniformly distributed around 24 circles centered at 24(*e*), $x=b/3$.
Double approach	8*D* in 96(*j*), $y_1=b\cos 9°\,44'$, $z_1=b\sin 9°\,44'$, 8*D* in 96(*k*), $x_2=(b/\sqrt{2})\cos 54°\,44'$, $z_2=b\sin 54°\,44'$.
Triple approach	12*D* in 96(*k*), $x_1=b/3\sqrt{3}$, $z_1=5b/3\sqrt{3}$, 4*D* in 32(*f*), $x_2=b/\sqrt{3}$.

The parameter b, the ratio of the $N-D$ distance to the unit cell edge, corresponded to $N-D=1.03$A. Separate temperature factors were assigned to each atomic species. The single approach model corresponds to free rotation about a single threefold axis of the ion oriented along a fourfold axis of the crystal.

For both substances the freely rotating ion model is in disagreement with the observed data, while the remaining three models achieve nearly equivalent agreement, satisfactory within experimental error. A number of other models for the bromide structure, in which no close approach of D to Br is achieved, were also found to be in disagreement with the data.

Stephenson, Landers, and Cole[4] have interpreted heat-capacity measurements on NH_4I and mixed crystals of NH_4I-KI to indicate ammonium ion rotation in both materials, in the latter even at very low temperatures. Their arguments, which are qualitative only, appear to apply as well to single-axis rotation as to free rotation. Further, the two nonrotating models here tested are highly disordered, and the corresponding ammonium-ion orientational potential of each has multiple equivalent minima to a high degree; it is to be expected that energy levels for rotatory motion of the ion would then be closely spaced. The qualitative interpretation of heat capacities of Stephenson *et al.* thus applies equally well to all models here considered.

Infrared absorption data from thin films of NH_4I and ND_4I has led Plumb and Hornig[5] to a model involving single-axis rotation identical with our single approach model.

We are grateful for several illuminating discussions of this problem with Professor Verner Schomaker, and for a conversation with Dr. R. C. Plumb.

* This work was performed under the auspices of the U. S. Atomic Energy Commission.

[1] H. A. Levy and S. W. Peterson, "Neutron diffraction determination of the crystal structure of ammonium bromide in four phases" (submitted to J. Am. Chem. Soc.)
[2] H. A. Levy and S. W. Peterson, Phys. Rev. 86, 766 (1952).
[3] The notation is that of *International Tables for Determination of Crystal Structure* (Edwards Brothers, Inc., Ann Arbor, Michigan, 1944).
[4] Stephenson, Landers, and Cole, J. Chem. Phys. 20, 1044 (1952).
[5] R. C. Plumb and D. F. Hornig, J. Chem. Phys. 21, 366 (1953).

Evidence for One-Dimensional Rotation in Ammonium Iodide

R. C. PLUMB* AND D. F. HORNIG
Metcalf Chemical Laboratories, Brown University, Providence, Rhode Island

(Received December 8, 1952)

PREVIOUSLY it has been demonstrated spectroscopically that the λ-point transitions in ammonium halides cannot involve free rotation since the torsional oscillation frequency of the ammonium ion in the lattice occurs in the phase above (*II*) as well as beneath (*III*) the transition temperature.[1] These results were subsequently confirmed by neutron diffraction studies.[2] However, it was noted by Wagner[3] and confirmed by the careful studies by Dinsmore[4] that in the face-centered cubic modification of NH_4I(*I*), which is stable above the first-order transition at −17.6°C, the combination of the triply degenerate bending vibration ν_4 at 1400 cm^{-1} with the lattice torsion ν_6 which occurs at 1685 cm^{-1} in phases *II* and *III* was absent. Instead the spectra showed only a weak diffuse absorption maximum at 1600–1650 cm^{-1} which persisted without much change in films in which phase *I* was supercooled

to −195°C. We have repeated this work with care and found the diffuse region mentioned before at approximately 1600 cm^{-1} and, in addition, noted that there were roughly exponential wings at the base of ν_4 in phase *I*. The width at half-height of the central peak changed from about 23 cm^{-1} in phases *II* and *III* to about 30 cm^{-1} in phase *I*.

These observations are consistent neither with a statically disordered model nor the 3-dimensional freely rotating structure suggested by the heat capacity studies of Stephenson *et al.*[5] The latter would require *P* and *R* branch maxima which do not exist.

According to a rough electrostatic calculation, the minimum potential energy occurs when one N−H bond is directed at an iodine ion. Such a model with free rotation about this $N-H\cdots I^-$ axis is consistent with the observed spectrum. The height of the barrier to this rotation, the frequency of the zero-point vibration, and the frequency of the perpendicular torsional oscillation were all computed from the electrostatic potential of an ammonium ion, represented with a charge $+0.43e$ located at the proton positions. This same model has been used successfully to calculate the torsional frequencies in NH_4Cl, NH_4Br, low ND_4Br, and NH_4I (*II* or *III*) and in no case did the effective charge vary outside the limits $0.42e$–$0.50e$.[6] The calculated torsional frequency was 203 cm^{-1}, in good agreement with the experimental combination band at 1600 cm^{-1}. The height of the barrier to rotation thus calculated was 35 cm^{-1}, with a zero-point vibrational level at 20 cm^{-1}. Consequently, the very first excited level would be above the barrier, and to a good approximation the ion can be thought of as freely rotating when $T>75°K$.

The selection rules for this model allow only the *Q* branch of the parallel component of ν_4, and only *P* and *R* branches of the perpendicular component, to appear in the infrared spectrum. However, the *P* and *R* branches of a one-dimensional rotator have no maxima; the band envelope is an error function with a missing central line. The predicted envelope of the line fits the experimental curve to within the experimental error and shows the correct effect of temperature on the wings. The diffuse nature of the combination band is roughly accounted for by rotational structure and rotation-vibration interaction.

Consequently, we conclude that the spectrum strongly indicates a structure for phase *I* of NH_4I in which one hydrogen bond is formed to I^-, and the ammonium ion rotates freely about this bond. A more detailed description of this work will appear at a later date.

Recent neutron diffraction studies of ND_4Br and ND_4I have also led Levy and Peterson to eliminate the model with 3-dimensional free rotation[7]; they find that two different static models and the one-dimensional rotator all give equally good agreement with their data.

The authors are indebted to Dr. C. C. Stephenson and Dr. H. A. Levy for conversations regarding their work.

* duPont Fellow in Chemistry, 1951–1952.
[1] E. L. Wagner and D. F. Hornig, J. Chem. Phys. **18**, 296 (1950); ibid. 305 (1950).
[2] H. A. Levy and S. W. Peterson, Phys. Rev. **86**, 766 (1952).
[3] E. L. Wagner (unpublished data).
[4] H. L. Dinsmore (unpublished data). See also L. F. H. Bovey, J. Opt. Soc. Am. **41**, 836 (1951).
[5] Stephenson, Landers, and Cole, J. Chem. Phys. **20**, 1044 (1952).
[6] D. F. Hornig and S. Millman (unpublished work).
[7] H. A. Levy and S. W. Peterson, J. Chem. Phys. **21**, 366 (1953).

The Effects of Neutron Bombardment on a Zinc Sulfide Phosphor

ALAN W. SMITH AND JOHN TURKEVICH
Department of Chemistry, Princeton University, Princeton, New Jersey
(Received December 1, 1952)

PREVIOUS studies of the effects of nuclear radiation on phosphors has been confined to the study of the interaction of alpha-particles on zinc sulfide and on cadmium sulfide.[1]

We wish to report results obtained by subjecting hexagonal zinc sulfide phosphor [0.006 percent Cu, NaCl (5) 1270°C 7 min] to neutron bombardment in the nuclear reactor of the Brookhaven National Laboratory.

Neutron bombardment produces marked changes in the properties of copper activated zinc sulfide phosphor. The luminescence efficiency, measured under comparable conditions, decreases exponentially with time of neutron irradiation. While the luminescence of the undamaged sample increases linearly with exciting light intensity, that of the damaged sample depends on the square of the intensity. Furthermore, the effect of the neutron bombardment is more marked, the higher the measurement temperature. Under x-ray excitation, the linear dependence of the excitation on the x-ray intensity is not affected by subjecting the phosphor to radiation damage, though the luminescence efficiency again decreases exponentially with duration in the pile. The sensitivity of phosphorescence of the zinc sulfide to infrared quenching is strongly enhanced by neutron damage.[2] The character of the thermoluminescence (glow curve) is often used to indicate the nature of the trapping of photoexcited electrons in the solid. It was found that neutron bombardment decreases the number of electrons that are trapped and that subsequently leave traps with light emission. In addition, the depth of traps is changed. The rate of decay of phosphorescence is increased by radiation damage, and the emission spectrum is shifted slightly to shorter wavelengths. The rise time of luminescence to a steady-state value on photoexcitation can be taken as a measure of the number of electrons trapped during the process of excitation. In the case of the undamaged sample, the rise time is rapid indicating that a small number of traps have to be filled before a steady state is established. In the damaged sample the rise time is slow indicating the presence of a large number of traps. Furthermore, the solid shows a memory in that once a steady value of luminescence is reached, the rise time is as fast as that for the undamaged sample. Keeping the damaged and light-saturated phosphor in the dark for two weeks restores it to the original state in that the slow rise time phenomenon is again observed. The transition of the electrons from the traps produced by the neutrons to the ground state is accompanied by radiation neither in the visible nor in the infrared part of the spectrum.

The changes in the dielectric properties of the phosphor on neutron bombardment were studied in an analogous way.[3] The increase in dielectric constant (100 kilocycles), normally observed in illumination of the phosphor, was about the same for both damaged and undamaged sample. In contrast to the effect of exciting light intensity on luminescence, the dielectric constant change was found to approach saturation at high light intensity. The dielectric constant change during thermoluminescence was found to be similar to the thermoluminescence curve and for the damaged sample was displaced to lower temperatures. The rise time of the dielectric constant change on illumination was increased, and the decay rate on removal of excitation decreased as result of pile irradiation.

Annealing the bombarded specimens at 200°C counteracts some of the effects of the damage produced by fast neutrons, but the temperature treatment must be carried out at about 900°C to remove completely the damage.

Grinding of the phosphor produces changes in the luminescent properties of the solid that are different from radiation damage. While the luminescence efficiency drops, the decay rate is slower. The thermoluminescence curve has a new high temperature peak indicating that grinding produces a new luminescence-active trap deeper than those already present. No evidence could be found for the production of nonradiative traps of a nature similar to those produced by neutron damage.

The results are explained in the following way: the normal phosphor contains emission centers, a filled band, an empty band, and isolated dislocations and/or vacancies. On photoexcitation, an electron is excited from the emission center into an excited state or the conduction band, leaving a hole in the emission center. The electron may go back to the conduction band with the emission of light (luminescence) or be trapped at the isolated dislocation or

vacancy. With time or with increase in temperature, the trapped electron is released via the conduction band to give rise to phosphorescence or thermoluminescence.

On neutron irradiation of the phosphor an occasional fast neutron transfers a small part of its high energy to a zinc or sulfur atom giving it high kinetic energy. These hot lattice atoms transfer their energy very efficiently to their neighbors producing a large number of highly localized dislocations.

On light irradiation, photoexcited electrons are captured very efficiently at these dislocations decreasing in this way the luminescence of the phosphor. Electrons thus captured are released from the killer traps not via the empty conduction band, but by a radiationless process involving the motion of holes from the emission center via the filled band to the killer trap. The dielectric constant changes which accompany both the radiative and the nonradiative processes seem to be associated not with the presence of electrons in traps but with the transfer *process* of electrons and holes in the solid.

This work was carried out under the sponsorship of the U. S. Atomic Energy Commission.

[1] E. Marsden, Proc. Roy. Soc. (London) **A83**, 548 (1910); E. Rutherford, *ibid.* **A83**, 561 (1910); P. Wolf and N. Riehl, Ann. Physik **17**, 581 (1933); E. Streck, *ibid.* **35**, 58 (1939); I. Broser and H. Kallmann, Z. Naturforsch. **5a**, 381 (1950); I. Broser and R. Warminsky, *ibid.* **6a**, 85 (1951).
[2] A. Becker, Z. Physik **125**, 475 (1949).
[3] G. F. J. Garlick, *Luminescent Materials* (Oxford University Press, London, 1949); W. deGroot, Physica **8**, 789 (1941).

The Rate of Combination of Methyl Radicals*

K. U. INGOLD† AND F. P. LOSSING
Division of Chemistry, National Research Council, Ottawa, Canada
(Received December 1, 1952)

THE rate constant (k_1) of ethane formation from methyl radicals

$$CH_3+CH_3 \xrightarrow{k_1} C_2H_6$$

has been re-examined by a modification of a method previously reported.[1,2] The concentrations of methyl radicals, ethane and methane, formed by the thermal decomposition of mercury dimethyl in a stream of helium were measured by continuous analysis of the gas stream using a mass spectrometer. A small portion of the gas entered the ionization chamber of the spectrometer through a small orifice in a quartz cone projecting into the stream.

In the present modification, the mercury dimethyl is almost completely decomposed to give methyl radicals by passing the stream of gas over a short movable furnace contained in a tubular quartz reactor. When the distance between the movable furnace and the orifice is small, the time available for combination of the radicals is very short ($<10^{-4}$ sec), and their concentration is nearly equivalent to the amount of mercury dimethyl which has been decomposed. As the contact time is increased by retracting the furnace from the orifice, the concentration of radicals decreases, and an equivalent amount of ethane appears. The rate of disappearance of the methyl radicals and formation of ethane with increasing time of contact has been examined by retraction experiments of this kind, using different concentrations of mercury dimethyl. It has been found that the combination proceeds by both a first-order and a second-order reaction. The effect of temperature on the second-order reaction has been studied, and it is found that the rate has a negative temperature coefficient. A plot of log collision efficiency [i.e., $\log(k_1/NZ)$ where N is Avogadro's number and Z is the collision frequency] against $1/T(°K)$ for this reaction gives a relation which is almost linear between 1100°K and 450°K and has a slope corresponding to -2.2 ± 0.5 kcal. No effect of total pressure was found over the range studied (i.e., 4.8 to 18.5 mm). A summary of the values obtained for the collision efficiency at different temperatures is given in Table I. These results will be presented in more detail in a forthcoming publication.

TABLE I. Effect of temperature and pressure on k_1. Values of $k_1T^{-\frac{1}{2}}$ are given in $(\text{moles/cc})^{-1}\,\text{sec}^{-1}\,(°K)^{-\frac{1}{2}}$.

Temp (°K)	$k_1T^{-\frac{1}{2}}\times10^{-12}$	Collision efficiency	He pressure (mm)
1087	0.144	0.024	9.0
873	0.200	0.033	9.0
713	0.242	0.039	9.0
617	0.344	0.055	9.0
551	0.414	0.066	9.0
502	0.520	0.085	9.0
466	0.540	0.090	9.0
434	0.655	0.105	9.0
1008	0.176	0.029	4.8
1008	0.163	0.027	18.5

* National Research Council Contribution 2925.
† National Research Council Postdoctorate Fellow.
[1] F. P. Lossing and A. W. Tickner, J. Chem. Phys. **20**, 907 (1952).
[2] Lossing, Ingold, and Tickner, Disc. Faraday Soc. (1952) (to be published).

Thermodynamical Study of the Water-Triethylamine System near Its Lower Critical Point

A. BELLEMANS
Faculty of Science, University of Brussels, Brussels, Belgium
(Received December 8, 1952)

AT a lower critical point (L.C.P.), one has[1]

$$\partial^2 g_m/\partial x_B^2=\partial^3 g_m/\partial x_B^3=0, \quad (1)$$
$$\partial^2 h_m/\partial x_B^2>0, \quad \partial^2 s_m/\partial x_B^2>0. \quad (2)$$

Using excess functions, defined by

$$h_e=h_m \quad \text{and} \quad s_e=s_m+k(x_A \lg x_A+x_B \lg x_B), \quad (3)$$

relations (1) and (2) give

$$\partial^2 h_e/\partial x_B^2>0, \quad \partial^2 s_e/\partial x_B^2>k/x_A x_B>0, \quad (4)$$
$$T_c(\partial^2 s_e/\partial x_B^2)>\partial^2 h_e/\partial x_B^2. \quad (5)$$

We shall now try to put relations (4) and (5) in a more explicit form, by making hypotheses on h_e and s_e. We shall assume that h_e and s_e are of the form

$$h_e=K_h x_A x_B \quad \text{and} \quad Ts_e=K_e x_A x_B. \quad (6)$$

Then, from (4) and (5), we get[1]

$$h_e<0, \quad Ts_e<0, \quad (7)$$
$$|Ts_e|>|h_e|. \quad (8)$$

It appears that the excess entropy is the decisive factor at a L.C.P. However, it must be noted that rigorous thermodynamic conditions are not (7) and (8), but (1) and (2), and (4) and (5).

The triethylamine-water solutions present a L.C.P. at 18.4°C, for a molar fraction of triethylamine of about 0.15. Roberts and Mayer[2] measured the vapor pressure of these solutions at temperatures between 13°C and 18°C. We measured the heat of mixing of this system at 16.0°C±0.1. Experimental apparatus consisted of a small metallic box, divided into two tight compartments, containing weighed quantities (about 1 g) of the pure components, which is hung in a calorimeter composed of a Dewar vessel, containing a known quantity of water. The Dewar vessel, supplied with a waterproof fastening, is completely immersed in a thermostat. After two or three hours, the temperature in the Dewar remains constant to 0.001°C. The box is then turned over and shaken, so that the two constituents mix. The temperature change is measured; the quantity of water in the Dewar vessel is chosen in order to get a rise of about 0.500°C. Precision of the results lies between 5 and 10 percent. Experimental results are shown in Fig. 1. Excess entropy has been obtained by sub-

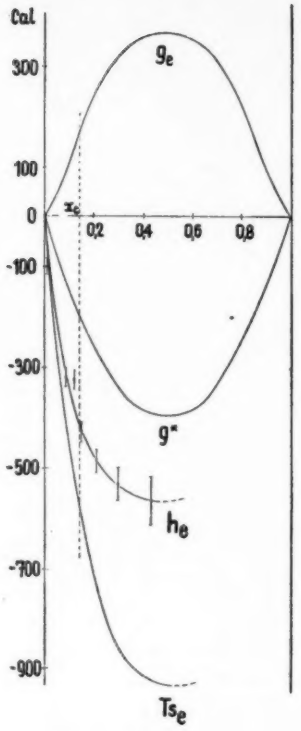

FIG. 1. Triethylamine-water system at 16°C. Excess thermodynamic functions in term of the triethylamine molar fraction. (g^* is the ideal free energy of mixing.)

tracting the excess free energy (deduced from the vapor pressure data[2]), from the excess enthalpy (deduced from our measurements). From Fig. 1, it appears clearly that relations (7) and (8) are entirely satisfied near the critical point.

We shall now discuss the molecular conditions of lower critical solution phenomena. The origin of a L.C.P. must be related to a modification of the internal degrees of freedom of the molecules in solution.[3,4] This will occur for strong anisotropic interactions between molecules, and particularly for associated substances. We made calculations on a mixture of molecules A and B giving a stable complex AB. When a complex AB is formed, there are a corresponding heat evolution ($h_e<0$) and an appreciable loss of entropy, arising from the fact that A and B lose their free rotation in the rigid complex AB.[5] When treating this solution as a perfect solution of molecules A, B, and AB, the second derivative of g_m is always positive and no demixtion can occur (see Fig. 2),

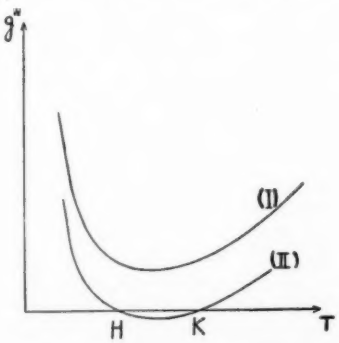

FIG. 2. Second derivative of g_m (for $x_B=0.5$), in function of temperature. (I) Perfect solution of A, B, and AB. (II) Solution of A, B, and AB, corrected by a positive term of Scatchard-Hildebrand.

though it appears that the situation is very favorable to it. And, if we add a positive enthalpy correction, related to the dispersion forces between molecules (term of Scatchard-Hildebrand), g_m'' will cross the abscissa. In Fig. 2 points H and K are, respectively, lower and upper critical points. Between them, there is a closed demixtion domain. Detailed calculations on this model will be published in the *Bulletin de la Classe des Sciences, Académie Royale de Belgique*. We thank Professor I. Prigogine, who suggested this work, for constant interest and advice.

[1] I. Prigogine and R. Defay, *Thermodynamique chimique* (Desoer, Liége, 1950).
[2] L. Roberts and J. E. Mayer, J. Chem. Phys. **9**, 852 (1941).
[3] J. S. Rowlinson, Proc. Roy. Soc. (London) **A214**, 192 (1952).
[4] A. Bellemans, J. Chem. Phys. **21**, 369 (1953).
[5] L. Saroléa-Mathot, Trans. Faraday Soc. (to be published).

Application of the Cell Method to the Statistical Thermodynamics of Solutions. III. Critical Solution Phenomena

A. BELLEMANS
Faculty of Science, University of Brussels, Brussels, Belgium
(Received December 8, 1952)

THE classical theory of strictly regular solutions states that

$$h_e=g_e=z(\epsilon_{AB}-\epsilon_{AA}/2-\epsilon_{BB}/2)x_Ax_B, \quad s_e=0, \tag{1}$$

where g_e, h_e, and s_e are excess free energy, excess enthalpy, and excess entropy, x_A and x_B are the molar fractions of constituents A and B, and z is the mean number of first neighbors. This model gives rise to an upper critical point in endothermic mixtures. It gives no explanation of lower critical solution phenomena.

It is well known that relations (1) are only first approximations. Two kinds of terms should be included in s_e:

(a) A configurational term, because of the fact that there is no random mixing.

(b) A term related to the change of the mean field acting on each molecule with composition. This term gives either positive or negative contributions to s_e.

The first of these terms has been studied extensively. Our purpose is to investigate the effect of the second one on critical solution phenomena.

In previous papers,[1,2] Prigogine and his co-workers extended to solutions the cell method of Lennard-Jones and Devonshire, first developed for pure liquids. For mixtures of spherical molecules, of same radius and with isotropic field of force, important corrections to the theory of strictly regular solutions, are obtained on both excess enthalpy and entropy by taking into account the volume change on mixing. All thermodynamical properties of the solution can be expressed in terms of two parameters δ and θ, defined by

$$\delta=(\epsilon_{BB}-\epsilon_{AA})/\epsilon_{AA}, \quad \theta=(\epsilon_{AB}-\epsilon_{AA}/2-\epsilon_{BB}/2)/\epsilon_{AA}. \tag{2}$$

One has

$$h_e=1.435x_Ax_Bz\epsilon_{AA}\theta+5.4kTv_e/v^*, \tag{3}$$

$$Ts_e=-12.8kTv_e/v^*, \tag{4}$$

where v_e is the excess volume[2] (negative for a contraction). We shall now apply these formulas to the problem of critical solution phenomena.

At the critical point, as it is well known,

$$\partial^2g_m/\partial x_B^2=\partial^3g_m/\partial x_B^3=0. \tag{5}$$

Moreover, the second derivative (with respect to x_B) of the enthalpy of mixing must be negative at an upper critical point (U.C.P.) and positive at a lower critical point (L.C.P.). These conditions fix the curvature of h_m and s_m near the critical temperature. Now, for nearly all known solutions and especially in the simple case considered here, the curvature of h_m (enthalpy of mixing) and s_m (entropy of mixing) keeps always the same sign through all the range of concentrations. So we may write

$$h_m>0; \quad s_m>0 \quad \text{at an U.C.P.}, \tag{6}$$

$$h_m<0; \quad s_m<0 \quad \text{at a L.C.P.} \tag{7}$$

The excess functions, defined by

$$h_e=h_m \quad \text{and} \quad s_e=s_m-s^*=s_m+k(x_A\lg x_A+x_B\lg x_B), \tag{8}$$

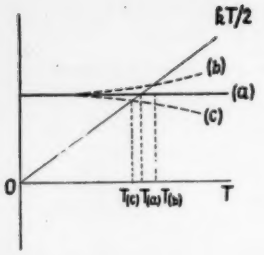

FIG. 1. Influence of excess volume on an U.C.P., from relation (11). (a) g_e in regular solutions ($v_e=0$), (b) g_e when contraction on mixing ($v_e<0$), (c) g_e when expansion on mixing ($v_e>0$).

may be put approximately in the form

$$h_e=K_h x_A x_B, \quad Ts_e=K_s x_A x_B, \tag{9}$$

owing to relations (3) and (4). K_h and K_s are independent of x_A and x_B but depend on temperature. From (9), the excess free energy becomes

$$g_e=(K_h-K_s)x_A x_B. \tag{10}$$

At the critical point, from relations (5) and (10), we get

$$x_{Ac}=x_{Bc}=\tfrac{1}{2}, \quad kT_c=(K_h-K_s)/2=2g_e(T_c, 0.5). \tag{11}$$

Relation (11) is very useful for a qualitative discussion: the critical temperature, if it exists, is given by the intersection of $kT/2$ and $g_e(T, 0.5)$ on a graphic.

(A) Upper critical solution phenomena occur in endothermic mixtures. There are two possibilities:

(a) There is a contraction on mixing. Then, from (3) and (4), g_e is higher than in the strictly regular solutions theory. Consequently, according to (11), the U.C.P. will be higher than in regular solutions. See Fig. 1. Exact calculations were made by taking the complete form of g_e in the case called "dispersion forces"[2] ($\theta\simeq-\delta^2/8$). The critical temperature is

$$kT_c/z|\epsilon_{AA}|=0.090\delta^2[1+0.36\delta^4(1+\delta/2)^{-3}], \tag{12}$$

while in strictly regular solutions it was

$$kT_c/z|\epsilon_{AA}|=0.090\delta^2. \tag{13}$$

The critical concentration is no more equal to 0.5 but is somewhat nearer to constituent A. Equations (12) and (13) are plotted on Fig. 2. Similar results have been obtained from another cell model, namely the harmonic oscillator model.[1]

(b) There is an expansion on mixing. Then, according to (3), (4), and (11), the U.C.P. will be lower than in the regular solutions theory. See Fig. 1. Exact calculations, made in the case called "association in inert solvent,"[2] show that the T_c is

$$kT_c/z|\epsilon_{AA}|=0.359\delta(1-1.8\delta+2.8\delta^2) \quad \text{for} \quad \delta\leqslant 0.3,$$

while for regular solutions,

$$kT_c/z|\epsilon_{AA}|=0.359\delta.$$

These two equations are plotted on Fig. 3. The results are compared to the quasi-chemical correction. The critical concentration is somewhat nearer to constituent B.

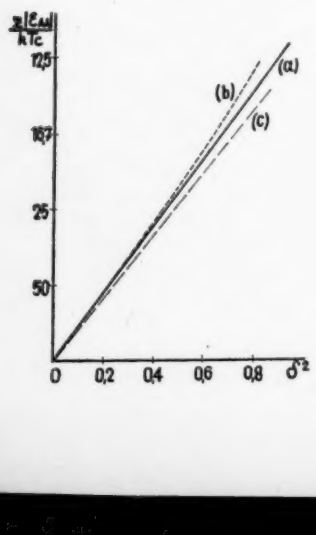

FIG. 2. Dispersion forces. Upper critical temperature in function of δ^2. (a) Strictly regular solutions; (b) cell model, taking into account the contraction on mixing; (c) quasi-chemical approximation.

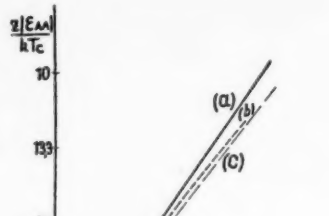

FIG. 3. Association in inert solvent. Critical temperature in function of δ. (a) Strictly regular solutions, (b) cell model taking into account the volume expansion, (c) quasi-chemical approximation.

(B) From relations (7) and (8), it follows that a L.C.P. can only occur in exothermic mixtures ($h_m<0$), where $s_e<-s^*$. This last condition cannot be filled at any reasonable temperature for the liquid state, even for large values of δ and θ. Such a model cannot give rise to a L.C.P., which must be related to other factors and especially to anisotropic interactions between molecules. These conclusions agree with those of Rowlinson[5] and reverse those of Ono,[6] who thought that a L.C.P. could occur in such simple solutions.

We are much indebted to Professor Prigogine, who suggested the present work, for constant interest and advice.

[1] I. Prigogine and G. Garikian, Physica **16**, 239 (1950).
[2] I. Prigogine and V. Mathot, J. Chem. Phys. **20**, 49 (1952).
[3] I. Prigogine and R. Defay, *Thermodynamique chimique* (Desoer, Liége, 1950), new edition.
[4] O. K. Rice, Chem. Rev. **44**, 65 (1949).
[5] J. S. Rowlinson, Proc. Roy. Soc. (London) **A214**, 192 (1952).
[6] S. Ono, Mem. Faculty Eng. Kyushu Imp. Univ. **12**, 201 (1950).

Interaction of Methylene Deformation Frequencies in Paraffin Crystals*

R. S. STEIN, *Department of Chemistry, University of Massachusetts, Amherst, Massachusetts*

AND

G. B. B. M. SUTHERLAND, *Department of Physics, University of Michigan, Ann Arbor, Michigan*

(Received December 11, 1952)

THE doublet at 14μ in the spectra of polythene and other polymethylene hydrocarbons has been discussed in several papers.[1-3] We should like to report the results of some investigations regarding the nature of this doublet which we have conducted and which will be reported in detail together with some more recent work in a forthcoming publication. We find that:

(1) The doublet consists of two components, one at 720 cm^{-1} (A) and one at 730 cm^{-1} (B).

(2) In all samples of unoriented polythene which we have studied, component (A) is more intense than (B). Component (B) is relatively more intense in samples having higher crystallinity.

(3) The ratio of the intensity of component (B) to that of (A) gradually decreases with increasing temperature in a manner similar to the decrease in crystallinity with temperature.

(4) The relative intensity of band (B) decreases appreciably on stretching (decreasing approximately to half in a 400 percent elongation).

(5) Both bands absorb most strongly with radiation polarized perpendicular to the direction of stretching the sample. The dichroic ratio for band (B) is much greater than that for (A).

(6) On cooling to liquid nitrogen temperature band (B) became appreciably sharper and shifted from 730 to 733 cm^{-1}. Band (A) was not appreciably affected.

(7) The spectra of a sample of a completely deuterated paraffin revealed that the counterpart of band (A) shifted to 518 cm^{-1} and

band (B) to 524 cm^{-1}, both bands decreasing in frequency in approximately the ratio $1/\sqrt{2}$. The counterpart of the 6.8μ band in polythene is also a doublet in the deuterated paraffin with two components at 1086 and 1093 cm^{-1}. This observation led to a reexamination of the 6μ band in polythene, which revealed that this is a doublet consisting of two components at about 1464 and 1473 cm^{-1}. The higher frequency component disappears on heating. This doublet changes with crystallinity, stretching polarization and temperature in a manner analogous to that of the 6μ doublet.

(8) An examination of a series of pure crystalline n-paraffins ranging from $C_{18}H_{38}$ to $C_{64}H_{110}$ revealed that the 14μ doublet is present in their spectra, with both components of equal intensity. On heating, component (B) disappeared sharply at a temperature corresponding to the transition temperature for these hydrocarbons identical with the temperature found by x-ray and specific heat methods.

All of these observations are consistent with the explanation that the spectra of polythene consists of a super-position of spectra of the crystalline and amorphous portions. The crystallites are oriented to a higher degree on stretching. The doublets occur only in the crystallite spectra in which case both components are of equal intensity in the unstrained crystallite. It can be shown[4] that splittings of this type may arise from coupling between normal vibrations of the CH_2 groups in adjacent hydrocarbon chains in the crystal lattice of a normal paraffin. Component (B) results from deformations in phase with those of nearest neighbors, while component (A) results from out-of-phase deformations. The magnitude of the separation of the components depends on the distance of closest approach of nearest neighbor hydrogens and on the degree of van der Waals interaction.

* This work was carried out while both authors were at the Department of Colloid Science, Cambridge University, England, 1948–1949. Mr. Stein's work was supported in part by a fellowship from the National Research Council.

[1] Elliot, Ambrose, and Temple, J. Chem. Phys. **16**, 877 (1948).
[2] H. W. Thompson and P. Torkington, Proc. Roy. Soc. (London) **184A**, 3 (1945).
[3] King, Hainer, and McMahar, J. Appl. Phys. **20**, 559 (1949).
[4] Stein and Montroll (to be published).

Investigation of the Heat of Vaporization of Carbon

WILLIAM A. CHUPKA, *Mallinckrodt Chemical Laboratory, Harvard University, Cambridge, Massachusetts*

AND

MARK G. INGHRAM, *University of Chicago and Argonne National Laboratory, Chicago, Illinois*

(Received December 1, 1952)

THE heat of vaporization of carbon is in considerable controversy. Three possible spectroscopic values for the dissociation energy of CO coupled with well established thermodynamic data give three possible values for this quantity. The three values are 136 kcal/mole, 141 kcal/mole, and 170 kcal/mole. The controversy revolves around two questions; the accommodation coefficient for evaporation, and the identity and relative amounts of the evaporating species. An accommodation coefficient near unity, assuming the evaporation occurs largely as C, would favor the highest value, according to available data on the rate of evaporation from a graphite surface. Doehaerd *et al.*[1] claim that the accommodation coefficient is actually about 0.001. If this is true, one of the lower heats of evaporation is correct. One of the above authors, Waelbroeck, claims that the major part of the species evaporating from a surface is C_2. This is in contrast with Brewers determination[2] where he finds the C_2 evaporation to be of the order of 0.0001 of the total evaporation. The main objection of Brewer to the experiments of Doehaerd *et al.* is the possibility of insufficient outgassing of their graphite sample.

One possible method of resolving these difficulties is to use a mass spectrometer to identify and measure the relative amounts of the various species evaporated from a graphite surface as a function of surface temperature. We have made preliminary measurements using this technique.

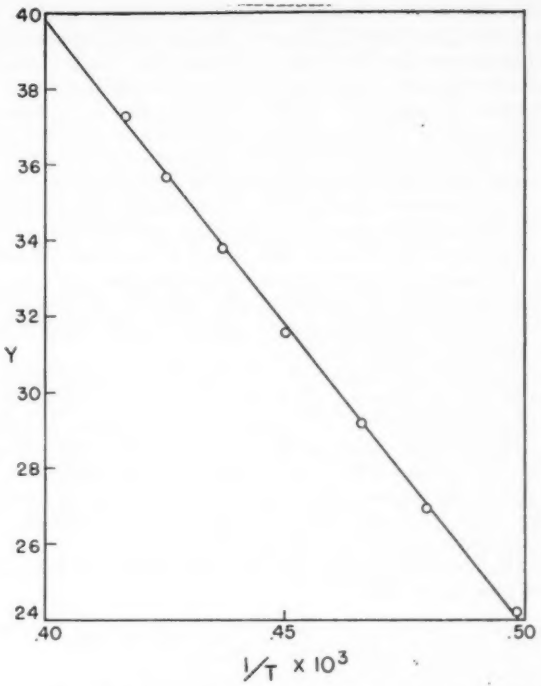

FIG. 1. Rate of evaporation of carbon atoms as a function of temperature. $Y = R \ln I(C^+)T - 2\Delta C_p 1000/T + \Delta C_p \ln 1000/T$, where $I(C^+)$ is the C^+ ion beam intensity and $\Delta C_p = -3.2$ cal/g atom degree. $I(C^+)T$ is proportional to the pressure of carbon atoms since $I(C^+)$ is proportional to the number of atoms crossing and the time spent in the ionization region. Slope of line $= -\Delta H$ (2000°K) (apparent) of the process C (graphite) $\rightarrow$ C(^5P) (gas).

The technique used consisted of bombarding the constituents evaporated from a carbon filament with controlled energy electrons and determining the mass of the ion produced with a standard single focusing magnetic analyzer. The constituents were thus identified both by mass and by appearance potential. The C^+ ion appeared at an electron bombarding energy of 11.1±0.5 volts, the C_2^+ appeared at 11.5±1 volts. The 11.1 volt appearance potential for C^+ ion indicates that the evaporation of C occurs in the ground state. This assumes that the half-life of the excited ^5S state is longer than the transit time between evaporation and ionization. The time of transit is about 5×10^{-6} sec while the half-life of the ^5S state is estimated to be of the order of $10^{-4}-10^{-5}$ sec from Shenstone's[3] line intensities.

In addition to mass resolution and appearance potentials, the ion beams were studied by retarding potential techniques. This served to show whether the evaporating species have kinetic energy in excess of thermal energies. According to a theory of Herzberg[4] carbon atoms may evaporate over a potential barrier which would give resulting atoms an excess kinetic energy in an amount equal to the difference between the heat of sublimation and the activation energy. Any excess kinetic energy would have to be subtracted from the apparent heat of vaporization obtained by temperature plots of evaporation from a surface in order to get the true heat of sublimation.

The variation of carbon atom evaporation with temperature is shown in Fig. 1. The slope yields an apparent ΔH(2000°K) of sublimation of 179.8±10 kcal/mole by a least squares analysis. This gives a ΔH(0°K) of 178.5±10 kcal/mole. This value agrees fairly well with the high spectroscopic value and eliminates the lower values as activation energies of sublimation.

Measurements of the energy of the C^+ ions showed them to have thermal energies within ±0.3 volt. This value is incompatible with Herzberg's suggestion of a potential barrier of the order of 1.5 volts. On the other hand, the proposal of Herzberg, Herzfeld, and Teller[5] is not affected by this observation so that a low accommodation coefficient is still possible.

The ratio of C/C_2, assuming equal ionization cross sections, was found to be 1.2 at 2300°K. This ratio, together with the assumption of an accommodation coefficient for C_2 near unity, tends to support a value for the heat of sublimation of C_2 in the neighborhood of 200 kcal/mole as suggested by Waelbroeck.[6] However, accurate measurements of the temperature dependence of this ratio have not yet been carried out because of interference of a strong Na^+ ion beam. Also, there still remains a slight possibility that the C_2^+ is formed from the free radical C_2H, since this appearance potential is unknown, and the value of the ionization potential of C_2 (12 ± 2 ev) determined by Kallmann and Rosen[7] is uncertain. The ratio C_2/C_2H, assuming equal ionization cross sections, was approximately unity. It is of interest to note that Gaydon[8] finds some evidence for a vapor pressure of C_2 which is roughly in agreement with that indicated by this work.

It was found that the intensity of hydrocarbons and free radicals went up with temperature. The ratio of carbon to total evaporation did improve throughout the course of an experiment. This indicates that spurious results might be obtained under conditions of insufficient outgassing and where mass resolution is not used.

Further experiments are planned to extend the temperature range of the experiment and to investigate more completely the accommodation coefficient and the ratio C/C_2.

The authors wish to thank Mr. Thomas L. Bailey for doing some of the preliminary work.

[1] Doehaerd, Goldfinger, and Waelbroeck, J. Chem. Phys. **20**, 757 (1952).
[2] Brewer, Gilles, and Jenkins, J. Chem. Phys. **16**, 797 (1948).
[3] A. G. Shenstone, Phys. Rev. **72**, 411 (1947).
[4] Herzberg, Chem. Revs. **20**, 145 (1937).
[5] Herzberg, Herzfeld, and Teller, J. Phys. Chem. **41**, 325 (1937).
[6] F. Waelbroeck, J. Chem. Phys. **20**, 757 (1952).
[7] Kallmann and Rosen, Z. Physik **61**, 332 (1930).
[8] Gaydon and Wolfhard, Proc. Roy. Soc. (London) **A201**, 570 (1950).

Thermoluminescence of Ice

EUGENE C. AVERY AND LEONARD I. GROSSWEINER
Chemistry Division, Argonne National Laboratory, Lemont, Illinois
(Received December 17, 1952)

THE investigation of the x-ray induced luminescence of ice[1] suggested the possibility that electrons might remain trapped in the ice after the excitation was removed. Samples of ice prepared from de-ionized water were irradiated with filtered 50 kv x-rays at −183°C and slowly warmed in a detection apparatus using cooled 1P28 photomultiplier tubes and pulse counting techniques.[2] Thermoluminescence was observed and a typical glow curve[3] is shown (Fig. 1). There is a principal peak at about −120°C and evidence of lesser peaks at higher and lower temperatures.

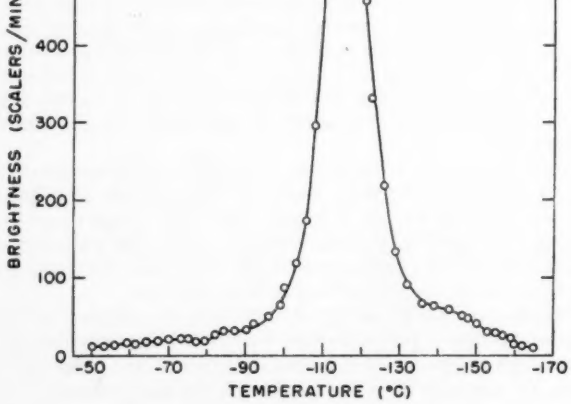

FIG. 1. Thermoluminescence of ice. Relative dosage: 20. Heating rate: 2.7°C/min.

TABLE I.

1[a] Relative dosage	2 Relative x-ray intensity	3 Glow peak (°C)	4 Heating rate (°C/min)	5[b] B^* (Scalers/min)	6 n^* (Scalers)	7 n^*/B^* (min)	8 E ev
1	4	−122	2.9	116	274	2.4	0.28
2	4	−121	2.7	126	390	3.1	0.24
2.5	1	−120	2.8	180	633	3.5	0.21
5	4	−119.5	2.6	313	1030	3.3	0.24
10	4	−113.5	2.4	385	1300	3.4	0.27
20	4	−115	2.7	555	1790	3.2	0.25

[a] A relative dosage of 1 corresponds to about 1750 roentgens.
[b] A scaler is 256 counts.

If the principal peak is associated with a first-order decay process and an electron trap of constant depth, the decay process can be represented by

$$B=-dn/dt=nse^{-E/kT}, \tag{1}$$

where n is the number of electrons in a trap of depth E, B is the measured brightness, and s is a rate constant. In these experiments the rate of heating was low so that the method suggested by Urbach[4] could be used to calculate E. Thus by differentiating Eq. (1), one finds

$$E/k=B^*T^{*2}/n^*\dot{T}, \tag{2}$$

where the asterisk refers to the glow curve maximum and $\dot{T}$ is the heating rate. Some results are summarized in Table I.

The light sum stored at the glow peak n^* was calculated from the peak and half-width (assuming a symmetrical peak) of the glow curve to minimize the effects of side bands. The nearly constant values of T^* (column 3) and of n^*/B^* (column 7) indicate the decay is first order in n. This being the case, E was calculated from Eq. (2), and its average value is 0.25 ± 0.02 ev. These calculations were checked by means of Eq. (1) for individual runs by plotting the $\log n/B$ against $1/T$, using average experimental values over 1 minute intervals for B and T and n^* from Table I. The agreement between E calculated from the slope and from Eq. (2) is good. A typical plot is shown in Fig. 2.

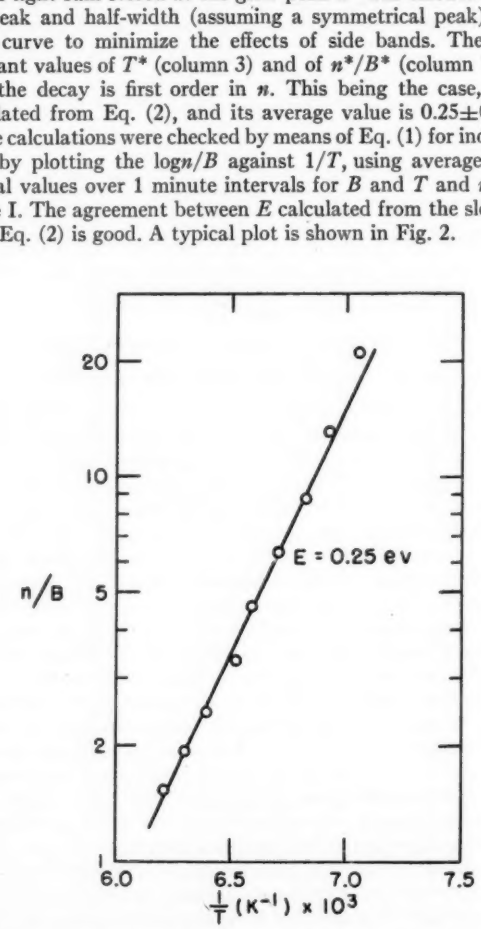

FIG. 2. Thermoluminescence of ice as a first-order process; plot of $\log n/B$ *vs* $1/T$. Relative dosage: 5. Heating rate: 2.6°C/min.

There appears to be a small shift of the glow peak to higher temperatures with higher concentration of filled traps. This may be interpreted as an increase in the trap depth, perhaps resulting from interaction between filled traps.

The spectral distribution has not been measured to date, but it is likely that this luminescence is the same as was observed during steady x-ray excitation of pure ice.[1] This latter has been observed with a Gaertner small quartz spectrograph to be a single peak at 385 mμ with a half-width of 95 mμ. Further work on thermoluminescence and fluorescence of pure ice and ice containing ionic additives is being carried out. It is a pleasure to acknowledge valuable discussions concerning this work with M. S. Matheson and B. Smaller of this laboratory.

[1] L. I. Grossweiner and M. S. Matheson, J. Chem. Phys. **20**, 1654 (1952).
[2] Smaller, May, and Freedman, Phys. Rev. **79**, 940 (1950).
[3] F. Urbach, Wien. Ber. IIa **139**, 353, 364, and 483 (1930).
[4] F. Urbach, *Solid Luminescent Materials* (John Wiley and Sons, Inc., New York, 1948), p. 124.

Electron Diffraction and Microwave Investigation of Tertiary Butyl Fluoride

FLEMMING ANDERSEN, JOHN RASTRUP ANDERSEN, AND BØRGE BAK
University of Copenhagen, Chemical Laboratory, Copenhagen, Denmark
AND
OTTO BASTIANSEN, EILIF RISBERG, AND LISE SMEDVIK
University of Oslo, Department of Chemistry, Oslo, Norway
(Received December 1, 1952)

FROM electron-diffraction studies of tertiary butyl chloride and bromide, Beach and Stevenson[1] were able to conclude that the interatomic distances were C−C=1.54±0.02, C−Cl =1.78±0.03, C−Br=1.92±0.03A, while the CCC angle was 111° 30′±2°, corresponding to the CCHal angle=107° 12′. The methyl groups were assumed to be tetrahedral with C−H =1.093A.

In a letter on the microwave spectra of tertiary butyl chloride, bromide, and iodide, Williams and Gordy[2] have discussed whether this CCC angle is compatible with reasonable values for the C−Hal bond lengths. Setting the CCC angle to 111° 30′, the HCH angle=109° 30′, the C−C distance=1.54, and the C−H distance=1.093A, they found that their microwave measurements were reproduced by C−Cl=1.82, C−Br=1.98, and C−J =2.19A. This is incompatible with the results by Beach and Stevenson. Moreover, these carbon-halogen distances deviate considerably from the corresponding distances in the methyl halides (1.78, 1.94, and 2.14A). Williams and Gordy showed that if one assumes that the CCC angle is tetrahedral or very nearly so, more reasonable values of the distances are obtained, *viz.*, C−Cl =1.78, C−Br=1.94, and C−J=2.14A. Harmony with the measurements of Beach and Stevenson now only exists if their determination of the CCC angle is assumed to be of maximum inaccuracy (2°).

As stated by Williams and Gordy the microwave spectra of tertiary butyl chloride, bromide, and iodide are not simple. The nuclear coupling of the halogen, the effect of centrifugal stretching, and the readily excited torsional vibrations of the methyl groups cooperate to make the spectra complex. Because of this, it was decided by the authors to examine the microwave spectrum of tertiary butyl *fluoride* (TBF) where there is no quadrupole coupling. Besides, the K-splitting is ignorable at the $J=1\rightarrow2$ transition which may conveniently be studied at 18 850 mhz. The absorption pattern due to restricted rotation remains as an interesting feature. As isotopic species of TBF are difficult to prepare, it was decided to investigate the electron-diffraction pattern simultaneously in the hope that a combination of the results from the two independent determinations might prove useful.

TABLE I.

CCF angle	CCH angle	C−F A
107° 28′	107° 28′	1.311
107° 28′	109° 28′	1.339
107° 28′	111° 28′	1.367*
109° 28′	107° 28′	1.321
109° 28′	109° 28′	1.349
109° 28′	111° 28′	1.377*
111° 28′	107° 28′	1.331
111° 28′	109° 28′	1.359
111° 28′	111° 28′	1.389

TABLE II. Dipole moments of primary and tertiary halogenides (Debye units)

	F	Cl	Br	J
CH_3X	1.83[a]	1.87[b]	1.80[a]	1.66[b]
$(CH_3)_3CX$	2.05[d]	2.04[c]	2.17[c]	2.20[c]

[a] Natl. Bur. Standards Circular 518, *Molecular Microwave Spectra Tables.*
[b] Townes, Shulman, and Dailey, Phys. Rev. **76**, 472 (1949).
[c] Shulman, Dailey, and Townes, Phys. Rev. **78**, 145 (1950).
[d] This investigation.
[e] A. Audsley and Frank Goss, J. Chem. Soc. **1942**, 497.

In its ground vibrational state TBF absorbs microwaves at 18 849.8 mhz. For a "staggered" model with C−C=1.54, C−H =1.093, the following combinations of the geometrical parameters are compatible with the observed microwave absorption frequency.

Table I shows that a Williams-Gordy model for TBF with tetrahedral angles and a C−F distance equal to the C−F distance in CH_3F(=1.384A) is excluded.

If it is assumed that the C−C distance=1.54A, it follows from the electron diffraction pattern that the C−F distance is 1.38 ±0.02A. Further, the electron-diffraction investigations leads to a CCF-angle of 108°±1.5°. The only combinations of Table I which agree with this are those marked with an asterisk. The agreement between the two combinations is, indeed, very satisfactory. We may, therefore, conclude that the CCF angle is about 1° smaller, that the CCH angle is about 2° larger, and that the CCC angle is about 1–2° larger than the tetrahedral. The C−F distance is 1.37±0.01A.

This is substantially in agreement with the results of Beach and Stevenson for the other tertiary butyl halogenides. Moreover, the deviation of the CCH angle from 109° 28′ is in the direction expected. The microwave spectrum of SiF_3CH_3[3] has successfully been interpreted by assuming that a repulsive force exists between the fluorine and the hydrogen atoms.

The approximate identity of the C−F distances in CH_3F and TBF is in harmony with the dipole moments of the two compounds which are given in Table II together with dipole moments for a few other primary and tertiary organic halogenides.

Probably, there are only very small differences (∼0.01A) between carbon-halogen bond distances in primary and tertiary compounds.

[1] J. Y. Beach and D. P. Stevenson, J. Am. Chem. Soc. **60**, 475 (1938).
[2] J. Q. Williams and W. Gordy, J. Chem. Phys. **18**, 994 (1950).
[3] Minden, Mays, and Dailey, Phys. Rev. **78**, 347 (1950).

Intensities of Vibration-Rotation Bands*

ROBERT C. HERMAN AND KURT E. SHULER
Applied Physics Laboratory, The Johns Hopkins University, Silver Spring, Maryland
(Received November 20, 1952)

MODERN advances in infrared techniques have led to improved vibration-rotation band intensity measurements and a renewed interest in the calculation of transition probabilities. The early work of Dunham[1] and Rosenthal[2] has been extended recently by Crawford and Dinsmore[3] and Heaps and Herzberg.[4] The last-mentioned authors have given explicit formulas for the matrix elements $(v'|u|v'')$ and $(v'|u^2|v'')$ using Morse wave functions with $u=r-r_e$.

During the course of our studies in flame spectroscopy we have independently obtained the following formula for the matrix element $(v'|u|v'')$ using Morse wave functions:

$$(v'|u|v'')=-[a(v'-v'')(k-v'-v''-1)]^{-1} \times\left\{\frac{v'!(k-2v'-1)(k-2v''-1)}{v''!\prod_{t=0}^{v'-v''-1}(k-v'+t)}\right\}^{\frac{1}{2}}, \quad (1)$$

where $ar_e=(\omega_e x_e/B_e)^{\frac{1}{2}}$ and $k=1/x_e$. By use of these expressions for a and k, one can rewrite Eq. (1) as

$$(v'|u|v'')=-\frac{r_e(B_e/\omega_e)^{\frac{1}{2}}x_e^{(v'-v''-1)/2}}{(v'-v'')[1-(v'+v''+1)x_e]} \times\left\{\frac{v'![1-(2v'+1)x_e][1-(2v''+1)x_e]}{v''!\prod_{t=0}^{v'-v''-1}[1-(v'-t)x_e]}\right\}^{\frac{1}{2}}. \quad (2)$$

This somewhat more compact result is equivalent to that obtained by Heaps and Herzberg.[4]

In the approximation $(v'+v'')x_e\ll 1$, Eq. (2) yields for the square of the matrix element with $v'=v''+n$,

$$|(v''|u|v''+n)|^2\cong\frac{r_e^2B_ex_e^{n-1}}{\omega_e}\frac{(v''+n)!}{n^2v''!}(1+v''x_e), \quad (3)$$

or

$$|(v''|u|v''+n)|^2\cong|(0|u|n)|^2\frac{(v''+n)!}{n!v''!}(1+v''x_e). \quad (4)$$

The last equation generalizes the restricted result for $n=1$, 2, and 3 obtained by Crawford and Dinsmore[3] using perturbation methods. It is interesting to note that within the above approximation both Morse and perturbed harmonic oscillator wave functions yield the same result.

As pointed out by Heaps and Herzberg, the use of Morse wave functions both with linear and higher terms in the dipole moment expansion does not give particularly accurate intensity formulas. The authors are therefore extending the perturbation treatments of Dunham and of Crawford and Dinsmore to include second-order corrections throughout.

* Supported by the U. S. Navy, Bureau of Ordnance.

[1] J. L. Dunham, Phys. Rev. **35**, 1347 (1930).
[2] J. E. Rosenthal, Proc. Natl. Acad. Sci. **21**, 281 (1935).
[3] B. L. Crawford and H. L. Dinsmore, J. Chem. Phys. **18**, 983 (1950).
[4] H. S. Heaps and G. Herzberg, Z. Physik **133**, 48 (1952).

Approximate Formulas for Many-Center Integrals in the Theory of Molecules and Crystals*

PER-OLOV LÖWDIN
Department of Physics, University of Chicago, Chicago, Illinois†
(Received November 25, 1952)

A FUNDAMENTAL problem in the theory of molecules and crystals is the evaluation of atomic many-center integrals of the type

$$(ab|cd)=\int\int\psi_a(1)\psi_b(1)\{e^2|r_{12}\}\psi_c(2)\psi_d(2)d\tau_1d\tau_2, \quad (1)$$

where the ψ-functions are normalized atomic orbitals associated with the nuclei a, b, c, and d, which in special cases also may coincide. Useful approximate formulas for these integrals have been given intuitively by Sklar[1] and by Mulliken,[2] who have expressed them in terms of overlap integrals[3]

$$\Delta_{ab}=\int\psi_a\psi_bd\tau=\delta_{ab}+S_{ab} \quad (2)$$

and two-center integrals of the Coulomb type. Recently, Rüdenberg[4] has shown rigorously that the Mulliken formula may be considered as being the first term in an infinite expansion of (1).

At the Shelter Island Conference in 1951, J. E. Mayer pointed out that charge densities (expressed in atomic units with $e=1$) of the form $\psi_a\psi_b-\Delta_{ab}\psi_a^2$ do not give any contribution to the total charge and that these "quasi dipoles" may be used in the interpretation of the energy expression.[5] The purpose of this note is to show that it is possible to use quantities of a similar type for deriving a generalization of the Sklar-Mulliken formulas.

For the sake of simplicity, let us assume that the charge distribution $\psi_a\psi_b$ has a "center of gravity" T, which is situated on the line connecting the nuclei a and b with respective distances α and β from them, and that similarly $\psi_c\psi_d$ has a center T' on the line connecting c and d with the distances γ and δ from them. We will then determine the coefficients in the expression $\lambda_a\psi_a^2+\lambda_b\psi_b^2$ from the condition that this quantity should have the same total charge and total moment as the density $\psi_a\psi_b$, which gives

$$\lambda_a=\Delta_{ab}(1+\alpha/\beta)^{-1},\quad \lambda_b=\Delta_{ba}(1+\beta/\alpha)^{-1} \quad (3)$$

with $\Delta_{ab}=\Delta_{ba}$. In comparison to Mayer's idea this means that we are here considering a quantity $\psi_{ab}-\lambda_a\psi_a^2-\lambda_b\psi_b^2$, which does not contribute to the total charge nor to the total moment. Neglecting the influence of higher moments, we obtain the approximate formula

$$\psi_a\psi_b\approx\lambda_a\psi_a^2+\lambda_b\psi_b^2, \quad (4)$$

and similarly

$$\psi_c\psi_d\approx\lambda_c\psi_c^2+\lambda_d\psi_d^2. \quad (5)$$

Substituting these expressions into (1), we get finally

$$(ab|cd)=\lambda_a\lambda_c(aa|cc)+\lambda_a\lambda_d(aa|dd) +\lambda_b\lambda_c(bb|cc)+\lambda_b\lambda_d(bb|dd). \quad (6)$$

Hence, it is possible to evaluate the many-center integral (1) approximately in terms of the overlap integrals Δ_{ab} and Δ_{cd}, the quotients α/β and γ/δ, and the Coulomb integrals.

For symmetrical charge distributions with $\alpha=\beta$ and $\gamma=\delta$, the right-hand side of (6) will reduce to the Mulliken formula. However, in the case of unsymmetrical charge distributions, as for instance in ionic crystals, Eq. (6) seems to be an essential improvement of the previous one, and, in such a case, it probably also indicates a method of improving the convergence of the Rüdenberg procedure by using unsymmetrical multiplication factors.

In order to derive the Sklar formula, we observe that the quantities $\Delta_{ab}\psi_T^2$ and $\Delta_{cd}\psi_{T'}^2$ have the same total charge and the same total moment as the given distributions $\psi_a\psi_b$ and $\psi_c\psi_d$, respectively. Neglecting higher moments, we therefore get

$$\psi_a\psi_b\approx\Delta_{ab}\psi_T^2,\quad \psi_c\psi_d\approx\Delta_{cd}\psi_{T'}^2. \quad (7)$$

Here ψ_T and $\psi_{T'}$ are atomic orbitals associated with the centers of gravity T and T', respectively, which have to be chosen in a suitable way.[1] Substitution of (6) into (1) gives then the approximate formula

$$(ab|cd)=\Delta_{ab}\Delta_{cd}(TT|T'T'), \quad (8)$$

which is essentially the Sklar formula. By combining the forms of (4) and (7), a still better result may sometimes be obtained by using a three-parameter formula and a third condition related to one of the higher moments.

The effect of the higher moments in general and the correction terms in (6) and (8) may be found by comparing these formulas with the exact expressions derived in another way.[6] However, a direct comparison with the numerical values of the integral (1) in special cases, previously obtained by us[7] for some alkali and alkali metals and with Lundqvist's[8] material for LiH, shows that formulas (6) and (8) in most cases have a surprisingly high accuracy, but also that there exist exceptional integrals of certain degenerate types which are better treated by more direct methods.

Equations (6) and (8) are intended for use, e.g., in the MO–LCAO method based on ordinary atomic orbitals (AO). If the molecular orbitals instead are built up from orthonormalized AO,[9] the use of (4) and (5) for the ordinary AO will lead to results which are related to those recently intuitively given by Parr.[10]

Finally, we wish to remark that the author's expressions[11] for the total and cohesive energies for the ground state of a molecule or crystal having its total wave function approximated by a single

determinant may be essentially simplified by using Eq. (6) and by summing the contributions from all matrix elements constituting the coefficients of the remaining Coulomb integrals; in this process it is even possible to treat the degenerate integrals separately. More details will be given in a survey of the various methods of evaluating many-center integrals to be published elsewhere.

I would like to express my sincere gratitude to Professor R. S. Mulliken for many valuable discussions and for his great hospitality during my stay in Chicago.

* Work assisted by the U. S. Office of Naval Research.

† Permanent address: Institute for Mechanics and Mathematical Physics, University of Uppsala, Uppsala, Sweden.

[1] A. L. Sklar, J. Chem. Phys. **7**, 984 (1939); A. London, J. Chem. Phys. **13**, 396 (1945).

[2] R. S. Mulliken, J. chim. phys. **46**, 497, 675 (1949), see particularly Eqs. (63) and (154b).

[3] Note the different meanings of the symbol S in papers by different authors; we have always used this notation for the *deviation* from normality and orthogonality for a set of functions, and, for $a=b$, we have therefore $S_{aa}=0$.

[4] K. Rüdenberg, J. Chem. Phys. **19**, 1433 (1951).

[5] See also Montet, Keller, and Mayer, J. Chem. Phys. **20**, 1057 (1952), and Keller's and Montet's Ph.D. theses, University of Chicago.

[6] S. O. Lundqvist and P. O. Löwdin, Arkiv Fysik **3**, 147 (1951).

[7] See P. O. Löwdin, J. Chem. Phys. **18**, 365 (1950); **19**, 1579 (1951), and references in these papers.

[8] S. O. Lundqvist, private communication.

[9] P. O. Löwdin, J. Chem. Phys. **18**, 365 (1950).

[10] R. G. Parr, J. Chem. Phys. **20**, 1499 (1952).

[11] P. O. Löwdin, J. Chem. Phys. **19**, 1570 (1951), Eqs. (33) and (51).

Hydrogen Peroxide Formation by Cobalt Gamma-Radiation

THOMAS J. SWORSKI

Chemistry Division, Oak Ridge National Laboratory, Oak Ridge, Tennessee

(Received December 1, 1952)

HYDROGEN peroxide formation in water irradiated with Co^{60} gamma-rays is shown in Fig. 1. The concentration in air-saturated pure water rises to a steady state measured after 16 hours of 143 μM/liter. The concentration in air-saturated 0.8N sulfuric acid, however, increases linearly with dose during the first hour and a concentration of 2840 μM/liter was measured after 17 hours. This acid effect is in agreement with the experiments of Ebert and Boag.[1] Hydrogen peroxide formation in helium-saturated 0.8N sulfuric acid, interpreted as the molecular yield, indicates the solution contains a radical remover. Since no measurable amount of hydrogen peroxide is observed in helium-saturated pure water, the radical remover may be the acid or an impurity contained in the acid (Baker and Adamson reagent grade). The presence of a radical remover may explain the linearity of hydrogen peroxide formation in air-saturated 0.8N sulfuric acid.

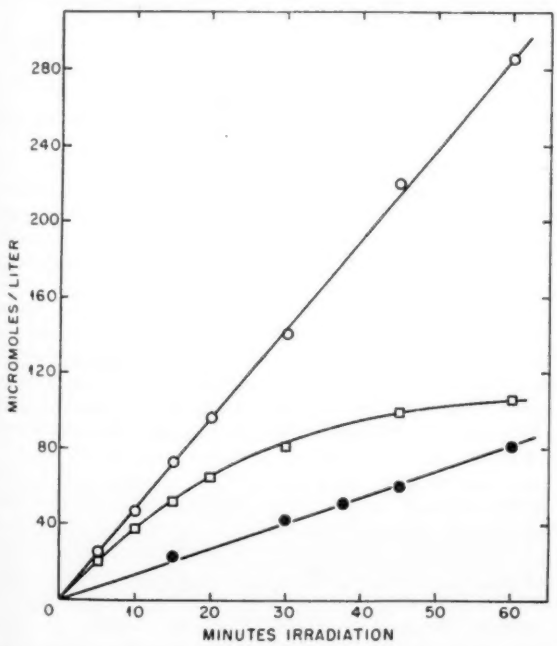

FIG. 1. Hydrogen peroxide formation by cobalt gamma-radiation: ○ air-saturated 0.8N H_2SO_4; □ air-saturated pure water; ● helium-saturated 0.8 N H_2SO_4.

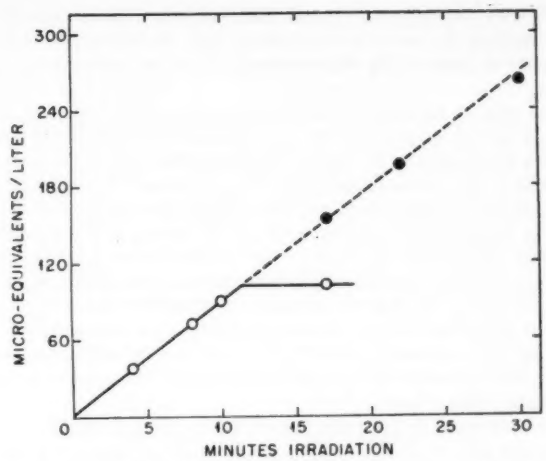

FIG. 2. Ceric sulfate reduction and hydrogen peroxide formation in air-saturated 0.8N H_2SO_4 by cobalt gamma-radiation: ○ cerous sulfate; ● hydrogen peroxide following complete ceric sulfate reduction.

The rate of hydrogen peroxide formation following complete ceric sulfate reduction is the same as that in air-saturated 0.8N sulfuric acid and is stoichiometrically equivalent to the rate of ceric sulfate reduction as shown in Fig. 2. This is in disagreement with the observations of Clark and Coe.[2] A similar stoichiometry has been reported between the reduction of chromate solutions and the formation of hydrogen peroxide in 0.8N sulfuric acid by x-rays.[3] The stoichiometry indicates that ceric sulfate reduction in solutions containing oxygen may take place through the intermediate formation of hydrogen peroxide and not by reaction

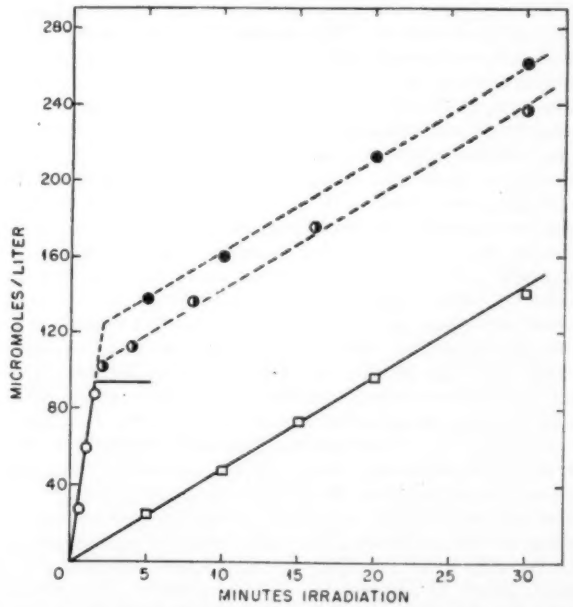

FIG. 3. Ferrous sulfate oxidation and hydrogen peroxide formation in air-saturated 0.8N H_2SO_4 by cobalt gamma-radiation: □ hydrogen peroxide formation in air-saturated 0.8N H_2SO_4; ○ ferric sulfate and ◑ hydrogen peroxide following complete ferrous sulfate oxidation, sample No. 1; ● hydrogen peroxide, sample No. 2.

either with OH radicals[4] or with HO_2 radicals.[5] The reduction of ceric sulfate is under investigation, and further experimental evidence substantiating this proposal will be presented in a later paper.

The rate of hydrogen peroxide formation following complete ferrous sulfate oxidation is the same as that in air-saturated 0.8*N* sulfuric acid as shown in Fig. 3. The higher initial rate of hydrogen peroxide formation reported by Fricke and Morse[6] is attributed to the build up of hydrogen peroxide during ferrous oxidation resulting in an "after irradiation effect" in ferrous sulfate concentrations 10^{-4} molar or less.[7,8] The concentration of hydrogen peroxide present when ferrous ions have been completely oxidized is a function of the time of continuous irradiation before complete ferrous oxidation. This is illustrated in Fig. 3 by a comparison of two samples containing initially 93.5 μM/liter of ferrous sulfate, No. 1 being intermittently irradiated and No. 2 being continuously irradiated during ferrous oxidation.

For values of 15.6 ferrous ions oxidized and 2.52 ceric ions reduced per 100 ev absorbed as the yields for the actinometers used,[7] the yield for hydrogen peroxide in air-saturated 0.8*N* sulfuric acid is evaluated as 1.26 molecules formed per 100 ev. A yield of 0.37 molecule of hydrogen peroxide per 100 ev for the molecular yield in 0.8*N* sulfuric acid is in agreement with the reported hydrogen yield[9] of 0.38 and the *p*H effect upon the molecular yield.[10]

[1] M. Ebert and J. W. Boag, Paper presented before The Faraday Society, Leeds, England, April 1952.
[2] G. S. Clark and W. S. Coe, J. Chem. Phys. **5**, 97 (1937).
[3] H. Fricke and E. R. Brownscombe, J. Am. Chem. Soc. **55**, 2358 (1933).
[4] Haissinsky, Lefort, and LeBail, J. chim. phys. **48**, 209 (1951).
[5] T. J. Hardwick, Can. J. Chem. **30**, 23 (1952).
[6] H. Fricke and S. Morse, Am. J. Roentgenol. Radium Therapy **18**, 430 (1927).
[7] C. J. Hochanadel and J. A. Ghormley, J. Chem. Phys. (to be published).
[8] F. S. Dainton, private communication; E. J. Hart, J. Am. Chem. Soc. **74**, 4174 (1952).
[9] C. J. Hochanadel, J. Phys. Chem. **56**, 587 (1952).
[10] E. R. Johnson and A. O. Allen, J. Am. Chem. Soc. **74**, 4147 (1952).

Photochemical Enrichment of Mercury 202

MURRAY ZELIKOFF, LEONARD M. ASCHENBRAND, AND PETER H. WYCKOFF
Geophysics Research Directorate, Air Research and Development Command, Air Force Cambridge Research Center, Cambridge, Massachusetts
(Received December 11, 1952)

THE original work on the photochemical separation of isotopes was performed by Mrowzowski.[1] The experiments to be described here were performed for the purpose of photochemically enriching mercury 202.

The light source used was an electrodeless discharge tube containing 91 percent mercury 202. This tube was constructed in a manner similar to that described elsewhere.[2] The lamp was excited in a microwave cavity[2] powered by a 2450-megacycle magnetron power supply. In order to produce unreversed Hg resonance radiation, the lamp was contained in a water jacket which, in turn, was surrounded by another tube through which was passed a stream of water vapor saturated with mercury. The pressure of water vapor was varied to some extent as was the pressure of nitrogen gas which was used as carrier in some of the experiments. Mercuric oxide deposited in a thermal precipitator through which the reaction mixture passed after exposure to the lamp. The mercuric oxide was collected, dissolved in dilute HNO_3, and the mercury plated out on a piece of copper wire. The product was analyzed on a Consolidated Engineering Corporation Analytical Mass Spectrometer (Model 21-103), precaution being taken to avoid contamination of the product by natural mercury.

The enriched product was found to vary in composition, depending on the conditions of the experiment. For example, at low H_2O (or H_2O+N_2) pressure, the enrichment appeared to be highest, about 20 percent; i.e., natural mercury contains 29.7 percent Hg 202 and the enriched product contained 35.5 percent Hg 202.

At very high pressures, 20 mm H_2O+740 mm N_2, no enrichment was detected. Thus, it appears that the extent of enrichment depends on the pressure-broadening of the absorption line. Some experiments showed that those isotopes whose hyperfine components lie close to that of Hg 202 were also enriched to an extent depending on the width of the absorption line which in turn depends strongly on the pressure of the absorbing gas. The Doppler broadening is probably unimportant here since the light source was water-cooled and the absorbing gas was at room temperature. A more detailed report of this work will be submitted.

Acknowledgment is made to the Oak Ridge National Laboratory for supplying the sample of Hg 202.

[1] S. Mrowzowski, Z. Physik **78**, 826 (1932).
[2] Zelikoff, Wyckoff, Aschenbrand, and Loomis, J. Opt. Soc. Am. **42**, 818 (1952).

Temperature Dependence of the Naphthalene Bands at 3200–2900A*

R. H. KNIPE AND H. SPONER
Department of Physics, Duke University, Durham, North Carolina
AND
C. D. COOPER
Department of Physics, University of Georgia, Athens, Georgia
(Received December 8, 1952)

FOR the weak absorption system of naphthalene at 3200–2900A, there are two possible assignments of current interest, ${}^1A_g-{}^1A_g$ [1-5] and ${}^1A_g-{}^1B_{3u}$.[6] According to the first assignment the band at 31 513 cm^{-1} would correspond to a 1−0 transition, and the stronger band at 32 454 cm^{-1} would be a 0−1 transition where the energy difference between the ground states has been taken as 476 cm^{-1}.[3,4] In the ${}^1A_g-{}^1B_{3u}$ assignment which characterizes a transition allowed by symmetry, the weakness of the system may be explained as result of an accidental cancellation of transition matrix elements. The assignment has in its favor that intensity changes upon substitution indicate the transition to be of the *g-u* type rather than of the *g-g* type[6] in naphthalene. In this assignment the transition moment lies in the molecular plane and along the long molecular axis. From measurements on the polarizations of fluorescence[7,8] and absorption[5] of naphthalene crystals, it became evident, however, that the transition moment is directed mainly along the short axis indicating ${}^1A_g-{}^1B_{2u}$ as effective transition. Accordingly, the interacting vibration in an electronic ${}^1A_g-{}^1A_g$ transition must be of type β_{2u}, and in a ${}^1A_g-{}^1B_{3u}$ transition of type β_{1g}. Raman line measurements do not include a line in the correct frequency region to be this β_{1g}. For the first interpretation to be valid the energy difference of 476 cm^{-1} must represent a β_{2u} vibration. This vibrational assignment has been proposed from polarized infrared studies.[9]

The interpretation of the system under consideration as a forbidden ${}^1A_g-{}^1A_g$ transition allowed by a 476 cm^{-1} vibration meets difficulties when extending it to completely deuterated naphthalene. Here the separation between the 1−0 and 0−1 bands is 912 cm^{-1} as compared to 941 in the ordinary compound, and the 476 vibration drops to a value of 403 cm^{-1}. As discussed previously,[3] it is quite unlikely that the interacting vibration in heavy naphthalene will have such a low value. Although, because of the great diffuseness of the bands in heavy naphthalene, the values of the 1−0 and 0−1 bands are less accurate than those in the light compound, their separation should not be much affected. It is of interest in this connection that the assignment of the 476 difference to a β_{2u} vibrational mode may not be final.[10]

There remains still another possibility by which the existing difficulties might be removed, namely, that the bands at 31 513 and 32 454 cm^{-1} are 0−0 bands of two separate but overlapping electronic systems of different intensities. It was thought that the slightly different fine structure of the two bands might be taken as being in favor of the last possibility, although it may not be impossible in the other assignment. It was also noticed that other weak bands in the system which do not fit well in the general analysis and which show the same fine structure as the 1−0 band could be linked with this band in a separate progression not

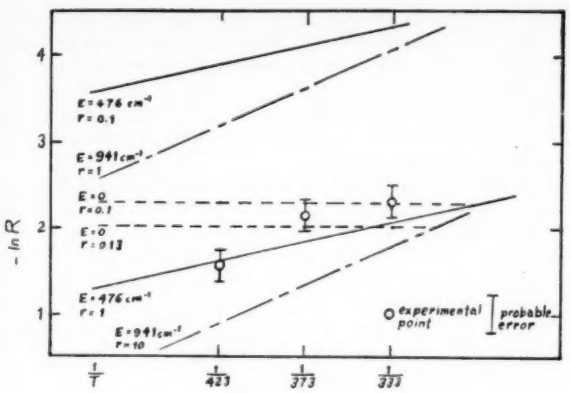

FIG. 1. Measured values of $-\ln R$ compared with theoretical curves of $-\ln R$ *versus* $1/T$ for possible values of E and r.

existing for the 0−1 band. The same situation is met in heavy naphthalene.

To test the different possibilities, the temperature dependence of the two bands has been investigated. Two methods have been used. First, the number of molecules in the absorption cell was maintained constant, and the two bands were photographed in first order with a 3 m grating spectrograph at 150°C, 100°C, and 60°C. The lower temperature is limited by the vapor pressure necessary to bring out the bands of interest, and the upper limit is determined by the Boltzmann factors. Unfortunately, this makes the useful temperature range very small. From the microphotometer traces of the plates, the quantity $R \simeq re^{-E/kT}$ could be measured. r is the transition probability of the 1−0 band relative to that of the 0−1 band, and E is the energy difference between the ground states of the two bands (Fig. 1). Second, the number of molecules in the absorption cell was varied by changing the pressure at a constant temperature of 100°C sufficient to compensate for the Boltzmann factor of an assumed 476 cm^{-1} vibration in the ground state of the 31 513 cm^{-1} band. r appeared to be the order of 1 (Fig. 2).

From the microphotometer traces of several exposures made at different exposure times, the measurements of optical density could be restricted to the region of the plates where it was found to be linear to within 10 percent. Probable errors were calculated on the basis of a 476 cm^{-1} difference between the two ground states neglecting the effect of deviations of naphthalene vapor from a perfect gas and the changing effect of collisions with pressure and temperature.

Examination of Fig. 1 suggests the existence of an energy difference between the ground states of the two bands. This result conforms to the assignment of a forbidden transition for the 3200–2900A system. Although these data should not be regarded as an actual measurement of the energy difference, the reasonable value of $r \sim 1$ requires that the difference be of the order of 500 cm^{-1}.

Although the method was somewhat crude and the results meager, they are presented here because it is felt that each additional contribution to the settlement of this assignment problem should be of value. This problem cannot be regarded as completely solved until all of the existing difficulties have been removed.

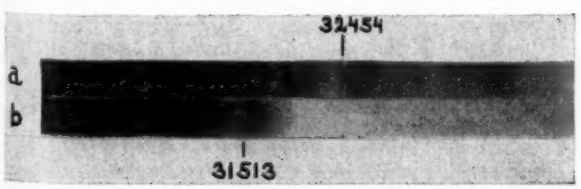

FIG. 2. Photographs from plates taken (a) at 100°C, 1.41 mm Hg, and (b) at 100°C, 8.84 Hg.

We would like to acknowledge the kind cooperation of Mr. B. W. Bullock and Dr. S. Silverman of the Applied Physics Laboratory (Silver Spring, Maryland) in obtaining the microphotometer tracings of our plates.

* Supported by the U. S. Office of Naval Research under Contract N6ori-107, T.O.I. with Duke University.

[1] D. P. Craig, Proc. Intern. Cong. Pure and Appl. Chem. **11**, 411 (1947).
[2] L. A. Blumenfeld, J. Phys. Chem. U.S.S.R. **21**, 529 (1947).
[3] H. Sponer and Gertrud P. Nordheim, Disc. Faraday Soc. **9**, 19 (1950).
[4] O. Schnepp and D. S. McClure, J. Chem. Phys. **20**, 1375 (1952).
[5] D. P. Craig and L. E. Lyons, J. Chem. Phys. **20**, 1499 (1952).
[6] John R. Platt, J. Chem. Phys. **17**, 484 (1949); **19**, 1418 (1951).
[7] S. Brodersen, Compt. rend. **233**, 1094 (1951); A. Kastler, Disc. Faraday Soc. **9**, 69 (1950).
[8] A. Prikhotjko, J. Phys. U.S.S.R. **8**, 257 (1944).
[9] George C. Pimentel and A. L. McClellan, J. Chem. Phys. **20**, 270 (1952).
[10] See remark on p. 1381 in reference 4.

The Pyrogenetic Formation of Ketones

R. I. REED
The University, Glasgow, Scotland
(Received December 12, 1952)

A MECHANISM, analogous to the "acetoacetic ester" condensation, proposed for the pyrogenetic formation of cyclic ketones,[1] has now been extended to include the formation of ketones from salts of the barium acetate type.[2] This mechanism is dependent on the presence of an α-hydrogen in the molecule, and thus it is necessary to attribute the formation of benzophenone to a special mechanism.

It is considered that this extension is not supported by the available evidence, and that the thermal decomposition of the alkali and the alkaline earth salts of benzoic, acetic, and isobutyric acids proceed by a mechanism involving free radicals.

The formation of benzaldehyde by the pyrolysis of mixtures of barium benzoate and barium formate at 450°C using an isotopic tracer technique, show that the aldehydic carbon is derived from the formate present.[3] The formation of benzene both in this reaction and in benzophenone formation is regarded as evidence of free radical formation, one of the reactions of the phenyl radical being the abstraction of a hydrogen to yield benzene.[4] The elevated temperatures necessary for significant reaction in this and similar compounds has already been adduced, in the case of acetaldehyde,[5] as evidence for a radical process.

The decomposition of sodium acetate is being studied in an attempt to determine the kinetic course of the reaction. These experiments are not yet concluded, but a series of measurements carried out in the temperature range 420°–500°C show that the reaction, followed by the formation of sodium carbonate, is of the order 3/2 with respect to the salt for at least 60 percent of the reaction, as shown in Fig. 1.

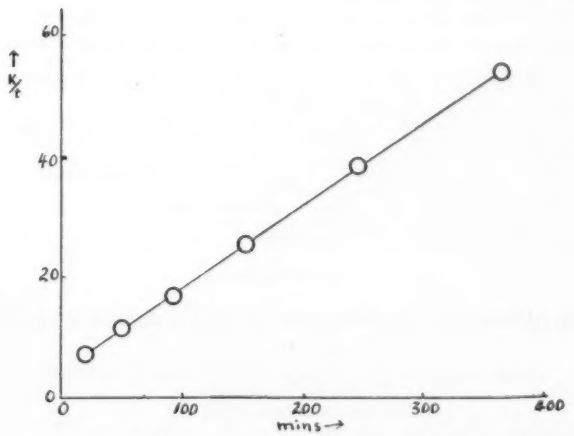

FIG. 1. K/t is plotted for values of the sodium carbonate formed, expressed as a percentage of the total possible reaction.

TABLE I.

Temp. °C	Ketone, as a % of the isobutyrate decomposed			
	Total	Di-*n*-propyl	Isopropyl-*n*-propyl	Di-isopropyl
380	100	43.1	43.7	13.2
420	100	44.9	41.9	12.2
460	35	19.0	12.0	3.7
500	13.3	8.8	3.4	1.1
540	8.0	5.7	1.8	0.4

An evaluation of the activation energy indicates that in the above temperature range, the value is nearly 50 kcal mol^{-1}. It is considered that this energy value and the nonintegral reaction order which is most readily interpreted as a chain reaction are consistent with a radical process.

The pyrolytic decomposition of isobutyric acid over a catalyst has been carried out with a careful analysis of all products.[6] In addition to the anticipated yield of di-isopropylketone, a small quantity of isopropyl-*n*-propylketone was obtained, and this was interpreted as resulting from an abnormal type of "Claisen" condensation. Attention was directed to the numerous other products, all of which could be obtained by the decomposition of the parent ketones. This variety of products has more recently been adduced as evidence for the radical nature of the reaction.[7]

Experiments on the pyrolysis of sodium isobutyrate[8] have yielded quantities of all three di-propylketones, as shown in Table I.

These experiments were carried out by pyrolyzing about one gram of sodium isobutyrate for a definite period of time at the appropriate temperature. The ketone formed was determined by preparing and weighing a derivative, and the decomposition of the isobutyrate was determined by estimating the sodium carbonate formed. The decomposition of the salt as a percentage of the original amount present, varied from 5–90 percent in these experiments.

These experiments are being continued in an investigation into the nature of the rearrangement. The results so far obtained are most readily interpreted by means of the following radical rearrangement:

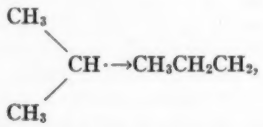

which has already been reported in the study of acetaldehyde formation.[5] A rearrangement of this type is implicit in one mechanism considered by Hamonet[9] as a means of interpreting the results of the electrolysis of potassium *n*- and *i*-butyric acids, and a similar explanation has been proposed in the photolytic decomposition of di-isopropylketone.[10]

These investigations are being continued and extended to include comparative studies on the formation of cyclic ketones.

[1] O. Neunhoeffer and P. Paschke, Ber. deut. chem. Ges. **72**, 919 (1939).
[2] K. B. Wiberg, J. Am. Chem. Soc. **74**, 4381 (1952).
[3] J. Bell and R. I. Reed (unpublished observations).
[4] D. H. Hey and W. A. Waters, Chem. Revs. **21**, 169 (1937). Evans, Braithwaite, and Field, J. Am. Chem. Soc. **63**, 2547 (1941).
[5] J. Bell and R. I. Reed, J. 1383 (1952).
[6] Miller, Cook, and Whitmore, J. Am. Chem. Soc. **72**, 2732 (1950).
[7] B. R. Brown, Quart. Rev. **5**, 146 (1951).
[8] W. A. O'Neill and R. I. Reed (unpublished observations).
[9] J. Hamonet, Compt. rend. **123**, 252 (1896).
[10] H. H. Glazebrook and T. G. Pearson, J. 1777 (1936).

Synthesis of Cyclobutene-d_6 and Cyclobutane-d_8

R. C. LORD
Department of Chemistry, Massachusetts Institute of Technology, Cambridge, Massachusetts
(Received December 12, 1952)

THE recent paper of Dunitz and Schomaker[1] serves to emphasize the fact that the spectroscopic work on cyclobutane reported in the literature some time ago needs to be repeated with the improved infrared equipment now available. This need was also seen in our laboratory, and study of the spectra of the molecule was undertaken. However, it seemed most desirable to study also the deuterium derivative cyclobutane-d_8, because of the well-known advantages[2,3] of isotopic molecules in the analysis of vibrational spectra.

Cope, Haven, Ramp, and Trumbull[4] have recently described a method of synthesis of cyclobutene that lends itself to the preparation of cyclobutene-d_6. In this procedure cyclo-octatetraene is reduced to 1,3,5-cyclo-octatriene, which is in equilibrium with bicyclo [4.2.0] octa-2,4-diene. A Diels-Alder addition of acetylene dicarboxylic methyl ester to the 2- and 5-positions of the bicyclo-octadiene then gives a tricyclic compound which cleaves readily on heating into dimethyl phthalate and cyclobutene. The latter can be hydrogenated easily to cyclobutane.

The changes in the synthesis of Cope *et al.*[4] to adapt it to the deuterium preparation are straightforward. Cyclo-octatetraene-d_8 is prepared by the polymerization of acetylene-d_2 [5] and is reduced to cyclo-octatriene-d_{10} by addition of lithium in ether with subsequent decomposition by deuterium oxide. Addition of the dimethyl acetylene dicarboxylate is then carried out as described by Cope *et al.*, as is the thermal decomposition of the adduct. Some 7.0 grams (0.12 mole) of cyclobutene-d_6 have been obtained by this procedure.

The cyclobutene-d_6 can be handled conveniently by addition of bromine to form the higher-boiling dibromo-cyclobutane, from which it is readily regenerated by treatment with zinc dust in alcohol.[6] Spectroscopic study of cyclobutene and cyclobutene-d_6 is now in progress and, upon completion of this study, that of cyclobutane and cyclobutane-d_8 will be carried out. This investigation is part of a general study of the spectra of simple hydrocarbons and their deuterium derivatives supported by the Office of Ordnance Research under Contract DA-19-020-ORD-896, Project TB5-0002(5).

[1] J. D. Dunitz and V. Schomaker, J. Chem. Phys. **20**, 1703 (1952).
[2] F. Halverson, Revs. Modern Phys. **19**, 87 (1947).
[3] B. L. Crawford, Jr., J. Chem. Phys. **20**, 977 (1952).
[4] Cope, Haven, Ramp, and Trumbull, J. Am. Chem. Soc. **74**, 4867 (1952).
[5] Lippincott, Lord, and McDonald, J. Am. Chem. Soc. **73**, 3370 (1951).
[6] G. B. Heisig, J. Am. Chem. Soc. **63**, 1698 (1941).

Absorption Band Systems of SiO and GeO in the Schumann Region

H. C. ROWLINSON AND R. F. BARROW
Physical Chemistry Laboratory, Oxford University, Oxford, England
(Received December 8, 1952)

ABSORPTION bands of SiO and GeO in the region 1250–2000A have been photographed on a 1-m normal incidence grating instrument with a reciprocal dispersion of about 8.5A/mm. A Lyman discharge was used as source of continuous radiation. The SiO systems were obtained by heating mixtures of Si and SiO_2 to temperatures in the range 1200–1500°C; the GeO bands were obtained by heating solid GeO to 750–800°C.

The vibrational analyses of two systems of red-degraded bands of each molecule have so far been completed. The constants for the states of these molecules now known are given in Table I. For both molecules, the strong bands of the $E-X$ systems are

TABLE I. Constants for the electronic states of SiO and GeO.[a]

State	SiO			GeO		
	ν_e	ω_e	$\chi_e\omega_e$	ν_e	ω_e	$\chi_e\omega_e$
F	68 562.5	1114.6	7.2	67 474.4	809.0	5.6
E	52 863.2	675	4.15	50 137.4	498.7	5.3
D	42 835.3	848.5	5.84	37 767	650.4	4.21
X	0	1242.03	6.047	0	985.5	4.29

[a] The constants for the states *X* have been taken from Herzberg (see reference 1); for the *D* state of SiO from Drummond (see reference 2); for the *D* state of GeO from Drummond and Barrow (see reference 3).

assigned to long $v''=0$ progressions; the values of v' for these systems are uncertain. The analyses of the much stronger $F-X$ systems are not in doubt, as in both cases the 0,0 band is the most intense. The 0,0 band of the $F-X$ system of SiO at 1459.9A is so strong as to appear in absorption on blank plates taken with a cold absorption tube, the SiO being formed from the silica capillary of the Lyman source.

It may be noted that some of the banded structure assigned by Pankhurst[4] to SiO_2 lies in the region for a transition $F\rightarrow D$ in SiO, and that the band at 6530A observed by Woods[5] is in the region for a transition $F\rightarrow E$ in SiO, but further work may show that these are accidental coincidences.

Comparison with other molecules of this group suggests that the dissociation energies of the E states may be about 45 percent of those given by linear extrapolations of the initial vibrational intervals. If this figure is assumed here, we obtain dissociation limits for SiO at 8.0_3 ev and for GeO at 6.8_2 ev. The analysis of thermochemical data leads to $D_0''(\mathrm{SiO})=7.15$ ev,[6] $D_0''(\mathrm{GeO})=6.81$ ev.[3] The closeness of the agreement in the case of GeO is no doubt fortuitous, and is best taken as evidence that $\mathrm{GeO}(E)\rightarrow \mathrm{Ge}(^3P)+\mathrm{O}(^3P)$. It seems most probable that the E state of SiO also dissociates into ground-state atoms; if this is so, then it appears that the present thermochemical value for $D_0''(\mathrm{SiO})$ may be a little too low.

[1] G. Herzberg, *Molecular Spectra and Molecular Structure. I. Spectra of Diatomic Molecules* (D. Van Nostrand Company, Inc., New York, 1950).
[2] G. Drummond (unpublished work).
[3] G. Drummond and R. F. Barrow, Proc. Phys. Soc. (London) **A65**, 277 (1952).
[4] R. C. Pankhurst, Proc. Phys. Soc. (London) **52**, 707 (1940).
[5] L. H. Woods, Phys. Rev. **63**, 426 (1943).
[6] L. Brewer and D. F. Mastick, J. Chem. Phys. **19**, 841 (1951).

Spectra of *p*-Fluorobenzonitrile in the Near Ultraviolet

C. Dewey Cooper
Physics Department, University of Georgia, Athens, Georgia
(Received November 19, 1952)

BOTH the solution and vapor absorption spectra of 1,4 FC_6H_4CN have been obtained between 3100–2200A. Two regions of absorption are observed. Using 2,2,4-trimethylpentane as the solvent, a strong absorption between 41 000 and 45 000 cm^{-1} has a maximum extinction coefficient of about 12 000 (see Fig. 1). The f values were not calculated for this transition because the absorption extends into the vacuum ultraviolet. A much weaker absorption with a maximum extinction coefficient of about 275 is found between 35 000 and 41 000 cm^{-1} (see Fig. 2).

The electronic transition involved in the weak region is the allowed A_1-B_1. Since one substituent on the ring is *meta* directing and the other *ortho-para* directing, the individual spectroscopic moments produced by each of the substituents are expected to be opposite in sign. In fact, these moments have been determined by Platt[1] to be -19 for CN and 21 for F. Then the predicted $\epsilon_{max}(sm)$ for 1,4 FC_6H_4CN is 154. From Fig. 2 the experimental value of $\epsilon_{max}(sm)$ is seen to be about 250, and the f value has been computed to be 3.9×10^{-3}. The difference in the predicted and experimental values is much greater than permitted by the accuracy quoted by Platt. A careful check shows that the experimental values are not excessively high due to an instrument error. In fact, we were able to reproduce, within 2 percent, the benzene curve reported in the A.P.I. Catalog of Ultraviolet Spectra Data,[2] Serial No. 26. The extinction coefficients for this curve were found to be lower than those in Serial[2] No. 40 which Platt used as a reference.

More than 500 bands have been measured in the vapor spectrum. These bands are very sharp and degraded toward the red in the weak transition region. The 0,0 band of this system is located at 36 616 cm^{-1} which represents a shift of 100 cm^{-1} toward the violet relative to the 0,0 band of benzonitrile.[3] This, along with the reported spectra of *p*-fluorotoluene,[4] *p*-fluorobenzotrifluoride,[4] and *p*-difluorobenzene,[5] indicates that the spectral shift produced by a fluorine atom substituted in the *para* position depends upon the directing power of the other substituent. If the first substituent is *meta* directing, then fluorine produces a violet shift; however, if the

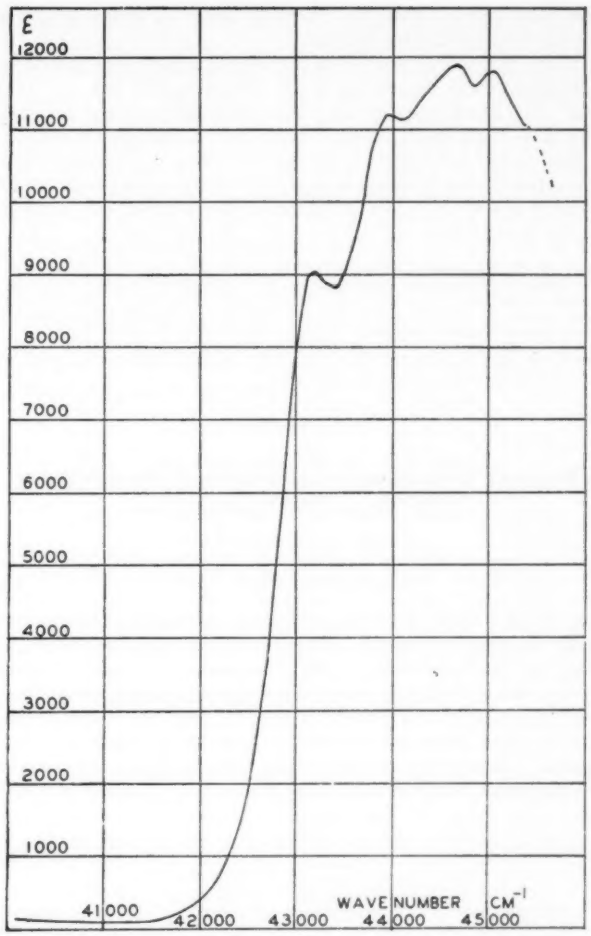

FIG. 1. Solution spectra of *p*-fluorobenzonitrile between 2450–2200A.

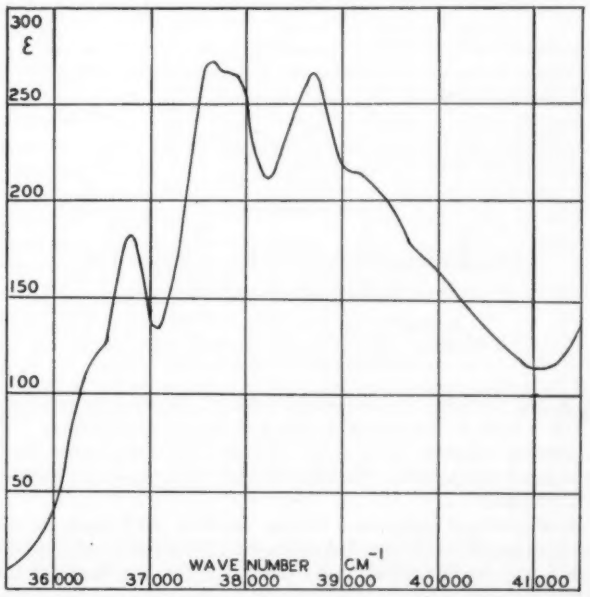

FIG. 2. Solution spectra of *p*-fluorobenzonitrile between 2800–2450A.

first substituent is *ortho-para* directing then a red shift is produced by the *para* substituted fluorine.

Bands in the weak portion of the spectrum have been associated with upper state frequencies of 147, 361, 499, 616, 794, and 1177 cm^{-1}. Also bands representing ground state frequencies of 178, 537, 644, 838, 1023, and 1242 cm^{-1} have been measured. Only broad diffuse bands are found in the strong absorption around 2200A. This transition is interpreted as an A_1-A_1 transition with the 0,0 band at 44 080 cm^{-1}. Further study of the spectrum is in progress at the present time.

[1] J. R. Platt, J. Chem. Phys. **19**, 263 (1951).
[2] *Catalog of Ultraviolet Spectrograms*, American Petroleum Institute Research Project 44, National Bureau of Standards (1945–1950), Serial No. 26 contributed by the Union Oil Company Serial No. 40 contributed by the Shell Development Company.
[3] R. C. Hirt and J. P. Howe, J. Chem. Phys. **16**, 480 (1948).
[4] W. T. Cave and H. W. Thompson, Disc. Faraday Soc. **9**, 35 (1950).
[5] H. Sponer, Phys. Rev. **87**, 213 (1952).

Nuclear Quadrupole Resonance in Some Metal Chlorides and Oxychlorides

H. G. DEHMELT*
Zweites Physikalisches Institut, Universität Göttingen, Germany
(Received December 8, 1952)

ABSORPTION lines due to nuclear quadrupole resonance[1] of the chlorine isotopes Cl^{35} and Cl^{37} have been detected in the compounds given below. As the chlorine atoms occupy different sites in the crystal lattices, the lines appear as multiplets. These multiplets spread out over a frequency range not wider than a few hundred kilocycles for the samples under discussion. Preliminary values for the frequencies, averaged over all lines in the multiplet ascribed to the Cl^{35} isotope, are given in Table I.

TABLE I.

Compound	Averaged frequency $\bar{\nu}(Cl^{35})$ Mc/sec	Number of lines in multiplet	Temperature
$AlCl_3 \cdot O(C_2H_5)_2$	11.30	2	liquid air
$SiCl_4$	20.35	4	liquid air
$SnCl_4$	24.09	4	liquid air
$SnCl_4 \cdot O_2NC_6H_5$	23.08	6	liquid air
$TiCl_4$	6.05	4	liquid air
$VOCl_3$	11.54	2	liquid air
CrO_2Cl_2	15.68	2	liquid air
MoO_2Cl_2	15.40	1	room

The lines due to the Cl^{37} isotope have been observed to occur at the frequencies expected from the known ratio $Q[Cl^{35}]/Q[Cl^{37}] = 1.26878 \pm 0.00015$.[2]

* Now at Duke University, Durham, North Carolina.
[1] H. G. Dehmelt and H. Krueger, Z. Physik **129**, 401 (1951).
[2] R. Livingston, Phys. Rev. **82**, 289 (1951).

The Proton Magnetic Resonance Line in Liquid Crystals

R. D. SPENCE, H. A. MOSES, AND P. L. JAIN
Michigan State College, East Lansing, Michigan
(Received December 1, 1952)

WE have observed the proton resonance in *para*-azoxyanisole both in the normal liquid and liquid crystal phase. The apparatus consisted of a twin-T bridge and the conventional associated components. The observations were made at a field of ~7300 gauss.

In the normal liquid state the line width is ≤ 0.1 gauss. As the temperature is reduced to below the transition point between the liquid and liquid crystal phase (135.8°C), the amplitude of the signal decreases greatly, and the line splits into three components as shown in Fig. 1. The separation between the two satellite peaks is about 3.3 gauss. As the temperature is decreased to below the transition point between the liquid crystal and crystalline phase (118°C) the signal again decreases, and we have been unable to obtain a satisfactory picture of the line shape.

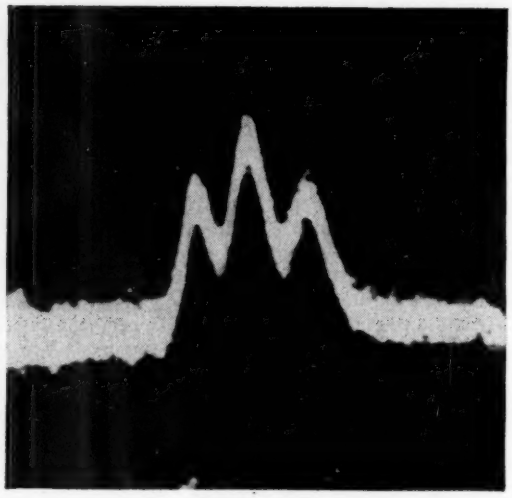

FIG. 1. Proton resonance signal from *para*-azoxyanisole in the liquid crystal phase.

The splitting in the liquid crystal phase may arise from a very strong hindering of the rotations of the methyl groups. An alternate possibility suggested by Dr. C. Kikuchi is that the protons in the benzene rings may be magnetically nonequivalent in the liquid crystal phase. We hope to extend these observations to the liquid crystal phases of *para*-azoxyphentole and *para*-azoxyanisolephentole.

Diffuse Spots of Pyrene at Higher Temperatures

M. N. DUTT
Department of Physics, Calcutta University, Calcutta, India
(Received December 17, 1952)

A PYRENE crystal was obtained by slow evaporation from a benzene solution. The substance crystallizes in the monoclinic system with $a=13.74$A, $b=9.22$A, $C=8.45$A, and $\beta=102°$ 30′. The space group of this crystal is

$$C_{2h}^5.$$

The number of molecules per unit cell is four. The crystal was mounted with the b axis vertical, and the x-ray beam was incident normally to $C(001)$ face of the crystal. The crystal shows extra Laue reflections from the $(\bar{3}10)$ and $(\bar{3}\bar{1}1)$ planes. These extra Laue reflections are found to be more intense as the temperature increases. At the temperature above 125°C, it was found that the lattice of the crystal is distorted.

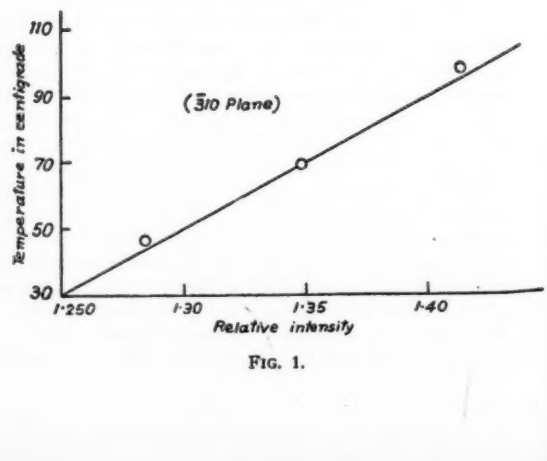

FIG. 1.

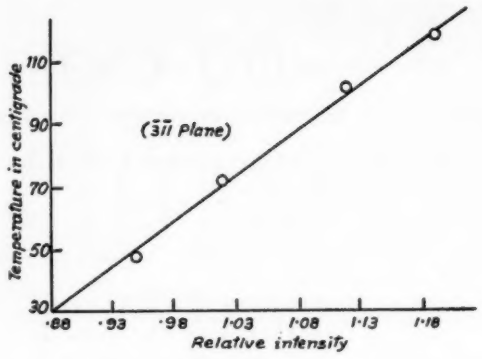

FIG. 2.

In order to have a standard for comparison of intensities of extra spots at different temperatures, a small quantity of aluminum powder was dusted over the crystal. The variation of the intensities of aluminum lines over the small range of temperature studied was neglected, however. The intensities were compared by means of a standard wedge, prepared according to the method of Robinson. The ratio of the (111) aluminum line to the maximum intensities of the extra spots were found by matching each of them against the standard wedge. It appears from the curve that intensities of extra spots increase very rapidly with the temperatures, and the variation of structure factor amplitude of two planes are different (see Figs. 1 and 2).

Erratum: Theory of Absorption Spectra of Carotenoids

[J. Chem. Phys. 20, 1661 (1952)]

GENTARO ARAKI
Faculty of Engineering, Kyoto University, Yosida, Kyoto, Japan

IN the previous letter[1] we attempted an explanation of the relation between absorption spectra and molecular lengths of carotenoids, making use of Tomonaga's method for electron gas with arbitrary couplings. We took into account the electron-spin for enumerating the number of electrons (occupying levels up to the Fermi maximum) only. If we take into account the spin degrees for wave functions we have, instead of Eq. (2) in the previous letter,[1] the following equation:

$$\delta=(L/\pi)^3(4/A)(N-2)^{-1}.$$

The empirical value of A thus becomes twice as large, $A=709.5$. The rest needs no change.

[1] G. Araki and T. Murai, J. Chem. Phys. 20, 1661 (1952).

Addendum: Directed Valence as a Property of Determinant Wave Functions

[J. Chem. Phys. 17, 598 (1949)]

HOWARD K. ZIMMERMAN, JR., *Department of Chemistry, Agricultural and Mechanical College of Texas, College Station, Texas*

AND

PIERRE VAN RYSSELBERGHE, *Department of Chemistry, University of Oregon, Eugene, Oregon*

IN his valuable recent review on "Quantum Theory, Theory of Molecular Structure and Valence" Professor Coulson[1] states that the idea of deriving directed valence properties from atomic wave functions (as written, for instance, under the form of determinants) "seems to have originated with Artmann,[2] but it has been "rediscovered" by Zimmerman and Van Rysselberghe[3]. . . ."

We wish to put on record that the tetrahedral valences of carbon were derived in this manner by one of us (P.V.R.) in 1933, that the calculations and results were communicated orally and by letter to several persons interested in the field, and that a communication to the editor of the *Journal of the American Chemical Society* giving a condensed presentation of this fundamental point was not published for reasons which, coupled with other preoccupations, resulted in our abandoning further work of this type. The problem was resumed in 1946 and led to our submitting a paper[3] to *The Journal of Chemical Physics* in July, 1948, publication following in July, 1949. In this paper we present the derivation of the tetrahedral valences of carbon in a manner identical with that of the intended communication of 1933, and we give reasons for offering our treatment of the whole problem of directed valences as an alternative to that of Artmann whose work had come to our attention through the abstract[4] published in September, 1947.

[1] C. A. Coulson, Ann. Rev. Phys. Chem. 3, 1 (1952), see p. 8.
[2] K. Artmann, Z. Naturforsch. 1, 426 (1946).
[3] H. K. Zimmerman, Jr., and P. Van Rysselberghe, J. Chem. Phys. 17, 598 (1949).
[4] Chem. Abstracts 41, 5785 (1947).

The Dissociation Energy of Fluorine*

PAUL W. GILLES AND JOHN L. MARGRAVE†
Department of Chemistry, University of Kansas, Lawrence, Kansas
(Received December 16, 1952)

RECENT spectroscopic data[1] on ClF imply a value for the dissociation energy of fluorine in the range 30–40 kcal/mol. Such a low dissociation energy would mean that considerable dissociation of diatomic fluorine into atoms must occur at relatively low temperatures. Doescher[2] and Wise[3] have reported experimental results that indicate a value for $D_0(F_2)$ between 36 and 39 kcal/mol.

The experiments reported here were carried out in 1950 on a sample of fluorine obtained from the Pennsylvania Salt Manufacturing Company. The pressure exerted by this sample of fluorine, when contained in a closed system of copper which had been previously treated with fluorine, was measured as a function of temperature over the range 300–860°K with a Bourdon type Dura gauge in two runs on different days. Between the two runs a slight leak into the system occurred so that about six percent of the gas was air in the second run.

When corrections are made (1) for the presence of this air in the second run on the basis that it did not react and (2) for the cooler zones of the system, the pressure calculated on the basis of no dissociation of an ideal gas agreed at all temperatures below 800°K with the experimentally observed pressure with standard deviations of ±0.02 inches of Hg for six points on the first day and of ±0.03 for six points on the second day.

Three measurements at temperatures above 800°K showed differences between observed and calculated pressures considerably greater than any found for the twelve lower temperature measurements. If it is assumed that these differences are caused by the partial dissociation of F_2 into atoms, one may calculate at each temperature the degree of dissociation, the dissociation equilibrium constant, and, by using the available data for the free energy functions of F and F_2,[4] the dissociation energy of F_2. Because of the corrections necessary for different temperatures in different parts of the system, the degree of dissociation α and the equilibrium constant K are not simply related to the pressure difference.

The data and results are shown in Table I, in which the calculated and observed pressures in the second run have been corrected for the air leak. The uncertainties listed are obtained by assigning to each pressure an uncertainty of ±0.03 inch of Hg.

TABLE I. Degree of dissociation, dissociation equilibrium constant, and dissociation energy of fluorine.

Run	T°K	Pobs (inches of Hg)	Pcalc (inches of Hg)	α	K (10^{-2} atmos)	$D_0(F_2)$ (kcal)
1	815	1.48	1.40	0.07±0.04	0.975±1.10	33.4±2.0
2	810	1.52	1.38	0.11±0.05	2.49 ±1.80	31.6±1.6
2	860	1.72	1.46	0.21±0.05	10.6 ±5.4	31.2±0.8

The weighted average of the values in the last column gives for $D_0(F_2)$ a value of 31.5±0.9 kcal/mol. Using the free energy functions[4] one calculates for the same quantity 36.5±1.0 from the data of Doescher[2] obtained in similar experiments at higher temperatures in a nickel container, and 39±1 from the graph of Wise.[3] It appears that the best value is 36±3 kcal/mol.

The electron affinity of fluorine may be related to the dissociation energy through a Born-Haber cycle. Studies by Ionov and Dukelskii,[5] in which positive and negative ion currents were observed during evaporation of alkali metal halides from a tungsten filament, allow calculation of the electron affinities of the halogen atoms if the proper work function for the tungsten surface is known. These experimenters found values for the electron affinities of chlorine, bromine, and iodine in good agreement with those given by other workers, when potassium halides were used and the work function for a clean tungsten surface was assumed. A similar treatment of their data on KF indicates a value of 83±3 kcal/mol for the electron affinity of F.

Metlay and Kimball[6] have studied the relative currents of negative ions and electrons emitted from a hot tungsten filament in the presence of fluorine. Although originally misinterpreted, the experimental data yield an average value for the electron affinity of 82±3,[7,8] in good agreement with the result of Ionov and Dukelskii.

If one uses the value 82±3 for the electron affinity of F in a Born-Haber cycle along with thermochemical data from the National Bureau of Standards Table "Selected Values of Chemical Thermodynamic Properties" and crystal energies of the alkali metal fluorides computed after Pauling,[9] he finds $D_0(F_2)=31\pm4$ kcal/mol, in agreement with the experimental value.

The authors are pleased to acknowledge the support of the U. S. Atomic Energy Commission in this work.

* Abstracted in part from a thesis presented by John L. Margrave in partial satisfaction of the requirements for the degree of Doctor of Philosophy at the University of Kansas, December 28, 1950.

† Present address: Department of Chemistry, University of Wisconsin, Madison, Wisconsin.

[1] A. L. Wahrhaftig, J. Chem. Phys. **10**, 248 (1942); H. Schmitz and H. J. Schumacher, Z. Naturforsch. **2a**, 359 (1947).

[2] R. N. Doescher, J. Chem. Phys. **19**, 1070 (1951); **20**, 330 (1952).

[3] H. Wise, J. Chem. Phys. **20**, 927 (1952).

[4] R. M. Potocki and C. W. Beckett, National Bureau of Standards Report 1294, December 1, 1951; L. Haar and C. W. Beckett, *ibid.* Report 1435, February 1, 1952.

[5] N. Ionov, Compt. rend. acad. sci. U.R.S.S. **28**, 512 (1940); N. Ionov and V. Dukelskii, Fiz. Zhur. **10**, 1248 (1940).

[6] M. Metlay and C. Kimball, J. Chem. Phys. **16**, 779 (1948).

[7] J. L. Margrave, thesis, University of Kansas (1950).

[8] R. B. Bernstein and M. Metlay, J. Chem. Phys. **19**, 1612 (1951).

[9] L. Pauling, *The Nature of the Chemical Bond* (Cornell University Press, Ithaca, New York, 1940), p. 340.

Partition Functions for Relating Entropy to Disorder in the Melting of Pure Metals

JOHN F. LEE
Mechanical Engineering Department, North Carolina State College, Raleigh, North Carolina

(Received December 11, 1952)

THE partition function due to Lennard-Jones and Devonshire[1] has been modified to avoid the controversial "communal entropy" following the suggestions of Ono.[2] Application has been made to the body-centered cubic lattice characteristic of some liquid metal coolants such as sodium.

The mean energy of an atom at a distance r from the center of its cell due to the nearest neighboring atom at a distance a from the same center is

$$\bar{u}(r)=\tfrac{1}{2}\int^{\pi} u\{(r^2+a^2-2ar\cos\theta)^{\frac{1}{2}}\}\sin\theta d\theta. \tag{1}$$

The energy of interaction of two spherical atoms separated by the distance r is

$$u(r)=4\epsilon_0\{(r_0/r)^{12}-(r_0/r)^6\}. \tag{2}$$

The energy $u(0)$ may be obtained by substituting Eq. (2) in Eq. (1) with the limit $r\to0$. Then the mean energy of the central atom is as follows, the number of nearest neighbors z being 8 for a body-centered cubic lattice:

$$z\bar{u}(r)-u(0)=z\epsilon_0\left\{\left(\frac{v_0}{v}\right)^4 l\left(\frac{r}{a}\right)^2-2\left(\frac{v_0}{v}\right)^2 m\left(\frac{r}{a}\right)^2\right\}. \tag{3}$$

Letting $y=(r/a)^2$ for convenience, the functions $l(y)$ and $m(y)$ are defined.

$$l(y)=(1+12y+25.2y^2+12y^3+y^4)(1-y)^{-10}-1,$$
$$m(y)=(1+y)(1-y)^{-4}-1.$$

The "free volume" is defined

$$v(0)=2\pi a^3 g, \tag{4}$$

and

$$g=\int_0^{y} y^{\frac{1}{2}}\exp\left\{-\frac{z\epsilon_0}{kT}\left[\left(\frac{v_0}{v}\right)^4 l\left(\frac{r}{a}\right)^2-2\left(\frac{v_0}{v}\right)^2 m\left(\frac{r}{a}\right)^2\right]\right\}dy,$$

where the upper limit of $y=(3/4\pi\sqrt{3})^{\frac{1}{2}}$ for a body-centered cubic lattice; or Eq. (4) may be expressed

$$v(0)=\int\exp\{-[z\bar{u}(r)-u(0)]/kT\}dr. \tag{5}$$

The integral extends over the cell.

The partition function for a single atom is

$$f=\left(\frac{2\pi mkT}{h^2}\right)^{\frac{3}{2}} v(0)\{-zu(0)/2kT\}. \tag{6}$$

The partition function for the whole assembly is found to be too low by a factor of e^N in the limit of the lower densities, this factor being in essence the "communal entropy." The partition function for the whole assembly is therefore

$$F=f^N e^N. \tag{7}$$

The "communal entropy" is avoided by regarding the existence of vacant sites which the preceding development ignores. If $x_i=N_i/N$ represents the ratio of the vacant sites to the total number of sites then zx_i is the number of vacant sites and $z(1-x_i)$ is the number of neighboring occupied sites. The energy at the center of the cell is $z(1-x_i)u(0)$, and the energy of the assembly is

$$u=\frac{z}{2}(N-\textstyle\sum_i x_i)u(0)+\sum_i (1-x_i)u_i. \tag{8}$$

The partition function for the assembly is

$$F=\left(\frac{2\pi mkT}{h^2}\right)^{3N/2}\Sigma\int dr_1\cdots\int dr_N\exp(u/kT). \tag{9}$$

When we substitute from Eq. (8),

$$F=\left(\frac{2\pi mkT}{h^2}\right)^{3N/2}\Sigma\exp\left[\frac{-z(N-\Sigma_i x_i)u(0)}{2kT}\right]\times\int\exp\{-(1-x_i)u_i/kT\}dr_i, \tag{10}$$

the generalized free volume being

$$v(x_i)=\int\exp\{-(1-x_i)u_i/kT\}dr_i. \tag{11}$$

When $x_i=0$, the neighboring sites are all occupied, and Eqs. (5) and (11) are identical. If $x_i=1$, the neighboring sites are all vacant. It is clear that some simple relationship must be found between $v(x)$ and x. Assuming $\ln v(x)$ to be linear in x, it can be shown that

$$\ln v(x)=x\ln v_1^*+(1-x)\ln v_0^*. \tag{12}$$

Following the suggestion of Ono modified for a body-centered cubic lattice,

$$v_0^*=v(0)=2\pi a^2 g=2\pi\sqrt{3}r_0^3(v/v_0)g,$$
$$v_1^*=v(1)=a^3/\sqrt{3}=r_0^3(v/v_0).$$

The solution now may be obtained using the methods of Fowler and Guggenheim.[3]

[1] Lennard-Jones and Devonshire, Proc. Roy. Soc. (London) **A163**, 53 (1937); **A165**, 1 (1938); **A169**, 317 (1939); **A170**, 464 (1939).

[2] Ono, Memoirs of the Faculty of Engineering, Kyushu University, Japan **10**, 190 (1947).

[3] R. H. Fowler and E. H. Guggenheim, *Statistical Thermodynamics* (Cambridge University Press, Cambridge, 1949), pp. 576–581.